PROCEEDINGS OF THE FIRST INTERNATIONAL SYMPOSIUM ON CLEANING TECHNOLOGY IN SEMICONDUCTOR DEVICE MANUFACTURING

SEMICONDUCTOR CLEANING TECHNOLOGY/1989

Edited by

Jerzy Ruzyllo
Pennsylvania State University
University Park, Pennsylvania

Richard E. Novak
FSI International
Chaska, Minnesota

Assistant Editors

M. Arienzo
A. Bowling
R. De Keersmaecker
K. Dillenbeck
D. Golland
M. Grunder
T. Ito
R. Reif
D. Tolliver

ELECTRONICS AND DIELECTRICS AND INSULATION DIVISIONS

Proceedings Volume 90-9

THE ELECTROCHEMICAL SOCIETY, INC., 10 South Main St., Pennington, NJ 08534-2896

Copyright 1990

by

The Electrochemical Society, Incorporated

Papers contained herein may not be reprinted and may not be digested by publications other than those of The Electrochemical Society in excess of 1/6 of the material presented.

Library of Congress Catalog Number: 90-81371

Printed in the United States of America

Preface

This softbound proceedings volume contains the papers presented during the First International Symposium on Wafer Cleaning Technology in Semiconductor Device Manufacturing held at the Electrochemical Society Fall Meeting in Hollywood, Florida, October 15-20, 1989. The symposium was sponsored jointly by the Electronics and Dielectrics and Insulation Divisions of the Society.

The papers in this volume are organized into seven sections according to subject. Within each section, papers are arranged in the order in which they were presented during the Symposium.

In passing this volume to the hands of the readers we would like to share a few observations related to semiconductor cleaning technology in general as well as the Symposium itself.

Wafer cleaning is the most frequently applied processing step in any IC fabrication sequence. In spite of this, an in-depth understanding of fundamental processes involved in cleaning, as well as influence of the numerous variables on the outcome of wafer cleaning operations appears to be insufficient. Consequently, all too often choices regarding wafer cleaning procedures are made on a "trial and error" basis rather than on sound recognition of interactions involved.

Although impressive progress has been made in wafer cleaning equipment and techniques, basic cleaning recipes have remained unchanged for over two decades. This has been caused by the uncertainty about exact capabilities and limits of present day wafer cleaning technology.This uncertainty is responsible for the reluctance to explore new avenues in wafer cleaning. However, for future applications new techniques and processes will have to be explored since it is believed that use of conventional wet cleaning operations will be severely restricted.

Wafer cleaning technology is at a crossroad and this Symposium, devoted solely to this topic, seemed to be both needed and timely. The goal of this First International Symposium on Wafer Cleaning Technology in Semiconductor Device Manufacturing was to make a step toward better

recognition of issues and problems pertinent to present, as well as future, semiconductor cleaning technology.

In retrospect, we may say the goal of this Symposium has been accomplished. As the organizers, we were particularly pleased with the quality and number of papers submitted and presented as well as the excellent attendance during all the sessions. We view this as an indication of growing awareness of problems facing wafer cleaning technology and the willingness of the research and industrial semiconductor community to participate in solving them. This awareness seems to be universal as a solid 40% of the papers contained in this volume were submitted and presented during this Symposium by authors from outside the United States.

To assure a continuing exchange of views and ideas on wafer cleaning technology, a decision was made to organize this symposium on a biannual basis. Consequently, the Second International Symposium on Wafer Cleaning Technology in Semiconductor Device Manufacturing will be held in 1991 during the Electrochemical Society Fall Meeting in Phoenix, Arizona.

We would like to take this opportunity to thank all symposium authors and participants who turned this Symposium into a very informative and productive meeting. In particular, we would like to thank all invited speakers, not only for their excellent contributions, but also for not turning our invitations down. Moreover, we are pleased to acknowledge our colleagues who assisted us in editing this volume and who chaired the Symposium sessions. Their help in the manuscripts revision process was particularly valuable.

This Symposium was initiated and organized on very short notice and was brought to fruition mainly due to support and decisive actions taken by the Chairmen of Electronics and Dielectrics and Insulation Divisions and the Society staff whom we would like to thank for their help and sponsorship.

Finally, we would like to acknowledge Mrs. F. J. Steffen at FSI International and Misses Kathy Miller and Wendy Woomer at Penn State for their assistance at various stages of Symposium and proceedings preparation.

Jerzy Ruzyllo
Richard E. Novak

TABLE OF CONTENTS

Preface *iii*

Overview 1

THE EVOLUTIONS OF SILICON WAFER CLEANING TECHNOLOGY, W. Kern (Invited) 3

Wet Cleaning Technology 21

CLEANING TECHNOLOGIES FOR HIGH-VOLUME PRODUCTION OF SILICON WAFERS, W. C. Krusell and D. I. Golland (Invited) 23

WET CHEMICAL PROCESSING IN A TRENCH, C. M. Tipton and R. A. Bowling (Invited) 33

INVESTIGATION OF H_2SO_4:H_2O_2 AND DILUTE HF SILICON WAFER CLEANING PROCESSES, L. A. Zazzera, L. S. Becker, P. E. Sobol, W. J. Eberle, and W. Katz 43

METALLIC CONTAMINATION ON Si WAFERS FROM CLEANING SOLUTIONS, J. Atsumi, S. Ohtsuka, S. Munehira, and K. Kajiyama 59

ADVANTAGES AND LIMITS OF WET ETCHING PROCESS IN SPRAY EQUIPMENT, D. Ross 67

CLEANING MECHANISM OF Si WAFER SURFACES BY THE SLIGHT ETCH METHOD, R. Takizawa and A. Ohsawa 75

THE USE OF REPROCESSED HF IN SEMICONDUCTOR QUARTZ AND WAFER CLEANING OPERATIONS, J. Davison, C. Hsu, E. Trautmann, and H. Lee 83

Dry Cleaning Technology 93

WAFER DRY CLEANING USING DILUTED ANHYDROUS HYDROGEN FLUORIDE GAS, T. Ohmi, N. Miki, H. Kikuyama, I. Kawanabe, and M. Miyashita (Invited) 95

A REVIEW OF UV/OZONE CLEANING TECHNOLOGY, J. R. Vig (Invited) 105

UV-ENHANCED DRY CLEANING OF SILICON WAFERS, T. Ito, R. Sugino, S. Watanabe, Y. Nara, and Y. Sato (Invited) 114

SEQUENTIAL VAPOR-PHASE WAFER CLEANING AND THIN FILM DEPOSITION, B. E. Deal, M. A. McNeilly, D. B. Kao, and J. M. de Larios 121

SURFACE DAMAGE DURING REMOTE PLASMA CLEANING OF SILICON WAFERS, D. G. Frystak and J. Ruzyllo 129

ELIMINATION OF METAL CONTAMINATION FROM PHOTORESIST BY USING THE OZONE ASHING TECHNIQUE, S. Onishi, K. Matsuda, K. Tanaka, and K. Sakiyama 141

ETCH PROPERTIES OF THERMALLY OXIDIZED SILICON NITRIDE. COMPARISON OF WET AND DRY ETCHING METHODS, L. M. Lowenstein and C. M. Tipton 148

EFFECTS OF LOW CONCENTRATION O_2 IN N_2 ON Si SURFACE CLEANING FOR SOLID PHASE EPITAXY, Y. Kunii 156

PARTICLES AND AIRBORNE CONTAMINANTS 165

REVIEW OF PARTICLE CONTROL METHODS DURING WET CHEMICAL CLEANING OF SILICON WAFERS, V. B. Menon and R. P. Donovan (Invited) 167

ULTRACLEAN ICE SCRUBBER CLEANING WITH JETTING FINE ICE PARTICLES, T. Ohmori, T. Fukumoto, T. Kato, M. Tada, and T. Kawaguchi (Invited) 182

STATISTICAL CONTRIBUTIONS TO THE SIZING OF PARTICULATES ON WAFERS BY LIGHT SCATTERING, S. Saadat, G. Kren, A. Neukermans, and J. Pecen 192

AIRBORNE CONCENTRATIONS OF ORGANIC VAPORS AND THEIR SURFACE ACCUMULATIONS ON WAFERS DURING PROCESSING IN CLEAN ROOMS, A. J. Muller, L. A. Psota-Kelty, J. D. Sinclair and P. W. Morrison 204

CHARACTERIZATION OF CLEANING 213

SURFACE COMPOSITION AND MORPHOLOGY OF Si WAFERS AFTER WET CHEMICAL TREATMENTS, M. Grundner, P. O. Hahn, I. Lampert, A. Schnegg, and H. Jacob (Invited) 215

ANALYSIS OF TRACE IMPURITIES ON WAFERS FROM CLEANING, R. S. Hockett (Invited) 227

IMPURITY ANALYSIS ON SILICON WAFER BY MONOCHRO TRXRF, K. Nishihagi and A. Kawabata 243

A DIFFERENTIAL REFLECTANCE STUDY OF THE CLEANING OF A SILICON SURFACE IN HYDROGEN FLUORIDE SOLUTIONS, U. S. Pahk and E. A. Irene 251

AUGER CHARACTERIZATION OF SILICON SURFACE CLEANED WITH H_2O_2 SOLUTION, P. M. Parimi and V. P. Sundarsingh 260

AN ANALYSIS FOR CLEANED SILICON SURFACE WITH THERMAL DESORPTION SPECTROSCOPY, N. Yabumoto, K. Minegishi, K. Saito, M. Morita, and T. Ohmi 265

SURFACE CHARGE ANALYSIS: A NEW METHOD TO CHARACTERIZE SEMICONDUCTOR/INSULATOR STRUCTURES: APPLICATION TO SILICON/OXIDE SYSTEM, E. Kamieniecki 273

CLEANING BEFORE THERMAL OXIDATION 281

THE EFFECT OF AQUEOUS CHEMICAL TREATMENTS ON Si SURFACE CHEMISTRY AND OXIDATION KINETICS, C. R. Helms, B. E. Deal, J. M. deLarios, and D. B. Kao (Invited) 283

THE IMPACT OF Si SURFACE CHARACTERISTICS ON MOS DEVICE YIELD, M. Heyns, C. Hasenack, R. DeKeersmaecker, and R. Falster (Invited) 293

THE INFLUENCE OF CLEANING ON THE OXIDATION MECHANISM OF SILICON, J.J. van Oekel 306

INFLUENCE OF THE PREOXIDATION CLEANING PROCEDURE ON OXIDE GROWTH RATE AND THE CHARACTERISTICS OF SUBOXIDE STATES, Z. M. Ling, L. H. Dupas, K. M. DeMeyer, J. Portillo, and W. Vandervorst 313

OXIDATION OF SILICON IN AIR OR NITROGEN AFTER VARIOUS HF ETCHES, P. A. M. van der Heide, H. W. L. Lindelauf, and H. J. Ronde 321

AGING OF HYDROPHILIC Si SURFACES AND ROUGHNESS OF THE Si/SiO_2 INTERFACE AFTER THERMAL OXIDATION, M. Grundner, P. O. Hahn and I. Lampert 328

EFFECT OF SILICON WAFER CLEANING ON PRE- AND POST-THERMAL OXIDATION CHARGES, A. Resnick, E. Kamieniecki, A. Philipossian, and D. Jackson 335

REMOVAL OF SURFACE ORGANIC CONTAMINANTS DURING THERMAL OXIDATION OF SILICON, S. D. Hossain, C. G. Pantano and J. Ruzyllo 341

THE EFFECT OF AMBIENT AIR INFILTRATION ON GROWTH RATE AND ELECTRICAL CHARACTERISTICS OF ULTRATHIN SILICON DIOXIDE GATE INSULATORS, A. Philipossian, D. Jackson, E. Kamieniecki, and A. Resnick 357

CLEANING OF III - V SEMICONDUCTORS 369

EPI GaAs SURFACE TREATMENT - IMPACT OF MIXED PHASES ON DEVICE PERFORMANCE, A. D. Warren and J. M. Woodall (Invited) 371

PROCESS DAMAGE AND CONTAMINATION EFFECTS ON SHALLOW SILICON IMPLANTED GaAs, H. Baratte, G. J. Scilla, T. N. Jackson, A. J. Fleischman, H. J. Hovel, and F. Cardone 377

IN-SITU SPECTROSCOPIC ELLIPSOMETRY STUDY OF THE CLEANING OF InP SURFACES, X. Liu and E. A. Irene 383

AUTHOR INDEX 393

SUBJECT INDEX 395

FACTS ABOUT THE ELECTROCHEMICAL SOCIETY, INC.

The Electrochemical Society, Inc., is a nonprofit, scientific, educational, international organization founded for the advancement of the theory and practice of electrochemistry, electrothermics, electronics, and allied subjects. The Society was founded in Philadelphia in 1902 and incorporated in 1930. There are currently over 5000 scientists and engineers from more than 40 countries who hold individual membership; the Society is also supported by more than 100 corporations through Patron and Sustaining Memberships.

The technical activities of the Society are carried on by Divisions and Groups. Local Sections of the Society have been organized in a number of cities and regions.

Major international meetings of the Society are held in the Spring and Fall of each year. At these meetings, the Divisions and Groups hold general sessions and sponsor symposia on specialized subjects.

The Society has an active publications program which includes the following.

JOURNAL OF THE ELECTROCHEMICAL SOCIETY - The JOURNAL is a monthly publication containing technical papers covering basic research and technology of interest in the areas of concern to the Society. Papers submitted for publication are subjected to careful evaluation and review by authorities in the field before acceptance, and high standards are maintained for the technical content of the JOURNAL.

EXTENDED ABSTRACTS - Extended abstracts of all technical papers presented at the Spring and Fall Meetings of the Society are published in serialized softbound volumes.

PROCEEDINGS VOLUMES - Papers presented in symposia at Society and Topical Meetings are published from time to time as serialized softbound Proceedings Volumes. These provide up-to-date views of specialized topics and frequently offer comprehensive treatment of rapidly developing areas.

MONOGRAPH VOLUMES - The Society has, for a number of years, sponsored the publication of hardbound Monograph Volumes, which provide authoritative accounts of specific topics in electrochemistry, solid state science and related disciplines.

OVERVIEW

THE EVOLUTION OF SILICON WAFER CLEANING TECHNOLOGY

Werner Kern

Lam Research Corporation, CVD Division
San Diego, California 92126

The purity of wafer surfaces is an essential requisite for the successful fabrication of VLSI and ULSI silicon circuits. Wafer cleaning chemistry has remained essentially unchanged in the past 25 years and is based on hot alkaline and acidic hydrogen peroxide solutions, the primary method used in the industry. What has changed is its implementation with optimized equipment: from simple immersion to centrifugal spraying, megasonic techniques, and enclosed system processing. Several alternative cleaning methods and wafer drying techniques have been investigated, including vapor etching and UV/ozone treatments. The evolution of wafer cleaning processes is traced from the 1950's to the present.

INTRODUCTION

The importance of clean substrate surfaces in the fabrication of semiconductor microelectronic devices has been recognized since the early days in the 1950's. As the requirements for increased device performance and reliability have become more stringent in the era of VLSI and ULSI silicon circuit technology, techniques to avoid contamination and processes to generate very clean wafer surfaces have become of critical importance. Besides, about 50% of yield losses in integrated circuit fabrication are due to contamination. Trace impurities, such as sodium ions, metals and particles, are especially detrimental if present on semiconductor surfaces during high-temperature processing (thermal oxidation, diffusion, epitaxial growth) because they may spread and diffuse into the semiconductor interior. Impurities must also be removed from surfaces before and/or after lower temperature steps, such as chemical vapor deposition, dopant implanting, and plasma reactions. Post- cleaning after photoresist stripping is necessary for every mask level through the production process.

Many wafer cleaning techniques have been tested and several are being used. The generally most successful approach for silicon wafers without metallization uses wet-chemical treatments based on hydrogen peroxide chemistry.

This process has remained essentially unchanged during the past 25 years, but important advances have been made in its technical implementation.

Impurities on silicon wafer surfaces occur in essentially three forms: (1) Contaminant films, (2) discrete particles, and (3) adsorbed gases that are of little practical consequence in wafer processing. Surface contaminant films and particles can be classified as molecular compounds, ionic materials, and atomic species. Molecular compounds are mostly particles or films of condensed organic vapors from lubricants, greases, photoresist, solvent residues, component from plastic storage containers, and metal oxides or hydroxides. Ionic materials comprise cations and anions, mostly from inorganic compounds that may be physically adsorbed or chemically bonded (chemisorbed), such as sodium ion, fluoride ions, and chlorine ions. Atomic or elemental species comprise metals, such as gold and copper, that may be electrochemically plated out on the silicon surface from HF-containing solutions, or they may consist of silicon particles or metal debris from equipment. Information on the nature, origin, detection and effects of contaminants is available from selected papers and reviews (1-13).

EARLY CLEANING PROCEDURES AND PROCESSES BASED ON HYDROGEN PEROXIDE MIXTURES

During the early stages of silicon wafer processing up to about 1970 one used organic solvent extraction, boiling nitric acid, aqua regia, concentrated hydrofluoric acid, and hot acid mixtures as cleaning chemicals. Mixtures of sulfuric acid-chromic acid led to chromium contamination and caused ecological problems of disposal. Mixtures of sulfuric acid and hydrogen peroxide caused sulfur contamination. Aqueous solutions containing hydrogen peroxide had long been used for cleaning electron tube components (14,15), but not for semiconductors. In general, impurity levels and particles in process chemicals were high and in themselves tended to lead to surface contamination. Particulate impurities were removed by ultrasonic treatment in detergent solutions or by brush scrubbing. The first caused frequent wafer breakage and the second often deposited more debris from the bristles than it removed from the wafer surfaces.

The first systematically developed cleaning process for bare or oxidized silicon wafers was based on a two-step oxidizing and complexing treatment with hydrogen peroxide solutions: 1) an alkaline mixture at high pH followed by 2) an acidic mixture at low pH (1). The choice of chemicals

was based on reaction chemistry, oxidation potentials, reagent purity, reagent volatility, safety and economy. The process was developed at RCA, introduced to device production in 1965, and published in 1970 (1).

In the first treatment step the wafers are exposed to a hot mixture of water-diluted hydrogen peroxide and ammonium hydroxide. This procedure was designed to remove organic surface films by oxidative breakdown and dissolution to expose the silicon or oxide surface for concurrent or subsequent decontamination reactions. Group IB and IIB metals and several other metals, including gold, silver, copper, nickel, cadmium, zinc, cobalt, and chromium are dissolved and removed by the complexing effectiveness of ammonium hydroxide; copper, for example, forms the $Cu(NH_3)_4^{+2}$ amino-complex.

The second treatment step exposes the rinsed wafer to a hot mixture of water-diluted hydrogen peroxide and hydrochloric acid. This procedure was designed to remove alkali ions, and cations such as Al^{+3}, Fe^{+3}, and Mg^{+2} that form NH_4OH-insoluble hydroxides in basic solutions. This second step also eliminates metallic contaminants that were not entirely removed by the first treatment, such as gold. Electrochemical displacement replating of heavy metals from the solution is prevented by formation of soluble complexes with the dissolved metals ions.

The solution compositions are based on ultrafiltered deionized water, electronic grade NH_4OH (29 w/w% as NH_3), electronic grade HCl (37 w/w%), and high-purity "unstabilized" H_2O_2 (30%). The hydrogen peroxide must be low in aluminum and stabilizer additives (sodium phosphate, sodium stannate, or amino derivatives) to prevent wafer recontamination. The usual volume ratios for the solution used in the first treatment step are 5 H_2O:1 H_2O_2: 1 NH_4OH; the mixture is known as "RCA standard clean 1 or SC-1". The usual volume ratios for the second solution are 6 H_2O:1 H_2O_2:1 HCl, "RCA standard clean 2, or SC-2". Treatments by the original immersion technique are typically 10 min at 75-80° C in each solution. Higher temperatures must be avoided to minimize excessive thermal decomposition of the hydrogen peroxide. Intermediate and final rinses in ultrafiltered deionized water are used.

The effectiveness of the process was demonstrated by sensitive radioactive tracer measurements with several radionuclides (1,16) and by capacitance-voltage bias temperature measurements of MOS capacitors (1). H_2O_2 solutions are unstable at elevated temperature, especially at high pH, rapidly decomposing to H_2O and O_2. The processing tempera-

ture should therefore be kept at 75-80° C to sufficiently activate the mixtures without causing excessively fast decomposition.

A preliminary clean up treatment with a hot H_2SO_4 - H_2O_2 mixture (2:1 vol.) can be used advantageously for grossly contaminated wafers having visible residues, such as photoresist layers. Another step, not noted in the original paper (1), concerns an etch in HF solution for bare silicon wafers. Since the hydrous oxide film from the SC-1 treatment may trap trace impurities, its removal before the SC-2 step should be beneficial. A 15-sec immersion in 1% HF-H_2O solution is sufficient to remove this film, as evidenced by the change from the hydrophilic oxidized surface to hydrophobic after stripping. However, unless high-purity and point-of-use ultrafiltered and particle-free HF solution is used under controlled conditions more harm than good can result. A silicon surface that was exposed to HF is highly reactive and immediately attracts particles and organic contaminants from solutions, D.I. water, and the ambient air. Contrary to SC-1, the subsequent SC-2 solution, which has no surfactant activity, will not eliminate these contaminants. It may therefore be preferable to rely on the dissolution action of SC-1 that dissolves and regrows the hydrated oxide layer at about the same rate. If the pre-clean is used, then the 1% HF step prior to SC-1 is acceptable since SC-1 will remove the contaminants. Exposure of bare silicon wafer to HF after SC-2 should not be done since it would destroy the passivated surface resulting from SC-2 and cause recontamination.

IMPLEMENTATION OF THE PEROXIDE PROCESS

The original RCA cleaning process was based on a simple immersion technique. Several different and improved techniques have been introduced over the years, as will be discussed. The immersion procedure is done in vessels of fused silica to prevent leaching of aluminum, boron, and alkalis if Pyrex glass were used. A batch of wafers is immersed in the SC-1 or SC-2 solution under the prescribed conditions. The reaction is terminated by overflow quenching with cold D.I. water before the wafers are transferred to a flow rinse system with ultrafiltered D.I. water, followed by spin drying in a wafer centrifuge. Several types of refined wet bench immersion systems for automated processing are now available for large-scale production (17-19).

In 1975 FSI Corporation introduced the first centrifugal spray cleaning machine specifically designed for automatic operation with corrosive chemicals. The wafers rotate past a stationary spray column. Filtered acids and

reagent solutions, including hot SC-1, SC-2, and D.I. water, are pressure-fed into a mixing manifold and then directed as a dispersed spray onto the spinning wafers. The spin-rinsed wafers are dried by high-speed spinning in heated nitrogen. A reduced volume of freshly mixed reagents is used and the process is faster than by immersion. The chemical cleaning efficiency, according to FSI, is comparable with that of immersion, but particles are removed more efficiently. Improved versions of this system (20) and other types of spray processing machines (17-19) are widely used, but tend to be maintenance extensive.

The original objective of the RCA cleaning process was the removal of contaminant films rather than particles. To complement this technique the megasonic particle removal system was developed at RCA and first described in 1979 (21). A highly effective non-contact scrubbing action on both front and backside surfaces of the wafers is achieved by ultrahigh frequency sonic energy while the wafers are submerged in the cleaning solution. The sonic waves of 850-900 kHz are generated by an array of piezoelectric transducers. Particles ranging in size from several micrometers down to about 0.3 µm can be efficiently removed with input power densities of 5-10 W/cm^2. For comparison, ultrasonic systems operate typically at 20-80 kHz and require power densities of up to 50 times that of the megasonic system, but are much less effective for removing very small particles. Megasonic cleaning made it possible to remove simultaneously contaminant films and particles in one operation by combining the peroxide treatments with megasonics. The system allows removal of particles, organic contaminant films, and lightly adsorbed contaminants with diluted SC-1 solution at the ambient bath temperature of only 35-42° C. Chemisorbed inorganics generally require higher temperatures (about 70° C) for complete desorption with SC-1 and SC-2, but no quantitative data are available as yet. A detailed paper on megasonic wafer cleaning was published in 1985 (22). Improved megasonic systems built under license from RCA have become available in the past few years from Verteq, Semiconductor Technology, and Estek.

A system termed Full-Flow^{TM}, developed in 1986 by CFM Technologies Inc., is based on keeping the wafers stationary and enclosed in the system during the entire cleaning, rinsing, and drying process (23). The vessel containing the wafers is hydraulically controlled to remain filled with hot or cold process fluids, including SC-1 and SC-2, that flow sequentially and continuously over stationary wafers loaded in cassettes. The repeated crossing through the gas/liquid

phase boundaries in the immersion techniques is thereby eliminated. The system thus avoids recontamination problems encountered when wafers are pulled out from a liquid.

CHRONOLOGICAL LITERATURE SURVEY

Beginning in 1972 independent investigators examined and verified by various analytical methods the effectiveness of the RCA cleaning method published in 1970 (1). This section reviews chronologically references on silicon wafer cleaning pertaining specifically to hydrogen peroxide solutions, up to mid-1989.

In 1972 Henderson published results on the evaluation of SC-1/SC-2 cleaning, using high energy electron diffraction and Auger electron spectroscopy as analytical methods (24). He concluded that the process is well suited for wafer cleaning prior to high-temperature treatments, as long as quartz ware is used for processing, as specified by us (1). An additional final etch in HF solution after SC-1/SC-2 caused carbon contamination and surface roughening during vacuum heating at 1100° C due to loss of the protective 1.5-nm thick C-free oxide film remaining after SC-2. Meek _et al._ (1973) investigated the removal of inorganic contaminants, including Cu and heavy metals, from silica-sol polished wafers by several reagent solutions (25). Using Rutherford backscattering, they concluded that SC-1/SC-2 preoxidation cleaning removes all elements heavier than Cl. Sulfur and chlorine remained after either SC-1, SC-2, or other cleaning procedures at $10^{13}/cm^2$. SC-1/SC-2 cleaning eliminated Ca and Cu much more reliably than did $HF-HNO_3$. Amick (1976) reported the presence of Cl on Si after SC-2 and S after $H_2SO_4-H_2O_2$; he used spark source mass spectrometric analysis (26). In 1976 Kern and Deckert published a brief review of surface contamination and semiconductor cleaning as part of a book chapter on etching (3). Murarka _et al._ (1977) studied methods for oxidizing Si without generating stacking faults and concluded that SC-1/SC-2 prior to oxidation is essential for this purpose (27). Gluck (1978) discussed removal of gold from Si by a variety of solutions. The desorption efficiency of SC-1 was more effective than that for SC-2, but the recommended sequential treatment of SC-1 followed by SC-2 was found the most effective method at high gold surface concentrations ($10^{14}/cm^2$ range) (28). Peters and Deckert (1979) investigated photoresist stripping by solvents, chemical agents, and plasma ashing. The SC-1 procedure was the only acceptable technique by which the residues could be removed completely (29). Burkman (1981) reported on desorption of gold

with several reagent solutions by centrifugal spraying. SC-1 type solution was much more effective than H_2SO_4-H_2O_2, while a SC-2 type alone showed poor efficiency (20).

Phillips et al. (1983) applied SIMS (secondary ion mass spectroscopy) to determine the relative quantities of contaminants on Si. Cleaned wafers were purposely contaminated with gross quantities of numerous inorganic materials and then cleaned by immersion or spray techniques with various aggressive reagents including aqua regia, hot fuming HNO_3, and H_2SO_4-H_2O_2. The lowest residual concentrations for most impurity elements were obtained by spray cleaning with H_2SO_4-H_2O_2 followed by the SC-1/HF/SC-2 type cleaning sequence (30). Goodman et al. (1983) demonstrated by minority-carrier diffusion-length measurements the effectiveness of SC-1/SC-2 for desorbing trace metals on Si (31). The author (1983) published a review of the subject on the occasion of the Citation Classic declaration of the original 1970-paper (32). In 1983 Watanabe et al. (33) reported dissolution rates of SiO_2 and Si_3N_4 films in SC-1. The rate of thermally grown SiO_2 in SC-1 during 20 min at 80° C was a constant 0.4 nm/min, a significant rate for structures with thin oxide layers. The etch rate of CVD Si_3N_4 was 0.2 nm/min under the same conditions. Measurements by the author in 1981 (and published in 1984), however, indicated much lower oxide dissolution rates under nearly identical conditions (34). Film thicknesses were measured by ellipsometry after each of four consecutive treatments in fresh 5:1:1 SC-1 at 85° C and totaled only 7.0 nm/80 min, or 0.09 nm/min. Under the same conditions, 6:1:1 SC-2 showed no loss. Similar results averaging 0.13 nm/min were obtained with thermal SiO_2 films grown on lightly or heavily doped Si. Wafers from the same sets were used to determine the etch rates of exposed Si in SC-1 solutions with decreasingly lower H_2O_2 content. No etching or attack of Si occurred until the H_2O_2 was reduced by more than 75% (34).

Bansal (1984, 1985) reported extensive results in particle removal by spray cleaning from Si wafers with SC-1/SC-2, H_2SO_4-H_2O_2, and HF solutions of various purity grades. He found the RCA cleaning solutions the most effective (35,36). Shwartzman et al. (1985) described simultaneous removal of particles and contaminant films by megasonic cleaning with SC-1 solutions (22). Ishizaka and Shiraki (1986) showed that atomically clean Si surfaces for MBE can be prepared below 800° C in UHV by thermal desorption of a thin (0.5-0.8 nm), passivating oxide layer that protects from C contamination (37). It is formed in a series of wet oxidation (HNO_3, SC-1) and HF-stripping steps, terminating with an SC-2 type treatment. Wong and Klepner (1986) used XPS analysis to examine Si after wet chemical

treatments. RCA cleaning without buffered HF stripping resulted in about 30% of the Si atoms in the top 1.0 nm being oxidized, whereas with a final BHF step less than one monolayer of suboxide coverage resulted (38). Grundner and Jacob (1986) conducted extensive studies of Si surfaces after treatment with SC-1/SC-2 or 5% HF solutions, using x-ray photoelectron and high-resolution electron energy loss-spectroscopy. Oxidizing solutions produced hydrophilic surfaces, whereas HF solution led to hydrophobic surfaces consisting mainly of Si-H with some $Si-CH_x$ and Si-F (39). In 1986 Becker et al. (40) reported on decontamination by different reagent sequences. SIMS analysis was used to test for the removal of Na, K, Ca, Mg, Cr, Cu, Al, and particle impurities. The best cleaning sequence for metallics was H_2SO_4-H_2O_2/SC-1/HF/SC-2. Reversing the order of SC-1 and HF was most effective for particle removal and slightly less so for metal ions. Kawado et al. (1986) found by SIMS that Al on Si wafers originated from impure H_2O_2 used in SC-2. Very high concentrations resulted if Pyrex vessels were used in the processing instead of fused quartz (41). In 1986 McGillivray et al. (42) investigated effects of reagent contaminants on MOS capacitors. Low field breakdown was more prevalent if preoxidation cleaning with SC-2 was terminated with HF solution instead of omitting it. No other significant differences in electrical properties resulted from these two treatments.

Lampert (1987) examined growth and properties of oxide films on Si in various aqueous solutions, including SC-1 and SC-2 (43). Gould and Irene (1987) studied the influence of preoxidation cleaning on Si oxidation kinetics (44). They found significant rate variations depending on treatment (SC-1/SC-2/HF, SC-1, SC-2, HF, no clean). Ruzyllo (1987) reported on similar experiments and found that various preoxidation cleans seem to affect structure and/or composition of the subsequently grown oxide rather than the reactivity of the Si surface (45). Slusser and MacDowell (1987) found that sub-ppm levels of Al in H_2O_2 used for SC-1/SC-2 causes a substantial shift (up to 0.2V) in the flat band voltage of a dual dielectric. Aluminum concentrates on the wafer surface, and basic media such as SC-1 lead to 5x higher levels than acid (SC-2) solutions (10). In 1987 Kern and Schnable reviewed wafer cleaning in a new chapter on wet etching (10). Probst et al. (1988) stated that for achieving predictable diffusion from implanted doped poly-Si into single-crystal Si an SC-1/SC-2 treatment of the substrate prior to poly-Si deposition is imperative (46). Khilnani (1988) discussed various aspects of semiconductor cleaning, including the RCA process (12). Peterson (1988) showed that the sequencing of cleaning solutions (H_2SO_4-H_2O_2, SC-1, SC-2, HF) can have dramatic effects on particle

levels (47). In 1989 Morita et al. (48) reported on the contamination of SC-1/SC-2 cleaned wafers by Na, K, Al, Cr, Fe, Ni, and Cu from solutions, showing that the absence or presence of an SiO_x layer on the Si surface strongly affect adsorption. Desorption of Al and Fe was most effective with HF-H_2O, and that of Cu and Cr with SC-2. The same authors (49) postulated that metals of high enthalpy of oxide formation adsorb on the oxidized Si surface by oxide formation, whereas metals of low ionization tendency deposit electrochemically on the bare Si. Gould and Irene (1989) studied the etching of native SiO_x and Si in NH_4OH-H_2O, BHF, and SC-1 by ellipsometry. Severe Si surface roughness resulted from NH_4OH, less with BHF, and none with SC-1 (50). Ohmi et al. (1989) compared particle removal efficiency of several cleaning solutions. They found that 5:1:1 SC-1 efficiently removes particles larger than 0.5um, but increased those smaller than 0.5um ("haze") unless the NH_4OH ratio was decreased to one half or less, in which case both types of particles were reduced efficiently. However, no processing conditions and effects of low-NH_4OH SC-1 on removal of chemical contaminant films were mentioned (51). Menon et al. (1989) evaluated effects of solution chemistry (5:1:1, SC-1, D.I. water) and particle composition on megasonic cleaning efficiency at various power levels. They concluded that cleaning efficiency depends on several factors and that megasonics can provide wafer cleanliness levels not previously attainable (52).

ALTERNATIVE METHODS: MECHANICAL, WET AND DRY CHEMICAL

Many techniques for cleaning silicon wafers have been tried over the years with various degrees of success. Some techniques are useful only for specific applications, or may introduce undesirable side effects. For example, glow discharge techniques (53), such as plasma etching, effectively strip photoresist films but leave inorganic contaminants and metals behind. Various types of sputter-etching (53) can cause surface damage. Some techniques remain restricted to certain applications, such as plasma treatments for preparing small-geometry devices for metallization (54), or wet-chemical etching of the silicon to remove entire surface layers by etch dissolution (3,11). The following few techniques have been found viable and, in some cases, can be a desirable addition or alternative to the processes based on hydrogen peroxide solutions.

The removal of large particles (e.g. after sawing and lapping operations) has been accomplished since the early days with wafer scrubbing machines that dislodge particles hydrodynamically with brushes made of a hydrophilic material (such as nylon) while D.I. water or isopropyl alcohol is ap-

plied to the surface (55). A thin layer of fluid must be retained between the brush and the wafers by careful mechanical adjustment to prevent surface scratching (22). While many contradictory claims have been made (56), if properly maintained, brush scrubbing can be very effective for removing particles larger than 1um from planar and preferably hydrophilic wafer surfaces.

High-pressure fluid jet cleaning consists of a high velocity jet of liquid sweeping over the surface at pressures of up to 4000 psi (55,56). The liquid can be D.I. water or organic solvents. The shear forces effectively dislodge submicron particles and penetrate into dense topography, but damage to wafer can result with improperly adjusted pressure (18).

Ultrasonic techniques use sonic energy of 20 kHz and above to dislodge particles. High intensity sound waves generate pressure fluctuations that result in cavitation bubbles which on collapsing release enough energy to dislodge and disperse particles, but can also lead to wafer damage (56). Menon _et al._ have recently investigated various cleaning liquids for removing particles from wafers by ultrasonic and spray jet techniques (57). D.I. water was best for removing polymeric particles, while ethanol-acetone (1:1) was best (better than Freons) for inorganic particles. Cleaning efficiency decreased with decreasing particle size. A unique acoustical cleaning system utilizing 20 kHz frequency and only D.I. water as medium was introduced by Estek in 1986 (18) but has been abandoned.

In contrast to the mechanical techniques for particle removal discussed in the previous section, choline cleaning is a chemical treatment that removes particles and some contaminant films, but at the same time appears to add certain contaminants to the surface. Choline, which is trimethyl-2-hydroxyethyl ammonium hydroxide, was first proposed by Asano _et al._ in 1976 (58) as a replacement for inorganic bases for etching and cleaning. It is a strong and corrosive base without alkali elements and etches silicon like other bases. A formulation of the chemical is available from Mallinckrodt under the tradename "Summa-Clean SC-15 M", which is a dilute choline solution containing a surfactant and methanol. Etching of Si can be prevented by adding H_2O_2 as an oxidant (59). There is very little published information on this subject, most data being contained in proprietary technical reports with contradictory results. Poly-flow Engineering manufactures an automatic dual-cassette spray machine that uses a warm choline-H_2O_2-H_2O mixture and a D.I. water spray rinse (18). In some procedures the mixture replaces only SC-1 in the RCA cleaning procedure. In 1989

Kaos discussed oxide defect densities as a function of various preoxidation cleans including choline-H_2O_2-H_2O, HF-H_2O, RCA cleans, and UV-ozone (60).

Irradiating a surface with short-wavelength UV from a mercury quartz lamp in the presence of oxygen is a powerful technique for removing many contaminants. Oxygen absorbs 185 nm radiation forming very active ozone and atomic oxygen (61). The technique is most suitable for oxidative removal of adsorbed organics, but is generally not effective for most inorganics or metals. Therefore, its use in the past has been limited to special applications, such as GaAs wafer cleaning. Improvements in oxide qualities have been attained by applying the technique after SC-1/SC-2/HF-H_2O, immediately before oxidation (62). Ruzyllo _et al._ (1989) have shown that UV-O_2 cleaning can replace SC-1 for removing organics (63), and Kaos reported improvements in properties of thermal oxide films (60).

Hoenig (1988) investigated the use of dry ice snow for removing particles from wafers (64). Clean, liquid CO_2 from a tank is allowed to expand to form dry ice snow, which is blown across the surface. The sliding snow is quite effective for mechanically removing particles. Particle detachment by electrostatic techniques has been investigated but found not practical (12). In 1987 FSI Corp. introduced a processing system for anhydrous HF gas phase etching of oxide and silicate films at room temperature (65). Applications to device processing were published in 1988 (66, 67). The contamination problems inherent with HF-H_2O solutions are avoided and in combination with the UV-ozone technique constitutes part of an ultra-pure, integrated dry cleaning process that can be carried out entirely in the gas phase and may replace conventional wet techniques. Removal of metallic impurities could be accomplished by use of a remote microwave plasma (68), by chlorine radical techniques (67), or by photo-induced desorption in reactant gases (69). These new processes being developed are all designed to remove contaminants at low temperatures as volatile compounds without damaging the surface.

WAFER RINSING AND DRYING

The last steps in wafer cleaning are rinsing and drying; both are extremely critical because clean wafers become recontaminated very easily if not processed properly. Rinsing after wet cleaning is done with flowing high-purity and ultrafiltered high-resistivity D.I. water, usually at room temperature (34). Megasonic rinsing is advantageous (52). Centrifugal spray rinsing (20) and rinsing in a closed system (23) have the advantage that the wafers are

closed system (23) have the advantage that the wafers are not removed between cleaning, rinsing, and drying. Wafer drying after rinsing must be done by physical removal of the water rather than by allowing it to evaporate. Spin drying accomplishes this and has been the most widely used technique. Hot forced air drying is a preferred technique with less chance for particle recontamination (21,22). Capillary drying is based on capillary action and surface tension to remove the water. Individual wafers are pulled out of D.I. water at 80-85° C; less than 1% of the wafer remains and evaporates, leaving a particle-free surface (70). In solvent vapor drying wet wafers are moved into the hot vapor of a high-purity solvent, usually IPA (isopropyl alcohol), which displaces the water. The wafers dry quickly and particle-free when the cassette is withdrawn above the hot vapor zone. Commercial drying systems for IPA and for non-flammable solvent mixtures are available (23,70). The purity of the solvent is extremely important, and the water content during processing must be closely controlled, preferably by continuous recycling (51,70).

CONCLUSION

Processes and techniques for cleaning, rinsing, and drying bare and oxide coated silicon wafers have been reviewed from the 1950's to the present. Wet chemical cleaning based on hydrogen peroxide solutions and implemented by several techniques is still the main process used in industry. However, new wafer surface preparation technologies based on dry processing in the gas or vapor phase are being developed that promise superior results. A great deal of research activity is taking place in this important area of technology, as evidenced by the scheduled presentations of over 40 papers at the First International Symposium on Wafer Cleaning Technology in Semiconductor Device Manufacturing, (October 16-18, 1989, Electrochemical Society National Meeting).

REFERENCES

1. W.Kern and D.Puotinen, "Cleaning Solutions Based on Hydrogen Peroxide for Use in Silicon Semiconductor Technology", RCA Review 31, 187-206 (1970).
2. W.Kern, "Radiochemical Studies of Semiconductor Surface Contamination-I.Adsorption of Reagent Components", RCA Review 31, 207-233 (1970).
3. W.Kern and C.A.Deckert, "Chemical Etching", Chap. V-1 in Thin Film Processes, J. L. Vossen and W. Kern, Editors, Academic Press, New York, 1978; pp. 411-413.

4. P.F. Schmidt and C.W. Pierce, "A Neutron Activation Analysis Study of the Sources of Transition Group Metal Contamination in the Silicon Device Manufacturing Process," Electrochem. Soc., 128 (3), 630-637 (1981).
5. W.T. Stacy, D.F. Allison, and T.C. Wu, "The Role of Metallic Impurities in the Formation of Haze Defects," in Semiconductor Silicon 1981, Proc. Fourth Internatl. Symp. on Silicon Mat. Sci. Technol., vol.81-5, H.R. Huff, R.J. Kriegler, and Y. Takeishi, Editors, The Electrochem. Soc., Inc., Pennington, NJ, 1981; pp. 344-353.
6. K. M. Eisele and E. Klausmann, "Effects of Heavy Metal Contamination from Corrosive Gas and Dopant Handling Equipment in Silicon Wafer Processing," Solid State Technol. 27 (10), 177-180 (Oct. 1984).
7. A. Licciardello, O. Puglisi, and S. Pignataro, "Effect of Organic Contaminants on the Oxidation Kinetics of Silicon at Room Temperature," Appl. Phys. Lett. 48 (1), 41-43, (1986).
8. J. Ruzyllo, "Pre-Oxidation Treatments to Reduce Defects and Contaminations," Technical Proc., Semicon/Europe '86, Zurich, March 3-6, 1986; pp. 10-17.
9. J. R. Monkowski, "Particulate Surface Contamination and Device Failures," Chap. 6 in Treatise on Clean Surface Technology, vol. 1, K.L. Mittal, Editor, Plenum Press, New York, 1987; pp. 123-148.
10. G.J. Slusser and L. MacDowell, "Sources of Surface Contamination Affecting Electrical Characteristics of Semiconductors," J. Vac. Sci. Technol. A-5 (4), 1649-1651 (1987).
11. W. Kern and G. L. Schnable, "Wet-Etching", Chap. 11 in The Chemistry of the Semiconductor Industry, S. J. Moss and A. Ledwith, Editors, Chapman and Hall, New York, 1987; pp. 235, 242-243.
12. A. Khilnani, "Cleaning Semiconductor Surfaces : Facts and Foibles," in Particles on Surfaces 1: Detection, Adhesion, and Removal, K. L. Mittal, Editor, Plenum, New York, 1988; pp. 17-35.
13. D.C. Burkman, C.A. Peterson, L.A. Zazzera, and R.J. Kopp, "Understanding and Specifying the Sources and Effects of Surface Contamination in Semiconductor Processing." Microcontamination 6 (11), 57-62, 107-111 (Nov. 1988).
14. D.E. Koontz, C.O. Thomas, W.H. Craft, and I. Amron, "The Purification of Ultraclean Electron-Tube Components by Chemical Etching", Symp. on Cleaning of Electronic Device Components and Materials; ASMT STP No. 246, pp. 136-145 (1959).
15. D.O. Feder and D.E. Koontz, "Detection, Removal, and Control of Organic Contaminants in the Production of Electronic Components," ibid, p.40.

16. W. Kern. "Radiochemical Studies of Semiconductor Surface Contamination-II. Adsorption of Trace Impurities", RCA Review 31, 234-264 (1970).
17. "Wafer Cleaning Equipment, 1986 Master Buying Guide, Semiconductor International 8 (13), 76-77 (1986).
18. K. Skidmore, "Cleaning Techniques for Wafer Surfaces," Semiconductor International 9 (9), 80-85 (August 1987).
19. P.H. Singer, "New Directions in Wet Chemical Processing," Semiconductor International 11 (8), 42-48 (July 1988).
20. D. Burkman, "Optimizing the Cleaning Procedures For Silicon Wafers Prior to High Temperature Operations", Semiconductor International 4 (7), 103-116 (July 1981).
21. A. Mayer and S. Shwartzman, "Megasonic Cleaning: A New Cleaning and Drying System for Use in Semiconductor Processing", J. Electronic Materials 8, 885-864 (1979).
22. S. Shwartzman, A. Mayer, and W. Kern, "Megasonic Particle Removal from Solid State Wafers," RCA Review 46, 81-105 (1985).
23. A.E. Walter and C.F. McConnell, "Stationary In Situ Wet Chemical Processing: The Impact on Wafer Surface Phenomena," 1988 Microcontamination Conf., Santa Clara, CA.
24. R.C. Henderson, "Silicon Cleaning with Hydrogen Peroxide Solutions: A High-Energy Electron Diffraction and Auger Electron Spectroscopy Study", J. Electrochem. Soc. 119, 772-775 (1972).
25. R.L. Meek, T.M. Buck, and C.F. Gibbon, "Silicon Surface Contamination: Polishing and Cleaning", J. Electrochem. Soc. 120, 1241-1246 (1973).
26. J.A. Amick, "Cleanliness and the Cleaning of Silicon Wafers", Solid State Technol. 47 (11), 47-52 (Nov. 1976).
27. S.P. Murarka, H.J. Levinstein, R.B. Marcus, and R.S. Wagner, "Oxidation of Silicon Without the Formation of Stacking Faults", J. Appl. Phys. 48, 4001-4003 (1979).
28. R.M. Gluck, "Gold Removal from Silicon with Dilute Peroxide Mixtures Containing NH_4OH and/or HCl", Electrochem. Soc. Ext. Abstr. 78-2, 640, (1978).
29. D.A. Peters and C.A. Deckert, "Removal of Photoresist Film Residues From Wafer Surfaces", J. Electrochem. Soc. 126, 883-886 (1979).
30. B.F. Phillips, D.C. Burkman, W.R. Schmidt, and C.A. Peterson, "The Impact of Surface Analysis Technology On the Development of Semiconductor Wafer Cleaning Processes", J. Vac. Sci. Technol. A-1 (2), 646-649 (1983).
31. A.M. Goodman, L.A. Goodman, and H.F. Gossenberger, "Silicon-Wafer-Process Evaluation Using Minority-Carrier Diffusion-Length Measurements by the SPV Method", RCA Review 44 (2), 326-341 (1983).

32. W. Kern, "Hydrogen Peroxide Solutions for Silicon Wafer Cleaning", RCA Engineer 28 (4) 99-105 (July/August 1983).
33. M. Watanabe, M. Harazono, Y. Hiratsuka, and T. Edamura, "Etching Rates of SiO_2 and Si_3N_4 Films in Ammonia-Hydrogen-Peroxide Cleaning Process", Electrochem. Soc. Ext. Abstr. 83-1, 221-222 (1983).
34. W. Kern, "Purifying Si and SiO_2 Surface with Hydrogen Peroxide," Semiconductor International 7 (4), 94-99 (April 1984).
35. I.K. Bansal, "Particle Contamination During Chemical Cleaning and Photoresist Stripping of Silicon Wafers," Microcontamination 2(4) 35-40 (Aug./Sept. 1984).
36. I.K. Bansal, "Autodoping and Particulate Contaminants During Pre-Diffusion Cleaning of Silicon Wafers," Solid State Technol. 29 (7), 75-80 (July 1986).
37. A. Ishizaka and Y. Shiraki, "Low Temperature Surface Cleaning of Silicon and Its Applications to Silicon MBE," J. Electrochem. Soc. 133 (4), 666-671 (1986).
38. C.Y. Wong and S.P. Klepner, "X-Ray Photoelectron Spectroscopy on Surface Oxidation of Silicon by some Cleaning Procedures," Appl. Phys. Lett. 48 (18), 1229-1230 (August 5, 1986).
39. M. Grundner and H. Jacob, "Investigations on Hydrophilic and Hydrophobic Silicon (100) Wafer Surfaces by X-Ray Photoelectron and High-Resolution Electron Loss- Spectroscopy," Appl. Phys. A-39, 73-82 (1986).
40. D.S. Becker, W.R. Schmidt, C.A. Peterson, and D. Burkman, "Effects of Various Chemistries on Silicon-Wafer Cleaning," in Microelectronics Processing: Inorganic Materials Characterization, Chap. 23, ACS Symp. Series No. 295, L.A. Casper, Editor, American Chemical Society, 1986; pp. 368-376.
41. S. Kawado, T. Tanigaki, and T. Maruyama, "SIMS Analysis of Aluminum Contaminants on Silicon Surfaces," Semiconductor Silicon 1986, Proc. Fifth Internatl. Symp. on Silicon Mater. Sci. Technol., H.R. Huff, T. Abe, and B. Kolbesen, Editors, The Electrochem. Soc., Inc., Pennington, N.J., 1986; pp. 989-998.
42. I.G. McGillivray, J.M. Robertson, and A.J. Walton, "Effects of Process Chemical Purity on MOS Capacitor Electrical Parameters," ibid., pp. 999-1010.
43. I. Lampert, "Influence of the Cleaning Method on the Chemical Behavior of Hydrophilic Silicon Surfaces," Electrochem. Soc. Ext. Abstr. 87-1, 381-382 (1987).
44. G. Gould and E.A. Irene, "Influence of Silicon Surface Cleaning Procedures on Silicon Oxidation," J. Electrochem. Soc. 174 (4), 1031-1033 (1987).
45. J. Ruzyllo, "Selected Aspects of Very Thin Oxide Growth Processes," ibid., pp. 1869-1870.

46. V. Probst, H.J. Bohm, H. Schaber, H. Oppolzer, and I. Weitzel, "Analysis of Polysilicon Diffusion Sources," J. Electrochem. Soc. 135 (3) 671-676 (1988).
47. C.A. Peterson, "Effect of Chemical Cleaning Sequencing on Particle Addition/Reduction on Silicon Wafers," in Particles on Surfaces 1: Detection, Adhesion, and Removal, K.L. Mittal, Editor. Plenum, New York, 1988; pp. 37-42.
48. E. Morota, T. Yoshimi, and Y. Shimanuki, "Adsorption and Reduction Behavior of Contaminant Metals on Si Wafer Surface (I)", Electrochem. Soc. Ext. Abstr. 89-1, 352-353 (1989).
49. T. Yoshimi, E. Morota, and Y. Shimanuki, "Adsorption and Reduction Behavior of Contaminant Metals on Si Wafer Surface (II)," ibid., pp. 354-355.
50. G. Gould and E.A. Irene, "An In Situ Ellipsometric Study of Aqueous NH_4OH Treatment of Silicon," J. Electrochem. Soc. 136 (4) 1108-1112 (1989).
51. T. Ohmi, H. Mishima, T. Mizuniwa, and M. Abe, "Developing Contamination-Free Cleaning and Drying Technologies," Microcontamination 7 (5), 25-32, 108 (May 1988).
52. V.B. Menon, A.C. Clayton, and R.P. Donavan, "Removing Particulate Contaminants from Silicon Wafers: A Critical Evaluation", Microcontamination 7 (6), 31-34, 107-108 (June 1989).
53. J.L. Vossen, "The Preparation of Substrates for Thin Film Deposition Using Glow Discharge Techniques," J. Phys. E: Sci. Instruments 12, 159-167 (1979).
54. J.L. Vossen, J.H. Thomas III, J.-S. Maa, and J.J. O'Neill, "Preparation of Surfaces of High Quality Interface Formation," J. Vac. Sci. Technol. A-2 (2) 212-215 (Apr.-June 1984).
55. P.S. Burggraaf, "Wafer Cleaning: Brush and High-Pressure Scrubbers," Semiconductor International 4 (8), 71-88 (July 1981).
56. J. Bardina, "Methods for Surface Particle Removal; A Comparative Study," in Particles on Surfaces 1: Detection, Adhesion, and Removal, K.L. Mittal, Editor, Plenum, New York, 1988; pp. 329-338.
57. V.B. Menon, L.D. Michaels, R.P. Donovan, and D.S. Ensor, "Effects of Particulate Size, Composition, and Medium on Silicon Wafer Cleaning," Solid State Technol. 32 (3), S7-S12 (March 1989).
58. M. Asano, T. Cho, and H. Muraoka, "Application of Choline in Semiconductor Technology," Electrochem. Soc. Ext. Abstr. 76-2, 911-913 (1976).
59. H. Muraoka, K.J. Kurosawa, H. Hiratsuka, and T. Usami, "Cleaning Solutions Based on Choline," Electrochem. Soc. Ext. Abstr. 81-2, 570-573 (1981).

60. P. Burggraaf, "Still Some Unknowns with Wafer Cleaning," Semiconductor International 11 (8), 15 (July 1989).
61. J.R. Vig, "UV/Ozone Cleaning of Surfaces," Chap. 1 in Treatise on Clean Surface Technology, Vol. 1, K.L. Mittal, Editor, Plenum Press, New York, 1987; pp. 1-26.
62. J. Ruzyllo, G.T. Duranko, and A.M. Hoff, "Preoxidation UV Treatment of Silicon Wafers," J. Electrochem. Soc. 134 (8), 2052-2055 (1987).
63. J. Ruzyllo, A.M. Hoff, D.C. Frystak, and S.D. Hossain, "Electrical Evaluation of Wet and Dry Cleaning Procedures for Silicon Device Fabrication," J. Electrochem. Soc. 136 (5), 1474-1476 (1989).
64. S.A. Hoenig, "Fine Particles on Semiconductor Surfaces: Sources, Removal, and Impact on the Semiconductor Industry," in Particles on Surfaces 1: Detection, Adhesion, and Removal, K.L. Mittal, Editor, Plenum Press, New York, 1988; pp. 3-16.
65. R. Cleavelin and G. Duranko, "Silicon Dioxide Removal in Anhydrous HF Gas," Semiconductor International 10 (12), 94-99 (Nov. 1987).
66. R.E. Novak, "Anhydrous HF Etching of Native SiO_2: Applications to Device Fabrication," Solid State Technol. 31 (3), 39-41 (March 1988).
67. N. Miki, H. Kikuyama, M. Maeno, J. Morota, and T. Ohmi, "Selective Etching of Native Oxide by Dry Processing Using Ultraclean Anhydrous Hydrogen Fluoride," IEDM Technical Digest 88, 730-733 (Dec. 1988).
68. J. Ruzyllo, "Evaluating the Feasibility of Dry Cleaning of Silicon Wafers," Microcontamination 3 (3), 39-43 (March 1988).
69. S.R. Palmer, "Your Surfaces Can Survive Atomic Cleaning," Research and Development 31 (5), 74-77 (May 1989).
70. K. Skidmore, "Dry Wafer Cleaning: Without Spinning," Semiconductor International 12 (8), 80-86 (July 1989).

WET CLEANING TECHNOLOGY

CLEANING TECHNOLOGIES FOR HIGH VOLUME PRODUCTION OF SILICON WAFERS

W. C. Krusell and D. I. Golland

MEMC Electronic Materials, Inc.
P.O. Box 8
St. Peters, MO 63376

ABSTRACT

This paper reviews the control of trace contaminants and surface particles during the production of silicon wafers in a high volume manufacturing environment. The efficacy of several wet processing schemes (HF strip, RCA chemistry, choline cleaning and ozone cleaning) are reviewed via SIMS analysis, gas chromatography, TXRF (Total Reflection X-ray Fluorescence Spectrometry) and electrical measurements. Particle control via the use of Clean Module technology is reviewed, with emphasis on the comparison of several types of automatic laser inspection equipment.

INTRODUCTION

The drive towards smaller device geometries and higher yields in VLSI and ULSI processing continues at a relentless pace. Silicon materials technology must support these developments with continuing improvements in bulk properties (crystal growth), mechanical parameters (slicing and polishing), and surface quality (cleaning and surface chemistry). This paper addresses the latter, specifically the control of trace contaminants and particulates on polished silicon surfaces.

In any discussion on silicon cleaning it is important to differentiate between the process technology used by materials manufacturers and that used in device houses. The former must remove gross contamination introduced during slice polishing. Major sources of contamination are shown in Table 1. In this paper we will describe approaches to organic, ionic, metallic and particulate control. The systematic reduction of contamination levels requires a combination of wet processing followed by stringent particle control in final wafer inspection and packaging.

WET PROCESSING

The sequence in wet processing generally involves organic removal, followed by oxide stripping, followed by surface oxidation.

Most wet cleaning schemes "peel the onion" in this sequence for the following reasons: First, organics are generally on the top surface of the silicon and if not removed will shield the oxide, resulting in residual metals and uneven oxidation in subsequent downstream processing. Second, oxide stripping is where the bulk of metal cleaning occurs. Finally, oxidation produces a hydrophilic surface which lends itself to particle removal and also yields a passivated surface for shipping.

This final step is where we see major differences in process approaches. For many years the RCA chemistry (1) was the workhorse of the industry. This involved a two-step treatment consisting of dilute NH_4OH and H_2O_2 in H_2O, followed by dilute HCl and H_2O_2 in H_2O. In recent years process deviations from the RCA approach have followed one of two paths. One approach has been to search for "cleaner" chemicals, as exemplified in the development of choline cleaning.(2) The other approach has involved a systematic reduction in the number of chemicals required to clean silicon (e.g. ozone cleaning).(3) The cleaning sequences evaluated in this paper are RCA clean, choline clean and ozone clean.

i) Organic Contamination

Table 2 shows organic contamination on silicon wafers cleaned by three chemical sequences. Contamination levels are expressed as total volatile organics measured by gas chromatography. Measurements were made on a Perkin-Elmer G.C. using a FID detector and fused silica capillary columns.

The "fresh" wafers were captured immediately after cleaning and placed in flamed pyrex Petri dishes for analysis. We see that wafers after ozone cleaning show considerably lower organic levels than those cleaned by either RCA or choline chemistry. This can be explained in terms of ozone digesting carbon contaminants in the cleaning baths and also providing a more passive surface. The latter effect is further demonstrated by the data after one hour exposure in a typical cleanroom environment. The effect of airborne organic vapors on wafer surfaces during cleanroom processing will be quantified by Muller et al at this Conference.(4) In Table 2 we see that the rate of organic deposition is probably highly dependent upon the as-cleaned surface condition.

ii) Oxide Stripping

Oxide stripping in dilute HF baths has been a mainstay in both silicon wafer production and in wafer fab lines for many years. Strip baths have generally been considered "dirty" because wafers removed from them typically have high particulate levels. Only with the advent of SIMS analysis, and its application to the analysis of

silicon cleaning, have we come to understand the efficiency with which metallic species can be controlled by HF treatments.

Table 3 shows the degree to which elements such as Na, Al, Fe, etc. can be reduced after treatment in a 10% HF solution. Table 3 also shows how the efficacy of the HF treatment is increased with the addition of HCl. The chloride ion from HCl complexes the Analytical Group III metal ions and heavy noble metals such as gold. Thus, the plateback of metal ions such as; Al^{+3}, Zn^{+2}, Ca^{+2}, Ni^{+2}, Mn^{+2}, Fe^{+3} and Cu^{+3} as well as Au^{+1} and Au^{+3} are greatly reduced by the formation of their soluble acid chlorides.

iii) **Surface Oxidation**

The aim in this step is to grow a hydrophilic passivating oxide. This step is generally considered necessary in a silicon manufacturers house in order to facilitate particle removal. However, this is also the step where the compromise between surface cleanliness with respect to metallic contamination and particulate removal begins. Like other investigators, we have seen a wide range of ionic contamination on wafers delivered by RCA chemistry due to variations in metal contaminant levels in semiconductor grade chemical reagents.(5) Wide fluctuations in wafer contamination frequently occur due to relatively narrow "permissible" (within-specification) variations of trace metals in NH_4OH, HCl and H_2O_2.

This issue can be addressed by either improving the quality of the chemicals in question, replacing the chemicals with others which serve the same function but which can be synthesized to higher purity (e.g. choline), or by systematically reducing the number of liquid chemicals (e.g. replace H_2O_2 with ozone gas). The effectiveness of the latter approach is clearly demonstrated in Tables 4 and 5 and is further validated in a sequential sampling experiment shown in Table 6. In this experiment, wafers were first processed through ozone oxidation baths and then half of the batch was transported directly to the RCA - "B" bath. The two groups of wafers were then analyzed by SIMS. The experiment was repeated with a new batch of chemicals and we see wide variation from batch-to-batch for the RCA "B" treatments.

The control of variability in metallic contamination translates directly to more consistent performance with respect to electrical characteristics, as shown in Table 7.

In addition to better control of metallic contamination, oxidation with ozone appears to provide better oxide surface coverage than H_2O_2 as evidenced by Auger spectroscopy (Figures 1-3) and by grazing angle ESCA (Table 8).

In the next section we will review the topic of particle control. As bridge to this topic the issue of metallic contamination from

autoscrubbing is worthy of mention. Autoscrubbing is used extensively in both the silicon materials industry and in wafer fabrication. It is well recognized that the use of dilute ammonia solutions on auto scrubbers can greatly increase the effectiveness of particle removal, but this is achieved at the expense of metallic contamination as indicated in Table 9.

PARTICLE CONTROL

The reduction of scaling of device dimensions has been the overriding trend in semiconductor technology for over a decade, and there is little sign of letup in the foreseeable future. The trend is summarized in Table 10. Linewidths will shrink from the 2 µm level required for 256K memory chips to ~0.25 µm for 16M BIT chips. With the generally accepted assumption that maximum defect size is 50% of linewidth, we see maximum particle sizes decreasing to ~0.1 µm within the next three to five years.

Particle control in high volume production situations requires close attention to air and water quality, and a high degree of process automation to eliminate operator interfaces. When particle control has been achieved at the final cleaning station, it must be maintained through final wafer inspection, packaging and delivery to the wafer fab line. A total system approach, The Clean Module, has been described previously.(6)

Keys to particle removal in the clean module are the four cleaning stations, each consisting of two sets of brushes and a spin-dry nest (Figure 4). Particle control from these stations must meet increasing demands imposed by continuing reductions in allowable defect sizes, as indicated in Table 10.

A major factor contributing to the effectiveness of the cleaning operation is the quality of water used at the brush and spin stations. Water is monitored and controlled for total oxidizable carbon (TOC), colloidal silica, dissolved ions, bacteria and particles as described by Craven, et al.(7)

Air quality is maintained at class 1/10 and is aided by the absence of operators. In addition to full robotic control within the wafer processing area, the Clean Module is designed such that key processing equipment (the four wafer autoscrubbers and the package cleaner) straddle the ultra clean processing area. Thus, unprocessed wafers and packages are fed into their respective cleaning systems outside the class 1/10 environment and only processed (cleaned) parts pass into the ultra clean area.

Wafer transportation within the module is achieved via a unique end-of-arm tooling on the Robots which utilizes edge-handling and hence avoids contamination on the backsides of the wafers. Finally,

wafer loading into cassettes and transportation of cassettes into final shipping containers is fully robotized.

PARTICLE MEASUREMENT

Developments in automatic inspection equipment are moving at a rapid rate, with several commercially available systems claiming detection limits of ~0.15 μm (e.g. Tencor Surfscan 5500, Estek WIS-850, PMS-SASP). Table 11 compares particle counts on 150 mm wafers measured on two different models of laser inspection equipment supplied by the same vendor (Estek). The WIS-150 instrument uses a red (helium-neon) laser, and the WIS-850 a more sensitive blue (argon ion) laser. Flaw counts 1, 2 and 3 approximate ultra-fine, medium and large particles. The major difference between the two laser systems is in flaw count 1, with the red laser having a detection limit at ~0.3 μm, and the blue laser at ~0.15 μm. Additionally, the latter has greater sensitivity in the whole flaw count 1 range. Advances in analytical capability invariably drive process technology, and the case of particle measurement and control is no exception.

SUMMARY

The twin issues of particulate control and reduction in metallic contamination must be addressed in the cleaning of silicon substrates for modern VLSI and ULSI applications. Recent advances in wet processing include high purity semiconductor grade chemicals and the replacement of liquid chemicals with ozone cleaning. Vapor phase cleaning may have a role to play in the next generation of silicon cleaning processes. Low particulates must be maintained through wafer inspection and packaging, areas which are being automated at a rapid pace. The Clean Module represents a fully integrated and automated approach to the final cleaning, inspection and packaging of silicon wafers. Major advances are being made in measurement methodology for both metallic contamination and particulates. Measurement capability will pace process technology.

REFERENCES

(1) W. Kern and D. A. Puotinen, RCA Rev. 31, 187 (1970).
(2) U. S. Patents 4,239, 661 and 4,172,005.
(3) W. C. Krusell, J. J. Farber and A. C. Sing, ECS Extended Abstracts, 86, 133 (1986).
(4) A. J. Muller, L. A. Psota-Kelty and J. D. Sinclair, ECS Extended Abstracts, 89-2, 554, (1989).
(5) Private Communication, A. C. Sing and J. N. Frank.
(6) D. I. Golland, P. D. Albrecht, W. C. Krusell and F. A. Puerto, Semiconductor International, 10, 1984 (1987).
(7) R. A. Craven, A. J. Ackerman and P. L. Tremont, Microcontamination, 4-11, 14 (1986).

Table 1

SOURCES OF CONTAMINATION

- MOLECULAR
  Organic residues (waxes, oils, polymers)
- IONIC
  Na, K, silicates
- ATOMIC
  Heavy metals (Au, Ag, Cu, Fe)
- PARTICULATE
  Silicas, air, water, and solution - borne particles

Table 2

TOTAL VOLATILE ORGANICS BY GAS CHROMATOGRAPHY

(TVC : E x 10^{-9}g/cm^2)

Cleaning Process	Immediately After Cleaning	After 1 Hour Exposure in Cleanroom*
RCA	2.8	4.2
Choline	2.4	3.6
Ozone	0.8	0.7

* Carbon/Hepa filtered air

Table 3

CLEANING OF HEAVILY CONTAMINATED WAFERS WITH 10% AND MODIFIED HF

	Contaminated Wafer*	After 10% HF Clean	After Modified HF Clean
Na	100,000	6	1
K	100	10	10
Al	100	7	1
Ca	110	60	10
Mg	20	8	4
Fe**	100	7	2

* Wafers were exposed to a two minute soak in 2.4 E-4 normal NaOH; almost no native oxide.

** Based on Fe mass 54 isotope. 56/54 ratios also came out in this order.

Table 4

SIMS AVERAGES AND STANDARD DEVIATIONS*

Cleaning Process	Na	K	Al	Ca	$Mg + C_2$
Modified RCA	4 (2)	5 (2)	38 (8)	19 (9)	19 (9)
Choline/H_2O_2	4 (2)	13 (8)	3530 (524)	28 (6)	28 (6)
MEMC Clean	4 (2)	4 (1)	3 (2)	8 (2)	8 (2)

* Based on absolute counts of $^{28}Si = 1e^5$.

Table 5

HEAVY METALS BY TXRF

Cleaning Process	Zn*	Br**
RCA	1.4	0.4
Ozone	0.3	N.D.

* $E12/cm^2$

** Swept 0 to 20.48 KeV.

ONLY SIGNALS DETECTED ABOVE ARGON.

Table 7

ELECTRICAL CHARACTERISTICS

P(100): MEDIUM RESISTIVITY

Process	FBVS (Volts)	Mobile Ion* $E\ 10/cm^2$	Std. Dev. $E\ 10/cm^2$
Modified RCA	0.15	3.30	1.1
Choline/H_2O_2	0.31	6.66	4.4
MEMC Clean	0.06	1.32	0.4

* Furance control 3.07 ± 2 $E\ 10/cm^2$

Table 6

MOBILE ION CONCENTRATIONS ON WAFERS FROM SEQUENTIAL SAMPLING BY SIMS *

Process	Li	Na	K	Al
Ozone	N.D.	5	1	1
RCA "B"	2.5	10	1	10
REPEAT NEW BATCH CHEMICALS				
Ozone	N.D.	1	1	1
RCA "B"	N.D.	5	1	1
"CONTROL" BATHS				
RCA "B"	N.D.	4	1	3
Ozone	N.D.	3	1	2

Table 8

GRAZING ANGLE ESCA DATA

Cleaning Process	O : Si
Modified RCA	1.37
Choline/H_2O_2	1.49
Ozone	1.58

Table 9

RELATIVE SURFACE CONCENTRATIONS OF CONTAMINANTS BY SIMS (O_2+)

Cleaning Process	Li	Na	K	Al	Ca	Mg
Ozone Clean + Autoscrub with NH_4OH	1	3	2	5	40	5
Ozone Clean + Autoscrub with H_2O	N.D.	3	N.D.	N.D.	20	2
Detection Limits (atoms/cm^2)	$3x10^7$	$1x10^9$	$2x10^8$	$2x10^{10}$	$8x10^8$	$4x10^9$

Table 10

EVOLUTION OF PARTICLE CONTAMINATION CRITERIA

	1985	1988	1990	1993
DRAM Bits	256K	1M	4M	16M
Linewidth (Microns)	2.0	1.0	0.5	0.25
Max. Defect Size (Microns)	1.0	0.5	0.25	0.125

Table 11

FLAW COUNT DATA FOR 150 MM WAFERS MEASURED ON ESTEK WAFER INSPECTION STATIONS

	Inspection Station WIS-150 (Red Laser)			Inspection Station WIS-850 (Blue Laser)		
FLAW COUNT	1	2	3	1	2	3
DEFECT SIZE (μm)	~0.3	0.3 to 2.0	>2.0	~0.15	0.15 to 2.0	>2.0
Counts:						
Mean	0.8	0.4	0.1	4.0	1.8	0.0
Std. Dev.	0.8	0.6	0.2	3.5	1.6	0.0
Mean + 3 S.D.	3.3	2.2	0.7	15.0	6.6	0.0
Sample Size	5,000 Wafers			250 Wafers		

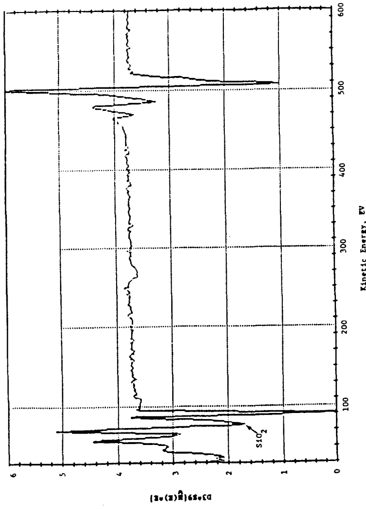

Figure 1 AES SURVEY (OZONE CLEANING)

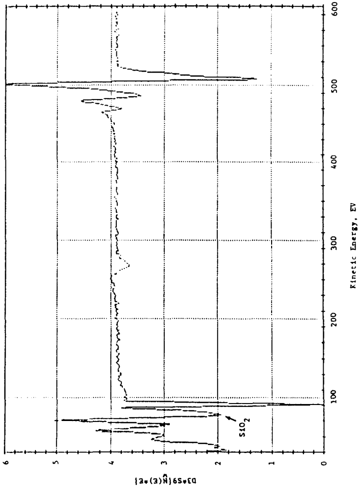

Figure 2 AES SURVEY (CHOLINE/H_2O_2 CLEANING)

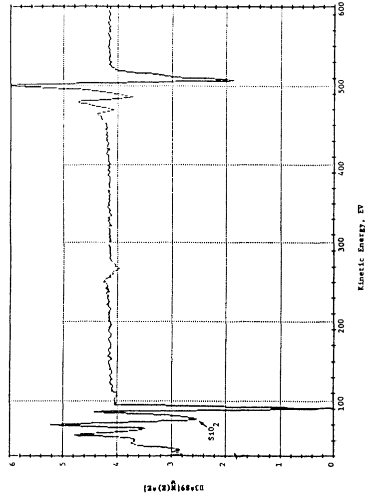

Figure 3 AES SURVEY (RCA CLEANING)

Figure 4 Clean Module Arrangement

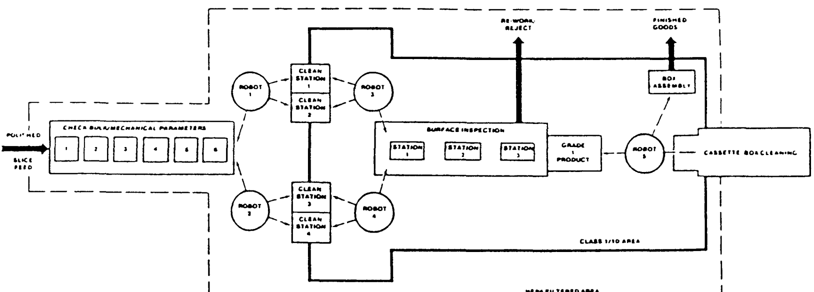

WET CHEMICAL PROCESSING IN A TRENCH

Charlotte M. Tipton and R. Allen Bowling

Semiconductor Process and Design Center, Texas Instruments Incorporated
P.O. Box 655012, MS 944, Dallas, TX 75265

ABSTRACT

Testing of wet chemical etching within trenches showed that liquids may penetrate very small openings via capillary forces. To test this mechanism, wet etching was first performed to generate small openings and second to measure the capillary forces. Failure to etch was not observed until a starting aspect ratio (depth:width) of 450:1. Changes in etch rates within a trench as compared to blanket surface etch rates are explained by comparisons with measured liquid-solid contact angles. For cases where the etchant contact angle on the etch-stop material which lines the trench was higher than the contact angle on the material being etched, trench etch rates were lower than blanket etch rates. For cases where the etchant contact angle on the trench lining was lower than on the material being etched, trench etch rates were higher than blanket etch rates. Differences in etch rates between initial etching and re-etching were observed. Within a trench by means of capillary forces, liquids with higher surface tensions more easily displace liquids with lower surface tensions. Differences in etch rates between initial trench etching and re-etching were explained by displacement of water. These differences thus raise concern over the subsequent ability to desorb structures with conventional drying techniques.

INTRODUCTION

As semiconductor devices become smaller, the ability for liquid chemicals to penetrate small openings becomes an issue [1]. Reports of etch nonuniformity due to high surface tensions of HF chemistries, with increased uniformity from lowering surface tensions with surfactants, are well known [2,3,4]. By similar means, high liquid surface tensions may inhibit liquid penetration into high aspect ratio structures, such as trenches. However, the effect of capillary forces must also be taken into consideration.

Trench technology is ideal for examining this issue. Where a typical aspect ratio for a contact may be on the order of 1:1, the aspect ratio for a trench may be 10:1. Structures being built within a trench may easily have an even higher aspect ratio. For example, by alternating film types in a trench, highly selective wet chemical etches may be used for etching in very high aspect ratio structures. Films to be etched may be as thin as 100Å within trench depths of 7 microns for aspect ratios of up to 700:1. Cross-sectional SEM micrographs of the trench may be used to determine the effectiveness of the wet etch.

EXPERIMENTAL

In this study, etch materials and wet etch chemistries were chosen to be representative of basic wet chemistries used within the semiconductor industry [5,6]. The material to be etched in a trench will be referred to as the trench wall and material to be used as an etch-stop which is surrounding the trench wall will be called the trench liner. A summary of etchant chemistries and corresponding trench wall and liner materials is listed in Table 1.

Liquid surface tensions were measured using a tensiometer (Fisher model 21). These measurements related to the surface tension of the liquid in air. Consequently, additional measurements were taken of the contact angle of the liquid in question on the appropriate substrate material. For this we used a Goniometer (Rame'-Hart model NRL 100-00), as shown in Figure 1. Contact angle measurements more directly reflected the relative interaction at the liquid-solid interface.

The 100mm diameter <100> silicon wafers used in these tests were prepared by first etching trenches to an approximate depth of 7 microns using a SiF_4:HBr chemistry plasma etch. The trenches were filled by layering materials to correspond to wet etch selectivities, with one trench wall material and one trench liner material, as outlined in Table 2. BHF is NH_4F-buffered HF solution; choline is an organic base solution.

A solution of 5.0% HF was used to etch SiO_2 with a high selectivity to silicon. Trenches for examining HF chemistries were filled by thermally growing SiO_2 of 1000Å, 500Å or 100Å thickness, followed by deposition of 8000Å of polycrystalline silicon. An HBr:HCl chemistry plasma etch was used to planarize the wafer stopping on the thermal oxide at the wafer surface, thus exposing the oxide trench wall. Wet etching was perfomed at ambient temperature in a stagnant immersion bath. After etching, wafers were rinsed in deionized (DI) water and dried using standard dump rinsing and on-axis spin rinse drying techniques. For samples with 100Å SiO_2 trench walls, an additional 2000Å thermal oxidation was performed after completion of the wet etching to broaden the etched region for improved viewing under a scanning electron microscope.

H_3PO_4 was used to etch Si_3N_4 with selectivity to SiO_2. Trenches for examining H_3PO_4 were filled by thermally growing 2000Å of SiO_2, depositing Si_3N_4 at low pressure for 2000Å or 1000Å thicknesses, followed by depositing 8000Å of SiO_2 at low pressure using a tetraethylorthosilicate (TEOS) source. Wafers were annealed at 800°C for 30 minutes in steam to densify the deposited SiO_2 for improved etch selectivity (Table 2). A CF_4 chemistry plasma etch was used to planarize the wafer stopping on the thermal oxide at the wafer surface, thus exposing the Si_3N_4 trench wall (Figure 2). Wet etching was performed by first deglazing wafers to remove any native oxide from the Si_3N_4 surface. A 0.5% HF solution buffered with ammonium fluoride was used in a stagnant bath at ambient temperature for 1 minute. After deglazing, wafers were rinsed in DI water and transfered to the H_3PO_4 etch. The H_3PO_4 etching was performed at 160°C and at boiling concentration. The etch tank was an Imtec model QN110 refluxed heated quartz bath with continuous DI water addition. The system uses a quartz tank with Inconel heaters. An inverted quartz tank with Teflon cooling coils mounted on the interior served as the reflux lid. DI water was added to the hot acid bath through a manifold in the lid. All wafers were rinsed in DI water and spin rinse dried as described above.

Choline was used to etch polysilicon with selectivity to SiO_2. Trenches for examining choline were prepared in identical fashion to those for H_3PO_4, with exception that polysilicon was deposited

at low pressure instead of Si_3N_4 (Figure 2). Because choline has such a high selectivity to SiO_2, removal of native oxide from the polysilicon surface was required to initiate the choline etch. In similar fashion to the Si_3N_4 wafers, deglazing was performed by processing wafers in a 0.5% HF solution buffered with NH_4F in a stagnant bath at ambient temperature for 1 minute. Wafers were then rinsed in DI water and transfered to a 5.0% choline bath. The choline etching was performed at 65°C in an Imtec model QZ110 heated quartz bath. No agitation was provided in the bath. Surfactant was added to the choline bath at a volume of 0.001% to provide for minimal etch uniformity (Table 3), as determined on blanket polysilicon wafers. As before, all wafers were rinsed in DI water and spin rinse dried.

The performance of an etchant was monitored in two ways: 1) comparison of etch characteristics on a blanket wafer surface to etch characteristics in the trench; and 2) by monitoring of etch characteristics in the trench during re-etching of trench walls. Initial etching in the trench was performed to various target depths. Wafers were then cleaved and additional etching was performed to a portion of the original wafers. Re-etching was performed to only one target depth.

All SEM micrographs were taken on a JEOL model JSM-845, calibrated according to procedures by the National Institue of Standards and Technology using Standard Reference Material 484. For difficult samples, backscattered electron imaging (BEI) enhancement techniques were employed.

RESULTS

Contact angle measurements showed that the three chemistries tested represented different cases with regards to the relative magnitudes of trench wall and trench lining contact angles, as summarized in Table 4. The HF had a very low contact angle on SiO_2 and a very high contact angle on Si. Choline also had a very low contact angle on SiO_2 with a high contact angle on deglazed Si. However, in the case of HF, the SiO_2 was being etched while surrounded by Si. In the case of choline, Si was being etched while surrounded by SiO_2. H_3PO_4 represented a more moderate case where contact angles for both the trench wall and lining materials were similar. Even so, the contact angles for H_3PO_4 were lower on the Si_3N_4 being etched than the surrounding SiO_2.

Table 5 summarizes etch rate results for each of the chemistries. Etch rates for both initial trench etching and re-etching are expressed as percentages of blanket wafer surface etch rates. For HF, initial etching occured at reduced rates from blanket etching, while re-etching occured at increased rates from initial etching. Figure 3 shows results from 6µm target HF initial etch and 2µm target HF re-etch of 1000Å, 500Å, and 100Å SiO_2 trench walls. For H_3PO_4, initial etching occured at reduced rates from blanket etching, while re-etching occured at reduced rates from initial etching. Figure 4 shows results from 6µm target H_3PO_4 initial etch and 2µm target H_3PO_4 re-etch of 1000Å Si_3N_4 trench walls. Finally, choline exhibited increased rates over blanket etching during initial trench etching. Re-etching showed the same etch rate as initial etching until a starting aspect ratio of 27.5:1 was achieved, at which point the etch rate was significantly reduced. Figure 5 shows results from (a) 1µm target choline initial etch and 1um target choline re-etch, and (b) 2µm target choline initial etch.

In only one case was a restriction found such that re-etching did not occur (Table 6). For the case of 100Å trench walls being etched by 5% HF, at an initial etch depth of 4.5µm, re-etching did not

occur for some trenches while adjacent trenches on the same sample did show additional etching. Figure 6 shows adjacent trenches with varying etch depths due to intermittent re-etching. As a result of thermal oxidation after re-etching, etch depths are noted by a thinning of trench walls. Oxidation will only occur where silicon is exposed by etching.

No changes in etch rate with increasing etch depth were noted for any of the cases. For the case of 5%HF, decreasing etch rates were seen correlating to decreasing trench wall thicknesses, as shown in Figure 7. This phenomenon was more pronounced for thinner trench wall thicknesses.

DISCUSSION

Initial etch rates in trenches were influenced by surface tensions. For cases where the etchant contact angle on the trench lining was higher than its contact angle on the trench wall, trench etch rates were lower than blanket etch rates. This was the case for HF and H_3PO_4. For HF, the contact angle on Si was very high while the contact angle on SiO_2 was very low. For H_3PO_4, the contact angle on SiO_2 was slightly higher than the contact angle on Si_3N_4. Because the etchant had to diffuse through regions of resistant forces (as evidenced by high contact angles), the diffusion rate, and hence the etch rate, was reduced. For the case where the etchant contact angle on the trench lining was lower than its contact angle on the trench wall, such as with choline, trench etch rates were higher than blanket etch rates. Because the choline diffused easily through SiO_2 trench liners to reach the polysilicon, as opposed to diffusing through a polysilicon surface as with blanket etching, the choline etch rate in the trench was accellerated.

Etch rates seen during re-etching in trenches were different from initial trench etch rates for all cases. For HF the second pass etch rate was higher than the initial trench etch rate, while for H_3PO_4 and choline it was lower than the initial trench etch rate. For blanket surface etching, a liquid with a lower surface tension will easily displace a liquid with a high surface tension. However, if we assume that changes in etch rates are due to displacement of rinse H_2O, which, due to capillary forces, never desorbed from the trenches, only the H_3PO_4 contact angles agree. To fully understand, we must first look more closely at the influence of capillary forces. Capillary forces within a tube may be expressed as

$$T = rhdg/2 \qquad (1)$$

where T is the liquid surface tension, r is the radius of the tube opening, h is the height to which the liquid will rise, d is the density of the liquid, and g is the gravitational constant. If r is constant, as T increases then so does h. Higher surface tensions generate stronger capillary forces. It follows then that due to capillary forces, liquids with higher surface tensions will more easily displace liquids with lower surface tensions within a trench. Thus, HF, with higher contact angles on Si than for H20, will more easily displace H_2O than it would displace itself. Hence it exhibited a higher etch rate during re-etch than during the initial etch.

Choline, with lower contact angles on SiO_2 than for H_2O, will not displace the water as easily as it would displace itself. It exhibited a lower etch rate during re-etch for higher aspect ratio starting points (>/= 27.5:1) than during the initial etch. Lower aspect ratio starting points showed the same elevated etch rate as initial etching (Table 6). This indicated that there was not H_2O present to diffuse through. Hence, trenches with aspect ratios < 27.5:1 were desorbed by standard spin rinse dry

techniques.

The H_3PO_4 results may be explained by noting that increased temperatures will lower liquid surface tensions [7]. All contact angles were measured at ambient temperatures, yet the H_3PO_4 was run at 160°C. Provided the heated bath lowered H_3PO_4 contact angles to below those for H_2O, the H_3PO_4 would not displace the H_2O as easily as itself, and an etch rate lower than the initial etch rate would be seen during re-etch.

CONCLUSION

Test results have shown that wet chemical etching may occur within high aspect ratio structures. Although some restrictions of liquid penetration were found, the limitations existed at aspect ratios greater than 50:1. Complications for wet processing within high aspect ratio structures appear to stem not from getting the liquid into the small opening, but rather in removing it. To fully understand the applicability of wet chemical processing for future device production, we must look not only at the benefits and restrictions of wet processing, but also at the effects that wet processing may have on subsequent device fabrication technologies.

ACKNOWLEDGMENTS

The authors would like to thank Sue Hughes for wet processing; Leslie Carlson and Don Dixon for surface tension and contact angle measurements; Fred Vaughn, John Truett, and John DeSimone for SEM micrographs; Richard Jackson and Jim Anderson for plasma etch planarization; and Doug Whitby for graphics.

REFERENCES

1. J. Ruzyllo, "Evaluating the Feasibility of Dry Cleaning of Silicon Wafers," **Microcontamination**, March 1988, p. 39.

2. R.J. Hopkins, "Wet Chemical Etchants for Silicon Dioxide Films," **Microelectronic Manufacturing and Testing**, March 1988, pp.42-43.

3. H. Kikuyama, and N. Miki, "Proceedings of the 9th International Symposium on Contamination Control," Los Angeles, California, 1988, p.45.

4. K.M. Shah, P. Mikkelsen, and W. Cummings, "Change Your Surfactant Formula and Use Etch Baths for a Week," **Semiconductor International**, Oct.

5. W. van Gelder, V.E. Hauser, "The Etching of Silicon Nitride in Phosphoric Acid with Silicon Dioxide as a Mask," **J. Electrochem. Soc.**, 114, 869 (1967).

6. A. Hariri, R.S. Hockett, "Evaluate Wafer Cleaning Effectiveness," **Semiconductor International**, Aug. 1989, pp. 74-78.

7. F. Daniels, and R.A. Alberty, **Physical Chemistry** (John Wiley & Sons, Inc., New York, 1955), p. 172.

TABLES

Table 1. Etchant and corresponding trench wall and liner materials.

ETCHANT	TRENCH MATERIALS WALL (etched)	LINER (etch stop)
$HF:H_20$	SiO_2	<100>Si, poly-Si
$H_3PO_4:H_20$	Si_3N_4	SiO_2
choline:surfactant:H_2O	poly-Si	SiO_2

Table 3. Effects of surfactant additions to choline poly-Si etch uniformity.

SURFACTANT (VOL %)	ETCH RATE	STD DEV (1 sigma)
-0-	3009 Å/min	982 Å/min
0.0001	2564 Å/min	500 Å/min
0.001	352 Å/min	21 Å/min
0.01	127 Å/min	10 Å/min

Table 4. Summary of measured contact angles (deg) and surface tensions (dynes/cm).

	CONTACT ANGLES				
SUBSTRATE	5%HF	0.5%BHF	H_3PO_4	5%CHOLINE	DI H_2O
<100> Si	76	--	--	37	19
poly Si	70	87	--	40	18
1000Å thermal ox	16*	31	45	11*	41
densified TEOS	10*	22	47	20	31
LPCVD nitride	9*	33	36	--	30
SURFACE TENSION					
	71.5	67.2	83.4	45.5	73.2

*=> angle was diminishing

Table 5. Trench etch rates for 1000Å trench walls expressed as percentages of blanket surface etch rates.

	5%HF	H_3PO_4	5%CHOLINE
Initial etch	83.3	87.5	236.3
Re-etch	93.0	72.6	86.0

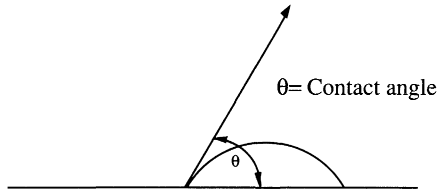

Figure 1. Technique used for measuring liquid contact angles against a solid.

Table 2. Material selectivities for wet etch chemistries used.

	ETCH RATES (Å/min)			
MATERIAL	5%HF	0.5%BHF	H_3PO_4	CHOLINE
<100> Si	~0	~0	--	--
poly-Si	~0	~0	--	350
thermal SiO_2	250	65	>0.1	~0
LPCVD SiO_2				
undensified	--	116	6	0.5
densified	--	114	0.5	0.5
LPCVD Si_3N_4	--	1.1	50	--

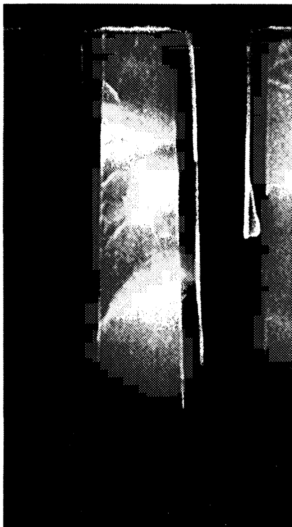

(a) (b)

Figure 2. Starting material for testing of (a) H_3PO_4 etch and (b) choline etch. Trench etch mask material was not removed for choline test material.

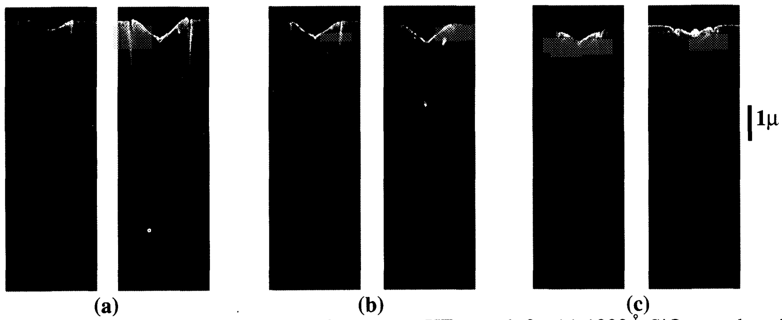

Figure 3. 6μm target initial HF etch and 2μm target HF re-etch for (a) 1000Å SiO_2 trench wall, (b) 500Å SiO_2 trench wall, and (c) 100Å SiO_2 trench wall.

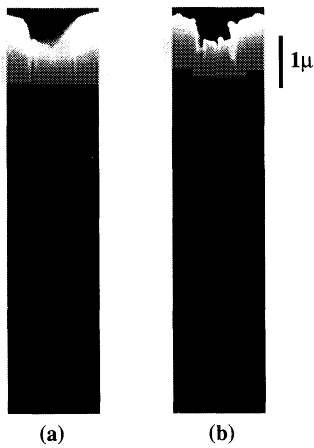

Figure 4. 6μm target initial H_3PO_4 etch and 2μm target H_3PO_4 re-etch for 1000Å Si_3N_4 trench

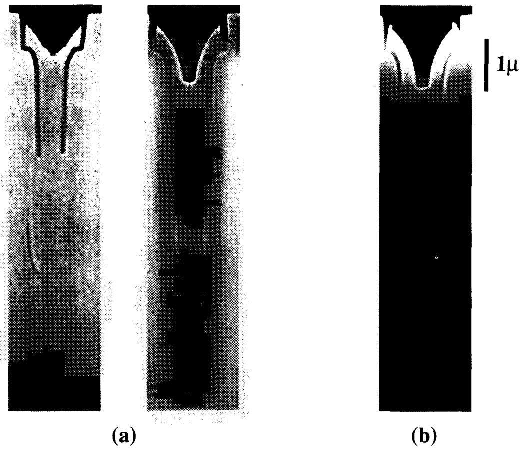

Figure 5. (a) 1μm target initial choline etch and 1μm target choline re-etch, and (b) 2μm target

Table 6. Summary of key aspect ratios tested.

	5%HF	H_3PO_4	5%CHOLINE
minimum aspect ratio tested for re-etch initiation	50:1	18:1	5:1
minimum aspect ratio where re-etch etch rate changed	50:1	18:1	27:1
maximum aspect ratio where successful re-etch occured	416:1	50:1	56:1
maximum aspect ratio tested for re-etch initiation	450:1	50:1	56:1

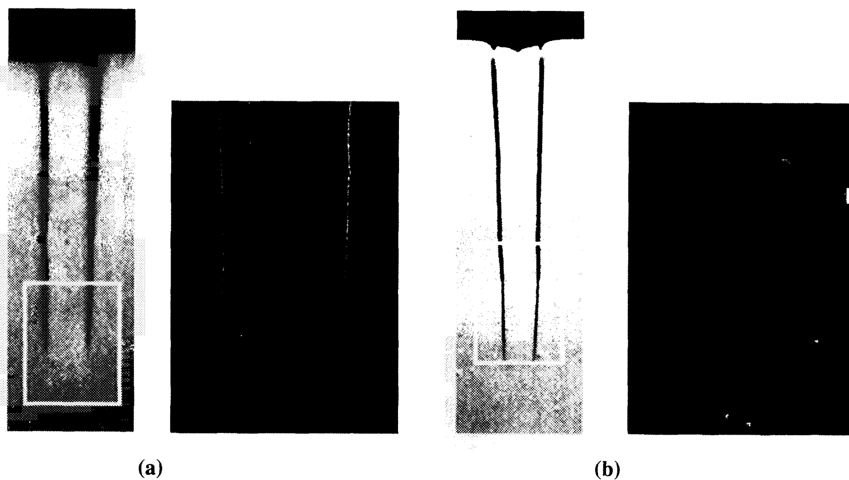

Figure 6. Attempted HF re-etch of 100Å SiO_2 from 4.5μm starting depth where (a) re-etch was successful, and (b) re-etch was unsuccessful in adjacent trenches.

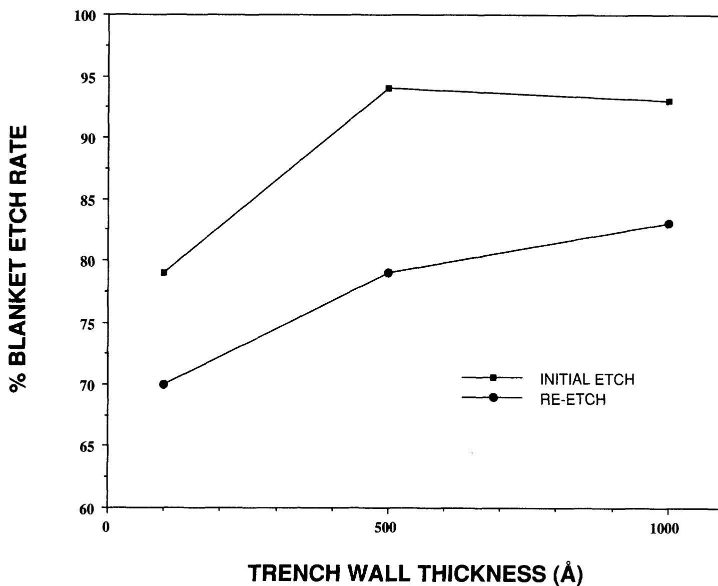

Figure 7. Decreasing etch rates with decreasing trench wall thickness seen for the case of 5% HF.

INVESTIGATION OF H_2SO_4:H_2O_2, DILUTE HF AND DI WATER SILICON WAFER CLEANING PROCESSES

L.C.. Zazzera and L.S. Becker
FSI International, Chaska, Minnesota 55318

W.J. Beery, P.E. Sobol and W. Chat
Perkin-Elmer, Physical Electronics Division,
Eden Prairie, Minnesota 55344

ABSTRACT

Fundamental silicon wafer cleaning processes based on a single acidic solution of either sulfuric or hydrofluoric acid followed by deionized water rinsing were studied. The utility of each clean was determined by extensive surface characterization after processing. The abbreviated cleans reduced trace metal impurities to $\leq 1x10^{11}$ atoms/cm^2 and also minimized particle and carbon contamination. The time and temperature of the final deionized water rinse influenced trace metal and particle contamination. Particle and carbon contamination following hydrofluoric acid was minimized by partially etching the native oxide; in this etch the wafer remains hydrophilic.

INTRODUCTION

The fabrication of semiconductor devices on silicon wafers involves a number of chemical processes which are performed at the wafer surface. The success of these processes are often highly sensitive to the chemical composition of the surface. The abundant surface atoms (Si, O, C and H) influence oxidation kinetics, epitaxial growth, wetting and adhesion (1,2,3,4). Trace metal impurities diminish the insulating quality of dielectric films grown on the surface and degrade the electrical characteristics of the active silicon region (5).

The nature of the wafer surface is controlled by cleaning. Cleaning usually consists of processes employing multiple chemical solutions. Each of the solutions is designed to control certain classes of contaminants. Investigation of the effects of these individual solutions

and the conditions used to apply them on wafer surface properties can lead to a fundamental understanding of cleaning and the development of more efficient cleaning procedures.

In this study, the effect on silicon wafer surface chemistry by processes composed of $H_2SO_4:H_2O_2$, dilute HF (DHF) and deionized (DI) rinse water was studied. $H_2SO_4:H_2O_2$ is commonly used to remove organic films where DHF is used to remove oxide and the impurities in the oxide. The acidic solutions were part of a two element cleaning process consisting of one acidic dispense followed by a rinse.

Various techniques were employed to determine the nature of the silicon surface. Particle contamination was measured with a laser defect scanner. Ellipsometry, x-ray photoelectron spectroscopy (XPS), and Auger electron spectroscopy (AES) were used to measure oxide thickness, carbon and chemical residue. Wettability was measured with a contact angle system. Secondary ion mass spectrometry (SIMS) and Total Reflection X-ray Fluorescence (TRXRF) were employed to yield information on trace metals.

The process parameters used in this experiment deviate from established optimal parameters usually employed in critical cleaning operations. Extending the parameters outside the optimal range increases the abundance of certain contamination. This was necessary to understand the nature of certain process parameters and their influence on surface contamination. Analysis involving XPS and TRXRF were performed at a different location which resulted in additional air exposure time during transportation. Prolong air exposure can give erroneously high values for adsorbed carbon and oxide thickness. TRXRF did not detect metals with atomic numbers $Z<20$. Hydrogen which is abundant on silicon surfaces was not monitored in this study.

Silicon wafer cleaning processes based on $H_2SO_4:H_2O_2$ or DHF removed trace metal impurities initially present in the native oxide. Particle contamination was minimum with the $H_2SO_4:H_2O_2$ clean. Particles after DHF were minimized using short dispense times, which did not remove all the SiO_2. Longer rinse times after the acidic solutions yielded higher sodium contamination. Hot deionized water minimized this sodium contamination but increased particle contamination.

EXPERIMENTAL

Materials - Close attention was given to cleanroom facilities, processing equipment and wafer handling

procedures. The silicon wafers used in this study were 100mm diameter, boron doped in the range of 4-15 Ω-cm, (100) orientation, and single side polished. The total number of particles ($\geq 0.3\mu m$) on each wafer was <10 before processing. Aqueous chemicals were low mobile ion semiconductor grade H_2SO_4 (96%), H_2O_2 (30%), and HF (49%). The deionized H_2O resistivity was >18 MΩ-cm at 25°C and had been passed through a 0.2μm filter prior to use. The sodium ion concentration in the DI water was <0.05ppb as determined by ion chromatography. Dry nitrogen was from a liquid nitrogen source. Airborne particle levels ($\geq 0.3\mu m$) averaged less than 4 per Ft^3.

Process - All cleans were performed in an FSI TITAN on center centrifugal spray processor. This highly automated processor utilizes an atomized spray for solution and rinse dispenses. The processes studied included H_2SO_4:H_2O_2 (4:1)-rinse, HF:H_2O (1:100)-rinse and rinse only. Variables included the dispense times of the hydrofluoric acid solution and water rinse. The sulfuric acid solution dispense time was always 60 s. The DI water temperature was either 20°C or 80°C as measured on the wafer with a thermocouple. The source for the cold and hot DI water was identical. Cold temperatures were obtained by passing water through the deactivated heater. Cleaning processes were always performed in a random order to minimize the influence of variation in the experimental environment.

Control wafers were used in all experiments. Control wafers received no processing beyond that of the manufacturer. Control wafers were transferred to and from the processor to monitor particle additions due exclusively to handling.

Surface Characterization - The surface of the wafers were characterized for particles, oxide thickness, hydrophobicity, trace metal impurities and elemental concentrations. Immediately before and after processing the wafers were measured for particle contamination with an Aeronca WIS 150 laser defect scanner. Pre and post particle levels for particles $\geq 0.3\mu m$ were measured. The net removal or addition of particles are included in the results.

Residue and oxide thickness measurements were measured with a Gaertner L116ALC automatic Ellipsometer. Five separate measurements were made on each wafer after completing the particle analysis. The data collected was useful in indicating relative amounts of oxide and residues present after processing.

Wetability measurements were performed with a Gaertner M2865 contact angle measurement system following the Ellipsometer analysis. The analysis included three contact angle measurements per wafer. In some cases the surface was so hydrophilic that contact angle analysis was not feasible. Instead 5-7μl of water were placed on the wafer and the drop diameter was measured with a ruler and a microscope.

Relative oxide thicknesses were measured via AES on the Perkin-Elmer model 590 Scanning Auger Microprobe. The primary electron beam was rastered to analyze a 2x2mm area. The beam current was 30μA, and the beam energy was 3 KeV. The operating pressure of the spectrometer was $1x10^{-9}$ torr. The model 590 SAM employs a cylindrical-mirror electron energy analyzer. Analysis involved monitoring the Si LMM peaks between 72-102 eV. The low energy peak in this window is indicative of oxide and the higher energy peak indicates unoxidized silicon. Relative oxide thicknesses are represented by the ratio of the oxidized peak area to the elemental peak area, $R=Si_{(OX)}/Si_{(EL)}$. The Auger analysis included one multiplex of Si, O, and C per wafer.

Oxide thicknesses, as well as carbon, sulfur and fluorine residues were measured by XPS. XPS measurements were performed using a Perkin-Elmer Model 500 LS XPS spectrometer, equipped with a 400W, 15 KeV Mg Kα (1253.6 eV) x-ray source. Photoelectrons were energy analyzed using a spherical capacitor analyzer operated at a constant pass energy of 17.9 eV. The base pressure of the spectrometer was $3x10^{-10}$ torr. XPS data was collected at θ=10 degrees; θ represents the angle between the plane of the sample and the detector. The average depth of analysis ($d=\lambda\sin\theta$), when based on the mean free path (λ=3.2nm(6)) of Si 2p photoelectrons in silicon dioxide, is 6Å. The XPS analysis included collection of the Si 2p, O 1s, C 1s, F 1s and S 2s photoelectrons. Percent concentration values were determined from the volume analyzed using atomic sensitivity factors. Oxide thickness values (Å) were calculated from the area ratio $R=Si_{(OX)}/Si_{(EL)}$ by using the reduced thickness algorithm (7).

$$d\text{Å}/\lambda=\sin\theta\ln(R/0.6+1)$$

Trace metal impurities were measured using a Perkin-Elmer 590 Scanning Auger Microprobe equipped with SIMS and a Perkin-Elmer Atomika X-ray Surface Analyzer XSA 8000. The SIMS analysis included rastering an Ar^+ primary beam in a 1x1 mm area. The beam diameter was 300μm, the beam current was 40 nA, and the beam energy was 4 KeV. An oxygen jet was used to enhance positive secondary ion yields. The operating pressure of the spectrometer was $5x10^{-7}$ torr.

SIMS analysis included three surveys per wafer, each survey was obtained by sputtering for 50 seconds while surveying atomic mass units 1-100.

Impurity concentrations from the SIMS analysis were expressed in relative elemental abundance (REA), a semiquantitative algorithm in which no assumptions are made as to the physical processes involved in secondary ion emission (8). The REA was obtained by dividing the intensities (counts/second) of the impurity peak of interest by the ^{28}Si peak and multiplying by 10^6. The relative elemental abundances for ^{23}Na, ^{27}Al, ^{40}Ca, and ^{64}Zn were reported.

Total Reflection X-ray Fluorescence (TRXRF) recently has been applied as a non-vacuum, non-destructive surface analysis technique by precisely positioning a X-ray beam on silicon wafers (9). TRXRF analysis involves restricting the x-ray beam to angles less than the critical angle needed to achieve total reflection at the surface. X-rays incident at angles less than the critical angle are reflected from a silicon wafer with 99% efficiency. In addition, reflection occurs within 50Å of the surface.

The XSA 8000 used in this study had minimum detection limits on the order of 10^{11} atoms/cm^2. The low background radiation simplifies quantitative analysis, since matrix effects are minimized. The XSA 8000 uses a molybdenum anode x-ray tube operated at 30 KeV and 60 mA. X-ray fluorescence is detected with a lithium drifted silicon detector. The TRXRF analysis included one survey per wafer. The concentrations of Ca, Fe, Cu, and Zn are reported in units of 10^{12} atoms/cm^2.

RESULTS

Particle characterization - The two principle parameters influencing particle contamination were DHF dispense time and rinse temperature. Table 1 lists the total number of particles added to the wafer after various processes employing hot and cold rinsing. The net particle addition values are represented by a mean (X) and standard deviation (σ) of at least ten wafers. The influence of HF dispense time on particle addition is illustrated in Figure 1. Rinse parameters after an extended DHF dispense also influenced particle addition and these results appear in Figure 2.

Silicon oxide thickness - Table 2 lists the Ellipsometer and XPS oxide thickness measurements (in

angstroms) in addition to the Auger $Si_{(ox)}/Si_{(EL)}$ ratio. Oxide thickness was measured with respect to DHF dispense time and rinse water temperature by Ellipsometry (Figure 3). The removal of oxide and the development of a hydrophobic surface was indicated by Auger spectroscopy and contact angle measurement (Figure 4).

Relative atomic concentrations - The relative atomic percent concentrations of Si, O, C, S, and F measured by XPS appear in Table 3. The percent concentration values are represented by a mean and standard deviation of at least five samples. Carbon adsorption during HF dispenses and subsequent rinsing was observed using the C 1s peak area (Figure 5). The C 1s peak area is directly proportional to the number of carbon atoms in the sampling volume.

Following a $H_2SO_4:H_2O_2$ dispense, the percent sulfur concentration with respect to rinse time was measured to study residue removal. Figure 6, plots the sulfur S 2s concentration, the $^{18}H_2O$ SIMS REA, and the Ellipsometer reading to characterize the hydrous sulfur residue and its removal.

Trace metal impurities - Trace metal impurities were removed as a result of the two acidic cleaning solutions. Table 4 summarizes the results of the SIMS surveys. The REA values are represented by a mean (X) and standard deviation (σ) of at least 10 wafers. Of particular interest was the increase in sodium abundance with longer rinse times following $H_2SO_4:H_2O_2$ and DHF processes (Figure 7). Sodium adsorption was also studied with respect to the DI water temperature (Figure 8).

TRXRF was used to measure the concentrations of Ca, Fe, Cu, and Zn after the different processes. Table 5 summarizes the TRXRF data. The concentration values are represented by a mean (X) and standard deviation (σ) from at least 5 wafers. Some trace metal concentrations decreased with only a DI water rinse. Figure 9 charts the Zn concentration (10^{12} atoms/cm^2) as a function of rinse time and temperature. The analysis of Zn after water rinsing involved a repetitive analysis/rinse sequence. This analysis measured the same area on the same wafer after each rinse process.

DISCUSSION

Particle characterization - The largest particle increases were observed after DHF-80°C rinse processes. The fewest particles added were observed after 20°C rinse only

and H_2SO_4:H_2O_2-20°C rinse processes. Removal of the native oxide had the greatest influence on increased particle contamination (Table 1). The number of particles added significantly increased with oxide removal.

Hot rinse temperatures increased particle densities on both hydrophilic and hydrophobic wafers. To test the influence of rinse temperature on hydrophobic wafers an extended (240 s.) DHF dispense was employed to yield surfaces with minimum oxide coverage regardless of rinse temperature. The increase in particle contamination from hot rinse water was observed in addition to the effect of oxide removal.

Information on the nature of the particles can be deduced from the ability of oxide removal and rinse temperature to affect particle contamination. Exposure to DHF removes the amorphous silica film referred to as the native or chemical oxide. Removing the native oxide transforms the hydrophillic wafer from a polar Si-OH surface, chemically similar to water, to a less polar surface which is hydrophobic. Molecules, colloids and particles with hydrophobic surfaces will always partition from water to a less polar environment. The increased particle additions observed on hydrophobic wafers is evidence that the surface of the particles are non polar and probably organic in nature. The two most abundant elemental impurities in DI water are typically Si and C. In water Si is present as extremely small particles of amorphous silica, the surface of which is hydrated as Si-OH. These colloidal silica particles are high molecular weight polymers of monosilicic acid $Si(OH)_4$ and have diameters $\geq$50Å. Carbon is present in a variety of forms. Silica can associate with organic compounds via hydrogen bonding with polar sections of an organic molecule, resulting in complexes with predominantly hydrocarbon surfaces.

The influence of higher temperatures on increased particle additions may be explained by the increased reaction rate between silicic acid polymer and larger colloidal silica particles. Polymerization involves condensation of adjacent silanol groups to form a siloxane (Si-O-Si) linkage and water. Higher temperatures combined with atomized spray can favor dehydration during the overall reaction:

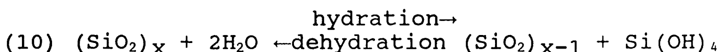

$$(10)\quad (SiO_2)_x + 2H_2O \underset{\leftarrow \text{dehydration}}{\overset{\text{hydration} \rightarrow}{}} (SiO_2)_{x-1} + Si(OH)_4$$

Increased particle contamination can also be due to evaporation. During evaporation the foreign matter in DI

water droplets is concentrated. The solvated matter becomes solid particles when the concentration exceeds the solubility. Evaporation is the basis for methods measuring non volatile foreign matter in DI water (11).

Considering the effects of oxide removal and rinse temperature on particle contamination DHF process parameters can be adjusted to yield minimum particle addition. A partial removal of the native oxide followed by a brief 20°C rinse was optimum with respect to particle contamination.

Silicon oxide thickness - The DHF dispenses were the only processes to significantly reduce the original native oxide thickness (Table 2). Data from Ellipsometry (Figure 3) and Auger (Figure 4) both indicated partial native oxide removal after 18 s. of DHF dispense and very little additional oxide removal for times longer than 42 s. The wafer surface remained hydrophillic after the partial oxide removal and became increasingly hydrophobic as the oxide thickness neared its minimum value. The surface continued to become more hydrophobic even though little change in oxide thickness was detected after 42 s of DHF. The wafer rapidly becomes hydrophobic due to the loss of the hydrophillic silica film. The removal of the silica is accompanied by the adsorption of hydrophobic species. The hydrophobic species continue to adsorb during the longer DHF dispenses, resulting in a more hydrophobic wafer. The adsorption of hydrophobic organic molecules after aqueous DHF processing was reported previously (12).

The increased DHF etch rate of oxide at elevated rinse temperatures is evident from Figure 3. A 30 second pre-rinse resulted in DHF mixing with hot water on the wafer surface.

Relative atomic concentrations - Carbon contamination increased with DHF dispense time (Table 3). However a partial oxide etch actually removed carbon before carbon started to adsorb at longer DHF dispense times. XPS C 1s binding energy data determined the chemical nature of carbon present after DHF etching of SiO_2. The majority of the carbon was associated with alliphatic hydrocarbons which are hydrophobic (13, 14).

The rinse time may have influenced carbon contamination shortly after the oxide is essentially removed as shown in Figure 5. Figure 5 is based on one set of data points and experimental variation may account for the different C 1s areas. However, if the difference seen at 42 s. is real, it indicates that the adsorption of carbon may be most rapid

immediately following oxide removal with the rate decreasing as the surface approaches saturation.

The C 1s area decreased after an 18 s. DHF dispense because the wafer is still hydrophillic. Some of the carbon initially present on the oxide is soluble in DHF and is removed from the wafer.

Characterizing the rinsing of residue left on the wafer following $H_2SO_4:H_2O_2$ solutions revealed a decrease in sulfur concentration with increasing rinse time. Rinsing also decreased other properties characteristic of the sulfur residue (Figure 6). Incomplete rinsing of the wafer following $H_2SO_4:H_2O_2$ resulted in a very hydrophillic surface. The hydrated surface was evident by a large SIMS signal at amu $^{18}H_2O$ and a large drop diameter during the wetting tests. The enhanced hydrophilicity is due to the nature of sulfur compounds like sulfonates and sulfates. These compounds are very hydroscopic because of their ability to form hydrogen bonds with water and help retain water on the wafer surface. The residue also contained trace metal impurities which will be discussed subsequently. The residue was essentially removed with rinse times exceeding 30 s.

Trace metal impurities - DI water alone greatly reduced Na and Ca contamination. The Zn atoms were more difficult to remove with DI water and Al was not removed with DI water. The acidic solutions containing H_2SO_4 and DHF were able to reduce the abundance of all the metal impurities monitored.

Sodium was observed to increase with rinse time after the acidic cleaning solutions (Figure 7). Sodium adsorption during rinsing appeared to be greatest after $H_2SO_4:H_2O_2$ solutions, intermediate after DHF and insignificant with rinsing only. The Na contamination was minimized with shorter rinse times and high water temperatures (Figure 8). The Na impurity at rinse times ≤ 24 s. after $H_2SO_4:H_2O_2$ solutions is present in the sulfur residue.

TRXRF analysis quantified trace metal removal. The Zn concentration (atoms/cm^2) was plotted with respect to rinse time and temperature in Figure 9. Hot water significantly increased the removal rate of Zn contamination. Removal of Zn to below the minimum detection limit ($<8 \times 10^{10}$ atoms/cm^2) was not accomplished with a 600 s. hot rinse. Both acidic solutions yielded surface impurity concentrations below the minimum detection limit of the XSA 8000.

When considering the behavior of trace metal impurities it is helpful to think of the native oxide as an ultra thin

ion exchange film. Before cleaning the negative charges associated with the oxygens in the silica network are balanced with a variety of metal cations. The strength of the bond increases with ionic charge and to a lesser extent the charge to radius ratio (15). Hence, the expected ease of removal is $Na^+ > Ca^{2+} > Zn^{2+} > Al^{3+}$. This is consistent with the data described above. The acidic solutions efficiently remove the Al and Zn by elevating the hydronium ion concentration. The excess H_3O^+ ions successfully compete with the less abundant cations for the negatively charged silica.

The readsorption of Na following acidic solutions involves an ion exchange with H_3O^+. Ion exchange involves weak chemical reactions (2 Kcal/mol) and the sorption of ions is a reversible process. After acidic cleans the surface is essentially free of all cations except excess H_3O^+. When this surface is exposed to water with even extremely low levels of cations, some exchange will take place. Similar adsorption has been seen with extended rinse times after cleaning with $HCl:H_2O_2$ solutions (16).

Wafers which received only a water rinse did not display an increase in Na contamination at extended rinse times. After water rinsing at pH 7 the surface still contains the stronger bound cations such as Al^{3+}. Unlike H_3O^+, present after an acidic solution, the Al^{3+} is not removed by rinsing. The ion exchange is prevented because Al^{3+} shields the negative silica matrix from Na^+ ions.

SUMMARY

The results discussed above indicate that the $H_2SO_4:H_2O_2$-rinse processes were consistently the cleanest with respect to particle and trace metal impurities. The DI water rinse following the sulfuric acid solution played a significant role in determining the amounts and nature of surface impurities. Particle contamination was removed or unchanged on wafers with initial densities of $\leq$ 10 (0.3μm) particles per wafer. DI water rinsing was necessary to remove sulfur residue and trace metals following $H_2SO_4:H_2O_2$. Trace metal impurities were < $1x10^{11}$ atoms/cm^2. Sodium contamination increased with extended rinse times after $H_2SO_4:H_2O_2$ dispenses. The readsorption of sodium was minimized with short rinse times and hot DI water.

The DHF-rinse processes varied widely with respect to particle and carbon contamination which was dependent upon the extent of oxide removal. Particle and carbon contamination was minimized with a partial oxide etch. The

shortened DHF dispense times did not remove all the SiO_2 and the wafer was hydrophilic. The trace metal impurities were below $1x10^{11}$ atoms/cm^2 and were not measurably influenced by the limited amount of oxide removed.

The DI water rinse only processes generally were low in particle contamination and removed many trace metals with out removing the native oxide. Particle contamination increased with higher rinse temperatures on wafers with native oxide as well as hydrophobic surfaces. The hot DI water rinses reduced the concentration of all the metal impurities except aluminum. The reduction of Zinc required extended rinsing at 80°C.

CONCLUSION

The chemical composition of a wafer surface following cleaning is highly dependent upon the chemical solutions and operating conditions used to perform the clean. Variables such as chemical dispense time, rinse time and water temperature can have a major impact on oxide thickness, particle contamination and the elemental composition of the surface. Cleaning conditions must be carefully defined and controlled to consistently obtain a surface with the properties required to perform subsequent processing. Silicon wafer cleaning processes based on single acidic solutions followed by a DI water rinse can be efficient alternatives to processes employing multiple chemical sequences.

ACKNOWLEDGEMENTS

The authors are grateful to D. Grant and P. Carr for their helpful discussions throughout this study, and to F.J. Steffen and D. Drakenberg for manuscript preparation.

REFERENCES

1. G. Gould and E. A. Irene, J. Electrochem. Soc., 134, 1031 (1987).
2. J.H. McFee, R.G. Swartz, V.D. Archer, and S.N. Finegan, ibid., 130, 214 (1983).
3. Y. Kunii, M. Tabe, and Y. Sakakibara, Jpn. J. Appl. Phys., 26, 1008 (1987)
4. R. Williams and A.M. Goodman, Appl. Phys. Lett., 25, 531 (1974).
5. P. Pan and C. Schaefer, J. Electrochem. Soc., 133, 1171 (1986).

6. M.F. Ebel and W. Liebel, J. Electron Spectrosc. Relat. Phenom., 16 463 (1979).
7. M.F. Ebel and G. Zuba, H. Ebel, J. Wernisch, and A. Jablonski, Spectrochim. Acta, 39B, 637 (1984).
8. A. Benninghoven, F.G. Rudenauer and H.W. Werner, "Secondary Ion Mass Spectrometry", P. 287, J. Wiley & Sons, Inc., New York (1987).
9. P. Eichinger, H.J. Rath and H. Schwenke, D.C. Gupta, Editor, Semiconductor Fabrication: Technology and Metrology, ASTM STP 990 (1988).
10. R.K. Iler, "The Chemistry of Silica", P. 4, J. Wiley and Sons, Inc., New York (1979).
11. Y. Koseki and S. Takahasi, J. Electrochem. Soc., 136, 2695 (1989).
12. A. Licciardello, O. Puglisi, and S. Pignataro, Appl. Phys. Lett., 48, 41 (1986).
13. M. Grunder and H. Jacob, Appl. Phys., A39, 73 (1986).
14. L.A. Zazzera and J.F. Moulder, J. Electrochem. Soc., 136, 484 (1989).
15. F. Helfferich, "Ion Exchange", P. 157, McGraw Hill, New York (1962).
16. L.S. Becker and L. A. Zazzera, "Effect of Final Rinse Processes on Sodium Contamination", FSI International, Technical Report 353, (1989).

Table 1. Particle characterization of various processes

Process	Net particle addition (0.3μm)	
	X	σ
No process	11	18
Rinse only 20°C	11	36
Rinse only 80°C	121	121
H_2SO_4:H_2O_2-20°C Rinse	3	14
H_2SO_4:H_2O_2-80°C Rinse	45	14
DHF-20°C Rinse	766	983
DHF-80°C Rinse	3184	1384

Table 2. Oxide thickness measurements of various processes

Process	Ellipsometer Å $\bar{X}$	Ellipsometer Å σ	Auger R Si$_{(OX/EL)}$ $\bar{X}$	Auger R Si$_{(OX/EL)}$ σ	XPS Å $\bar{X}$	XPS Å σ
No process	16	1	1.7	0.3	9.2	1.0
Rinse only	15	1	1.6	0.1	8.3	0.2
$H_2SO_4:H_2O_2$	14	1	1.7	0.2	8.5	0.7
DHF(18s.)	11	1	0.8	0.3	7.6	0.1
DHF(42s.)	8	1	0.2	0.2	3.1	0.1
DHF(240s.)	6	1	0.1	0.1	2.3	0.1

Table 3. Relative atomic concentrations of various processes

Process	Si 2p $\bar{X}$	Si 2p σ	O 1s $\bar{X}$	O 1s σ	C 1s $\bar{X}$	C 1s σ	S 2s $\bar{X}$	S 2s σ	F 1s $\bar{X}$	F 1s σ
No process	27.0	3.7	50.4	9.9	23.0	7.0	0.4	0.4	0.2	0
Rinse only	27.5	0.5	56.3	0.8	16.2	1.3	<0.1%		<0.1%	
$H_2SO_4:H_2O_2$	28.3	2.6	54.8	5.0	14.8	2.1	0.4	0.5	<0.1%	
DHF(18s.)	36.1	0.2	55.5	0.1	8.3	0.4	<0.1%		.1	.2
DHF(42s.)	36.6	0.8	26.6	6.9	36.5	7.7	<0.1%		.3	.2
DHF(240s.)	35.3	0.2	14.0	0.4	50.6	0.7	<0.1%		.1	.1

Table 4. Trace metal impurities Relative Elemental Abundance

Process	^{23}Na $\bar{X}$	^{23}Na σ	^{27}Al $\bar{X}$	^{27}Al σ	^{40}Ca $\bar{X}$	^{40}Ca σ	^{64}Zn $\bar{X}$	^{64}Zn σ
No Process	1024	2781	26917	41780	4063	3251	683	416
Rinse only	37	35	33276	41634	681	580	234	211
$H_2SO_4:H_2O_2$	102	93	1540	113	96	17	15	8
DHF	60	52	3575	1668	137	74	37	27

Table 5. Trace metal impurities 10^{12} atoms/cm^2

Process	Ca $\bar{X}$	Ca σ	Fe $\bar{X}$	Fe σ	Cu $\bar{X}$	Cu σ	Zn $\bar{X}$	Zn σ
No process	8.7	3.2	0.21	0.29	0.12	0.2	36	15
Rinse only	<1.0		<0.1		0.16	0.31	6.3	9.5
$H_2SO_4:H_2O_2$	<1.0		<0.1		<0.06		<0.08	
DHF	<1.0		<0.1		<0.06		<0.08	

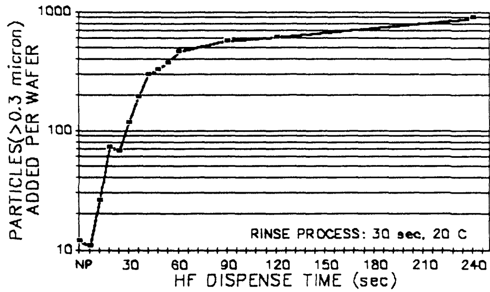

Fig.1 Particle contamination increased with longer HF dispense times.

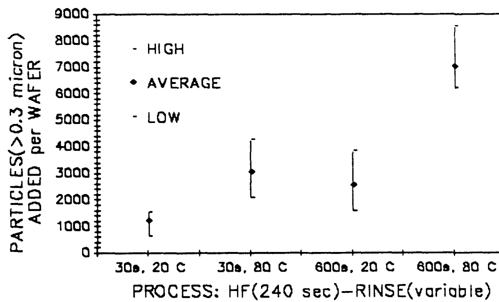

Fig.2 Wafer particle additions were increased with longer rinse time and hotter rinse temperatures on hydrophobic wafers.

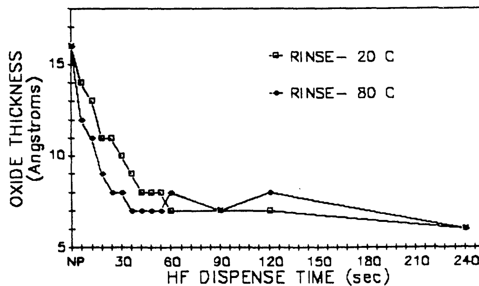

Fig.3 Ellipsometry indicated the rate of oxide removal was increased by higher rinse temperature.

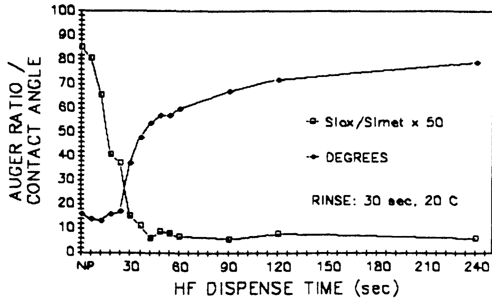

Fig.4 Oxide removal was measured by Auger and Contact Angle. Note the continued increase in contact angle did not correspond to further oxide removal.

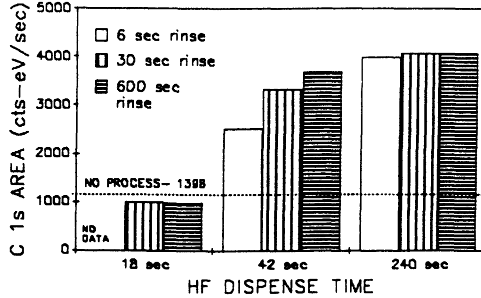

Fig.5 Carbon adsorption increased with longer HF dispense times. Rinse time may also influence carbon adsorption shortly after oxide removal (42 second dispense time).

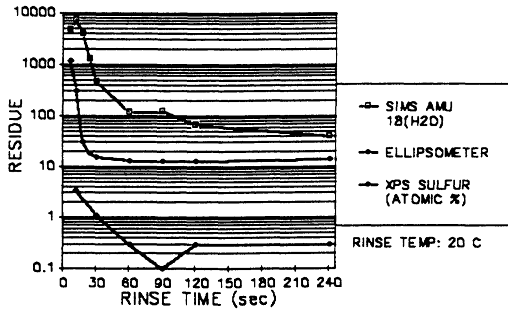

Fig.6 Sulfur residue was present on wafers following a 60 second H_2SO_4:H_2O_2 dispense. Residue removal as a function of rinse time was monitored.

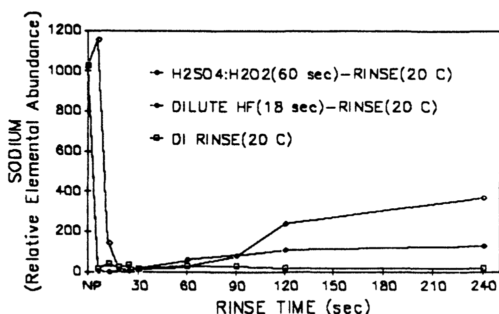

Fig.7 Longer rinse times after acid solutions increased sodium contamination.

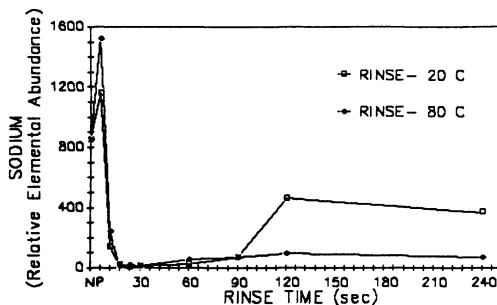

Fig.8 The higher rinse temperature after $H_2SO_4:H_2O_2$ dispense minimized the sodium contamination. Note the initial increase in sodium contamination as a result of incomplete rinsing of the $H_2SO_4:H_2O_2$ residue.

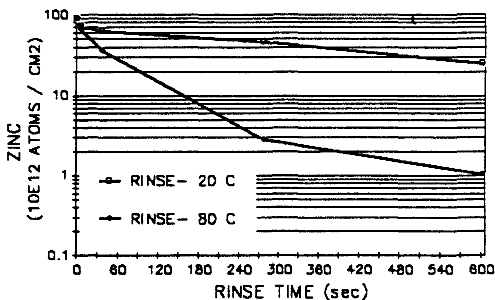

Fig.9 Rinsing alone reduced Zinc contamination. TRXRF analysis measured the same are on the same wafer between successive rinses.

METALLIC CONTAMINATION ON Si WAFERS FROM CLEANING SOLUTIONS

Jun Atsumi, Susumu Ohtsuka, *Syuuji Munehira and Kenji Kajiyama

Materials Research Laboratory-III Nippon Steel Corp.
NSC Electron Corp.
3434 Shimata, Hikari-shi, Yamaguchi Pref., 743, Japan

ABSTRACT

Metallic contamination on Si wafers from some cleaning solutions was evaluated by measuring lifetime by photo-conductivity decay method.

Lifetime of the wafers cleaned in $NH_4OH+H_2O_2$ solution was shorter than that processed in $HCl+H_2O_2$ solution or in dilute HF solution.

In case of $NH_4OH+H_2O_2$ solution with little amount (~1ppb) of Fe, lifetime shortening was observed, but with Cu, it was not observed.

In case of $HCl+H_2O_2$ solution no remarkable lifetime shortening was observed.

In case of dilute HF solution lifetime shortening was observed with Au and Cu whose ionization tendency was lower than Si.

1. INTRODUCTION

Small amount of metallic contamination in VLSI fabrication process degrades electronic functions of VLSI. Therefore chemical solutions are carefully selected and applied to decrease contamination, but in some cases it is observed chemical solutions may increase contamination. We studied preferential metallic contamination from cleaning solutions.

2. TEST PROCEDURE

CZ silicon wafers of 5" N-type, ρ =8~12Ωcm and (100) were cleaned in different solutions which consist well kown RCA cleaning method (Table 1). 0.5~500ppb amount of metallic impurities were intentionally added to each solution. After dipped in these solutions the wafers were rinsed in deionized water twice for 5min. per time, followed by spin drying. The wafers were oxidized in dry O_2 at 1000℃ for 70 min., when clean wafers were interposed between contaminated wafers to avoid cross contamination. Contamination on these wafers was evaluated by measuring lifetime by use of micro-wave reflecting lifetime measuring apparatus (LEO Corporation LTA-330A ;9040Å exciting wave length). To check experimental error and/or repeatabi-lity, two wafers were evaluated at each test condition.

Direct analysis of the surface of contaminated Si wafers was performed as follows. Three contaminated wafers were etched in approx. 75ml of HF/HNO_3 solution(1/10ratio) to an extent of some 5μm per

side, and the etchant was, after evaporation to dryness, redissolved in 3.2ml of HNO_3(1/1ratio) and diluted to 25ml to obtain 1N HNO_3 sölution. This etchant was analyzed by flameless atomic absorption spectrophotometry(Hitachi Z-8000). The lower detection limit for this analysis was approx. $4x10^{11}$ atoms/cm^2.

3. TEST RESULTS AND DISCUSSION

3.1 Lifetime Dependence on Cleanings

Lifetime value for dopant type and cleaning solutions to which no contaminants were intentionally added are shown in Fig. 1. The reason why N-type shows higher values of lifetime than P-type is considered that the diffusion coefficient for the minority carriers of N-type, i.e. holes, is smaller than that of P-type, i.e. electrons. Various cleaning solutions yield significantly differnt value, particularly those ending $NH_4OH+H_2O_2$ cleaning show very low level.

One potential reason for such lifetime difference by cleaning solutions is considered that SiO_2/Si interface may changed the surface condition and thus surface reconbination effect may be different by cleaning solutions. In order to determine surface reconbination effect, the wafers were etched by hydrofluoric acid to strip-off the oxide film and then reoxidized. The lifetime values measured for these wafers are shown in Fig. 2. Notwithstanding above processing, lifetime of the wafers cleaned in $NH_4OH+H_2O_2$ solution before initial oxidation remains short. This indicates that certain metallic contaminants that can be cause of shortening lifetime were deposited on the surface of the wafers by $NH_4OH+H_2O_2$ solution. Such contaminants could not be removed by hydrofluoric acid etching, because they diffused into wafers during the first oxidation.

Also in Fig. 2, wafers cleaned in dilute HF solution show a little decrease after further oxidation, while the wafers cleaned in $NH_4OH+H_2O_2$ solution show a little increase. This is considerd that the former were less contaminated, so they were influenced by contamination from the furnace during second oxidation, while in the latter case contamination remain in the oxide film or interface was removed as a result of the oxide film etching.

It is known from Secondary Ion Mass Spectroscopy (SIMS) analysis that $NH_4OH+H_2O_2$ cleaning causes contamination of Al in the solution.[1)2)] It is also reported that similar alkaline cleanings in which choline is used instead of ammonum hydroxide cause deposition of Al as well.[3)]

However, since Al is not sensitive metal to lifetime shortening[4)], it is considered that different metallic contaminants may deposit. Such metallic contamination can not be detected by this SIMS analysis because of a trace amount, and no relevant data are available in the above report.[1)2)3)]

3.2 Contamination by $NH_4OH+H_2O_2$ Cleaning

The relation between metallic concentration of Fe and Cu added to $NH_4OH+H_2O_2$ solution and lifetime is shown in Fig. 3. It should be noted that addition of even such as small as 0.5ppb amount of Fe can

cause drastic shortning of lifetime. Below 50ppb lifetime decrease according to Fe added, while 50 to 100ppb this decrease saturated. Lifetime dependence on Cu concentration in the solution is rather unique, and even 50ppb additive makes little decrease in lifetime. This indicates that a trace amount of Fe in the cleaning solution deposits on the surface of wafers, but Cu does not.

There are given in Table 2 for reference the results of analysis of impurity concentration in chemicals which were used in the experiment. These values are below electronic grade level, and both ammonium hydroxide and hydrogen peroxide have no higher impurity concentration than other chemicals. Therefore, the fact that lifetime level for $NH_4OH+H_2O_2$ solution without intentional contamination is shorter than those for dilute HF and $HCl+H_2O_2$ solutions is attributable to deposition of 0.1ppb order of Fe in $NH_4OH+H_2O_2$ solution.

Estimation of mechanism that a trace amount of Al and Fe in the solution for alkaline cleanings containing oxidants such as $NH_4OH+H_2O_2$ solution deposit on the surface of wafers but Cu does not is made as follows. Scince oxide formation enthalpies($-\Delta H_f^\circ$)of Al and Fe are greater than that of Si, Al and Fe are preferentially oxidized over Si and deposit in oxide film while the oxide film is formed. These elements are insoluble in the alkaline solution and so stay on the surface of wafers. On the other hand, because oxide formation enthalpy of Cu is smaller than that of Si, it is difficult to deposit in the oxide film while it is formed. In addition, as Cu form a complex with ammonium hydroxide to turn into soluble ions it is difficult to stay on the surface of wafers. Oxide formation enthalpies are given in Table 3.

Furthermore, lifetime of wafers processed in the solution with 5 and 10 ppb Cu significantly increased. This was confirmed by retesting. If the reason of lifetime shortening in case of $NH_4OH+H_2O_2$ cleaning without addition of contaminants is considered as deposition of Fe in the solution, then it may be possible that a little amount of additive Cu could disturb Fe deposition. However, further details remain to be studied.

3.3 Contamination by $HCl+H_2O_2$ Solution

The lifetime of wafers cleaned in $HCl+H_2O_2$ solution to which Fe or Cu was added in 50ppb concentration is shown in Fig. 4. Dissimilarly to $NH_4OH+H_2O_2$ solution, almost no shortening of lifetime for both Fe and Cu is observed, and it is understood that no contaminants deposit on the wafers.

The proposed reason for this is that both Fe and Cu turn into soluble ions at low pH by hydrochloric acid.

3.4 Contamination by dilute HF Solution

The lifetime of wafers dipped in dilute HF solution with 50ppb of metallic impurities for 60min. is shown in Fig. 5. Significant lifetime shortening occers for Cu and Au, although little shortening occers for Fe, Zn and Ni.

This is because metallic impurities with lower ionization tendency (Table 4) are adsorbed on the surface of wafers electrochemically.

5) 6)

3.5 Analysis of Wafers by Atomic Absorption Spectrophotometry

The result of atomic absorption analysis of contamination on the surface of Si wafers cleaned in $NH_4OH+H_2O_2$ and $HCl+H_2O_2$ solutions to which Fe and Cu were added is shown in Fig. 6. For $NH_4OH+H_2O_2$ solution, Fe deposition increases in proportion to the amount of Fe added in $NH_4OH+H_2O_2$ solution at 0.5ppb to 50ppb, and saturates above 50ppb up to 500ppb. As compared with Fe, Cu plots are lower than the detection limit of atomic absorption analysis even for 50ppb additive solution concentration. Furthermore, for $HCl+H_2O_2$ solution both Fe and Cu plots stay below the detection limit. In this way, behavior of Fe and Cu contamination of wafers in $NH_4OH+H_2O_2$ and $HCl+H_2O_2$ solution was comfermed by atomic absorption spectorophotometry, which was same as the one previously confermed by lifetime measurements.

Notwithstanding the foregoing, the hypothesis based on the measurements of lifetime that Fe contamination of wafers processed in $NH_4OH+H_2O_2$ solution free from intentional contamination would be higher than that of wafers processed in $HCl+H_2O_2$ solution with 50ppb Fe additive could not be proved because the values obtained were lower than the detection limit of atomic absorption analysis.

4. CONCLUSIONS

(1) A trace amount of Fe in $NH_4OH+H_2O_2$ solution deposits on the surface of wafers. Deposited Fe causes lifetime shortening even if the concentration is less than 1ppb.

(2) In case of $HCl+H_2O_2$ solution, deposition of various metals is hard to occur.

(3) In case of dilute HF solution, metallic impurities whose ionization tendency is lower than Si are adsorbed electrochemically.

5. ACKNOWLEDGEMENTS

The authors would like to thank M. Inamitsu and S. Yamamoto for sample preparation and measurement works.

REFERENCES

1) Kawado, S. et al; Proc. of the 5th Int. Symp. on Silicon Materials Science & Technology, P961 (1986)
2) Becker, C. et al; FSI Technical Report TR251 (1984)
3) Krusell, W. C. et al; Ext. Abst. of Spring Meeting of Electrochemical Soc. 169th, P331 (1986)
4) Atsumi, J. et al; Proc. of the 33rd Symp. on Semiconductors & Integrated Circuits Technology, P61 (1987) in Japanese
5) Miki, M. et al; Proc. of the 5th Symp. on ULSI Ultra Clean Technology, P235 (1987) in Japanese
6) Kern, W.; RCA Engineer, **28-4**, p.99 (1983)

Solutions	Recipe
Dilute HF	$HF:H_2O=1:99$ RT. 60sec or 60min
$NH_4OH+H_2O_2$	$NH_4OH:H_2O_2:H_2O=1:1:5$ 80^0C 10min
$HCl+H_2O_2$	$HCl:H_2O_2:H_2O=1:1:5$ 80^0C 10min
$H_2SO_4+H_2O_2$	$H_2SO_4:H_2O_2=3:1$ 100^0C 10min

Table-1 List of Cleaning Solutions

(ppb)

Chemicals	Al	Ca	Cr	Cu	Fe	K	Mg	Na	Ni	Zn
HF	3.02	0.14	0.18	<0.05	0.43	<0.05	<0.05	0.08	<0.05	0.11
HCl	4.36	1.92	0.11	<0.05	0.88	0.64	2.92	0.80	0.07	0.07
NH_4OH	0.32	0.56	0.05	0.05	0.06	<0.05	<0.05	0.78	<0.05	<0.05
H_2O_2	1.71	2.35	1.10	<0.05	0.13	0.07	<0.05	0.31	<0.05	<0.05

Table-2 Analysis of Chemicals Used in Experiment

OXIDE	$-\Delta H^{\circ}_{f}$
Al_2O_3	1675.3
Fe_3O_4	1118
SiO_2	910.9
CuO	157

(KJ/mol) at 293K

Table-3 Oxide Formation Enthalpies

Ionization Tendency	Zn>Fe>Ni>Si>Cu>Au
Electronegativity	1.6 ¦ 1.8 ¦ 1.8 ¦ 1.8 ¦ 1.9 ¦ 2.4

Table-4 Ionization Tendency & Electronegativity

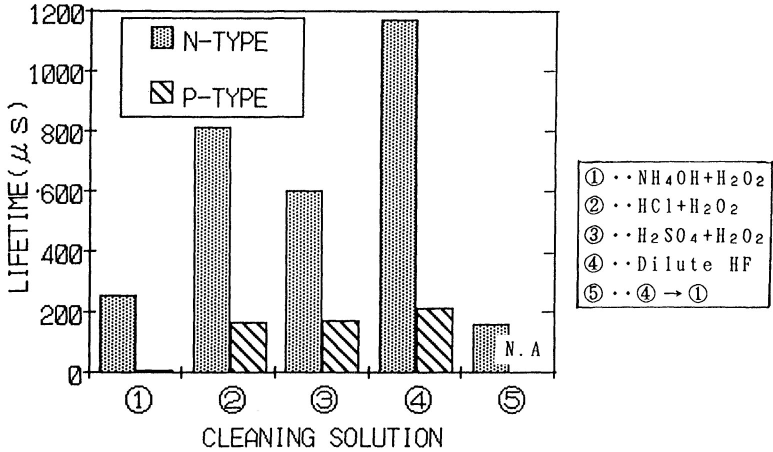

Fig.-1 Lifetime vs. Cleaning solution & P/N Type

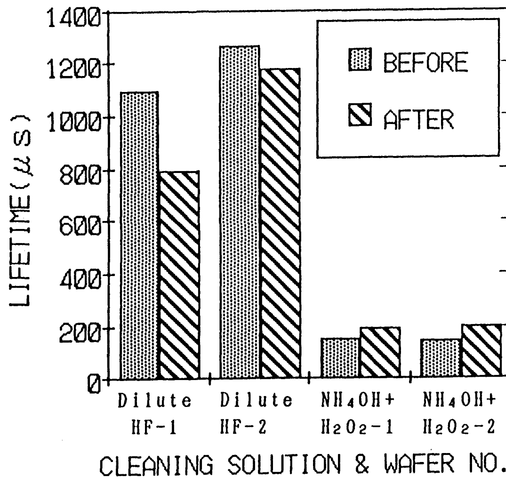

Fig.-2 Lifetime Before & After Reoxidation

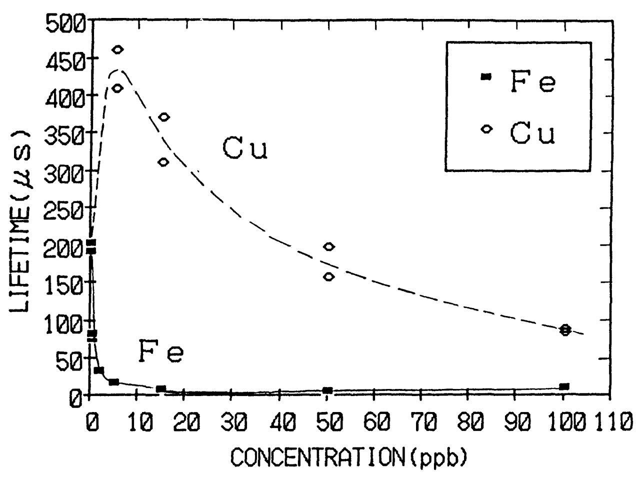

Fig.-3 Lifetime vs. Metallic Concentratin in $NH_4OH+H_2O_2$ Solution

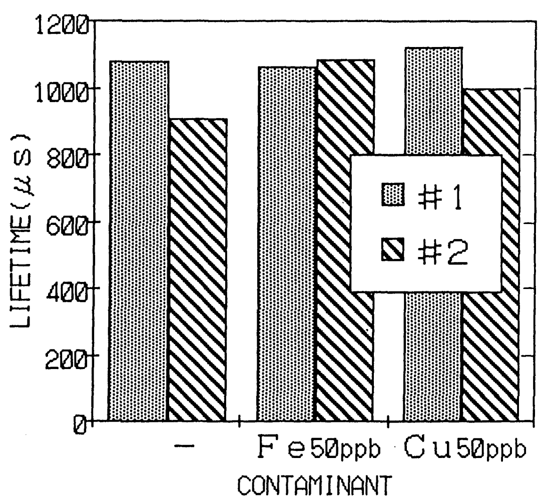

Fig.-4 Lifetime Shortening by 50ppb Fe or Cu in $HCl+H_2O_2$ Solution

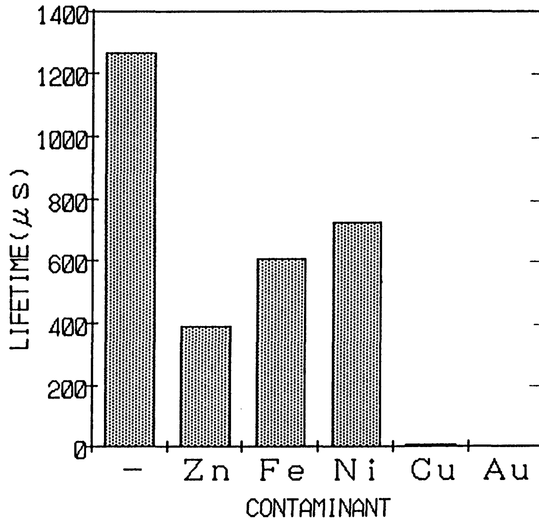

Fig.-5 Lifetime Shortening by Several Metals of 50ppb in Dilute HF Solution

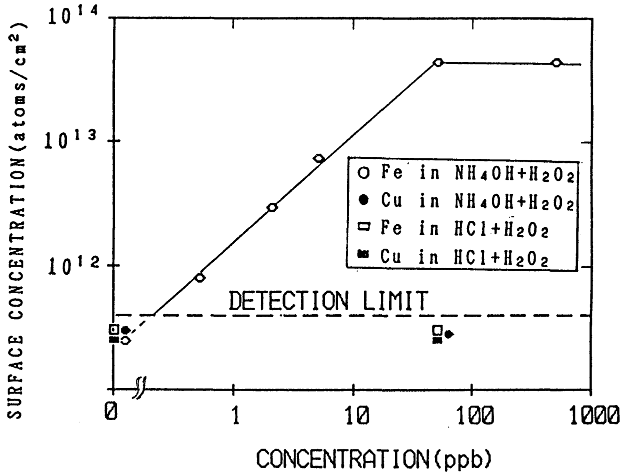

Fig.-6 Surface Concentration vs. Solution of various metals Concentration

Advantages and Limits of Wet Etching Process in Spray Equipment

Detlef Roß
Siemens AG
Semiconductor Department
8000 Munich 83, Germany

Abstract

Spray process equipment is well known in cleaning applications. Wet etching processes are carried out mostly in tank or wet bench systems. Many of the cleaning processes contain overetch steps with HF solutions. These steps remove the top layer of silicon dioxide as well as the impurities located on the surface. For special applications a buffered HF (BOE) solution is used. Very cost effective is it to combine wet etching and the preceding or following cleaning step in one machine. This paper will discuss possible applications of buffered HF solutions and diluted HF in spray process equipment in combination with cleaning processes.
At constant temperature the oxide removal depends on the etching time, the flow rate of the etching solution and the concentration of the etching solution. Speed of rotation and atomizer pressure were found to have no influence on the removal rate. The range of the oxide removal increases with the time and the flow of the etching solution but decreases with the atomizer pressure.

Introduction

Every four years a new DRAM (Dynamic Random Access Memory) generation will be developed. Each generation needs new sophisticated equipment and processes. The smallest possible structure width dropped from about 3 um to 0.8 um in the last 10 years. This needs highly sophisticated instruments such as Scanning Electron Microscopes to control such dimensions. The development in the wet chemistry was more quiet. Most people expected the near end of wet chemical process steps, but the percentage of wet processes has kept constant (7). Progress in wet chemistry lies in the better removal of particles and processes better adapted to the following process steps such as Oxidation, CVD or Sputtering. This adaptation requires the use of HF solutions. In former days HF processes were known as very dirty processes, in spite of the fact that the aqueous hydrofluoric acid is one of the cleanest solutions. It is available with particle levels of 10 - 20 particles/ml (> 0.2 um) and metal contents of less than 10 ppb for each element.

Experimental

Equipment and Materials

For the experiments a commercially available FSI Multi Position spray processor (SATURN) of a standard configuration was used. Figure 1 shows the cross section through the process chamber. The silicon wafers are located horizontally in the turn table. The hot and cold DI water was supplied by a central supply system. For the experiments we used different concentrations of HF containing solutions. The diluted HF solutions were delivered by an automatic blending station, varying the concentration from 0.5% to 5% These solutions were then further diluted in the spray processor to a concentration in the range from 0.1% to 1% on the wafer surface. The original buffered oxide etch solution (30 wgt.% NH_4F and 6 wgt.% HF) was only diluted in the spray processor. All chemicals were MEGA Selectipure grade.
The used wafers were of p-type, <100> oriented and had 150 mm in diameter. The oxides were grown by wet thermal oxidation (720 nm thickness) or by chemical vapor deposition with TEOS (Tetraethoxisilane) as a silicon source (750 nm thickness).
Oxide thicknesses before and after etching were determined by means of interferometry.

Cleaning Processes

A lot of different cleaning processes are being used throughout the world in the semiconductor industry. Nearly all of them are based on principles of the so called RCA Clean developed by W. Kern (4,5,6). Figure 2 gives an overview of the derived cleaning processes. Three principal usages of HF are shown:

1 HF as a first step
2 HF as an intermediate step
3 HF Last

HF as a first step is used for pre gate oxide oxidations. The HF removes the existing native oxide and during the following cleaning step the oxide will be rebuilt by the applied chemistry. This ensures a defined origin of the native oxide before gate oxidation (8).
HF in the middle of a cleaning sequence is used for more rigid cleaning steps. At first a layer of organic contaminants must be removed then the HF etches a contaminated oxide layer. After these steps predominantly acidic chemicals give a very clean surface. Another application of the HF step is the removal of so called Plasma Polymers. The HF underetches the polymers and the following rinse removes them.
HF Last is only used before sputtering. Here the HF removes the native oxide layer. The following rinsing is not sufficient to renew this oxide layer.

Process Parameters

Every process during manufacturing of semiconductor devices is characterized by a special set of control parameters. HF cleaning steps are normally carried out in tanks and wet benches respectively or in spray process systems. Nowadays single wafer processing machines enter the market. But nevertheless cleaning is one of the typical batch processes. Figure 3 shows a set of parameters for each type of equipment. The most important parameters for the HF etching processes are the amount of removed oxide or as an equivalent the removal rate and the uniformity within the wafer and the carrier. These results are influenced by process and machine parameters such as concentration of the used HF solution, temperature, process time and a certain number of parameters special to the used equipment.
HF application in a cleaning process has to remove only a small quantity of oxide, typically 4 nm within the range of ± 2 nm. For larger amounts the range within the wafer and the carrier should be much better than 10%.
An important parameter too is the particle density at the end of a complete cleaning step. An acceptable number typically is the increase of less than 30 particles (> 0.5 u m) per wafer.

Measurements

To solve the problem of undefined temperature in the spray process equipment a special program was developed which cooled down the whole chamber to reproducible constant temperature. This is important because the temperature of the process chamber depends on the previous process. The required uniformity of the etch rates does not allow for variations due to an undefined temperature.
To define the influence of the parameters a full factorial design (2 values and 4 parameters) was used. The results can be expressed by a polynomial equation such as

$$\text{Response} = a_0 + a_1 p_1 + a_2 p_2 + a_{12} p_1 p_2 + \dots \qquad (1)$$

where p_i are the parameters and a_{ii} the coefficients of the polynome.

Results

Figure 4 shows the general results of the experiments.

Rate of Oxide Removal
Three parameters have the strongest influence on the amount of oxide removal. These are the chemical dispense time, the flow rate and the product of dispense time and flow rate. They all show a comparatively large positive coefficient. Figure 5a shows the response surface of these parameters. The interdependence between time and flow gives a slight

bow of the surface. The rotation speed of the turn table has a minor influence which is less than a tenth compared to the parameters above. By increasing the rotation speed the amount of removed oxide will also increase. Figure 5b shows the response surface for the parameters flow and rotation speed (RPM).

Removal Range within a Wafer

The influence on the removal range within a wafer is more complicated. The major effect have chemical dispense time, flow rate and the product of time and flow rate. The corresponding coefficients have the same magnitude. This leads to a stronger curvature of the response surface (Figure 6a).
More surprising is the influence of the other parameters. Rotation speed and the atomizer pressure have a negative coefficient. Figure 6b shows the response surface plot of this result. Therefore high rotation speed and high atomizer pressure are the adequate process parameters for a HF dispense step.

Variations within the Carrier

Figure 7 shows a typical result. The amount of removed oxide shows a minimum which is not at the center of the wafer carrier. The explanation lies in the nature of the chemical dispense. As can be seen in Figure 1 the spray post has only a limited number of openings for chemicals and atomizing nitrogen which do not cover all wafers equally from top to bottom.

Particle Density

The particle problem depends on the type of the remaining wafer surface. If an oxide surface on the wafer remains after the HF step almost no particle formation is observed. The increase is less than 10 particles per wafer. On the other hand a bare silicon surface leads to a not reproducible number of particles from run to run. This is not an effect of the HF dispense steps itself. At the end of an oxide strip process with anhydrous HF the wafers show a low particle density but after rinsing in a spray system the particle level is very high. An overflow rinse of such wafers in a bench gives a normal low particle number.

Model of Particle Formation

After a HF etching step a perfect silicon surface is covered with hydrogen (1). Therefore mostly Si-H bondings are present. A small percentage is also covered with fluoride or hydroxyl groups. These are points of invisible structural defects on the single crystal, i. e. the Si- Si bondings are weakened. At these sites the growth of the native oxide starts. Figure 8 shows a schematic summary of the resulting reaction mechanism. During the rinse step the number of adsorbed hydroxyl groups increases. Due to condensation Si-O-Si bridges are formed and this leads to a further weakening of the crystal lattice. After drying the wafer no native silicon dioxide is detectable. By adsorbtion of oxygen from the

air the native oxide starts to grow. The growth rate is about 10-7 nm/s (1,2).
If the oxygen content in the rinsing water is high or the water is being sprayed another possible reaction path arises. At the sites where adsorbtion starts the production of silicic acid can occur in a faster mechanism . The growth rate is about 10-2 nm/s. This leads to a particle growth on the silicon surface. The consumption of silicon is very small. To create ten thousand particles of 5 um in diameter only a thousandth of a Si monolayer is needed.

Summary

Etching in spray process equipment is a good method to achieve an smooth surface with a small removal range. The amount of oxide removal depends linearly on the etching time. The uniformity increases with decreasing HF concentration. The time consumption for dispensing the chemicals is negligible compared the total rinse time. Therefore it is possible to get a uniformity batter than 1%. This is not possible in a tank process because the range of oxide removal always increases with the etching time. The temperature can be stabilized if cold DI water with a constant temperature is available. The consumption of chemicals, roughly estimated, results in 0.5 ml/nm/wafer of buffered oxide etchant above mentioned.
The disadvantage and therefore a limitation lies in the particle problem on a bare silicon surface. A model for the growth of this type of particle formation is proposed but no solution was found to avoid the particle generation.

Acknowledgment

I wish to thank Miss B. Schneider for carrying out the experiments.

References

1) D. Gräf, M. Grundner, R. Schulz, J. Vac. Sci. Technol., A7(3), 808 (1989).
2) L. Mühlhoff, T. Bolze, Fresenius Z. Anal. Chem., 333:527-530 (1989).
3) W. Huschka, Diplomarbeit, TU München 1987.
4) W. Kern, Semicond. Int., 4, 94 (1984).
5) W. Kern, RCA Engeneer., 28(4), 99 (1983).
6) W. Kern, D. A. Puitonen, RCA Review, 6, 187 (1970).
7) D. Ross, Technic. Proceed. Semicon Europe, 1 (1989).
8) G. Gould, E. A. Irene, J. Elechtrochem. Soc., 134(4), 1031 (1987).

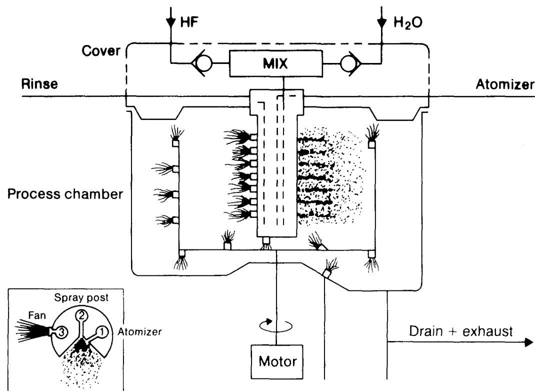

Figure 1: Cross section and functional diagram of a FSI Saturn/MP cleaner.

Chemicals \ Sequenz	A	B	C	D	E
(dil.) HF	O				
Mixture 1	O	O		O	O
(dil.) HF		O			
Mixture 2		O	O	O	
(dil.) HF			O		
Final rinse	O	O	O	O	O
Dry	O	O	O	O	O
Usage before	Gate Oxidat. / Sacrif. Oxide	Compl. Clean	Sputtering	Overall Clean	Particle Removal

Examples of mixtures

Mixture 1: H_2SO_4/H_2O_2, $NH_3 \cdot aq/H_2O_2{:}H_2O$, Choline/$H_2O_2/H_2O$

Mixture 2: Choline/H_2O_2/H_2O, $HCl/H_2O_2/H_2O$

Figure 2: Process sequences of typical cleaning steps.

	Process Parameter	Target Parameter
Tank	Temperature, Concentration, Flow, Time, Design	Material removal Range Particle count
Spray batch	Concentration, Flow, Time, Atomizer pressure, RPM, Total flow, Temperature	
Single wafer	RPM, Concentration, Flow, Time	

Figure 3: Process and target parameters for cleaning processes.

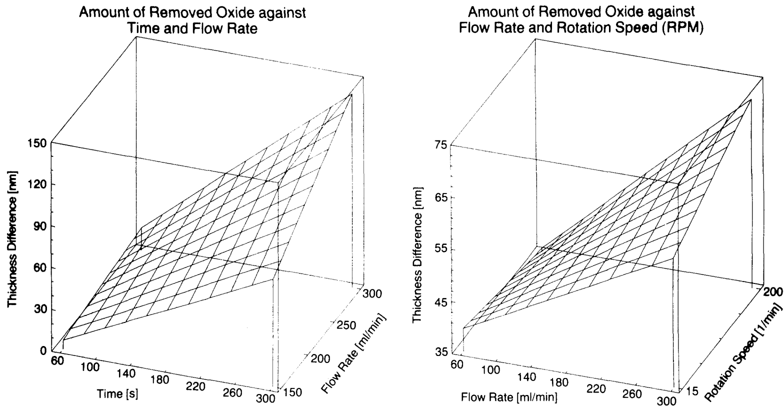

Figure 5: Amount of removed oxide against time and flow rate (a), flow rate and rotation speed (b).

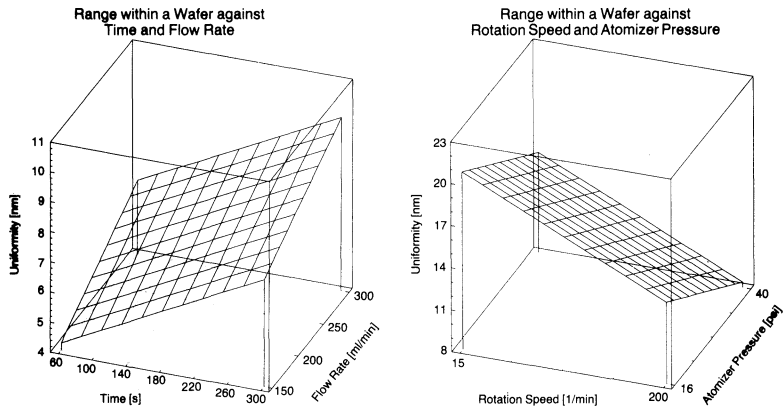

Figure 6: Range within a wafer against time and flow rate (a), rotation speed and atomizer pressure (b).

1) Removal rate / 2) Range	Time	Flow	Total flow	RPM	ATM
Time	++ / ++	+	○	○	○
Flow	++	++ / ++	○	+	○
Total flow	○	○	○ / ○	○	○
RPM	○	○	○	± / –	○
ATM	○	○	○	○	○ / –

1) $RR = b_0 + b_1\,(time) + b_2\,(flow) + b_{12}\,(time) \cdot (flow)$
2) $R = C_0 + C_1\,(time) + C_2\,(flow) + C_{12}\,(time) \cdot (flow) + C_3\,(RPM) + C_4\,(ATM)$

Figure 4: General results of the experiments.

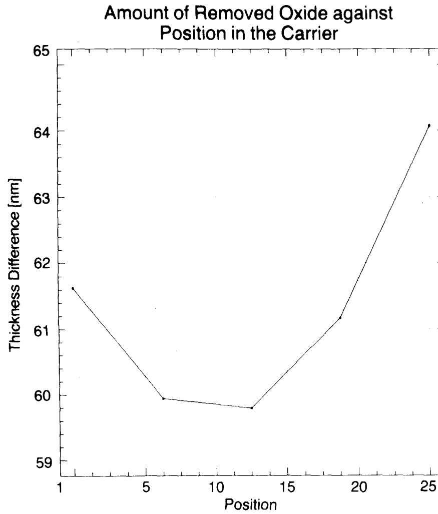

Figure 7: Amount of removed oxide against position in the carrier.

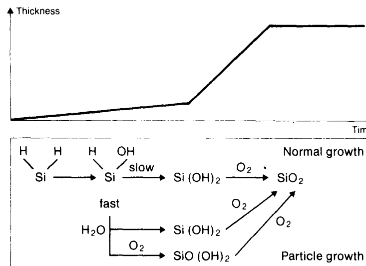

Figure 8: Growth model of native oxide or particles.

CLEANING MECHANISM OF SI WAFER SURFACES BY THE SLIGHT ETCH METHOD

R. Takizawa and A. Ohsawa

FUJITSU LABORATORIES LTD.
1015 Kamikodanaka, Nakahara-ku
Kawasaki 211, Japan

The slight etch method is a new, previously reported cleaning technique which uses HNO_3-HF solution. It reduces the surface Fe concentration by a factor of 10 after RCA, and improves MOS device characteristics.

The cleaning effect of SE is not simply caused by its etching action but by the nature of the cleaning solution itself. The number of Fe ions from the SE solution adhering to the Si surface is about 4 orders of magnitude less than that from NH_4OH/H_2O_2. The concentration of Fe introduced to the Si surface during SE decreases with the square root of the etch rate. We analyzed this behavior by applying Freundlich's adsorption formula.

1. Introduction

Significant amounts of impurities, such as heavy metals and particles, are unintentionally introduced on the Si wafer surfaces during wafer and device fabrication. In order to remove such contamination, RCA cleaning (1, 2) and/or a modified method are generally used. However, it is not easy to reduce Fe impurities below a concentration of 10^{11} cm^{-2} (3). We have already reported a new cleaning technique called the slight etch **(SE)** method (4, 5), which dissolves the Si wafer surface with an HNO_3-HF solution having an extremely low HF concentration. Etching to a depth of 30-nm after RCA reduced the surface Fe concentration by a factor of 10 and Ca and Mg by one-third. Improved C-t retention time and SiO_2 defect density of planer and trench MOS diodes were also confirmed.

To study how the SE reduces surface metal concentration, we took note of Fe impurities removed remarkably by the SE and investigated the adsorption behavior of Fe from cleaning solutions to the Si surface. In this paper, we first briefly introduce the fundamental characteristics and practical effects of SE, and then describe the cleaning mechanism of the Si wafer surface by SE.

2. Fundamental characteristics and cleaning effects

Boron-doped 9-11 ohm-cm (100) CZ Si wafers 100 mm in diameter were used. SE cleaning was performed using a mixture of 60% nitric acid and 0.025-0.1% fluoric acid. The fundamental characteristics of SE cleaning are listed in Table 1. Native oxides about 1 nm thick are produced, suggesting that the etch reaction is determined by the dissolution rate of the oxide in the extremely low HF concentration. The etch rate of the Si can be controlled from 3 to 60 nm/min by adjusting the HF concentration. The etch uniformity for thermal oxide patterned wafers is less than 5% for both Si and the oxide. Since the etch selectivity of Si is more than 10 for the oxide (Si/SiO_2), and 1-0.8 for poly-Si (Si/p-Si), SE is also suitable for patterned wafers.

Surface roughness changes caused by SE following RCA (NH_4OH/H_2O_2-HF-HCl/H_2O_2-NH_4OH/H_2O_2) was characterized using a Mirau optical profilometer (**TOPO-2D**, Wyko Corp.) (6) and reflection electron microscopy (REM) (7). The profilometer can reveal roughness with a period of about 5-500 µm using a 1024-detector charge-coupled device. Rrms is the root mean square of the height at 1024 points. REM is able to reveal roughness with a period of about 20-5000 nm. Figure 1 shows the dependence of roughness on the etch depth. Since Rrms does not depend on etch depth to 270 nm, the roughness with a period of 5-500 µm is not degraded by SE. The periodic asperity of about 100 nm revealed by REM, however, is degraded by a factor of 2 in height after 270 nm removal.

Figure 2 compares the surface metal concentrations among as-received, RCA only, and RCA + SE (30 nm etch) wafers. The concentration was determined by atomic absorption spectrophotometry with HF vapor-phase decomposition. The surface concentration of as-received wafers was found to be 10^{11}-10^{13} cm^{-2} for Fe, Ca, Mg, Na, and Al. RCA cleaning reduces these impurities by a factor of 10-100. Removal of 30 nm by SE after RCA reduces the concentration of Fe by a factor of 10, and the concentrations of Ca and Mg by one-thirds. The dependence of the C-t retention time at 50°C and SiO_2 defect density on the etch depth is graphed in Fig. 3 (4). It is evident that the removal of 30 nm improves the retention time by a factor of 2 and the defect density by one-third compared to RCA only, but etching beyond 30 nm affords no further improvement.

3. Cleaning mechanism

To clarify the SE cleaning mechanism, we take note of Fe impurities removed remarkably by the SE. The dependence

of surface Fe concentration on the etched depth using NH_4OH/H_2O_2 or SE solutions (Fig. 4) was first studied to clarify whether the cleaning effect of the SE was caused simply by the removal of the surface. An NH_4OH/H_2O_2 solution also etches Si by about 5 nm per cleaning. Though the initial Fe concentration (about 5×10^{11} cm^{-2}) is reduced by a factor of 10 by RCA (surface removal is about 10 nm), surface removal by NH_4OH/H_2O_2 after RCA does not significantly reduce the surface Fe. Surface removal by SE, however, reduces further Fe impurities. This suggests that the cleaning effect of SE is not simply caused by its etching action but by the nature of the cleaning solution itself.

Consequently, the relationship between the surface Fe concentration and the Fe concentration in the cleaning solutions was investigated as shown in Fig. 5. All wafers were first cleaned by RCA. The log of Fe concentration on the Si increases linearly with the log of that in the cleaning solutions, other than HNO_3 at low Fe concentrations. This diversion from the line is due to residue on the Si surface. Because the action of an HNO_3 solution is oxidizing rather than etching, it is difficult to remove the contamination completely. NH_4OH/H_2O_2 and SE solutions, however, have an etching action. Therefore, surface Fe concentration was directly determined by the adsorption equilibrium of Fe ions. The number of Fe ions from the NH_4OH/H_2O_2 solution adhering to the Si surface is about 4 orders of magnitude greater than that from the SE solution. The reason why the surface Fe concentration is rarely reduced below 7×10^{10} cm^{-2} by RCA is that the concentration is determined by the Fe concentration in the NH_4OH/H_2O_2 solution used for the final cleaning of RCA. When we used super-purified NH_4OH/H_2O_2 solution **(TAMAPURE-AA-100)**, the surface Fe concentration could be reduced to about 10^{10} cm^{-2}. This result is indicated by the closed square in the figure. On the other hand, Fe ions in the SE solutions are about 10 times less likely to adhere than those in HNO_3. This seems to be due to the disorption effect of etching. The dependence of surface Fe concentration on the etch rate, R, by SE with an Fe concentration of 100 ppm is shown in Fig. 6. Surface concentration decreases as etch rate increases.

During the SE cleaning, Fe ions react with the native oxides (about 1 nm in thickness) to form an Fe(III)-O complex (3) by HNO_3 agent, and the HF agent dissolves the oxide attending with exhaustion of Fe impurities. This behavior is analyzed empirically by applying Freundlich's adsorption formula (8). The formula is useful for isothermal adsorption of solute in solutions. The surface Fe concentration, C_s (cm^{-2}) is given by

$$C_s = k\ C_o^{1/n}.$$

C_O (ppm) is the Fe concentration in the solution, and k and n are constants determined empirically. k and 1/n were determined from the results shown in Fig. 5 using the method of least squares, and are summarized in Table 2. The 1/n value of NH_4OH/H_2O_2, HNO_3, SE are 0.94, 0.76, and 0.72 respectively, and the latter two are almost the same. Therefore the disorption effect by etching action is dependent on k, not on 1/n. The dependence of k on the etch rate, R, was calculated from the results shown in Fig. 6, and is shown in Fig. 7. k decreases linearly with the square root of the etch rate. Accordingly the disorption of Fe ions increases with the square root of the etch rate of the Si surface.

4. Conclusions

To study the SE cleaning mechanism, we investigated the adsorption behavior of Fe from cleaning solutions to Si surfaces. The cleaning effect of SE is not simply caused by its etching action but by the nature of the cleaning solution itself. The number of Fe ions from the the SE solution adhering to the Si surface is about 4 orders of magnitude less than that from NH_4OH/H_2O_2. Surface Fe also decreases with the square root of the etch rate of the Si surface. SE cleaning can clean Si surfaces more effectively to control the etch rate.

Acknowledgments

The authors would like to thank Messrs. H. Ishikawa and K. Honda for their discussions and encouragement.

References

1) W. Kern and D. A. Puotinen, RCA Rev. 31, 187(1970).
2) W. Kern, RCA Engineer 28-4,99(1983).
3) R. Takizawa, T. Nakanishi, and A. Ohsawa, J. Appl. Phys. 62, 4933(1987).
4) R. Takizawa, T. Nakanishi, K. Honda, and A. Ohsawa, Jpn. J. Appl. Phys. 27, L2210(1988).
5) A.Ohsawa,R.Takizawa, K.Honda, T.Matsutani, and K.Imaoka, IEEE IEDM'88 Digest of Technical Papers, 35-1(1988).
6) B. Bhushan, J. C. Wyant, and C. L. Koliopoulos, Appl. Opt. 24, 1489(1985).
7) K.Honda, R.Takizawa, and A. Ohsawa, J. Appl. Phys. 63, 2637(1988).
8)D.J. Shaw,Introduction to Colloid and Surface Chemistry (Butterworth, London, 1970).

Table 1. Fundamental characteristics of SE cleaning.

Native oxide	About 1 nm thick
Etch rate of Si	3–60 nm/min (HF: 0.025–0.1%)
Etch uniformity	< 5% within 4"ϕ wafer
Etch selectivity	Si/SiO_2 : > 10
	Si/p-Si : 1 - 0.8

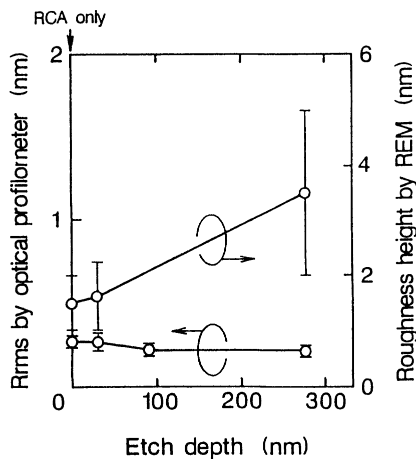

Fig.1. Dependence of surface roughness on the etch depth by SE.

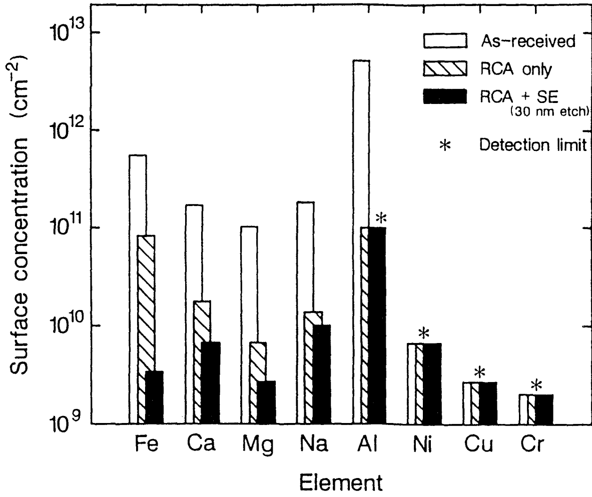

Fig. 2. Difference in surface metal concentration among as-received, RCA only, and RCA + SE.

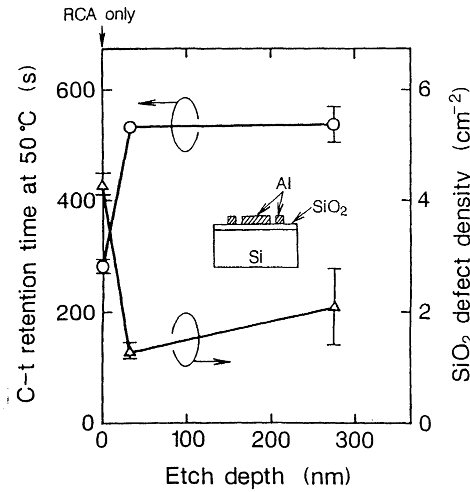

Fig. 3. Improvement of MOS diode characteristics by SE.

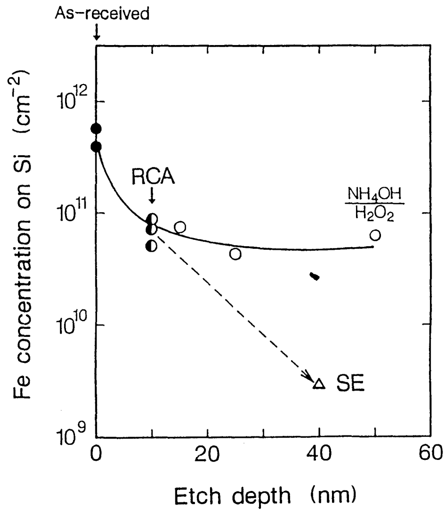

Fig. 4. Dependence of surface Fe concentration on the etch depth using NH_4OH/H_2O_2 or SE solution after RCA.

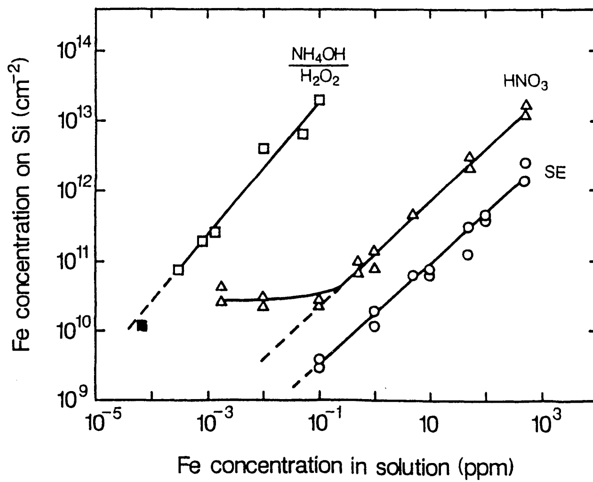

Fig. 5. Relationship between surface Fe concentration and Fe concentration in cleaning solutions.

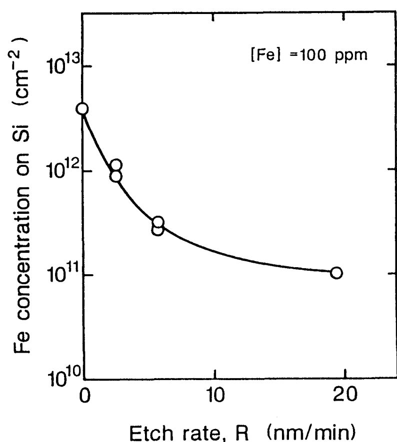

Fig. 6. Dependence of surface Fe concentration on the etch rate by SE with 100 ppm Fe concentration.

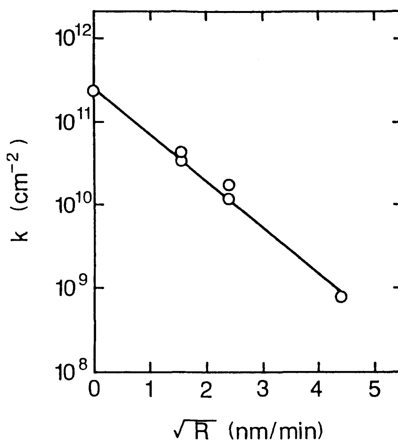

Fig. 7. Dependence of k on the square root of the etch rate.

Table 2. Empirical constants of Freundlich's adsorption formula and correlation coefficient of the method of least squares.

Solution	$\frac{NH_4OH}{H_2O_2}$	HNO_3	SE
1/n	0.94	0.76	0.72
k (cm^{-2})	1.6×10^{14}	2.5×10^{11}	1.8×10^{10}
Correlation coefficient	0.986	0.995	0.987

THE USE OF REPROCESSED HF IN SEMICONDUCTOR QUARTZ AND WAFER CLEANING OPERATIONS

John Davison and Chung Hsu
ATHENS CORP
Oceanside, California 92056

Erwin Trautmann and Howard Lee
TEXAS INSTRUMENTS, DMOS IV
Dallas, Texas 75265

ABSTRACT

In a cooperative project, a chemical reprocessor was developed to recycle and repurify the hydrofluoric acid (HF) solutions used in semiconductor quartz and wafer cleaning operations. The reprocessor removes ionic and particulate impurities via ion exchange and filtration, respectively. The reprocessed HF is ultrapure. HF from a "non-phosphorus" quartz cleaner was reprocessed and used in subsequent quartz and wafer cleaning tests. In the quartz cleaning evaluation, the reprocessed HF proved to be as good as the production acid as determined by FCGOI tests. Split lot wafer cleaning tests indicated no difference in 1 megabit DRAM yield or FCGOI performance when reprocessed HF was used in a critical cleaning step. The HF reprocessor is now being used in production to reclaim quartz clean acid.

INTRODUCTION

Aqueous hydrofluoric acid, HF, is one of the essential liquid chemicals used in the manufacture of silicon semiconductor devices. HF solutions of 10-20 wt% are commonly used to clean the furnace tubes and other miscellaneous quartzware used in device fabrication. Quartz cleaning operations often consume the largest volumes of HF in a fab. Also, HF solutions of 0.5-10 wt% are frequently used to remove oxides from the silicon wafers themselves. A typical device might undergo six or more oxide removal steps.

The cleanliness and purity of the HF used in the quartz and wafer cleaning operations directly impacts device yield and reliability. This is especially true for the oxide removal operations where the HF directly contacts the wafer substrate. Particulate impurities from the HF that adhere to the wafers produce defects that cause failures and lower yields. Ionic impurities that adhere to the wafers cause device reliability problems. For these reasons, the tendency is to use ultrapure HF for a short period of time and then discard it. This activity creates a costly consumption and disposal problem.

In a cooperative project, we recently built and tested an HF reprocessor. This project had the dual goals of converting used HF from a quartz cleaning operation into ultrapure HF, and of substantially reducing the associated HF consumption and disposal costs. This paper describes how the reprocessor works and how the reprocessed HF was tested to evaluate its suitability in quartz and wafer cleaning operations.

DESCRIPTION OF THE HF REPROCESSOR

The HF reprocessor was designed to treat 50 gallon batches of HF coming from a horizontal tube cleaner. Since tube cleaning is a batch process, it was decided that the reprocessing operation could likewise be a batch (vs. continuous) process.

Our analyses of used quartz cleaning solutions found that they contained thousands of particles $\geq$ 0.5 u per ml, and ionic impurities in the multiple ppm range. Obviously an HF reprocessor would, among other things, have to remove particulate and ionic impurities.

These objectives are accomplished by the HF reprocessor shown schematically in Figure 1. Used HF from a quartz cleaner collects in the used acid tank. Then it is pumped through a "coarse" (e.g. 1 u) filter, an ion exchange system, a "medium" (e.g. 0.5 u) filter, and into the ion-free HF tank. This phase of the process removes the large particles and the ionic impurities.

In the second part of the process, the HF is recirculated through a "fine" (e.g. 0.1 u) filter, a special conductivity sensor, and back into the ion-free HF tank. The final filter removes whatever particles are still in the solution at that point. Downstream from the filter, an on-line PMS laser particle counter measures the particle levels in the product HF. The HF is not considered acceptable unless the particle counts are below some predetermined threshold value, e.g. $\leq$ 10/ml of $\geq$ 0.5 u. A conductivity sensor determines the concentration of the reprocessed HF. The control system adds either DI water or 49% HF to the ion-free tank as necessary to adjust the concentration of the reprocessed acid to the predetermined value. The reprocessor can also interface with an optional on-line atomic absorption (AA) spectrometer to monitor ppb levels of sodium in the product stream. The AA is used to determine when the cation exchange column needs to be regenerated. Only when the product HF meets the specs for particles, ions (sodium) and concentration is it pumped back to the quartz cleaner.

A key component in the HF reprocessor is the ion exchange system. Ion exchange works because HF is a weak acid, so there are relatively few H^+ and F^- ions to compete with cationic and anionic impurities, respectively, for the active sites on the ion exchange resins. Also, the resins have very little affinity for small, monovalent ions like H^+ and F^-. Thus, HF passes quickly through the resin beds while impurity ions

are retained. Eventually, however, the impurity ions elute from the resins one by one. When this occurs, the cation and anion resins must be chemically regenerated by rinsing with dilute, ultapure sulfuric acid and ammonium hydroxide, respectively. Not surprisingly, we have found that the ionic purity of the reprocessed HF depends greatly on the purity of the regeneration chemicals.

Accumulated particulate impurities are periodically removed by replacing the filter cartridges.

EXPERIMENTAL

The original intent of these tests was simply to qualify the reprocessor for tube cleaning. However, after reviewing the analytical data and the tube clean test data, the scope of the tests was expanded to include wafer cleaning.

The reprocessor was facilitized with DI water, 49% HF, 96% sulfuric acid and 30% ammonium hydroxide from the in-house chemical delivery systems. During the tests, all chemicals were analyzed by ICP/MS, ICP and AA and found to be equivalent to ULSI-grade.

The HF reprocessor was interfaced with a horizontal quartzware cleaner. Quartz furnace tubes from the production fab were cleaned with 50 gallons of 11-15 wt% HF. Each 50 gallon batch was used to clean five "non-phosphorus" tubes before it was reprocessed. (In many fabs, the furnace tubes and their cleaners are dedicated to either "phosphorus" or "non-phosphorus" applications.) Thirty such batches were reprocessed over a two-month period. The reprocessor adjusted the concentration of each batch to 10%. "Before" and "after" reprocessing samples were collected and analyzed by ICP/MS and AA for 35 elemental impurities. Multi-gallon samples of reprocessed HF from various batches were also collected in one gallon polyethylene bottles. These samples were later used in the wafer cleaning tests.

Tube Cleaning Tests

One furnace tube was dedicated to this test. It was cleaned in thirty consecutive batches of reprocessed acid (that had been used to clean five production-line non-phosphorus tubes). The cleanliness of the tube was periodically evaluated via two tests.

The first test was the FCGOI or "Full Chip Gate Oxide Integrity" test. The test chip represented a 256K DRAM structure after LOCOS isolation (LOCal Oxidation of Silicon). A sacrificial oxide was grown in the substrate region of the test wafers. This oxide was then removed with 5% HF during a subsequent pre-oxidation wet chemical clean. A 20 nm clean oxide was then grown in the furnace tube, and a polysilicon top plate deposited. The polysilicon was patterned so as to isolate the chips on the 150 mm wafers. The active gate oxide area of each test

chip was approximately 0.1 cm^2. Approximately 500 chips per wafer were tested. The breakdown voltage (BV) of the grown oxide was determined by ramping the applied voltage at 1 V/50 msec while monitoring the current to the failure point of 10 uA. The BV test on such a large capacitor is an excellent way to detect minute differences in pre-oxidation cleans and/or oxidation processes in terms of defect related, non-intrinsic oxide breakdown characteristics.

Measurement of the capacitance-voltage (CV) characteristics of the chips served as the second test monitor. CV measurements are commonly used to characterize oxide quality parameters (1, 2). Work function differences, insulator charges, and surface states are evaluated via these tests. The test device was another MOS capacitor of the same oxide used on the FCGOI test wafers. Flatband voltage (VFB), stress VFB, surface state density (QSS) and capacitance rise time (CT) were used as comparison criteria.

Wafer Cleaning Tests

The FCGOI test was also used in the wafer cleaning tests to determine the characteristics of the oxide grown on the clean silicon surface. Reprocessed 10% HF was diluted to 5% and used to remove the sacrificial oxide from 3 test wafers immersed in a recirculating filtered bath. For comparison, the same number of wafers were cleaned in an identical bath containing 5% ULSI HF, the production standard. Any trace contaminants on the wafers at this point would effect the CV/CT performance. The FCGOI-BV test on the large capacitor area is very effective in detecting particulate contamination problems.

A second wafer cleaning evaluation involved the use of standard 1 megabit DRAM production wafers. Two lots of 24 wafers each were split and processed as above, half in reprocessed HF, and half in the ULSI HF. The HF etch step chosen was one of the most critical within the device process flow. Like the FCGOI monitor, it is highly sensitive to both particulate and ionic contamination. It involves the growth of an oxide in a critical MOS capacitor used within each memory cell of the DRAM device. Any failure of one of these capacitors will cause a bit loss and, therefore, a degradation in the final device yield.

RESULTS AND DISCUSSION

Analytical Results

Results of the trace impurity analyses were dramatic. As shown in Figure 2, the acid coming from the tube cleaner often had impurity levels (measured for 35 elements) totaling several ppm. (The 35 elements represented in Figure 2 do not include silicon which was determined separately.) However, the trace impurity levels in the HF after reprocessing averaged only 43 parts per billion in the first nine batches. The high ion level in reprocessed batch 10 was due to aluminum

eluting from the anion column. Normally, the ion exchange columns would be regenerated **before** ion elution occurs. However, for the purposes of this test, the columns were not regenerated in an effort to observe when different ions would elute.

Tube Cleaning Tests

FCGOI-BV and CV tests were performed on test wafers representing several different batches of reprocessed HF. The intent was to note any performance differences that could be attributed to the different impurity levels in the acid. The results are shown in Table 1.

TABLE 1. FCGOI-BV and CV data from tube cleaning tests.

Batch No.	Total PPB Impur.	Brkdwn. Volts	VFB V No Stress	VFB V -5V Stress	VFB V +5V Stress	QSS Ions/cm	CT Sec
1	32.3	NA	-.880	.012	.017	4.45E10	340
5	25.3	22.2	-.855	.014	.007	4.63E10	310
9	67.2	22.6	-.894	.005	.011	5.47E10	300
15	294.4	25.4	-.888	.008	.021	5.03E10	330
20	320.2	23.9	-.876	.016	.001	4.57E10	330
Control		23.5	-.872	.033	.039	4.00E10	310

There were no significant differences between any of the reprocessed test groups and the control. All of the reprocessed HF data conformed to the normal distributions of the standard database. This was despite the fact that there was over a ten-fold difference in impurity level between the best and worst batch of reprocessed HF. It should be mentioned that serious ion elution began in batch 10, so that is why batches 15 and 20 were of such relatively low quality.

Having passed this test, the HF reprocessor was released for production cleaning of quartz furnace tubes.

Wafer Cleaning Tests

In these tests, reprocessed HF of two different qualities was compared to ULSI HF. Besides processing in the usual manner, some of the wafer test splits were subjected to a modified process intended to maximize sensitivity to trace impurities. The modified process consisted of eliminating all post-HF treatments. Thus, the wafers did not receive an RCA SC-2 clean (H_2O-H_2O_2-HCl) which is known to remove inorganic contaminants (3). Likewise, the furnace tubes were not treated with gaseous HCl to getter ionic impurities during the furnace oxidation step. The FCGOI-BV and CV data are shown in Table 2.

TABLE 2. FCGOI-BV and CV data from wafer cleaning tests.

	BV	SIG	VFB	QSS	CT	VFB STRESS -5V	VFB STRESS +5V
Test #1:							
- Reprocessed HF Batch #5, std. hood/furnace	18.0		-.848	3.24E10	470	.043	.105
- No HCl	17.5	2.91	-.795	3.37E10	460	.020	.010
- ULSI HF, std. hood/ furnace	19.8	3.53	-.845	3.16E10	410	.015	.084
- No HCl	17.7	3.48	-.793	4.22E10	470	.004	.034
Test #2:							
- Reprocessed HF Batch #23, std. hood/furnace	16.7	2.57	-.847	3.13E10	470	.012	.002
- No HCl	15.7	2.30	-.799	4.29E10	460	.046	.031
- ULSI HF, std. hood/ furnace	16.9	2.92	-.847	3.41E10	450	.050	.089
No HCl	16.3	2.72	-.784	4.83E10	460	.007	.004

The purity levels in reprocessed HF batches 5 and 23 that were used in these tests are shown in Table 3.

TABLE 3. Total ppb levels for 35 ionic impurities in reprocessed HF.

Element	Batch #5	Batch #23
Ag	0.5	< 0.3
Al	< 0.3	163.4
Au	0.4	< 0.3
Ca	4.0	< 1.0
Cr	4.4	4.3
Cu	1.0	4.3
K	3.0	4.0
Mg	1.3	7.5
Na	2.0	13.0
Pb	0.9	< 0.3
Ti	4.7	45.9
Zn	2.7	< 0.3
TOTAL	**24.9**	**242.4**

The other 23 elements were not detected.

Since the reprocessed HF was diluted 1:1 for the wafer cleaning tests, the ion levels in the cleaning bath should have been approximately half of those listed in Table 3.

Once again there were no significant differences noted between the reprocessed HF groups and the ULSI HF groups.

Table 4 shows the differences in final die yield and single bit failures. Statistical tests on these results indicated that there was no significant difference between the ULSI and the reprocessed HF. Distribution plots from these tests are shown in Figures 3 and 4.

TABLE 4. Yield and single bit failure data from wafer cleaning tests.

1 Megabit DRAM	Delta % (Reproc - Std.)	Reproc. Sigma	ULSI Sigma
Final probe yield	+ 4.4	9.4	8.7
Single bit failures	- 4.4	11.8	14.6

The FCGOI and yield tests were unable to differentiate between reprocessed batches 5 and 23 containing 25 and 242 ppb ionic impurities, respectively. One possible reason for this is that the HF was diluted about 1:1 so that the ion levels in the wafer cleaning baths were actually about half of the original levels. Another possible reason is that the levels of the particular elements present were just too low to noticeably effect the performance of the test devices.

CONCLUSIONS

The HF reprocessor met its original goal for producing quality HF for cleaning quartz tubes. The low ionic impurity content of the reprocessed HF was confirmed through FCGOI performance. The HF reprocessor is now being used in production to clean furnace tubes.

The data from the initial wafer cleaning tests appears very promising. Indications are that the reprocessed HF has potential for use in wet chemical cleaning processes. However, for mass production, repeatability and reproducibility are key attributes which must be further demonstrated.

REFERENCES

1. A.S. Grove, "Physics and Technology of Semiconductor Devices", pp. 271-285, John Wiley & Sons, New York, N.Y. (1967).

2. A.H. Nicollian and J.R. Brews, "MOS Physics and Technology", pp. 71-96 and 409, John Wiley & Sons, New York, N.Y. (1982).

3. W. Kern and D.A. Puotinen, RCA Review, 31, 187 (1970).

FIGURE 1. Schematic Diagram of HF Reprocessor

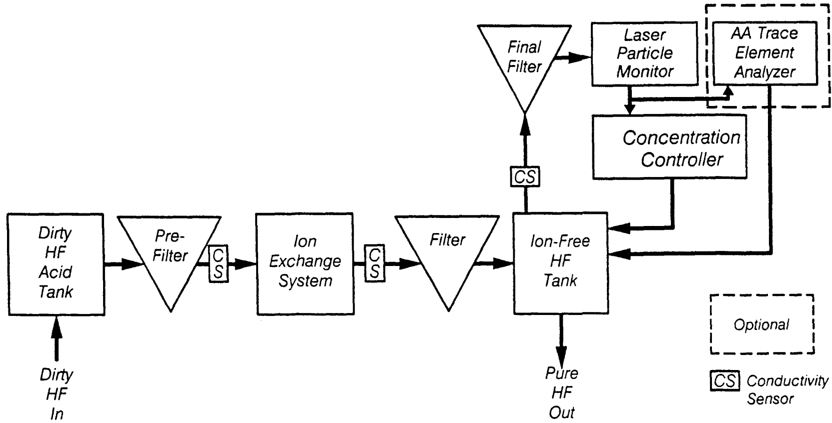

FIGURE 2. Total Ionic Impurity Level in HF Measured by ICP/MS, ICP and AA

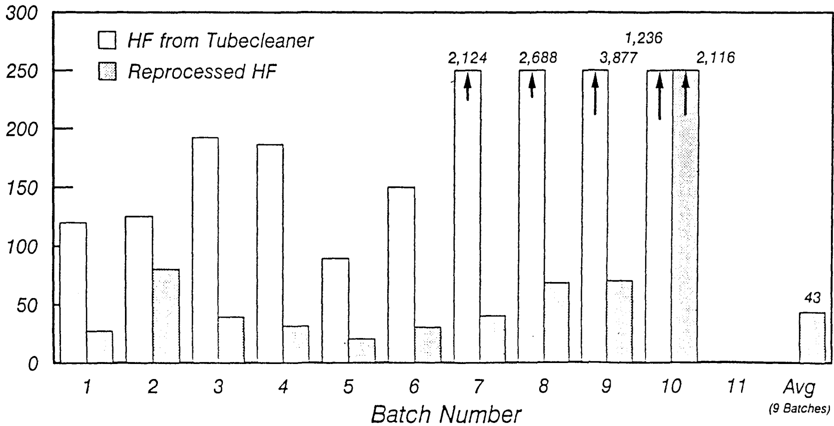

Total Detectable Levels for 35 Elements

FIGURE 3. Final Probe Yield from Wafer Cleaning Tests

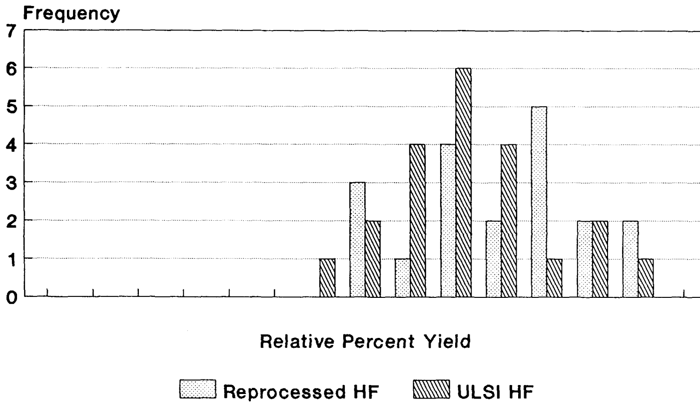

Sigma (Reprocessed) = 9.4
Sigma (ULSI) = 8.7

FIGURE 4. Single Bit Failures from Wafer Cleaning Tests

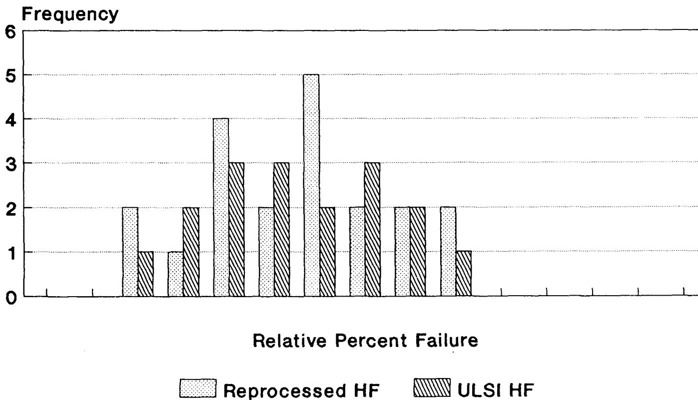

Sigma (Reprocessed) = 11.8
Sigma (ULSI) = 14.6

DRY CLEANING TECHNOLOGY

WAFER DRY CLEANING USING DILUTED ANHYDROUS HYDROGEN FLUORIDE GAS

T.Ohmi, N.Miki*, H.Kikuyama*, I.Kawanabe and M.Miyashita

Department of Electronics,Faculty of Engineering, Tohoku University,Sendai,980,Japan

*Hashimoto Chem.Ltd.,Kaizan-cho,Sakai 590,Osaka,Japan

ABSTRACT

The gas-phase removal of a native oxide film from a silicon substrate, at room temperature and atmospheric pressure, has been developed. The technique is uses gas-phase, anhydrous hydrogen fluoride (AHF) in a fluorine passivated system. It is found that after removal of the native oxide, atomic fluorine remains adsorbed onto the bare silicon surface, which is detrimental to the processes that follow. This paper describes the technology of removing both the native oxide film from the silicon substrate and the terminating fluorine which results from this process.

INTRODUCTION

The down-scaling of device dimensions has rendered performance highly susceptible to dark and leak currents, which are mainly caused by wafer surface contamination: a mixture of of organic substances, metallic materials and native oxide films. Removal of these impurities and the native oxide is an essential requirement for ULSI process technologies such as low temperature silicon epitaxy and is necessary to obtain low contact resistance and high quality thin oxide films. Other wafer surface cleaning technologies such as removal the of metallic material by chlorine radicals, or dry cleaning of organic contamination using ozone. However, ozone cleaning is, inevitably, accompanied by the oxidation of the bare silicon surface at room temperature i,e.,an appearance of native oxide. Gas-phase selective etching of native oxide films using diluted hydrogen fluoride (HF) has been used[1]-[4] to resolve these problems.

This paper describes wafer dry cleaning technology,

particularly native oxide etching using moisture-free HF gas.

EXPERIMENTAL APPARATUS

Figure 1 shows wafer dry cleaning system. It is completely corrosion, moisture and contamination free and features a continuous monitoring system. An all-metallic structure was used to suppress outgassing from plastic materials[5]. Additionally, these metal materials are passivated using pure fluorine gas[6]-[9]. Therefore the inner surface is highly resistant to even very aggressive chemicals, such as wet HF gas. A dewpoint (DP) meter and infrared (IR) spectrometer are used to measure moisture content in the reacted gas stream. Ultrapure nitrogen (1.8 ppb moisture and 0.1 ppb maximum hydrocarbon content) is used as a carrier gas. The HF gas is also ultrapure, as it is generated from HF liquid with a very low moisture content and the vapor-liquid equilibrium favors any dissolved moisture remaining in the liquid phase. because of using low temperature gas-liquid equilibrium. The moisture concentration in HF gas decreases with decreasing the vessel temperature which is precisely controlled in the range of -70°C to -40°C steps.

XPS to determine if native oxide and/or adsorbed fluorine remain on the wafer surface. The dry-cleaned silicon wafer is then evaluated by subsequent low-temperature sputtering of epitaxial silicon [10]-[12], oxidation and Jet-CVD [13].

RESULTS

It was found that the reaction did not occur, at atmospheric pressure and room temperature, below a certain concentrations of HF. We call these points the "HF critical concentration ".

Figure 2 shows the relationship between HF critical concentration in N_2 and the moisture level in the system for various oxides of silicon. The vertical axis is the HF critical concentration and the horizontal axis is the moisture level in the system. For example, thermal oxide film does not react with HF when its concentration is less than 4.7% or greater than 4.7%. It may be seen in Fig. 2 that the HF critical concentration decreases with increasing moisture level in the reaction environment and the HF critical concentration is different for various kinds of SiO_2. The critical concentrations for native oxide range from 0.25% to 0.58%, depending on the conditions (e.g. clean air

condition, wet chemical oxidation and ozone oxidation) under which it was formed. Since a bare silicon surface is immediately oxidized by the presence of oxygen and moisture, even at room temperature[14][15], it must be removed just before starting each subsequent process in order to improve the process quality.

Figure 3 shows the XPS spectra from wet-cleaned and dry-cleaned silicon surfaces. The Si2p XPS peak at about 104 eV indicates the presence of a native oxide film. It may be seen from Fig.3, that a native oxide film is clearly present on the wet-cleaned silicon surface. This native oxide film is a result of final rinsing in deionized (DI) water, which contains O_2 at a level of 0.6 ppm. On the dry-cleaned silicon surface, the Si2p spectrum peak is very weak, but the F1s spectrum (having binding energy of 686 eV) from fluorine is clearly recognized. This indicates that the silicon surface after dry-cleaning is covered by fluorine.

The influence of adsorbed fluorine on subsequent processes is evaluated by two methods. Table 1 summarizes the results of low-temperature sputtering silicon epitaxy on three different silicon surfaces: a fluorine-terminated silicon surface, native oxide having a thickness of 7Å and wet cleaned silicon surface having 0.4Å native oxide. These Si films are evaluated using reflection electron diffraction (RED). The sheet resistivity is measured using a four point probe method. Single-crystal silicon found on the wet cleaned surface, whose resistivity is 100 Ω . On the other hand, the structures of the dry-cleaned surface and the native oxide surface are, respectively, polycrystalline silicon having the sheet resistivity of $5x10^8$ Ω and amorphous silicon having a sheet resistivity of $3\text{-}5x10^6$ Ω .

Figure 4 shows MOS capacitance-voltage curves for oxide films formed on Si(100) p-type substrates after wet- and dry-cleaning, where the oxide thickness is about 200Å. It is seen from Fig.5 that an inversion layer is formed quickly in MOS diode on the dry-cleaned silicon surface compared to that the wet-cleaned surface. Thus, it is concluded that chemically-combined fluorine degrades the generation life-time of carriers after high temperature oxidation.

Both of these experimental results highlight the need to remove adsorbed fluorine.

Procedures for eliminating adsorbed fluorine have been investigated. Figure 5 shows the results of thermal treatment to eliminate chemically-combined fluorine. The peaks of the F1s XPS spectra indicate the presence of a fluorine-terminated surface. It is seen

that terminated fluorine could not be eliminated by heating silicon wafer up to 930°C in N_2 at atmospheric pressure. The F1s spectra peaks intensity dose not change at all after heating.

Low kinetic energy Ar ion bombardment has been confirmed to be very effective at removing absorbed impurities from bare silicon surfaces, particularly adsorbed moisture . It was tried as a technique for removing adsorbed fluorine. The F1s spectra from fluorine-terminated silicon surface are shown for three different processing conditions in Fig.6, where the effects of thermal treatment in ultra-high vacuum environment and for different ion bombardment energies are examined. The peak height of F1s spectra decreases with an increase in Ar ion energy. But, the elimination of adsorbed fluorine is not sufficient, even when the Ar ion energy is increased up to 10 eV, as shown in curve (4).

Figure 7 shows F1s XPS spectra from a fluorine terminated silicon surface before and after irradiation with a Xe lamp having power density of about 10 W/cm^2 under reduced pressure of $1x10^{-8}$ torr. It is confirmed in Fig.8 that the Xe lamp irradiation removes adsorbed fluorine from silicon surfaces within 1 minute. Single-crystal silicon epitaxy has been obtained on dry-cleaned substrates at 700°C by the Si_2H_6 CVD procedure where Xe irradiation has been used to remove adsorbed fluorine[13]. The crystallinity of grown film has been evaluated by RED analysis, as shown in Fig.8. Where the RED pattern of the film grown on the dry-cleaned silicon surface shows clear Kikuchi-lines similar to that of the wet-cleaned silicon surface.

CONCLUSIONS

HF gas, diluted with ultra-pure nitrogen has proved successful in removing native oxide films from silicon wafers. However, the surface is immediately re-oxidized, even at room temperature, in typical wafer processing environments: cleanroom air, ultrapure D.I. water, etc., and fluorine is adsorbed on the resulting bare silicon surface.

The fluorine-terminated surface behaves similar to a native oxide surface in film depositions and degrades generation lifetime of carriers in high temperature processes such as oxidation. The chemically-combined fluorine must be removed before subsequent processing. Xe lamp irradiation at reduced pressure is effective in removing adsorbed fluorine from silicon surfaces.

ACKNOWLEDGMENTS

This work is mainly carried out in the Superclean Room of Laboratory for Microelectronics,Research Institute of Electrical Communication,Tohoku University.

REFERENCES

[1] H.Kikuyama, M.Maeno, I.Kawanabe, M.Miyashita, K.Maruhashi, T.Ishida, N.Miki, and T.Ohmi, "Wafer dry cleaning," in Proceedings of 7th VLSI Ultra Clean Technology Symposium, pp.171-207, Tokyo, Jul., 1988.

[2] H.Kikuyama, N.Miki, M.Miyashita, I.Kawanabe, M.Morita and T.Ohmi, "Selective Etching of Native Oxide," in Proceedings of 8th VLSI Ultra Clean Technology Symposium, pp.195-222, Tokyo, Jan., 1989.

[3] N.Miki, H.Kikuyama, M.Maeno, J.Murota, and T.Ohmi, "Selective Etching of Native Oxide by Dry Processing Using Ultra Clean Anhydrous Hydrogen Fluoride," Tech. Dig. of International Electron Devices Meeting, pp.730-733, San Francisco, Dec., 1988.

[4] N.Miki, H.Kikuyama, I.Kawanabe, M.Miyashita and T.Ohmi "Gas Phase Selective Etching of Native Oxide" to be published in IEEE Transactions on Electron Devices, Jan.,1990.

[5] O.Uchizawa, T.Hatayama, Y.Kanno, and T.Ohmi, "Metal Sealed Diaphragm Valve," in Proceedings of 8th VLSI Ultra Clean Technology Symposium,pp.27-48, Tokyo,Jan.,1989.

[6] M.Maeno, K.Maruhashi, Y.Nakagawa, N.Miki, and T.Ohmi, "Fluorine Passivation Technology of Metal Surface," in Proceedings of 8th VLSI Ultra Clean Technology Symposium, pp.119-139, Tokyo, Jan., 1989.

[7] N.Miki, M.Maeno,K.Maruhashi, Y.Nakagawa and T.Ohmi, "FLUORINE PASSIVATION OF METAL SURFACE FOR SELF-CLEANING SEMICONDUCTOR EQUIPMENT" to be published in IEEE Transactions on Semiconductor Manufacturing, Feb.,1990.

[8] N.Miki, M.Maeno, K.Maruhashi, Y.Nakagawa and T.Ohmi"FLUORINE PASSIVATION OF STAINLESS STEEL", SIXTH INTERNATIONAL SYMPOSIUM ON PASSIVITY, Sapporo,Sep.,1989.

[9] M.Maeno, N.Miki and T.Ohmi, "FLUORINE PASSIVATION OF STAINLESS STEEL", MICROCONTAMINATION 89 CONFERENCE AND EXPOSITION ,Anaheim,California,Oct.,1989.

[10] T.Ohmi, K.Matsudo, T.Shibata, T.Ichikawa, and H.Iwabuchi, "Very-Low-Temperature Epitaxial Silicon Growth By Low-Kinetic-Energy Particle Bombardment," Jpn. J. Appl. Phys., vol.27, No.11, pp.2146-2148, Nov.,1988.

[11] T.Ohmi, T.Ichikawa, T.Shibata, K.Matsudo, and H.Iwabuchi, "In situ substrate-surface cleaning for very low temperature silicon epitaxy by low-kinetic-energy particle bombardment," Appl.Phys.Lett., vol.53, No.1,pp.45-47, Jul.,1988.

[12] T.Ohmi, K.Matsudo, T.Shibata, T.Ichikawa, and H.Iwabuchi, "Very-Low-Temperature Epitaxial Silicon Growth By Low-Kinetic-Energy Particle Bombardment," Extended Abstracts of the 20th Conference on S.S.D.M., pp.49-52,Tokyo,Aug.,1988.

[13] T.Ohmi, H.Kumagai, M.Morita, M.Itoh, T.Kochi, M.Kosugi, and G.Tei, "Surface reaction film formation utilizing free jet molecular flow," in Proceedings of first international symposium on ADVANCED MATERIALS FOR ULSI, P.Vol.88-19, pp.36-43,1988.

[14] T.Ohmi, M.Morita, E.Hasegawa, M.Kawakami, K.Suma, "Control of Native Silicon Oxide Growth in Air or in Water," 2nd International Symposium Ultra Large Scale Integration Science and Technology, Extended Abstracts of 1989 ECS Meeting, Vol.89-1, pp.227-228, Los Angeles, May, 1989.

[15] M.Morita, T.Ohmi, E.Hasegawa, M.Kawakami, and K.Suma, "Control factor of native oxide growth on silicon in air or in ultra pure water", to be published in Appl. Phys. Lett.,Aug.

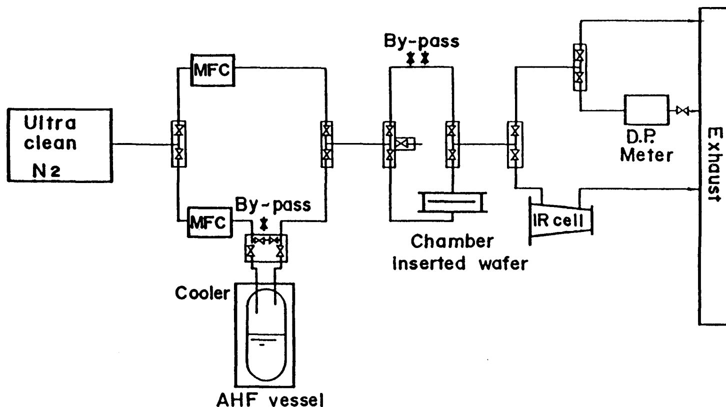

Fig.1. Ultra-clean surface dry cleaning system using HF gas.

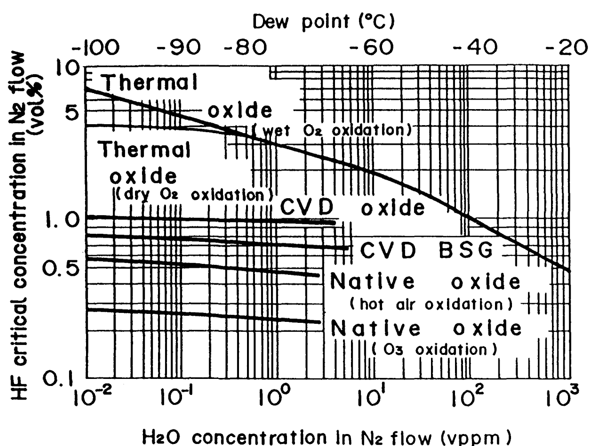

Fig.2. Relationship of HF critical concentration and moisture level at room temperature for various oxide films.

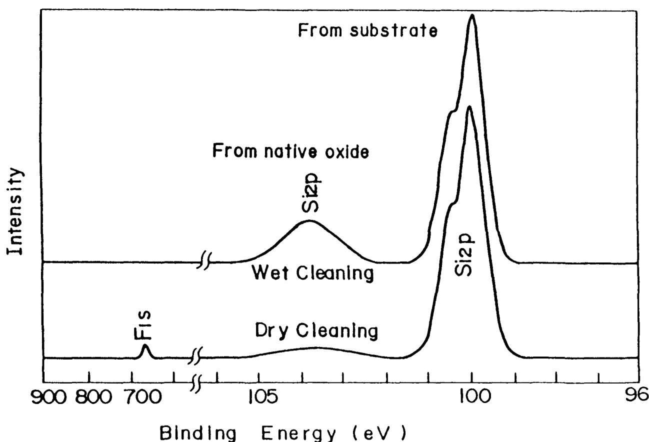

Fig.3. Si_{2p} and F_{1s}XPS spectra from wet and dry HF cleaned silicon surface.

Cleaning condition

1)Pretreatment	:	$H_2SO_4:H_2O_2$ (4:1 vol) 5min
Wet cleaning	:	0.5%HF aq. solution 1min
Over flow rinse	:	Ultra Pure DI water 10min
2)Pretreatment	:	$H_2SO_4:H_2O_2$ (4:1 vol) 5min
Dry cleaning	:	1.0%HF gas (D.P. -100°C)

Table I Resistivity of sputtering epitaxial silicon

Silicon Substrate [1]		Epitaxial Silicon	
HF cleaning	SiOx film thickness (Å) (x>0.5)	Crystal structure [2]	Sheet resistivity [3] (Ω/□)
Before cleaning	7	Poly-crystal	5×10^{6}
Wet cleaning	0.4	Single-crystal	100
Dry cleaning	0.3	Amorphous.	$3\sim5\times10^{6}$

1) Pretreatment
H_2SO_4:H_2O_2(4:1vol)⟶ DI water⟶IPA vapor drying
2) Crystal structure : Reflection electron diffraction
3) Sheet resistivity : Four point probe method

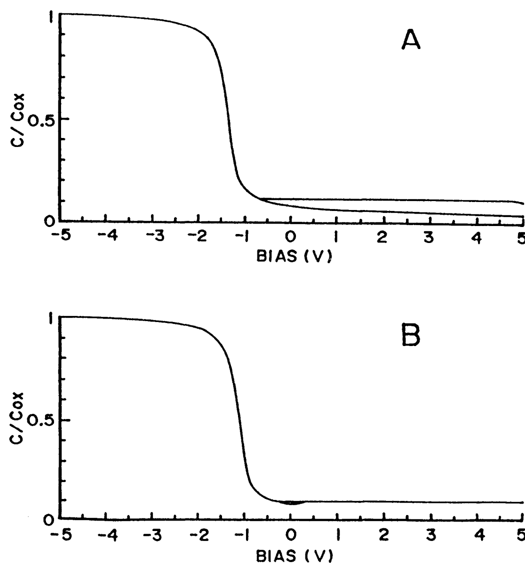

Fig.4. MOS capacitance-voltage curves for oxide films having a thickness of 200 Å after wet and dry cleaning, where frequency is set at 1 MHz.
A : Wet cleaning, B : Dry cleaning

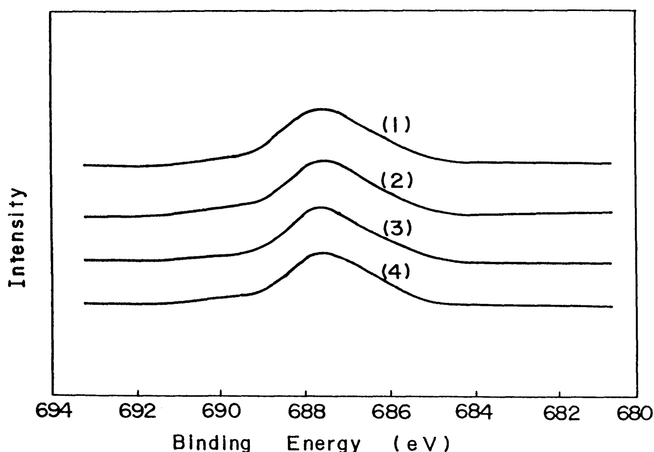

Fig.5. F_{1s} XPS spectra from fluorine terminated surfaces heated up to various temperatures in N_2 treatment condition, (1) R.T. 760 Torr, (2) 80^oC 1hr 760 Torr, (3) 630^oC 1hr 760 Torr, (4) 930^oC 1hr 760 Torr.

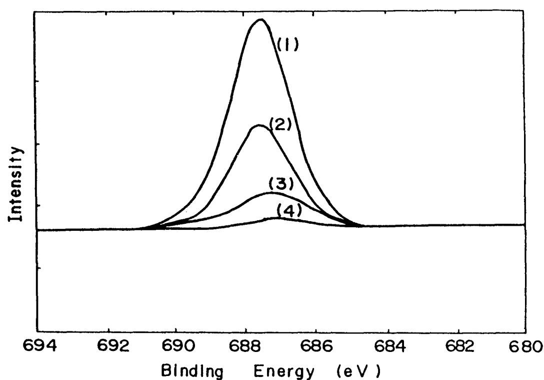

Fig.6. Variation of F_{1s} XPS spectra from fluorine terminated surface by low energy Ar bombardment, (1) Dry cleaned surface, (2) Substrate temperature 300^oC, base pressure 5x10^{-9} Torr, (3) Substrate temperature 300^oC, Ar gas pressure 8x10^{-3} Torr, Bombarding Ar ion energy of ~3 eV, (4) Substrate temperature 300^oC, Ar gas pressure 8x10^{-3} Torr, Bombarding Ar ion energy of ~10 eV.

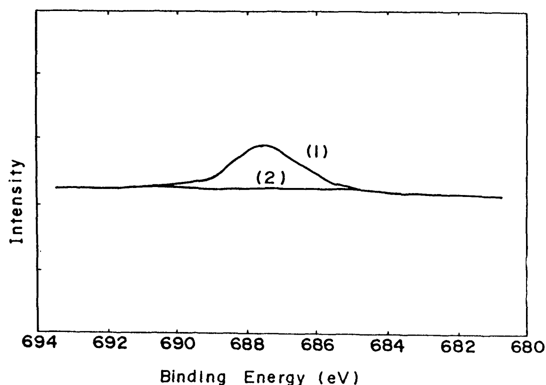

Fig.7. Variation of F_{1s} XPS spectra from fluorine terminated surface by an irradiation of Xe lamp, (1) Before irradiation, (2) After irradiation.

Xe lamp energy : 1.13-4.13 eV
Irradiated condition : 1min, 10 W/cm^2
$1x10^{-8}$ Torr

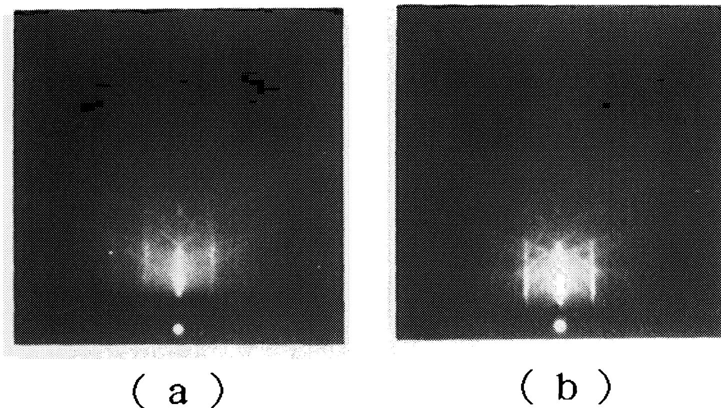

Fig.8. Reflection electron diffraction pattern of epitaxial silicon on dry and wet cleaned surface, (a) Epitaxial silicon on dry cleaned surface, having a Xe lamp irradiation as a pretreatment of fluorine removal, (b) Epitaxial silicon on wet cleaned surface.

UV/OZONE CLEANING OF SURFACES

John R. Vig
US Army Electronics Technology and Devices Laboratory
Fort Monmouth, New Jersey 07703-5000

ABSTRACT

The (UV)/ozone surface-cleaning method, which is reviewed in this paper, is an effective method of removing a variety of contaminants from surfaces. It is a simple-to-use dry process which is inexpensive to set up and operate. It can rapidly produce clean surfaces, in air or in a vacuum system, at ambient temperatures. Placing properly precleaned surfaces within a few millimeters of an ozone-producing UV source can produce clean surfaces in about one minute. The technique can produce near-atomically clean surfaces, as evidenced by Auger electron spectroscopy, ESCA, and ISS/SIMS studies. Topics discussed include the variables of the process, the types of surfaces which have been cleaned successfully, the contaminants that can be removed, the construction of an UV/ozone cleaning facility, the mechanism of the process, UV/ozone cleaning in vacuum systems, rate-enhancement techniques, safety considerations, effects of UV/ozone other than cleaning, and applications.

Introduction

The capability of ultraviolet (UV) light to decompose organic molecules has been known for a long time, but it is only since the mid-1970's that UV cleaning of surfaces has been explored (1-6). Since 1976, use of the UV/ozone cleaning method has grown steadily. UV/ozone cleaners are now available commercially. This paper is a greatly condensed version of a book chapter of the same title (6).

The Variables of UV/Ozone Cleaning

a. The Wavelengths Emitted by the UV Sources. Since only the light which is absorbed can be effective in producing photochemical changes, the wavelengths emitted by the UV sources are important variables. The low-pressure mercury discharge tubes generate two wavelengths of interest: 184.9 nm and 253.7 nm. Whether or not these wavelengths are emitted depends upon the lamp envelopes.

The 184.9 nm wavelength is important because it is absorbed by oxygen, thus leading to the generation of ozone (7). The 253.7 nm radiation is not absorbed by oxygen, therefore, it does not contribute to ozone generation, but is absorbed by most organic molecules (8,9) and by ozone (7). The absorption by ozone is principally responsible for the destruction of ozone in the UV box. Therefore, when both wavelengths are present, ozone is continually being formed and destroyed. An intermediate product, both of the formation and of the destruction processes, is atomic oxygen, which is a very strong oxidizing agent. While both UV light without ozone and ozone without UV light (10) can produce a slow cleaning effect in air, the combination of short-wavelength UV light and of ozone, such as is obtained from a quartz UV lamp (11), produces a clean surface orders of magnitude faster. In the UV/ozone cleaning experiments of Vig et al. (4,5), contact angle measurements, wettability tests, and Auger electron spectroscopy (AES) were used to monitor the surface cleanliness (5,12,15). Later, others also used AES, ESCA and ISS/SIMS (15-17) in studying UV/ozone cleaning.

b. Distance Between the Sample and UV Source. Another variable that can greatly affect the cleaning rate is the distance between the sample and the UV source. Ozone has a broad absorption band (7,18,19) centered at about 260 nm. At 253.7 nm, the absorption coefficient is

130 cm^{-1} atm^{-1}. The intensity I of the 253.7 nm radiation reaching a sample therefore decreases as

$$I = I_0 e^{-130pd},$$

where p is the average ozone pressure between the sample and the UV source in atmospheres at 0^oC, and d is the distance to the sample in centimeters. Therefore, to maximize the cleaning rate, the samples should be placed as close as practicable to the UV source.

c. The Contaminants. Vig et al. found that the UV/ozone cleaning procedure is effective on a variety of contaminants. Among the contaminants were: human skin oils (wiped from the forehead of one of the researchers); contamination adsorbed during prolonged exposure to air; cutting oil (20); beeswax and rosin mixture; lapping vehicle (21); mechanical vacuum pump oil (22); DC 704 silicone diffusion pump oil (23); DC 705 silicone diffusion pump oil (23); silicone vacuum grease (23); acid (solder) flux (24); rosin flux from a rosin core lead-tin solder; cleaning solvent residues, including acetone, ethanol, methanol, isopropyl alcohol, trichloroethane, and trichlorotrifluoroethane; ion-implanted Kodak Micro Resist 747 (25); and carbon films.

After contamination, the wafers were precleaned, then exposed to UV/ozone by placement within a few millimeters of the tube in UV box 1. After a 60 s exposure, the steam test and AES indicated that all traces of the contaminants had been removed. Inorganic contaminants, such as dust and salts, cannot be removed by UV/ozone and should be removed in the precleaning procedure. UV/ozone has also been used for waste-water treatment and for destruction of highly toxic compounds (26-29). It has also been shown (30) that using the combination of UV and ozone is more effective than using either one alone in destroying microbial contaminants (E. coli and streptococcus faecalis) in water. Contaminants such as thick photoresist coatings and pure carbon films can be removed with UV/ozone, without any precleaning, but, in general, gross contamination cannot be removed without precleaning.

Many chemicals respond to radiation in various ways, depending upon whether or not oxygen is present. For instance, in the presence of oxygen, many polymers degrade when irradiated; whereas, in the absence of oxygen (as would be the case for the bulk of a thick film) these same polymers crosslink. In the study of the radiation degradation of polymers in air, the "results obtained with thin films are often markedly different from those obtained using thick specimen...." (31). For the UV/ozone cleaning procedure to perform reliably, the surfaces must be precleaned.

d. The Substrate. The UV/ozone cleaning process has been used with success on a variety of surfaces, including: glass, quartz, mica, sapphire, ceramics, metals, silicon, gallium arsenide, and a conductive polyimide cement. Quartz and sapphire are especially easy to clean with UV/ozone since these materials are transparent to short wavelength UV. Also, reference 32 shows that photocatalytic oxidation of hydrocarbons, without the presence of gaseous oxygen, can occur on some oxide surfaces.

The process has been used successfully to clean quartz resonators which have been bonded with silverfilled polyimide cement (33). Teflon (TFE) tape exposed to UV/ozone in UV box 1 for ten days experienced a weight loss of 2.5 percent (34). Also, the contact angles measured on clean quartz plates increased after a piece of Teflon was placed next to the plates in a UV box (35). Similarly, Viton shavings taken from an O-ring experienced a weight loss of 3.7 percent after 24 hours in UV box 1. Semiconductor surfaces have been successfully UV/ozone cleaned without adversely affecting the functioning of the devices (36).

e. Rate Enhancement Techniques. UV/ozone cleaning "rate enhancement" techniques have been investigated by Zafonte and Chiu (37). Photoresist removal rates of 800 to 900 A/min for positive photoresists and 1500-1600 A/min for negative photoresists (38) were reported by one manufacturer of UV/ozone cleaning equipment (38).

The Mechanism of UV/Ozone Cleaning

The available evidence indicates that UV/ozone cleaning is primarily the result of photosensitized oxidation processes. The contaminant molecules are excited and/or dissociated by the absorption of short wavelength UV light. Atomic oxygen and ozone (18,19) are produced simultaneously when O_2 is dissociated by the absorption of UV with wavelengths less than 245.4 nm. Atomic oxygen is also produced (18,19) when ozone is dissociated by the absorption of the UV and longer wavelengths of radiation. The excited contaminant molecules and the free radicals produced by the dissociation of contaminant molecules react with atomic oxygen to form simpler, volatile molecules, such as CO_2, H_2O, and N_2. Mattox (39) found that mild heat increases the UV/ozone cleaning rates. Bolon and Kunz (1), on the other hand, had found that the rate of ozone depolymerization of photoresists did not change significantly between 100°C and 300°C. The rate of destruction of microorganisms was similarly insensitive to a temperature increase from room temperature to 40°C (30). One manufacturer of UV/ozone cleaning equipment claims that the rate of photoresist stripping by UV/ozone increases severalfold as the temperature is raised from 20°C to 300°C (38).

UV/Ozone Cleaning in Vacuum Systems

Sowell et al. (2) reported that, when 10^{-4} torr pressure of oxygen was present in a vacuum system, shortwavelength UV desorbed gases from the walls of the system. During UV irradiation, the partial pressure of oxygen decreased, while that of CO_2 and H_2O increased.

One must exercise caution in using a mercury UV source in a vacuum system because, should the lamp envelope break or leak, mercury can enter and ruin the usefulness of the system. Caution must also be exercised when using UV/ozone in a cryopumped vacuum system, since cryopumped ozone is potentially explosive (40), particularly during regeneration of the cryopump. A convenient method of dealing with this potential hazard is to use two kinds of UV sources, one an ozone-generating source, the other an "ozone killer" source (41). (See next section.)

Safety Considerations

In constructing a UV/ozone cleaning facility, one should be aware of the safety hazards associated with exposure to short-wavelength UV light which can cause serious skin and eye injury within a short time (42-44). Another safety hazard is ozone, which is highly toxic. In setting up a UV cleaning facility, one must ensure that the ozone levels to which people are exposed do not exceed 0.1 ppm, the OSHA standard (45). Ozone is a potential hazard in a cryopumped vacuum system because cryopumped ozone can become explosive under certain conditions (40). One method of minimizing the hazards associated with ozone is to use two types of short-wavelength ultraviolet sources for UV/ozone cleaning (41): one, an ozone generating UV lamp, e.g., a low-pressure mercury light in a fused quartz envelope, the other, a UV lamp that does not generate ozone but which emits one or more wavelengths that are strongly absorbed by ozone, e.g., a low-pressure mercury light in a high-silica glass tube which emits at 253.7 nm but not at 184.9 nm. Such a non-ozone generating UV source can be used as an "ozone killer" (44-47). The decomposition of ozone can also be greatly accelerated through the use of catalysts (48).

UV/Ozone Cleaning Facility Construction

The materials chosen for the construction of a UV/ozone cleaning facility should remain uncorroded by extended exposure to UV/ozone. Some commercially available UV/ozone cleaners are now constructed of stainless steel (49,50).

The most widely available sources of short-wavelength UV light are the mercury arc lamps. Low-pressure mercury lamps in pure fused quartz envelopes operate near room temperature, emit

approximately 90 percent at the 253.7 nm wavelength, and generate sufficient ozone for effective surface cleaning. Approximately five percent of the output of these lamps is at 184.9 nm. Microwave-powered mercury vapor lamps are also available (51). Other available sources of short-wavelength UV include xenon lamps and deuterium lamps. The samples should be held as close to the UV source as is possible. In one UV/ozone cleaning box, the UV lamp was built into the bottom of the box so as to allow the parts to be cleaned to be placed directly onto the UV tube (52).

Applications

The UV/ozone cleaning procedure is now used in numerous applications. A major use is substrate cleaning prior to thin film deposition. The process is also being applied in a hermetic sealing method which relies on the adhesion between clean surfaces in an ultrahigh vacuum (14,53-55). The adhesion phenomenon between clean (UV/ozone cleaned) gold surfaces has been applied to the construction of a novel surface contaminant detector (56,57). The process has also been applied to improve the reliability of wire bonds, especially at reduced temperatures (58,59,60). UV/ozone is also being used for cleaning alumina substrate surfaces during the processing of thin film hybrid circuits (61).

Other applications which have been described are: the cleaning of thermal/flash protective electrooptic goggles (62), photoresist removal (1,5,13,38), the cleaning of vacuum chamber walls (2), photomasks (63), silicon wafers (63-65), lenses (63), mirrors (63), solar panels (63), sapphire (63) (before the deposition of HgCdTe) and other fine linewidth devices (63,64,66), inertial guidance subcomponents (glass, chromium-oxide surfaced-gas bearings, and beryllium) (63,67), gallium-arsenide wafers (68,69,75), the cleaning of stainless steel for studying a milk-stainless steel interface (70), and the cleaning of adsorbed species originating from epoxy adhesives (71). Since short-wavelength UV can generate radicals and ions, a side benefit of UV/ozone cleaning of insulator surfaces can be the neutralization of static charges (71). UV/ozone cleaning of silicon substrates in silicon molecular beam epitaxy (MBE) has been found to be effective in producing near defect-free MBE films (72). In the processing of semiconductor wafers, a single UV/ozone exposure has been found to be capable both of "descumming" and of stabilizing (73,74).

Effects Other Than Cleaning

Short wavelength UV, ozone, and the combination of the two can have effects other than surface cleaning. Among the more significant of these effects are: oxidation (47,72,75-78), UV-enhanced outgassing (79), other surface/interface effects (34,80-84), and etching (85-89).

Conclusions

The UV/ozone cleaning procedure has been shown to be a highly effective method of removing a variety of contaminants from surfaces. It is a simple-to-use dry process which is inexpensive to set up and operate. It can produce clean surfaces at room temperature, either in a room atmosphere or in a controlled atmosphere.

References and Notes

1. Bolon, D. A. and Kunz, C. O., "Ultraviolet Depolymerization of Photoresist Polymers." Journal of Polymer Engineering Science, Vol. 12, pp. 109-111, (1972).

2. Sowell, R. R., Cuthrell, R. E., Mattox, D. M., and Bland, R. D., "Surface Cleaning by Ultraviolet Radiation." Journal of Vacuum Science Technology, Vol. 11, pp. 474-475, (1974).

3. Vig, J. R., Cook, C. F. Jr., Schwidtal, K., LeBus, J. W., and Hafner, E., "Surface Studies for Quartz Resonators." in: Proceedings of 28th Annual Symposium on Frequency Control, Philadelphia, PA, 1976, AD 011113, pp. 96-108, 1974.

4. Vig, J. R., LeBus, J. W., and Filler, R. L., "Further Results on UV Cleaning and Ni Electrobonding." in: Proceedings of the 29th Annual Symposium on Frequency Control, Philadelphia, PA, 1977. pp. 220-229, 1975, AD A017466.

5. Vig, J. R. and LeBus, J. W., "UV/Ozone Cleaning of Surfaces," IEEE Trans. Parts, Hybrids, and Packaging, Vol. PHP-12, pp. 365-370, 1976.

6. Vig, J. R., "UV/Ozone Cleaning of Surfaces" in: Treatise on Clean Surface Technology, Vol. 1 (K. L. Mittal, ed.), pp. 1-26, Plenum Press, NY 1987.

7. Calvert, J. G., and Pitts, J. N. Jr., Photochemistry, pp. 205-209, 687-705, John Wiley & Sons, New York, 1966.

8. Fikhtengolts, V. S., Zolotareva, R. V., and L'vov, Yu A., Ultraviolet Spectrum of Elastomers and Rubber Chemicals, Plenum Press Data Div., New York, 1966.

9. Lang, L., Absorption Spectra in the Ultraviolet and Visible Region, Academic Press, New York, 1965.

10. See, e.g., "Encyclopaedic Dictionary of Physics," Vol. 5, p. 275, Pergamon Press, New York, 1962.

11. The author used in his experiments a Model No. R-52 Mineralight Lamp, UVP, Inc., San Gabriel, CA 91778.

12. Schrader, M. E., "Surface-Contamination Detection Through Wettability Measurements," in: Surface Contamination: Its Genesis, Detection and Control, (K. L. Mittal, ed.), Vol. 2, pp. 541-555, Plenum Press, New York, 1979.

13. Holloway, P. H., and Bushmire, D. W., "Detection by Auger Electron Spectroscopy and Removal by Ozonization Photoresist Residues," in: Proceedings of the 12th Annual Reliability Physics Symposium, pp. 180-186, IEEE, Piscataway, NJ, 1974.

14. Peters, R. D., "Ceramic Flatpack Enclosures for Precision Crystal Units, in: Proceedings of the 30th Annual Symposium on Frequency Control, pp. 224-231, Philadelphia, PA, 1976, AD A046089.

15. Bryson, C. E., and Sharpen, L. J., "An ESCA Analysis of Several Surface Cleaning Techniques,"in: Surface Contamination: Its Genesis, Detection and Control, (K. L. Mittal, ed.), Vol. 2, pp. 687-696, Plenum Press, New York, 1979.

16. Benson, R. C., Nall, B. H., Satkiewitz, F. G., and Charles, H. K. Jr., "Surface Analysis of Adsorbed Species from Epoxy Adhesives Used in Microelectronics,"Applic. Surf. Science, Vol. 21, Vol. 21, pp. 219-229, 1985.

17. Braun, W. L., "ISS/SIMS Characterization of UV/03 Cleaned Surfaces,"Appl Surface Sci., Vol. 6, pp. 39-46, 1984.

18. McNesby, J. R., and Okabe, H., "Oxygen and Ozone," Advances in Photochemistry, (Noyes, W. A. Jr., Hammond, G. S., and Pitts, J. N., eds.), Vol. 3, pp. 166-174, Interscience Publishers, New York, 1964.

19. Volman, D. H., "Photochemical Gas Phase Reactions in the Hydrogen-Oxygen System," Advances in Photochemistry, (Noyes, W. A., Hammond G. S., and Pitts, J. N., eds.), Vol. 1, pp. 43-82, Interscience Publishers, New York, 1963.

20. P. R. Hoffman Co., Carlisle, PA. 17013.

21. John Crane Lapping Vehicle 3M, Crane Packing Co., Morton Grove, IL 60053.

22. Welch Duo-Seal, Sargent-Welch Scientific Co., Skokie, IL 60076.

23. Dow Corning Corp., Midland, MI 48640.

24. Dutch Boy No. 205, National Lead Co., New York, NY 10006.

25. Eastman Kodak Co., Rochester, NY 14650.

26. Prengle, H. W. Jr., Mauk, C. E., Legan, R. W., and Hewes, C. G., "Ozone/UV Process Effective Wastewater Treatment," Hydrocarbon Processing, Vol. 54, pp. 82-87, Oct 1975.

27. Prengle, H. W. Jr., Mauk, C. E., and Payne, J. E., "Ozone/UV Oxidation of Chlorinated Compounds in Water," Forum on Ozone Disinfection, 1976; International Ozone Institute, Warren Bldg., Suite 206, 14805 Detroit Ave., Lakewood, OH 44107.

28. Prengle, H. W. Jr., and Mauk, C. E., "Ozone/UV Oxidation of Pesticides in Aqueous Solution." Workshop on Ozone/Chlorine Dioxide Oxidation Products of Organic Materials, EPA/International Ozone Institute, November 1976.

29. Prengle, H. W. Jr., in: Proceedings of the International Ozone Symposium, Warrren Bldg., Suite 206, 14805 Detroit Avenue, Lakewood, OH 44107, 1978.

30. Zeff, J. D., Barton, R. R., Smiley, B., and Alhadeff, E. UV-Ozone Water Oxidation/Sterilization Process, US Army Medical Research and Development Command, Final Report, Contract No. DADA 17073-C-3138, Sep 1974, AD A0044205.

31. Boenig, H. V., Structure and Properties of Polymers, p. 246, Wiley, New York, 1973.

32. Filimonov, V. N., Elementary Photoprocesses in Molecules, (B. S. Neporent, ed.), pp. 248-259, Consultants Bureau, New York, 1968.

33. Filler, R. L., Frank, J. M., Peters, R. D., and Vig, J. R. "Polyimide Bonded Resonators," Proceedings of the 32nd Annual Symposium on Frequency Control, Philadelphia, PA, pp. 290-298, 1978.

34. LeBus, J. W., and Vig, J. R., U.S. Army Electronics Technology and Devices Lab., Fort Monmouth, NJ 07703, unpublished information, 1976.

35. Kusters, J., Hewlett Packard Co., Santa Clara, CA 95050, personal communication, 1977.

36. Lasky, E., Aerofeed Inc., Chalfont, PA, personal communication, 1978.

37. Zafonte, L., and Chiu, R., Technical Report on UV-Ozone Resist Strip Feasibility Study, UVP, Inc., 5100 Walnut Grove Avenue, San Gabriel, CA 91778, September 1983; presented at the SPIE Santa Clara Conference on Microlithography in March 1984.

38. Application Note, "Photoresist Stripping With the UV-1 Dry Stripper," March Instruments Inc., Concord, CA 94520.

39. Mattox, D. M., "Surface Cleaning In Thin Film Technology," Thin Solid Films, Vol. 53, pp. 81-96, 1978.

40. Chen, C. W., and Struss, R. G., "On the Cause of Explosions in Reactor Cryostats for Liquid Nitrogen." Cryogenics, Vol. 9, pp. 131-132, April 1969.

41. Vig, J. R. and LeBus, J. W., "Method of Cleaning Surfaces by Irradiation With Ultraviolet Light," US Patent No. 4,028,135, issued June 7, 1977.

42. Peak, M. J., Peak, J. G., and Jones, C. A., "Different (direct and indirect) Mechanisms for the Induction of DNA-Protein Crosslinks in Human Cells by Far and Near-Ultraviolet Radiations (290 and 405 nm)." Photochemistry and Photobiology, Vol. 42, pp. 141-146, 1985.

43. Kubitschak, K. S., Baker, K. S., and Peak, J. M., "Enhancement of Mutagenesis and Human Skin Cancer Rates Resulting From Increased Fluences of Solar Ultra-violet Radiation," to be published in Photochemistry and Photobiology.

44. Tucker, M. A., Shields, J. A., Hartge, P., Augsburger, J., Hoover, R. N., and Fraumeni, J. F. Jr., "Sunlight Exposure as Risk Factor for Intraocular Malignant Melanoma." New England Journal of Medicine Vol. 313, pp. 789-792, 1985.

45. Occupational Safety and Health Standards, Vol. 1, "General Industry Standards and Interpretations." Oct. 1972, Pt. 1910, 1000, Table Z-1, "Air Contaminants," p. 642,4 as per change 10, June 26, 1975.

46. Ehlers, D. A., Ozone Generation and Decomposition by UV in the ERADCOM QXFF, Report No. PT81-004, General Electric Neutron Devices Dept., P.O. Box 2908, Largo, FL 34924, Jan 26, 1981.

47. Matheson Gas Data Book, Published by Matheson Gas Products Co., East Rutherford, NJ, 6th Edition, pp. 574-577, 1980.

48. Bonacci, J. C., Egbert, W., Collins, M. F., and Heck, R. M., "New Catalytic Abatement Product Decomposes Ozone in Jet Aircraft Passenger Cabins," International Precious Metals Institute Proceedings, 1982; reprint and additional literature on DEOXO Catalytic Ozone Converters is available from Englehard Corp., Specialty Chemicals Div., 2655 U.S. Rt. 22, Union, NJ 07083.

49. UVOCS Div., Aerofeed Inc. P.O. Box 303, Chalfont, PA 18914.

50. UVP, Inc., 5100 Walnut Grove Ave., San Gabriel, CA 91778.

51. Petelin, A. N., and Ury, M. G., "Plasma Sources for Deep-UV Lithography," VLSI Electronics: Microstructure Science, Vol. 8, Plasma Processing for VLSI (Einspruch, N. G., and Brown, D. M., eds.), Academic Press, 1984.

52. R. D. Peters, General Electric Neutron Devices Dept., P.O. Box 2908, Largo, FL 34924, personal communication, 1976.

53. Vig, J. R., and Hafner, E., Packaging Precision Quartz Crystal Resonators, Technical Report ECOM-4134, US Army Electronics Command, Ft Monmouth, NJ, July 1972, AD 763215.

54. Hafner, E., and Vig, J. R., "Method of Processing Quartz Crystal Resonators," US Patent No. 3,914,836, Oct 28, 1975.

55. Wilcox, P. C., Snow, G. S., Hafner, E., and Vig, J. R., "New Ceramic Flatpack for Quartz Resonators," Proceedings of the 29th Annual Symposium on Frequency Control, Philadelphia, PA, pp. 202-210, 1975. See Ref. No. 4 above for availability information.

56. Cuthrell, R. E. and Tipping, D. W., "Surface Contaminant Detector," Rev. Sci. Instrum., Vol. 47, pp. 595-599, 1976.

57. Cuthrell, R. E., "Description and Operation of Two Instruments for Continuously Detecting Airborne Contaminant Vapors," Surface Contamination: Its Genesis, Detection and Control, (Mittal, K. L., ed.) Vol. 2, pp. 831-841, Plenum Press, New York, 1979.

58. Jellison, J. L., "Effect of Surface Contamination on the Thermocompression Bondability of Gold," IEEE Trans. Parts, Hybrids, Packaging, PHP-11, pp. 206-211, 1975.

59. Jellison, J. L., "Effect of Surface Contamination on Solid Phase Welding - An Overview," Surface Contamination: Its Genesis, Detection and Control, (Mittal, K. L., ed.), Vol. 2, pp. 899-923, Plenum Press, New York, 1979.

60. Weiner, J. A., Clatterbaugh, G. V., Charles, H. K. Jr., and Romensko, B. M., "Gold Ball Bond Shear Strength," Proc. 33rd Electronic Components Conference, pp. 208-220, 1983.

61. Tramposch, R., "Processing Thin Film Hybrids," Circuits Manufacturing, Vol. 23, pp. 30-40, March 1983.

62. Wagner, J. A., "Identification and Elimination of Organic Contaminants on the Surface of PLZT Ceramic Wafers," Surface Contamination: Genesis, and Control, (K. L. Mittal, ed.), Vol. 2, pp. 769-783, Plenum Press, New York, 1979.

63. Lasky, E., UVOCS Div., Aerofeed Inc., Chalfont, PA 18914, personal communication, 1983.

64. J. Ruzyllo, G. T. Duranko, and A. M. Hoff, "Preoxidation UV Treatment of Silicon Wafers," Journal of the Electrochemical Society, Vol. 134, No. 8, pp. 2052-2055, August 1987.

65. B. S. Krusor, D. K. Biegelsen, R. D. Yingling, and J. R. Abelson, "Ultraviolet-Ozone Cleaning of Silicon Surfaces Studied by Auger Spectroscopy," J. Vac. Sci. Technol. B7(1), pp. 129-130, Jan/Feb 1989.

66. Smith, H. I., Massachusetts Institute of Technology, unpublished class notes on Cleaning of Oxides, and personal communications, 1982.

67. Stemniski, J. R., and King, R. L. Jr., "Ultraviolet Cleaning: Alternative to Solvent Cleaning," Adhesives for Industry, pp. 212-228, Technology Conferences, El Segundo, CA 1980.

68. McClintock, J. A., Wilson, R. A., and Byer, N. E., "UV-Ozone Cleaning of GaAs for MBE." Journal of Vacuum Science Technology, Vol. 20, pp. 241-242, Feb 1982.

69. S. Ingrey, W. M. Lau, and N. S. McIntyre, "An X-Ray Photoelectron Spectroscopy Study on Ozone Treated GaAs Surfaces," J. Vac. Sci. Technol. A4(3), pp. 984-988, May/Jun 1986.

70. Almas, K. A., and Lund, B., "Cleaning and Characterization of Stainless Steel Exposed to Milk," Surface Technology, Vol. 23, pp. 29-39, 1984.

71. Baird, D. H., Surface Charge Stability on Fused Silica, Final Tech. Report, TR 76-807.1, Dec. 1976, AD A037463.

72. Tabe, M., "UV Ozone Cleaning of Silicon Substrates in "Silicon Molecular Beam Epitaxy," Appl. Phys. Lett., Vol. 45, pp. 1073-1075, 1984.

73. Gardner, W. L., Engelhard Millis Corp., Millis, MA, 02054, personal communication, Nov, 1985.

74. Matthews, J. C., and Wilmott, J. I. Jr., "Stabilization of Single Layer and Multilayer Resist Patterns to Aluminum Etching Environments," presented at SPIE Conference, Optical Microlithography III, Santa Clara, CA, March 14-15, 1985; reprints available from Semiconductor Systems Corp., 7600 Standish Place, Rockville, MD 20855.

75. McClintock, J. A., Martin Marietta Laboratories, Baltimore, MD 21227, personal communication, 1981.

76. Janousek, B. K., and Carscallen, R. C., "Photochemical Oxidation of (HgCd)Te: Passivation Process and Characteristics," Journal of Vacuum ScienceTechnology, pp. 195-198, Jan-Feb 1985.

77. Graedel, T. E., Franey, J. P., and Kammlott, G. W., "Ozone-and Photon-Enhanced Atmospheric Sulphidation of Copper," Science, Vol. 224, pp. 599-601, 1984.

78. Clatterbaugh, G. V., Weiner, J. A., and Charles, H. K. Jr., "Gold-Aluminum Intermetallics: Ball Shear Testing and Thin Film Reaction Couples," Proceedings of the 34th Electronic Components Conference, pp. 21-30, 1984.

79. Altemose, V. O., "Outgassing by Ultraviolet Radiation," Vacuum Physics and Technology, Weissler, G. L., and Carlson, R. W., eds., Vol. 14 of Methods of Experimental Physics, Academic Press, 1979, New York, Chapter 7, pp. 329-333.

80. Tagieva, M. M., and Kiseler, V. F., "The Action of Radiation on the Surface Properties of Silica," Russian Journal of Phys. Chem. Vol. 35, pp. 680-681, (1961).

81. Hair, M. L., "The Molecular Nature of Adsorption on Silica Surfaces," Proceedings of the 27th Annual Symposium on Frequency Control, AD 771042, pp. 73-78, 1973.

82. White, M. L., "Clean Surface Technology," Proceedings of the 27th Annual Symposium on Frequency Control, AD 771042, pp. 79-88, 1973; also, "The Detection and Control of Organic Contaminants on Surfaces," Clean Surfaces: Their Preparation and Characterization for Interfacial Studies, (Goldfinger, G., ed.), pp. 361-373, Marcel Dekker, Inc., New York, 1970.

83. Lamb, R. N., and Furlong, D. N., "Controlled Wettability of Quartz Surfaces," Journal of Chemical Soc., Faraday Trans. Vol. 1, 78, pp. 61-73, 1982.

84. Caplan, P. J., Poindexter, E. H., and Morrisson, S. R., "Ultraviolet Bleaching and Regeneration of Si-Si03 Centers at the Si/SiO Interface of Thinly Oxidized Silicon Waters," Journal of Applied Physics, Vol. 53, pp. 541-545, 1982.

85. Srinivasan, R., "Conference on Lasers and Electrooptics." as reported in: "Clean Cuts for Notched Hairs," Science News, Vol. 123, p. 396, June 18, 1983.

86. Srinivasan, R., and Braren, B., "Ablative PhotoDecomposition of Polymer Films by Pulsed Far Ultraviolet (193 nm) Laser Radiation: Dependence of Etch Depth on Experimental Conditions," Journal of Polymer Science: Polymer Chemistry Edition, Vol. 22, pp. 2601-2609, 1984.

87. Alberts, G. S., "Process for Etching Organic Coating Layers," U.S. Pat. No. 3,767,490, issued Oct 23, 1973.

88. Wright, A. N., "Removal of Organic Polymeric Films from a Substrate," U.S. Pat. No. 3,664,899, issued May 23, 1972.

89. Robinson, L., "The Development of Ozone Resistant Materials for Wire and Cable," IEEE Electrical Insulation Magazine, Vol. 1, pp. 20-22, 1985.

UV-ENHANCED DRY CLEANING OF SILICON WAFERS

Takashi Ito, Rinshi Sugino, Satoru Watanabe,
Yasuo Nara, and Yasuhisa Sato

Fujitsu Laboratories Ltd.,
Semiconductor Devices Laboratory,
10-1 Morinosato-Wakamiya, Atsugi, Japan 243-01

The UV-enhanced dry cleaning with highly purified chlorine radicals can be suitable for an ultra-clean process in VLSI/ULSI production. It is advantageous especially in submicron or deep-submicron device fabrication. Metallic contaminant concentrations such as Fe, Mg, Al, and Cu ramaining on a wafer surface can be reduced much less than those of the state-of-the-art wet cleaning. This dry cleaning results in improvements of carrier lifetime, epi-film quality, thin gate oxide integrity, and SiO_2-Si interface characteristics.

INTRODUCTION

Wafer surface cleaning is important in LSI device manufacturing because contaminants such as hydrocarbon, alkaline and heavy metal degrade device performance and reliability. It is done prior to thermal oxidation, impurity diffusion, epitaxial growth of silicon films, chemical vapor deposition, dry etching, and other thermal processes. Wet cleaning processes are predominant for those purposes till now, which are exclusively useful to remove both particles and contaminants remaining on wafer surfaces after each process.

A much higher level of cleanliness is required for wafer surfaces of submicron devices. Conventional wet cleaning processes have some problems for those productions and are not fully cost-effective because huge amounts of chemicals are required for many or large wafers. Disposal of the chemicals causes cost and safety problems.

UV-enhanced dry cleaning with reactive gases is more attractive than wet or other dry cleaning techniques such as plasma or ion methods which damage or contaminate the wafer surfaces. UV-enhanced ozone-cleaning is useful for removing organic particles. For inorganic materials such as metals, UV-excited halogen-radical cleaning is effective. Combination of UV-enhanced and wet cleaning resulted in significant improvements of cleanliness(1)(2).

UV-enhanced dry cleaning alone has several advantages over conventional techniques as follows:

(1)As the devices become smaller and smaller, it will be more and more difficult for wet chemicals to clean abrupt contact holes and deep trenches. UV-excited halogen-radical cleaning makes the both processes possible.
(2)Gases are exhausted from a chamber much easier than wet chemicals. There is less recontamination on the cleaned surface.
(3)The amount of chemicals required is usually much smaller for gas. So the system and process is more economical.
(4)Dry cleaning technique does not require drying process, which often causes problems such as watermark.
(5)Process chambers are similar to those of CVD or etching. The process is compatible with automated ULSI production line.

This paper describes the possibility of all-dry cleaning process demonstrating cleaner surfaces of UV-enhanced chlorine etching than wet etched ones.

CLEANING MECHANISM

There are two cleaning mechanisms in UV-excited halogen radical cleaning as shown in Fig.1. One of them is its direct reaction with contaminative metal atoms which results in volatile halogen compounds. Chlorine gas was first used as the halogen reaction gas because it produces radicals under UV irradiation by a low-pressure mercury lamp. The other is a lift-off process. The chlorine radicals adsorbed on a wafer become negative ions by obtaining electrons from the silicon lattice and penetrate into the wafer. The process becomes more active when the substrate is irradiated with UV and electron-hole pairs are genarated. Silicon-chloride compounds are produced and spontaneous etching occurs. Metal contaminants can be removed by the lift-off process.

CLEANING PROCEDURE

Etching a silicon wafer greatly depends on the surface conditions. Very thin native oxides disturbe chlorine radicals to diffuse into the surface resulting in morphologies on the etched surface. Figure 2 shows the etching depth dependence on the UV irradiation time at a substrate temperature of 150℃, where microwave-excited UV lamp was used. The UV intensity was 22 mW/cm^2 for wavelengths ranged from 200 to 350 nm.

Despite a native oxide on the surface, there is no delay at the begining of the etching. UV-excited chlorine radicals probably diffuse through the thin native oxide and react with silicon atoms producing volatile species like $SiCl_2$ and $SiCl_4$. Controlled native

oxides formed with hydrogen peroxide and ammonium hydroxide result in very uniform etched surfaces. This is in contrast with those formed in nitric acid as shown in Fig.3. We could not distinguish both structures but the amounts of suboxides in those native oxides were found different. All the suboxides were mostly localized at the silicon interface in the controlled sample(3).

ESTIMATION OF CLEANLINESS

Because the substrate surface is covered with native oxide and chlorine radicals penetrate into the oxide, very small amount of chlorine atoms are only detected on the surface as just seen in Fig. 4. Auger signal from hydrocarbon residue becomes smaller than that of the wet cleaning.

Concentrations of various elements on silicon wafer surfaces were examined by SIMS and atomic absorption spectrometry. UV-excited dry cleaning with chlorine was done mostly in a clean quartz chamber at 150℃ and 2.7 kPa. Specially purified chlorine gas of 5 nine was used. Concentrations of Fe, Mg, Ca, and Na were much less than those after the conventional wet cleaning such as RCA cleaning as shown in Fig.5. Other elements such as Ni, Cr, Al, and Cu were below the detection limits. The amount of metal impurities remaining in the halogen gas determined the lower limit of the cleanliness.

Potassium and sodium chlorides are less volatile. But hydrogen gas annealing has been found effective to remove them. Figure 6 compares SIMS ion counts between hydrogen annealing and UV-excited cleaning/hydrogen annealing at 980 ℃.

ELECTRICAL PROPERTIES

Metallic impurities remaining on the wafer surfaces degrade the electrical characteristics of devices, and decrease the carrier lifetimes in silicon. Those are probably attributed to impurities in resist materials and process environmental contamination.

Figure 7 shows hystograms of dielectric breakdown stengths of MOS structures with about 15 nm thick oxides. The gate oxides were grown just after the UV-enhanced dry cleaning. The distribution of dielectric strengths of fabricated MOS structures was sharp and a little higher than the reference, where the UV-enhanced dry cleaning was followed by NH_4OH/H_2O_2 cleaning and deionized water rinsing. Thermal oxide films grown on clean silicon surfaces, however, are scarcely influenced by the wet cleaning.

The interface state density of the MOS structure revealed almost the same value between the UV-excited dry and conventional wet cleaning, in the order of $10^{10}cm^{-2}eV^{-1}$ as shown in Fig.8.. Although it is not clear what factors directly influenced the Si/SiO

$_2$ interface characteristics and whether much lower values are obtained or not, this result indicates that, at least, the UV-excited dry cleaning with chlorine can be used as a process of MOS gate oxidation.

The improvement corresponds with the decrease in surface recombination velocity which was calculated from MOS Zerbst plots. Figure 9 shows the etching depth dependence of surface recombination velocity. The deviation of the velocities is also improved.

The dry cleaning technique was applied to clean a silicon surface just prior to epitaxy. Following the photo-excited chlorine cleaning, a thin native oxide and volatile chloride compounds were removed by thermal treatment in hydrogen. To estimate the cleanliness, 1μm of an epitaxial silicon film was grown at 850 ℃ using Si_2H_6 and H_2. No defects were observed at the interface between the epi and substrate. The epi-wafer was followed by dry oxidation to obtain a 20 nm-thick SiO_2 film. The average breakdown fields were 9.6 MV/cm for H_2 and over 11 MV/cm for the photo-excited dry cleaning as shown in Fig.10, respectively. This means the clean surface formed by the UV-enhanced dry cleaning is used to grow a high quality silicon epitaxial film.

CONCLUSION

In conclusion, the UV-enhanced dry cleaning can be an ultra-clean process for VLSI/ULSI. It is advantageous in submicron- or deep submicron-device production. Subjects that we should plan are further investigation of the cleaning mechanism, optimization of the cleaning conditions depending on the surface conditions of respective wafer, fully-automated cleaning equipments and direct cleanliness-evaluation technique of higher level.

REFERENCES

(1) T.Ito, R.Sugino, T.Yamazaki, S.Watanabe, and Y.Nara, Proc. Symp. on Dry Processes, ECS, Vol.88-7, 287 (1988)

(2) R.Sugino, Y.Nara, T.Yamazaki, S.Watanabe, and T.Ito, Ext. Abst. 19th Conf. on SSDM, 207 (1987)

(3) T.Hattori, K.Takase, H.Yamagishi, R.Sugino, Y.Nara, and T.Ito, Jpn.J.Appl.Phys.,28, 2, L296 (1989)

(4) K.Takase, H.Yamagishi, R.Sugino, Y.Nara, T.Ito, and T. Hattori, Abst. 21th Conf. on SSDM, 393 (1989)

(5) S.Watanabe, R.Sugino, T.Yamazaki, Y.Nara, and T.Ito, Dig. of Papers, 1989 2nd MicroProcess Conference, B-1-4, 120 (1989)

(6) R.Sugino, R.Takizawa, H.Sato, and T.Ito, Abst. 21th Conf. on SSDM, 417 (1989)

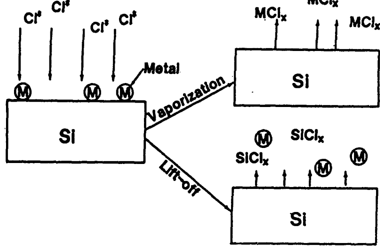

Fig.1 Two cleaning mechanisms in UV-excited halogen radical cleaning

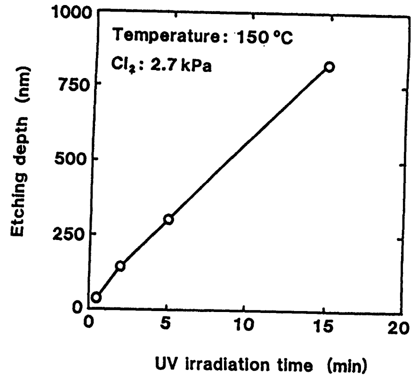

Fig.2 Etching depth dependence of silicon on UV irradiation time at 150 ℃

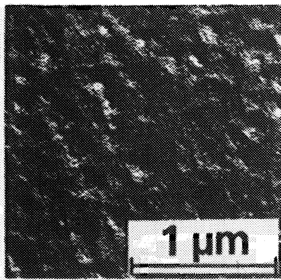

(a)HNO_3

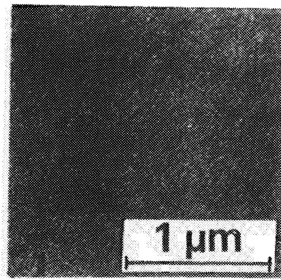

(b)NH_4OH

Fig.3 Surface morphologies of etched silicon pretreated in different solutions

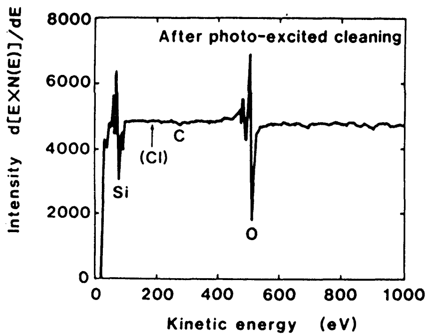

Fig.4 Auger signals from UV-excited chlorine cleaned surface

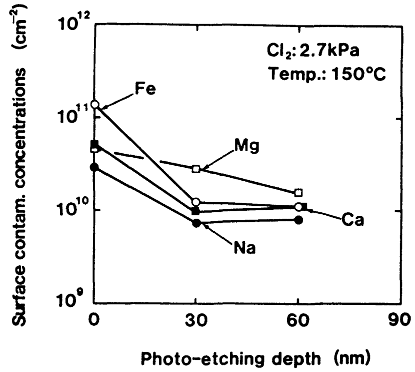

Fig.5 Trace impurities on silicon surfaces measured by atomic absorption spectrometry

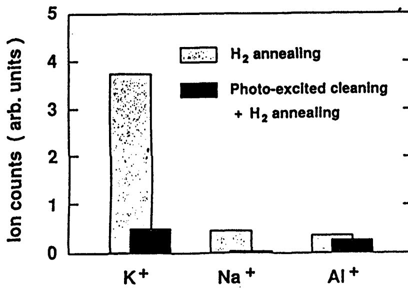

Fig.6 SIMS signals of silicon surfaces cleaned by UV-excited chlorine and hydrogen annealing

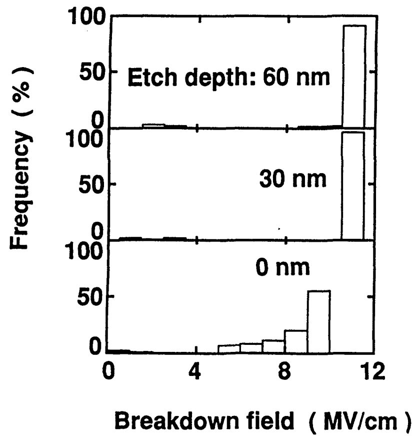

Fig7. Hystograms of dielectric breakdown voltages of 15 nm thick silicon- dioxide films

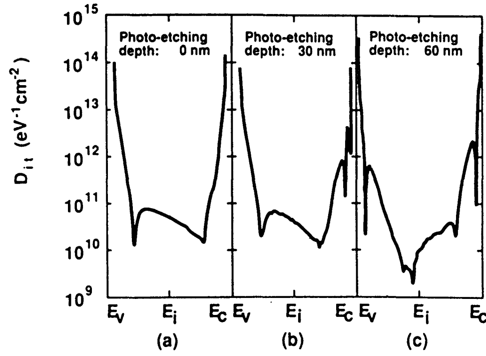

Fig.8 Interface state desities of MOS structures
(a) wet cleaned (0 nm etched), (b) 30 nm etched, (c) 60 nm etched

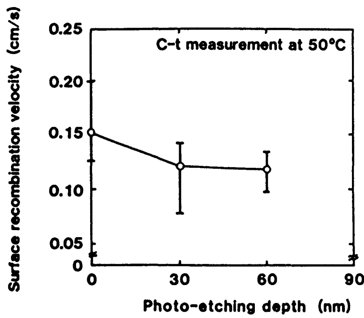

Fig.9 Etching depth dependence of surface recombination velocities

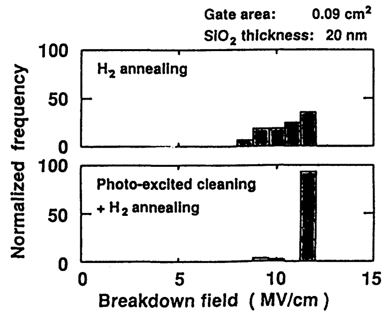

Fig.10 Hystograms of dielectric breakdown voltages of 15 nm thick silicon-dioxide films grown on epi-layers

VAPOR-PHASE WAFER CLEANING, OXIDE ETCHING, AND THIN FILM GROWTH

B.E. Deal, M.A. McNeilly, D.B. Kao, and J.M. deLarios

ADVANTAGE Production Technology, Inc.
820 Kifer Road
Sunnyvale, CA 94086

ABSTRACT

A newly developed reactor and associated vapor phase processes for the fabrication of high density, sub-micrometer semiconductor device structures during fabrication are described. The reactor, constructed of a specially formulated silicon carbide material, permits contamination-free, in-situ wafer cleaning, oxide etching, and native oxide regrowth, with the potential for sequential thermal oxidation and CVD processing. Wafers up to 150 mm in diameter are processed individually at reduced pressure, and in a vertical position to minimize contamination. Initial results involving oxide etch-back and native oxide removal using HF/H_20 chemistry along with native oxide regrowth characteristics are reviewed. Future development plans concerning new cleaning chemistries and sequential cleaning/deposition processing steps at elevated temperatures are summarized.

INTRODUCTION

The procedures employed for cleaning semiconductor wafers during device fabrication have not changed appreciably in thirty years (1). However, current silicon technology being developed, which involves integrated circuits having upwards of one million components and feature sizes well below one micrometer, will obviously require drastically improved cleaning methods. Even so, many device manufacturers seem to be "content in their ways" with respect to advanced cleaning technologies when surveyed regarding their current activities in this area (2).

Two concepts have been proposed to improve the cleanliness and perfection of surfaces and interfaces with regard to pretreatment and subsequent thin film deposition. One of these is vapor phase cleaning. It has been demonstrated that many of the current and anticipated problems associated with liquid cleaning processes - such as contamination, lack of penetration into deep geometries, environmental effects and the like - may be greatly minimized or eliminated by so-called "dry" processing (3 - 11). At the same time, radiation-producing processing must be avoided to prevent device degradation (12, 13).

A second concept for future megabit device fabrication involves sequential or in-situ, multi-step processing. It is known that surface films ("native oxides") tend to form rapidly on the bare silicon surface after such films are removed in hydrofluoric acid solutions. These films are uneven, of varying composition, and tend to degrade resulting film/device properties. A good example is that thermal oxidation has been found to be greatly affected by impurities in the pre-oxidation cleaning reagents (14 - 16). Other

effects have been reported for metal contacts (17), epitaxial deposition (18), and poly-Si emitter structures (19). The adoption of sequential, in-situ processing, where the device wafer is not exposed to a reactive ambient between cleaning and subsequent processing, will make it possible to minimize contamination and oxide regrowth, and thus improve device performance, yield, and reliability.

Because of the above, a system and associated processes have been developed which will permit vapor-phase wafer cleaning to be carried out at reduced pressure prior to and sequentially with various device processing steps. The reaction chamber consists of a unique silicon carbide material, and may be designed in a single or multi-chamber configuration. In this paper, a single-chamber system is described, along with an HF/H_20 cleaning/etching process. Silicon oxide etch characteristics, contamination aspects, and native oxide removal are discussed. Future directions, involving concepts such as multi-chamber, in-situ processing, other cleaning chemistries, and potential CVD processing are also briefly presented.

CLEANING SYSTEM AND PROCEDURE

The current vapor phase clean/etch reaction chamber is shown in Fig. 1, which includes a schematic of the overall process system. The material used to construct the chamber is a specially formulated silicon carbide composite manufactured by Norton Company (20). It consists of two concentric spheres connected by a center ring or block. The diameter of the outer sphere is approximately 24 cm and will accommodate one or two silicon wafers up to 150 mm in diameter. The wafer is placed vertically in the chamber. As indicated in Fig. 1, process gases may be admitted into one side of the chamber through the inner sphere, while evacuated by a vacuum pump through the outer sphere. Thus a considerable amount of flexibility in gas phase dynamics is possible by controlling gas flows and vacuum supply. The silicon carbide material is inert to essentially any reactant gas. A special low mass, resistance heater has been designed to heat the wafer(s) up to 1000 °C (21).

Figure 1 also includes mass flow meters, gas sources, two vaporizers, and vacuum pump. Gas lines from the vaporizer and other gas sources are heated, as are the valves (not shown). All reactant transport components outside the reactor are fabricated from teflon-based materials.

A typical sequence for cleaning or etching a device wafer is indicated in Fig. 2. The procedure is as follows: after insertion of the silicon wafer in the chamber, the door is clamped and the chamber evacuated to one Torr in less than 10 sec (I). This tends to vaporize absorbed moisture and other volatile species-even from high aspect ratio trenches. Nitrogen or argon is then admitted to the system to about 350 Torr. Next, the cleaning or etching mixture (HF in H_20) flows through the chamber in the carrier gas (II). After the prescribed cleaning or etching time (generally 20 - 40 sec), the gas flows are stopped and the system once more is evacuated in less than 10 seconds to the milliTorr range. After a suitable pumping time for desorption and evacuation of gases including reaction products, atmospheric pressure nitrogen (argon) is readmitted to the chamber and the wafer removed for evaluation or additional processing. All of the above procedures are computer programmed and controlled.

For evaluation purposes, various wafer and film surface properties are measured before

and after processing. These may include particle density, film thickness and uniformity, and contamination analysis (SEM, SIMS, Auger, TXRF, etc.). In addition, gas phase composition is monitored during the process using residual gas analysis. The environment around the loading end of the system and monitoring equipment is maintained at Class 10 or better.

RESULTS

Oxide Etchback: One of the primary methods of evaluating the vapor phase clean/etch system and associated processing described above is to characterize thermal oxide etching. This was done by removing varying amounts of oxides under selected process conditions, and determining etch rates, etch uniformity, and reproducibility of etching from run to run. Typical results are shown in Fig. 3. In the upper plot, oxide thickness data across a 100 mm thermally oxidized wafer are shown before and after removing 1150 A oxide. Differences in these two plots (thickness of oxide etched) are shown below. Total deviation of oxide etched for this example is $\pm 1.3\%$. Other etching conditions were P_{vap} HF = 1.4 Torr, P_{vap} H_2O = 20 Torr, P_{total} = 250 Torr, N_2 flow rate = 9 l/m, substrate temperature = 25 °C, and etch time 60 sec. Similar results were obtained for 125 and 150 mm diameter wafers and for various process conditions.

In Fig. 4, thermal oxide removed (etched) is plotted against H_2O/HF exposure time. For the conditions indicated, an etch rate of 33.9A/sec is obtained. A slight offset along the time axis may be noted, which is discussed briefly below. Other etch rate data have been obtained for varying HF/H_2O vapor pressures and range from 10 to 50 A/sec. Further such evaluations are in progress.

A similar plot showing the etch characteristics of borophosphosilicate glass (BPSG) is included in Fig. 5. Boron and phosphorus concentrations are each approximately 5% by weight in this deposited oxide dielectric. Etch conditions for the BPSG were the same as those indicated in Fig. 4. Note that the BPSG etch rate is approximately twice that of thermal oxides. This same ratio has been noted for etching in conventional aqueous HF solutions. If no boron were present in the film, the etch rate of the BPSG dielectric would probably be ten times or more greater than that of thermal oxides (22).

The mechanism of thermal oxide etch-removal in HF/H_2O vapor mixtures is being investigated. It has been found, however, that the actual etching occurs by the action of a thin condensed layer of HF in H_2O on the oxide surface (see Fig. 6). This can explain the very good uniformity of etching and a lesser dependence on gas dynamics. It also helps to explain the importance of the operation at reduced pressure during the etch cycle and the final evacuation of the reaction chamber in removing reactants, reaction products, and contamination in a matter of seconds. The time offsets observed in Figs. 4 and 5 are probably due to the time required for this film to form. Thus, the surface condition of the oxide plays an important role in the etching mechanism. A more detailed description of the mechanism of vapor transport and vapor HF etching of dielectric films on silicon will be reported in the near future (23).

Native Oxide Removal and Regrowth: An important aspect of cleaning or removing native oxides on silicon prior to subsequent film deposition steps is to maintain the surface as free from oxide regrowth as possible. An investigation was carried out to monitor the effects of various ambients on native oxide regrowth of HF vapor etched silicon. These

included wet and dry N_2 and O_2, and exposure to light or the dark. The results were compared with room ambient exposure, as well as treatment in aqueous HF solutions plus deionized water rinse. Oxide thicknesses were measured using a Gaertner Model No. L115B mapping ellipsometer.

Typical results of native oxide regrowth are presented in Fig. 7. Data for 24-hour exposure of an HF vapor etched silicon surface to dry nitrogen and filtered room air are shown. Note that the initial native oxide thickness was 12 A (as measured by the ellipsometer) while after HF vapor etch, it was 4 A. A thickness of 12 A was obtained after 24 hours in room air, while the dry N_2 exposure resulted in less than 7 A, or an increase of 1 -2 A. Note that oxide thicknesses measured by an ellipsometer in the 1-15A range tend to be thicker (almost 2:1) than when measured by an electron beam technique such as Auger spectroscopy.

General observations of results obtained thus far are as follows with regard to native oxide regrowth after vapor phase HF etching of silicon.

* Dry N_2 and O_2 give minimum regrowth.
* A dark environment generally reduced oxide growth.
* Wet gases increase oxide regrowth 2-3 times.
* Room air (R.H. = 40%) increases regrowth up to 10 times. The effects of other variables such as silicon properties, are being investigated.

These observations tend to agree with those of other authors (24 - 26) although the ledge growth kinetics reported by Ohmi (24) have not been observed.

Particulate and Metallic Contamination: Contamination effects, both particulate and metallic, have been monitored on an on-going basis. It has been found that the vapor phase HF system tends to be very clean and does not add particles to the wafer. In a series of twelve runs where the native oxide was etched from the silicon surface, an average of 1.5 particles equal to or greater than 0.4 um were removed per run. Measurements were made with a Tencor Model 5500 Surfscan particle analyzer. Average starting (pre-etch) counts were 9 particles $\geq$ 0.4 um per 150 mm wafer.

With respect to metallic contaminants, various beam techniques have been used to monitor impurities on the surface before and after vapor HF treatment. These include Auger, SIMS, XPS, SEM, and TXRF (Total Reflection X-ray Analysis). These analyses, especially TXRF, indicate that no metallic impurities are added by the system. In fact, two separate evaluations indicated that Pb, Fe, Cu and Ni are typically reduced in concentration by more than 50% during native oxide removal by the HF vapor process. Pre-etch values were 0.5 to 1.0 x 10^{12} atoms/cm^2 as received from the supplier.

FUTURE DIRECTIONS

A vapor phase cleaning system dealing primarily with HF/H_20 chemistry has been discussed; however, several other chemistries are possible and are being investigated. Initially, we will investigate gas phase analogs of conventional aqueous cleaning processes, such as ammonium hydroxide/hydrogen peroxide and hydrochloric acid/hydrogen peroxide. Other vapor systems will also be explored, with primary interest directed towards removal of metallics, organics, alkalis, and even particulates.

In addition to cleaning chemistries, the reactor described in this paper is ideally suited for the chemical vapor deposition (CVD) of thin films, such as epitaxial and polycrystalline silicon, dielectrics, interconnect and contact metals, and even growth of thermal oxides. The deposition of these films will be investigated using a specially designed heater and appropriate processes developed. Subsequently, the cleaning and deposition processes will be combined into one multichamber system, such as is depicted in Fig. 8. In this figure, a surface contamination removal module (SCR) is shown which is connected to an interprocess robot chamber. It is possible to move the cleaned wafer in vacuum to the next module for additional cleaning, native oxide regrowth, or possibly CVD. Thus, it should be possible to carry out sequential process steps which will eliminate many of the current and future problems associated with the fabrication of high density, sub-micrometer device structures.

In summary, a novel, single wafer reactor, along with appropriate vapor phase cleaning/etching processes, for use in semiconductor device fabrication, has been described. This system exhibits several important features. First, the unique design of the silicon carbide reaction chamber is compatible with all types of chemistries over a wide range of temperature and pressure. Next, vapor phase processing used in conjunction with this reactor will be an important aspect of sub-micrometer device fabrication in the future -- especially with respect to wafer cleaning. Specific to this system is the use of reduced pressure during the cleaning and etching steps; of equal value is the desorb cycle capability which results in the significant reduction of impurities, particles, and reaction products from the wafer surface. Finally, the system described has the potential for in-situ and sequential cleaning, oxidation, and CVD processing steps. This latter capability will be a critical requirement in the fabrication of complex device structures used for future ULSI applications.

ACKNOWLEDGEMENTS

The authors thank Professors C. Robert Helms of Stanford University and Rafael Reif of MIT for their valuable suggestions and consultation during the course of this investigation.

REFERENCES

1. Proceedings of "Symposium on Cleaning of Electronic Device Components and Materials," ASTM, STP No. 246, Am. Soc. Test. Matls., (1959).
2. A. Khilnani, "Cleaning Semiconductor Surfaces: Facts and Foibles" in Particles on Surfaces 1, Detection, Adhesion, and Removal, K. L. Mittal, Ed., Plenum Press, New York, p. 17 (1986).
3. P. J. Holmes and J. E. Snell, Microelectronics and Reliability, 5, 337 (1966).
4. R. E. Novak, Solid State Tech., 31 (3), 39 (1988).
5. T. Ohmi, Proc. Microcontamination Conf. and Expo., Santa Clara, CA (1988).
6. P. A. M. van der Heide, M. J. Baan Hofman, and H. J. Ronde, J. Vac. Sci., Tech., A7, 1719 (1989).
7. D. B. Fenner, D. K. Biegelsen, and R. D. Bringans, J. Appl. Phys., 66, 419 (1989).
8. R. L. Bersin and R. F. Reichelderfer, Solid State Tech., 20(4), 78 (1977).
9. E. A. Irene, Proc. Deposition and Growth Limits for Microelectronics, G. W. Rubloff, Ed., Am. Inst. Physics No. 167, New York, p. 74 (1987).
10. J. Ruzyllo, Microcontamination, 6 (3), 39 (1988).

11. J. R. Vig, J. Vac. Sci. Tech., A3, 1027, (1985).
12. G. S. Oehrlein, G. J. Coyle, J. C. Clabes, and Y. H. Lee, Surf. Interface Ana., 9, 275 (1986).
13. K. F. Galloway, S. Mayo, and P. Roitman, J. Electrochem. Soc, 126, 2245 (1979).
14. F. N. Schwettmann, K. L. Chiang, and W. A. Brown, Paper No. 276 in Spring Meeting of The Electrochemical Society, p. 688 Extended Abstracts 78-1, Seattle, WA (1978).
15. G. Gould and E. A. Irene, J. Electrochem. Soc., 134, 1031 (1987).
16. J. M. deLarios, D. B. Kao, B. E. Deal, and C. R. Helms, Appl. Phys. Lett., 54, 715 (1989).
17. W. T. Stacy, E. K. Broadbent, and M.H. Norcott, J. Electrochem. Soc., 132, 444 (1985).
18. T. J. Donahue and R. Reif, J. Electrochem. Soc., 133, 1691 (1986).
19. G. L. Patton, J. C. Bravman, and J. D. Plummer, IEEE Trans. Electron Devices, ED-33, 1754 (1986).
20. Norton Company, 1 New Bond Street, Worcester, MA 01615.
21. M. A. McNeilly, U.S. Patent 4,778,559, issued Oct. 18, 1988.
22. W. E. Beadle, J. C. C. Tsai, and R. D. Plummer, Quick Reference Manual for Silicon Integrated Circuit Technology, John Wiley and Sons, New York, p. 5-8 (1985).
23. C. R. Helms, B. E. Deal, D. B. Kao, and J. M. deLarios, manuscript in preparation.
24. T. Ohmi, M. Morita, E. Hasegawa, M. Kawakami, and K. Suma, in Proc. VLSI Symposium, The Electrochemical Society, Los Angeles, CA (1989); see also Appl. Phys. Lett., 55, 562 (1989).
25. S. I. Raider, R. Flitsch, and M. J. Palmer, J. Electrochem. Soc., 122, 413, (1975).
26. R. J. Archer, J. Electrochem. Soc., 104, 619 (1957).

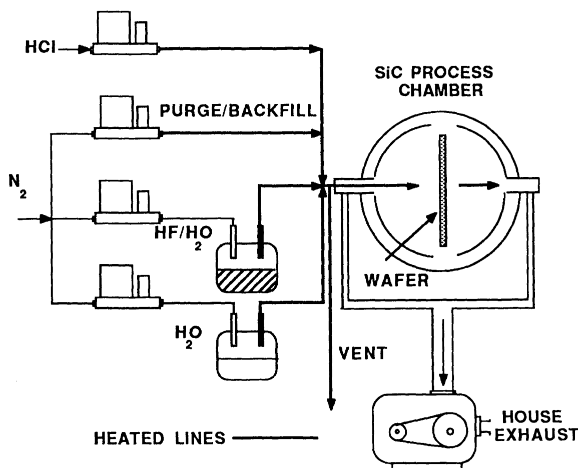

Fig. 1 Schematic of process system for vapor-phase HF cleaning and etching of silicon wafers.

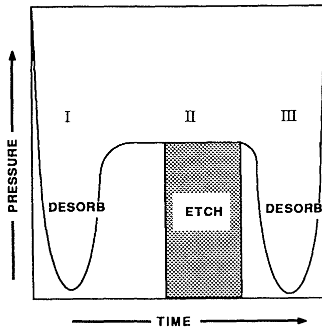

Fig. 2 Pressure - time cycle for HF vapor-phase etching of thermal oxide.

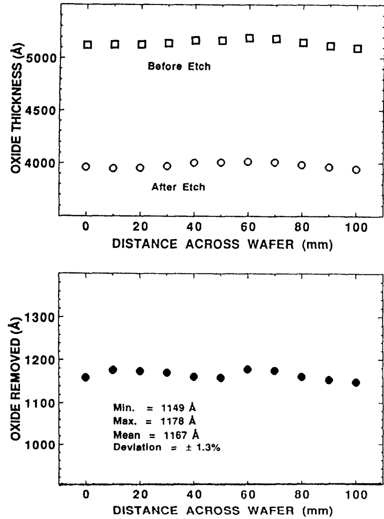

Fig. 3 Thermal oxide thickness before and after vapor-phase HF etching (above) and total oxide etched (below). Conditions: 25% HF in H_2O at 30°C, 9 l/min N_2, 250 Torr, 60 sec etch time, 100 mm dia. Si at 25°C.

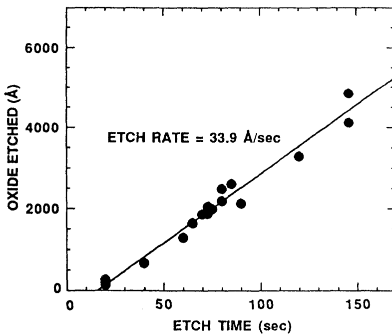

Fig. 4 Etching of thermal SiO_2 in vapor-phase HF. Conditions: 25% HF in H_2O at 50°C, 16 l/min N_2, 350 Torr, 150 mm dia. Si at 25°C.

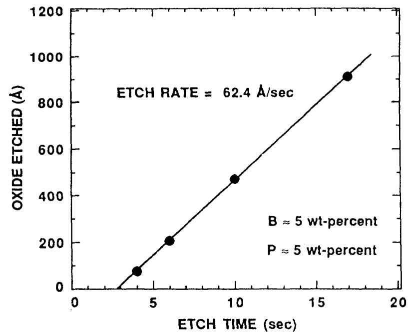

Fig. 5 Etching of borophosphosilicate glass film in vapor-phase HF. Conditions same as Fig. 4.

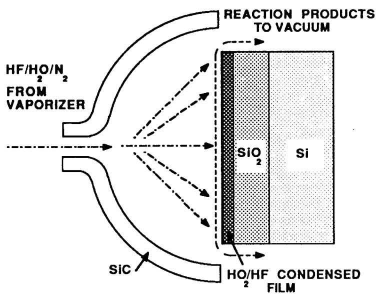

Fig. 6 Mechanism involved in vapor-phase HF etching of oxidized silicon wafer.

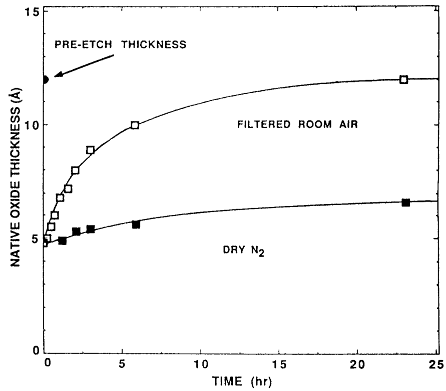

Fig. 7 Regrowth of "native" oxide on silicon wafer after removal of oxide in vapor-phase HF.

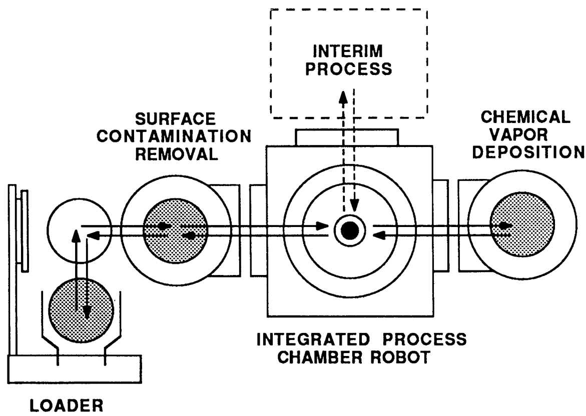

Fig. 8 Schematic of proposed integrated processing system.

SURFACE DAMAGE DURING REMOTE PLASMA CLEANING OF SILICON WAFERS

David C. Frystak and Jerzy Ruzyllo
Center for Electronic Materials and Processing
Department of Electrical Engineering
The Pennsylvania State University
University Park, PA 16801

Cleaning of silicon surfaces in chlorine based remote plasma can lead to roughening of the cleaned surface. In this paper, correlation between surface damage and various parameters of the remote plasma cleaning are determined. An ultrathin oxide grown prior to cleaning or addition of oxygen to the gaseous cleaning mixture are studied as a means to control surface damage.

INTRODUCTION

Remote plasma cleaning using an HCl/Ar gas mixture has shown promise as a technique to remove metallic impurities from the surface of silicon wafers [1,2]. An undesired side effect of this process however, is the formation of surface roughness due to pitting of the silicon during exposure to the HCl/Ar afterglow mixture [3].

In this experiment, efforts were carried out to gain an improved understanding of the nature of the development of surface roughness under these particular process conditions. This understanding is needed to introduce modifications to the afterglow process which will minimize its damaging effects, but maintain at the same time its cleaning capabilities.

EXPERIMENTAL

P-type, (100) oriented silicon doped with boron in the range of 2-7 ohm-cm resistivity was used in this study. Two types of samples were prepared for experiments. Uncontaminated silicon samples were used to evaluate the impact that HCl/Ar remote plasma cleaning has on silicon substrates alone, while samples intentionally contaminated with copper were used to study the cleaning efficiency of a given remote plasma process.

All samples were cleaned via the standard RCA procedure [4] prior to any further processing. Clean samples were then treated in afterglow mixtures of hydrogen chloride, argon and, in some cases,

oxygen in the remote plasma apparatus shown in Fig. 1. It consists of a conventional resistance heated furnace with a microwave generator attached to it. The chemically active products of a gas discharge taking place in the fused silica tube located in the microwave cavity are allowed to flow at a high rate into the reaction chamber to interact with the wafer. The parameters of the afterglow process, including gas composition, exposure time and substrate temperature, were varied in an effort to determine the conditions under which no damage to the substrate occurs. HCl concentrations in argon were varied from 1 to 10 percent. The substrate temperature was held in the range of 200°C to 400°C, and time of exposure to the afterglow gas was varied from 30 seconds to 5 minutes. Plasma afterglows were generated at a pressure of 1 torr which corresponded to a gas flow rate of 2 standard liters per minute for the given reactor geometry and pumping speed.

Except for the wet chemical cleaning step, the samples intentionally contaminated with copper were processed in the same fashion as the control samples, and were likewise tested in the same fashion. The metallic impurities were deposited by means of chemical plating from solution. This technique was used to prescisely deposit elemental Cu in surface concentrations in the range of 1E14 to 1E16 atoms/cm^3.

After plasma cleaning was performed, the samples were thermally oxidized at 1000°C in O_2 to grow oxides in the thickness range of 200 to 250 angstroms. Aluminum evaporation was used to form MOS capacitors on the samples for oxide breakdown measurements. In this last case, oxides were stressed with a d.c. voltage ramp of 1V/sec while a current threshold of 1μA was set as the criterium for oxide failure.

Samples were also inspected immediately after dry cleaning. The bare substrates were examined using optical microscopy as an initial test for the presence of damage caused by the afterglow exposure. Further investigation included scattering of white light from the sample surfaces, the scattering of polarized laser light from the sample surfaces and SEM studies. In addition, mechanical profiling of the surface was used in the case of excessively damaged and/or etched surfaces. Occasionally, preferential wet chemical etching was used to magnify the observed surface features.

RESULTS AND DISCUSSION

It was determined that surface roughness introduced during the HCl/Ar afterglow treatment was the cause for inferior breakdown statistics of oxides grown on dry cleaned substrates [3]. Nonuniform etching of the Si surface by excited species of HCl and Cl takes place during the afterglow exposure. Prevention of this roughness is

necessary in order to implement this technique as a useful VLSI/ULSI cleaning step.

Dependence of roughness on the process parameters of the HCl/Ar treatment was studied. It was determined that roughness was dependent primarily on process temperature and time of wafer exposure to afterglow gas. Formation of roughness was not strongly dependent on the concentration of HCl in the gas mixture or pressure over a range of investigation. Properties of oxides grown on substrates processed under various conditions are presented in Fig. 2. Samples were treated with various concentrations of HCl in the gas mix for a time of 30 seconds for three different temperatures. Results for the addition of oxygen in the afterglow gas mixture are also shown, and will be discussed later in this report. Results for samples treated at a substrate temperature of 200°C (Fig. 2a) show that the afterglow treatment does not have a detrimental effect on the quality of the subsequently grown thermal oxides. 50% cumulative failure of capacitors formed on these samples occurred at fields of 10 MV/cm or greater making them comparable in quality to the control samples, i.e. those not exposed prior to thermal oxidation to the HCl/Ar afterglow. As the processing temperature is increased to 300°C and 400°C, Fig. 2b and Fig. 2c, the oxide breakdown field characteristics are degraded. At both temperatures, 50% cumulative failure of capacitors tested occurred at applied fields of 5 MV/cm or less. This is due to the effects that surface roughness has on both the growth of the thin oxide film and the local enhancement of the electric field across the dielectric [5].

Extended time of exposure to the HCl/Ar afterglow allows for more Si to be etched and more opportunity for roughness to form. Surface roughness evaluation for samples exposed for various times to 10% HCl/Ar afterglow at a substrate temperature of 400°C is presented in Fig. 3. After 300 seconds exposure, the sample surface is very rough as compared to the undamaged control sample. The surface appeared very hazy and exhibited a maximum value of peak to peak roughness of 1150 angstroms as measured with a surface profilometer. Even after 30 seconds, damage is evident at this temperature in the form of haze observed through light scattering measurements and the occurance of etch pits on the surface. The increase in roughness with time of exposure correlates with the decrease of oxide quality with time of exposure as shown in Fig. 4. The greater the extent of roughness and damage, the lower the breakdown field. Thus, apart from any other means of controlling surface roughness, as short as possible an afterglow exposure time is desirable.

The thickness of the chemical oxide on the Si surface was found in this experiment to have a strong impact on the etch rate of Si as well as on the formation of surface roughness. The difference in the protective nature of two chemical oxide film thicknesses is very clearly displayed in Fig. 5. Shown is a silicon wafer which had an

initial chemical oxide of 27Å. This oxide was removed on one half of the wafer with dilute HF leaving behind a chemical oxide of about 5Å. The entire wafer was then treated in 10% HCl/Ar afterglow for 5 minutes at 400°C. After this treatment, the surface with initially 5Å of chemical oxide was found to be very rough (Fig. 5). On the other hand, 27Å of native oxide protected the Si surface from etching, leaving it far less damaged by this process. Measurements of the surface profile show that a 1 micron step is present at the boundary between two halves of the wafer corresponding to an etch rate of silicon of 0.2 micron/min (Fig. 5). In a separate experiment, etch rates for 10% HCl/Ar at 200°C were 0.08 to 0.14 micron/min through a 5Å oxide film, again with 27Å of chemical oxide retarding the etching process.

A summary of surface etching and damage for various initial chemical oxide thicknesses is presented in Fig. 6. For 7Å chemical oxide, a 200°C, 1 minute exposure to HCl/Ar does not produce any evident damage to the surface whereas a 5 minute exposure leaves the surface hazy as determined by scattering of white light from the surface of the processed sample. A 20Å thick chemical oxide is enough to prevent etching of Si at a process temperature of 200°C, although it needs to be very uniform to avoid haze which may occur due to nonuniform etching through the oxide. At the same time, 20Å is not enough to protect the surface in the case of 400°C HCl/Ar treatment. A 27Å chemical oxide allows only a slight haze to develop at a processing temperature of 400°C under the listed conditions.

The ideal situation would be to not etch Si at all while removing transition metals from the silicon surface during dry cleaning. This would be an ultimate solution to the issue of preventing nonuniform etching of Si resulting in surface roughness. The reality however, is that the Si etching can not be avoided in the process of formation of volatile metal chlorides. This is because silicon chlorides are much more volatile than chlorides of transition and akali metals. In other words, Si etching is an integral part of the proposed dry cleaning mode, and hence, must be kept under control.

In this context, the key issue is how to etch Si, and complex metals at the same time, without introducing surface roughness. In light of the before mentioned properties of thin chemical oxide films in preventing roughness, two approaches toward this issue were investigated: the use of oxygen in the HCl/Ar gas mixture during cleaning, and the use of an oxygen afterglow to grow an ultrathin oxide film prior to HCl/Ar exposure. Oxygen in the afterglow gas may lead to in-situ oxidation and subsequent control of etching. A thin oxide film formed prior to cleaning prevents nonuniform etching being at the same time permeable to Cl species. This approach was successfully applied in UV enhanced dry cleaning [6].

The use of O_2 in concentrations of 0.5% to 1.0% in mixtures of HCl/Ar increased observed surface damage of the processed samples, and had a detrimental effect on the oxide breakdown characteristics. Referring back to Fig. 2, in each case the use of O_2 in the afterglow composition resulted in the poorest overall oxide breakdown characteristics for a given process temperature. The damaged surface of a sample exposed to an $HCl/O_2/Ar$ treatment is presented in Fig. 7. The surface was Yang etched [7] to enhance the feature of the defects and is compared to a control sample. The observed damage was formed during a 1 minute treatment at 200°C. The cause of this phenomena may be the reaction of HCl with O_2 in the nonequilibrium plasma producing a greater Cl content in the afterglow or enhancement of nonuniform etching due to nonuniform oxidation. Locally grown oxide will prevent etching in some areas, while the etching will be proceeding in the other areas resulting in increased surface roughness.

Much more promise is shown by the second approach in which an ultrathin oxide is formed on the surface prior to HCl/Ar treatment. The growth of an ultra thin 22 Å oxide film by means of an O_2 afterflow prior to HCl/Ar dry cleaning proved to be useful in preventing the formation of surface roughness. Samples exposed to 10% HCl/Ar afterglow for 5 minutes at 400°C are presented in Fig. 8. The sample treated in O_2 afterglow appears essentially undamaged at this magnification as opposed to the other sample which is extremely rough. Prior to dry cleaning, these samples each had about 20 Å of chemical oxide on the surface following the RCA cleaning process. Following the O_2 afterglow step at substrate temperatures of 400°C or less, the thin oxide film was measured to be 22 Å. In spite of only a slight change in oxide thickness, its performance during subsequent cleaning was substantially different suggesting higher oxide quality and more uniform surface coverage in the latter case. In the extreme case of dry cleaning at 400°C, this modified chemical oxide was much more able to protect the silicon surface. Oxide breakdown statistics for samples treated with O_2 afterglow prior to dry cleaning in HCl/Ar afterglow are presented in Fig. 9. The characteristics are much better than of the samples treated at the same temperature without the oxidation step (Fig.2c). In this case, 50% cumulative failure of capacitors tested occurs at applied fields of as high as 8 MV/cm. This improvement is attributed to the reduction of surface roughness due to the thin oxide film. The results of SIMS characterization not discussed in this paper indicate that the presence of the oxide does not prevent cleaning providing its thickness is adequately controlled.

CONCLUSION

Surface roughness produced by HCl/Ar afterglow cleaning of Si wafers is responsible for inferior breakdown statistics of MOS capacitors formed on these samples. Damage is proportional to both time and temperature of the treatment. Process temperatures of 200°C and times of 30 seconds are found to be appropriate for avoiding

damage. The thickness of the chemical oxide found on the sample surface can influence etching and roughness formation during HCl/Ar afterglow. The use of an O_2 afterglow oxidation step to modify the chemical oxide on the sample surface has been shown to be successful in preventing the formation of surface roughness. This oxidation step may be useful in controlling the uniformity of the ultra thin chemical oxide and allowing the time and temperature range of HCl/Ar afterglow cleaning to be expanded while not inhibiting the cleaning action of the process.

ACKNOWLEDGMENTS

The authors would like to acknowledge Texas Instruments, Inc. for financially assisting with this project, as well as for assistance in preparing contaminated samples for this experiment.

REFERENCES

1. D. Frystak and J. Ruzyllo, in Proceedings of the Seventh Symposium on Plasma Processing, Eds. G.S. Mathad, G.C. Schwartz, and D.W. Hess, The Electrochem. Soc., 1988, p. 125.

2. J. Ruzyllo, A.M. Hoff, D.C. Frystak and S.D. Hossain, J. Electrochem. Soc., 136, 1474 (1989).

3. D.C. Frystak and J. Ruzyllo, J. Electronic Materials, submitted for publication.

4. W. Kern and D. Puotinen, RCA Review, Vol. 31(2), p. 187, June 1970.

5. A Bhattacharyya, C. Vorst and A.H. Carim, J. Electrochem. Soc., 132, 1900 (1985).

6. T. Ito, R. Sugino, S. Watanabe, Y. Nara and Y. Sato, This Volume.

7. K.H. Yang, J. Electrochem. Soc., 131, 1140 (1984).

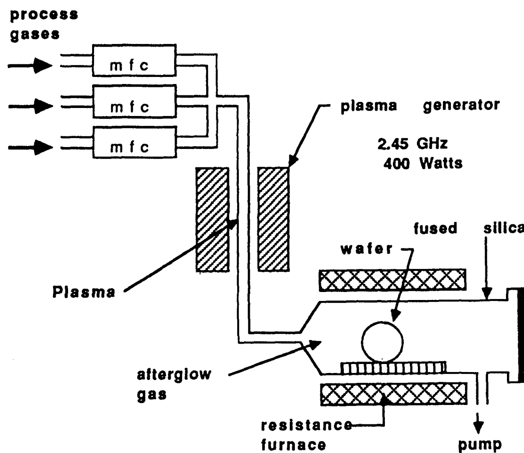

Fig. 1. Remote plasma reactor used in this study.

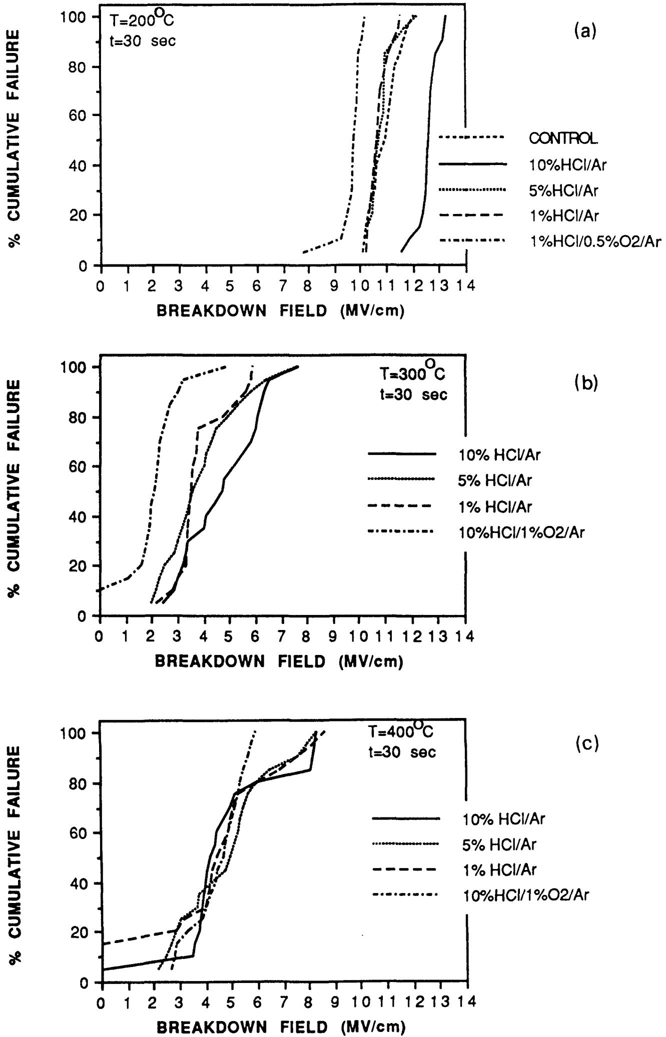

Fig. 2. Oxide breakdown statistics for afterglow processed samples.

Evaluation of Surface Roughness (R)		
Exposure time (secs)	Rpp max (Å)	Light Scattering
0 (Control)	- - -	- - -
30	- - -	Haze
300	1150	Haze

Fig. 3. Development of roughness with time of exposure for samples treated in 10%HCl/90%Ar afterglow at a substrate temperature of 400°C.

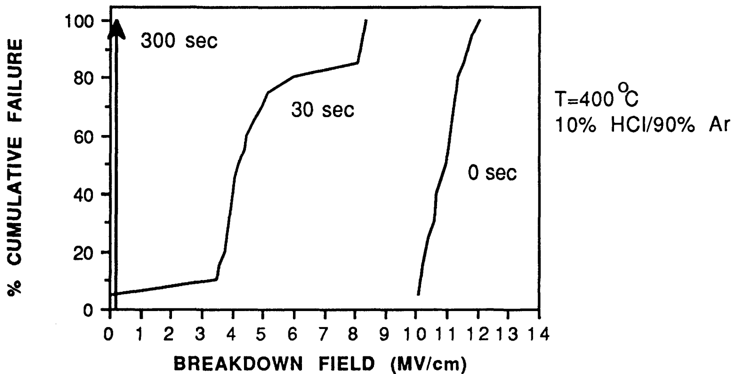

Fig. 4. Degradation of oxide quality with time of exposure of samples treated in 10%HCl/90%Ar afterglow at a substrate temperature of 400°C.

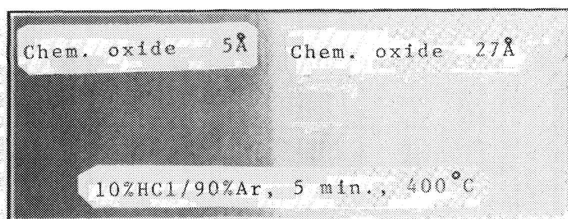

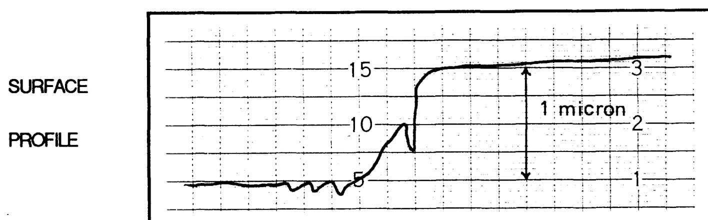

Fig. 5. Rough and undamaged surface regions of a sample processed in 10%HCl/Ar afterglow for 5 min. at 400°C. Roughness is related to the thickness of the chemical oxide on the surface.

Temp	Oxide Thickness	Time	Si Etched	ETCH RATE	Nature of Surface Damage
(°C)	(Å)	(min)	(microns)	(micron/min)	
200	7	1	0.07	0.07	
200	5-7	5	0.4-0.72	0.08-0.14	Roughness, Haze
200	20	5	0	0	Haze
400	5	5	1.0	0.2	Very Rough
400	20	5	1.0	0.2	Very Rough
400	27	5			Slight Haze

Fig. 6. Summary of etching and surface damage observed for samples with different initial oxide thickness. Samples were treated in a 10%HCl/90%Ar afterglow gas mixture at the temperatures and times listed.

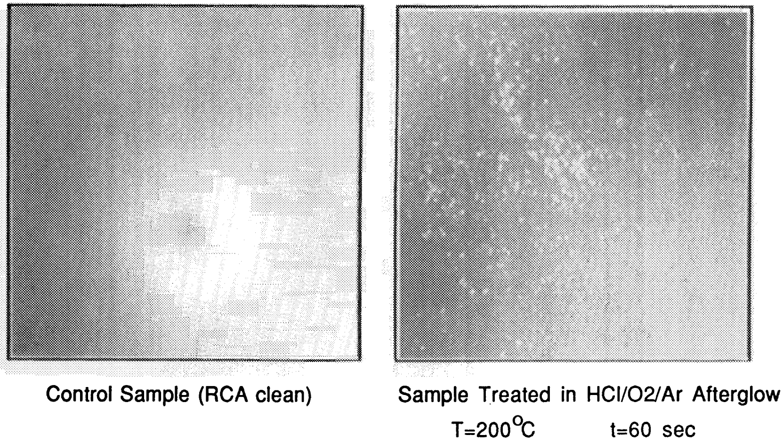

Fig. 7. Severe damage as a result of exposure to $HCl/O_2/Ar$ afterglow for 60 sec. at $200^{\circ}C$. Surfaces were Yang etched for 20 seconds to enhance visibility of the damage.

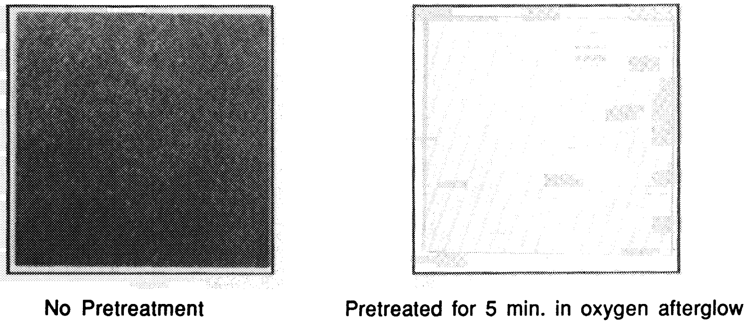

Fig. 8. Prevention of surface roughness observed when the sample is pretreated in O_2 afterglow prior to 10%HCl/90%Ar afterglow exposure for 5 minutes at $400^{\circ}C$.

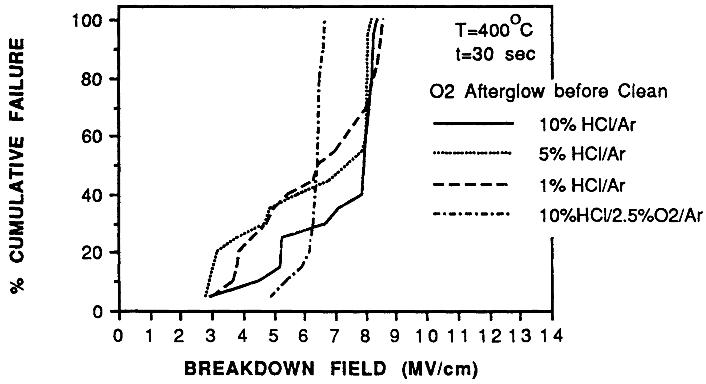

Fig. 9. Oxide breakdown statistics for samples treated with O2 afterglow prior to dry cleaning in HCl/Ar afterglow.

ELIMINATION OF METAL CONTAMINATION FROM PHOTORESIST BY USING OZONE ASHING TECHNIQUE

Shigeo Onishi, Kenzo Matsuda, Kenichi Tanaka, and Keizo Sakiyama

Sharp Corp., IC-Group, A1136 Project Team,
2613-1, Ichinomoto-cho, Tenri-city, Nara 632, Japan

ABSTRACTS

The effect of preventing metal contamination during photoresist ashing has been found by using oxygen radicals generated by thermal decomposition of ozone gas. During photoresist ashing treatment, various kinds of metals in the photoresist accumulate at the sample surface. This residue consists largely of heavy metals rather than lighter metals. In O_2 plasma ahing, metal impurities in the photoresist are easily knocked on into the samples. Especially, most of Na^+ atoms residue in the sample and this causes a shift in the V_{FB} of MOS devices. On the other hand, the ozone ashing treatment does not exhibit the knock-on phenomenon, so that metal impurities on the sample can be easily removed by a subsequent cleaning process (H_2SO_4).

INTRODUCTION

As device dimensions has been scaled down, dry etching technology has been at the fore. However, dry etching is usually performed in a plasma environment, so damage introduction to the device can be a serious problem.[1-3] Generally, the following three phenomena are considered as "damage". First, Si-Si and Si-O bonds in the silicon crystal or the SiO_2 film are cut because of energetic particle bombardment to the sample, and crystalline defects and traps are formed. Second, metal impurities are knocked on into the sample because of collisions of energetic particles. Third, gate oxide films are destroyed by the charge-up phenomenon associated with the charged particle in the plasma environment.

For some time, O_2 plasma ashing has been in general use for photoresist ashing processes, and many problems has been reported concerning damage introduction. Fujimura reported that heavy metals in the photoresist were knocked on into the underlying silicon substrate during O_2 plasma ashing and minority carrier lifetimes were degraded. Tsumura reported that the flat band voltage in MNOS (Metal-Nitride-Oxide-Silicon) structures shifted because of the charge-up phenomenon during photoresist ashing. Degradation of gate oxide films occures in actual LSI fabrication processes.

From this background, the ozone ashing technology has been developed for the prevention of damage introduction. In this technique, photoresist is ashed by utilising oxygen radicals generated by thermal decompotition of

ozone gas, so the ozone ashing is considered to be useful in preventing device damage. In this work, photoresist ashing was performed with the ozone ashing equipment, and it has been found that this method is effective in preventing metal contaminations from the photoresist into the samples.

EXPERIMENTAL

Metal contaminations were investigated by utilizing BT (Bias and Temperature) stress tests of MOS diodes, atomic absorption analysis and SIMS (Secondary Ion Mass Spectroscopy). As shown in Table 2, the photoresist used in this work contains several metal impurities (Na, Al, Cr, Mo, Cd). Also, the comparison was made with both O_2 plasma ashing and ozone ashing equipment that are commonly used in a production process. Fig. 1 shows the temperature dependence of the ashing rate for ozone ashing equipment. The ashing rate abruptly increased above 250°C. A throughput equivarent to O_2 plasma ashing was obtained at temperatures above 300°C , so metal contamination was evaluated at ozone ashing temperatures above 300°C. The typical condition for O_2 plasma ashing was with RF power at 800W, and ashing temperature at 150°C. A 100% overetch was performed for both O_2 plasma and ozone ashing treatments.

MOS diodes were fabricated according to the process flow shown in Fig. 2. Oxide films of 200Å in thickness were grown on p-type (100) silicon substrates, then four groups of samples were fabricated. First, photoresist (1.2µm) was coated on the sample, then removed in boiling H_2SO_4. Second, an O_2 plasma or ozone ashing treatment was performed without a photoresist coating, then a boiling H_2SO_4 treatment was done. Third, an O_2 plasma ashing treatment was performed after photoresist coating, then a boiling H_2SO_4 was performed. Forth, a reference wafer was treated with only the boiling H_2SO_4. The above process was repeated five times, then n^+-polysilicon films were deposited and MOS diodes were fabricated by patterning polysilicon. The BT stress test conditions were an applied voltageof +5V and -5V, and heat treatment at 280°C for 10 min.

For the SIMS analysis samples, photoresist was coated on silicon wafers after growing thermal oxide films (200Å), and photoresist ashing with a following boiling H_2SO_4 treatment was performed. SIMS and atomic absorption analysis were done for samples both before and after the H_2SO_4 treatment.

RESULTS AND DISCUSSION

Table 1. shows the results ($\triangle V_{FB}$ values) obtained from BT stress tests of MOS diodes. When O_2 plasma ashing was performed after photoresist coating, large $\triangle V_{FB}$ values of about -1.0V were obtained. When photoresist removal was performed by a boiling H_2SO_4 treatment, or O_2 plasma treatment was performed without photoresist coating, $\triangle V_{FB}$ values hardly shiftedand were equivalent to that of the reference sample. From these results, it is supported that mobile ions contained in the photoresist were knocked-on into the underlying SiO_2 films. Next, the depth profile o mobile ions in the SiO_2 films were examined. A boiling H_2SO_4 treatment was

performed after photoresist ashing (repeated five times), then the SiO_2 films were etched in an HF solution. Fig. 3 shows the depth profile of $\triangle V_{FB}$ values and mobile ion concentrations as calculated from the $\triangle V_{FB}$ changes. The $\triangle V_{FB}$ monotonously decreased against the etched thickness of the SiO_2 films and mobile ions of about 10~15ppm were knocked-on above 100Å of SiO_2 thickness. On the other hand, for the ozone ashing treatment, a very small $\triangle V_{FB}$ value, equivalent to the reference wafer, was obtained. Similar results were obtained for ozone ashing between 300°C and 400°C.

The following results of the metal impurities investigation were obtained from SIMS analysis. Fig. 4 shows the depth profile of Na^+ concentration after photoresist ashing and after H_2SO_4 treatment. After photoresist ashing it was found that the Na^+ concentration for ozone ashing was one order of magnitude higher at the sample surface and was lower in the SiO_2 films, compared with the O_2 plasma ashing treatment. When the sample was analysed after H_2SO_4 treatment, Na^+ ions in the oxide film were completely removed and the concentration was below the detectable limits. For O_2 plasma ashing, however, Na^+ ions in the oxide film were not removed and the concentration of about 2 ~3 ppm was detected. This value corresponds to the concentration of mobile ions for one ashing as obtained from the BT stress test. The following conclusions are obtained from the results shown in Fig. 4. For O_2 plasma ashing, Na^+ ions were knocked on into the oxide films and could not be removed by a boiling H_2SO_4 treatment. For ozone ashing, Na^+ ions were simply adsorbed at the SiO_2 surface and were easily removed by the H_2SO_4 treatment.

Table. 2 shows the results obtained from SIMS for other metals. Metal impurities (Na, Ca, Al, Cr, Mo, Cd) were detected after photoresist ashing for both O_2 plasma and ozone ashing. These impurities were contained in the photoresist itself, and were not detected when the ashing treatment was performed without the photoresist coating. Thus, it is believed that metal impurities contained within the photoresist accumulated at the sample surfaces. Fig. 5 shows the ratio of metal impurities on the oxide films after photoresist ashing to metal impurities in the photoresist. Light metals (Na, Al, Ca) had little accumulation on the samples during photoresist ashing, however, heavy metals (Cr, Mo, Cd,) accumulated to a greater extent. When a boiling H_2SO_4 treatment was performed after ozone ashing, mosts of metal impurities were removed and very small impurity concentrations, equivalent to the reference wafers, were obtained. This effect was confirmed at ashing temperatures between 300°C and 400°C. On the other hand, for O_2 plasma ashing, metal impurities were difficult to remove in boiling H_2SO_4, and remained on the samples. Fig. 6 shows the ratio of metal impurities after H_2SO_4 treatment to metal impurities after photoresist ashing. Mosts of the Na atoms in the O_2 plasma sample could not be removed by the H_2SO_4 treatment and remained as residue. The ratio of metal impurities remaining in the samples decreased with an increased mass number.

From the results of SIMS analysis, a mechanism of metal contamination due to the ashing process is introduced as follows. During resist ashing treatment, various kinds of metals in the photoresist accumulate at the sample surface. At this time, heavy metals (Cr, Cd, Mo) accumulate to a

greater degree than do the lighter metals (Na, Al). In the case of the O_2 plasma ashing treatment, metal impurities are knocked-on into the samples due to the bombardment of energetic particles. On the other hand, for the ozone ashing treatment, it is believed that most of the metal impurities are adsorbed at the sample surface. Thus, these impurities can be easily removed by cleaning in boiling H_2SO_4. It is concluded that the ozone ashing process is effective in preventing metal contamination from the photoresist in the temperature region between 300 °C and 400°C where throughput higher than O_2 plasma ashing throughputs can be obtained.

CONCLUSIONS

Metal contamination due to photoresist ashing was evaluated by using both O_2 plasma and ozone ashing equipment, and the following conclusions are offered.

1) Metal impurities contained within the photoresist accumulated at the sample surface during the photoresist ashing. Heavy metals accumulated to a greater degree than light metals.

2) For O_2 plasma ashing, metal impurities were knocked-on into the samples. In particular, most of the Na atoms were left as residue in the sample, inducing V_{FB} shift in actual MOS devices.

3) For ozone ashing, metal impurities were adsorbed at the sample surface without the knock-on phenomena, so they were easily removed by cleaning in a boiling H_2SO_4 solution. In actual MOS devices, V_{FB} did not shift and was stable.

ACKNOWLEDGMENT

The authors would like to thank R. Miyake for his helpful support.

REFERENCES

1) N. Hayasaka and H. Okano, 1988 Dry Process symp. (1988) 125.
2) Y. Yoshida and T. Watanabe, Proc. 5th Symp. Dry Process (1983) 4.
3) H. Akiya, K. Saito and K. Kobayashi, Jpn. J. Appl. Phys., (1981) 20

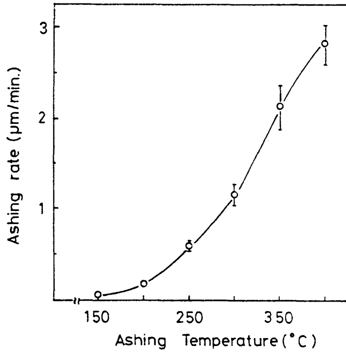

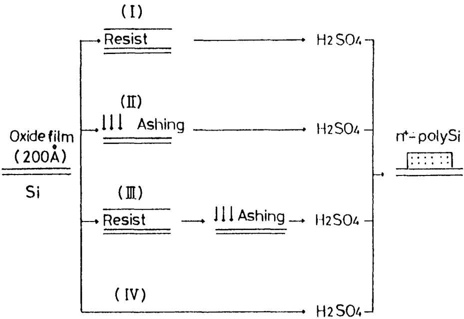

Fig. 1 Temperature dependence of the ashing rate for ozone ashing equipment.

Fig.2 Fablication process flow of MOS diodes for evaluating BT stress test.

Process	(I) Resist + H_2SO_4	(II) O_2 plasma + H_2SO_4	(III) Resist + O_2 plasma + H_2SO_4	(III) Resist + Ozone + H_2SO_4	(IV) H_2SO_4
ΔV_{FB}(V)	- 0.01 ~ - 0.03	- 0.01 ~ - 0.05	- 0.65 ~ - 1.0	- 0.03 ~ - 0.05	- 0.02 ~ - 0.03

Table.1 ΔV_{FB} values obtained from BT stress test

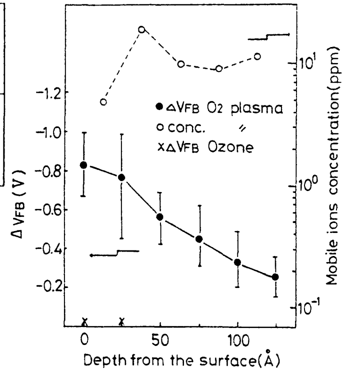

Fig.3 Depth profile of ΔV_{FB} values and mobile ion concentrations as calculated from the ΔV_{FB} changes.

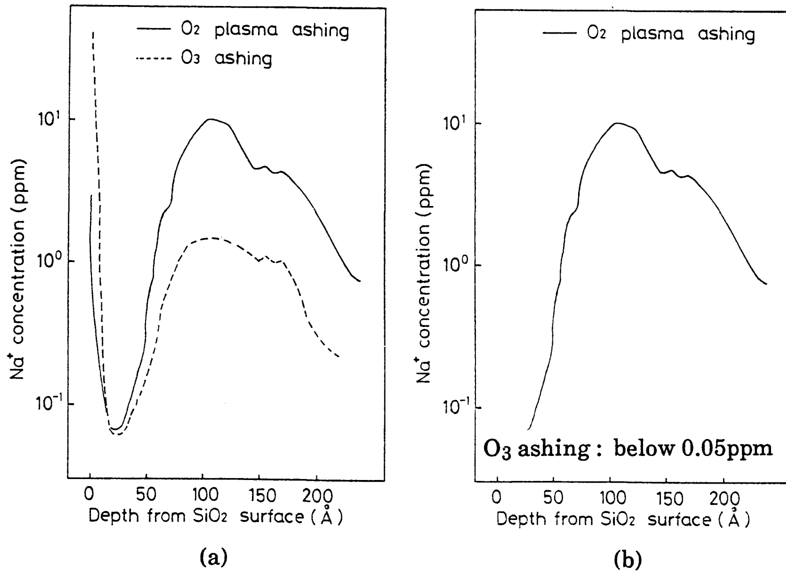

Fig.4 Depth profile of Na atoms (a) after photoresist ashing ,and (b) after H_2SO_4 treatment.

	Na	Al	Ca	Cr	Mo	Cd
Photoresist(ppm)	2.0	8.2	3.1	0.7	0.5	0.4
O_2 plasma(ppm)	3.5	4.7	0.82	1.6	1.3	4.9
O_2 plasma+H_2SO_4(ppm)	3.7	0.72	0.29	0.024		
Ozone(ppm)	5.0	4.4	0.55	17.6	0.7	2.8
Ozone+H_2SO_4(ppm)	—	0.18	0.05	—	—	—
Ozone(no resist)(ppm)	—	0.15	0.06	—	—	—
Reference(ppm)	—	0.14	0.06	—	—	—

Table. 2 Concentration of metal impurities obtained from SIMS analysis

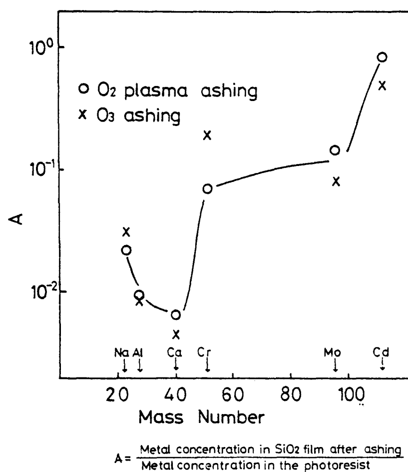

Fig.5 Ratio of metal impurities on the oxide films after photoresist ashing to metal impurities in the photoresist.

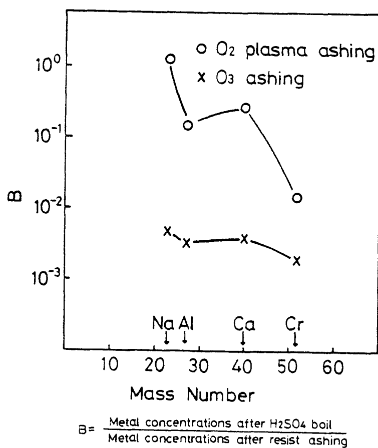

Fig.6 Ratio of metal impurities after H2SO4 treatment to metal impurities after photoresist ashing.

ETCH PROPERTIES OF THERMALLY OXIDIZED SILICON NITRIDE: COMPARISON OF WET AND DRY ETCHING RESULTS

Lee M. Loewenstein and Charlotte M. Tipton

Semiconductor Process and Design Center
Texas Instruments Incorporated
Dallas, TX 75265

ABSTRACT

The ability to etch silicon nitride changes after this material is exposed to an oxygen ambient, as a result of the partial oxidation of the silicon nitride to form a silicon oxynitride. We have measured the etch rate of silicon nitride exposed to different temperatures and oxygen pressures, to determine how these parameters affect the cleanup steps needed in local oxidation of silicon-based processing sequences. Both wet (hydrofluoric acid and phosphoric acid) and dry (SF_6-based remote plasma) cleanup methods are described and correlated to Rutherford backscattering measurements. Our results show the presence of an oxidized layer which requires process modification for removal.

INTRODUCTION

The use of Si_3N_4 as a masking material for local oxidation of Si is commonly employed during device manufacture. The technique involves using a thin oxide layer, or "pad" oxide, beneath the Si_3N_4 mask as an etch stop when removing the mask. As geometries grow smaller, pad oxide thicknesses are driven thinner to minimize encroachment of the newly grown oxide into desired masked regions. Thinning of pad oxides requires higher Si_3N_4:SiO_2 selectivity etches for removal of Si_3N_4 masks.

The use of higher selectivity etches also requires a greater understanding of the effects of surface oxidation of Si_3N_4 films during oxidation processing. This paper will compare wet and dry etching techniques for removal of Si_3N_4 films. Furthermore, due to issues such as the "bird's beak" phenomenon[1] which effect device performance and consequently determine the choice of oxidation conditions, a variety of oxidation conditions are examined.

Wet chemical etching of Si_3N_4 in a bath of H_3PO_4 is well known[2], and is standard in Si wafer processing. A substantial overetch may be performed to ensure complete Si_3N_4 removal as the process is highly selective to SiO_2 (see Table 1). Since the surface of the Si_3N_4 is oxidized during the formation of an isolation oxide, removal of the Si_3N_4 must actually begin with a HF etch or "deglaze" to remove SiO_2 and any mixed SiO_xN_y.

The dry method of removing the SiO_xN_y, Si_3N_4, and also the poly-Si, depends on the use of a downstream or remote microwave plasma system. The etch selectivities of one material to another may be altered by adjusting the wafer temperature as well as the gas composition. This has been shown for SiO_2 etching with respect to Si[3], and Si_3N_4 etching with respect to SiO_2[4,5]. Since the wafer does not lie on an electrode, and the discharge region is, in fact, substantially removed from the process chamber, there should be minimal damage to the substrate either by

ions or by radiation. In addition, processes performed in remote plasma reactors will be isotropic, and thus potentially direct substitutes for wet stripping processes.

EXPERIMENTAL

The Si_3N_4 was grown by low pressure chemical vapor deposition. Combinations of temperature (875 and 975 °C) and oxygen pressure (1, 10 and 25 atm) were used to produce SiO_xN_y of varying composition and thickness. The oxidation times were varied for the different process conditions so 8000 Å of thermal SiO_2 would be grown by the oxidation of 100 mm diam. Si <100> under those conditions. The conditions are summarized in Table 1.

The wet etching consisted of etch procedures using either 5% HF or 0.5% buffered HF aqueous solution at 20 °C to strip the oxynitride layers, followed by boiling H_3PO_4 at approximately 160 °C to etch the underlying Si_3N_4. The buffering agent for the 0.5% HF solution was 40% NH_4F. The HF chemistries were run in stagnant immersion baths, while the H_3PO_4 was run in a commercially available refluxed heated quartz bath (Imtec, model QN110) with continuous deionized (DI) water addition capability. The system used a quartz tank with Inconel heaters bonded to the exterior of the quartz walls for heating. An inverted quartz tank with Teflon cooling coils mounted on the interior served as the reflux lid. DI water was added to the hot acid bath through a manifold in the top of the lid at a rate of 4.2 ml/min. All wafers were rinsed in DI water following the acid treatments, and spin-rinse dried.

The dry method used a microwave-based remote plasma reactor constructed at Texas Instruments, and has been described previously[3,4]. The gases used included SF_6 (45 sccm), and N_2 (1500 sccm), which passed through the discharge, and H_2 (25 sccm), which bypassed the discharge. This gas chemistry is known to etch thermal Si_3N_4 with reasonable selectivity to SiO_2.[4] The process temperature was 100 °C, and the pressure 2.0 Torr. Microwave power at 2.45 GHz was about 600 W.

The etches were halted periodically to measure film thicknesses and to infer etch rates, using an ellipsometer (Gaertner, model L115B).

RESULTS

A. Wet etching

Wet etching results showed an increasing oxynitride thickness with increasing temperature and pressure used during oxidation. Relative oxynitride thicknesses were determined by repetitive etching of wafers in HF solutions. Since HF chemistries etch SiO_2 with significant selectivity to Si_3N_4, changes in etch rate can indicate a change in film type. Wafers representative of each set of oxidation conditions (see Table 1) were processed through multiple passes of each of the two HF solutions, 5% HF and 0.5% buffered HF. Ellipsometric measurements were made to determine the total film thickness (SiO_xN_y and underlying Si_3N_4) before and after each pass through the etchant. The etch run where a drop in etch rate occurred marked entry into the underlying Si_3N_4, as shown in Fig. 1. The total etch time before this run was recorded as the time required to remove the SiO_xN_y film. A summary of these etch times is presented in Table 1. Failure to adequately remove the oxynitride with HF resulted in gross nonuniformities in subsequent Si_3N_4 etching with H_3PO_4. The H_3PO_4 etched the SiO_xN_y in a slow, nonuniform fashion which was exaggerated by the relatively rapid etching of the underlying Si_3N_4 once it was exposed.

Once the SiO_xN_y layer was removed, etching with H_3PO_4 of the Si_3N_4 films showed a shift in etch rates which was dependent on the temperature, but independent of the pressure, of the local oxidation process. Initial film thickness measurements were made after an HF treatment adequate to remove all SiO_xN_y. Final film thickness measurements were made after a 20 minute etch time in the H_3PO_4. Higher temperature oxidations resulted in lowering Si_3N_4 film etch rates, while oxidation pressure had no effect. A summary of etch rates is listed in Table 1.

B. Dry etching

The thicknesses of the Si_3N_4 layer after etching for given amounts of dry etching time are shown respectively in Figs. 2 and 3 for samples either first deglazed according to the wet chemical procedure described above or etched solely according to the dry remote plasma chemistry. For comparison, the etch behavior of SiO_2 and Si_3N_4 standards are also presented in the figures. The HF deglazed samples all etched similarly, regardless of the prior oxidation conditions, while the completely dry etched wafers showed substantial variability. For the Si_3N_4 wafers having undergone the oxidation procedure, etch behavior appeared initially similar to the SiO_2 standard, whereas at a later time the etch behavior appeared more like Si_3N_4. A transition region existed between these two extremes. The time of onset of this transition region depended on the oxidation conditions, with the earliest transition being for the 875 °C/1 atm oxidation and the latest for the 975 °C/10 and 25 atm oxidations.

The etch rate-film thickness relationships for the deglazed and as-grown Si_3N_4 films are shown respectively in Figs. 4 and 5a-b. Fig. 4 shows the slowly increasing etch rates deeper in the film, for the films once they have been deglazed. Figs. 5a-b show the etch rates increasing with depth, generally in a sigmoidal fashion. The lowest temperature, lowest pressure oxidation (850 °C, 1 atm) resulted in a film whose etch rate was proportional to a film depth of about 250 Å. Below this depth, the etch rate was approximately constant (600 Å/min). The two other Si_3N_4 films that were oxidized at 850 °C showed etch rates that were constant or slowly rising (15-25 Å/min) below a depth of 30 Å. Then they entered a transition region where the etch rate increased with depth, as with the 1 atm-grown film. At a depth of nearly 800 Å, the etch rates reached a plateau where the etch rate was 700-800 Å/min. Similar results were obtained for the Si_3N_4 films that were oxidized at 975 °C. It is noteworthy that the etch rate at the native surface is lower than that of thermal SiO_2 prepared by direct oxidation of the Si (150 Å/min under the dry etch conditions employed). The etch rate behavior is presented in Table 2.

From the log-log plots of Figs. 5a-b, it appears that the etch rate had an exponential dependence on the film thickness in the transition region:

$$R \sim d^n \qquad (1)$$

Values for n are presented in Table 2.

DISCUSSION

The variation in dry etch rates as we etched through the films can be explained by a model of the film that consists of three layers subsequent to oxidation. On the surface of the film is a layer of approximately stoichiometric SiO_2. Beneath this layer is a region that is graded in composition from SiO_2 to Si_3N_4, i.e., SiO_xN_y. At the base of this film is a layer of Si_3N_4 which has not been

oxidized, but may be altered in some way (e.g., densification) by the application of a combination of high temperature and pressure.

To study the nature of the film, we have employed Rutherford backscattering (RBS). The composition of each SiO_xN_y layer was derived from depth profiles with units of areal density (g/cm^2). Linear combinations of density of SiO_2 and Si_3N_4 were used to derive densities for each layer. A representative depth profile using this method is shown in Fig. 6. Fig. 7 highlights the dependence of the O level on film depth. The thickness of each SiO_xN_y layer was determined from the depth profiles assuming that the interface of the SiO_xN_y/Si_3N_4 layer occurs when the oxygen atomic fraction has fallen to half its initial value. The layer compositions and densities used are tabulated in Table 3, along with the computed thicknesses.

The layer composition agrees in general with the level of oxidation of the Si_3N_4 that might be expected following oxidation. Low temperature/low pressure oxidation has the least effect on the film, which consequently has the highest Si_3N_4 composition and density of the post-oxidation films. Conversely, the films processed under the most strongly oxidative conditions were largely SiO_2, with only a small amount of Si_3N_4 remaining.

The oxidation conditions affect dry etch rates according to the amount of oxygen incorporated into the film, and also by any densification of the film. Fig. 4 shows two effects for HF-deglazed samples: (1) etch rates slowly increase with depth, presumably as the vestigal oxygen concentration declines; and (2) the 850 °C and 975 °C-oxidized wafers have etch rates that tend to cluster together as separate groups. This may be due to densification of the Si_3N_4 film.

The convention of choosing the interface position as a drop by one-half of the atomic oxygen signal results in thickness values that are approximately half of those that we obtained by etch rate measurements. The average ratio of the etch rate thickness to the RBS thickness is 2.1 ± 0.5, in good agreement with the hypothesis. Consequently, in the transition region, we can reasonably assume that the etch rate is dependent to the compositional balance, with the resultant etch rate being proportional to the linear combination of etch rates for the mixed materials.

Wet etch rates were different from the dry etch rates in several respects. No very low etch rate was seen at the top of the oxidized Si_3N_4. While the wet etch methods, 0.5% BHF and 5% HF, agreed in the depth of the oxidized layer, the thicknesses which they determined were in accordance with the unadjusted RBS values rather than the dry etch ones. This difference may result from the higher selectivity of the wet etches as compared to the dry one: once the film is much more like nitride than oxide, the etching stops completely, while for the dry etch, which was designed primarily to etch Si_3N_4, the etch begins slowly in the oxide, then speeds up as the material become more of a nitride.

CONCLUSIONS

The Si_3N_4 film used as a mask for the local oxidation of Si may be removed by either wet or dry means. The condition of the Si_3N_4 after the oxidation must be understood and accounted for when etching this film. When using HF/H_3PO_4, the variation of the oxidized film thickness requires longer HF deglaze times for more strongly oxidizing conditions. The hot H_3PO_4 process to remove the underlying Si_3N_4 must also be adjusted, as the etch rate of Si_3N_4 depends to some extent, as well, on the prior oxidizing environment. Dry etching must encompass an SiO_xN_y etch rate that increases with time, reaching a plateau value for the underlying Si_3N_4 that is dependent on the prior oxidation step. As the SiO_xN_y film is so slow to etch, small variations in either the

nature of the deposited Si_3N_4 or the oxidizing environment may have large effects on the time needed to remove the Si_3N_4 film entirely. As a consequence, an endpoint system is highly desirable.

ACKNOWLEDGMENTS

The RBS measurements were taken by J. Keenan. R.K. Pohlmeier, G. Schneider, S. Hughes and M. Kasner assisted us in this work. The research was sponsored in part by the DARPA Defense Sciences Office and the AF Wright Research and Development Center, Manufacturing Technology Directorate and Electronics Technology Laboratory under contract F33615-88-C-5448.

REFERENCES

1. T.A. Shankoff, T.T. Sheng, S.E. Haszko, R.B. Marcus, and T.E. Smith, J. Electrochem. Soc. **127**, 216 (1980).
2. W. van Gelder and V.E. Hauser, J. Electrochem. Soc. **114**, 869 (1967).
3. L.M. Loewenstein, J. Vac. Sci. Technol. A **6**, 1984 (1988).
4. L.M. Loewenstein, J. Vac. Sci. Technol. A **7**, 686 (1989).
5. S. Suto, N. Hayasaka, H. Okano and Y. Horiike, J. Electrochem. Soc. **136**, 2032 (1989).

TABLES

Table 1. Wet etch rates of thermal SiO_2, LPCVD Si_3N_4, oxidized Si_3N_4 and its underlying Si_3N_4 in HF and H_3PO_4.

Oxidation Conditions			0.5% HF		5% HF		H_3PO_4
T(°C)	P(atm)	t(min)	d(Å)	Rate[a]	d(Å)	Rate[a]	Rate[a]
850	1	1107	36	100	45	158	44
850	10	105	190	126	178	326	44
850	25	49	317	194	289	501	44
975	1	266	164	170	163	496	41
975	10	23	334	159	335	433	41
975	25	16	507	181	484	472	42
	Thermal SiO2		-	70	-	250	<1
	LPCVD Si3N4		-	<1	-	8	50

[a]Units: Å/min

Table 2. Dry etch properties of as-oxidized Si_3N_4: apparent film thicknesses, d, etch rates, R, and transition region exponent, n.

Oxidation Cond.		Top film		Mid.	Lower film	
T(°C)	P(atm)	d(Å)	Rate[a]	n	d(Å)	Rate[a]
850	1	-	-	1.3	250	600
850	10	40	20	1.9	300	600
850	25	45	25	1.7	700	700
975	1	200	20	1.3	400	500
975	10	60	23	2.0	400	600
975	25	100	30	2.4	600	700

[a]Units: Å/min

Table 3. RBS compositional analysis of oxidized Si_3N_4.

Oxidation		Layer composition			Density	d(Å) SiO_xN_y		d(Å)
T(°C)	P(atm)	Si_3N_4/SiO_2/Si			(g/cm³)	RBS[a]	RBS[b]	Si_3N_4
850	1	5	2	0	3.14	100	50	2010
850	10	3	5	0	2.74	190	180	2110
850	25	1	4	5	2.43	240	290	2050
975	1	2	3	0	2.76	170	170	1980
975	10	1	4	1	2.50	250	340	2050
975	25	1	2	0	3.69	240	310	1950

[a]Computed from integrated area
[b]Computed from peak height

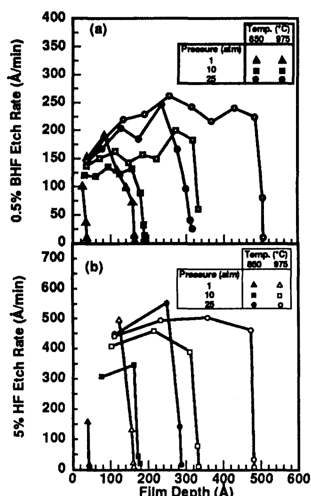

Fig. 1. Wet etch rate as a function of film depth for as-oxidized Si^3N^4 films: (a) 0.5% buffered HF, (b) 5% HF.

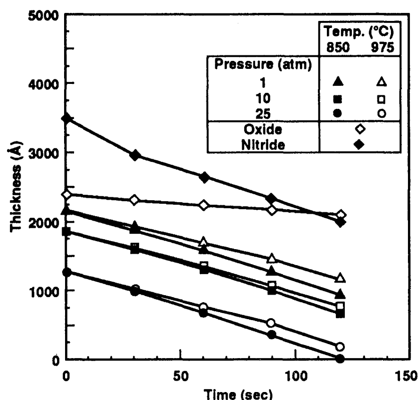

Fig. 2. Dry etch behavior of HF-deglazed Si_3N_4, thermal SiO_2, and LPCVD Si_3N_4. Thicknesses have been offset by constant factors for display purposes.

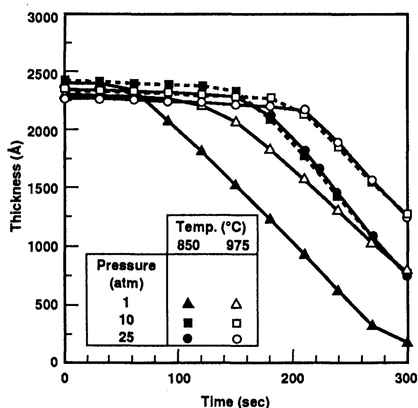

Fig. 3. Dry etch behavior of as-oxidized Si_3N_4.

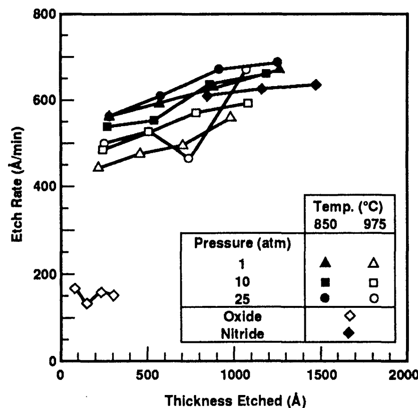

Fig. 4. Etch rate as a function of film depth for HF-deglazed Si_3N_4 films, thermal SiO_2, and LPCVD Si_3N_4.

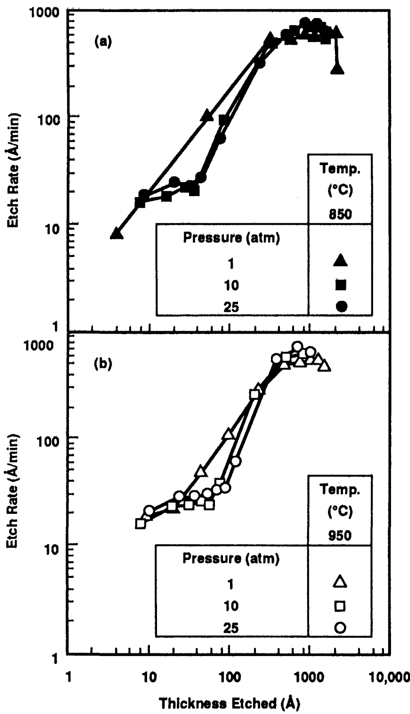

Fig. 5. Etch rate as a function of film depth for as-oxidized Si_3N_4 films:
(a) 850°C, and (b) 975°C.

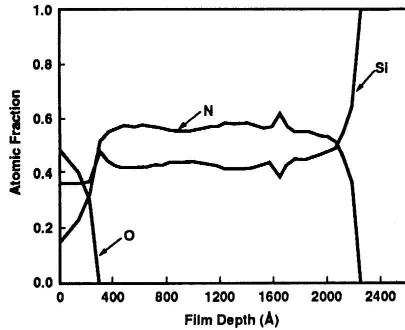

Fig. 6. Sample RBS depth profile of Si, O, and N for as-Oxidized Si_3N_4 film (25 atm, 975°C).

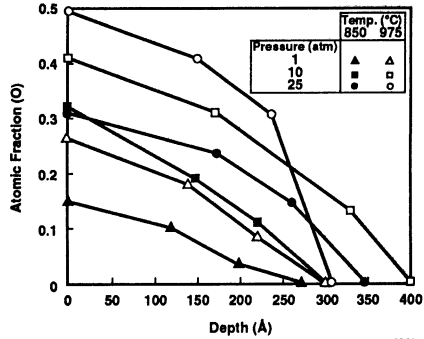

Fig. 7. RBS depth profiles of O for as-oxidized Si_3N_4 films.

EFFECTS OF LOW-CONCENTRATION-O_2 IN N_2 ON Si SURFACE CLEANING FOR SOLID PHASE EPITAXY

Yasuo KUNII

NTT LSI Laboratories,
Nippon Telegraph and Telephone Corporation,
3-1, Morinosato Wakamiya, Atsugi-shi,
Kanagawa, 243-01 Japan.

The oxygen adsorption and reaction process on Si clean surface in N_2 with low-concentration O_2 is examined for surface cleaning prior to solid phase epitaxy of CVD a-Si. Si clean surface is shown to be oxidized up to 2-4 A in N_2 with O_2 (<10 ppb) at 600℃, and up to 7-10 A at 900℃. Measuring the O_2 concentration increase after O_2 addition (330 ppb) to N_2 at 800-900℃, information about Si surface cleanness in a CVD reactor is obtained.

INTRODUCTION

Solid phase epitaxy (SPE) of deposited amorphous Si (a-Si) is a promising technique for realizing 3-dimensional integration of electronic devices (1-9). The crystalline quality of SPE layers plays a key role in fabricating devices, and it is very sensitive to the degree of interface cleanness between the deposited layer and the substrate. In the surface cleaning process for SPE of CVD a-Si, surface native oxide is removed by H_2 gas etching (1) or Si_2H_6 gas etching (7). However, some contaminates will be adsorbed after the gas etching, and deteriorate the interface cleanness.

The relationship between the interface cleanness and crystallinity has been studied using secondary ion mass spectrometry (SIMS), cross-sectional transmission electron microscopy (XTEM), etc. (5,7,8). The results are summarized below.

Small contrast centers with twins at the bottom of vertical-SPE (V-SPE) layer, dislocations in V-SPE layer and dips of V-SPE growth front were observed by XTEM (8), as schematically shown in Fig. 1. The defects in V-SPE layers were mainly dislocations extending from contrast centers to dips of V-SPE growth front. Also, small twins were observed near the contrast centers. The twin region is restricted near the contrast center. In the surface

cleaning process of this sample, the native oxide layer at the substrate surface was removed by Si_2H_6 gas etching (7), and a thin vertical vapor phase epitaxial layer (V-VPE) was formed after the removal of the native oxide. Therefore, the lowest layer in Fig. 1 is denoted as "V-VPE & Sub.".

The suspected contaminates between the deposited a-Si layer and the substrate are oxygen and carbon. The concentration of O_2 and H_2O gases contained in the carrier gas of the present CVD system is of the order of 10 ppb. Also, some carbonic gases will be contained in the carrier gas. SIMS measurement showed that, in the region between V-SPE layer and substrate, the detected oxygen peak was $1x10^{20}$ cm^{-3}, whereas the carbon concentration was $<3x10^{17}$ cm^{-3} (7). Therefore, oxygen will be the most dominant contaminate at the interface.

Accordingly, oxygen will be contained in the contrast centers at high concentrations. The presence of oxygen deforms the Si lattice, and the strained lattice creates contrasts in TEM image. These centers were probably formed through segregation of oxygen before V-SPE. The speculated formation process of dip, twin, and dislocation is shown in Fig. 2. The dip was formed by the high concentration of oxygen presented in the contrast centers, because the presence of oxygen decreases SPE growth rate (10). The twin could be easily formed on {111} facets existing at the dip (4). The dislocation was probably formed by coalescence of strained growth fronts at the dip.

As shown by the previous results, the origin of the defects in V-SPE layer is the high concentration of oxygen. The origin of oxygen in the contrast center is probably O_2 or H_2O in the carrier gas of the CVD system. Although purified N_2 gas is used as a carrier gas for the a-Si CVD in our experiments, the ambient gas in the reactor contains a low-concentration of O_2. This probably comes from the residual O_2 in purified gas, small leaks, out-diffusion from the reactor wall, etc.

Therefore, clarifying the oxygen adsorption and reaction process in a low-concentration range is important for studying surface cleaning prior to the a-Si CVD for SPE. In this paper, oxygen adsorption and reaction process on Si clean surface in N_2 has been studied in the O_2 concentration range between <10 ppb (purified N_2) and 330 ppb (purified N_2 + O_2).

EXPERIMENTAL

The substrates used were p-type Si (100), (110), and (111) wafers 100 mm in diameter, and their resistivities were in the 4-6 Ω cm range. The substrates were precleaned using H_2SO_4+H_2O_2, HCl+H_2O_2+H_2O, HF+H_2O, H_2O rinse and drying. The substrates were loaded into an atmospheric pressure RF-heating reactor with a silicon-coated susceptor.

The Si surface of substrates and susceptor was cleaned by H_2 gas etching at 1080℃ for 2-8 min. The ambient in the reactor was pumped and analyzed by a dew-point meter and an O_2 concentration meter (Fig. 3). The H_2O concentration was measured by an electric-capacitance-type meter. O_2 concentration was measured by a galvanic-cell-type meter. The concentration of H_2O and O_2 in the ambient gas was normally <10 ppb after H_2 gas etching.

After the substrate temperature was lowered to the intended temperature, the ambient was switched from H_2 to N_2. After that, a small amount of O_2 was added into the N_2 for some experiments. The amount of added O_2 was constant through the experiments. The oxide thickness of Si substrates was measured by automated ellipsometry within 20 min after exposing the substrates to air. The refractive index of thin oxide film was assumed to be a constant value (n=1.465).

OXIDATION OF Si CLEAN SURFACE IN N_2

The thickness of oxide grown on the Si clean surface was measured for 3 temperature history cases in N_2 after surface cleaning. The three cases are as follows: (A) room temperature (R.T.), (B) from 600℃ to R.T., and (C) from R.T. to 900℃ and to R.T. The oxide thickness of the substrates was 1 A or less for case (A), while the thickness was ~3 A for case (B) and ~9 A for case (C) (Table I). These results show that the clean Si surface is oxidized in the ambient N_2 gas by a small amount of O_2 or H_2O at T>600℃ .

The measured thickness was almost the same for substrates with different orientations ((100), (110), and (111)). Therefore, oxidation of a polycrystalline Si surface will be almost the same as that of a single crystalline Si substrate surface in the present experimental conditions. Some following experiments were carrieu out without loading substrates on the polycrystalline Si coated

susceptor. The results were almost the same between experiments with and without Si substrates.

INCREASING THE O_2 CONCENTRATION BY ADDING O_2

The O_2 concentration increase curve, after a small amount of O_2 was added to purified N_2, provides information about Si surface cleanness in the reactor. The increase of O_2 concentration ($\Delta C(O_2)$) after addition of O_2 at time (t) = 0 min is shown in Fig. 4. In this case, the substrate temperature was lowered to R.T. in H_2 after Si surface cleaning, and raised to 800-900℃ in N_2 ambient. Then a small amount of O_2 was added to N_2 ambient. $\Delta C(O_2)$ increases quickly to 30 ppb after adding O_2 and then increases gradually to a saturation value. When O_2 was stopped after saturation and added again (900℃ (2nd) in Fig. 4), O_2 concentration increased quickly to the saturation value.

These results can be explained by the O_2 consumption from the oxidation on Si surface in the reactor. The O_2 concentration in the ambient does not increase quickly to the concentration level corresponding to the addition of O_2, because a large amount of O_2 is consumed in the early stage of oxidation. When O_2 was added again after saturation, O_2 concentration increased promptly with the relatively short time constants of diffusion in the reactor and of sample gas pumping.

The oxide thickness was ~15 A after O_2 addition for 2 hrs at 900℃ . The thickness increase (5-8 A) roughly corresponds to the O_2 consumption in the experiment. It should also be noted that, with the temperature decrease, $\Delta C(O_2)$ increases more rapidly, and the saturation value becomes higher (Fig. 4). This is because the oxide growth rate decreases with the temperature decrease. The saturation value at 800℃ was 330 ppb, and roughly corresponded to the amount of added O_2.

RELATION BETWEEN SURFACE CLEANNESS AND O_2 CONCENTRATION INCREASE CURVE

In the experiments of Fig. 4, Si surface was covered with a 7-10 A thick oxide, because Si clean surface at high temperature was exposed to N_2 for a long time. The O_2 addition experiment was performed on a cleaner Si surface by the process shown in Fig. 5. In this case, O_2 was added after a short N_2 purge time (4-5 min), therefore the Si surface is cleaner than that in the experiment of Fig. 4.

After a quick increase and plateau at time (t) = 5-15 min, $\Delta C(O_2)$ shows another plateau at t = 20-25 min for 800℃ (Fig. 6). The first plateau corresponds to the oxide growth with a constant growth rate in the very early stage, and the second plateau corresponds to the oxide growth with a constant growth rate slower than the first. The decrease of the "linear constant" with an increase of oxide thickness has been also reported in the 10-50 A oxide growth stage at 800-950℃ with O_2(1-10 %)/Ar (11).

The O_2 concentration increase curve, after a small amount of O_2 was added to purified N_2, is strongly affected by the degree of Si surface cleanness in the reactor. The dependence of $\Delta C(O_2)$ curve on N_2 purge time at 900℃ is shown in Fig. 7. Increasing N_2 purge time at high temperature degrades surface cleanness, and $\Delta C(O_2)$ increases more rapidly. This result shows that this technique will provide a sensitive parameter of surface cleanness and the gas purity.

CONCLUSION

The oxygen adsorption and reaction process in O_2 concentration range between <10 ppb (purified N_2) and 330 ppb (purified N_2 + O_2) was studied for surface cleaning for SPE of CVD a-Si.

The observation shows that

(1) Si clean surface is oxidized up to 2-4 A at 600℃, and up to 7-10 A at 900℃ in purified N_2 (O_2<10 ppb).
(2) Measuring O_2 concentration increase after O_2 addition to purified N_2, the information about Si surface cleanness in the reactor can be obtained.
(3) The plateaus in the $\Delta C(O_2)$ curve at 800℃ correspond to the oxide growth with constant growth rates in the early stage.

As shown by the experimental results, the O_2 concentration increase is strongly affected by oxidation of Si clean surface, i.e., the degree of surface cleanness essential for SPE of CVD a-Si. It is believed this technique provides a sensitive parameter of surface cleanness and gas purity, if O_2 concentration is measured more precisely.

ACKNOWLEDGEMENTS

The author is grateful to Mr. Yutaka Sakakibara and Mr. Tetsushi Sakai for fruitful discussions and for reading the manuscript.

REFERENCES

1. Y.Kunii, M.Tabe and K.Kajiyama, Jpn.J.Appl.Phys., **21**, 1431 (1982).
2. Y.Kunii, M.Tabe and K.Kajiyama, J.Appl.Phys., **54**, 2847 (1983).
3. H.Ishiwara, H.Yamamoto, S.Furukawa, M.Tamura and T.Tokuyama, Appl.Phys.Lett., **43**, 1028 (1983).
4. Y.Kunii, M.Tabe and K.Kajiyama, J.Appl.Phys., **56**, 279 (1984).
5. Y.Kunii, M.Tabe and Y.Sakakibara, Jpn.J.Appl.Phys., **26**, 1008 (1987).
6. K.Kusukawa, M.Moniwa, E.Murakami, M.Miyao, T.Warabisako and Y.Wada, Extended Abstracts 19th Conf. Solid-State Devices and Materials, 1987, p.179.
7. Y.Kunii and Y.Sakakibara, Jpn.J.Appl.Phys., **26**, 1816 (1987).
8. Y.Kunii, Y.Sakakibara, T.Ueno, K.Suzuki, and I.Ohdomari, Abst. of FED 3D WORKSHOP, (1988), Miyagi-Zao, p.183.
9. N.Hirashita, T.Katoh and H.Onoda, IEEE Trans. Electron Devices, **36**, 548 (1989).
10. E.F.Kennedy, L.Csepregi, J.W.Mayer and T.W.Sigmon, J.Appl.Phys., **48**, 4241 (1977).
11. H.Z.Massoud, J.D.Plummer and E.A.Irene, J.Electrochem.Soc., **132**, 2685 (1985).

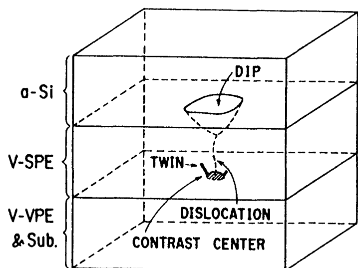

Fig. 1 Schematic view of V-SPE sample.

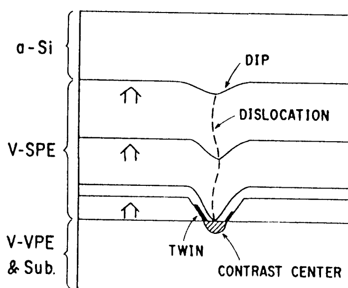

Fig. 2 Formation process of dip, twin, and dislocation during V-SPE.

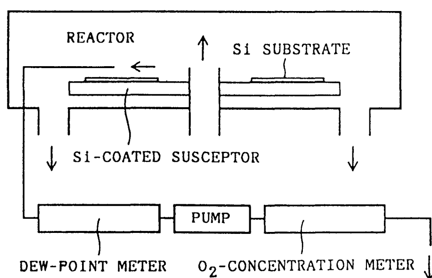

Fig. 3 Schematic view of reactor and ambient analyzing system.

Table I. Oxidation in N_2 with O_2(<10 ppb).

Case	A	B	C
Max. temp.	R.T.	600℃	900℃
Oxide thickness	0-1 A	2-4 A	7-10 A

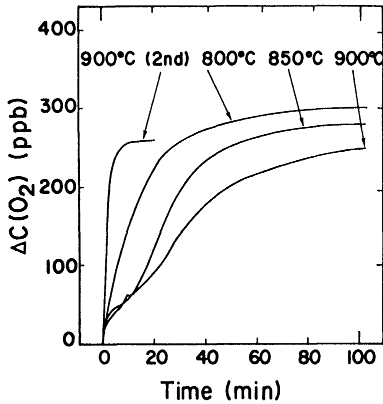

Fig. 4 Increase in O_2 concentration after a long N_2 purge and addition of O_2.

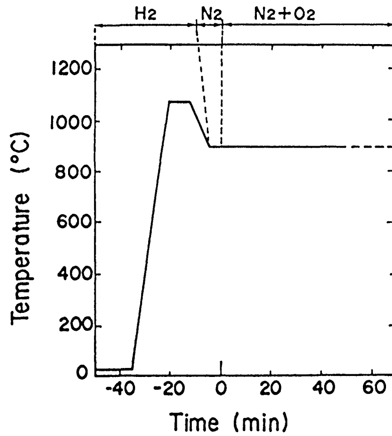

Fig. 5 Process diagram of O_2 addition experiment with a short N_2 purge time.

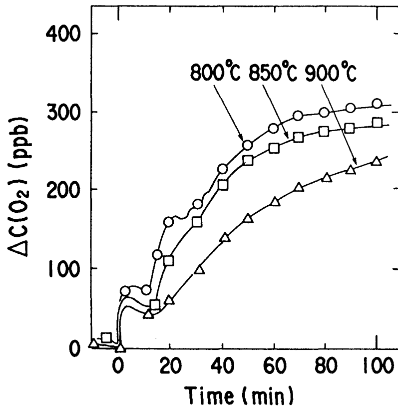

Fig. 6 Increase in O_2 concentration after a short N_2 purge and addition of O_2.

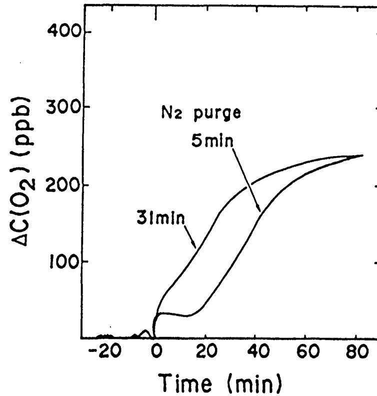

Fig. 7 Effect of the N_2 purge time on the O_2 concentration increase curve.

PARTICLES AND AIRBORNE CONTAMINANTS

REVIEW OF PARTICLE CONTROL METHODS DURING WET CHEMICAL CLEANING OF SILICON WAFERS

V. B. Menon and R.P. Donovan*

SEMATECH
2706 Montopolis Drive
Austin, Texas 78741

*Research Triangle Institute
P.O. Box 12194
Research Triangle Park, North Carolina 27709

Particles get entrained in liquid chemicals at various stages of chemical production, distribution and use. The probability that these particles deposit onto wafers during wet chemical cleaning is a function of filter performance, physicochemical interactions between the wafer surface and the chemicals, and the dynamics of liquid flow in recirculation baths. In addition, the configuration of the rinse tank, and the quality of the dryer are important variables that determine the final particle levels on wafers exiting a wet chemical cleaning sequence. This paper reviews the major particle contamination issues associated with wafer cleaning and describes particle control strategies to minimize wafer contamination.

INTRODUCTION

There are many wet chemical cleaning sequences that are routinely used for removing organic, inorganic, and ionic materials from wafer surfaces. These include the use of hydrofluoric acids to etch oxide films; sulfuric acid-hydrogen peroxide mixtures to remove heavy organics such as photoresist; hydrochloric acid-hydrogen peroxide-water mixtures to remove ionics; and ammonium hydroxide-hydrogen peroxide-water solutions to remove light organics and particles. Some of these chemical solutions are notorious for adding particles to wafers, while others aid in the particle removal process.

The major components of a wet chemical cleaning system are (i) the chemical distribution system, (ii) the process tank (iii) the rinse tank, and (iv) the dryer. The major variables are chemical purity, process effects, and cleanliness of the rinse and dry process.

CHEMICAL PURITY

While many IC fabrication plants still supply chemicals manually in bottles, the trend is towards the use of chemical distribution systems that automatically dispense chemicals into process tanks. These systems improve safety and reliability, eliminate the need to bring bottles into the cleanroom, incorporate multiple prefiltering stations to reduce particles, and reduce the variability associated with manual operation (1). The final quality of chemicals at the point of use depends on the compatibility and cleanliness of incoming chemical drum material, the filtration scheme, the particle generation characteristics of pumps and valves, and any dead legs in the supply lines.

Present day IC production typically requires chemicals with particle levels less than 1 particle/ml of size greater than 0.5 um. While chemical vendors are working towards such levels of particulate contaminants in incoming chemicals, the purity at the point of use depends entirely on the filtration scheme in the chemical distribution system and at the recirculating process tank. Filters capable of efficiently removing particles of size less than 0.2 um are available; however, there are compatibility issues that must be carefully looked at before selecting a filter for a specific process. Fluorocarbon resins such as PFA, PVDF and PTFE are generally compatible with most inorganic acids and alkalis (2). Often, the membrane of a filter is compatible with the chemical being filtered, but the cartridge material is not. This can result in change in material composition, leading to gas permeation, polymer degradation, particle shedding, and overall loss of chemical quality. Hence, a systematic program for selection, maintenance and replacement of filters is essential to successfully controlling particles in a wet chemical process tank.

Table 1 depicts a comparison of the purity of selected chemicals, delivered using a chemical distribution system, with low particle bottle specifications (3). Figure 1 shows the effect of chemical type on the delivered chemical particle concentration (3). For sulfuric acid, hydrogen peroxide, ammonium hydroxide, and hydrochloric acid, 6 - 10 minutes of operation in a recycle mode is sufficient to bring particle counts well below those observed in bottled chemicals. The particle concentrations at 0.3 um size, are typically 3 - 5 times that at 0.5 um.

Most wafer cleaning and etching processes are conducted in an immersion tank or spray processor. Recirculation tanks, with continuous filtration, are only available for processes which are conducted at temperatures below approximately 80° C owing to limitations in filter availability and pump materials of construction. With recent advances in polymeric materials technology, higher temperature recirculation tanks are slowly becoming available. Even in a recirculation tank, it takes more than an hour for the particle level ($\geq$ 0.5 um) to attain its steady state value. Figure 2 depicts the change in particle level with time for a filtered, recirculating buffered HF

tank (4). For particles greater than 0.3 um, this process takes several hours. When chemicals are supplied manually, in bottles, to such a recirculating tank, it is necessary to provide adequate time for particle levels to stabilize.

PROCESS CHEMISTRY

Table 2 lists the most common chemical combinations used for wafer cleaning and their applications. The RCA cleaning chemistry (5) is meant to remove oxide films, organic residues and ionic species, but not particles. Indeed, a typical RCA cleaning sequence consisting of the following chemical combinations, can add a significant number of particles. In a recent study of particles added/removed by a typical RCA clean, the following components were investigated (4).

	Process Title	Process Description
1.	Alkaline (SC-1)	$H_2O:NH_4OH:H_2O_2$ (5:1:1) Conditions: 300 s, 70°C Overflow DI rinse, 450 s
2.	Acid (SC-2)	$H_2O:HCl:H_2O_2$ (5:0.8:1) Conditions: 300 s, 70°C Overflow DI rinse, 450 s
3.	BOE(buffered HF)	10:1 buffered oxide etch Conditions: 10 s, 70°C Overflow DI rinse, 450 s

In all cases, the wafers were spun dry, with no rinsing in the dryer. Figure 3 depicts the number of particles, in the size range 0.2-0.5 um, added during each step of the cleaning sequence, and for the entire clean (4). The SC-2 and BOE treatment added particles to the wafer, while the SC-1 treatment removed a few particles. The overall number of particles added to the wafer was very close to that added during the BOE process (the last process). The addition of the particle contributions from the individual steps of the cleaning sequence does not equal the particles added for the entire clean. This implies that some of the particles added during one cleaning steps are removed during a following step, possibly due to interfacial effects or chemical dissolution (6, 7).

Use of HF solutions has generally been known to add particles to wafers (8, 9). Stripping an oxide film from a silicon wafer renders the surface hydrophobic. When this wafer is immersed in the DI-water rinse tank, the hydrophobicity causes organic particles in the DI-water to be preferentially deposited on the wafer surface. Hence, particle levels on wet-etched wafers generally correlate well with particle levels in

the rinse tank, and not the HF bath (4). In a later section, various rinse tank configurations to minimize particle deposition, are discussed.

The hydrophobic or hydrophilic nature of a surface is defined by the "contact angle" of a drop of water on that surface. A surface with a contact angle of zero degrees is completely hydrophilic, while a contact angle of 180° defines a completely hydrophobic surface. The contact angle of water with a silicon surface, freshly etched in BOE, is approximately 66 - 85°, while a drop of buffered HF on a hydrophobic surface makes a contact angle of around 70° (10, 11). The wettability of buffered HF is not significantly different from that of water. To improve the wettability of the etchant, Ohmi (10) recommends the use of hydrocarbon surfactants. His studies have shown that the use of carefully selected surfactants can significantly reduce the particle contamination in wet-etch processing. However, the application of surfactants in chemical solutions, especially in pre-gate oxidation cleans, should be approached very carefully. Surfactant molecules are often sources of carbonaceous residue. Aggregates of these molecules, called micelles, are in the submicron size range and can represent an added source of particles. Also, many surfactants cause foaming, which can leave stains on the wafer surface, and cause uneven etching.

The hydrophilic/hydrophobic nature of wafer surfaces after various chemical cleaning steps is shown in Table 3 (11). The SC-1 and SC-2 chemical treatments leave the wafer extremely hydrophilic. Generally, HCl has been easier to filter than NH_4OH, and particle specifications for bottled HCl have been lower than those for bottled NH_4OH. Yet, Figure 3 shows that SC-2 adds particles on a wafer surface, while SC-1 actually removes a few particles. Both SC-1 and SC-2 leave the wafer hydrophilic, and the surface tensions of both chemical solutions are close to each other (12), hence, the differences in particulate removal behavior must be attributed to chemical interactions at the liquid-wafer interface. Kern (13) reports that SC-1 etches SiO_2 at an etchrate of about 0.5 A/min, whereas, SC-2 shows very little change in oxide thickness. Thus, SC-1 chemistry results in particle removal, while SC-2 does not, probably because SC-1 removes a very thin surface oxide layer, which carries with it any particles present on the surface.

Mishima et al. (14) have investigated the effect of different concentrations of NH_4OH, in an ammonium hydroxide-water-hydrogen peroxide mixture, on particle removal. They recommend that the SC-1 solution should have lower NH_4OH content (0.5 to 0.1 times that conventionally used) to improve the particle removing capability by a factor of two, without any increase in surface roughness. Figures 4 and 5 (14) show the influence of NH_4OH ratio on particle removal efficiencies for polystyrene and silica particles on silicon wafers. In another study of wafer cleaning chemistries and their influence on oxidation induced stacking faults Hariri et al. (15) conclude that choline/surfactant solutions may be more effective than RCA solutions in removing heavy metals from the wafer surface. The impact of such a chemistry on removal of organic species and particles has not been evaluated extensively, but some, limited comparisons are presented in the next section.

MEGASONIC CLEANING

The use of megasonic energy in a tank containing the SC-1 solution enhances the particle removing capability of this solution. Commercial megasonic wafer cleaning systems typically operate at a frequency of about 700-900 KHz. Megasonic transducers are piezoelectric crystals, which are usually mounted at the bottom of the chemical tank. The sonic pressure waves travel through the liquid, in a direction parallel to the wafer surface. Wafer cleaning is accomplished by the impact of these pressure waves on the particle surface.

The force required to remove a particle from the wafer surface must equal, or exceed, the force of adhesion. This adhesive force is a function of particle size, particle and wafer surface composition, and the nature of the liquid medium (16). For a silica particle of 1 micron diameter (and mass = 5×10^{-13} g), adhered to a bare silicon surface, the force of adhesion in water is approximately 4×10^{-4}dynes (17). This is the van der Waals force of adhesion. The applied megasonic force acting on this particle is

$$F_{meg} = \text{Mass x Acceleration.}$$

The acceleration produced by a megasonic transducer vibrating at a total power of 300 watts is approximately 2.5×10^{8} cm/s^2 (18). Thus, the megasonic force = 1.25×10^{-4} dynes. The megasonic force is approximately equal to the force of adhesion; hence, some 1 micron diameter particles should be removed from silicon wafers in a megasonic tank containing water. Here again the hydrophilic/hydrophobic nature of the wafer surface influences particle removal. Table 4 compares particle removal data from high contact angle surfaces with those from low contact angle surfaces (19). For all three particle types and both wafer conductivity types, the low contact angle surfaces retain fewer particles after cleaning than the high contact angle surfaces; they also exhibit higher cleaning efficiencies.

When SC-1 chemistry is used in lieu of water, the particle removal efficiency is further increased because of some of interfacial effects discussed in the previous section. Figure 6 shows a comparison of the megasonic cleaning efficiencies of DI-water, SC-1 solution, and a choline-hydrogen peroxide solution (11), for particles of size greater than 0.5 microns. The use of SC-1 was found to consistently produce high cleaning efficiencies and relatively small variability between runs. The lowest cleaning efficiencies, and the largest variabilities were seen with DI-water. The results for the choline-peroxide system were intermediate to those of DI-water and SC-1. This solution did not however, include a non-ionic surfactant as did the choline results reported by Hariri and Hockett [15]

Megasonic cleaning is a very effective method for removing submicron particles from silicon wafers. However, its effectiveness at particle sizes below 0.2 microns has not been demonstrated. One possible approach to removing submicron particles

from wafers is to combine the inherent advantages of chemical dissolution with megasonic energy. Chemical dissolution as a means to particle removal becomes more effective as particle size decreases. Megasonic cleaning, on the other hand, becomes more effective as particle size increases. For example, when wafers contaminated with metal particles are subjected to megasonic cleaning in a solution containing hydrochloric acid, the acid will dissolve the small particles, while megasonic energy will dislodge the large particles. Alternatively, the acid treatment can precede megasonic cleaning with conventional SC-1 solution. For particles that are predominantly made up of SiO_2, a mild HF treatment before megasonic cleaning may be more effective than megasonic cleaning alone.

Because the megasonic wafer cleaner is a tool for removing particles, it is often forgotten that this system can also generate particles. Deteriorating seals and gaskets, and bad transducer bonding materials can shed particles when the transducers are vibrated. A worthwhile experiment would be to monitor the particles in the megasonic tank (use DI-water instead of SC-1) using a liquid particle counter, as a function of duration of vibration. If the particle count in the bath increases with every additional cycle of vibration, then the megasonic unit is generating particles.

RINSING AND DRYING

A major source of particulate contamination during wet chemical cleaning is often in the rinse tank and spin dryer, and not in the chemical bath. Careful selection of rinse tank and dryer configuration is therefore critical. The most commonly used rinse tank mode is the quick dump with top spray. The advantage of this configuration is that it removes chemicals from the wafer surface very rapidly, periodically dumping the water containing the chemicals. However, spray nozzles tend to generate particles and grow bacteria. Also, quick dump rinse (QDR) tanks generally produce turbulent convective currents in the water, which increase particle mobility to the wafer surface. Hence, the QDR is a poor choice from a particle control point of view.

Particle control in the rinse tank becomes especially critical for wet etch processes using HF chemistry. Hydrophobic wafers exiting from the HF bath and entering the rinse tank are very susceptible to particle deposition. Figure 7 depicts a comparison of various rinse tank configurations for cleaning etched hydrophobic wafers (16). The cascade overflow configuration adds the least number of particles to the wafer surface. Rinse tanks with megasonic transducers also perform well.

Routine correlation of particle counts in the DI-water with overall water quality is useful in determining the cause of particle excursions. For HF-etched wafers, variations in the TOC level in the rinse tank can cause major changes in the number of particles added to wafers.

It is common practice in the semiconductor industry to expose wafers leaving the rinse tank to another level of rinsing in the spin dryer. A spin dryer contains moving parts, spray nozzles, and various kinds of gaskets and seals. These components are sources of particles. Conducting a centrifugal rinse in the dryer results in the generation of micrometer and sub-micrometer size water droplets which may not be effectively removed in the dry cycle. A dry-only mode is, by far, a lower particle adder than a rinse-and-dry mode. As a general practice, it is recommended that the rinsing process be accomplished in the rinse tank, and not the spin dryer. An efficient dryer in the dry-only mode can add fewer than 10 particles (>= 0.2 microns) on a 6-inch diameter wafer.

Viscous chemicals such as sulfuric acid and phosphoric acid are not effectively removed from the wafer surface in a cold cascade overflow rinse. For such systems, the use of hot DI-water or a good DI-spray has generally proven to be effective. While a hot DI- cascade rinse is more expensive than a QDR with spray nozzles, it adds fewer particles.

IPA vapor dryers were introduced to achieve particle-free wafer drying. These dryers do not have the particle problems associated with centrifugal drying in a spin dryer. Ohmi et al. (20) report that the water content in the IPA, the IPA heating system, and the IPA vapor velocity are major variables affecting the performance of a vapor dryer. So far, the number of particles added using an IPA vapor dryer have not been significantly lower than that added in a well-functioning spin dryer. These dryers are also slower than spin dryers. With improvements in design and throughput, IPA vapor dryers could, in the near future, take the place of spin dryers.

CONCLUSION

An effective particle control strategy during wet chemical cleaning of silicon wafers requires (i) stringent control of chemical purity, (ii) an understanding of the interactions between the wafer and the chemicals, and (iii) the implementation of a rational rinse and dry protocol. This strategy also requires periodic monitoring of particles in the in-coming chemicals, the process tank, the rinse tank, the dryer, and on wafers. Correlation of the results of these monitoring experiments with bacteria analysis and TOC levels in the DI-water, and the particle levels in the cleanroom ambient around the wet processing tool, in a proactive manner will help resolve particle problems quickly with short down-times.

REFERENCES

1. S. Hashimoto, M. Kaya, and T. Ohmi, Microcontamination, 7, 25 (1989).

2. V. Krygier, Microcontamination, 4, 20 (1986).

3. D. C. Grant, and W.R. Schmidt, paper presented at the Seventh Annual Millipore Microelectronics Technical Symposium, Semicon West, San Jose, CA, May (1989).

4. V.B. Menon, L.D. Michaels, A.C. Clayton, and R.P. Donovan, Solid State Technology, in press.

5. W. Kern, and D.A. Puotinen, RCA Review, 31, 187 (1970).

6. V.B. Menon, L.D. Michaels, L.A. Hollar Jr., R.P. Donovan, and D.S. Ensor, Proceedings of the Institute of Environmental Sciences, pp. 382-289 (1988).

7. V.B. Menon, L.D. Michaels, R.P. Donovan, and D.S. Ensor, Solid State Technology, 32, S7 (1989).

8. T.A. Milner, and T.M. Brown, Proceedings of the Microcontamination Conference and Exposition, pp. 146-156 (1986).

9. K. Dillenbeck, Tutorial on Contamination Engineering Principles for Semiconductor Wafer Fabrication, Microcontamination Conference and Exposition (1988).

10. H. Kikuyama, N. Miki, J. Takano, and T. Ohmi, Microcontamination, 7, No. 7, 25 (April 1989).

11. V.B. Menon, L.D. Michaels, A.C. Clayton, and R.P. Donovan, Proceedings of the Institute of Environmental Sciences, pp. 320-324 (1989).

12. Handbook of Chemistry and Physics, 63rd edition, CRC Press, Boca Raton, Florida, 1984.

13. W. Kern, Semiconductor International, pp. 94-99, April (1984).

14. H. Mishima, T. Yasui, T. Mizuniwa, M. Abe, and T. Ohmi, IEEE Transactions on Semiconductor Manufacturing, 2, 69 (1989).

15. A. Hariri, and R.S. Hockett, Semiconductor International, pp. 74-77, August (1989).

16. V.B. Menon, A.C. Clayton, and R.P. Donovan, Microcontamination, 7, 31 (1989).

17. M.B. Ranade, Aerosol Science and Technology, 7, 161 (1987).

18. Pre-Tech Inc. Japan, Technical Bulletin, 1988.

19. R.P. Donovan, unpublished data.

20. T. Ohmi, H. Mishima, T. Mizuniwa, and M. Abe, Microcontamination, 7, No. 5, 25 (May 1989).

Table 1. **Comparison of purity of bulk distributed chemicals* with bottled chemicals (3)**

Operating Time (Hrs.)	Particles/ml > 0.5 um in H_2SO_4	NH_4OH	H_2O_2	HCl
0.1	27	28	0.06	0.02
0.5	10	4.3	0.04	0.01
1.0	7.0	1.9	0.03	0.01
2.0	4.6	0.85	0.03	0.01
4.0	3.1	0.38	0.02	<0.01
6.0	2.4	0.24	0.02	<0.01
8.0	2.0	0.17	0.02	<0.01
Bottled Chemicals Specification**	60	500	100	40

* FSI ChemFill™ system

** CleanRoom™ low particulate grade chemicals (1 gallon bottles) from Ashland Chemical Company, Columbus, OH.

Table 2. **Common wet chemical cleans and their applications**

Chemicals	Application
1. HF - H_2O	etching SiO_2 layers
2. H_2SO_4 - H_2O_2	removing heavy organics
3. NH_4OH - H_2O_2 - H_2O (SC-1)	removing light organic residue and particles
4. HCl - H_2O_2 - H_2O (SC-2)	removing metallic species

Table 3. Effect of cleaning chemistry on contact angle[11]

System	Contact Angle (°) +/- Standard Deviation
1. Bare wafer after cleaning with DI-water	16 +/- 1.3
2. Bare wafer after cleaning* with $5H_2O:1H_2O_2:1NH_4OH$	10 +/- 0.8
3. Bare wafer after cleaning with $5H_2O:1H_2O_2:1HCl$	9 +/- 0.5
4. Bare wafer after cleaning with choline-peroxide solution	16 +/- 0.5
5. Bare wafer after cleaning with $10H_2O$:1 buffered HF solution	66 +/- 2.1

* All cleans were followed by a DI-water rinse which preceded the measurement of contact angle using a goniometer.

Table 4. Megasonic Wafer Cleaning in DI-Water at 200 Watts(19).

Particle type	Mean contact angle (°) of starting wafer surface	Mean no. of particles after deposition	Mean no. of particles after cleaning
	p-type wafers		
glass beads	12.3 ± 1.5	731.0 ± 773.7	7.3 ± 2.8
silicon dust	11.7 ± 1.5	693.3 ± 922.2	25.3 ± 18.0
1 μm PSL	11.7 ± 1.2	761.7 ± 653.8	9.0 ± 8.7
glass beads	64.3 ± 0.6	1,116.7 ± 1,256	80.7 ± 19.7
silicon dust	61.3 ± 2.3	910 ± 753.1	152.3 ± 36.1
1 μm PSL	60.0 ± 0	914.3 ± 646.7	81.0 ± 15
	n-type wafers		
glass beads	16.3 ± 1.5	882.4 ± 821.6	3.0 ± 2.7
silicon dust	14.7 ± 0.6	298.0 ± 238.6	46.4 ± 45.2
1 μm PSL	16.7 ± 0.6	682.7 ± 603.4	9.7 ± 1.5
glass beads	60.0 ± 6.1	3,869.3 ± 3,347	68.0 ± 33.2
silicon dust	64.3 ± 1.2	825.0 ± 754.9	89.7 ± 13.8
1 μm PSL	62.3 ± 1.5	820.3 ± 623.3	67.3 ± 39.6

± gives the standard deviation.

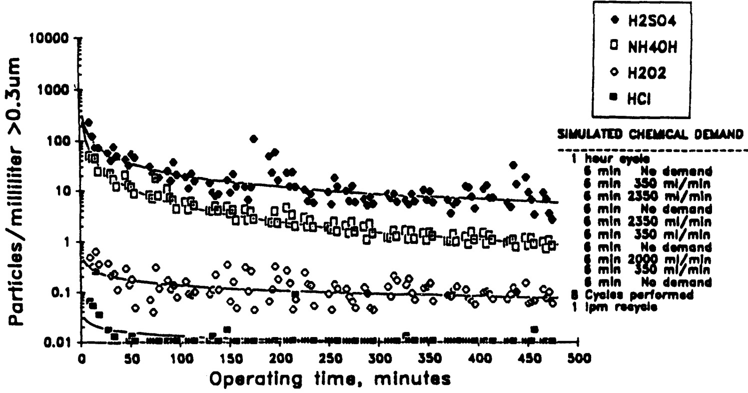

Figure 1: The Effect of Chemical Type on Chem Fill Delivered Chemical Particle Concentrations (>0.3μm) (Ref. 3)

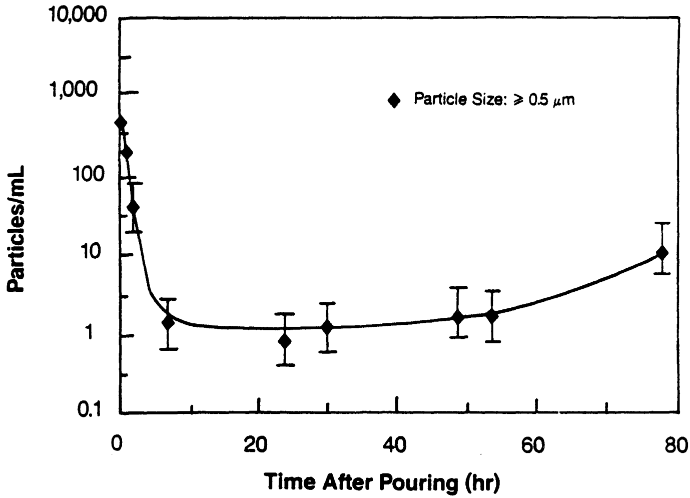

Figure 2: Time variation of particle concentration in recirculating buffered oxide etch bath (Ref. 4)

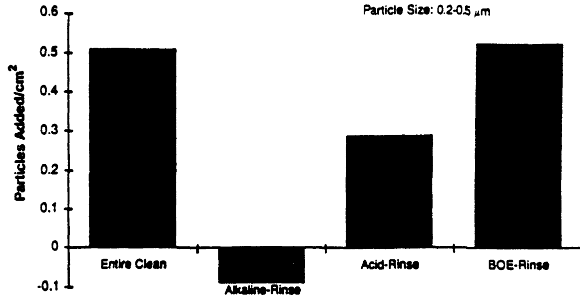

Figure 3: Particle deposition on wafers during a wet chemical cleaning sequence (Ref. 4)

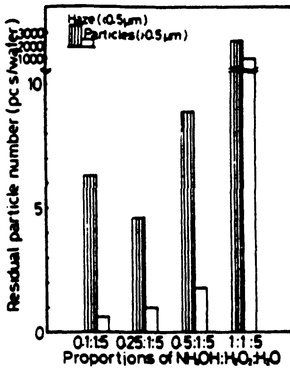

Figure 4: Influence of the NH_4OH ratio on particle removal efficiencies when polystyrene latex spheres were adhered to wafers (Ref. 14)

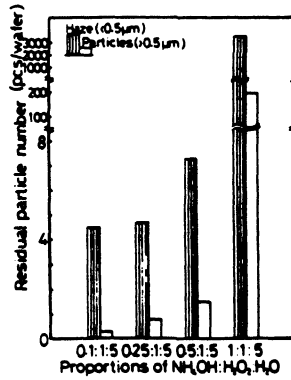

Figure 5: Influence of the NH_4OH ratio on particle removal efficiencies when silica latex spheres were adhered to wafers (Ref. 14)

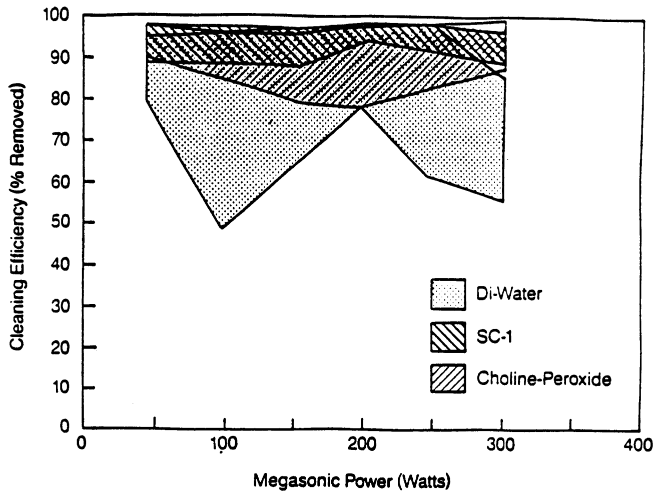

Figure 6: Variation of particle removal efficiency with megasonic power for different cleaning media (Ref. 11)

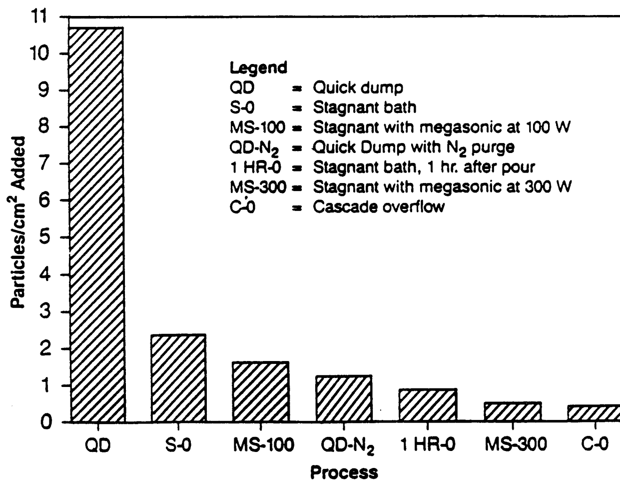

Figure 7: Effect of rinse tank configuration on particulate contamination on etched wafers (particle size: 0.2-0.5 μm; initial particle count $\leq 1.2/cm^2$.) (Ref. 16)

Ultra Clean Ice Scrubber Cleaning with Jetting Fine Ice Particles

Toshiaki Ohmori, Takaaki Fukumoto and Tadao Kato
LSI Research and Development Laboratory, Mitsubishi Electric Corporation, Itami City, Hyogo 664, Japan
AND
Masuo Tada and Toshiaki Kawaguchi
Taiyo Sanso Co.LTD, Osaka City, Osaka 556, Japan

ABSTRACT

A low temperature cleaning method with jetting fine and ultra clean ice particles (Ice scrubber cleaning) is proposed. These ultra clean ice particles are produced by spraying ultra pure water into low temperature gas N2 (-80 ~-150℃). It is possible to control the ice particle size between 30 μm and 300 μm in diameter. Particulate contaminants and organic thin films on semiconductor wafer surface are more effectively removed with ice scrubber cleaning than dry ice cleaning, brush scrubber cleaning and megasonic cleaning. It is possible to control the impact onto wafer surface by adjusting the solidity (hardness) of ice particles, the jet pressure and the jet angle. In this paper, the method of producing of fine and ultra clean ice particles, the impact control onto substances to be cleaned, the cleaning mechanism and the application are described.

1. Introduction

In recent ULSI fabrication process, the importance of cleaning technology has been increasing more and more, for contaminants such as resist residue, submicron particles, organic thin films and native oxide are major factors to worse the yield and degrade the device quality. In regard to submicron devices, we have to remove particulate contaminants larger than 0.1 μm in diameter. Conventionally many kinds of cleaning methods with brush scrubber, high-pressure water, megasonic wave, dry ice and chemicals, have been utilized and improved.(1)(2)(3) Brush scrubber cleaning has an effect to remove contaminants which have adhered to semiconductor wafers hard, but little to remove submicron particulate contaminants. On the contrary megasonic wave cleaning has an effect to remove submicron particulate contaminants, but little to remove contaminants which have adhered hard. We have developed a new cleaning method, ice scrubber cleaning, having the both effect and aiming at the removal of submicron particles on semiconductor wafers after chemical vapor deposition (CVD). This new cleaning method is done by jetting fine and ultra clean ice particles onto the surface of semiconductor wafers. These particles are between 30μm and 300 μm in diameter.

2. Constitution of equipment

This equipment consists of five units, an ice generating unit, a cleaning unit, a drying unit, a transfer unit and a control unit. In the drying unit, we applied Isopropyl alcohol (IPA) vapor drying system. The followings are about the ice generating unit and the cleaning unit.

2.1. Ice generating unit

The principle of producing ice particles is shown in figure 1. We got fine and ultra clean ice particles by freezing fine drops of pure water sprayed from a spiral spray nozzle into low temperature gas N2 (-80℃~-150℃).(4) In this equipment, liquid N2 was supplied at the flow rate of 0.24 kg/min into the freezing chamber (450 mm in length× 450 mm in width ×1000 mm in height). And ice particles between 30μm and 300 μm in diameter were produced by spraying pure water at the flow rate of 0.1ℓ/min in this freezing chamber. (Fig. 2) If all cooling capacity of liquid N2 works to freeze pure water of 23℃ and cool ice particles on the above-mentioned condition, it is possible to get ice particles of about -132 ℃. It is calculated with some constants that evaporating latent heat of liquid N2 is 48.8 cal/g, specific heat of gas N2 is 0.25 cal/g ·℃, melting latent heat of ice is 79.7 cal/g , specific heat of ice is 0.25 cal/g·℃. But actually all thermal energy of liquid N2 isn't transferred to pure water and ice particles, because of the incomplete heat insulation of the freezing chamber. The freezing temperature influences the hardness of ice particles. The relation between the freezing temperature and the hardness of ice particles is shown in figure 3. Mohs hardness of ice particles is 3 to 4 at the freezing temperature under -50 ℃. Above -50 ℃ the hardness of ice particles decreases according as the freezing temperature rises. And the hardness decreases temporarily due to the change of the crystal structure of ice at about -80 ℃. It is possible to freeze many kinds of liquid (chemicals) which have freezing points above the boiling point of liquid N2 (-196℃) with this method. For example, Mohs hardness is 1 to 2 in frozen methanol and is 2 in frozen glycerin and trichloro-trifluoroethane.
In regard to the size of ice particles, it is influenced by the characteristics of a spiral spray nozzle and the spray pressure. A frequency distribution of particulate size is shown in figure 4. This is a result in using a spiral spray nozzle whose orifice is 0.5 mm in diameter. We got ice particles which had a peak at about 200μm in diameter in the condition of spraying pure water with the pressure of 1.5 kg/ cm² and which had a peak at about 130μm in diameter with the pressure of 4.0kg/cm². It is possible to produce ice particles between 30 μm and 300 μm in diameter with this method. And we succeeded in producing smaller ice particles between 0.1μm and 30μm in diameter by supplying steam into the freezing chamber.
In the ice generating unit it is important to use ultra pure water and ultra clean valves and remove particulate contaminants in liquid N2 in order to get ultra clean ice particles.

2.2. Cleaning unit

Ice pariticles are jetted from the fixed jet nozzle with dry clean air or ultra pure gas N2 onto the wafer surface, after the wafer is set in the holder. During jetting the wafer is revolved and moved horizontally in order that ice particies hit all of the wafer surface. The jet angle with the wafer surface is variable adusting the jet nozzle. But it is necessary to think out an adequate method of jetting ice particles for cleaning an uneven surface. It is one idea to jet ice particles from multi-nozzles at the same time. The cleaning unit has an automatic cleaning system including a blower, a HEPA filter and an ionizer in order to prevent particulate contaminants blown out of the wafer surface from adhering to it again. When ice particles were blown on silicon wafer with the pressure of 4kg/cm² without using the ionizer, we observed the voltage of about minus 5 kv had occured. Therefore the power of the ionizer must be set adequately according to the substances to be cleaned.

3. Jet condition and impact control

The impact given to substances to be cleaned is decided by the hardness of the substances, the jet pressure, the jet time, the jet angle and the distance between the jet nozzle and the substance. We measured the surface roughness of aluminum plates blown by ice particles in various jet conditions. Table 1. shows the surface roughness of the aluminum plate whose Brinell hardness is 44. The surface roughness between 0.32μm and 0.84μm occurred in the case that the jet pressure was between 2 and 4 kg/ cm². In this evaluation the jet distance was 100 mm and the jet angle was 70 ° . Table 2 shows the surface roughness of aluminum plates which have various hardness after jetting. The jet pressure was 4 kg/cm², the jet distance was 50 mm and the jet angle was 80° throughout this evaluation. The roughness of 3.0μm occurred on the surface of the aluminum plate whose Brinell hardness was 44. On the other hand it was 0.01 μm in the case that the hardness was 105. The ice particles give the damage to the substances for example aluminum or copper whose Mohs hardness is 3 to 4. But this damage doesn't occur on the surface of slicon or silicon-oxide whose hardness is 7. The following shows a result of evaluating the damage to thin silicon-oxide film. We measured the break-down rate of silicon -oxide film of about 100A thickness. (Table 3) Poly-silicon film of about 2500A thickness was deposited on this silicon-oxide film. The ice particles of 200μm in diameter were blown with the jet distance of 50 mm. When the ice particles were blown vertically with the jet pressure of 4 kg/ cm², the break-down rate of silicon-oxide films increased according as the jet time became longer. But when the ice particles were blown with the low jet pressure for example 2 kg/ cm² or with the low jet angle, the break-down of silicon-oxide films didn't occur. It is necessary to adjust the condition of jetting ice particles for the material and structure of the substances to be cleaned.

4. Application

4.1. Removal of particulate contaminants

At first we studied the effect of removing polystyrene standard particles of 0.322 μm in diameter which were scattered on the silicon wafer. Table 4 shows a result of comparing ice scrubber cleaning with other cleanings. We got a best removing rate (about 95 %) with ice scrubber cleaning. And the removing rate of dry ice cleaning which is similar to ice scrubber cleaning was about 69 %. Next we studied the effect of removing particulate contaminants which adhered to the back surface of wafers. Recently process equipments have been improved not to contaminate the wafer surface. But it is still a fact to contaminate the back surface of wafers with belts and stages in process equipments. A result of removing contaminants on the back surface is shown in figure 5. We think that submicron particulate contaminants on the wafer surface are able to be removed according to the cleaning mechanism shown in figure 6. Model 1 shows how to remove submicron particulate contaminants. Ice particles are smashed into smaller particles and scrub the wafer surface in the case that the wafer surface is harder than the ice particles. The contaminants are removed from the wafer surface with the works of these smaller ice particles. On the other hand ice particles melt partially and are frozen again in the moment that ice particles run on the wafer surface. At this time the contaminants are taken in the ice particles and removed with the ice particles, when other particles hit them. Model 2 shows how to remove organic films. While the wafer is cooled from room temperature to about -30 ℃ during ice scrubber cleaning, organic films contract and the adhesion between organic films and the wafer decreases. Organic films on the wafer surface are removed owing to this effect and the impact of ice particles.

4.2. Removal of particulate contaminants after CVD

The abnormal growth of CVD film whose example is shown in figure 8. occurs, if there are contaminants on the wafer surface before CVD. We observed the surface of poly-silicon films treated with ice scrubber cleaning, brush scrubber cleaning and high pressure water cleaning.

<u>With ice scrubber cleaning</u>

Almost all of contaninants had been removed as shown in figure 9. But in some case poly-silicon film was stripped off with these contaminants.

<u>With brush scrubber cleaning</u>

Almost all of contaminants had been removed and the strip of poly-silicon film was observed as well as ice scrubber cleaning. The scar occurred on the wafer surface as shown in figure 10. It was because a removed contaminant scrubbed the wafer surface with the brush.

<u>With high pressure water cleaning</u>

Almost all of contaminants hadn't been removed.

Ice scrubber cleaning is most effective to remove these contaminants that have adhered to the wafer surface.

4.3. Removal of greese and oil

Chlorofluoro-carbons, trichloroethylene and other solvents have been used to remove greese and oil. But the use of chlorofluoro-carbons will be prohibited by the year 2000 because they deplete the stratospheric ozone layer, while trichloroethylene is subject to regulations as a carcinogenic substance. The followings are about the effect of removing greese and oil with ice scrubber cleaning. We compared ice scrubber cleaning with chemical cleaning of trichloro-trifluoroethane and trichloroethylene on the effect of removing oil ink, fingerprints, greese and oil which have adhered to the wafer surface. (table 5) Oil ink and fingerprints were removed perfectly with ice scrubber cleaning. But some residues remained in greese and oil. This evaluation was done with a microscope. Next we studied the effect of removing five kinds of oil which have different melting points. (table 6) Oil which has melting point above -10 ℃ was removed perfectly with ice scrubber cleaning. This result proves on the model 2 of cleaning mechanism shown in figure 6, that the low temperature effect makes it easy to remove oil on the wafer surface.

5. Summary and conclusion

As a new cleaning method for ULSI device, We have developed ice scrubber cleaning with jetting fine and ultra clean ice particles between 30μm and 300 μm in diameter and evaluated its performance. As a result of this evaluation we realized that this cleaning method has an effect of removing submicron particulate contaminants which have adhered to the wafer surface hard and it is possible to remove greese and oil with this method. We already developed another method of producing smaller ice particles between 0.1μm and 30μm in diameter. And now we are developing an equipment using these smaller ice particles. This technology of taking advantage of fine and ultra clean ice particles is possible to be applied to cleaning of other various substances besides semiconductor wafers and surface processing of various substances whose hardness are lower than ice particles.

6. Acknowledgments

The authors acknowledge the assistance and encouragement of many persons of Mitsubishi Electric Corp. and Taiyo Sanso Co.LTD engaged in the ice scrubber cleaning system. This development was carried out under cooperation of Mitsubishi Electric Corp. and Taiyo Sanso Co.LTD.

REFERENCES

1. P.Buggraaf: "Wafer Cleaning:Brush and High-Pressure Scrubbers" Semiconductor Internatl.71(1981-7)
2. W.Kern: "Megasonic Particle Removal from Solid-State Wafers" RCA Review 46,81(1985-3)
3. S.A.Hoenig: "New Technology For The Detection And Control of Contamination in The One Micron Semiconductor Manufacturing Environment" SEMI Technology Symposium '85,G-1-1(1985-12)
4. T.Hata:Japanese Patent Filing No.61-238695, Oct. 6, 1989.

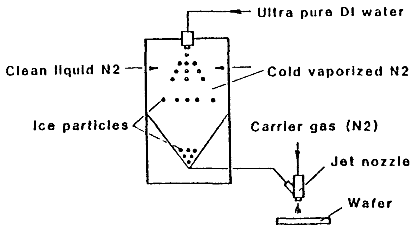

Fig.1 The principle of ice scrubber cleaning

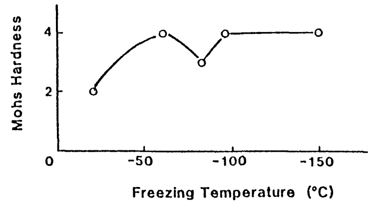

Fig.3 The relation of freezing temperature and hardness in Mohs

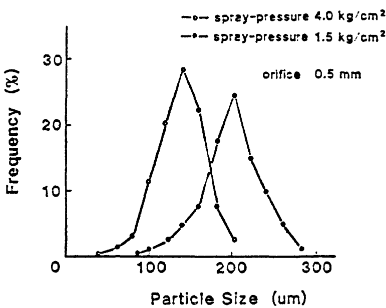

Fig.4 Distribution of ice particles

Table 1 Surface roughness on aluminum plates

Jet-Pressure (kg/cm^2)	2	3	4
Roughness (Ra) (um)	0.32	0.35	0.84

Table 2 Surface roughness on aluminum plates

Brinell Hardness	44	68	105
Roughness (Ra) (um)	3.8	0.16	<0.01

Table 3 The break-down of silicon dioxide films in several condition of jetting ice particles

Jet-Condition			Rate of Break-Down
Pressure (kg/cm^2)	Angle (°)	Time (sec)	(%)
4	80	240	45
4	80	120	31
4	90	60	18
4	5	60	2
2	90	60	4
Reference			8

Table 4 The effect of removing polystyrene standard particles by various cleaning methods

Cleaning Methods	Removal Rate (%)	Condition
Ice Scrubber	97.6	Pressure $3kg/cm^2$ Angle 80° Time 30sec
	94.0	Pressure $2kg/cm^2$ Angle 80° Time 30sec
Megasonic	95.0	Frequency 950kHz Time 10min
Brush Scrubber	87.4	Brush-pressure $0.8kg/cm^2$ Time 40sec
High-Pressure Water	84.4	Water-Pressure $100kg/cm^2$ Time 40sec
Ultrasonic	83.9	Frequency 27kHz Time 15min
Dry Ice Scrubber	68.9	Time 30sec

Table 5 The effect of removing grease and oil

Cleaning Methods	Oil Ink	Fingerprints	Grease	Oil
Ice Scrubber	○	○	△	△
Trichloroethylene	×	△	△	△
Trichloro-trifluoroethane	×	△	△	△

○ No Residue △ A Little Residue × No Removal

CONDITION

Ice Scrubber	Jet-Pressure $4kg/cm^2$ Jet-Angle 80°	Distance 30mm Time 60sec
Trichloroethylene	Boil	Time 40min
Trichloro-trifluoroethane	Boil	Time 60min

Table 6 The relation between melting points and removal effect

Contaminants	Melting Points (°C)	Removal Effect
Sesame Oil	-2	○
Salad Oil	-3	○
Machine Oil	-7.5	○
Grease	-20	△
Oil for vacuum pump	-20	△

○ No Residue △ A Little Residue

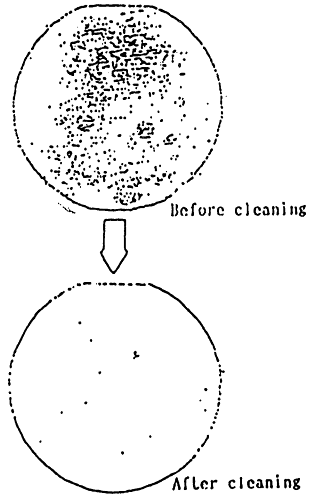

Fig.5 A result of applying to cleaning back surface of wafers

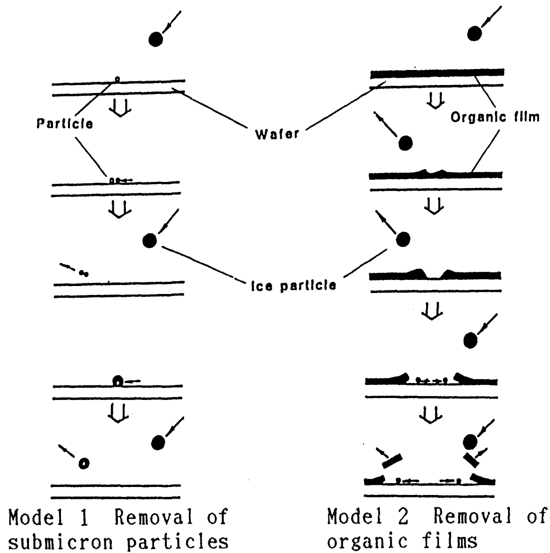

Model 1 Removal of submicron particles

Model 2 Removal of organic films

Fig.6 Mechanism of ice scrubber cleaning

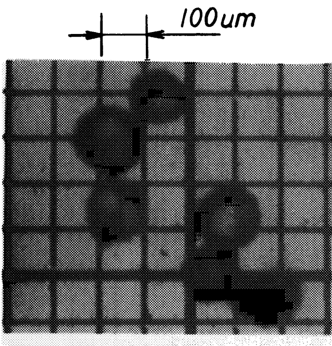

Fig.2 Fine and ultra clean ice particles

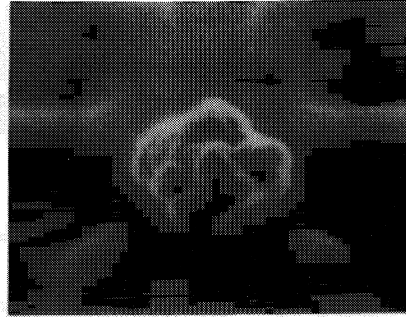

Fig.7 Abnormal growth of CVD film

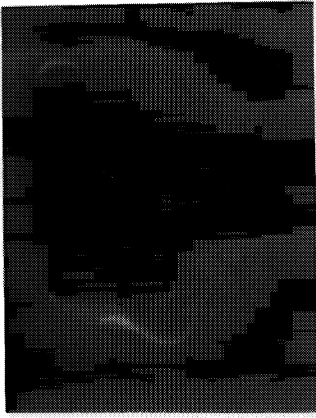

Fig.8 After cleaning with ice scrubber

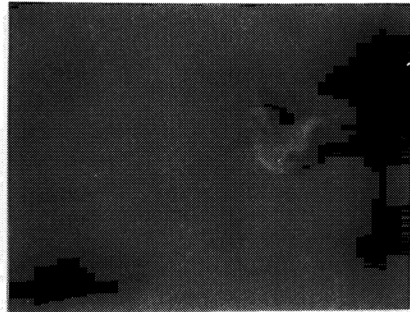

Fig.9 After cleaning with brush scrubber

STATISTICAL CONTRIBUTIONS TO THE SIZING OF PARTICULATES ON WAFERS BY LIGHT SCATTERING

S.Saadat, G.Kren, A.Neukermans, J.Pecen
Tencor Instruments
2400 Charleston Rd.
Mountain View, CA 94043

Sizing of particulates through light scattering is the standard way of measuring contamination on semiconductor wafers. Although extremely powerful and convenient, the technology suffers from a number of deficiencies. For example, the particle shape and orientation, the presence of underlying dielectric films and the nature of the substrate all affect the amount of scattered light, and hence, the apparent size. These are fundamental limitations, inherent to the method, and difficult to improve upon. However, other limitations, such as photo noise, arise because of the desired very high wafer throughput. These are described in detail, together with techniques to alleviate some of the short comings.

Sizing and counting of particulates by light scattering, although simple and fast in its application, suffers from a number of deficiencies because the size of the particle cannot unambiguously be determined. For example, the orientation of the particle with respect to the substrate, the nature of the substrate, the presence of underlying dielectric films affecting the reflectivity, and the dielectric constant of the particle all affect the amount of scattered light.[1] These difficulties are fundamental, and difficult to improve upon. In addition however, there are a number of limitations which are less fundamental. Most of them arise because we require a fast throughput in the operation of these machines. For example, in many of the laser scanning based instruments, the beam speed is on the order of 300-400 m/s; hence, with a beam diameter of a hundred micron, the dwell time on a defect is only a few hundred nanoseconds. For submicron particles, the number of both scattered and collected photons become rather, and hence, the statistical variations, inherent in the detection, become more pronounced. This phenomenon appears to be characterized by Poisson statistics, therefore, if N is the number of detected photons, then N is the expected standard deviation of N. These effects are easily seen in the histograms of monodisperse particles, as the particle size decreases.

Fig.1 illustrates a histogram of 1.08um latex spheres, deposited on a bare silicon wafer, and scanned with a He-Ne laser (λ=.63 micron). The standard deviation of this peak is about 6.5% of the mean value. This finite width is caused by various factors, some of them systematic, others statistical in nature. Non-uniform illumination of the field, finite sampling, varying beam speed, and varying collection uniformity, plus the intrinsic width of the particle distribution itself (2%), all affect the measurement spread of the peak value. The number of photoelectrons being collected in this case is estimated to be 800 and therefore, the contribution to the peak broadening is estimated at 3.5% (Gaussian quadrature applies). Hence, the photon "starvation" effect is rather mild.

However, when we measure a .20 micron particle, we find a distribution as given in Fig.2. Note that the light level is down by more than a factor of 100, from the previous figure, and now, by and large, the photon starvation effect is the dominant one. The standard deviation of this distribution is approximately 33% of the mean, which is in agreement with what we expect from the number of available events. If we plot the standard deviation as a fraction of the mean, measured for various particle sizes (using monodisperse spheres) against scattering cross-sections we obtain the curve illustrated in Fig.3. The slope of the curve in this logarithmic plot is 0.5, which is characteristic of a Poisson distribution. At high cross-sections, deviations occur because of the other peak broadening effects described above.

There are some significant implications of this phenomenon in the use of particle detection which most users seem somewhat reluctant to accept. One cannot assign a single value to the scattering cross-section (i.e. the amount of scattered light) for a given size particle. Within a 2σ limit of confidence, the scattering cross-section of a 0.2um particle, may vary from .003 to .012um^2, a factor of 4. As stated, this is not a fundamental limitation since, by slowing down the measurement, we might improve the measurement accuracy. Fortunately, the limitation is only particularly significant for small particles, which generally exhibit a very steep dependence of the scattered light on their size; hence, the sizing is not as drastically affected.

Fig.4 shows the measured scattering cross-sections versus size for various spheres and deformed spheres. Fig.5 compares the analytic expression with more general data on spheres and other particles (2). In the region of

concern, there is a very steep dependence (fifth power) on particle diameter d. The definition of the size of a particle is also somewhat arbitrary; usually the size is defined as illustrated in Fig.6, (3), which gives the particle projection in some view of a microscope. The size associated with this particle is then: d= D_1D_2.

In many clean rooms, the total number of particles, above a given size, follows a $1/d^2$ distribution, at least for diameters larger than 0.05um.(4) Much less data is available for the distribution of particles collected on wafers, but let us assume that the trend is similar. Hence, we can always expect there to be many more small particles than big ones in the distribution. When we, therefore, count the number of particles present on a wafer, we may expect there to be significant statistical variation in the result.

This is readily seen in Fig.7: the percentage of the histogram above the threshold represents the probability that the particle will be counted, and there are many particles present, with a probability less than one.

If we make two successive scans with identical thresholds on such a wafer, we will find that the total number of observed particles above the threshold is very close to each other; in fact, it turns out to be very close to the true number that is present on the wafer. But, if we compare in detail, the presence or absence of individual particles, then we will notice that there are significant differences, especially for particles near the threshold. As many as 20 to 30% of the observed particles have disappeared, and have been replaced by others in the next scan. Obviously, to the user who wants to compare, in detail, two particle maps, before and after a process step, this situation is difficult, if not bewildering.

We have developed two techniques, dual thresholding and scan averaging, which, when used in conjunction, drastically lower the observed statistical effects. Hence, it becomes possible to affirm with a great degree of certainty, which particles have been removed or added at a particular wafer location. We call this process map-to-map comparison.

Dual thresholding is illustrated in Fig.8. A lower threshold Tc is defined (collection threshold), together with an upper threshold Tm (map to map threshold). The addition of the lower threshold Tc allows us to gain additional information, at the expense of working at a slightly higher effective threshold Tm.

When comparing scans, the following algorithm is used: if a particle is observed at least once above Tm in one of the scans, and is not detected above Tc in the other scan, then the particle is considered either a true addition or deletion. We call these particles "difference" particles. All other cases do not result in difference particles. Of course, it is also required that we consider only particles in the same spatial location on the wafer.

The use of this buffer zone between Tc and Tm greatly reduces the ambiguity that is usually observed. This can be readily studied using a Monte Carlo technique. Through simulation, we distribute over the wafer, a known number of particles, between .15 and 1 micron, according to a $1/d^2$ cumulative distribution (or any other distribution).

Table 1. Difference Particles with Dual Thresholding

Tc um^2	Tm um^2	# particles on wafer	# particles detected(avg)	% diff.part. (mean)
.008	.008	608	605.9	17.5 %
.008	.008	61	62.1	22.1 %
.006	.008	580	584.4	10.0 %
.004	.008	572	572.9	4.54%

The averages are for 10 simulations with the same number of particles on the wafer.

To each particle is assigned an appropriate scattering cross-section (Fig.4) and the associated statistical variation in its measurement (Fig.3). The results are shown in Table 1. The "before" and "after" scans in this case are exactly identical, and hence, the number of difference particles expresses the error of the technique. The case that the average number of particles detected is quite close to the true number present, in almost all cases. But the percentage "difference" particles drops very drastically when Tc is lowered below Tm. At a ratio of Tm/Tc=2, the number of difference particles is usually down to 4 or 5% of the total number, versus 20 to 30% for the single threshold case. The exact fraction is generally a function of the threshold setting, and the particle distribution.

A second method can be used to further increase the accuracy of the measurement. If we scan the wafer not once, but several times, in the "before" condition, and average the scans together, we can construct a prototype

of a "before" scan, which is more accurate than a single scan. Likewise, we can construct an averaged "after" scan.

Whereas dual thresholding forced a higher effective threshold, the penalty we pay in scan averaging is, of course, in the increased measurement time. However, in critical applications, such as equipment acceptance, the greatly improved accuracy may well warrant the necessary increase in time. The number of required repetitive measurements is generally quite small, particularly when used in conjunction with dual thresholding.

Table 2. Difference Particles with Tm/Tc=2

Tc um^2	Tm um^2	# particles on wafer	# particles detected(avg)	N	% diff.part. (mean)
.004	.008	572	572.9	1	4.54%
.004	.008	585	588.2	2	1.20%
.004	.008	596	589.2	3	.44%
.004	.008	576	579.5	4	.20%
.004	.008	605	602.7	5	.03%

The averages are for 10 simulations with the same number of particles on the wafer. N is the number of identical scans averaged.

Table 3. Difference Particles with Tm/Tc=1.33

T1	T2	# particles on wafer	# particles detected(avg)	N	% diff.part. (mean)
.006	.008	580	584.4	1	10.1 %
.006	.008	605	605.8	2	5.6 %
.006	.008	603	602.6	3	3.2 %
.006	.008	585	590.5	4	2.14%
.006	.008	610	612.7	5	1.35%
.006	.008	613	617.8	6	1.06%

The averages are for 10 simulations with the same number of particles on the wafer. N is the number of identical scans averaged.

Table 2 lists the results observed with an increasing number of scans averaged, used in conjunction with a setting Tm/Tc=2. It is seen that just rescanning the wafer once, drastically drops the remaining inaccuracy by another factor of almost 4, bringing the error close to the 1% level. In Table 3, Tm/Tc is smaller and we require

more scans, namely 5, to bring the error down to the 1% level. But if averaging twenty scans, the error is still on the order of 4%. Clearly, a judicious combination of both techniques is much more powerful than either of them by itself.

All of the above has tacitly assumed that the particle maps can be spatially-superimposed, so that it can be unambiguously determined that we are considering the same spatial location when applying the above criteria. In practice, the wafers may have been rotated, a large number of particles may have been added or removed, and pattern matching must be used to overlay the maps. Prominent particles are selected from one scan, and a number of polygons are constructed. In the second scan, the computer attempts to reconstruct these polygons, with high degree of congruency. Once these are reconstructed, the specifics of the coordinate transformation can be determined. To correct for a non-uniform beam velocity during the scan, the beam scan is calibrated with the aid of a special wafer, having known defects on a metric grid.

Fig.9 illustrates an example of such scans produced on Tencor 4500 Surfscan. (Note that the particles here are clustered, and cannot be resolved on the screen). It is necessary to allow for some spatial inaccuracy in the particle location when comparing two maps. Therefore, a small region of "diffusion" is allowed around each particle. However, if dense clusters of particles do occur, the above technique no longer works. It then becomes necessary to apply some of the pattern matching techniques to the cluster itself. Note, however, that in many uses of before and after comparison, the original defect may have changed size, even if it stayed in place. For example, in a CVD of epi reactor, the size of the defect may have changed after the deposition.

The above discussion brings out in considerable detail the limitations that must be taken into account when sizing or counting particles on a wafer. These limitations must be taken into account when using these particle monitors for acceptance criteria for cleanliness. For example, an acceptance criterion such as "No more than 5 particles, of .5um and above" is of limited usage. As indicated, subsequent measurements on the same wafer may either give 4 or 6, causing either acceptance or rejection. It is therefore, much more logical to look at the cumulative histogram, which plots at each cross-section, the sum of all particles having a cross-section larger or equal than the present one. This has several advantages:

a) If a particle is "erroneously" sized, it still makes a contribution to the histogram, but does not cause a drastic acceptance or rejection.

b) The whole contamination distribution is taken into account, with the instrument using its full range of sensitivity. Small particles (<.5um) do not enter in the definition above; yet if a large number of them is present, they may drastically alter the defect density.

c) The integration inherent in the cumulative distribution brings out trends and patterns which are difficult to see in a regular histogram.

d) The method is similar to the classic cleanroom definition of cleanliness.

Plotting both quantities (cumulative number and scattering cross-section) on log-log scales, we may often, although not always, obtain a straight line, Fig.10. Acceptance or rejection of a wafer is then based on the line of the histogram laying above or below a given acceptance criterion. Note that the full range of contamination, with the full power of the instrument, can be used in this approach, rather than concentrating on one point of the graph. Conversion to particle size can be done, if necessary (Fig.11).

Fig.12 illustrates point c) above. It can be clearly determined that the last point is not part of the distribution, and therefore, is likely to be caused by excessive electronic noise.

Fig.13 illustrates the power of the cumulative histogram, and point c), in a different way. Particles have been distributed according to a $1/d^2$ dependence. In the regular histogram the law is barely, if at all perceptible. By contrast, the cumulative histogram clearly brings out the powerlaw. Clearly, this approach makes much better use of the capabilities of the instrument, while at the same time recognizing its limitation.

Conclusions

The user of contamination monitoring equipment must recognize the limitations caused by the trade offs between measurement accuracy and throughput of these instruments. Lack of photons appears as the main limitation; however, through judicious use of dual thresholding, scan averaging and cumulative histograms, many of the statistical limitations can be overcome.

REFERENCES

1) L.Galbraith, A.Neukermans, SPIE Vol.774, 13, 1987.

2) T.Shiraiwa et al, 2nd Symposium on Particles on Surface, Detection, Adhesion, Fine Particle Society Proceedings, Santa Clara, 1988.

3) E.Hansen, J.Daniel, Journal of Applied Physics 18, 1967.

4) B.Lin, B.Fardi, K.Ahn, Proceedings, 32nd IES Meeting, 1986.

List of Figures

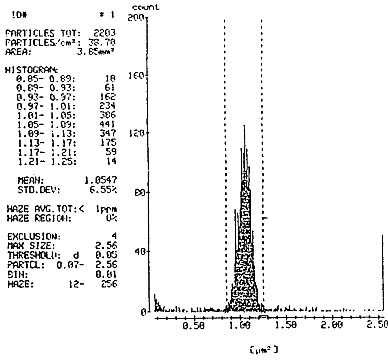

Fig.1 Histogram of monodisperse 1.08 spheres; standard deviation: 6.5% of the mean.

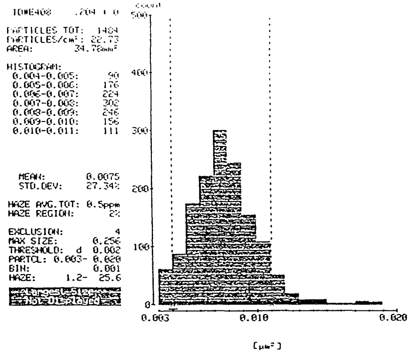

Fig.2 Histogram of .20 micronspheres; standard deviation: 33% of the mean.

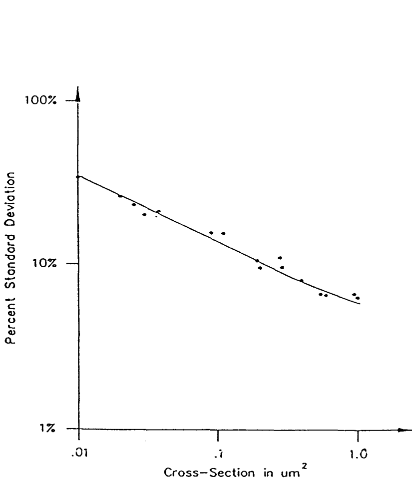

Fig.3 Standard deviation, as a percent of the mean, for various scattering cross-sections. The slope of the curve is 0.5, as expected from photon statistics.

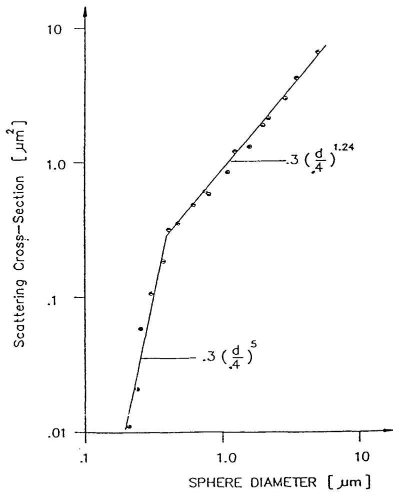

Fig.4 Scattering cross-section versus particle diameter, from spheres and deformed spheres measurements.

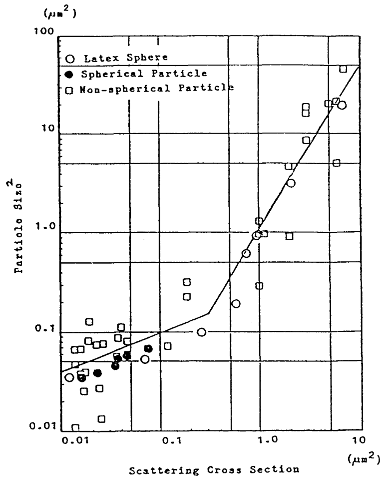

Fig.5 Comparison with other experimental data on arbitrary shaped particles.

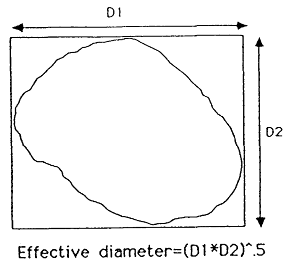

Fig.6 Definition of an effective particle diameter.

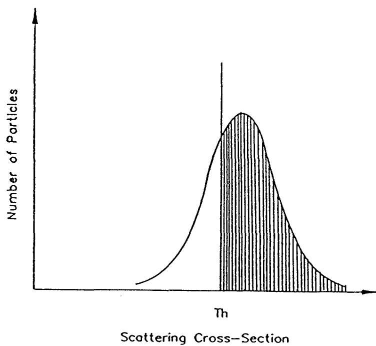

Fig.7 The fraction of the histogram above the detection threshold represents the probability of detection of the particle.

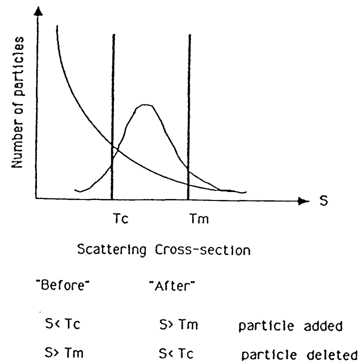

Fig.8 Dual thresholding technique; only the listed cases cause addition or deletion of particles.

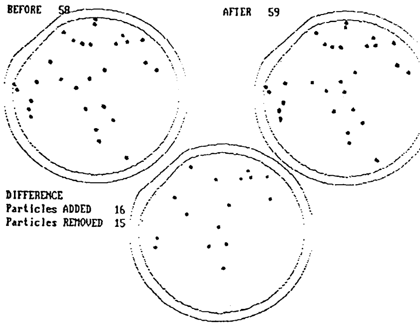

Fig.9 Comparison of two maps, "before" and "after", as presented on the Surfscan 4500 (most of the particles here are clusters).

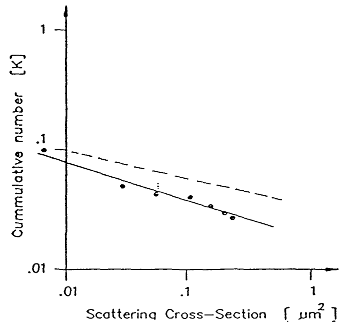

Fig.10 Cumulative histogram versus scattering cross section (dotted line is an example of acceptance curve).

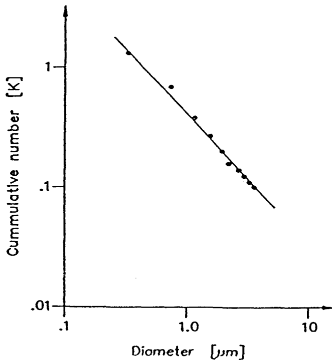

Fig.11 Cumulative histogram, plotted versus particle diameter.

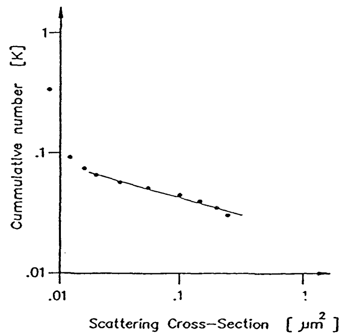

Fig.12 The cumulative histogram easily detects the error in the last measurement point.

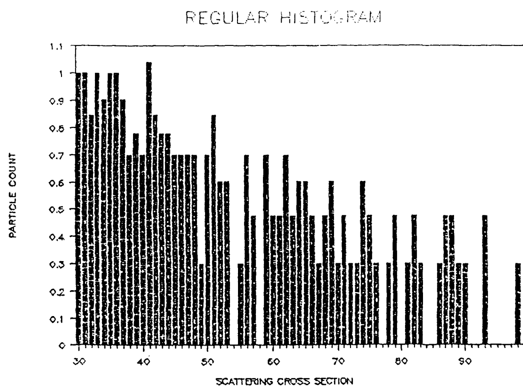

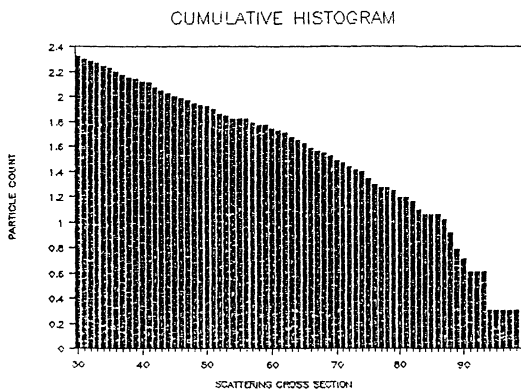

Fig.13 $1/d^2$ powerlaw, easily seen on cumulative histogram, barely detectable on the regular histogram.

CONCENTRATIONS OF ORGANIC VAPORS AND THEIR SURFACE ARRIVAL RATES AT SURROGATE WAFERS DURING PROCESSING IN CLEAN ROOMS

A. J. Muller, L. A. Psota-Kelty, J. D. Sinclair

AT&T Bell Laboratories, Murray Hill, NJ 07974

P. W. Morrison

AT&T-Microelectronics, Orlando, FL 32819

ABSTRACT

Sampling and analysis methods for characterizing vapor phase organic compounds in clean rooms have been developed. Two separate schemes have been devised to monitor airborne concentrations of organic vapors and their surface arrival rates onto an intially clean surface. The airborne concentrations and surface arrival rates of selected organic species have been quantified at three manufacturing locations. The total airborne concentration of organic vapors was found to be in excess of 100 $\mu g/m^3$ at all sampling locations. Both internal and external sources contribute importantly to this total hydrocarbon abundance. The total surface arrival rate at the static collection device of all species that have been quantified is typically >2 pg/cm^2sec and sometimes >20 pg/cm^2sec. This contrasts with an expected deposition rate for particles (using an estimated average deposition velocity of 0.001 cm/sec) of approximately 10^{-6} pg/cm^2sec in clean rooms operated at the Class 10 limit.

Introduction

Characterization of airborne contamination in clean rooms for semiconductor device manufacturing has usually been limited to periodic measurements of the concentrations of particles >0.3 μm diameter and to laser scan evaluations of such particles deposited on wafer surfaces. Until recently, convenient methods to conduct multipoint repetitive analysis of particles <0.3 μm or of contaminant vapors have not been available. In the case of organic vapors there has also been little consideration given to potential effects on device yield or reliability.

Recently, researchers have begun evaluating the airborne concentrations of organic vapors in office buildings and in homes (1-3). In one study that examined three sites in different regions of the United States (1), the indoor concentrations of semi-volatile organic compounds (vapor pressure in the range $10\text{-}10^{-4}$ mm) in electronic equipment rooms were typically 30 $\mu g/m^3$ (total abundance) and values as high as 1000 $\mu g/m^3$ were found when construction was in progress. Outdoor concentrations at the same sites ranged from 1-35 $\mu g/m^3$. These concentrations contrast with an upper limit particle mass concentration in Class 10 clean rooms of roughly 2 ng/m^3, assuming the average particle size is 3 μm (a conservative estimate) and the density is that of ammonium sulfate. Organic species with vapor pressures less than roughly 10^{-2} mm can be expected to condense to appreciable extents on available surfaces. Of course, highly volatile organic species such as methanol, acetone, and low

molecular weight alkanes are also likely to be present in clean rooms and to quickly produce monolayer coverage on clean surfaces, but their high volatility prevents accumulation much beyond a monolayer. Substances with vapor pressures $>10^{-4}$mm are also likely to be present at very low concentrations but are not considered in this paper. Since clean room air handling systems typically do not filter organic vapors, the concentrations of these vapors and their deposition rates to wafer surfaces are likely to be significant, even in the absence of internal generation. The deposition velocities for organic molecules are larger than those for typical clean room particles (0.01-5 μm), due to their much larger diffusivity in air. Consequently, the arrival rate of organic contamination at initially clean wafer surfaces, on a mass basis, is expected to greatly exceed the arrival rate for particles. Clearly, if successful manufacture of integrated circuits requires Class 10 or better environments with respect to airborne particles, then the potential effect of organic vapors on yield and reliability needs further investigation. While particles typically cause defects at or in close proximity to the point of deposition, the effects of organic contamination on wafer surfaces are likely to be less well defined. The effects may include: (1) poor adhesion of metallization, passivation, polysilicon, photoresist, or encapsulant; (2) nucleation irregularities on surfaces; and (3) variations in oxide growth. The intent of this continuing study is to develop a sampling and analysis protocol for characterizing organic contamination relevant to integrated circuit processing in clean room manufacturing environments and then to use the analytical procedures to determine the sources, surface accumulation rates, and effects of these contaminants.

Experimental

Both passive and active sampling techniques were used to collect organic vapors. Static charcoal collection badges fitted with polymer screen membranes (#3500 Organic Vapor Monitors from 3M Company) were used for determining airborne concentrations and arrival rates of organic vapors at surfaces. The amount of air sampled is somewhat dependent on the the air flow characteristics, as will be discussed. Adsorbent tubes (Carbotrap 300 Multi-bed Thermal Desorption Tubes from Supelco) connected to the house vacuum lines through flow limiting orifices were used to collect organic vapors. The flow rate through the critical orifices was designed to be 6.5 ml/min. Two tubes were used in series and the second tube was used to detect breakthrough of the most abundant compounds. Sampling was carried out over a period of several months and the typical sampling interval was four weeks for both the tube and badge samplers. For the tubes, the four week interval represented a total sampled volume of approximately 0.25 m^3 (250 l). After sampling and analysis were completed, it was discovered that even though calibration in the laboratory showed that the flow rates through the charcoal tubes matched those expected for the critical orifices, some of the adsorption tubes from some lots restricted the flow to values appreciably below the intended flow rate. In a typical lot, the flow rates have been found to be at least 75 percent of the expected flow rates, but in about 10 percent of the cases, the flow rates were as low as 20 percent of normal. The indicated concentrations for the tube samplers could be low by as much as a factor of five.

The organic species collected by the samplers were identified and quantitated using gas chromatography/mass spectroscopy (GC/MS). All analyses were done using a Hewlett-Packard 5890 Capillary Gas Chromatograph interfaced to a 5970B Mass Selective Detector and equipped with a 0.2 mm x 12 m 5% phenyl/methyl silicone column (Ultra-2). Compound identities were confirmed by comparison to the mass spectra of known compounds.

Compound concentrations were determined using external calibration.

The charcoal badges were extracted with 2 ml of carbon disulfide. The extraction continued for at least an hour and then the extract was concentrated to 0.3 ml and 5 μl were injected into the GC/MS. The GC oven was temperature programmed from 0°C to 280°C at a rate of 8°C/min. The arrival rate, R, at the charcoal surface is calculated using $R=m/At$, where m is the weight of a given compound determined by GC/MS, A is the area of the sampler (7.07 cm^2), and t is the sampling time. Since transport from the polymer screen to the charcoal is by Brownian diffusion, the arrival rate at the polymer screen must be larger than that at the charcoal and R may be taken as a lower limit for the arrival rate at the screen. The arrival rate at the polymer screen should be roughly equivalent to that of an initially clean wafer. As contamination accumulates on the wafer, the surface will eventually saturate. Ambient vapor concentrations (C) can be calculated using Fick's First Law of Diffusion, where the diffusion path is the region between the polymer screen and the charcoal adsorbent. The form of Fick's First Law used here is $C=m/tur$ where r is the recovery coefficient and u is the uptake rate. The uptake rate is equal to DA/l where D is the diffusion coefficient, A is the geometric area of the charcoal collection badge, and l is the length of the diffusion path (1.0 cm). The uptake rate is assumed to be constant for each compound. This assumption holds if: (1) the total compound mass is significantly less than the capacity of the adsorbent; and (2) the mass transfer resistance across the boundary layer is negligible, which is true for flow rates > 20 m/min but for lower flow rates introduces increasingly significant error on the low side (4). Tables of values for r and u are available from the badge supplier.

The adsorbent tubes were thermally desorbed using a Supelco Model 850 Thermal Desorption Unit operated at a desorption temperature of 330°C. The desorption time was 15 minutes. During the desorption period, the GC column was maintained at -25°C to cryofocus the released compounds. After the desorption period, the GC oven was ramped to 25°C at a rate of 50°C/min, then to 100°C/min at a rate of 10°C/min, and finally to 280°C at a rate of 5°C/min. Vapor concentrations, C, were calculated using $C=m/f(t)$, where m is the weight of the compound as determined in the GC/MS analysis, f is the flow rate, and t is the sampling time.

The capacity of the charcoal badges (all species combined) was 25 mg, and in this study, the total compound weight was never over 0.5 mg. The recovery for compounds smaller than hexadecane was usually 100%, and the detection limit was 10 ng (0.1 ppb in air). The capacity of the adsorbent tubes was quite variable depending on the substance, recovery was typically 90-100%, and the detection limit was approximately 10 ng.

Results and Discussion

Sampling for organic vapors using the passive charcoal collection badges was conducted at three locations, designated CR I, CR II, and CR III. Two of these were in rural environments (CR I and CR II) and one was in an urban environment (CR III). Sampling using the charcoal adsorbent tubes was also conducted at CR I.

Airborne Concentrations and Surface Arrival Rates From Charcoal Badge Samplers - A typical chromatogram for samples collected with the charcoal badge samplers is shown in Figure 1. Major components seen in nearly all samples include toluene, butyl acetate, cellosolve acetate, xylenes, and C_3 alkyl benzenes (ethyl toluene and trimethyl benzene isomers). Straight chain aliphatic hydrocarbons (C_9 to C_{14} hydrocarbons), ethyl benzene,

trichloroethylene, tetrachloroethylene, and branched hydrocarbons were usually present at lower concentrations. Many other minor and trace components are evident in the chromatogram. No attempt was made to identify every detectable peak since >90 percent of the mass is contained in roughly 10 of the components.

The average airborne concentrations and arrival rates for selected compounds found at each location are given in Table I. The compounds selected for quantitation shown in Table I were chosen to cover a range of molecular weights, polarities, and functional groups. These compounds were not always the most abundant at a given location. Table II gives some less significant components from each location that were detected but not quantified. More than half of the species found in each clean room were present as substantial components at all three locations. Typical compounds found at all locations in each clean room include toluene, ethyl benzene, and nonane. Sampling at multiple points (See Figure 2) across the CR I clean room shows, as seen in Figure 3, that the concentrations of these species span a narrow range for each sampling period consistent with their sources being either external to the clean room or from construction materials or housekeeping chemicals present throughout the room. Automobile emissions are a well known source for many of these species (1-3). Each clean room was also found to contain some species with concentrations that were quite variable across the room, as seen in Figure 4. Very high concentrations of butyl and cellosolve acetate were encountered at two locations, strongly suggesting that these contaminants were derived from processing taking place near these sampling locations. This array of compounds found in CR's I, II, and III is similar to the components found in office buildings using the same sampling and analysis methods (1), except for the species derived from processing, such as butyl and cellosolve acetate. The concentrations of toluene and ethyl benzene in the clean rooms are compared in Figure 5 with data from office buildings housing electronic equipment (1). The outdoor concentrations at CR III are also indicated and show that the external environment contributes substantially to the observed concentrations of these two components at the CR III location.

Vapor Concentrations From Adsorption Tubes - A typical chromatogram obtained from a CR III sample is given in Figure 6. In general, chromatograms from the charcoal badges and adsorption tubes were very similar in appearance and all of the major compounds were present in both chromatograms for a given location. Tube sampling, however, generally provided better detectibility for the most volatile compounds such as isopropanol and chlorofluorocarbons. Most of the peaks seen in Figure 1 for the CR I location are also found in Figure 6, though the relative intensities are quite variable, reflecting the differences in relative concentrations at different sampling sites within the clean room. Average values of concentrations at CR I are given in Table III.

Comparison of Adsorption Tube and Charcoal Badge Samplers - The agreement between Tables I and III is only fair. This is more easily visualized in Figure 7. The flow rate uncertainty already discussed for the adsorbent tube samplers is probably the dominant contributor to the discrepancy. The variation in air flow characteristics at the polymer screens of the charcoal badge samples may also contribute.

In principal, a lower limit for the mass transfer coefficient for transport across the external boundary layer of the passive samplers, which should be equivalent to the initial phase of transport to an initially clean 2 inch wafer placed in the same configuration, can be determined by taking the ratio of the arrival rate at the polymer screen to the airborne concentration. The

data for the passive samplers provides a lower limit arrival rate at a clean wafer surface which, when divided by the airborne concentration from the active sampler, provides an estimate of the mass transfer coefficient. These are given as ranges in Table IV. The ranges in the arrival rates are known with a high level of certainty and accurately reflect the variation in arrival rates across the CRI cleanroom. The appreciable uncertainty discussed above for the airborne concentrations contributes substantially to the ranges in airborne concentrations and the mass transfer coefficients.

These lower limit estimates of the mass transfer coefficients assume that no loss of organic vapors takes place across the polymer screen of the charcoal badges. If this loss rate is not negligible, then the indicated range would be low. However, these estimates are probably representative of the lower limit of the accumulation rates on wafers during the initial exposure of a freshly formed or cleaned surface to the clean room environment. Further work will be required to determine how long it takes for accumulation rates to be slowed to insignificant levels by the desorption of previously condensed material, i.e. the rate of arrival and desorption become equal.

Summary and Conclusions

The vapor concentrations and surface arrival rates of selected airborne organic species have been quantified at three manufacturing locations. The total vapor concentration of organic vapors was found to be in excess of 100 $\mu g/m^3$ at all sampling locations. Both internal and external sources contribute significantly to this total abundance. The total surface arrival rate of all species that have been quantified is typically >2 pg/cm^2sec and sometimes >20 pg/cm^2sec. This contrasts with an expected deposition rate for 0.5 μm particles (using an estimated deposition velocity of 0.1 cm/sec) of roughly $10^{-6}g/cm^2sec$ in clean rooms operated at the Class 10 limit. Clearly, if successful manufacture of integrated circuits requires Class 10 or better environments with respect to airborne particles, then the potential effect of organic vapors on yield and reliability needs further investigation.

Acknowledgements

The authors thank P. Yannes, E. T. Eckroth, J. Rauchut, A. J. Murphy and R. F. Karoly for important contributions throughout the course of this work.

REFERENCES

1. H. C. Shields, C. J. Weschler, *J. Air Polln. Contr. Assoc., 37(9),* 1039 (1987).
2. M. A. Cohen, P. B. Ryan, Y. Yanagisawa, J. D. Spengler, H. Ozkaynak, *J. Air Polln. Contr. Assoc., 39(8),* 1086 (1989).
3. S. A. Edgerton, M. W. Holdren, D. L. Smith, *J. Air Polln Contr. Assoc., 39(5)* 729 (1989).
4. R. G. Lewis, J. D. Mulik, R. W. Coutant, G. W. Wooten, C. R. McMillin, *Anal. Chem., 57,* 214 (1985).

Table I. Airborne Concentrations Determined By Passive Samplers* (µg/m³)

Compound	CR I	CR II	CR III
Toluene	3.3 ± 1.2	1.4 ± 0.7	10.5 ± 1.9
Ethyl benzene	1.8 ± 1.1	0.58 ± 0.51	2.15 ± 0.94
Butyl acetate	59.5 ± 80.8	0.65 ± 1.07	4.6 ± 4.1
Cellosolve acetate	31.8 ± 40.0	1.50 ± 1.84	22.4 ± 21.8
n-Nonane	1.6 ± 0.9		
n-Decane	2.7 ± 0.9		
n-Undecane		1.4 ± 0.6	

*Average of ten sampling sites in each clean room

Table II. Components Identified

Trichloroethane	Cellosolve acetate
Trichloroethylene	Hexamethylcyclotrisiloxane
Tetrachloroethylene	Octamethylcyclotetrasiloxane
Dichlorobenzenes	3-Methylhexane
Benzene	Trimethylhexane
Toluene	Dimethylcyclohexane
Ethylbenzene	Tetrachloroethane
Xylenes	Propylbenzene
C_3-Alkylbenzenes	3-Ethyltoluene
Methylcyclohexane	4-Ethyltoluene
n-Nonane (Nonane)	1,3,5 Trimethylbenzene
n-Decane (Decane)	2-Ethyltoluene
n-Undecane	1,2,4 Trimethylbenzene
C_{12}-C_{16} n-alkanes	Butyl acetate

Table III. Airborne Concentrations at CR I Determined by Active Samplers* (µg/m³)

Toluene	3.3 ± 3.3
Ethylbenzene	2.0 ± 1.2
Butyl acetate	21.1 ± 33.0
Cellosolve acetate	2.41 ± 2.54
n-Nonane	2.14 ± 1.92
n-Decane	4.38 ± 4.63

*Average of ten sampling sites

Table IV. Comparison Of Ambient Concentrations and Arrival Rates

Compound	Arrival Rate (At Charcoal) µg/(cm²sec)	Concentration (Active Samplers) µg/cm³	Ambient Mass Transfer Coefficient * cm/sec
Toluene	3.0 - 5.3 x 10^{-7}	0.5 -8.9 x 10^{-6}	0.006 - 0.65
Ethylbenzene	0.7 - 1.3 x 10^{-7}	0.2 - 3.7 x 10^{-6}	0.02 - 0.43
Butyl acetate	8.9 - 88 x 10^{-7}	2.6 - 88 x 10^{-6}	0.08 - 2.4
Cellosolve acetate	4.3 - 10.2 x 10^{-7}	0.6 - 4.2 x 10^{-6}	0.1 - 1.67
Nonane	0.6 - 1.91 x 10^{-7}	0.18 - 4.7 x 10^{-6}	0.14 - 0.44
Decane	1.3 - 2.6 x 10^{-7}	0.36 - 11.9 x 10^{-6}	0.014 - 0.46

*Mass Transfer Coefficient = Arrival Rate/Ambient Concentration

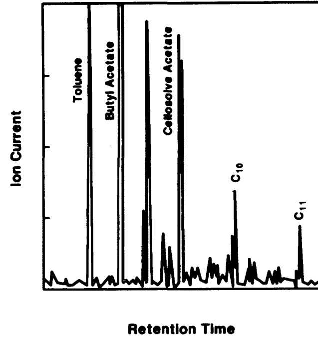

Figure 1. Typical chromatogram for a sample collected at CR I using the charcoal badge samplers.

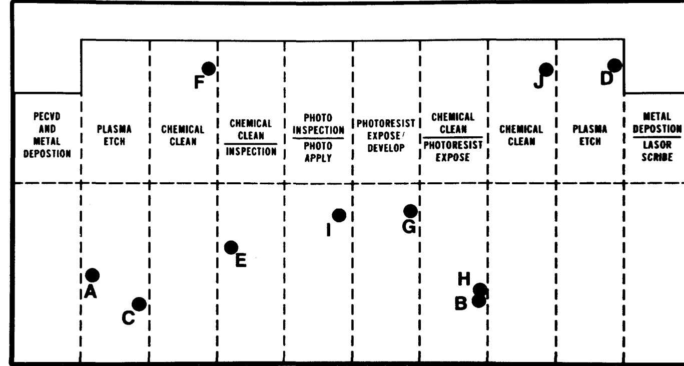

Figure 2. Sampling locations at CR I.

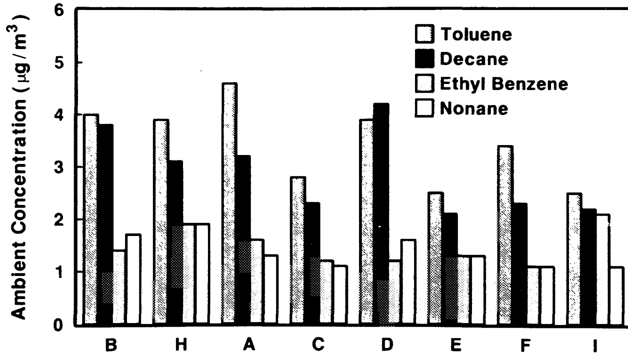

Figure 3. Vapor concentrations of selected components at the indicated locations in CR I.

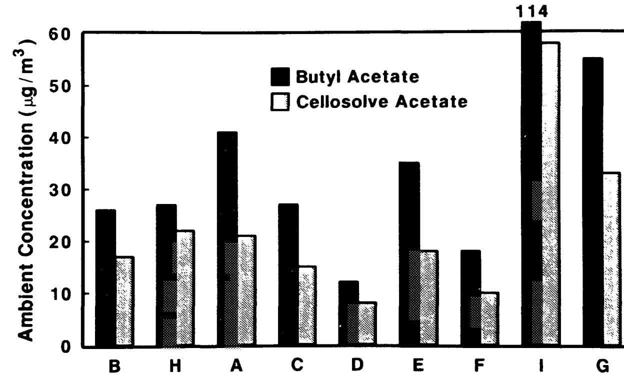

Figure 4. Vapor concentrations of selected components at the indicated locations in CR I.

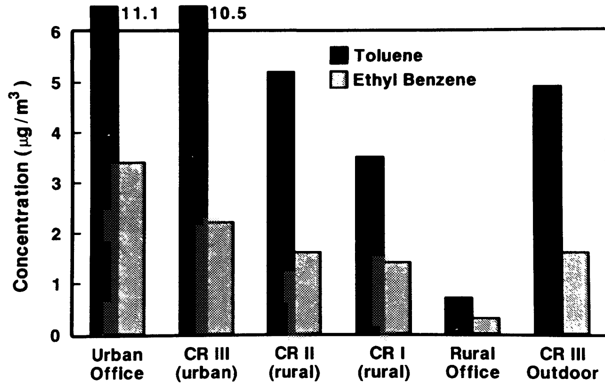

Figure 5. Vapor concentrations of selected components at clean room and office building locations.

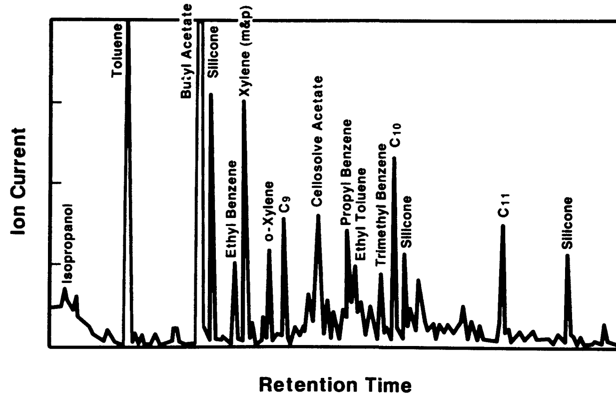

Figure 6. Typical chromatogram for a sample collected at CR I using the adsorption tube samplers.

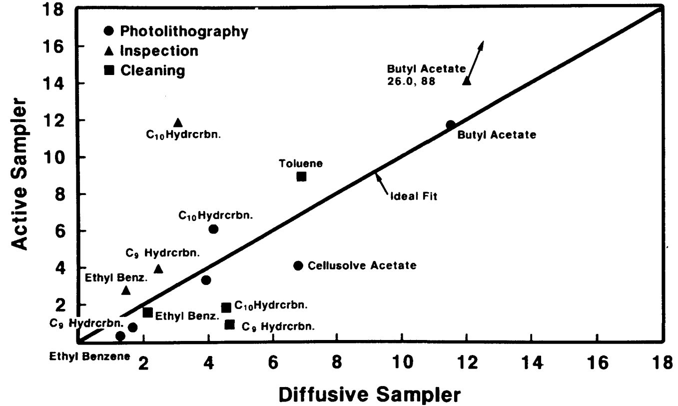

Figure 7. Comparison of vapor concentrations ($\mu g/m^3$).

CHARACTERIZATION OF CLEANING

SURFACE COMPOSITION AND MORPHOLOGY OF SI WAFERS AFTER WET CHEMICAL TREATMENTS

M. Grundner, P.O. Hahn, I. Lampert, A. Schnegg, and H. Jacob
Wacker-Chemitronic GmbH, Research and Development,
Postfach 1140, D-8263 Burghausen, FRG

ABSTRACT

Wafer production or processing demands the application of chemical treatments for the sake of cleaning, dissolving dielectric layers or surface conditioning. The chemical state of the silicon surface after usual treatments with HF, water, and fast oxidizing media has been studied by means of XPS (X-Ray Photoelectron Spectroscopy) and HREELS (High Resolution Electron Energy Loss Spectroscopy). Storage effects are included, too. Specifically it is shown that the hydrophobic state obtained by a HF dip is due to Si-H groups and hydrophilicity is caused by Si-OH groups. Conclusions on reaction paths are drawn, if possible. Morphological changes during or after treatments are characterized by means of ARLS (Angle Resolved Lightscattering), which yields the correlation lengths of surface inhomogeneities in the micron range.

I. INTRODUCTION

Wet chemical treatments play an important role in the course of wafer production. A crucial step is the final clean providing in a reproducible way a homogeneous "nonreactive" surface state with metallic and ionic contaminants on a level as low as possible. The semiconductor industry applies wet chemical treatments as part of a sophisticated process technology. In fact more than 40 % of all processes in submicron technology are based on wet chemical treatments and more specifically about 10 % are cleaning procedures.
A wafer surface thus comes into contact with various reactive species. They leave the surface with a distinct chemical composition, which has impact on following processing steps and on electrical properties (1).
It is the main concern of the paper to shed some light on the chemical state of the surface after usual treatments

and to conclude on reaction pathways, if possible. Storage effects are investigated, too, because of their practical relevance. First the surface state after an HF dip is examined and the chemical passivation of the surface is proved by a slow interaction with water and air. Fast wet oxidations performed with treatments based on the famous RCA clean will be characterized. Morphological changes occur during or after treatments, which refer to roughness of the Si surface in the case of the HF dip and to the homogeneity of the hydrophilic oxides on storage.

II. EXPERIMENTAL

The investigations of the chemical surface state were performed in a combined HREELS/XPS apparatus equipped with a load lock for fast insertion of the samples. The surfaces were prepared either in an adjacent clean room (sample insertion time $\sim$ 2 min) or in a nitrogen box connected to the load lock. No differences in the spectra could be detected. Structural investigations were performed with a newly developed light scattering method (2). ARLS measurements of the diffuse scattered light of a laser beam offer the possibility to detect different Fourier components of the surface structure in the micron range (0.17-10 um).
Samples were polished silicon wafers, boron doped in the range 3-30 Ohmcm, with (100) or (111) oriented surfaces. The preparations were performed in electronic grade media (HF, NH_4OH, HCl, H_2O_2) and the water used for rinsing had a base resistivity of 18 MOhmcm. During the measurements the pressure was in the low 10^{-9} mbar region or less.

III. MEASUREMENTS

1. The surface state after a HF treatment.

Despite the ubiquitous use of HF treatments in microelectronic production the surface state attained has long been disputed and the general opinion was that hydrophobicity was due to a coverage by fluorosilyl species (3) with the exception of a recent paper by Jablonovitch et al (4).
A survey spectrum of Si after a HF dip (40 % HF, 1 min) with no water rinse is depicted in Fig. 1. We observe the Si 2p 3/2, 1/2 and Si 2s lines and minor quantities of C, O, and F as contaminants.
Spectra taken after a HF dip at lower concentration (5 %, 1 % HF) exhibited similar features with somewhat changed intensities, however. In general the oxygen signal rose from below $10^{14}/cm^2$ to 1-1.5 x $10^{14}/cm^2$ and the F signal declined (5). The carbon concentration was between 1-2 x

$10^{14}/cm^2$ for all measurements reported here. The carbon peak could always be deconvoluted in C-C or C-H and a minor C-O bonding component, as observed by different authors (e.g. 6).
The fluorine coverage turned out to be a function of the HF concentration. In the case of the (100) surface coverages range from $3 \times 10^{13}/cm^2$ to $\sim 1 \times 10^{14}/cm^2$ with an approximate logarithmic dependence on HF activity. The (111) surface showed an enhanced F coverage for the very low HF concentration due to the fact that the removal of the native oxide was not completely performed. The F coverage was also time dependent. The fluorosilyl concentration rose by nearly a factor of two within two hours. Obviously fluoridating reactions slowly occur during storage.
The XPS measurements prove that the total surface coverage is well below a monolayer equivalent. Hence the surface must be saturated by species not detectable by XPS. HREELS measurements will help to establish a consistent picture of the HF dipped Si surface in the following.

The vibrational spectra of a Si (100) and a Si (111) surface after a 1 min, 40 % HF dip are shown in Fig. 2. The spectrum starts with the "no loss" peak of elastically scattered electrons. The loss peaks can be identified by a comparison with published spectra of UHV cleaned and atomic hydrogen dosed Si samples (7). The spectrum of the (100) surface corresponds closely to that of a dihydride covered (1x1) Si surface state. This dihydride structure exhibits losses due to a stretching mode at 2100 cm^{-1}, a scissor mode at 900 cm^{-1}, a wagging or bending mode at 640 cm^{-1} and a fourth mode around 480 cm^{-1}, whose origin is as yet unclear.
According to the surface structure essentially monohydride should exist on (111). This is indeed the case, the stretching mode at 2080 cm^{-1} and bending mode at 640 cm^{-1} dominating the spectrum. There is a small peak at 900cm^{-1}, which is not expected to occur on an ideal (1x1) termination of the Si lattice. This may be explained by edge atoms on the steps of a well ordered surface, resulting from a misorientation between the wafer surface and the crystal lattice. Such edge atoms can form $Si\text{-}H_2$ groups and give rise to a scissor vibration.
The only vibrations which did not originate from Si-hydride were hydrocarbon related. We observe contributions from the stretching vibrations of CH_x (x = 1,2 or 3) around 2950 cm^{-1} and deformation vibrations around 1350 cm^{-1} on both types of surfaces.
The Si-F vibronic excitation, which should be situated at 800 cm^{-1} could not be detected for two reasons: Firstly, the oscillator strength is weak (8) and secondly the

vibration is covered by the stronger hydride contributions in this region.

2. Interaction of HF treated Si surfaces with water/air

2a. Interaction with water

The interaction of water with a Si surface is of fundamental importance because water is certainly the most abundant chemical with which a wafer comes into contact. Moreover it is the dissolution medium for chemicals used in cleaning, etching and layer removing techniques.

Regarding the fate of the fluorine coverage during a water rinse a rapid decline of nearly one order of magnitude within some minutes could be oberved. Fluorine is replaced during rinsing by an oxygen containing species, which can be inferred from Fig. 3, exhibiting the oxygen coverage (left scale) as a function of rinsing time. The oxygen concentration rises approximately by an amount equal to the vanished fluorine coverage during the first minutes of rinsing. In the course of further oxygen uptake two logarithmic branches are clearly discernible with a break after 3-5h.

Two additional points in Fig. 3 show the oxygen coverage of (111) samples cleaved in water after 10 sec and 1300 min of water contact. The surface concentration of oxygen after cleaving is slightly more than a monolayer equivalent. This fast reaction proves that passivation of the HF treated surfaces is solely due to the hydride coverage.

The lower curve in Fig. 3 refers to the growth of SiO_{2-x} (chemical shift >3.4 eV) during oxygen uptake. A nominal SiO_{2-x} thickness is indicated on the right scale. Oxygen coverage and SiO_{2-x} thickness are mutually adjusted, the difference being due to Si in a lower oxidation state. SiO_{2-x} is the prevalent constituent of the oxide already before a monolayer coverage is reached. Oxide growth in H_2O hence proceeds by island formation of SiO_{2-x}. The same conclusion can be directly drawn from the Si2p spectra, of course. They show that lower oxides are present but do not increase very much in the course of oxidation. Further incorporation of oxygen occurs preferentially at already partially oxidized sites to yield SiO_{2-x}.

Typical HREELS spectra after different rinsing times are shown in Fig. 4 in the case of a (100) wafer. Already after 30 sec of rinsing a feature around 3640 cm^{-1} develops, which is the stretching vibration of OH groups. Hence Si-F exchanges with water to yield Si-OH. After approximately 5 min the first weak signs of an asymmetric Si-O-Si vibrations around 1000 cm^{-1} appear and after 18 min the vibration is quite marked. The invasion of oxygen into Si-

SiH backbonds gets evident, too, in the development of a chemically shifted component of the Si-H stretching vibration (9), as indicated above. The spectrum after 300 min clearly shows that part of the surface is not oxidized yet, in accordance with the oxide coverage derived from XPS data (Fig. 3). In the course of still longer rinsing times a strong Si-OH vibration develops.

2b. Interaction with air

Although the interaction of a HF treated surface with air does not direcly belong to the category "wet chemical treatments", it is of practical relevance in this context. Analogous to Fig. 3 the curves in Fig. 5 show the oxygen coverage (left scale) and the respective oxide thickness of SiO_{2-x} (right scale) as a function of storage time. There is a great similarity in the principal shape of the growth curves in water and air. Both show a logarithmic rise and a changing rate constant after reaching approximately a monolayer coverage by oxygen. The break, however, occurs a factor of 20 later with air than with water. A monolayer equivalent of oxygen is reached after approximately one week. Again the preferred oxidation state is SiO_{2-x}.
The corresponding HREELS spectra show that there is only a minor indication of a Si-O-Si vibration after 10 min, and the main features of course derive from the hydride coverage of the surface. After a week of storage the Si-H stretching vibration is composed of an unshifted and a shifted component, indicating that a part of the surface is still unoxidized in accordance with the data of Fig. 5. The chemical passivation of the surface is thus proved again.

IV. CHEMICAL CONSIDERATIONS

Chemical aspects of the interaction of Si with HF, H_2O and air shall now be discussed. The hydride coverage after a HF dip is at odds with former publications (3), which assumed that the dangling bonds are saturated by fluorine. The reasoning was mostly based on the higher stability (bond strength) of Si-F compared to Si-H. The criterion is, however, not bond strength but rather more the spatial selectivity of the attack, which is explained by Fig. 6.
The dissolution of the oxide (native or thermal) by HF leads to Si-OH and Si-F groups. These groups with their high electronegativity lower the electron density of an adjoining Si-Si bond, inducing a strong partial charge (δ++) on the next (α) and a lesser positive charge (δ+) on the Si atom (β) neighboring to that. The polarization thus induced on the $Si^{\delta+} - Si^{\delta++}$ backbond directs the attack of H^+F^- in such a way that F^- bonds to (α)Si and H^+ to the (β)Si. After further reaction the (α) Si is dissolved, forming finally SiF_6^{2-}.

The selectivity induced by the above mentioned polarization is rather high (90 % in 40 % HF and still higher in lower concentrated HF). Si-F residues are quickly hydrolyzed by water rinsing, exchanging OH for F.
The electronegativity of H is about that of Si and does not induce much of a polarization. Si-H bonds and Si-Si backbonds remain therefore stable under conditions of a low pH value.

During a water rinse the OH^- activity is high enough for a nucleophilic attack on Si-H bonds:

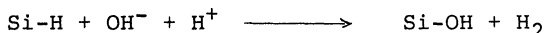

$$Si\text{-}H + OH^- + H^+ \longrightarrow Si\text{-}OH + H_2$$

The Si-OH groups are the sites for the preferential attack of water on Si-Si backbonds, as shown in Fig. 7. The reasoning is again based on the polarization induced by electronegative surface species (OH). After rupture of the Si-Si bond Si-OH and Si-H are facing. Further attack of OH^- on the interior Si-H leads to neighbouring Si-OH groups which finally condense to yield Si-O-Si bridges. Si-Si bonds next to interior Si-OH or Si-O-Si are polarized, too, and may be subsequently attacked by water. Hence oxide nuclei develop which finally coalesce.
Occasionally all of the backbonds of a surface Si atom will be broken before condensation occurs, which leads to a soluble silicate. The consequence is a roughening of the surface, which was measured with the lightscattering technique. Fig. 8 shows the roughness increase during storage in H_2O of different pH value. The measurements prove that the attack of water occurs by a bond rupture mechanism and furthermore that OH^-ions play a decisive role (10).
At oxidation in air two logarithmic branches are obtained, too, confirming that the origin of the break is not due to the respective attacking species but rather more a property of the oxide (strain). The induction period extends to much longer times owing to the fact that OH^- is a much more aggressive species than O_2.

V. HYDROPHILIC TREATMENTS

The last step in cleaning a Si surface is generally a hydrophilic treatment like the RCA clean (11). It involves after a HF dip a two step wet oxidizing treatment referred to as SC1 and SC2 clean. The first (SC1) is a base (NH_4OH, H_2O_2, H_2O) and the second step (SC2) an acid (HCl, H_2O_2, H_2O) catalyzed oxidation. The oxide obtained is reported to be mainly SiO_2 in the thickness region of 0.6-1 nm (12-14), depending on the detailed conditions during the treatment.

We shall concentrate here on some generic features of these oxides using essentially HREELS as they are not easily detectable by XPS.
Fig. 9 depicts spectra after a SC1 and a SC2 clean. Common to the spectra is a strong asymmetric Si-O-Si vibration, centered around 1160 cm^{-1} for SC1 and with somewhat weaker intensity around 1120-1130 cm^{-1} for SC2 treated samples. In addition all spectra exhibit a strong OH stretching vibration from singular OH groups (silanols) at 3740 cm^{-1} and from mutually hydrogen bonded (associated) groups or hydrogen bonded water around 3500 cm^{-1}. The number of the latter needs however not to be large because of the strong intensity of the OH stretch in hydrogen bonded systems. Quite obviously the OH groups are the reason for hydrophilicity.
Subtle differences between SC1 and SC2 treatments show up in the band around 2200 cm^{-1}. The double loss of the strong Si-O-Si vibration falls into this region, but on the other side oxygen backbonded Si-H groups could contribute, too. The intensity of this peak relative to the Si-O-Si asymmetric stretch is stronger on acid than on base catalyzed oxides. From this we conclude, that at least after the SC2 treatment residual Si-H groups are present. Thus the Si^{3+} oxidation state which is normally detected by XPS, e.g. (13), may at least partially be explained by configurations like Si-[O_3H] in the case of the SC2 treatment and by remaining Si-Si bonds otherwise.

Some conclusions concerning the structure of such hydrophilic films can be drawn from spectra after a 1 min isochronal anneal in UHV. Up to temperatures of 200 °C the OH tail disappears, hence it is most probably caused by hydrogen bonded water. Singular OH groups finally disappear between 400 and 500 °C. Thereafter the frequency of the Si-O-Si vibration shifts to higher wavenumbers ($\sim$ 1170 cm^{-1}) before decomposition of the oxide occurs. The shift of the asymmetric stretch may be explained by a growing average angle of the Si-O-Si bridge during thermal relaxation of the oxide, as discussed in more detail in (12). In conclusion acid catalyzed oxides appear to be less interconnected because of terminating Si-H bonds and subjected to more bond strain than the more vigorously oxidized surfaces after SC1 treatment.

The concentration and location of Si-OH were investigated by the treatment of a hydrophilic (SC1) wafer with hexamethyldisilazane (HMDS), normally used as a coupling agent in photoresist deposition. HMDS reacts with Si-OH groups according to (15)

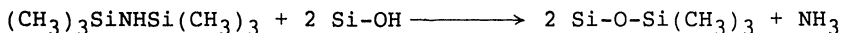

$$(CH_3)_3SiNHSi(CH_3)_3 + 2\ Si\text{-}OH \longrightarrow 2\ Si\text{-}O\text{-}Si(CH_3)_3 + NH_3$$

After the reaction the surface is densely covered by hydrophobic trimethylsilyl groups. The OH vibration in HREELS spectra loses 70% - 80% of the initial intensity, indicating that at least this percentage of silanols is located on top of the oxide. HMDS is not expected to react with subsurface groups because of space requirements of the $Si(CH_3)_3$ moiety.
An assessment of the coverage of silanols was performed from the number of $Si(CH_3)_3$ groups measured by XPS, which turned out to be $2x10^{14}/cm^2$. This agrees reasonably well with an expected maximum areal density of $2.5 \times 10^{14}/cm^2$ of $Si(CH_3)_3$ groups on account of their size of 0.4 nm^2. Not all of the silanols reacted, however, hence a coverage of Si-OH in the range $2.5 - 3 \times 10^{14}/cm^2$ is deduced. Roughly each second Si atom of the oxide surface bears a silanol group.

VI. MORPHOLOGY AFTER TREATMENTS

In recent papers it was shown by LEED that the polished surface of a wafer after stripping the native oxide by an HF dip, exhibits the 1x1 structure of the bulk silicon (16). Edge atom density of the surface of perfectly polished wafers is less than a few percent. LEED, however, integrates over an area of 1 mm^2 and is therefore not very sensitive to local defects, arising from the polishing process or chemical treatments. STM on the other side provides the best local resolution. In general STM confirms the perfectness of the interface, the structural inhomogeneities found are, however, difficult to interprete (17). Recently Chabal et al showed by ATR-FTIR measurements on thermally oxidized and HF stripped samples that, apart from dihydride, mono- and trihydride is present on (100) surfaces and additionally di- and trihydride on (111) (18). This suggests that the HF dip itself might create defects on the surface.
Light scattering and a prolonged storage were used to assess the influence of HF on the Si surface structure. Fig. 10 exhibits angle resolved measurements on (111) surfaces dipped in HF for various times. A wafer with definite misorientation of the surface was taken, which resulted in a bragg peak in the scattered light intensity corresponding to a terrace length of 0.35 µm and an otherwise very low level of diffuse scattered light. After 2 h in 50% HF the level slightly increased and after 6 h all correlation lengths in the accessible region > 0.35 µm up to 10 µm (limited by the specular beam) showed enhanced scattered light intensity. This result clearly reveals that there is an ongoing slow corrosion reaction of the surface with HF, and even a short HF dip can be assumed to enhance

roughness.

A second example for morphology changes provide hydrophilic wafers which are stored in humid air. Usually there is no difference in lightscattering between a wafer with or without a hydrophilic oxide layer present. After storage of the hydrophilic surfaces in humid air (preferentially > 60% r.h.) remeasurement of the wafer after some days yielded an enhanced level of scattered light. After simply dipping this wafer in H_2O the original low level was attained again. Hence a mere roughness effect can be excluded, the oxide itself developed microregions in the order of the correlation lengths with somewhat different optical density. On the other side a HMDS treated wafer with a dense and homogeneous coverage of $Si(CH_3)_3$ groups, which excludes reaction with water vapour during storage, did not show any deterioration.
From this we conclude that condensation-hydrolization reactions during storage generate inhomogeneity of the hydrophilic oxide, that is regions with different ratio OH/bridging oxygen develop. They give rise to diffuse lightscattering and also to effects in thermal oxidation (19).

VII. CONCLUSIONS

It is generally recognized in semiconductor industry that the surface state of wafers is of exceptional importance for reliability and yield in microelectronic production. A thorough knowledge of the chemical surface composition after treatments and of possible changes during storage times is therefore essential in "wafer surface engineering". Knowing the reactive species on the surface allows for a better understanding of the interplay between treatments and subsequent processes. Moreover the varying adsorptive properties of differently treated surfaces, especially against metals in solutions, become understandable (20). Thus surface analysis contributes to the effectiveness of microelectronic production techniques.

REFERENCES

1. H. R. Huff and F. Shimura, Solid State Technol. 26 (3), 103 (1985)
2. P.O. Hahn and M. Kerstan, Proc. SPIE Vol. 1009, 172 (1988)
3. B.R. Weinberger, G.G. Peterson, T.C. Eschrich, and H.A. Krasinski, J. Appl. Phys. 60 (9), 3232 (1986)
4. E. Yablonovitch, D.L. Allara, C.C. Chang, T. Gmitter, and T.B. Bright, Phys. Rev. Lett. 57 (2), 249 (1986)

5. M. Grundner and R. Schulz, AIP Conf. Proc. No. 167, 329 (1988)
6. L.A. Zazzera and J. F. Moulder, J. Electrochem. Soc., Vol. 136 (2), 484 (1989)
7. J.A. Schäfer, F. Stucki, J.A. Anderson, G.J. Lapeyre, and W. Göpel, Surf. Sci. 140, 207 (1984)
8. N.D. Shinn, J.F. Morar, and F.R. Mc Feely, J. Vac. Sci. Technol. A2, 1593 (1984)
9. J.A. Schäfer, D. Frankel, F. Stucki, W. Göpel, and G.J. Lapeyre, Surf. Sci. 139, L 209 (1984)
10. D. Gräf, M. Grundner, and R. Schulz, J. Vac. Sci. Technol. A7 (3), 808 (1989)
11. W.A. Kern and D.A. Puotinen, RCA Rev. 31, 187 (1970)
12. M. Grundner and H. Jacob, Appl. Phys. A 39, 73 (1986)
13. T. Hattori, K. Takase, H. Yamagishi, R. Sugino, Y. Nara, and T. Ito, Jpn. J. Appl. Phys. 25, L 296 (1989)
14. F.J. Grunthaner and P.J. Grunthaner, Materials Science Reports 1(2-3), 65 (1986)
15. W. Hertl and M.L. Hair, J. Phys. Chem., 75 (14), 2181 (1971)
16. P.O. Hahn, Mat. Res. Soc. Symp. Proc. Vol. 54, 645 (1986)
17. P.O. Hahn, M. Grundner, A. Schnegg, and H. Jacob in: The Physics and Chemistry of SiO_2 and the Si-SiO_2 Interface (Editors C.R. Helms and B.E. Deal), 401 (1988)
18. Y.J. Chabal, G.S. Higashi, and K. Raghavachari, J. Vac. Sci. Technol. A7 (3), 2104 (1989)
19. M. Grundner, P.O. Hahn, and I. Lampert, these proceedings
20. E. Morita, T. Yoshimi, and Y. Shimanuki, Electrochem. Soc. Extended Abstr. 89-1, 352 (1989)

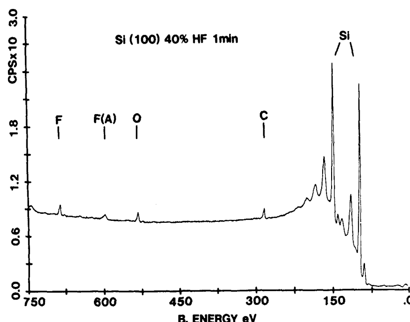

Fig. 1: Wide scan spectrum of a Si(100) surface after a HF dip (40% HF, 1 min), showing Si2s,2p, C1s, O1s, F1s and F(Auger) lines.

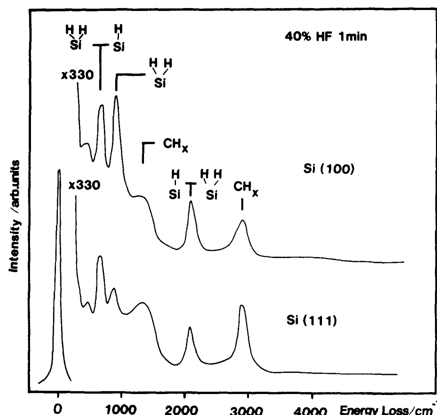

Fig. 2: Vibrational spectra of Si(100) and Si(111) surfaces after a HF dip (40 % HF, 1 min). Si-hydride and hydrocarbon lines contribute to the spectra.

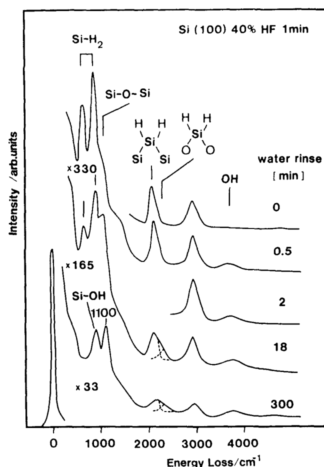

Fig. 4: Vibrational spectra after different water rinsing times. OH groups appear after 0.5 min. The Si-H stretching vibration at 2100 cm^{-1} develops a chemically shifted component, indicated as O_2-SiH_2 above.

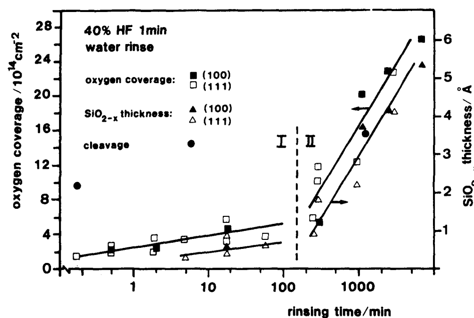

Fig. 3. Oxygen coverage (left scale) and corresponding SiO_{2-x} thickness as a function of rinsing time. Both branches of the growth curve follow a logarithmic time law.

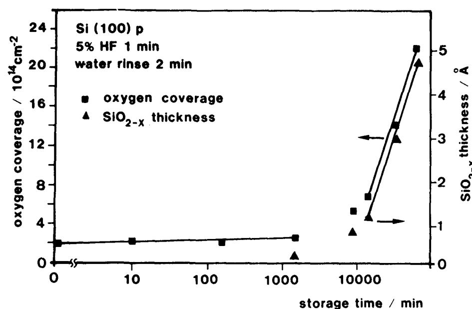

Fig. 5: Oxygen coverage (left scale) and corresponding SiO_{2-x} thickness as a function of storage time in air. Note the expanded time scale in comparison to Fig. 3.

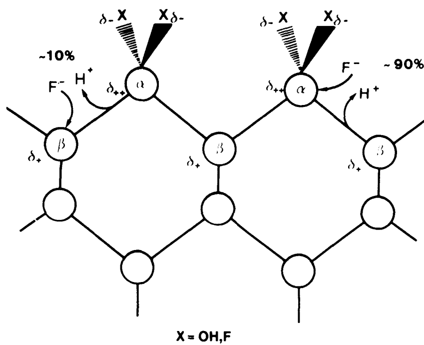

Fig. 6: Electronegative substituents X (X=F, OH) induce a polarization of the Si-SiX bond. The attack of H^+F^- leads to F bonding to (α) Si and H bonding to (ß) Si.

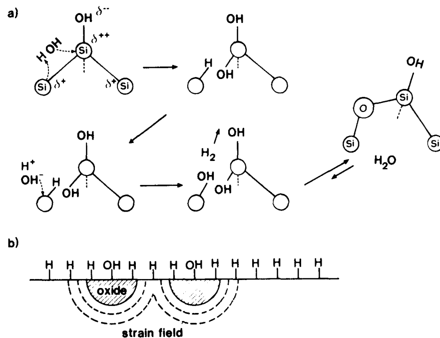

Fig. 7a: The attack of water proceeds by a bond rupture mechanism. Condensation of Si-OH finally leads to Si-O-Si bridges.
Fig. 7b: Local development of oxide nuclei around Si-OH groups.

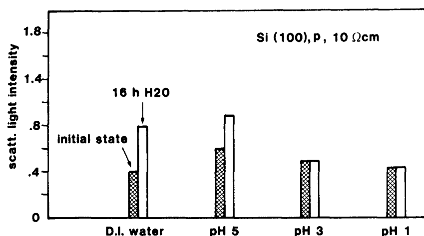

Fig. 8: Scattered light intensity versus storage in D.I. water of different pH value.

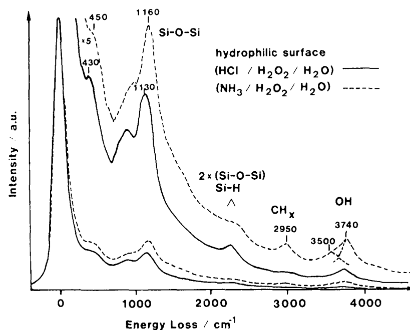

Fig. 9: Vibrational spectra of acid (HCl) and base (NH_3) catalyzed hydrophilic oxides. Si-OH groups (3740 cm^{-1}) characterize the oxides. The Si-O-Si vibrations differ in peak position and intensity.

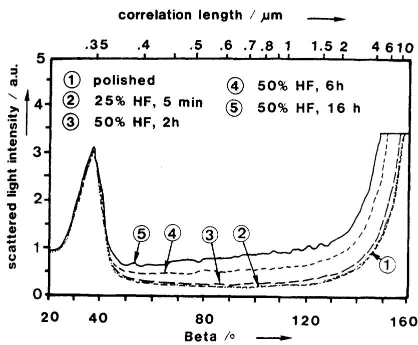

Fig. 10: The scattered light intensity increases after prolonged HF exposure due to increasing roughness of the surface.

ANALYSIS OF TRACE IMPURITIES ON WAFERS FROM CLEANING

R. S. Hockett
Charles Evans & Associates
Redwood City, CA 94063

ABSTRACT

This paper reviews three surface analytical techniques for measuring trace elemental contamination on the surface of semiconductor substrates after cleaning: (1) qualitative analysis using Secondary Ion Mass Spectrometry (SIMS) with an oxygen jet; (2) quantitative analysis using polyencapsulation/SIMS (PC/SIMS) for low atomic number elements with detection limits in the range of 10^9-10^{11} atoms/cm^2; and (3) quantitative analysis using Total reflection X-Ray Fluorescence (TXRF) for high atomic number elements with detection limits in the range of 10^{11}-10^{12} atoms/cm^2. The applications will be for silicon and GaAs.

INTRODUCTION

The cleaning processes for semiconductor substrates are to result in substrates surfaces without elemental trace contamination. The measurement of this contamination has been addressed most recently by secondary ion mass spectrometry (SIMS), polyencapsulation/SIMS (PC/SIMS), Total reflection X-Ray Fluorescence (TXRF), and HF vapor phase decomposition followed by atomic absorption spectroscopy (VPD/AAS). The purpose of this paper is to review the first three techniques: SIMS, PC/SIMS, and TXRF as applied to surface elemental trace contamination after cleaning. The VPD/AAS technique is reviewed elsewhere [1,2]. A novel combination of VPD and TXRF is also presented elsewhere [3].

QUALITATIVE SIMS

The SIMS analysis of silicon wafer surfaces after cleaning came to fruition in the early to mid 1980's [4-6]. The technique uses a primary ion beam (e.g., noble gas ions He^+, Ar^+, Xe^+, or reactive ions O_2^+, Cs^+), often with an oxygen jet focused on the analysis area, to sputter ionize the elemental trace impurities in the native oxide region. The ejected ions are then detected in a mass spectrometer, either of a quadrupole design or magnetic sector design. The purpose of the oxygen jet is to stabilize the ion yields during the analysis through the native oxide region. This effect is shown in Figure 1 where a Xe^+ primary ion beam was used for sputter ionization and a quadrupole mass spectrometer was used for detection of secondary positive ions corresponding to ^{28}Si and $^{44}(SiO)$. The figure shows that without the oxygen jet the ^{28}Si signal

changes several orders of magnitude during the analysis; this is due to the $^{28}Si^+$ ion yield change from changing oxygen content in the sample as the sputtering process moves through the native oxide. The figure demonstrates that the oxygen jet largely eliminates this artifact.

Qualitative SIMS Comparison of Cleaning Processes

As an example of the use of qualitative SIMS to develop commercial scale cleaning processes for silicon wafers, Table 1 lists the relative SIMS signals (relative to a 10^5 ^{28}Si matrix measurement) for Na, K, Al, Ca and Mg+C_2 for three cleaning processes: modified RCA, Choline/H_2O_2, and a Monsanto clean. The standard deviation of the measurements is shown in each parenthesis. This work used a Xe^+ primary ion beam, an oxygen jet, and a quadrupole mass spectrometer on a Perkin-Elmer Phi 560 instrument with a SIMS II probe.

TABLE 1 QUALITATIVE SIMS COMPARISON OF CLEANING PROCESSES [5]
(units are integrated counts ratioed to 10^5 ^{28}Si counts)

	Na	K	Al	Ca	Mg+C2
modified RCA	4(2)	5(2)	38(8)	19(9)	10(4)
Choline/H_2O_2	4(2)	13(8)	3530(524)	28(6)	7(2)
Monsanto clean	4(2)	4(2)	10(2)	8(2)	4(1)

The role of surface Al after cleaning and its effect upon thermal oxidation rate has received attention lately both in the U.S. [7] and in Japan [8]. The effect of Al in different RCA baths upon subsequent thermal oxide thickness is shown in Figure 2 [9]. The data indicate that a small amount of Al in an NH_4OH/H_2O_2 bath can inhibit thermal oxide growth as much as a much greater amount of Al in an HCl/H_2O_2 bath. A correlation between surface Al in the bath and on the wafer was done by qualitative SIMS.

Qualitative SIMS Deficiencies

In spite of the oxygen jet, the technique is only qualitative, because standards have not been developed which can produce representative ion yields similar to the real analysis. Furthermore, there are major mass resolution problems for some elements of interest (e.g., Si_2 for Fe; Si_2 and SiO_2 for the isotopes of Ni; SiCl for the two isotopes of Cu; SiH for P; and SiC_2 for Cr). Reports in the literature of surface Cr, Cu, Fe and Ni at low levels have been misleading when this technique was used. The technique has primarily been used for the qualitative measure of Na, Mg, Al, K and Ca. However, even these can at times be misleading depending upon mass interferences [10]. For example, the surface Al for levels in the range of $>10^{12}$ atoms/cm^2 are easily amenable to measurement by qualitative SIMS, but lower levels may find significant C_2H_3 interferences which cannot be discriminated against using a quadrupole spectrometer. The attempt to use high mass resolution spectrometers to eliminate the mass interferences has not been very successful, because the ion beam erosion rates must be very small to obtain a significant sample of the native oxide region, and

under high mass resolution there is often not enough signal to accurately tune the magnet. Furthermore, if electronegative elements are of interest, the oxygen jet reduces ion yields and therefore detection limits.

POLYENCAPSULATION/SIMS (PC/SIMS)

The polyencapsulation/SIMS (PC/SIMS) technique [11], was developed in 1980 to overcome the difficulties listed above, but was not reported in use until much later [12-13]. In PC/SIMS the silicon wafer is covered with a thin layer of polysilicon or amorphous silicon which translates the difficult to quantitate surface region away from the polished silicon surface of interest by "burying" the original surface deeper than the non-linear region. The encapsulation material is usually polysilicon or amorphous silicon, although CVD oxide can be used if an O_2^+ beam or an oxygen jet is also used for the analysis of electropositive (but not electronegative) elements. The chosen thickness of the encapsulant is a balance between being greater than the thickness of the non-linear ion yield region, but thin enough to avoid loss of the interface signal due to dilution mixing. Typical thicknesses have been 50 to 120 nm. Since the surface impurities are now fully encapsulated in a silicon matrix: (a) the original surface is protected from subsequent contamination, (b) SIMS non-linear ion yield effects are minimized, (c) ion implants can be used to effectively quantitate the SIMS ion signals, (d) high mass resolution can be used when required, and (e) a Cs^+ primary beam can be successfully used to optimize ion yields of the electronegative elements.

Encapsulation Artifacts

The polyencapsulation/SIMS technique is, in principle, capable of detecting all trace elements quantitatively with a wide range of detection limits due to the widely ranging ion yields for elements across the periodic table. However, the limitation in PC/SIMS is often due to artifacts from the encapsulation itself.

Care must be taken to determine if the encapsulation process itself introduces, or removes, impurities in the analytical region of interest. A recommended procedure to assess the first issue is to perform the encapsulation twice, so that the interface between the first and second polysilicon layers provides an analytical measure of the impurities introduced by the encapsulant process, and the interface between the polysilicon and crystal provides an analytical measure of the original surface impurities, plus those impurities introduced by the encapsulation process. Because the reactivity of fresh polysilicon is much greater than a native oxide, a subtraction procedure between the two interface measurements is not recommended. Also, because the issue is impurities introduced by the encapsulation process, the wafers should not be exposed to air (even clean room air) after the first poly layer is deposited. A study of several different methods for depositing

polysilicon or amorphous silicon has shown the encapsulation process itself can easily introduce impurities, as illustrated in Figure 3.

Care must also be taken to assess whether the encapsulation process removes impurities of interest. This removal might occur by two different mechanisms: (1) desorption to the chamber ambient; or (2) diffusion into the encapsulant or into the crystal. An assessment of this issue was made for heavy metals by measuring the heavy metal areal densities first by Total reflection X-Ray Fluorescence (TXRF), performing a double polyencapsulation via CVD polysilicon deposition, and then measuring the interfacial metals using SIMS. The results revealed surface Zn was removed by the encapsulation process (probably desorption), surface Cu diffuses into the polysilicon, and surface Br desorbs down to a level of 10^{11} atoms/cm^2.

PC/SIMS Quantification

As mentioned, the intent of the polyencapsulation is to provide a constant ion yield in the analytical region of interest, i.e., the poly/crystal interface. This region has a native oxide which is cascade mixed [11] into both the polysilicon and the crystal by the primary ion beam, so that the amount of oxygen remaining at the interface from the native oxide is about 4% atomic, as measured by Cs^+ beam SIMS. This amount may introduce minor ion yield artifacts, which can be experimentally assessed by implanting silicon with oxygen (7×10^{16} atoms/cm^2 at 100 keV) and then co-implanting with the element of interest such that the co-implant peak coincides with the oxygen peak. A comparison of SIMS profiles and calculated Relative Sensitivity Factors (RSF's) with and without the oxygen implant provides a measure of the ion yield effect of the cascade mixed native oxide. Studies of this type for a variety of elements have shown that there is no ion yield enhancement for most elements and only up to 20%-50% enhancement for others. The same kind of oxygen implant can be used to measure the amount of voltage offset required to remove oxygen-containing molecular interferences at the polysilicon/crystal interface.

Quantification is achieved using ion implants of known dose into silicon to calculate an RSF which is then used for the polyencapsulation/SIMS measurement. In practice it is the areal density of the impurity which is desired, and this is easily calculated from the SIMS depth profile (a depth calibration is required) and the RSF.

PC/SIMS Detection Limits

As with any analytical technique, detection limits are influenced by numerous factors. In our case these include: instrumental background, molecular interferences, signal-to-noise, and impurity introduction by the encapsulation process. Some estimated detection limits for polyencapsulation/SIMS are listed in Table 2, where the practical problem of contamination from polyencapsulation (CVD poly using a local service) is included.

TABLE 2 ESTIMATED DETECTION LIMITS (DL) FOR PC/SIMS
(Units of atoms/cm^2)

	DL		DL		DL
Li	2E09	B	5E10	Al	2E10
Na	1E10	P	1E10	Mg	2E09
K	2E09			Ca	2E10
				Fe	2E11

PC/SIMS Comparison of Cleaning Processes

The surface Al, Ca and Mg after an RCAI and RCAII clean sequence were measured earlier by this technique to be 1.3, 4, and 0.7 $x10^{12}$ atoms/cm^2 respectively [13]. A very recent comparison of commercial wafers from five different silicon vendors (different cleaning processes) was completed using PC/SIMS. All wafers were encapsulated at the same time. The results are shown in Table 3. Both dopants P and B are detectable even though these wafers are both n- and p-type. We also can detect the alkalis Na and K, and the metals Mg, Ca and Al. The wafers have similar levels of P, B, Na, Mg and Ca (D-2 is an exception for Ca). The "A" group has much lower K and Al compared to the others.

TABLE 3 PC/SIMS COMPARISON OF CLEANING PROCESSES
(Units of 10^{12} atoms/cm^2)

	P	B	Na	K	Mg	Ca	Al
A-1	0.2	p+	0.1	0.009	0.06	0.1	<0.003
A-2	0.1	p+	0.1	<0.009	0.07	0.3	0.003
B-1	0.09	1	0.08	0.2	0.1	0.2	0.07
B-2	0.07	1	0.07	0.2	0.04	0.1	0.1
C-1	0.08	1	0.08	0.02	0.06	0.08	0.06
C-2	0.1	1	0.09	0.1	0.07	0.3	0.3
D-1	0.08	1	0.1	0.2	0.07	0.1	0.08
D-2	0.1	1	0.08	0.3	0.1	3	2
E-1	0.1	1	0.1	0.03	0.07	0.07	0.0
E-2	0.06	2	0.1	0.1	0.1	0.1	0.2

The PC/SIMS concept also works for GaAs when a low temperature poly GaAs is deposited on the crystal. When using PC/SIMS to measure Fe, Ni and Cu on the surface of GaAs by PC/SIMS care must be taken to avoid molecular interferences from Si, Cl, Ca, Al, and O containing species at the poly/crystal interface (i.e., Si_2 and CaO for ^{56}Fe, Si_2 for ^{58}Ni, SiO_2 for ^{60}Ni, SiCl for ^{63}Cu and ^{65}Cu, and Al_2 for ^{54}Fe.)

TOTAL REFLECTION X-RAY FLUORESCENCE

In TXRF [14,15] using an ATOMIKA XSA-8000 X-Ray Surface Analyzer, x-rays from a conventional molybdenum x-ray anode impinge the surface of the silicon wafer at a glancing angle, below the critical angle (1.83 milliradians) for total external reflection, thereby greatly reducing the background silicon fluorescence signal commonly experienced in conventional x-ray fluorescence. The surface fluorescence x-rays from the top 3-4 nm of surface atoms are then detected using a conventional Li-drifted silicon detector which functions as an energy dispersive spectrometer. The system is normally operated at 30 kV and 60 mA in air using full diameter wafers up to 150 mm. The analysis area is 8 mm in diameter.

Quantification is achieved using a silicon substrate which has been intentionally contaminated with Ni of a known areal density using a diluted wet chemistry standard. Once the calibration for Ni is completed, the calibration for the other metals is completed using sensitivity factors which were measured once when the instrument was manufactured. Precisions (one relative standard deviation) depend upon the specific element and its amount, but practical examples include <15% for zinc at 0.4×10^{12} atoms/cm^2 and for iron at 0.9×10^{12} atoms/cm^2. The TXRF technique using a Mo anode is sensitive to surface metals with atomic numbers in the ranges of 20-35 and 56-83. The optimum interference-free detection limits on silicon are on the order of 10^{11} to 10^{12} atoms/cm^2 as shown in Figure 4. These measurements assume a Mo anode, analysis in air, and 1000 second integration.

It has been shown both experimentally [14] and theoretically [16] that the change in the TXRF signal as a function of the incident angle is different for plated contamination (e.g., one thousandths of a monolayer of copper) than for residue contamination (e.g., Ni atoms dispersed in a 50 nm thick organic residue). This difference can be used to qualitatively distinguish between particulate contamination and plated contamination, so that in the same series of measurements the contamination related to particles and to plating can be in principle distinguished.

Correlation of TXRF, RBS and VPD/AAS

We have recently completed a surface measurement correlation on silicon wafers contaminated with Fe, Ni, Cu and Zn by a spin coating process [18]. The surface analytical techniques included: VPD/AAS by Kyushu Electronic Metals Co., TXRF (Perkin-Elmer XSA-8000) at Charles Evans & Associates and at GeMeTec (Munich, West Germany), and RBS (N-beam) at GeMeTec.

Four wafers were intentionally contaminated by Kyushu Electronic Metals Co. with Fe, Ni, Cu and Zn at a target level of 10^{11} atoms/cm^2, then four with 10^{12} atoms/cm^2, and finally four more with 10^{13} atoms/cm^2. The contamination process was previously characterized by VPD/AAS. The vapor phase HF decomposition was performed on the native oxide rather

than a thermal oxide. A BLANK was also provided with VPD/AAS impurity measurements for Fe, Ni, Cu and Zn of 1.0, <1.0, <0.23, and 0.11 $x10^{10}$ atoms/cm^2; this BLANK represented the starting impurity levels for the intentionally contaminated wafers.

The TXRF measurements were made at several spots per wafer, both at Charles Evans & Associates and at GeMeTec. Different wafers were analyzed at Charles Evans & Associates compared to GeMeTec; a wafer swap and remeasurement is scheduled. Both companies used the same model of TXRF, but different quantification procedures were used. Charles Evans & Associates uses a diluted and dried wet chemistry standard containing Ni, and GeMeTec uses a Cu contaminated (low rate sputter deposition) silicon wafer which has been made into a standard by nitrogen-beam RBS.

The nitrogen-beam RBS was done at GeMeTec at only one point at half the radius, and the RBS data reduction assumed the contamination was localized on the top surface. Although RBS cannot mass resolve these metals, it was possible to measure the sum total of these metals and compare that number against the sum total by TXRF and by VPD/AAS. The nitrogen-beam RBS is capable of detection limits in the 10^{10} atoms/cm^2 range.

The correlation between TXRF and VPD/AAS for the average TXRF reading for two wafers per company and multi-spots per wafer for all four elements is shown in Figure 5. The data reveal that the TXRF at Charles Evans & Associates reads 1.6X higher on the average compared to the TXRF at GeMeTec, for the two more highly contaminated wafer groups (10^{12} and 10^{13} atoms/cm^2.) But there is good agreement for the lower levels of contamination of Fe, Ni, and Zn.

The correlation to VPD/AAS appears linear for Cu, Ni and Zn, but the lower Fe level falls out of linearity. In order to check for an instrumental Fe background for TXRF, one of the BLANKs was analyzed by TXRF at Charles Evans & Associates for 5.6 hours with the result of only detecting Cu at $7x10^{10}$ atoms/cm^2, which is assumed to be an instrumental Cu background. Thus the non-linearity for Fe does not arise from a TXRF instrumental background. The TXRF measurements read higher than the VPD/AAS measurements, however, the two techniques agree within a factor of X3 or less for Fe, Ni and Zn. The correlation for Cu is not as good, but it is not certain that the VPD collected all the surface Cu.

The correlation between RBS, TXRF and VPD/AAS is shown in Figure 6 for the summation of all four elements. The data show a systematic difference between VPD/AAS and RBS, with RBS reading higher than VPD/AAS. However, RBS reads within a factor of X3 of VPD/AAS.

TXRF Comparison of Cleaning Processes

A comparison of the surface impurities on 100 mm diameter prime silicon wafers taken from four world-scale silicon manufacturers was made using TXRF [18]. Two of the manufacturers are Japanese. One cassette per vendor was used to provide twenty-five wafers per vendor.

The average data for the 25 wafers per vendor are summarized in Table 4. The results show statistically valid differences between wafers taken from the four cassettes for Cu, Fe, Zn, Ca and Br. Furthermore, one of the cassettes (B) has wafers with surface Cu out of statistical control (Cu varying over two orders of magnitude within the cassette of wafers) while the other surface impurities on these same wafers are in statistical control. This indicates the importance of using a multi-element characterization technique for characterizing cleaning.

TABLE 4. TXRF COMPARISON OF CLEANING PROCESSES
(units of 10^{12} atoms/cm^2)

Cassette	Fe	Cu	Zn	Ca	Br
A	0.5	0.5	2.5	<2	0.3
B	0.6	60	0.5	<2	<0.2
C	0.4	0.8	1.5	3.5	0.2
D	<0.3	0.5	0.5	<2	2

Others have shown TXRF Ca and Fe surface maps on a 100 mm diameter silicon wafer [19]. A total of over 60 measurement points are included. The maps reveal distinct patterns which can help the cleaning process engineer identify and control the sources of these cleaning defects. The maps reveal axial heterogeneity, suggestive of heterogeneous plating of contamination, and some non-symmetric heterogeneity, suggestive of particulate contamination.

Others have shown the plating efficiency of metals from chemicals used in two different cleaning chemistries [14,20]. The data reveal that Cu is especially plated to silicon in buffered HF chemistry and Fe is especially plated to silicon in ammonium hydroxide: hydrogen peroxide chemistry.

A TXRF multi-point spectra of an oxide wafer which had received a rinse in a Semitool revealed heterogeneous contamination. The TXRF angle variation in this case revealed the Fe and Zn contamination was particulate rather than a heterogeneous plating. In contrast, the TXRF angle variation of a bare substrate cleaned by an RCA1 type chemistry, which has been shown [20] to plate out Fe, revealed plated Fe contamination, as expected.

TXRF Analysis of GaAs

TXRF can also be used to measure Fe and Cu on GaAs surfaces, although the detection limits are about one order of magnitude higher than for silicon surfaces. The reason for this is the very intense Ga and As fluorescence signals must be reduced because of very high detector dead time, and the methods for their reduction also reduce the fluorescence signals from the surface contaminants. In addition the Ga and As lines provide interferences for some elements which are detectable on silicon. In practice it is possible to analyze for Si, S, Cl, Ca, Ti, V, Cr, Mn,

Fe, Cu, Pb, and Hg. We have seen Fe and Cu on commercial GaAs wafers.

SUMMARY

In summary, three different analytical techniques have been reviewed for their capability of characterizing semiconductor substrate surfaces after cleaning. The PC/SIMS is capable of providing quantitative information for the light elements, while TXRF is capable of providing the same for heavy elements. If polyencapsulation is not available, or if it is not clean enough, then qualitative SIMS with an oxygen jet can be useful for the light elements. These tools are sensitive enough to detect trace element contamination on commercially cleaned semiconductor substrates, so that analytical tools are available for cleaning process development.

ACKNOWLEDGEMENTS

The author would like to thank Mr. J. Norberg of Charles Evans & Associates for the PC/SIMS data, Dr. N. Fujino of Kyushu Electronic Metals Co. for the spin-coated wafers and the VPD/AAS data, and Dr. P. Eichinger of GeMeTec for the N-beam RBS data and TXRF data from his ATOMIKA XSA-8000 instrument.

REFERENCES

1. A. Shimazaki, H. Hiratsuka, Y. Matsushita, and S. Yoshii, Extended Abstracts of the 16th (1984 International) Conference on Solid State Devices and Materials, Kobe, p. 281 (1984).

2. T. Shiraiwa, N. Fujino, S. Sumita, and Y. Tanizoe, Semiconductor Fabrication: Technology and Metrology, ASTM STP 990, Dinesh C. Gupta, editor, American Society for Testing and Materials, 1989.

3. A. Huber, H. J. Rath, P. Eichinger, Th. Bauer, L. Kotz and R. Staudigl, Diagnostic Techniques for Semiconductor Materials and Devices, edited by Thomas J Shaffner and Dieter K. Schroder, ECS Proceedings Vol. 88-20, 109 (1988).

4. B. F. Phillips, D. C. Burkman, W. R. Schmidt, and C. A. Peterson, J. Vac. Sci. Technol. A1, 646 (1983).

5. W. C. Krusell, J. J. Farber, and A. C. Sing, Abstract No. 229, ECS Extended Abstracts 86-1, Spring Meeting, Boston (1986), p. 331.

6. L. A. Zazzera and J. F. Moulder, J. ECS 136, 484 (1989).

7. J. M. deLarios, D. B. Kao, C. R. Helms, and B. E. Deal, Appl. Phys. Lett. 54, 715 (1989).

8. A. Maeda and S. Yoshii, Abstracts of the Japan Applied Physics Society Meeting, Spring 1988, Abstract no. 30p-N-2.

9. R. J. Falster, R. D. Wingrove, R. S. Hockett, R. A. Craven, and D. I. Golland, "The Total System Approach to Wafer Ecology," SEMICON Europe 86, Zurich, March 1988.

10. G. Stingeder, M. Grundner, and M. Grasserbauer, Surface and Interface Analysis, 11, 407, 1988

11. Peter Williams and Judith E. Baker, Appl. Phys. Lett. 36, 842 (1980).

12. G. J. Slusser and L. MacDowell, J. Vac. Sci. Technol. A5, 1649 (1987).

13. R. S. Hockett, Rapid Thermal Processing of Electronic Materials, edited by Syd. R. Wilson, Ronald Powell, and D. Eirug Davies, Mat. Res. Symp. Proc. Vol. 92, (Materials Research Society, Pittsburg) p. 41 (1987)

14. Peter Eichinger, Heinz J. Rath, and Heinrich Schwenke, Semiconductor Fabrication: Technology and Metrology, ASTM STP 990, edited by Dinesh Gupta, American Society for Testing and Materials, 1988.

15. R. S. Hockett, S. M. Baumann, and E. Schemmel, Diagnostic Techniques for Semiconductor Materials and Devices, edited by Thomas J Shaffner and Dieter K. Schroder, ECS Proceedings Vol. 88-20, 113 (1988).

16. W. Berneike, J. Knoth, H. Schwenke, and U. Weisbrod, Fresenius Z. Anal. Chem. 333, 524 (1989).

17. M. Hourai, T. Naridomi, Y. Oka, K. Murakami, S. Sumita, N. Fujino and T. Shiraiwa, Jap. J. Appl. Phys. 27, L2361 (1988).

18. R. S. Hockett and William Katz, accepted for publication by the J. ECS.

19. P. Eichinger, "Metallic Trace Contamination in IC Technology: Impact, Origin, and Analytics," STEP Europe Conference, October 27-28, 1989, Brussels.

20. V. Penka and W. Hub, Fresenius Z. Anal. Chem. 333, 586 (1989).

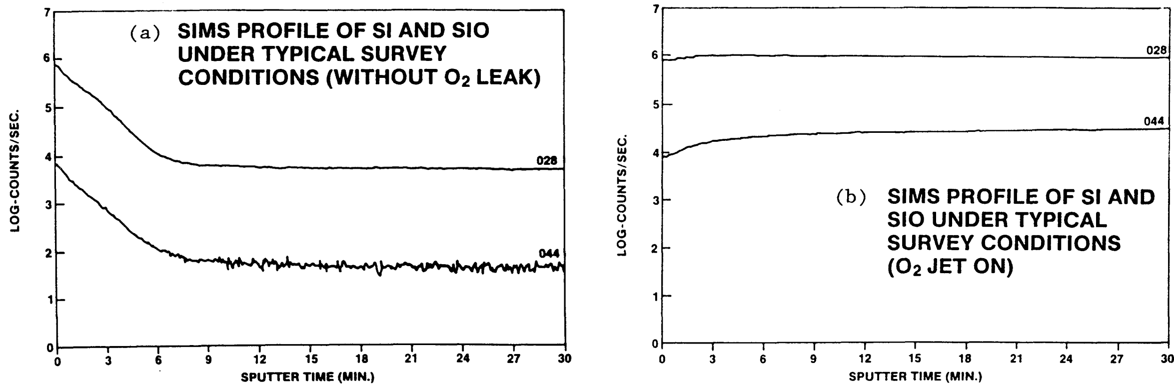

Fig. 1 Effect of oxygen jet (or leak) upon Si and SiO ion yields in native oxide region when using Xe^+ primary ion beam and quadrupole mass spectrometer. (a) without oxygen leak; (b) with oxygen leak.

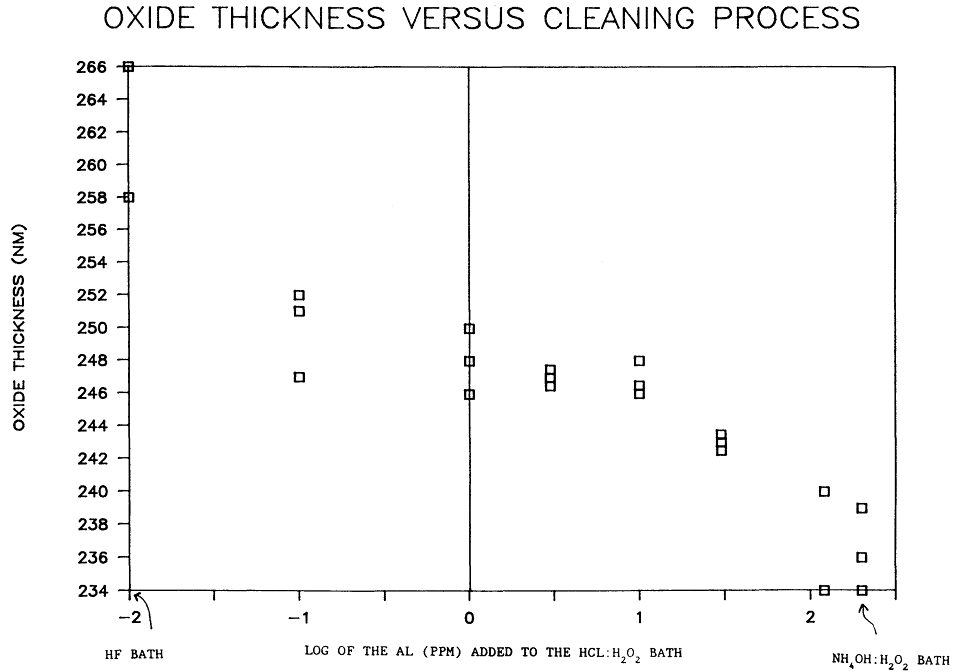

Fig. 2 Thermal oxide thickness as a function of cleaning process where Al has been intentionally introduced into the HCl:H_2O_2 at different levels and the same H_2O_2 was used for the HCl and NH_4OH baths.

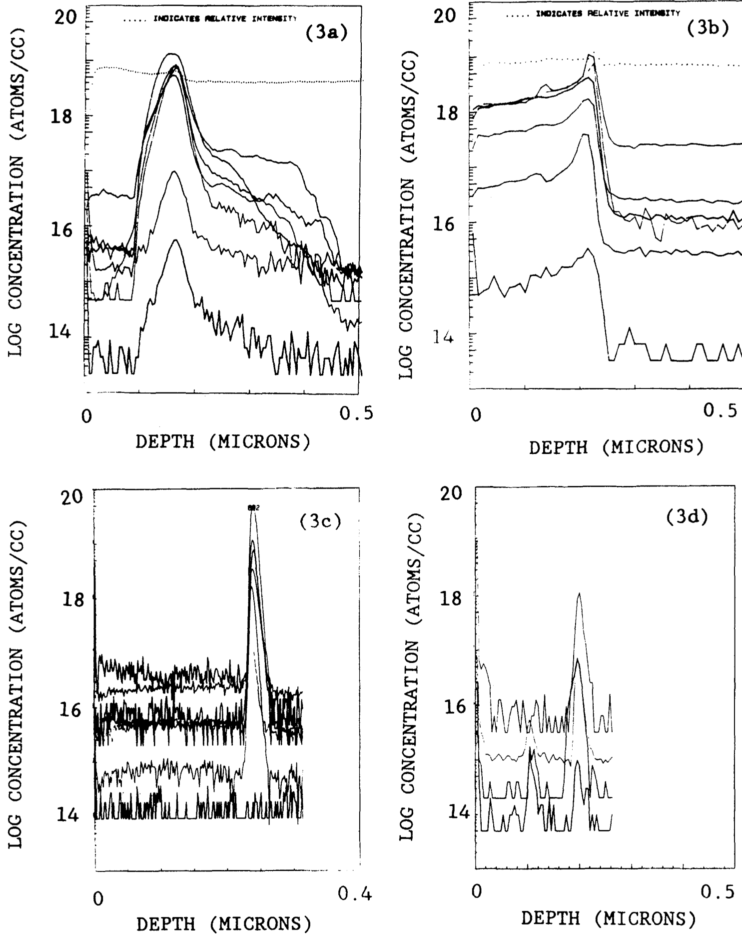

Fig. 3 SIMS profiles through double encapsulation layers (120 nm thick each) for (a) plasma deposition A, (b) sputter deposition, (c) plasma deposition B, and (d) CVD polysilicon deposition.

OPTIMUM TXRF DETECTION LIMITS ON SILICON USING A MO X-RAY ANODE

LIMITS OF DETECTION

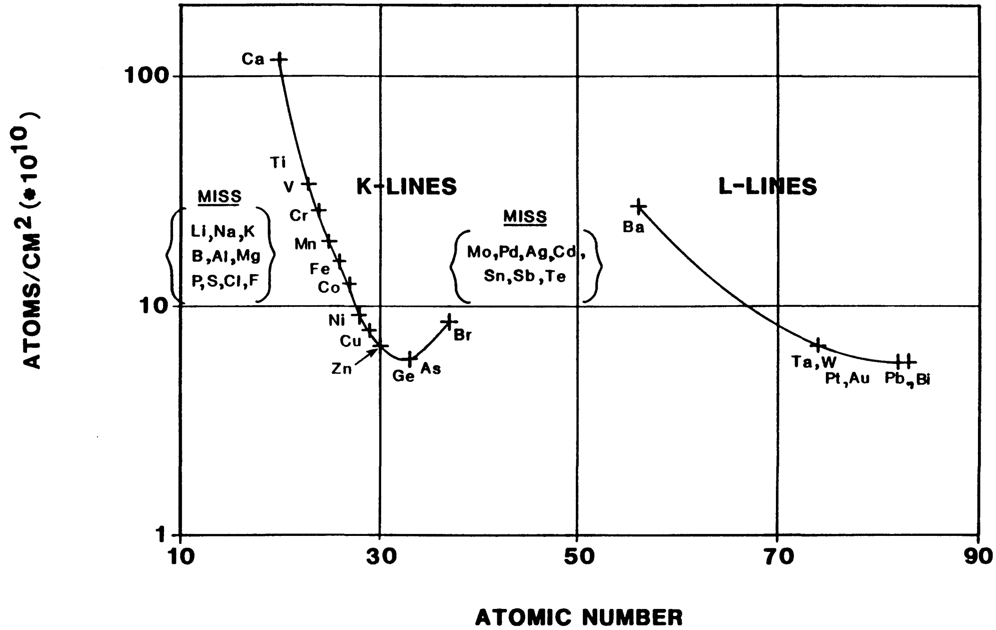

Fig. 4 TXRF interference-free detection limits for silicon surfaces.

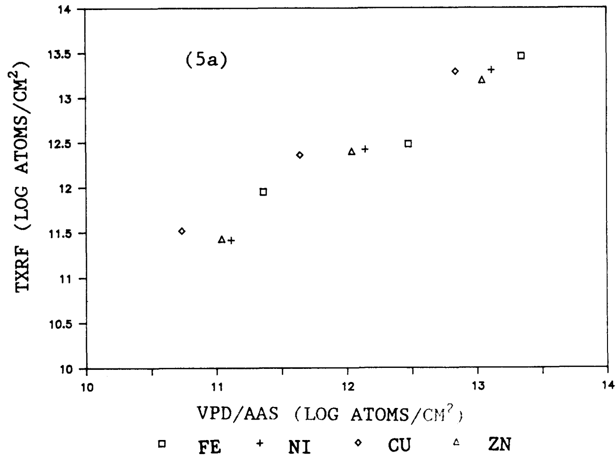

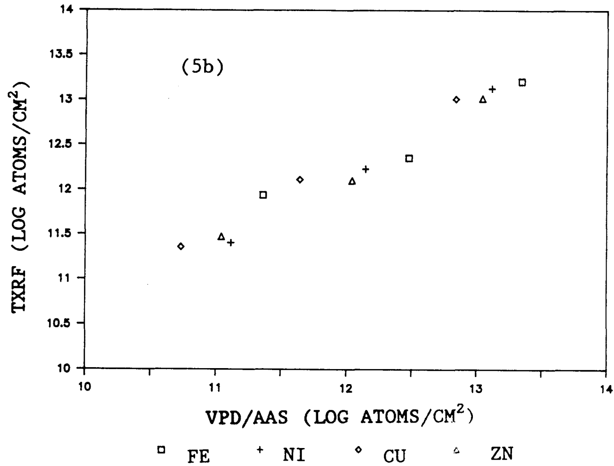

Fig. 5 Correlation between TXRF and VPD/AAS for Fe, Ni, Cu and Zn: (a) Charles Evans & Associates TXRF; (b) GeMeTec TXRF.

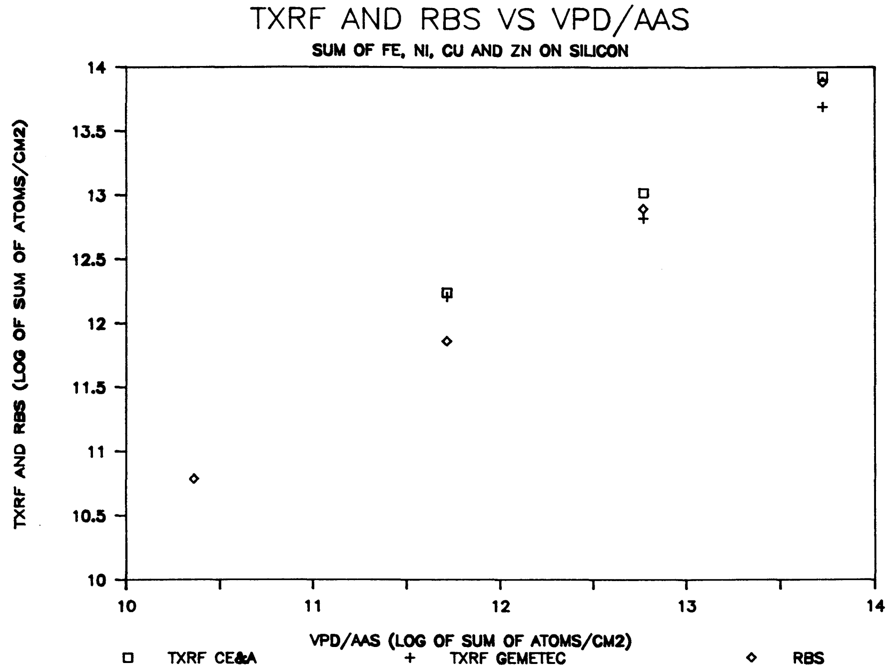

Fig. 6 Correlation between TXRF (GeMeTec and Charles Evans & Associates), RBS (GeMeTec) and VPD/AAS for summed Fe, Ni, Cu and Zn contamination on spin-coated wafers.

IMPURITY ANALYSIS ON SILICON WAFER BY MONOCHRO TRXRF

K. Nishihagi, A. Kawabata, *T. Taniguchi, **S. Ikeda

Technos Co., Ltd.;
*Osaka Electro Communication University
**Ryukoku University
2-23 Hayako-cho, Neyagawa City, Osaka 572, Japan.

ABSTRACT

Ordinary TRXRF and other analytical methods have poor sensitivity to detect contamination on silicon wafer. New TRXRF performes higher sensitivity and lower background using rotating anode as excitation source, and monochromator. The contamination of 10^{10} atoms/cm^2 can be distinguished.
Wide information to silicon wafer can be obtained from distribution analysis and depth profile.

1. INTRODUCTION

Surface impurity on silicon wafer makes big influence in characteristic of semiconductor as final products. But the quantity of impurity is too small to detect by ordinary analytical methods. Only the information of the surface is interested. Comparison of typical analytical methods for checking of contamination of silicon wafer is shown in Table 1. Auger Electron Spectroscopy (AES) and X-ray Photoelectron Spectroscopy (XPS) are surface analysis methods, but the sensitivity is too poor. Secondary Ion Mass Spectroscopy (SIMS) is also surface analysis method and has middle sensitivity , but the information of first several tens angstromes from surface is not used for sputtering process. Furthermore, the estimation of result is too difficult to get quantitative value. Atomic Absorption Spectroscopy (AAS) has high sensitivity in case of efficient sample preparation. But it takes half a day to get sample solution from silicon wafer. Water and reagents must be clean. And handling must be done very carefully. Furthermore ,the information of AAS is limited to average values of surface. Distribution and depth informaiton can't be obtained. Total reflection X-ray fluoresence (TRXRF)is very sensitive method and is obtained the information from surface. TRXRF performes low background by reducing scattering from silicon substrate. Detection limits of ordinary TRXRF are 10^{11} to 10^{12} atoms/cm^2 for transition metals. These levels are not always satisfactory for silicon vendors. Detection limits depend on the sensitivity and the background. Using bright X-ray source is the most effective method for prompting sensitivity. Rotating anode is adopted instead of conventional sealed X-ray tube as excitation source. The power of rotating anode is 5 to 10 times bigger than sealed X-ray tube. Excitation by monochromized beam

instead of continuous beam is suited for reducing background. Only characterlistic line from target material is used for excititation of impurity elements. The high energy X-ray causes background by immersing into substrate deeply because of unsatisfying critical condition of total reflection . Unwanted high energy X-ray is removed by monochromator. The background of monochro TRXRF is reduced to 1/20 tol/50 smaller than that of conventional TRXRF. Detection limits of monochro TRXRF performes 10^9 to 10^{10} atoms/cm^2.

2. INSTRUMENTATION

2-1 Excitation source

Rotating anode is used as excitation source instead of sealed tube. The maximum power of rotating anode is 30kv-300mA. The power of sealed tube is usually 30kv-40mA at actual measurement. Therefore the intensity of rotating anode is expected to be approximately 10 times bigger than that of sealed tube. Maximum kv is suppressed to 30kv because efficiency of excitation decreases over 3 times of excitation voltage. Excitation voltage of tungsten LII is 11.5keV. Target material is tungsten. There are two reasons for selection of tungsten target. (1) Big atomic number has high efficiency for excitation of X-ray from target. (2) Characteristic line of tungten has high efficiency for excitation of fluorescence X-ray of transition metals on silicon wafer.

2-2 Monochromator

LiF(200) is used for monochromator. Characteristic line ($L\beta_1$) of tungsten is selected from primary beam by monochromator. Tungsten $L\beta_1$ (9.67keV) is the most effective line for excitation of transition metals. Tungsten $L\beta_1$ has not enough energy to form scattering by immersing into silicon substrate deeply.

2-3 Detector

SSD (Solid State Detector) of Si(Li) is used for detector. The effective area of detector is 80mm^2. Big area of detector increases sensitivity and high resolution of 160 eV improves accuracy.

2-4 Adjusting glancing angle

Higher stability of vertical position of silicon wafer is required, because small glancing angle is needed for total reflection method. The accuracy of vertical position is needed less than 1 micron meter. It is very difficult to keep it by only mechanical reproducibility. This accuracy and reproducibility can be obtained by automatic servo system. This automatic servo system consists of excitation source, scintillation counter as detector and Z , θ axis driving motors .

2-5 Distribution analysis

Distribution analysis is necessary to know the origin of cotamination. Resolution of distribution analysis is 10 mili meters diameter by limiting to area of detector. R and θ axis driving method is adopted for positioning.

2-6 Depth profile

Depth profile is necessary to know the diffusion of each impurity element in depth direction. Glancing angle is adjustable from keyboard.

3. EXPERIMENTAL

Standard sample are contamineded by a spin coater method. Several ml of dilute solution with intentionally contaminated are dropped on virgin silicon wafer and are spun after 1 min. The contaminated elements are Fe, Ni, Cu, Zn. These samples are measured by TREX610 at Technos. The schematic arrangement of monochro TRXRF is shown in Fig.1 . Measuring conditions are shown in Table 2 . The layer of natural silicon oxide is removed on H.F environment and estimated by AAS .

4. RESULTS AND DISCUSSION

4-1 Peak profile

Peak profile of $5*10^{13}$ atoms/cm^2 contaminated silicon wafer is shown in Fig.2 . Peak height of Fe-Kα and Ni-Kα are smaller than Cu-Kα and Zn-Kα, mainly due to difference of fluorescence yield and mass absorption coefficient for tungsten Lβ1. Peak profile of $1*10^{11}$ atoms/cm^2 contaminated silicon wafer is shown in Fig.3 . The peak of each element is clearly observed . Background is extremely low compared with conventional TRXRF .

4-2 Working curve

The relationship between concentration of surface impurity on silicon wafer and X-ray intensity is linear and dynamic range of working curve has four figures as shown in Fig.4 . Same working curves can be obtained for other elements except slope .

4-3 Detection limit

Detection limits of transition metals on silicon wafer as impurity element are 10^9 to 10^{10} atoms/cm^2 as shown in Table 3 . Detection limits are calculated using background of blank sample (no contamination) and slope of working curve . Detection limit is

$$L.L.D. = 3 * K * \sigma_B$$

where K and σ_B are slope of working curve and standard deviation of X-ray intensity of background .

4-4 Reproducibility

Reproducibility of X-ray intensity for each element is within 10 percent for five measurements at same sample .

4-5 Distribution analysis

The result of distribution analysis for $5*10^{11}$ atoms/cm^2 contaminated standard sample is shown in Fig.5 . Standard sample is not

necessarily uniform contaminated .

4-6 Depth profile

Deeper information for contamination of silicon wafer can be obtained by larger glancing angle . Relationship between X-ray intensity and glancing angle for $5*10^{13}$ atoms/cm^2 contaminated standard sample is shown in Fig.6 . The differrence of variation of X-ray intensity for each element is assumed to be caused by the difference of diffusion speed of each element into silicon substrate.

4-7 Example of actual sample

Peak profile of abnormal or troubled samples are shown in Fig.7 and Fig.8 .

5. Conclusions

(1) Detection limit of 10^9 to 10^{10} atoms/cm^2 for transition metals can be obtained by adopting rotating anode and monochromator .

(2) Automatic analysis can be done using servo system for adjusting glancing angle .

(3) Wider information can be obtained by combination with distribution analysis and depth profile .

6. Acknowledgements

The authors thank Matsushita and Tsuchiya of Toshiba , Yakushiji of Showa Denko Silicon , Kyoto of Sumitomo Industries and Atsumi of Nippon Steel for their helpful suggestions and sample preparation .

7. References

(1) M.Hourai, T.Naridomi, Y.Oka, K.Murakami, S.Sumita, N.Fujino and T.Shiraiwa : Jpn.J.Appl.Phys.,27(1988)2361.

(2) A.Iida, A.Yoshinaga, K.Sakurai and Y.Goshi : Anal.Chem.,58(1986) 394

(3) L.T.Canham, M.R.Dyball and K.G.Barraclough : J.Appl.Phys.,60(198 9)920

Table 1

Comparison of Typical Analytical Methods for Checking of Contamination of Si Wafer

	Advantage	Disadvantage
TRXRF	Non-destructive Surface analysis	
AES,XPS	Surface analysis	Low-sensitivity Local analysis
AAS ICP-AES	Cheap	Destructive Pretreatment Average estimation
ICP-MS	High sensitivity	Expensive Hard-handling
SIMS	High sensitivity	Semi-destructive

Table 2 Measuring Conditions

Target	W
Applied Voltage	30kV
Emission Current	200mA
Detector	Si(Li) 80mm^2
Measuring Time	1000 sec

Table 3

Detection limits of impurity elements on silicon wafer by Monochro TRXRF

Element	Fe	Ni	Cu	Zn
Detection limit (10^9atoms/cm^2)	7.4	6.4	3.7	3.2

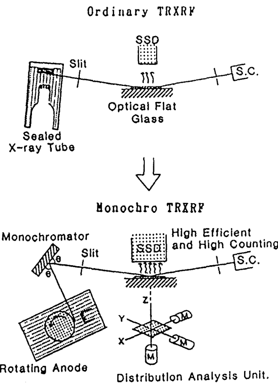

Fig. 1 Comparison between Ordinary TRXRF

and Monochro TRXRF

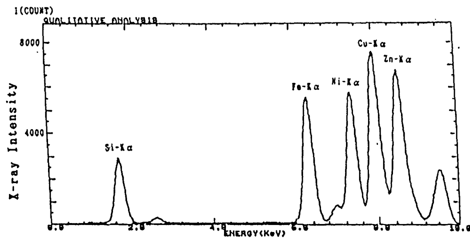

Fig.2 Peak profile of $5\cdot10^{13}$atoms/cm^2 contaminated silicon wafer

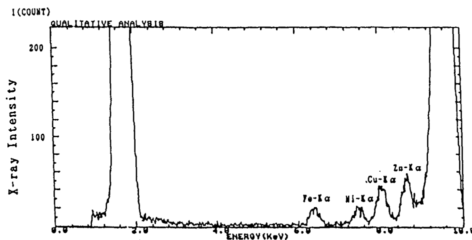

Fig.3 Peak profile of $1\cdot10^{11}$atoms/cm^2 contaminated silicon wafer

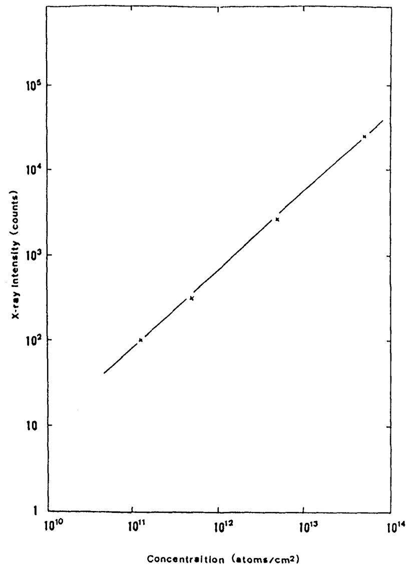

Fig.4 Working curve of Ni

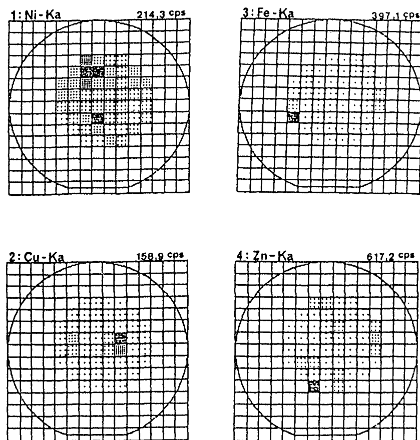

Fig.5 Distribution Data

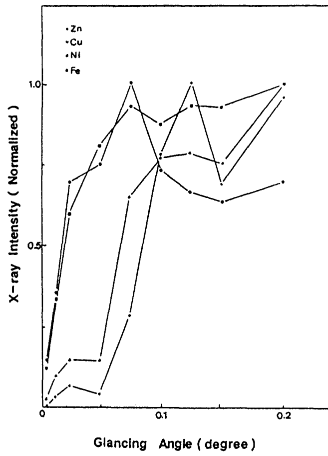

Fig.6 Relationship between X-ray intensity and glancing angle

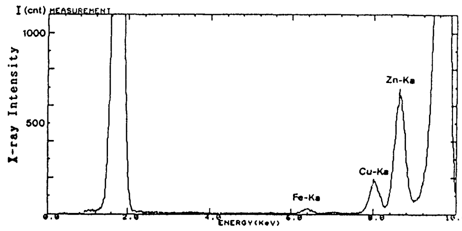

Fig.7 Peak profile of abnomal silicon wafer NO.1

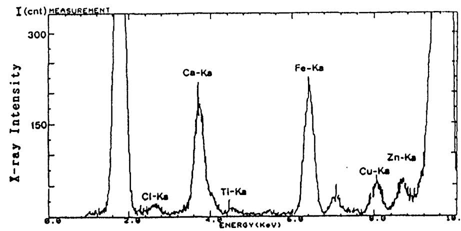

Fig.8 Peak profile of abnormal silicon wafer NO.2

IN-SITU DIFFERENTIAL REFLECTANCE STUDY OF THE ETCHING OF SiO_2 FILMS

Uean-Sin Pahk, S. Chongsawangvirod and E. A. Irene
Department of Chemistry CB# 3290
University of North Carolina
Chapel Hill, N.C. 27599-3290

Abstract

A differential reflectance technique has been applied to study the etching of SiO_2 films on Si substrates in-situ in the liquid (HF/H_2O) environment as well as ex-situ. Essentially, the technique scans an incident optical beam in the spectral range of 200-800 nm across two adjacent samples at near normal incidence and the reflected beams are detected using lock-in amplification so as to measure only the difference in the reflectance spectra. This study demonstrates the great sensitivity of the technique to follow the etching experiment in-situ, and in conjunction with simulated spectra and ex-situ results, a new spectral feature is seen which may be evidence for an electric double layer at the Si surface in the etch solution.

Introduction

In microelectronics processing, the cleaning of silicon substrates prior to processing and the etching of SiO_2 films on Si for various lithographic procedures often involves the use of aqueous HF solutions. Previous studies(1,2) have shown that the use of HF alters the Si surface and the oxidation kinetics. More recent studies(3,4) have confirmed these results and indicate that the major effect is at the Si surface. Studies aimed at the elucidation of the specific role of HF and other typical cleaning and etching media such as NH_4OH have employed such in-situ techniques as ellipsometry and contact angle measurements in the etching solutions during the processing(5,6). From these studies, the HF in solution has been observed to cause the formation of a hydrophobic film on Si which is absent in NH_4OH solutions. The film is likely a hydrocarbon or fluorocarbon film. Some recent studies have shown only the appearance of H at the Si surface(7,8) although F and other impurities have also been reported(9). From these studies the specific nature and role of the etching solutions has been elucidated but not fully characterized. For example, it is now clear that HF solutions modify the Si surface, but the nature of the modification, the specific role of the modification on subsequent processing steps, the change of barrier height, interface states and charge are all open questions. For resolution of these detailed and basic issues more incisive experimental results are needed. It is preferable that the experiments be performed in-situ in the processing media, so as to avoid the ambiguity of other ambients and even vacuum conditions on the treated surface. To this end the present study reports on the use of differential reflectance, DR, techniques to study the HF solution etching of SiO_2 on Si. The technique can be employed both in-situ and ex-situ and is found to be extremely sensitive. Using one version of DR techniques in which different samples to be compared with respect to reflectivity are placed side by side and sequentially scanned, it was shown(10-12) that differential reflectometry is very sensitive to the small changes in both composition of alloys and damage caused by ion bombardment on the surface of a Si sample. The differential nature of the technique cancels out effects of experimental environment such as the solution in an in-situ solution measurement thereby rendering the measurement sensitive only to the change of the sample. Other versions of DR techniques compare different spectra of the same sample before and during surface treatments(13), however, we do not use that technique here and we will not consider it further.

Experimental Procedures

The details of the DR technique used in the present study, as well as experimental studies

have been reported (see for example references 10-12) and are briefly discussed below. Essentially, the technique is a type of reflectance modulation spectroscopy in which both chemical and physical changes made to a surface are sensitively detected relative to an adjacent reference. The measurement of optical reflectance is performed near normal incidence using a rapidly rastered beam incident upon two adjacent samples which are subtly different in composition or surface condition. The detected reflected light is measured with the use of lock-in amplification tuned to the rastering frequency thus only the difference, ΔR, between the two samples is obtained.

The normalized difference of the intensity of the reflected light, $(\Delta R)/R$, from two adjacent samples is measured as a function of wavelength from 250 nm to 750 nm. The differential reflectance is defined as follows:

$$\frac{\Delta R}{R} = \frac{R_1 - R_2}{(R_1 + R_2)/2} \qquad (1)$$

where R_1 and R_2 are the reflectance of sample 1 and sample 2, respectively.

Figure 1 shows a block diagram of the apparatus. The 600 W Xe-high pressure arc lamp is used as a wide band light source in the visible to near uv spectral range that is scanned in wavelength using a monochromator. The light from the monochromator is focused onto the samples at near normal incidence by a focusing lens. A galvanometric optical scanner is placed between the samples and the focusing lens, in order to raster the incident beam equally over two samples. The frequency of the scanner is variable, but we used 250 Hz so as to be above usual interferences. The reflected beam from the samples is collected and focused onto a photomultiplier tube by a concave mirror. A uv-grade diffuser is placed in front of the photodetector to avoid an effect due to the inhomogeneous response of the detecting surface. The signal from the photomultiplier tube is simultaneously fed into a lock-in amplifier and a low-pass filter. Thus, both the difference, ΔR, and average, R, of the signal which is proportional to the difference and average of the reflectivities from two samples, respectively, are measured. The ratio, $\Delta R/R$, is obtained by a dividing circuit in the lock-in amplifier, and stored on a small computer for further analysis. The wavelength of the incident light is automatically controlled by a stepping motor driver also using a personal computer. All optics are enclosed within a light proof box to shield from laboratory light. It should be noticed that any environmental chamber can be used to house the samples providing the samples can be scanned, the reflected light can be detected, and the light path does not alter the beams except for that from the samples.

Commercially obtained device quality silicon wafers of (100) and (111) orientations, both n and p type in the 2 ohm cm resistivity range were cleaned by following a slightly modified RCA cleaning procedures prior to oxidation(14). The samples were thermally oxidized in a fused silica tube furnace in clean dry oxygen which yields MOS quality SiO_2 films on Si. After oxidation a sample is cleaved into two pieces having straight and sharp sides. Before each experiment, the optics are aligned and calibrated by using two identical samples to yield a null background of $\Delta R/R$. With properly aligned optics, it is routine to obtain a background spectra within $\pm 0.2\%$ and without any spectral features.

Both ex-situ and in-situ experiments have been performed to study etching of SiO_2 films in HF-H_2O solutions. For ex-situ experiments, after the desired processing, two samples are mounted vertically side by side in room ambient on the sample holder. For the experiments reported below we started with two samples of equal film thickness, and then one of the samples was etched by dipping in a dilute HF solution of about 450 parts deionized water to

one part HF(49% by volume), rinsed in deionized water, and dried by nitrogen gas. The thickness of the SiO_2 film was measured by ellipsometry. Then, the sample was remounted along side the unetched sample and $\Delta R/R$ spectrum was obtained. The procedure was repeated until the etched sample was bare Si with only a native oxide.

For in-situ experiments, two Si substrates, each with different SiO_2 film thicknesses, are mounted on a teflon sample holder and placed in a fused silica sample cell. The sample cell has an optical window perpendicular (a deviation from perpendicular is best to avoid reflections from the window) to the optical axis of the incident beam, and the cell has an inlet and outlet so as to permit the addition of etchant or change the solution without otherwise interrupting the experiment or exposing the samples to the laboratory ambient. With the samples in the cell containing 16-18 Mohm deionized water, the background spectra are obtained. Subsequently, HF solution is introduced so as to attain the desired concentration of the HF etching solution. The differential reflectance spectra are obtained as a function of exposure time in the solutions, in order to follow the etching process. Essentially, the in-situ DR experiment observes two SiO_2 films etching simultaneously. However, the two films are initially of unequal thickness, hence the interface will be reached for one sample sooner than for the other. In the experiment, the differences are recorded during etching and finally with both Si substrates bare.

Using a simple optical model of a homogenous film on a planar substrate surface, classical electromagnetic theory permits a simulation of the reflectance spectra based on literature values for the optical properties of the film and substrate in the wavelength range studied. Hence, a comparison of theory and experiment will provide information relative to the assumptions in the model. The ex-situ and in-situ experimental results along with simulations of the experiments will be shown below.

Results and Discussion

Simulations

The reflectance of a Si substrate covered with a SiO_2 film is calculated using the complex-amplitude reflection coefficient, r, for the ambient-film-substrate system given as(15):

$$r = \frac{r_{01} + r_{12}\exp(-j2\beta)}{1 + r_{01}r_{12}\exp(-j2\beta)}$$

$$\beta = 2\pi(d/\lambda)N_1 \qquad (2)$$

where subscripts 0, 1, and 2 represent ambient, film, and substrate, respectively. r_{01} and r_{12} represent the Fresnel reflection coefficients at the ambient-film and film-substrate interface, respectively. d is the film thickness, λ is the wavelength of the incident light, and N_1 is the complex refractive index of the film. r_{01} and r_{12} are functions of the complex refractive index of the ambient, film, and substrate. Equation 2 includes the multiple reflections of the incident light in the film. β is the phase change experienced by the multiply-reflected waves inside the film on a single traverse between boundaries. Reflectance, R, is calculated from the product:

$$R = rr^* \qquad (3)$$

where r^* is the complex conjugate of r. In the simulation, the subscripts 0, 1, and 2 represent air, SiO_2, and silicon substrate, respectively. Optical constants of SiO_2 and Si were found in the literature(16).

Figure 2 shows the simulated reflection spectra as a function of wavelength for different

thickness of SiO_2, and the spectrum corresponding to zero thickness of SiO_2 is the reflection spectrum of the bare silicon. All the simulated spectra have two major peaks at around 275 nm and 365 nm in the 250 nm to 800 nm spectral range which is experimentally scanned. These two peaks are due to the interband transitions in bulk silicon, viz. $L'_3 \rightarrow L_1$(3.4 eV) and Σ(4.2 eV), and there is a small peak at 225nm (5.6eV) which is due to $L'_3 \rightarrow L_3$, but which is on the borderline of detection in the present experiment(12). In the wavelength range investigated SiO_2 is transparent, hence the effect of the presence of the SiO_2 film on silicon substrate is merely to decrease the overall reflectivity via interference, but not to change the main features of the reflection spectrum due to Si. The reflectivity decrease is due to the interference between the incident light reflected from the top surface of SiO_2 and from the SiO_2-Si interface and therefore the effect will be a function of both the path difference in the silicon dioxide layer and the incident wavelength and the effect is larger for both shorter wavelengths and thicker films.

With the reflectance spectra calculated using equation (1), and shown in Fig. 2, differential reflectance spectra are also simulated and relevant examples are shown in figure 3 for the wavelength range 250nm - 750nm. For this simulation the thickness of oxide on one sample was fixed at 26 nm while on the other sample the thickness was varied as shown in Fig. 3. These specific thicknesses and wavelength range correspond to some actual ex-situ experimental conditions which will be shown below. In the figure, all spectra can be characterized by two silicon peaks (at about 275nm and 365nm), and a gradual increase above 400 nm. The sign of $\Delta R/R$ is negative in the figure, because the reflectance of a sample with a thinner oxide film (large R) is subtracted from the thicker one (smaller R). Also, the absolute value of $\Delta R/R$ increases with large thickness differences between two samples as expected. It should be noted that only the pure interference effect due to a non-absorbing SiO_2 film has been taken into account in the calculations. Thus, any deviations of experimental $\Delta R/R$ spectra from the simulations can be attributed to physical and/or chemical phenomena other than interference. Among the many possibilities are two for which precedent exists, namely, the formation of a surface film due to a chemical reaction(5) and/or a possible change of the Si lattice structure due to the release of the film stress by virtue of the etching back the oxide film(17).

Ex-Situ Differential Reflectance Experiments

The ex-situ experimental results shown in Fig. 4 a and b explore the etching of SiO_2 films grown on both Si(100) and Si(111) surfaces, respectively, in HF-H_2O solutions. Both Si(100) and Si(111) samples were cleaned and oxidized together in order to insure identical experimental conditions. For the Si(100) samples the oxide thickness for the left hand side sample was constant at 25nm, while the other sample was etched back to the values shown in Fig. 4a. In the case of Si(111), the left hand side sample had a fixed thickness of 26nm, while the right hand side was etched back to the values shown in Fig. 4b. In both experiments the thermal oxide was etched completely but the native oxide re grew during the measurement. The simulated spectra corresponding to the ex-situ Si(111) experiments are shown in Fig. 3. and a featureless background spectra is shown in Fig. 4c. The one sample background is obtained from a rastered beam across a single sample and tests the alignment of components while the two sample background is the centered spectrum taken across two adjacent identical samples, and tests the ability to align the samples.

Firstly, the spectral features in Fig. 4a and b are the same except for the anticipated and predictable intensity differences due to optical interference effects. No Si substrate orientation effect was observed in these experiments, however more detailed studies on this issue are underway and will be reported separately. Secondly, the experimental spectra in Fig. 4 b are very well correlated with the simulated spectra in Fig. 3, showing the same spectral shape with two silicon peaks, a smoothly shaped valley between two peaks, and gradual increase above 400 nm.

Any small discrepancy of the absolute value of $\Delta R/R$ for the equivalent thickness of oxide might be due to the error possibly resulting from the thickness measurement by ellipsometry. In both Fig. 4 a and b, a noticeable broad feature above 650 nm is evident. Since the time that this experiment was performed, the apparatus was improved with the inclusion of a wider bandwidth photomultiplier tube and spectral filters and this feature disappeared as is shown below in the spectra in Figs. 5 and 6. No spectral features are seen in the ex-situ DR spectra that have not been included in the simulations. The great sensitivity of the present DR technique to SiO_2 thicknesses of less than 3nm is routinely accomplished.

In-Situ Differential Reflectance Experiments

In contrast with the ex-situ experiments above, for the in-situ situation both samples are simultaneously and continuously etched until a bare Si surface is reached, but until this condition is attained there always exists a difference in thickness, since the experiment commences with different oxide thicknesses. The bottom most spectrum in Fig 5, 1, shows the $\Delta R/R$ for starting oxide thicknesses of 23.4nm vs. 4nm oxide in deionized water. After replacing the H_2O with the HF containing etching solution, 400:1 = H_2O:HF(49%), which had an SiO_2 etch rate of about 4nm/min, the changes in the spectra as a function of time are to be seen by comparing spectra 1 through 8 as shown in Fig. 5.

In all of the spectra shown in Fig. 5 except the initial two at the bottom of the figure which were taken within 10 min of the addition of the etching solution, we estimate that the sample with the initially thinner oxide of 4 nm has reached the Si surface, while for the adjacent sample the oxide is thinning. Firstly, the observed overall decrease of the absolute value of $\Delta R/R$ with time can be explained by the decreasing thickness difference of the oxides as etching of both samples, being initially thick, proceeds to the Si surface. Secondly, the spectral features for Si near 275nm and 365nm are present as is the overall increase in $\Delta R/R$ for longer wavelengths as expected, and in concordance with the simulations. However, despite the increased noise for the in-situ measurement, especially at longer wavelengths, the gradual increase in $\Delta R/R$ as predicted in Fig. 3 and seen for the ex-situ experiments is here in spectra 4 - 7 replaced by a decrease in $\Delta R/R$ up to about 550nm and then the expected increase. Comparing the top three spectra, 5,6,7 with the bottom spectra, 1 and 2, where the differences in SiO_2 thicknesses are greatest, the broad feature showing a decrease in $\Delta R/R$ until 550nm is clearly visible. In order to uncover possible artifacts with the in-situ measurement we show in Fig.6 a comparison of in-situ and ex-situ spectra. From these spectra it seems clear that neither the in-situ cell nor liquid in the cell contributes to the decrease in $\Delta R/R$ above 400nm although the magnitude of the overall spectra is affected by both the cell and more so by liquid. However, the spectral features are unchanged and the spectra agree with the simulations in Fig. 3. In addition Figure 7 shows that the long time background as well as the fully etched samples spectra show a flat response as anticipated in the region of interest, but the other spectra, 4 through 7 in Fig. 5, shows the decreasing slope in the 400-550nm range. Thus, the broad feature appears to be real.

The broad feature in this 400-550nm region is likely another interference effect associated with a surface film. Evidence for this kind of an effect was presented by Hummel et al for buried layers in ion beam damaged samples(12). While at the present time we are not certain of the origin, we speculate that an electric double layer at the Si surface may be responsible. Under this assumption we explore the consequences of the existence of a double layer adjacent to the Si surface in the solution. First, an electric double layer film would not be observed for the ex-situ experiments. The spectra of Fig. 4 compared with Fig. 5 confirm that the spectral feature is seen only in the in-situ experiments and from Fig. 6 is not an artifact due to the in-situ cell or liquid. Secondly, the optical effects on the in-situ DR spectra can be simulated,

viz., the observed decrease in $\Delta R/R$ in the long wavelength regime. Fig. 8 shows four relevant simulated spectra. Spectra 1 and 2 demonstrate that a transparent film with an index near to that of SiO_2 cannot cause the spectral feature, nor can a transparent film with a higher index in spectrum 5. Spectra 3 and 4 show that an absorbing film with a higher index yields a decreasing $\Delta R/R$ in the proper spectral range. For the simulation we chose amorphous Si because R data is available(16), but no implication about the nature of the film is otherwise implied. The 400-550 nm broad feature is reproduced with the a-Si R data in the DR spectra, but the relative intensities of the higher energy peaks is not reproduced. Before additional simulations are profitable, further information relative to the surface film is required. For the present purpose the postulation of a higher density double layer film is consistent with the observed in-situ spectra. Recently, using in-situ ellipsometry to extend previous work on the etching of SiO_2 on Si(5), we have uncovered further evidence for the existence of a high index film, only in solution, at or very near the bare Si surface in HF/H_2O solutions(18). Further work is required to determine the precise nature of the film.

Conclusions

The differential reflectance technique has been shown to be sensitive to small differences in SiO_2 film thicknesses on Si substrates. The etching of SiO_2 can be followed with this technique both ex-situ and in-situ in the HF/H_2O ambient. Spectral features can be simulated with simple optical models and can provide the bases for interpretation. Some evidence for the existence of a double layer on a bare or nearly bare Si surface is given.

Acknowledgement

This research was supported in part by the Office of Naval research, ONR.

REFERENCES

1. F. N. Schwettmann, K. L. Chiang, and W. A. Brown, 152rd Electrochem Soc. Meeting, Abs. No. 276, May 21-26, 1978.
2. F. J. Grunthaner and J. Maserjian, IEEE Trans. Nucl. Sci., NS-24(6), 2108 (1978).
3. G. Gould and E.A. Irene, J. Electrochem. Soc., 134, 1031 (1987).
4. J.M. DeLarios, C.R. Helms, D.B. Kao and B.E. Deal, Appl. Surface Sci., 30, 17 (1987).
5. G. Gould a/nd E.A. Irene, J. Electrochem. Soc., 135, 1535 (1988).
6. G. Gould and E.A. Irene, J. Electrochem. Soc., 136, 1108 (1989).
7. E. Yablonovitch, D.L. Allara, C.c. Chang, T. Gmitter and T.B. Bright, Phys. Rev. Lett., 57, 249 (1986).
8. V.A. Burrows, Y.J. Chabal, G.S. Higashi, K. Raghavachari and S.B. Christman, Appl. Phys. Lett., 53, 988 (1988).
9. K.D. Beyer and R.H. Kastl, J. Electrochem. Soc., 129, 1027 (1982).
10. R.E. Hummel, Phys. Stat. Sol.(a), 76, 11 (1983).
11. J.A. Holbrook and R.E. Hummel, Rev. Sci. Inst., 44, 463 (1973).
12. R.E. Hummel, W. Xi, P.H. Holloway and A. K. Jones, J. Appl. Phys., 63, 2591 (1988).
13. P. Chiaradia, G. Chiarotti, S. Nannarone, and P Sassaroli, Solid State Comm. 26, 813 (1978); S.Selci, F Ciccacci and G. Chiarotti, J. Vac. Sci. Technol.A, 5, 327 (1987).
14. W. Kern and D.A. Poutinen, RCA Rev., 31, 285 (1962).
15. R.M.A. Azzam and N.M. Bashara, "Ellipsometry and Polarized Light", North Holland Publishing Co., New York (1977).
16. E.D. Palik, Ed., "Handbook of Optical Constants of Solids", Academic Press, Orlando Fla, (1985).
17. E. Kobeda and E.A. Irene, J. Vac. Sci. Technol. B, 6, 574 (1988).
18. X. Liu and E.A. Irene, to be published.

Differential Reflectometry Apparatus

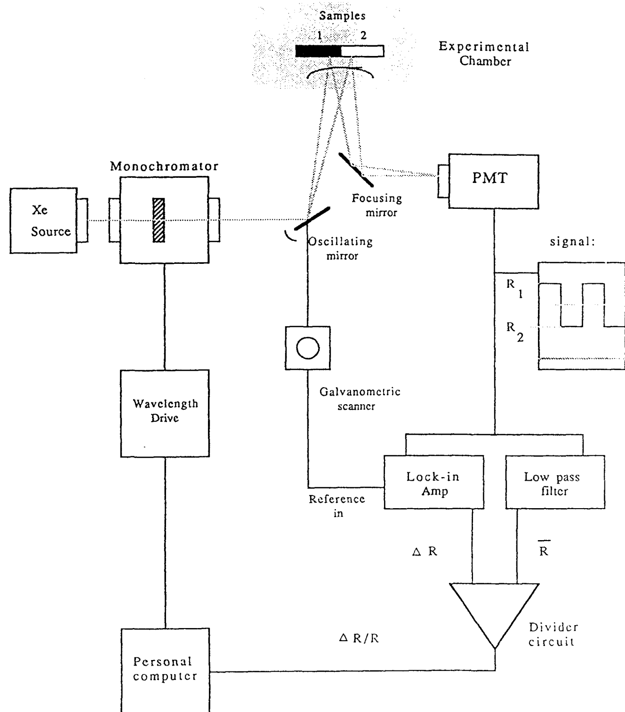

Figure 1. Block diagram of differential reflectance apparatus.

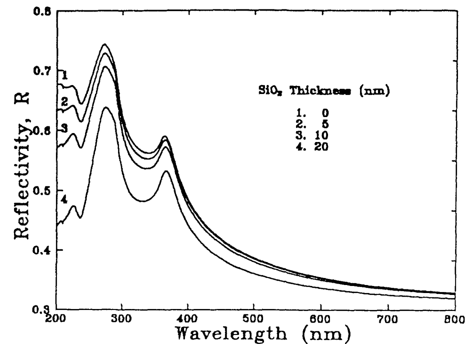

Figure 2. Simulation of the reflectivity, R, from SiO_2 films of varying thicknesses on a single crystal Si substrate.

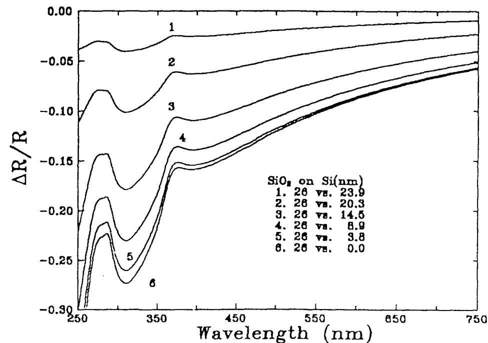

Figure 3. Simulated differential reflectance spectra for two adjacent samples with different SiO_2 film thickness on Si substrates.

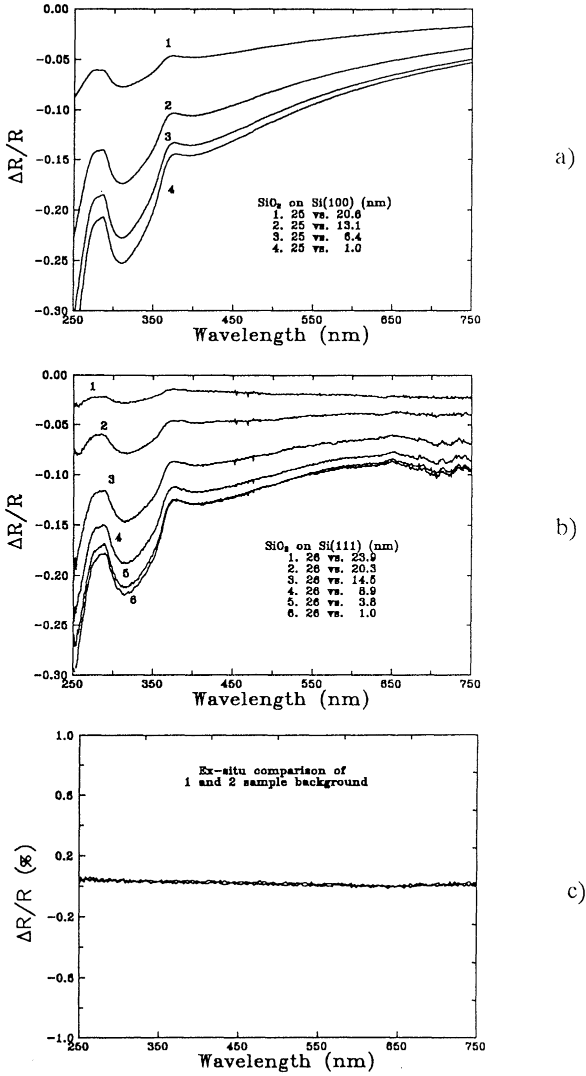

Figure 4. Ex-Situ experimental results of etching SiO_2 films in HF/H_2O solutions: a) SiO_2 on Si(100), b) SiO_2 on Si(111) and c) background spectrum.

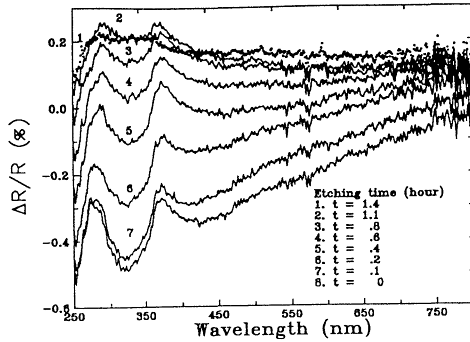

Figure 5. In-Situ experimental results of SiO_2 of 23.4 nm thickness versus 4 nm on (100) Si with 1 the initial spectrum proceeding to 8 at the times indicated on the figure. Background was subtracted from each spectrum.

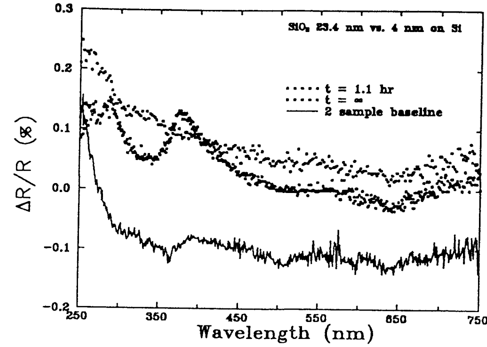

Figure 7. In-situ two sample background spectrum compared with spectrum 7 and 8 from Fig. 5.

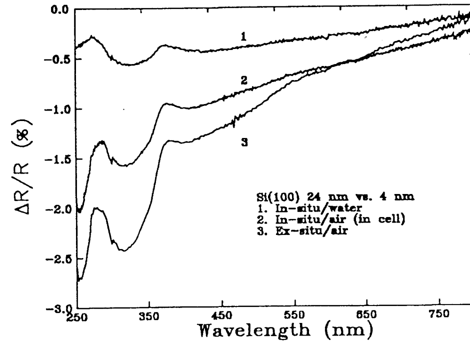

Figure 6. A comparison of in-situ and ex-situ spectra with the in-situ spectra in air but in the in-situ cell, 2, and in water in the cell, 1, with ex-situ in air, 3, and all with the same samples of 24nm SiO_2 versus 4nm both on Si(100) substrates.

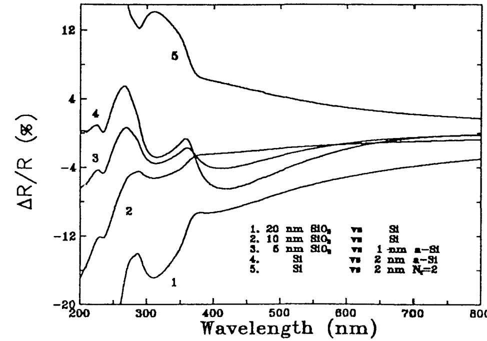

Figure 8. Simulated ΔR/R spectrum. Spectra 1 and 2 are a 20nm and 10nm SiO_2 film adjacent to Si surface, respectively; spectra 3 and 4 are for a 1 and 2 nm a-Si film adjacent to a 5 nm SiO_2 film on Si surface and a bare Si surface, respectively; and spectrum 5, is for a 2 nm transparent film with an index of 2.0 and a Si surface.

AUGER CHARACTERIZATION OF SILICON SURFACE CLEANED WITH H_2O_2 BASED SOLUTIONS

Prasad M. Parimi * and V. P. Sundarsingh**
** Electrical Eng. Dept., I.I.T Bombay, Powai, Bombay-400076.

ABSTRACT

Auger electron spectroscopy has been used to evaluate the chemical state of silicon surfaces cleaned by a specific technique. This method was used to clean wafer surfaces before depositing a spin-on source. Hydrogen peroxide based solutions have been used since they are very effective for the removal of organic contaminants. Small traces of iron were noticed on the untreated sample. The other most common impurities observed were carbon and oxygen. The application of a brief etch in dilute HF solution after the cleaning process enhanced the propensity of the silicon surface for adsorption of hydrocarbons, as HF removed the native oxide from the surface and left behind a very active bare surface.

In recent years, with the increased demand for performance and reliability in semiconductor devices, great emphasis has been laid on the development of improved processing techniques. The wafers must be thoroughly cleaned and dried to achieve uniform surface concentration and adhesion before depositing the dopant film. Any cleaning procedure must be performed correctly, otherwise the wafer will be contaminated rather than cleaned. It is necessary to remove organic contaminants before it is possible to effectively remove the more troublesome ionic contaminants. When large quantities of contaminants are present, an oxidizing acid solution, such as sulfuric acid - hydrogen peroxide is preferred since the necessary cleaning time for alkaline peroxide mixtures exceeds the life of the solution (1). The advantages of cleaning a silicon substrate using the acidic or basic hydrogen peroxide solution have been extensively studied. The only drawback of H_2O_2 solutions are that they decompose faster at higher pH's and in the presence of metal contaminants. Another potential problem is, when the peroxide concentration gets too low in a basic solution, the solution will etch the silicon surface (2). In the present article, Auger spectroscopy studies have been carried out to characterize the cleaning procedure adopted, using H_2O_2 solutions. The significant feature of using the AES technique is that the spectra originates from atoms on or very near the surface of the specimen.

* Present address: LSI Logic Corp., 3115 Alfred St, Santa Clara, CA-95054.

Experimental

The samples used in this study were boron doped silicon wafers of 10 ohm-cm resistivity and they were cleaned by adopting the following procedure.

1. The substrates were dipped in trichloroethylene at room temperature for one minute.
2. The wafers were etched in $HF + H_2SO_4 + HNO_3$ solution.
3. They were rinsed in DI water.
4. They were boiled in either 4:1 $H_2SO_4 - H_2O_2$ or 4:1 $HCl - H_2O_2$ solution at 95 ^oC for 5 minutes.
5. They were rinsed in DI water.
6. Then, they were dipped in 5% HF acid for 30 seconds.
7. Finally, the substrates were thoroughly rinsed in DI water.

The Auger analysis was carried out by using a PHI Model 551 electron spectrometer interfaced to a PDP 11/04 computer. The UHV chamber was evacuated to a vacuum less than 5×10^{-9} torr, using the ion and titanium sublimation pumps. The Auger spectra were recorded using a 3 KV, 20uA electron beam of 5um diameter. The AES spectra recorded in the present work are in their differentiated form dN(E) / d(E) vs E. The spectra were recorded on a pre-calibrated energy scale. The samples were placed in the high vacuum chamber as soon as possible in order to avoid possible contamination.

The Auger spectra obtained from the samples in different stages of cleaning are presented in the Figure 1. Figure 1(a) represents the spectrum obtained from the original wafer. It is interesting to note that in addition to Si, C and O peaks, there are 3 more peaks at 591 eV, 650 eV and 700 eV. These are found to correspond to iron. There is no peak at 179 ev indicating the absence of boron as the boron doping level is too small to be detected (3) and this also indicates that the substrate is free from Pyrex glassware contamination. By etching the silicon sample, the iron contamination was eliminated as shown in Figure 1(b). Figure 1(c) presents the spectrum obtained from the wafer surface after treatment in boiling in $H_2SO_4 - H_2O_2$ solution. It can be observed that the amount of carbon was reduced and that a peak corresponding to sulfur was not seen. After etching, the sample was boiled in $HCl - H_2O_2$ solution instead of $H_2SO_4 - H_2O_2$ solution and Figure 1(d) indicates the presence of chlorine (b.e is 180 eV), whose peak resulted from the LMM transition on the surface. It is observed that the presence of chlorine is helpful in eliminating metallic impurities. As a final cleaning step, the substrate was dipped in 5% HF solution to remove the oxide layer on the surface and it was observed that the carbon contamination had increased. This is because the silicon surface after the removal of the oxide layer will be highly reactive and absorbs carbon compounds either from the HF directly or from the atmosphere (4). It can be observed that in all these spectra, the Si peaks are obtained from cross Auger transitions.

Summary and Conclusions

The above results are summarized as follows:

a. The iron contamination on the fresh wafers was removed when sample was etched for surface polishing.
b. Both acidic and basic hydrogen peroxide solutions were found to be very effective for wafer surface cleaning.
c. A considerable amount of chloride ions were found to be present on the wafer surface after cleaning the samples in hydrochloric acid - hydrogen peroxide solution.
d. The presence of sulfur was not detected on the wafer surface after the sulfuric acid - hydrogen peroxide clean.
e. The amount of carbon contamination on the wafer surface was increased after the final HF etch.

From the above results, it is concluded that the method employed for cleaning the silicon substrates for circuit processing can be implemented successfully with the following recommendations.

1. It is preferable to avoid the usage of Pyrex glassware to eliminate boron contamination.
2. The presence of HCl is preferable to that of sulfuric acid along with hydrogen peroxide so that chloride ions can remove the metallic contamination.
   A still greater drawback to using the sulfuric acid - hydrogen peroxide cleaning procedure is the possibility that a sulfur residue can be left behind on the wafer surface, even though its presence was not noticed in this study.
3. Since the final HF etch process removes the hydrous oxide film formed during the initial cleaning procedure, it enhances the carbon contamination and so this process step should be omitted.
   Otherwise, the HCl - H_2O_2 clean should follow this brief etch in dilute HF solution to enhance the bare silicon surface purification (5). It also reduces the particulate contamination that resulted from the HF dip (6).

Acknowledgements

The authors wish to thank Dr. R.Krishnan and Mr. S.K.Sharma of Metallurgy Division, Bhabha Atomic Research Center, Bombay for extending the Auger spectroscopic fecilities.

REFERENCES.

1. D. Burkman, Semiconductor International, **4** (7), 103 (1981).
2. W. Kern and D. Puotinen, RCA Review, **31**, 187 (1970).
3. J.H. Thomas III and J.M. Morabito, Surface Science, **41**, 629 (1974).
4. R.C. Henderson, Jn. Electrochem Soc., **119**, 772 (1972).
5. W. Kern, Semiconductor International, **7** (4), 94 (1984).
6. D.S. Becker, W.R. Schmidt, C.A. Peterson and D.C. Burkman, " Microelectronics Processing: Inorganic Materials Characterization, " p.366, ACS (1986).

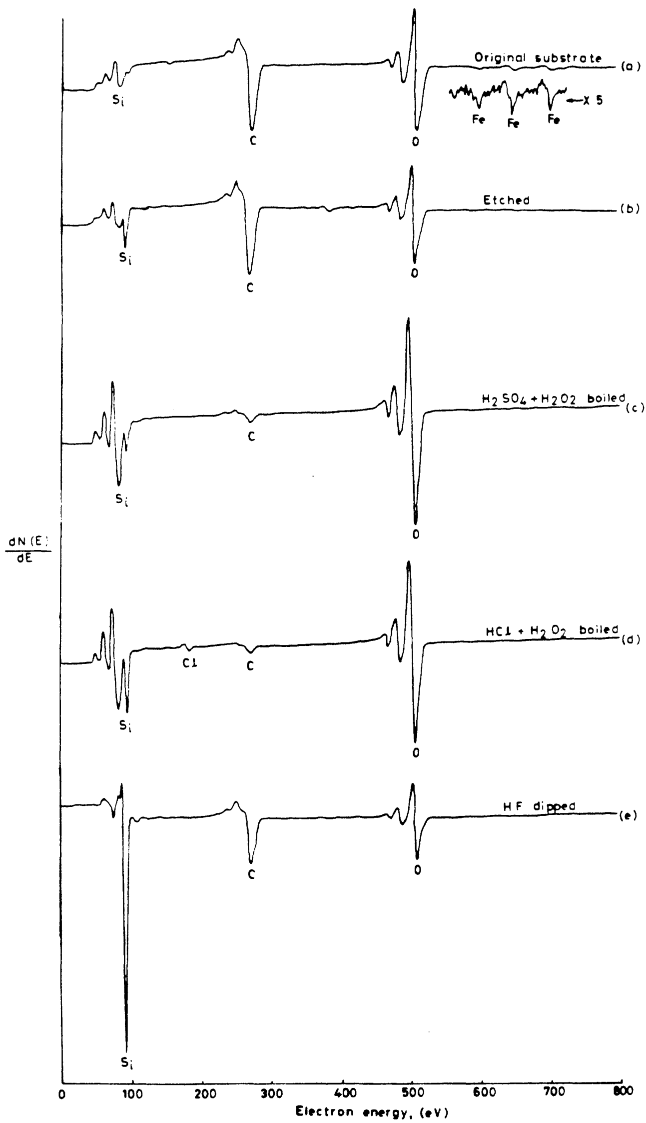

Figure 1. Auger electron spectra from a silicon wafer after various cleaning procedures.

AN ANALYSIS FOR CLEANED SILICON SURFACE WITH THERMAL DESORPTION SPECTROSCOPY

Norikuni YABUMOTO, Kazushige MINEGISHI, Kazuyuki SAITO, Mizuho MORITA*, and Tadahiro OHMI*

NTT LSI Laboratories, 3-1, Morinosato Wakamiya, Atsugi-shi Kanagawa, 243-01, JAPAN
*Department of Electronics, Tohoku University, Aramaki Aoba-ku, Sendai-shi, Miyagi, 980, JAPAN

An improved thermal desorption spectroscopy is developed to remove the backgrounds of gas desorption from the sample chamber and several kinds of cleaned Si(100) wafers are evaluated. By both wet HF solution cleaning and dry HF gas cleaning, about 99% dangling bonds of silicon surfaces are terminated by hydrogen atoms with desorption peaks at 380 and 520°C. The next most desorbed molecules are H_2O and C_2H_4. They have main desorption peaks at 340 and 490°C, respectively. HF gas cleaning methods decrease Si-OH bonds but increased Si-F bonds compared with HF solution cleaning methods. Isopropyl alcohol (IPA) vapor decrease fluorine contaminants but increase trace IPA-derived contaminants.

INTRODUCTION

As ULSI yield is strongly affected by silicon wafer surface conditions, evaluation for different wafer cleaning methods is important. Electron energy loss spectroscopy, X-ray photoelectron spectroscopy and Fourier transform infrared spectroscopy studies revealed that the HF treated silicon surface was mainly terminated by hydrogen atoms. It was also covered by small amounts of hydroxyl groups, hydrocarbons and traces of fluorine(1), (2). Thermal desorption spectroscopy (TDS) is able to determine the binding states of adsorbed molecules from the peak temperature of the desorption spectrum(3). This method has high sensitivity when removing background signals.

This paper presents an adsorbed molecule analysis on the silicon surface after various kinds of cleanings using TDS. We have developed an improved TDS system to remove background signals. Wet HF solution cleaning methods and dry HF gas cleaning methods are compared. Drying methods using inert gas and isopropyl alcohol (IPA) at a final treatment are also compared.

EXPERIMENTAL

The samples were both side mirror-polished, n-type CZ Si(100) wafers with 30 $\Omega\cdot$cm. The sample size was 2 cm x 5 cm. Figure 1 shows the wafer cleaning methods. In the first step, the wafers were washed using conventional wet cleaning methods, i.e., dipping H_2SO_4-H_2O_2, diluted HF, boiling in NH_4OH-H_2O_2-H_2O and HCl-H_2O_2-H_2O. In the second step, samples A and B were dipped in a 1% HF solution, rinsed in de-ionized (DI) water. After these treatments, Sample A was dried with hot Ar gas. Sample B was exposed to IPA vapor. Samples C and D were treated with dry cleaning methods using a 1% anhydrous HF gas in N_2 gas instead of HF solution. Sample C was dried with N_2 gas. Sample D was exposed to IPA vapor. Moisture concentrations of the gases, Ar, N_2 and HF, were less than 10 ppb.

Figure 2 shows a drawing of a TDS apparatus. TDS analyses were carried out with a heating rate of 20 °C/min under a background pressure of less than 1 x 10^{-8} Torr. First, the sample chamber was heated to 1000°C to remove adsorbed gases such as H_2 and H_2O. Next, the sample chamber was heated again to record background data. Finally, the sample was transported by a magnet from position A to position B. The chamber heating was repeated three times, and gas desorptions were measured. This method enabled measurements of trace H_2O desorption just from the Si surface.

Secondary ion mass spectroscopy (SIMS) with high mass resolution, $M/\Delta M>3000$, was applied to detect trace contaminants such as F, S and Cl from the cleaning solutions, and to distinguish them from hydrocarbons. Oxygen concentrations were measured with Auger electron spectroscopy (AES).

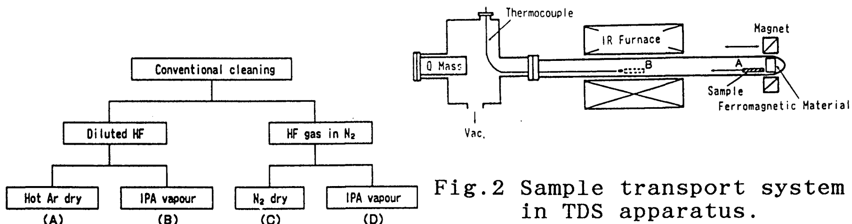

Fig.2 Sample transport system in TDS apparatus.

Fig.1 Wafer cleaning methods.

Main Molecules of Desorption

The previous papers(1), (2) reported that Si-H, Si-OH and hydrocarbons were present on the HF cleaned silicon surfaces. TDS analyses were carried out, watching these spectra. Figure 3 shows typical TDS spectra from sample A. The spectra of M/e=2, 18 and 28 correspond to H_2, H_2O and C_2H_4 or CO molecules, respectively. The main part of M/e=28 spectrum was judged to be C_2H_4, because the spectrum of M/e=28 was similar to those of M/e=26,27,29, which corresponded to C_2H_2, C_2H_3 and C_2H_5. The solid lines are the raw spectra from the Si surface including the background signals and the dotted lines are the background signals from the sample chamber. H_2 was detected over 50 times more than H_2O and C_2H_4, which were the next most desorbed molecules in all the desorption components. The ratio of transmission efficiency for a quadruple mass filter of H_2, H_2O and C_2H_4 is 1 : 5 : 6(4). Consequently, about 99% dangling bonds of the surfaces are terminated by hydrogen atoms. Small amounts of hydrocarbons, such as CH_x(x=2,3) and C_2H_y(y=2,3,5), and fluorocarbons were also detected. These hydrogen, water, hydrocarbon and fluorocarbon molecules were also detected on samples B, C and D with sample A.

Oxygen concentrations on the cleaned silicon surfaces measured with AES are summarized in Table 1. Oxygen concentrations of silicon surfaces at immediately measurements after cleaning were several percents. The increments of oxygen concentrations for 7 days after

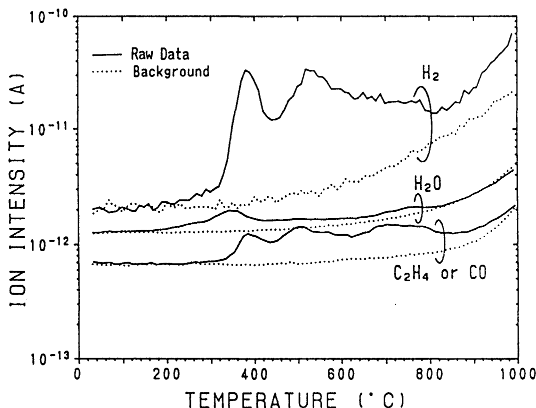

Fig.3 Thermal desorption spectra of H_2, H_2O, and C_2H_4 or CO from sample A.

Table 1 Oxygen concentrations on the silicon surface at immediately after cleaning and 7 days after cleaning.

	Immediately after cleaning	7days after cleaning
A	5.8	9.0
B	3.7	8.2
C	5.3	13.3
D	3.8	8.4

cleaning were 8% at most, because surface terminated hydrogen atoms protect oxidation of silicon. Detailed analysis of adsorbed molecules for different cleaning methods are mentioned in the following paragraphs.

Water Adsorbed States

The thermal desorption spectra of H_2O for four kinds of cleaning methods are shown in Fig.4, where the vertical axis is linear scale. These spectra were corrected to coincide the raw spectra with the background spectra at room temperature and at 900°C. All of the spectra were noticed in the range of 100 to 800°C, and showed main peaks at 340°C. Small peaks at about 500°C and at 750°C were also observed. These pretty high temperatures suggest that water molecules chemisorb on the surface. The spectra might depend on the surface conditions such as the formation of native oxide islands and steps.

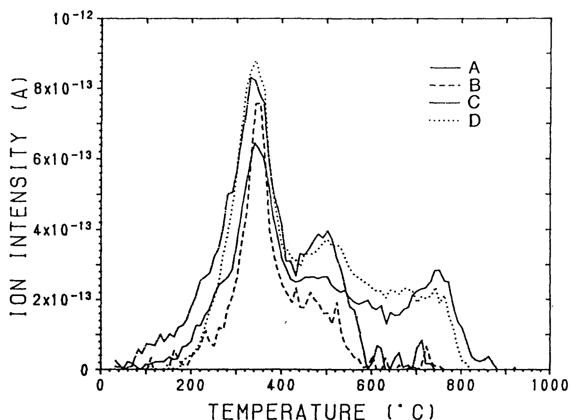

Fig.4 Thermal desorption spectra of H_2O for the four kinds of cleaning methods.

Hydrogen Adsorbed States

The spectra of hydrogen desorption for the four kinds of cleaning methods are compared in Fig.5. The peak heights at 380°C for the wet HF solution cleaning methods, A and B, were higher than those for the dry HF gas cleaning methods, C and D. While the peak heights at 520 °C were almost the same for all cleaning methods. The peaks at 380 and 520°C have been speculated to Si-OH and Si-H(3). This assignment was also confirmed by the above results. Hydroxyl groups are a much amount using HF solution cleaned samples compared with by HF gas cleaned samples, because they are adsorbed from the cleaning solution.

When a TDS measurement was repeated for the same sample, only 520°C peak appeared again. If dangling bonds are present on the silicon surface, the hydrogen that exists in the chamber even at a vacuum of 1 x 10^{-8} Torr combines to form Si-H bonds. Therefore, the second peak represents the hydrogen of Si-H terminated the dangling bonds. The Si-H peaks of samples B and D have shoulders over 600°C. These are considered to be desorbed from the native oxide islands(3). However, the relationships between the cleaning methods that caused the formation of native oxide islands and the H_2 and H_2O desorption have been not found.

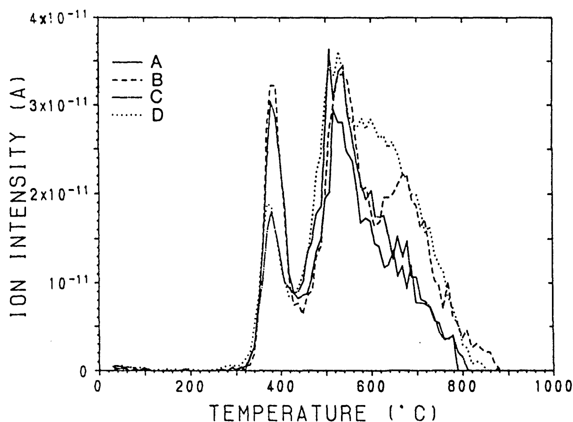

Fig.5 Thermal desorption spectra of H_2 for the four kinds of cleaning methods.

Trace Contaminants

Trace contaminants, C, O, F, S, Cl are measured with SIMS and are summarized in Table 2. Oxygen concentrations were several percents that were the same levels as the results of AES measurements. These oxygen volumes are originated from oxygen atoms of Si-OH bonds and adsorbed H_2O molecules in addition to those of native oxide islands.

The HF gas cleaning methods formed a F-rich surface compared with the wet HF solution cleaning methods. This is because Si-F bonds are hydrolyzed in the solution to form Si-OH by the following reaction : Si-F + $H_2O \longrightarrow$ Si-OH + HF(1). IPA treatment was effective for washing fluorine from the surface. Fluorine of Si-F bonds is removed by IPA vapor, because it dissolves in alcohol.

The other trace contaminants, such as S and Cl, which were intruded from the washing solutions, were also detected less than 2×10^{11} atoms/cm^2.

Table 2 Contaminant concentrations determined with SIMS (atoms/cm^2).

	C	O	F	S	Cℓ
A	2.0×10^{13}	5.6×10^{13}	2.1×10^{11}	2.0×10^{11}	6.4×10^{10}
B	1.4×10^{13}	4.8×10^{13}	0.4×10^{11}	1.8×10^{11}	6.9×10^{10}
C	0.7×10^{13}	4.8×10^{13}	7.4×10^{11}	1.9×10^{11}	8.4×10^{10}
D	0.6×10^{13}	5.6×10^{13}	5.6×10^{11}	1.0×10^{11}	7.6×10^{10}

SUMMARY

An improved TDS system was developed to remove the influence of gas desorption from the sample chamber, and several kinds of cleaned Si(100) surfaces were evaluated. About 99% dangling bonds on the HF cleaned silicon surfaces after both wet solution methods and dry gas methods were terminated by hydrogen atoms with desorption peaks at 380 and 520 °C. Small amounts of water and hydrocarbons were also detected. Their main desorption peaks were 340 and 490 °C. HF gas cleaning methods decreased Si-OH bonds but increased Si-F bonds compared with HF solution cleaning methods. IPA vapor treatment decreased fluorine but increased small amounts of IPA-derived $CH_3CH(OH)$ and $(CH_3)_2CH$ contaminants.

Hydrocarbon Adsorbed States

Many kinds of hydrocarbons were detected by TDS. Desorbed volumes were ordered by carbon numbers, that is C_2H_y > C_3H_z > CH_x. In these hydrocarbons of each carbon numbers, the most desorbed volume molecules are shown in Fig. 6, which compares relative desorbed volumes of hydrocarbons for the four kinds of cleaning methods. Each desorbed volume was normalized with C_2H_4 volume of cleaning method D. The desorbed volume of hydrocarbons was small in wet cleaning compared with dry cleaning. When using IPA, C_3H_7 molecules were increased. The increments were caused by IPA fragment, $(CH_3)_2CH$. However, the differences of total desorbed volumes of hydrocarbons were less than twice in the all cleaning methods.

The remarkable difference using IPA appeared in spectra M/e=45($CH_3CH(OH)$). However, the relative volume was about 0.03. Figure 7 shows the thermal desorption spectra for $CH_3CH(OH)$. The use of IPA vapor at the end of the cleaning increased these IPA-derived $CH_3CH(OH)$ and $(CH_3)_2CH$. The desorption of IPA molecules themselves were not detected.

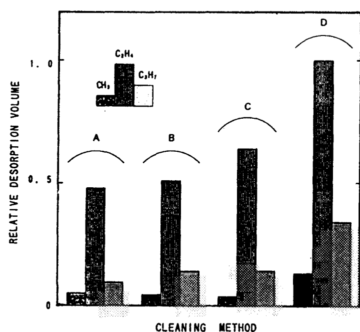

Fig.6 Relative desorption volumes of hydrocarbons for the four kinds of cleaning methods.

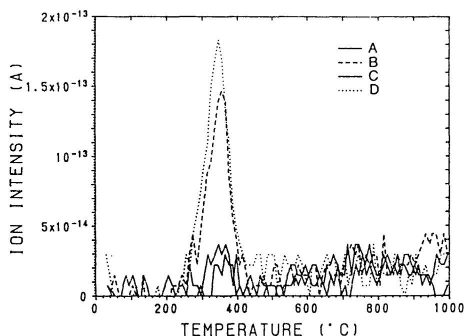

Fig.7 Thermal desorption spectra of $CH_3CH(OH)$ for the four kinds of cleaning methods.

ACKNOWLEDGMENTS

The authors thank Dr. Eisuke Arai and Dr. Hiroyuki Harada of NTT LSI Laboratories for useful discussion and encouragement, and Eiji Hasegawa of Tohoku University and Yukio Komine of NTT LSI Laboratories for valuable technical assistance.

References

(1) T. Takahagi, I. Nagai, A. Ishida, H. Kuroda and Y. Nagasawa, J. Appl. Phys., Vol.64 (1988)3516.
(2) M. Grundner and H. Jacob, Appl. Phys., A39 (1986)73.
(3) N. Yabumoto, K. Minegishi, Y. Komine and K. Saito, Jpn. J. Appl. Phys., to be submitted.
(4) T. C. Ehlert, J. Phys. (E), Vol.3 (1970)237.

SURFACE CHARGE ANALYSIS: A NEW METHOD TO CHARACTERIZE SEMICONDUCTOR/INSULATOR STRUCTURES APPLICATION TO SILICON/OXIDE SYSTEM

Emil Kamieniecki
SemiTest Incorporated, Billerica, MA 01821

ABSTRACT

A novel technique, surface charge analysis (SCA), is introduced. The method allows for immediate and non-destructive characterization of electronic properties of semiconductor/insulator system. Unlike conventional capacitance techniques it does not require formation of the gate electrode and direct electrical contacts. It determines the electronic properties of the system from surface photovoltage measurements of the depletion layer width as a function of an external electrical field. The method allows for determination of the doping type, doping concentration at the semiconductor surface, dielectric (oxide) charge, and energy distribution of the interface state density. Capabilities of the SCA technique extend from bare surface to several micron thick dielectric coatings. These have been demonstrated for Si wafers in such applications as monitoring of contamination in preoxidation cleaning, cleaning of oxidized wafers, etching and oxidation processes.

INTRODUCTION

The operation of integrated circuits based on silicon critically depends on electronic properties of the narrow region at the Si/SiO_2 interface. There is a well established need for a rapid and non-destructive technique which can be used to characterize the Si/SiO_2 interface region in the early stages of the IC production cycle. Conventionally, characterization of the electronic properties of the interface region is performed utilizing measurements of electrical admittance of a metal-oxide-silicon (MOS) structures such as capacitance-voltage characteristics.(1,4) While such measurements might be relatively rapid, need for formation of the gate electrode and hence MOS structure is cumbersome and time consuming. Additional processing steps also introduce uncertainty in evaluation of the Si/SiO_2 interface and oxide properties.

In this report a novel technique, surface charge analysis (SCA), is introduced. It allows for characterization of electronic properties of a semiconductor/insulator system, including silicon with submonolayer dielectric coating (e.g., bare silicon), without a need for formation of the gate electrode or direct electrical contacts with the wafer. The method makes use of the Surface Photovoltage Measured Capacitance (SPMC) (2,3) technique to determine relationships between the ac voltage generated at the semiconductor surface due to chopped light and the width of the surface depletion layer (depletion capacitance). The surface photovoltage

signal generated in the semiconductor is capacitively detected by an external electrode. Unlike the conventional admittance methods which require intimate contact between a gate electrode and the semiconductor/oxide structure (1,4) the external electrode used in the present method is not in contact with the evaluated semiconductor structure. The electronic properties of the Si/SiO_2 system are determined from the analysis of the variation of the depletion layer width induced by an external electrical field. The SCA method allows for determination of the doping type and doping concentration of the semiconductor surface region, the oxide (dielectric) charge, value and energy distribution of the interface state density. The capabilities of the SCA technique are illustrated in such applications as monitoring of the effect of preoxidation cleaning on bare Si wafers and on subsequent oxidation, cleaning of oxidized wafers, and oxidation processes (5-8).

SCA - PRINCIPLES OF OPERATION

The Surface Charge Analyzer (SCA) system measures the ac Surface Photovoltage (SPV) generated in the semiconductor when a beam of chopped light of a photon energy greater than the semiconductor bandgap is incident on the semiconductor surface. The illumination is adjusted to a level at which the generated SPV signal is proportional to the intensity of the incident light. It was previously shown (2,3) that under such conditions the ac SPV signal is proportional to the depletion layer width (reciprocal of the depletion layer capacitance).

The block diagram of the SCA system is shown in Figure 1. The electrical coupling to both front and back surface of the wafer is purely capacitive. The chopped light from the green light emitting diode (LED) is brought to the surface of the wafer via the Mylar spacer (about 12 μm thick) coated on the side opposite the wafer with an optically transparent, conductive film. The conductive film on the Mylar spacer serves as an electrode which, due to capacitive coupling to the semiconductor surface, detects the SPV signal. Variable voltage bias (up to 1000V) applied to the conductive film induces an electrical charge in the semiconductor, Q_{ind}, which is the sum of the changes in the space charge layer and in the interface states.

DOPING CONCENTRATION

The typical dependence of the imaginary component of the SPV signal (and therefore depletion layer width, W_d) vs. Q_{ind} is shown in Figure 2 for p-type Si with 250Å thermal oxide. Note that at accumulation (positive Q_{ind} in Figure 2) the SPV signal vanishes. On the other hand the SPV signal and depletion layer width, W_d, achieves its highest, saturation values under inversion conditions (negative Q_{ind} in Figure 2) when a formation of an inversion layer prevents further expansion of the depletion layer. The relationship between maximum depletion layer width and the doping concentration, N_{sc}, in the space charge region (4) is used first to calibrate the SCA system using a reference wafer of a known doping concentration and later used to determine or confirm doping concentration of other wafers.

DOPING TYPE

The polarity of the SPV signal, and especially the imaginary component, depends on the doping type. The change in polarity of the SPV signal results from the difference in the sign of the surface potential barrier under depletion condition for n- and p-type semiconductors. At the same time the shape of the curve of Figure 2 will change depending on the doping type of the material. While in p-type inversion occurs at more negative Q_{ind} than accumulation, in n-type it will be the opposite.

DENSITY OF INTERFACE TRAPS

Induced charge, Q_{ind}, represents the sum of the changes from the zero bias conditions in the semiconductor space charge, Q_{sc}, and in the interface trapped charge, Q_{it},

$$Q_{ind} = \Delta Q_{sc} + \Delta Q_{it} . \quad (1)$$

At zero bias $Q_{ind}(0) = 0$ and the oxide charge is compensated by the total of the space charge, Q_{sc}, and the interface trap charge, Q_{it}, ,

$$Q_{ox} = -[Q_{sc}(0) + Q_{it}(0)] , \quad (2)$$

where $Q_{sc}(0)$ and $Q_{it}(0)$ are values at zero bias.

Since the oxide charge, Q_{ox}, is independent of bias, and at any bias

$$Q_{sc} = Q_{sc}(0) + \Delta Q_{sc}$$
$$Q_{it} = Q_{it}(0) + \Delta Q_{it},$$

we get

$$Q_{ind} = Q_{ox} + Q_{sc} + Q_{it} . \quad (3)$$

The density of interface traps, $D_{it}(E)$, is defined as (4)

$$D_{it}(E) = dQ_{it}/qdE , \quad (4)$$

with the energy

$$E = E_{Fs} - E_{is} = E_F - (E_i - q\psi_s) , \quad (5)$$

where, E_F is the Fermi level in the bulk, E_i is the intrinsic level, and q is the elementary charge. The surface potential is given by

$$\psi_s = qN_{sc}W_d^2/2\varepsilon , \quad (6)$$

where ε is the semiconductor permittivity (4). From Equation 3

$$dQ_{it} = dQ_{ind} - dQ_{sc}, \quad (7)$$

where $|dQ_{sc}| = qN_{sc}dW_d$. An energy distribution of the interface state density determined for the wafer of Figure 2 using the above described method, Equations 4-7, is shown in Figure 3.

OXIDE CHARGE

Under flat band conditions $Q_{sc}(FB) = 0$, and hence, using Equation 3,

$$Q_{ind}(FB) = Q_{ox} + Q_{it}(FB). \quad (8)$$

Since the depletion layer capacitance in the Surface Photovoltage Measured Capacitance (2,3) and in the admittance methods (4) can be defined similarly, as a derivative of the semiconductor space charge over surface potential, the depletion layer width under flat band conditions, $W_d(FB)$, in both cases is given by the extrinsic Debye length, L_D (4). Knowledge of the doping concentration from the saturation of the SPV (see Figure 2) allows calculation of L_D, and hence $W_d(FB)$ and $Q_{ind}(FB)$, from the curve of Figure 2. $Q_{ind}(FB)$ is the total charge in the oxide and in the interface states (see Equation 8) related to the flat band voltage that is used in the capacitance voltage techniques (1,4).

It is postulated here that a better measure of the total oxide charge than that offered by Equation 8 will be the value extracted from the induced charge, $Q_{ind}(MG)$, measured with the semiconductor biased to align the surface Fermi level with the intrinsic level; that is $E = 0$ in Equation 5 and $q\,\psi_s(MG) = E_i - E_F$. Considering that, due to compensation of the charges of the interface states located above and below the intrinsic level, the interface trapped charge usually vanishes at such surface bias, $Q_{it}(MG) = 0$, and from Equation 3.

$$Q_{ox} = Q_{ind}(MG) - Q_{sc}(MG). \quad (9)$$

where $Q_{ind}(MG)$ is determined from the curve of Figure 2 using $W_d(MG)$ from Equation 6, and $|Q_{sc}(MG)| = qN_{sc}W_d(MG)$.

Additionally, inaccuracy of such an approach assuming $Q_{it}(MG) = 0$ is minimized due to the interface state density reaching a minimum at the energies close to the mid-gap (see Figure 3).

APPLICATIONS

The SCA technique presented allows for rapid and non-destructive characterization of the electronic properties of the semiconductor/insulator structures. SCA uses neither a gate electrode nor direct electrical contact and so eliminates the additional processing steps required before testing by the C-V technique. This major simplification of the test procedure:

* Makes it applicable to a wide range of dielectric thicknesses from zero to at least several microns,
* Reduces ambiguities in interpretation of measurement (due to elimination of additional processing steps),
* Allows easier differentiation of contamination created in individual stages of the semiconductor fabrication process,
* Shortens the time required to identify and correct failures in the production process.

SCA, as a real-time method, provides the capability of determining, in-process, a basic electrical characteristic of the silicon wafers and, therefore has the ability to monitor process variations during manufacturing. The SCA technique has already found application in monitoring contamination in preoxidation cleaning, cleaning of oxidized wafers, and oxidation processes (5-8).

REFERENCES

1. E.H. Nicollian and J.R. Brews, MOS (Metal Oxide Semiconductor) Physics and Technology (Wiley, New York, 1982).
2. E. Kamieniecki, J. Vac. Sci. Technol. 20, 811 (1982).
3. E. Kamieniecki, J. Appl. Phys. 54, 6481 (1983).
4. S.M. Sze, Physics of Semiconductor Devices (Wiley, New York, 1981), Chapter 7.
5. A. Resnick, E. Kamieniecki, A. Philipossian, and D. Jackson, "Effect of Silicon Wafer Cleaning on Pre and Post Thermal Oxidation Charges," this symposium.
6. V. Murali, D.B. Fraser, E. Kamieniecki, A. Resnick, "On the Electrical Nature of Native Oxides Formed By Various Cleaning Techniques and Their Effect on Thermal Oxide Quality," this symposium.
7. V. Murali, D.B. Fraser, and E. Kamieniecki, "Quantitative Measurement of Electrically Active Impurities on Bare Silicon and Silicon Oxide Surfaces," this symposium.
8. A. Philipossian, D. Jackson, E. Kamieniecki, and A. Resnick, "The Effect of Ambient Air Infiltration on Growth Rate and Electrical Characteristics of Ultra-Thin Silicon Dioxide Gate Insulator," this symposium.

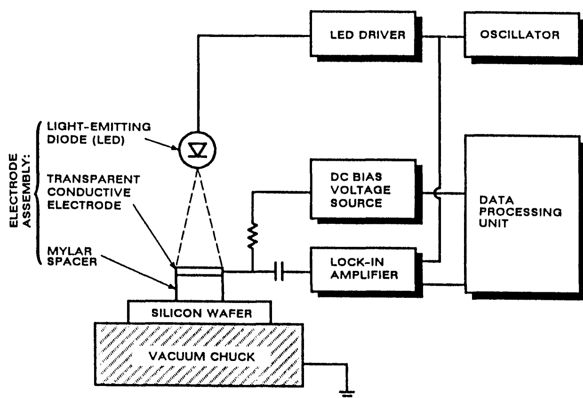

Figure 1. Block diagram of the SCA system.

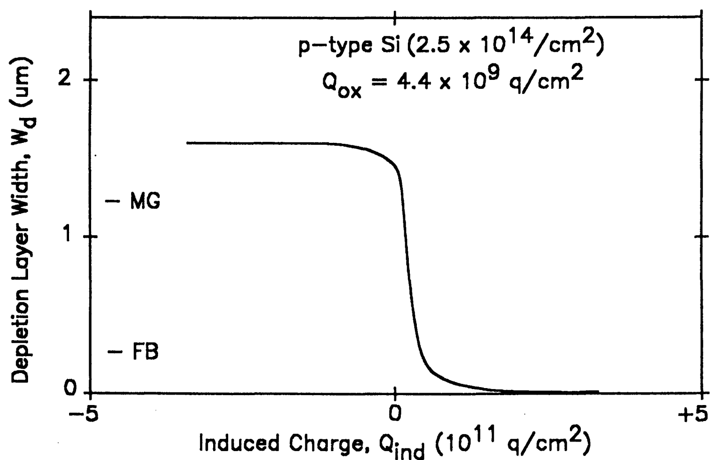

Figure 2. Typical dependence of the depletion layer width, W_d, on the induced charge, Q_{ind}.

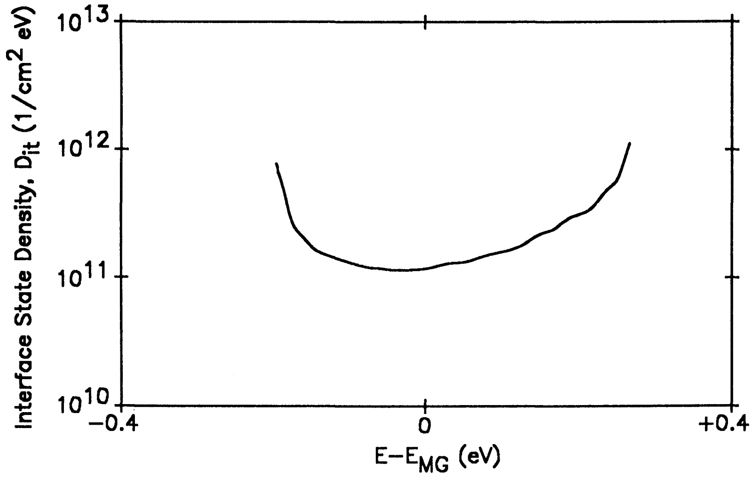

Figure 3. Energy distribution of the interface state density, D_{it}, for the wafer of Figure 2.

CLEANING BEFORE THERMAL OXIDATION

THE EFFECT OF AQUEOUS CHEMICAL TREATMENTS ON SI SURFACE CHEMISTRY AND OXIDATION KINETICS

C. R. Helms*, B. E. Deal+, J. M. deLarios+**, D. B. Kao+
*Department of Electrical Engineering, Stanford University Stanford, California 94305
+Advantage Production Technology, 820-SC Kifer Road, Sunnyvale, CA 94086
**Work performed while author was at Stanford

ABSTRACT

This paper presents a review of recent studies of the chemistry of surface residues left after popular aqueous chemical cleaning sequences and the effect of these residues on subsequent oxidation kinetics. Except for a final step involving NH_4OH:H_2O_2:H_2O (with or without a water rinse) seemingly quite different surface chemistries lead to nearly identical oxidation kinetics. Al deposited on the Si surface from the NH_4OH:H_2O_2:H_2O is responsible for the effects observed leading to oxidation kinetics which are first accelerated and then retarded compared to the other cleans.

It has long been realized that the previous chemical history of the silicon surface can have a substantial effect on the kinetics of subsequently grown thermal oxides [1]. In particular the final "cleaning" step employed, normally in aqueous solutions, can lead to differences in oxide thickness for a particular set of growth conditions of up to 25% [2]. The purpose of this paper is to review the recent work on the effect of preoxidation cleans on oxidation kinetics and to attempt to illustrate the particular chemical cause of these effects as well as determine what physical mechanism is being effected during oxidation.

This latter goal is made difficult since there is currently no general agreement as to the dominant mechanisms that control the oxidation process itself. Although the purpose of this paper is not to review oxidation models, a brief discussion is in order to provide a comparison of limiting behavior we will use below. Proposed mechanisms for the rate limiting step in dry oxidation of silicon fall primarily into three categories: interface reaction controlled, "bulk" transport controlled via Fickian diffusion in a concentration gradient, and electrochemical field controlled. In addition, multiple reaction paths associated with parallel diffusing species have been suggested [3,4]. In the first case the interface may be the Si-SiO_2 interface or the SiO_2/O_2 gas interface and mechanisms associated with the reaction of O_2 with Si [5], dissociation of O_2 at the interface [3,6], and absorption of O_2 into the SiO_2 have been all suggested as being important [3,7]. If more than one mechanism is important then we would normally think of the interface mechanisms as being more important for thin oxides. However, in some of the parallel path models this is not necessarily required. Mechanisms involving transport of the oxidant through the oxide would normally be assumed to dominate for thick oxides although as will be discussed below for dry oxidation, thicknesses approaching 1μm are necessary for this effect to dominate. Electrochemical fields due to the possible presence of charge or stress during oxidation have also been suggested as important mechanisms [5,8,11]. Indeed these mechanisms have led different workers to suggest on the one hand that the electrochemical effect on transport is the only rate limiting step [12] whereas others have suggested that the effect on interface reactions[13] is the only rate limiting step.

Irrespective of the actual mechanisms involved it is important to establish a method to assess the preoxidation cleaning kinetic effects, especially as a function of oxide thickness. In addition, it is also critical that the effects be determined over a sufficient thickness range so that meaningful conclusions can be reached. With this in mind we will illustrate a method to quantitatively compare the experimental results to the prediction of an oxidation model. To illustrate this, if we take the simplest form of the linear parabolic model

$$x^2 + Ax = Bt \qquad (1)$$

We wish to assess the effect of the clean on the rate constants B and B/A. This can be done quantitatively by determining the percentage change in thickness for given oxidation times for cleans to be compared. Mathematically the effect can be calculated by relating dx/x to dB/B and d(B/A)/(B/A) so that we obtain a relationship for a percentage change in thickness associated with a percentage change in the rate constants. This gives

$$\frac{dx}{x} = \frac{x\left(\frac{dB}{B}\right) + A\frac{d(B/A)}{(B/A)}}{2x + A} \qquad (2)$$

$$\text{as } x \rightarrow o \qquad \frac{dx}{x} \rightarrow \frac{x\left(\frac{dB}{B}\right)}{A} + \frac{d(B/A)}{(B/A)} \qquad (3)$$

$$\text{as } x \rightarrow oo \qquad \frac{dx}{x} \rightarrow \frac{1}{2}\left(\frac{dB}{B}\right) + \frac{A \; d(B/A)}{2x(B/A)} \qquad (4)$$

For data analyzed by this model a plot of dx/x versus x (or t) makes a qualitative determination of which rate constant is being affected by a clean possible. In equation 3, effects associated with B are reduced by the x term so that deviations in kinetics for thin oxides must be associated with B/A. For thicker oxides (eqn. 4) effects of deviations in B/A are reduced by the 1/x term allowing an assessment of the effect on B. However as we have pointed out before [2,3] the thin and thick limits, at least for this model, are typically never approached as the model breaks down for x<500Å and data is not usually available for x>1µm.

Indeed, such plots as shown in Figure 1 comparing $HF:H_2O$ and $NH_4OH:H_2O_2:H_2O$ final cleans to be discussed in more detail below show more complex behavior with dx/x changing sign at approximately 200Å and showing a peak for the 900 and 1000°C cases. Although it is clear the simple model of equation (1) is insufficient in describing the kinetics for dry oxidation, the method outlined above allows for a quantitative comparison of kinetic data through which a model may be evaluated.

In some ways it is surprising that preoxidation cleans have any substantial effect on oxidation kinetics. The oxidation process is usually preceded by insertion into a furnace in an "inert" gas such as N_2 and brought up to temperature. Such a step has a major effect on the residues left by the preoxidation cleaning. This is illustrated in Figure 2 where Auger spectra are shown for surfaces after a 1:2:5 $NH_4OH:H_2O_2:H_2O$ treatment

followed by a water rinse (top spectra), an HF dip in 1:50 HF/H_2O (also followed by a water rinse - middle spectra), and a spectra obtained on either surface after a push-pull into and out of the furnace at 1000°C in N_2 (bottom spectra). The high temperature N_2 exposure effectively removes carbon and leads to a thicker oxide. These two effects may well be due to O_2 or H_2O impurities in the furnace. In addition, although the hydrogen surface concentration was not determined, it desorbs at significantly lower temperatures (<500°C [17]) and has undoubtedly been removed by the 1000°C N_2 exposure. It thus becomes clear that any cleaning effect on oxidation kinetics must be due to factors other than the dominant surface chemistry after the clean. Such factors might be structural (roughness) or due to minority chemical constituents left on the surface after the cleans. Indeed, in our own work in this area the sole cause of kinetic differences in oxidation due to silicon precleaning (at least for oxides thicker than ~200Å) was low level contamination (as little as $10^{13}cm^{-2}Al$) deposited on the surface during the clean ($NH_4OH:H_2O_2:H_2O$) [14]. Major differences in surface chemistry induced by the cleans led to little apparent difference in oxidation kinetics.

The first paper reporting the sensitivity of thermal oxidation to surface cleans was by Grunthaner and Maserjian [1]. N-type (100) wafers were given a "standard" clean followed by an extended 30 minute rinse in deionized water. Wafers given no further treatment were referred to as having a hydroxylated surface. These cleaned wafers were compared to wafers given an additional HF clean. For oxidation in dry O_2 at 1000°C over the thickness range from 200 to 700Å, the HF cleaned surface produced a thicker thermal oxide. An interesting aspect of the kinetics is the presence of cross-over point where the hydroxylated surface formed a thicker oxide below approximately 175Å. This corresponds to the zero crossing in our own data in the dx/x plot of Figure 1.

The dependence of oxidation kinetics on the surface preparation was shown by Schwettmann et al for thicker oxides [18]. Wafers cleaned with a sulfuric-peroxide solution produced a considerably thicker thermal oxide when compared to the "no-clean" wafers (these were cleaned only by the vendors) and the ammonium hydroxide-hydrogen peroxide clean. They noted that the effect of the clean on the oxidation rate continued to be observed over the entire oxidation time. As their minimum measured thickness was over 300Å, they did not observe the thickness/time cross-over between the cleans as did Grunthaner et al [1]. The linear and parabolic rate constants were extracted from using the Deal-Grove linear-parabolic model [5], indicating that the parabolic rate constants for all the cleans were essentially the same, while the linear rate constants varied by a factor of two for the sulfuric and ammonium hydroxide cleans. The exact nature of the "no-clean" surface treatment was not known, but it was believed to include a final DI water rinse.

A recent study by Gould and Irene [19] concentrating on variations of the standard RCA clean was initiated to investigate the effect of surface cleans for even thicker oxides. Their results were similar to those of Schwettmann et al [18], where the slowest oxidation rate was observed for the ammonium hydroxide-hydrogen peroxide cleaned sample. However, the $HCl:H_2O_2$ clean produced nearly the same retardation as the $NH_4OH:H_2O_2$ clean. A HF clean gave the most rapid oxidation. Oxidation rates were calculated by fitting their data to a second order polynomial which is indeed equivalent to the mathematics of the linear parabolic model.

Using Gould and Irene's values for the oxidation rates, the linear-parabolic rate constants were calculated and are listed in Table 1 for the HF, $HCl:H_2O_2$, and $NH_4OH:H_2O_2$ cleaned surfaces. There is little variation in the parabolic rate constant with surface clean. The ammonium-hydroxide and hydrochloric-peroxide based cleans

resulted in an 8% increase in B compared to the HF clean. The major change is in the linear parameter. The $NH_4OH:H_2O_2$ and $HCl:H_2O_2$ cleans have a reduced linear parameter of approximately 33% compared to the HF clean. Gould and Irene's analysis of their data concentrated on a comparison of the oxidation rate as a function of thickness and surface treatment. Since there was a substantial variation in the oxidation rate for thicker oxides (2,750Å), they concluded that either 1) the interface reaction rate and other interfacial effects must extend to a greater thickness than expected or 2) that the bulk SiO_2 is modified by the chemical treatments. Our previous analysis [3] shows that the reaction at the Si/SiO_2 interface is important for thickness well over 2000Å at the temperature of 980°C used by Gould and Irene. The second conclusion of Gould and Irene, is supported by ellipsometric analysis of the thermal oxides which indicates that the ammonium hydroxide oxides have a larger index of refraction and are therefore denser than the HF oxides. However, this is inconsistent with the extracted parameters in Table 1. In fact, the oxidation parameters suggest that the ammonium hydroxide oxides have an increased solubility-diffusion coefficient product (lower density) compared to the oxides formed after the HF clean. The trends found in the oxidation parameters in Gould and Irene's study are in general agreement with both the work of Schwettmann et al. and our results. The main exception is that our $HCl:H_2O_2$ cleans did not retard the oxidation kinetics while the $HCl:H_2O_2$ cleans of Gould and Irene resulted in a retardation similar to the $NH_4OH:H_2O_2$ clean.

The effect of surface cleans on thin oxides was studied by Ruzyllo [20,21] for an RCA clean followed by a HF treatment and DI rinse, a variation of the RCA clean with no HF treatment, and a sulfuric-peroxide clean. No substantial effect of cleaning procedure on the oxide growth rate in the range of oxide thicknesses under 250Å was observed for the "original RCA" clean, with a final HF etch, and the "standard RCA" clean, with a final $HCl:H_2O_2$ step. Since earlier studies had shown that a clear impact on oxidation rates was found for thicker oxides, it was suggested that the primary effect of pre-oxidation treatments was on the diffusion controlled regime of silicon oxidation rather than during the initial surface controlled oxidation. This lack of dependence on surface cleans is a direct result of the fact that all of the cleans used in Ruzyllo's study do indeed show similar oxidation rates. In addition, the crossover in rates already mentioned which occurs at approximately 200Å yields little sensitivity to the cleans over this thickness range.

Our results on the effect of various cleans on oxidation kinetics are illustrated in Figure 3, where thickness versus time data is shown for wafers, after an RRCA clean or RRCA clean plus HF (all cleans are followed by a water rinse). In addition, a number of other cleans were investigated [15,16]. All cleans except the RRCA gave identical kinetics representative of the "HF Clean" (RRCA + HF) in the figure. There is a clear difference in kinetics for the cleans all the way up to nearly 1 μm in thickness except for the 1200°C case, which shows no effect of the cleans whatsoever.

With this data we can of course obtain fits to various oxidation models in an attempt to determine what physical process is being effected by the clean. The plot of $\Delta x/x$ vs x shown in Figure 1 from the data of Figure 3 show, however, that the mechanism may be quite complex and therefore such fitting approaches without additional data will quite possibly lead to erroneous conclusions. Indeed, the linear parabolic model of (1) cannot explain even the qualitative features of Figure 1 without allowing a substantial variation in the "initial" oxide thickness (from 30-200Å), which is clearly not physically reasonable.

Indeed, determination of the mechanisms for the effects observed has been illusive. Based on the previous discussion and the fact that the data plotted in Figure 1 (at least for the 900 & 1000°C cases) shows the cleaning effect is diminishing with thickness, we assume that the effect of the cleans on the transport of oxidant through the SiO_2 is less important than interface mechanisms, for if it were (see eqn. 2) the cleaning effect on $^{\Delta x}/x$ would reach a limiting value as $x \rightarrow \infty$. For the 800°C case it might be argued that such a limiting value is being reached. However, for such a low temperature, many models indicate that the kinetics are only minimally effected by oxidant transport for thickness reached in these experiments. Therefore, we would anticipate that such a fall-off in $^{\Delta x}/x$ observed for the 900° and 1000°C cases might also be expected for lower temperature oxidations if thicker oxides were studied. The 1200°C case may seem curious; however, as we have shown previously, the chemical cause for the deviation in kinetics associated with the NH_4OH:H_2O_2:H_2O treatment is removed at high (1200°C) temperatures. The interface mechanism normally assumed to dominate the kinetics is associated with reaction of oxygen with silicon at the Si-SiO_2 interface (possibly involving O_2 dissociation as the rate limiting step. However, our data show that the retardation in oxidation rate (thickness > 200Å) associated with the NH_4OH:H_2O_2:H_2O final cleaning step can be removed in a two step oxidation by etching away only a few tens of angstroms of the SiO_2 surface in between the steps [14-16].

This led us to investigate if any impurities (albeit at a low concentration) left on the Si surface after the cleans were also present on the oxide surface after oxidation. SIMS measurements of the surface are shown before oxidation in Figure 4 and after oxidation in Figure 5. Although numerous impurities are observed it is clear Al is present in much higher concentrations on the RRCA cleaned surface as well as the SiO_2 after a subsequent oxidation [14-16]. Calibrations of the SIMS with evaporated Al standards yields ~$2x10^{13}cm^{-2}$Al present after the RRCA clean and <$2x10^{11}cm^{-2}$ after an HF clean. Indeed, further experiments including the deposition of Al onto a surface prior to oxidation and treatments of SiO_2 surfaces with NH_4OH:H_2O_2:H_2O prior to a subsequent oxidation [14-16] yield a retardation in oxide growth rates. It is therefore clear that this retardation is associated with the aluminum and, in addition, is due to important chemical process occurring at the SiO_2/O_2 surface during oxidation.

Although this work clearly establishes the cause of the growth rate retardation associated with the RRCA clean for thicknesses greater than 200Å, the cause of the rate increase for thinner oxides has not been concretely established. However, irrespective of the actual mechanism, the effect gives additional support for the idea that there exists a distinct rate limiting step for oxidation in this thin range, different from those important for thicker oxides.

The concept of an important chemical process at the outer SiO_2 surface effecting kinetics, although not discussed in most papers on oxidation modeling, has been suggested in the past [5]. However, within the framework of a linear-parabolic type model, for such a process to cause a factor of two change in the interface reaction rate constant implies that the Si-SiO_2 interface mechanism certainly does not dominate and indeed the SiO_2 surface mechanism may dominate. Although some recent modeling efforts have taken these results into account, others need to be reexamined and, indeed, models based solely on transport as the dominate rate limiting step seem inconsistent with the present findings.

Although a detailed discussion of fits to kinetics models is beyond the scope of this paper we present in Tables 2 and 3 the parameters extracted from the data of Figure 3 for the popular linear parabolic model (Table 2) and a form of the parallel oxidation model

$$\frac{dx}{dt} = \frac{B}{2x + A}\left(1 + \frac{\beta}{2x}\right) \qquad (5)$$

Both fits yield nearly constant parabolic rate constants but linear rate constants differ by about a factor of two. The rate constant β associated with oxidation for thin oxides also varies by a factor of two causing the negative values of $\Delta x/x$ in Figure 1; this effect is also manifested in the large variation in τ observed.

This work was supported by SRC Contract 88-SP-101 and gift funds from the Fairchild Research Center at National Semiconductor.

REFERENCES

1. F. J. Grunthaner and J. Maserjian, IEEE Trans. on N.S., NS-24, 2108 (1977).
2. J. M. deLarios, C. R. Helms, D. B. Kao, and B. E. Deal, Appl. Surf. Sci. 30, 17 (1987).
3. C. R. Helms, J. deLarios in "The Physics and Chemistry of SiO_2 and the Si-SiO_2 Interface" C. R. Helms, B. E. Deal, eds. P. 25, Plenum, New York (1988) and references therein.
4. C. J. Han and C. R. Helms, J. Electrochem. Soc. 134, 1297 (1987).
5. B. E. Deal, A. S. Grove, J. Appl. Phys. 36, 3770 (1965).
6. R. Ghez and Y. J. Van der Meulen, J. Electrochem. Soc.119, 1100 (1972).
7. S. M. Hu, J. Appl. Phys. 55, 4094 (1984).
8. P. J. Jorgensen, J. Chem. Phys. 37, 874 (1962).
9. E. A. Irene, J. Appl. Phys. 54, 5, 416 (1983).
10. R. H. Doremus, Thin Solid Films, 122, 191 (1984).
11. A. Fargeix, G. Ghibaudo, G. Kamarinos, J. Appl. Phys. 54, 2878 (1983).
12. R. H. Doremus, Thin Solid Films, 122, 191 (1984).
13. A. Reisman, E. H. Nicollian, C. K. Williams, C. J. Merz, J. Elect. Mats. 16, 45 (1987).
14. J. M. deLarios, D. B. Kao, C. R. Helms, B. E. Deal, Appl. Phys. Lett. 54, 715 (1989).
15. K. B. Kao, B. E. Deal, J. M. deLarios, C. R. Helms in "The Physics and Chemistry of SiO_2 and the Si-SiO_2 Interface" C. R. Helms, B. E. Deal, eds. P. 421, Plenum, New York (1988) and references therein.
16. J. M. deLarios, Ph.D. Dissertation, Stanford University, 1989.
17. T. Sakurai, H. D. Hagstrom, Phys. Rev. B14, 1593 (1976).
18. F. N. Schwettmann, K. L. Chiang, and W. A. Brown, Abst. No. 276, Extended Abstracts, Vol. 78-1, The Electrochemical Society Spring Meeting, Seattle, Washington, May 212-16, 1978.
19. G. Gould and E. A. Irene, J. Electrochem. Soc., 134, 1031 (1987).
20. J. Ruzyllo, J. Electrochem. Soc., 134, 1869 (1987).
21. J. Ruzyllo, in "The Physics and Chemistry of SiO_2 and the Si-SiO_2 Interface" C. R. Helms, B. E. Deal, eds. P.391, Plenum, New York (1988) and references therein.

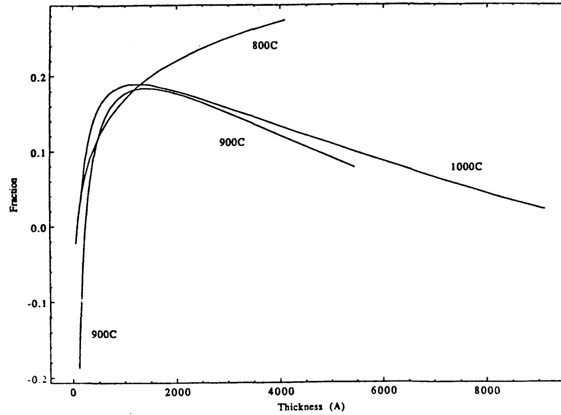

Figure 1: Fractional change in oxide thickness ($\Delta x/x$) vs thickness comparing an $HF:H_2O$ cleaned surface to an $NH_4OH:H_2O_2:H_2O$ cleaned surface from the data of references 2, 3, 14, 15, 16.

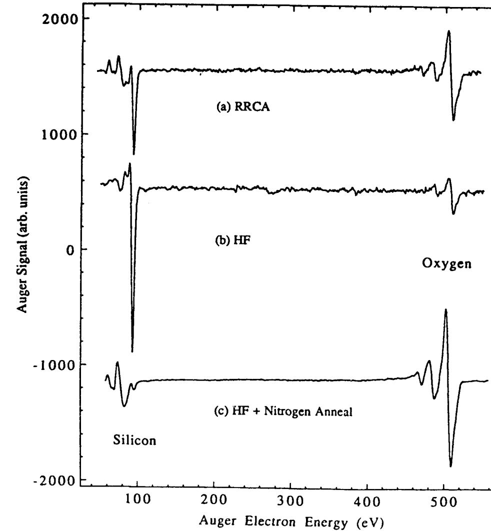

Figure 2: Auger spectra are shown for surfaces after a 1:2:5 $NH_4OH:H_2O_2:H_2O$ treatment followed by a water rinse (top spectra), an HF dip in 1:50 HF/H_2O (also followed by a water rinse - middle spectra), and a spectra obtained on either surface after a push-pull into and out of the furnace at 1000°C in N_2 (bottom spectra). The locations of the silicon and oxygen regions of the spectra are included.

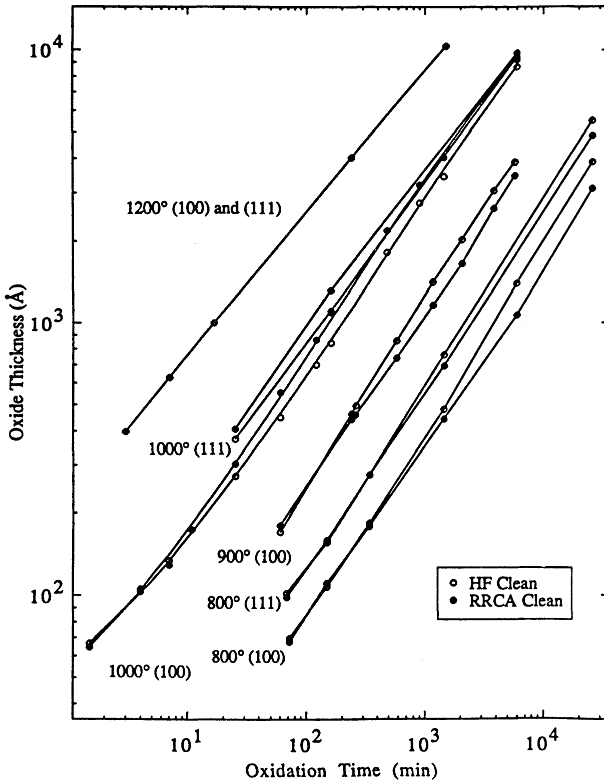

Figure 3: Oxide thickness vs oxidation time for dry oxidation of Si(100) and (111) at 800°C, 1000°C, and 1200°C and Si(100) at 900°C for wafers given RRCA and RRCA+HF cleans.

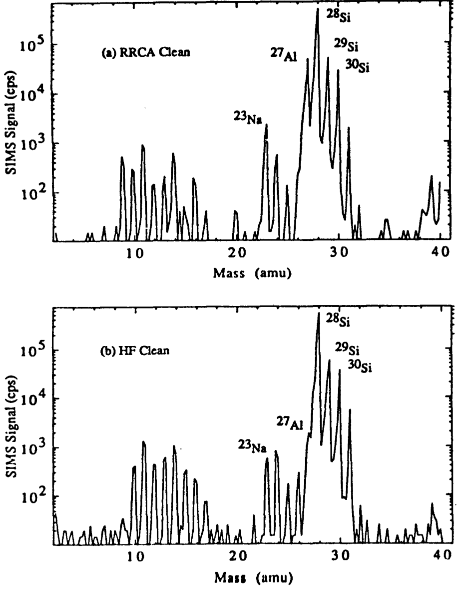

Figure 4: SIMS spectra of (a) RRCA and (b) HF cleaned surfaces showing the increased Al signal associated with the RRCA cleans.

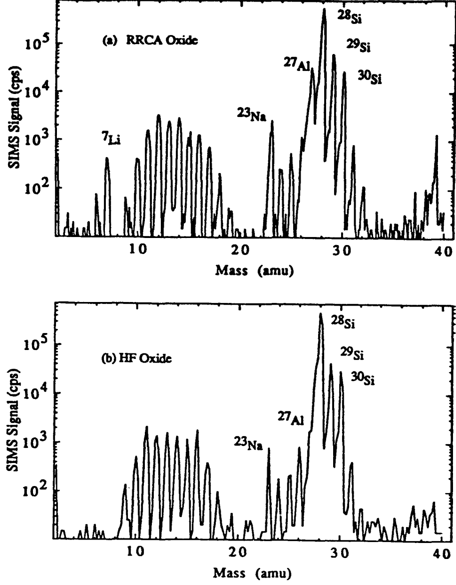

Figure 5: SIMS spectra of (a) RRCA and (b) HF cleaned surfaces that were subsequently oxidized showing the increased Al signal associated with the RRCA cleans.

Table 1. Oxidation parameters calculated from Gould and Irene's oxidation rate data [19].

	HF	$HCl:H_2O_2$	$NH_4OH:H_2O$
B ($Å^2$/min)	13800	15000	15100
B/A (Å/min)	7.51	5.16	4.94

Table 2. Si (100) dry oxidation parameters at 800°, 900°, 1000°, and 1200°C [15] for the linear-parabolic oxidation model [5].

Temperature (°C)	*B* ($Å^2$/min)		*B/A* (Å/min)		τ (min)	
	HF	RRCA	HF	RRCA	HF	RRCA
800°	1100	1120	0.31	0.17	271	1325
900°	4530	4740	1.7	1.0	90	230
1000°	16200	16900	11.1	5.3	13	43
1200°	74100	74100	235	235	0.9	0.9

Table 3. Si (100) dry oxidation parameters at 800°, 900°, 1000°, and 1200°C for the advanced parallel oxidation model [3,4].

Temperature (°C)	*B* ($Å^2$/min)		*B/A* (Å/min)		β (Å)	
	HF	RRCA	HF	RRCA	HF	RRCA
800°	1100	1110	0.31	0.15	170	400
900°	4600	4600	1.6	0.80	250	550
1000°	19100	19100	7.3	3.7	350	600
1200°	73900	73900	82	82	650	650

THE IMPACT OF Si-SURFACE CHARACTERISTICS ON MOS DEVICE YIELD

M. HEYNS, C. HASENACK, R. DE KEERSMAECKER and R. FALSTER*

Interuniversity Microelectronics Center (IMEC vzw)
Kapeldreef 75, B-3030 Leuven - Belgium

* *Monsanto Electronic Materials Company*
Featherstone Road, Wolverton Mill South
Milton Keynes, Buckinghamshire MK12 5TB - United Kingdom

ABSTRACT

Electrical characterization of thermally grown oxide layers on variously preconditioned Si-wafers is used to demonstrate the important effect of the Si-surface characteristics on MOS-device yield. The study includes the effect of various cleaning and pre-oxidation heat treatments and of a sacrificial oxidation step on the thermal oxide quality. Total Reflection X-Ray Fluorescence Analysis measurements, Scanning Tunneling and Scanning Optical Microscopy were used to investigate the origin of the observed effects.

1. INTRODUCTION

As the gate oxide thickness in Metal-Oxide-Semiconductor (MOS) transistors becomes thinner and its yield and reliability requirements more stringent, an increasing number of previously secondary parameters contribute to the final oxide quality. Among these, the topographical as well as the chemical characteristics of the Si-substrate surface and the Si-bulk properties have been shown to be important [1].

The chemical state of silicon wafer surfaces is often classified into two categories: hydrophobic and hydrophillic. Usually, as-received wafers exhibit a hydrophillic character as a consequence of a native oxide. However, it is the hydrophobic surface - in practice usually obtained with an HF-dip followed by a rinse in deionized (DI) water - which is technologically important. HF-dipped silicon surfaces contain mostly H (~80%) and some O, F and C (~20% together) [2-5]. It is claimed that it is mainly due to the large H-coverage that silicon exhibits its hydrophobic character after the HF-dip [1]. One of the drawbacks of the HF-dip is that surfaces treated in such a way contain usually more carbon than RCA-cleaned [6] wafers [3,5] which may result in a reduction of the dielectric strength of thermally grown oxides. Techniques to reduce the carbon contamination include performing an anhydrous HF-etch instead of an (aqueous) HF-dip [3], exposing the wafer to UV/ozone [4] or performing the HF-dip in a solution with ethanol [7]. Rinsing the wafer after the HF-dip (as usually done) was also found to slightly lower the carbon contamination [4]. With respect to the HF-dip, it was also suggested that, due to the fact that it leaves the silicon surface highly reactive, the silicon surface would become very susceptible to metallic contamination [10].

In this paper some results on the effect of chemical (metallic) contamination on the quality of oxides grown on different substrate types will be discussed. It will be shown that metallic contamination problems are less pronounced for final-HF-dipped wafers than for RCA-cleaned ones. Furthermore, it will be shown that the silicon surface topography has a strong effect on the oxide quality. In addition, it will be demonstrated that while for some types of substrates a certain pre-oxidation treatment ultimately results in good oxide quality, for other substrate types the same treatment may yield a drastic degradation of the oxide characteristics.

2. EXPERIMENTAL CONDITIONS

In this work 4 and 5 inch Si wafers with a <100> orientation were used. Both highly-doped wafers ($\sim10^{17}$ cm^{-3}) and lightly-doped wafers ($\sim10^{15}$ cm^{-3}) were investigated. For each of the doping levels, our experiments included float-zone (FZ), Czochralski (CZ) and EPI(taxial) wafers. In addition, the CZ substrates were divided into 3 groups according to their initial interstitial oxygen content: <27 ppma, 30±2 ppma and 35±2 ppma (below referred to as CZ-A, CZ-B and CZ-C, respectively). The interstitial oxygen content is given according to the ASTM-F121-76 calibration, as determined by Fourier Transform Infrared Spectrometry. The interstitial oxygen content of the substrates used for the p+ EPI wafers was 30 ppma.

With respect to cleaning treatments, 3 RCA-based cleans were studied: i) the original RCA-clean; ii) the FULL clean, consisting of the original RCA-clean preceded by the PIRANHA clean (H_2SO_4:H_2O_2,4:1 followed by HF); iii) the RCA(or FULL)+HF-clean consisting of the original RCA(or FULL)-clean followed by a 30 s dip in a 2% HF solution which in addition was usually followed by a rinse-step in DI water. Drying of the wafers was carried out in a spin-dryer equipment. In case the rinsing was not performed after the HF-dip, the spin-dryer was operated without the addition of water.

Some of the wafers were submitted to a pre-oxidation heat treatment (POHT) aiming at the formation of an oxygen-depleted zone at the surface and at oxygen precipitation in the bulk of the wafers. The POHT consisted of a three-step anneal carried out in Ar as follows: i) 10 hours at 1025°C; ii) 4 hours at 750°C and iii) 6 hours at 1000°C. A double-walled quartz-tube furnace with Ar flowing in the annular cavity was used in order to minimize the contamination in the furnace ambient [11]. The oxidation was carried out in the same furnace tube after adding the wafers which were not to receive a POHT. For the experiments involving a sacrificial oxidation step, a wet oxide layer of 100 nm thickness was first grown at 975°C on FULL-cleaned wafers. Eventually, the sacrificial oxidation step was carried out in dry O_2 ambient with 1,1,1,-trichloroethane added (TCA; 1% HCl equivalent). After this step, the wafers were taken out of the furnace and the sacrificial oxide was removed with buffered HF. During this etch-step (including the following rinse-step) FULL-cleaned control wafers were added to the sacrificially oxidized wafers. All samples were then oxidized together.

Oxidation was normally carried out at 900°C in dry O_2 to a nominal thickness of 20 nm. Immediately after oxidation the samples received an in-situ anneal in Ar at 900°C for 20 min. Loading and warm-up was always performed in either 100% flowing Ar or 95% Ar plus 5% O_2. Cooling-down and unloading was always carried out in 100% Ar. Immediately after the oxidation, Al or P-doped poly-Si gate capacitors with various areas were prepared using standard wet lithography. Poly-Si doping was performed using

solid-source doping and drive-in at 900°C. After backside contacting with a magnetron-sputtered Al layer the samples received a sintering in forming gas at 420°C for 20 min.

The MOS capacitors were submitted to voltage-ramp irreversible breakdown measurements and constant-current stressing measurements. Cleaning efficiency was assessed by means of Total Reflection X-Ray Fluorescence Analysis (TRXFA) employing the XSA 8000 X-Ray surface analyzer from PHI Atomika, which has the capability of quantifying heavy metal contamination down to a level of 10^{11} at/cm^2 [12]. Scanning Tunneling Microscopy (STM) of the samples was performed in a NANOSCOPE (I or II) microscope. Measurements were carried out in air on samples which had either been HF-dipped to remove any native oxide or on samples which had been covered with a Au-layer deposited on top of a chemically-grown oxide. Scanning Optical Microscopy (SOM) measurements were carried out using a Confocal Scanning Optical Microscope SOM 100 from LaserSharp.

3. CLEANING AND PREOXIDATION HEAT TREATMENTS : CHEMICAL EFFECTS

Si-surface contamination

Cleaned wafers often have low levels of surface transition metals contamination (such as Zn and Cu) with concentrations in the range of a few times 10^{11}/cm^2 when the cleaning is not performed properly. In order to evaluate the influence of these contaminants during oxidation, such contaminated CZ and FZ wafers were submitted to a dry gate oxidation together with non-contaminated EPI-wafers. The CZ and FZ wafers were contaminated with Cu and Zn with a concentration of 3×10^{11}/cm^2 and 9×10^{11}/cm^2, respectively. Some of the wafers first received a POHT. Special care was taken to avoid cross-contamination between the CZ and FZ-wafers and the non-contaminated EPI-wafers. In this experiment wafer-loading was carried out in a 95% Ar - 5% O_2 mixture so as to grow a thin oxide during furnace-loading and ramp-up. Immediately after the POHT it was detected that the FZ material exhibited a hazy appearance, the haziness being more pronounced close to the wafer's edge. A closer inspection of this wafer by means of optical microscopy revealed a large amount of defects. SEM micrographs showed these defects to be protrusions into the silicon lying, however, underneath the loading-induced oxide. The defects look similar to what has been observed for SiO void growth [13-15] and on many defective places, the oxide overlayer had been perforated. Because of the existence of these defects, the POHT FZ wafer was not further processed.

The results of the breakdown measurements carried out on this batch of POHT and non-POHT wafers are shown in fig.1. It can be seen from this figure that the effect of the presence of metallic contaminations during oxidation is relatively small when no POHT has been given. This is obvious when the results of the CZ and FZ-wafer are compared with that of the non-contaminated EPI-wafer. This result indicates that a critical metallic contamination level (related to the critical size and density of the metal precipitates) is probably necessary before a severe oxide breakdown degradation can be detected. However, upon POHT a drastic increase in defect-related breakdowns occurs for the contaminated CZ wafer as around 60% of the capacitors did not survive stressing to an electric field of 5 MV/cm. The POHT has almost no effect on the breakdown characteristics of the non-contaminated EPI-wafers.

Cleaning efficiency

Figure 2 shows a typical evolution of the metal surface contamination levels found monitoring ab initio contaminated wafers after several cleaning steps using TRXFA. The ammonium-peroxide step of the RCA-clean (1st RCA step) removes a large part of the Zn contamination but adds Fe to the wafer surface. This Fe is efficiently removed by the following HCl-step. The latter step, however, adds a large Br contamination which, in turn, is largely removed by a short HF-dip. The Br concentration is also strongly suppressed (to levels which are undetectable with TRXFA) when the samples are furnace-loaded to 900°C. This Br was found to be highly volatile and, therefore, easily evaporates upon heating. At room temperature, however, it was observed that large densities can persist on the surface after several months. An important finding illustrated in fig. 2, which is also in agreement with recent literature [16], is that the HF-dip is effective in removing metallic contamination still present on the wafer's surface after the HCl step and that no metal plating occurs during the HF-dip.

Effect of an HF-dip before POHT

The beneficial cleaning effect of the HF-dip, as discussed in the foregoing paragraph, was further evidenced by means of oxide breakdown measurements on POHT wafers. Upon POHT a secondary breakdown peak was found to appear in the breakdown histograms around 5 MV/cm for the RCA-cleaned wafers. This peak was not present for the RCA+HF-cleaned wafers (for the same capacitor areas tested). This behavior was observed independently of the substrate type but was present for only about 50% of the wafers which had undergone the FULL clean (instead of the RCA-clean). This suggests that this phenomenon can be related to contamination in the native oxide present before the cleaning which degrades the oxide quality after POHT. However, TRXFA measurements carried out on these virgin wafers did not reveal the existence of any metallic contamination. It is thought that either the contamination level is sufficient to cause electrical effects (although below TRXFA detection limit) or other contaminants not detectable by TRXFA (such as organic contaminants) are the cause of the observed degradation. The latter hypothesis is supported by the fact that the wafers used for this test had been stored in their original boxes for at least 2 years before processing. FULL-cleaned wafers which were not stored for such a long time did not display the secondary breakdown distribution for the same gate areas tested. Therefore, organic contamination from the storage box could be the origin of the secondary breakdown peak. However, additional experiments are needed to confirm the storage effect.

From these experiments we can conclude that (at least in our facility) wafers which receive a final HF-dip are less prone to metallic contamination than non-HF-dipped ones. In addition, these experiments show that a POHT in combination with oxide breakdown measurements constitutes an extremely sensitive tool for the detection of low contamination levels. It has, of course, the drawback of giving information neither about the chemical nature nor about the source of the contaminants.

Effect of an HF-dip: particles and chemical effects

Performing an HF-dip followed by a rinsing-drying step was found to seriously degrade the oxide quality of non-POHT wafers. This is illustrated in fig. 3 (see "FULL+HF+rinse" curve). The detrimental effect of the HF-dip was not observed when no rinsing was performed. At first we attempted to correlate these observations with the particle density on the Si-surface as, in agreement with literature, it was observed that the

particle density on a wafer strongly increases by an aqueous HF-dip followed by a rinsing-drying step [8,9]. (Typically FULL+HF+rinsed wafers exhibit at least one order of magnitude higher particle densities than FULL- or RCA-cleaned wafers.) However, no consistent difference in particle density between rinsed and non-rinsed wafers could be found, while a large difference in the breakdown characteristics exists (see fig.3). Therefore, the mere particle <u>density</u> after cleaning can not explain these observations. Possibly not all particles necessarily cause detrimental effects upon inclusion in the oxide and their effect may be partially compensated by the surface condition which is likely to be affected by the final aqueous treatment (with or without rinsing). Furthermore, it was experimentally established that particles may be lifted off from the surface of the wafer upon furnace heating. Thus, the particle density at the onset of oxidation may be completely different from the particle density directly after cleaning. This could explain why the detrimental effect of an HF-dip is not observed after a POHT where, due to the long treatment at high temperature, a large portion of the particles may be removed. The particle sticking probability depends on both the nature of the particle (chemical constituents, size, shape) and on the chemical condition of the Si-surface (e.g. the F and C concentration on the Si-surface). Both parameters again are affected by the nature of the final aqueous treatment preceding oxidation. Thus, according to our present understanding, the Si-surface condition is a key factor in determining the effect which a given quantity of adhering particles will cause.

4. SUBSTRATE EFFECTS

Although, as was illustrated, contamination plays an important role in the determination of the oxide quality, there exists a more fundamental effect related to the Si-substrate and, more specifically, to the Si-surface. If one is not aware of this, poor breakdown characteristics may erroneously be attributed to cleaning or processing deficiencies alone.

Si-surface characteristics

That Si-surface effects alone, of whatever origin, play an important role in oxide breakdown characteristics is illustrated in a striking manner by fig.4. In the upper part of the figure the Weibull plots calculated from the breakdown data corresponding to CZ-A and CZ-C substrates are shown to have quite distinctly different characteristics with the CZ-C substrates having higher defect densities. For this lot of wafers this was consistently observed during several runs, independent of the pre-oxidation cleaning and only slightly affected by POHT. Initially, we erroneously attributed this effect to a (bulk) oxygen content effect [17]. However, further experiments indicated that after polishing off 2 µm from not -yet- oxidized wafers of the same lot, the effect was no longer present (lower part of fig. 4) and a 'normalization' of the breakdown curves occurred.

This clearly indicates that the cause for the detrimental effect displayed in the upper part of fig.4 must be related to the Si-surface characteristics. Since the bulk oxygen precipitation induced by a POHT or during oxidation favors intrinsic gettering, the effect is a priori not due to contamination because the most efficient gettering is expected for the CZ-C substrate. Unless, of course, the surface of the 'bad' CZ-C substrates contain additional factory-induced damage so that metals could also getter (and precipitate) there. It is clear, however, that after the polishing the Si-surface has a 'fingerprint' which persists through the cleaning and pre-oxidation heat treatments and drastically affects the oxide breakdown characteristics. Additional evidence that Si-surface characteristics, and

not bulk characteristics, are dominant was provided by another wafer lot where the CZ-A material consistently exhibited worse breakdown characteristics than any of the other substrates, irrespective of the cleaning procedures used. The lower intrinsic gettering capability of this material could not be held responsible for the observed degradation in this case as the oxides grown on the FZ-substrates (which have only a low gettering capability) showed excellent breakdown properties.

Si-surface roughness

In order to find the origin of this 'fingerprint' the surface characteristics of poor CZ-wafers (in terms of breakdown characteristics) were compared with that of good wafers. STM measurements on Au-covered samples revealed the surface of the 'bad' CZ-C substrate lot to be clearly rougher than that of the good substrates, as shown by the typical results of fig. 5. SOM measurements also revealed the surface of the 'bad' CZ-C wafer lot to be approximately twice (peak to peak) rougher than that of a 'good' CZ-C wafer lot. (No absolute roughness values could be assigned with this technique.) This demonstrates that Si-surface roughness has to be considered in explaining breakdown characteristics, as was already claimed in ref. 1.

Additional experiments in which gate structures were prepared on the backside of soft-damaged wafers (which is an extremely rough surface) also yielded degraded breakdown characteristics. The effect was, however, not as pronounced as for the bad CZ-C substrate and could be strongly suppressed when large quantities of Cl where used during the oxidation. This already suggests that, although a correlation between surface roughness and breakdown characteristics exists, these roughness effects can not explain all the observed effects and the contribution of metal contamination can not be completely discarded. This is further evidenced by the fact that the EPI material had a very rough surface (peak to peak roughness ~2x that of a good CZ wafer as determined by STM and SOM measurements) while the breakdown characteristics of oxides prepared on these substrates showed excellent properties. This may be related to the high gettering capability of these substrates due to the presence of a backside poly-Si layer together with the intrinsic gettering of the CZ-substrate upon which the epi-layer is grown. It is, however, also possible that the surface roughness is only an indirect indication of the presence of a specific Si-surface defect on polished wafers which acts as a precipitation center for metals (thereby causing the low-field breakdowns). Following this line of thought, it can then be conceived that, although the Si-surface of EPI-wafers is rather rough, this defect is not present due to the fabrication procedure for these wafers. In general, these experiments suggest that both a rough Si-surface (or large Si-surface defect density) and a low-level metallic contamination, must be simultaneously present to degrade the breakdown characteristics.

Sacrificial oxidation

A simple way to change the Si-surface characteristics is by performing a sacrificial oxidation. Figure 6 shows the effect of a sacrificial oxidation step before the dry gate oxidation for the various substrates. While the characteristics of the oxides grown on the FZ substrates became strongly degraded, the characteristics of the 'bad' CZ-C substrate were improved. Since sacrificial oxidation consumes about 40 nm of the Si-wafer (and because we know from previous runs that the POHT in itself does not cure the bad CZ-wafers) this once more evidences that we are dealing with a Si-surface effect. The improvement with sacrificial oxidation, however, was not complete for the bad CZ-C wafer since constant-current stressing measurements revealed that the charge-to-

breakdown which could be injected did not reach the level of the other substrates. With respect to the FZ material, the degradation of the breakdown characteristics indicates that either enhanced contamination or surface roughening took place during the sacrificial oxidation. Repeating the sacrificial oxidation in dry oxygen environment with TCA (1% HCl equivalent) added, yielded similar results. Therefore, under the assumption that this amount of TCA is sufficient for the gettering of metal contamination [18], the observed degradation is likely to be associated with a surface roughening effect of the FZ wafers. Upon repeating the experiment with FZ wafers from a completely different lot, a less severe degradation of the breakdown characteristics was observed. This suggests the existence of a different fingerprint for various FZ-lots. The main conclusion here is that a sacrificial oxidation is not necessarily a beneficial treatment. Its effects, from breakdown point of view, strongly depends on the fingerprint of the starting substrate.

5. CONCLUSIONS

It was demonstrated that the Si starting material plays a major role in determining the breakdown characteristics of thermally grown oxides. The Si effect (which was termed the wafer 'fingerprint') persists through a complete cycle of cleaning and pre-oxidation heat treatments. The nature of this fingerprint and its exact effect on the thermally grown oxide layer remain somewhat unclear. Surface roughness (as determined by STM and SOM measurements) seems to be a very good candidate for explaining our results, although the roughness in itself is not sufficient to degrade the breakdown characteristics. It is believed that there is a complex interplay between the Si-surface roughness (both long range and on a local scale), the low-level contamination (metallic and organic), the pre-oxidation processing (heat treatments and sacrificial oxidation) and the electrical characteristics of thermally grown oxide layers. The importance of these results with respect to the yield of MOS-devices justifies a further study of the interrelation between the oxide properties and the Si-surface characteristics on one hand and the effect of various processing steps on the other hand.

6. ACKNOWLEDGEMENTS

The authors would like to thank Lieve Stockman (Physics department, K.U. Leuven) for assistance with the STM-measurements, Dr. Allan Pidduck (RSRE) for the SOM analysis and E. Dooms (IMEC) for helping with the figures. The MONSANTO-company is gratefully acknowledged for supporting the investigations.

7. REFERENCES

1) P.O. Hahn, M.Grundner, A. Schnegg and H. Jacob in "The Physics and Chemistry of SiO_2 and the Si-SiO_2 Interface", Eds. C.R. Helms and B.E. Deal (proceedings of the 173rd Meeting of The Electrochemical Society, Atlanta, Georgia, May 15-20, 1988), p.401
2) B.R. Weinberger, G.G. Peterson, T.C. Eschrich and H.A. Krasinski, J.Appl.Phys. 60, 3232 (1986)
3) G.T. Duranko, D.J. Syverson, L.A. Zazzera, J. Ruzyllo, and D.C. Frystak, FSI Technical Report TR329 (1988)
4) L.A. Zazzera and J.F. Moulder, J.Electrochem.Soc. 136, 484 (1989)

5) M. Grundner and H. Jacob, Appl.Phys. A39, 73 (1986)
6) W. Kern and D.A. Puotinen, RCA Rev. 31, 187 (1970)
7) J.L. Prom, J. Castagne, G. Sarrabayrouse and A. Munoz-Yague, IEE Proc. 135, 20, (1988)
8) D.J. Syverson and G.T. Duranko, Solid State Technology, October, 101 (1988)
9) C.A. Peterson, FSI Technical Report TR325 (1988)
10) K.D. Beyer and T.H. Yeh, IBM Techn. Discl. Bull. 20, 1741 (1977)
11) M.W. Hillen, R.F. De Keersmaecker, M.M. Heyns, S.K. Haywood and I.S. Daraktchiev in "Insulating Films On Semiconductors", Eds. J.F. Verweij and D.R. Wolters (North-Holland, Amsterdam), p.85 (1983)
12) P. Eichinger, H.J. Rath and H. Schwenke: "Application of Total Reflection X-Ray Fluorescence Analysis for Metallic trace Impurities on Silicon Wafer Surfaces" in "Semiconductor Fabrication: Technology and Metrology, ASTM STP990", Ed. D.C. Gupta, American Soc. for Testing and Materials (1988)
13) K. Hofmann, G.W. Rubloff, M. Liehr and D.R. Young, Appl.Surf. Sci. 30, 25 (1987)
14) M. Liehr, G.B. Bronner and J.E. Lewis, Appl.Phys.Lett. 52, 1892 (1988)
15) M. Liehr, H. Dallaporta and J.E. Lewis, Appl.Phys.Lett. 53, 589 (1988)
16) R. Wiget, H. Ryssel and W. Aderhold, in proceedings of "SEMICON/EUROPA 89" March 7-9, 1989, Zurich, Switzerland
17) C. Hasenack, M. Heyns, R. Falster and R. DeKeersmaecker in "The Physics and Chemistry of SiO_2 and the Si-SiO_2 Interface", Eds. C.R. Helms and B.E. Deal (proceedings of the 173rd Meeting of The Electrochemical Society, Atlanta, Georgia, May 15-20, 1988), p.437
18) G.J. Declerck in "Solid State Devices 1979", Ed. H. Weiss (The Institute of Physics, Bristol and London, 1980), p.133

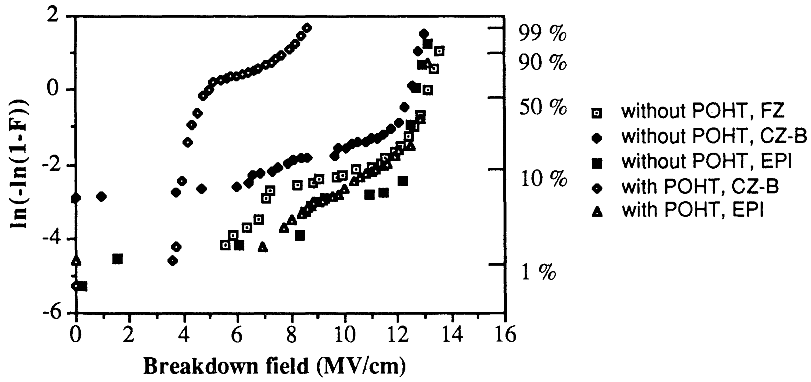

FIGURE 1: *Weibull plots corresponding to Cu and Zn contaminated FZ and CZ-B wafers and a "clean" EPI wafer with or without the POHT before gate oxidation. The Cu and Zn contamination level was approximately $3x10^{11}/cm^2$ and $9x10^{11}/cm^2$, respectively. Gate area=$3.14x10^{-4}$ cm^2. Gate material: P-doped poly-Si. The Weibull plot for the POHT FZ wafer is missing because a high defect density was observed on the wafer after POHT.*

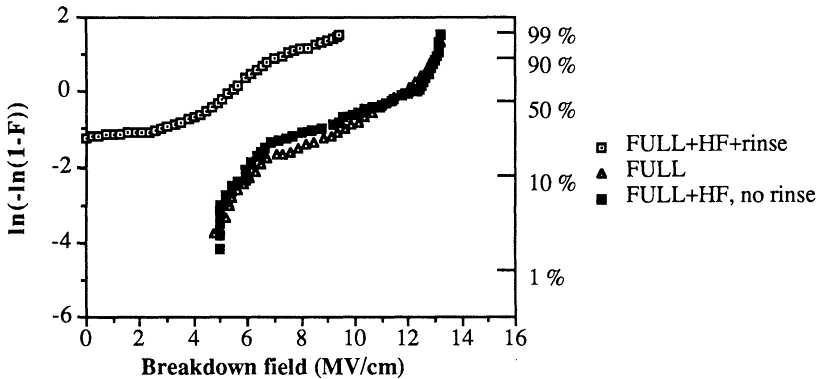

FIGURE 3: *Weibull plots showing the effect of the rinse step after the final HF-dip on the oxide breakdown characteristics. Gate area = $1.2x10^{-2}$ cm^2. Gate material: P-doped poly-Si. CZ-B substrate.*

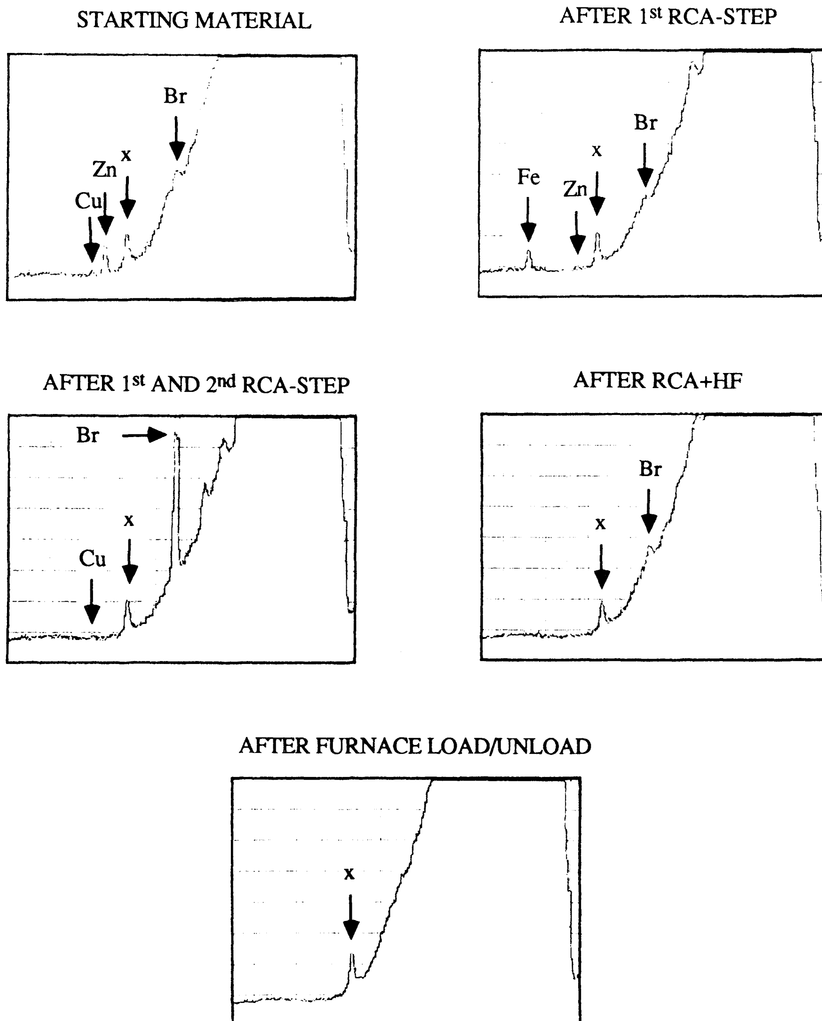

FIGURE. 2: *TRXFA spectra showing the evolution of surface contamination levels during the cleaning steps of a standard RCA-clean. The Br-concentration after the 1st and 2nd RCA-step is typically a few times $10^{12}/cm^2$. The level of all other indicated contaminations is in the $10^{11}/cm^2$ range. The peak labeled "x" is system-related.*

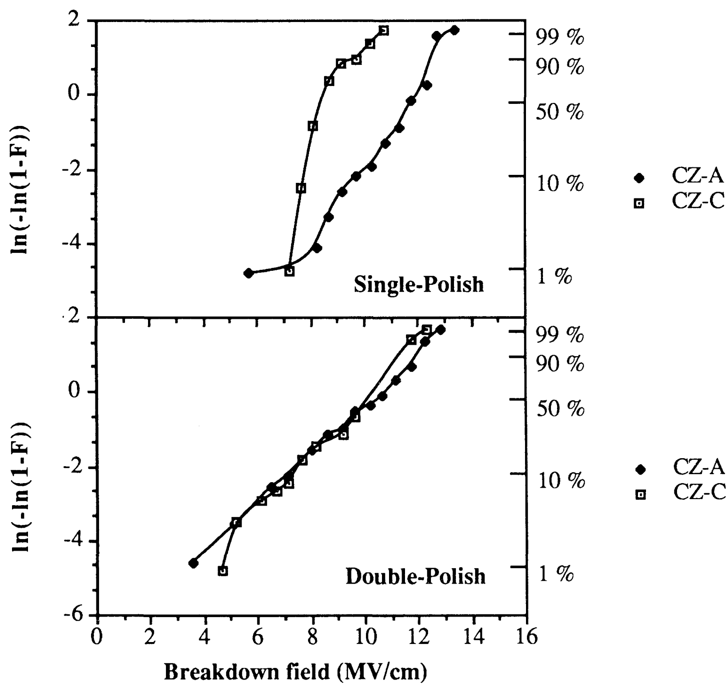

FIGURE 4: *Effect of the Si-surface characteristics on the breakdown histograms of thermally grown oxide layers. Upper part: single-polished wafers. Lower part: double polished wafers (from same wafer lot as the single-polished ones). Gate area =* $1.26x10^{-3}$ cm^2*. Gate material: Al.*

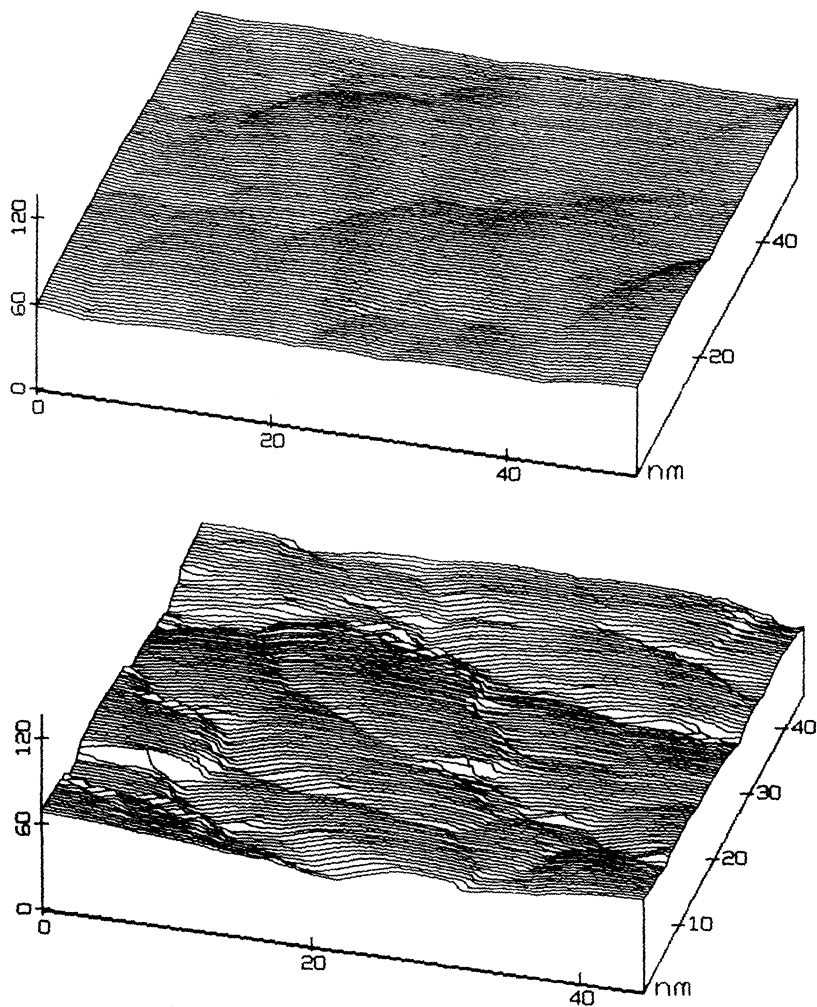

FIGURE 5: *STM pictures of the surface of Au evaporated Si. Upper plot: typical exemple of a 'good' Si-material (picture shown for FZ material). Lower plot: 'bad' CZ-C material.*

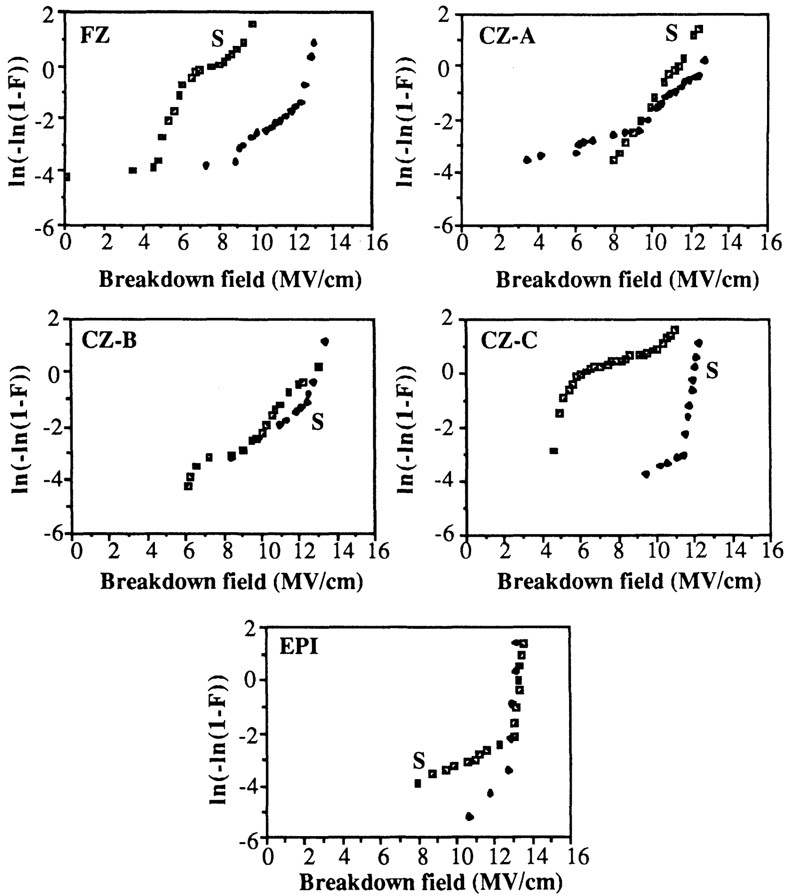

FIGURE 6: *Weibull plots corresponding to 5 different 4" substrates with (curves labelled 'S') or without (no label) a sacrificial wet oxidation to 100 nm before gate oxidation. Gate area = 3.14x10^{-4} cm^{2}. Gate material: P-doped poly-Si.*

THE INFLUENCE OF CLEANING ON THE OXIDATION MECHANISM OF SILICON

J.J. van Oekel and P.M. Snee
Philips Research Laboratories, P.O. Box 80.000
5600 JA Eindhoven, The Netherlands

The correlation between pre-oxidation cleaning procedures and various aspects of thermal oxidation of silicon is studied. It is shown that the RCA-1 clean affects the top layer of the oxide.

INTRODUCTION

In this paper the relationship between cleaning and a wet or dry oxidation of silicon is investigated. The type of wafer cleaning is known to have a significant influence in case of a dry oxidation (1,2). Especially, after an RCA-1 clean (see Table 1) the oxidation rate, compared to the other cleans, is relatively low. An investigation has been carried out into whether the bulk, top or bottom of the oxide is altered by the RCA-1 clean.

In the experiment the RCA-1 clean is compared with the RCA clean. Supposing that the RCA-1 clean changes the top layer of the oxide grown after the clean, then removal of this top layer by an etchback will result in an oxidation rate equal for both types of cleaned wafers. However, when the bulk of the oxide is affected by the RCA-1 clean then the oxidation rate will still be lower.

Experiments were done on wafers preoxidized at 900°C during 77 minutes since this yields 250 Å oxide independent of the precleaning.

EXPERIMENTAL

In order to investigate the influence of different cleaning steps on dry and wet oxidation the following experiments were done. Two batches of 25 wafers each (Wacker, 4", (100), 17-23 Ohm-cm) were submitted to several cleans. See Table 1 for the cleaning conditions. The wafers were randomized and subsequently oxidized (wet oxidation 1000°C, 120 min., 88% H_2O in O_2; dry oxidation 1000°C, 190 min., 7.5 SLM O_2). The oxide thickness was measured for all wafers with an ellipsometer (3x standard deviation $\leq$ 1%).

In the following experiment attention was paid to the influence of the RCA-1 clean on a dry oxidation. The

set-up for the experiment is shown in Figure 3. A batch of 25 wafers (Wacker, 4", (100), 17-23 Ohmcm) is split in two: half is given the RCA clean, half the RCA-1 clean. The wafers are randomized and preoxidized in one run to 250 Å (dry oxidation, 900°C, 77 min., 7.5 SLM O_2).

Most wafers were etched back in 1% HF during 15, 90 or 300 s. The oxide thickness was measured for all wafers with an ellipsometer. The wafers were randomized and oxidized a second time in one run (dry oxidation, 1000°C, 190 min., 7.5 SLM O_2). Thickness and refractive index were measured with an ellipsometer.

RESULTS AND DISCUSSION

The results for wet oxidation are shown in Figure 1 and for dry oxidation in Figure 2. The influence of cleaning on wet oxidation is negligible. For dry oxidation however, the RCA-1 clean results in a significantly lower oxide thickness.

In the following we will focus on the RCA-1 clean and a dry oxidation. The results are shown in Figure 4.

No influence of cleaning on the oxidation rate could be shown for oxides grown at 900° C during 77 min. For both the RCA and RCA-1 cleaned wafers, the thickness is 249 ± 2 Å. The oxides are however different: a second oxidation results in different oxide thicknesses. This difference could not be nullified by an RCA clean after the first oxidation. The RCA-1 cleaned wafers have a thinner oxide (1170 ± 16 Å) compared to the RCA cleaned wafers (1220 ± 12 Å). The refractive index is equal for both types of cleaned wafers (1.463 ± 0.001). The densities of both oxides must be equal since the density is related to the refractive index via the Lorentz-Lornez relationship (1).

The RCA cleaned wafers, etched back after the first oxidation, yield a thinner oxide after the second oxidation.

RCA-1 cleaned wafers etched back 20 Å yield a thicker oxide after the second oxidation. A further etchback naturally yields thinner oxides. The results are in accordance with data published recently by Delarios et. al. (3). The difference in oxidation rate between the two type cleaned wafers has practically vanished if both type wafers are etched back 20 Å. From this observation we can

conclude that the top layer of the oxide causes the lower oxidation rate in the case of the RCA-1 cleaned wafers.

The lower oxidation rate can be explained by:

1. Negative charge introduced on the wafer surface due to the caustic clean:
   $Si\text{-}OH + OH^- \rightarrow Si\text{-}O^- + H_2O$
   The negative oxide charge may retard the diffusion of negatively charged oxygen species through the oxide. This is in accordance with the space charge limited oxidation model (4).
2. The presence of Al on the wafer surface. With high-resolution-time-of-flight-static SIMS it could be shown that Al is reproducibly deposited on the wafer surface by an RCA-1 clean. The relative intensity of the Al^+ peak compared to the Si^+ peak is 0.16 after the RCA-1 clean and 0.03 in case of no cleaning. The deposition may be due to trapping on SiO^-.

More research is required to elucidate the cause of the lower oxidation rate.

CONCLUSIONS

Cleaning has no influence on the oxide thickness after a wet oxidation. In case of dry oxidation it is shown that, compared to other cleans, an RCA-1 clean results in a lower oxidation rate of silicon. It has now been proven that the RCA-1 clean affects the top layer of the oxide. The retardation in oxidation rate vanishes by removal of at least 20 Å of the oxide.

ACKNOWLEDGMENTS

The authors wish to thank Dr. D.R. Wolters for the fruitful discussions and Dr. H. van der Wel for the static SIMS analysis.

References

1. G. Gould and E.A. Irene, J. Electrochem. Soc., 134(4), 1031 (1987)
2. F.N. Schwetmann, K.L. Chiang, and W.A. Brown, El. Chem. Soc. Ext. Abstr., 78-1, 688 (1978)
3. J.M. Delarios, D.B. Kao, C.R. Helms, and B.E. Deal, Appl. Phys. Lett., 54(8), 715 (1989)
4. D.R. Wolters and A.T.A. Zegers-Van Duijnhoven, J. Appl. Phys., 65, 5134 (1989)

Table 1. Cleaning conditions applied in the experiments

RCA clean	: $NH_3/H_2O_2/H_2O$= 1/1/5 (T= 70 °C, t= 180 s) rinse, $HCl/H_2O_2/H_2O$= 1/1/5 (T= 70 °C, t= 180 s) rinse, dry
RCA-1 clean	: $NH_3/H_2O_2/H_2O$= 1/1/5 (T= 70 °C, t= 180 s) rinse, dry
fuming HNO_3	: fuming HNO_3 (15 min), rinse, dry
HF	: 1% HF (1 min), rinse, dry

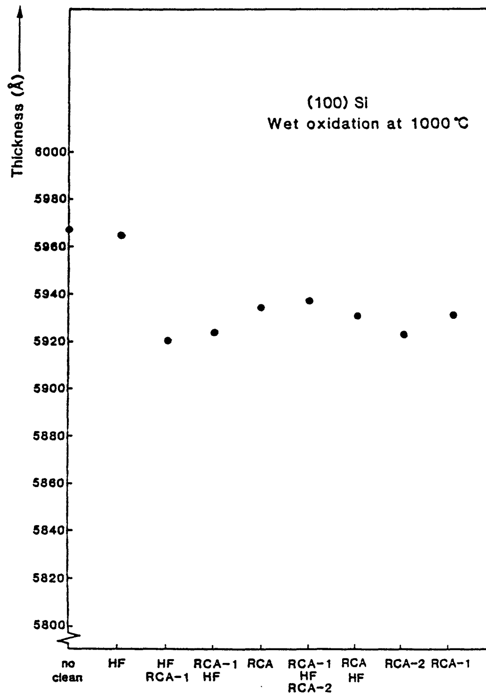

Figure 1. The influence of different cleaning steps on the oxide thickness after a wet oxidation (1000 °C, 120 min). See Table 1 for the process conditions.

Table 1. Cleaning conditions applied in the experiments

RCA clean	: $NH_3/H_2O_2/H_2O$= 1/1/5 (T= 70 °C, t= 180 s) rinse,
	$HCl/H_2O_2/H_2O$= 1/1/5 (T= 70 °C, t= 180 s) rinse, dry
RCA-1 clean	: $NH_3/H_2O_2/H_2O$= 1/1/5 (T= 70 °C, t= 180 s) rinse, dry
fuming HNO_3	: fuming HNO_3 (15 min), rinse, dry
HF	: 1% HF (1 min), rinse, dry

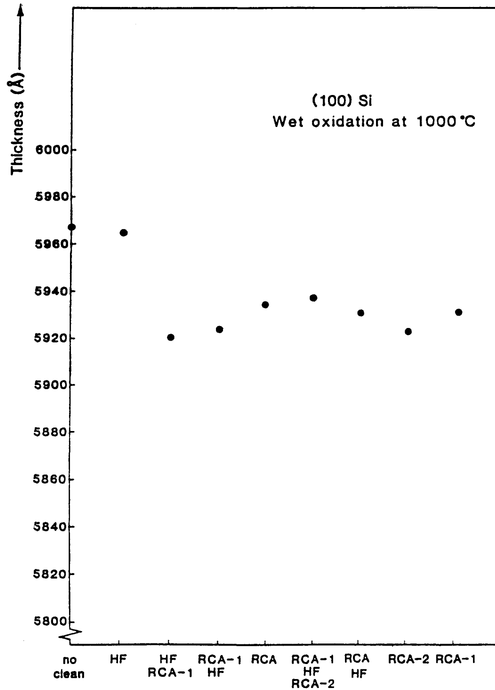

Figure 1. The influence of different cleaning steps on the oxide thickness after a wet oxidation (1000 °C, 120 min). See Table 1 for the process conditions.

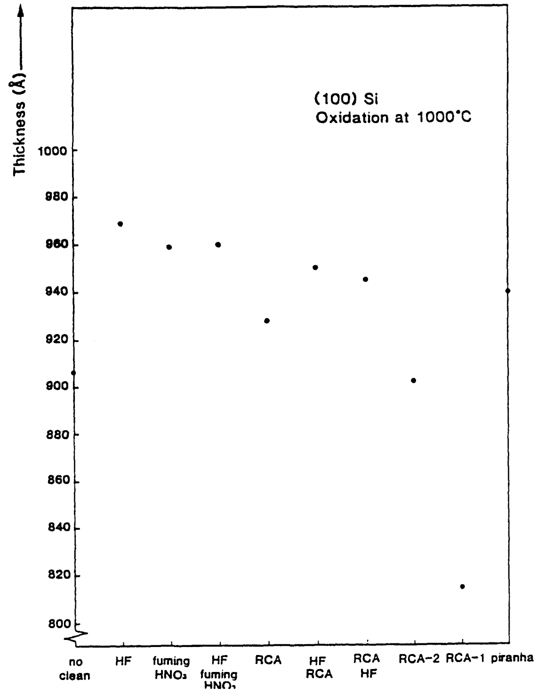

Figure 2. The influence of different cleaning steps on the oxide thickness after a dry oxidation (1000 °C, 190 min). See Table 1 for the process conditions.

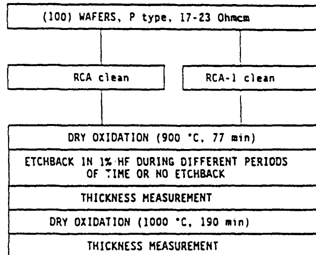

Figure 3. Experimental set-up.

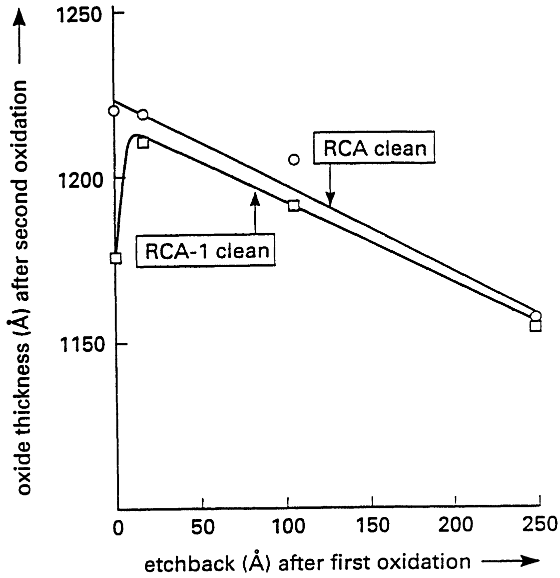

Figure 4. Influence of etchback of oxide grown after an RCA or RCA-1 clean on the oxide thickness after a second oxidation. After an RCA or RCA-1 clean and oxidation to 250 Å the wafers were etched back and oxidized again.
In case of no etchback a difference in oxidation rate shows up after the second oxidation. In case 20 Å or more is etched off no significant difference in oxide thickness is observed after the second oxidation.

INFLUENCE OF THE PREOXIDATION CLEANING PROCEDURE ON OXIDE GROWTH RATE AND THE CHARACTERISTICS OF SUBOXIDE STATES

Zhi-Min Ling, Luc H. Dupas,
Joachim Portillo, Wilfried Vandervorst and Kristin M. De Meyer *
IMEC, Kapeldreef 75, B-3030 Leuven, Heverlee, Belgium

Abstract

The purpose of this work is to study the influence of the preoxidation cleaning procedure on the oxide growth rate in dry, wet and in chlorine ambients, as well as the influence of preoxidation cleaning procedures on the characteristics of suboxide states of thermally dry grown oxides. Also, ESCA measurements of Si $2p$ peaks as a function of the preoxidation cleaning procedure is performed. Finally, the influence of the preoxidation cleaning procedure on the oxide growth rate is correlated to the various of suboxide state characteristics measured from these samples.

1 Introduction

The chemical cleaning procedure is an important component of many of the process steps used in device fabrication. It is intended to reduce the contamination and improve the yield and reliability. Recently, in the area of silicon oxidation, more attention has been given to chemical cleaning and its effects on the silicon surface, oxide kinetics, and gate oxide electrical properties. It is well established that the dry oxide growth rate depends on the preoxidation cleaning procedures. Several mechanisms for the influence of preoxidation treatments on the oxidation kinetics are proposed. For instance, some include various refractive indices of thermally grown oxides under different preoxidation cleaning treatment [1]. Others include different levels of residual aluminium contamination on the silicon surface resulting from different preoxidation cleaning procedures [2].

In this work, the influence of the preoxidation cleaning procedure on the silicon oxide growth rate is observed in dry oxygen and wet oxygen ambient, as well as in chlorine containing ambients. To gain more insight in the mechanism of the influence of preoxidation treatments on the silicon oxidation kinetics, the surface analysis tool ESCA is used to investigate the surface and near surface of the SiO_2/Si system grown in oxygen ambients with different preoxidation cleaning procedures. Furthermore, it is found that the influence of the preoxidation cleaning procedure on the oxide growth rate can be related to the variety of suboxide states characteristics as measured by ESCA.

*Professor at the Katholieke Universiteit, Leuven. Research Associate of the Belgian National Found for Scientific Research

2 Sample Preparation and SE Measurement.

As the first part of this work, the influence of the preoxidation cleaning procedure on the oxide growth rate in different oxidation ambients is studied.

Preoxidation Cleaning Procedure. The p-type (100) silicon wafers used in this work are initially cleaned with a sequence of $H_2SO_4 : H_2O_2 : H_2O$, DI rinse, HF dip, DI rinse and spin dry. These initially cleaned wafers are then split into two groups. One group of wafers, further on called HF-wafers, were cleaned with a sequence of $NH_4OH : H_2O_2 : H_2O$, DI rinse, $HCl : H_2O_2 : H_2O$, DI rinse, HF dip and DI rinse. Another group of wafers, further on called ammonia-wafers, were cleaned with a sequence of $NH_4OH : H_2O_2 : H_2O$ and DI rinse. Both HF- and ammonia-wafers were directly loaded together into the thermal oxidation furnace after wafer cleaning and being spin dry with N_2 gas. The oxidations are performed at T=950°C for different oxidation times in dry oxygen, wet oxygen and in a chlorine (TCA/O_2=0.3%) ambient, respectively. The oxide thickness and refractive index of these samples are measured by Spectroscopic Ellipsometry (SE).

Growth in Dry Oxygen. The oxide thickness versus oxidation time curves are plotted in *fig* 1 (marked as squares), and the experimental data set is listed in *table* 1. In dry oxidation, for oxides thicker than 200Å, it is observed that for each given oxidation time, the oxide on the HF-wafers is always thicker than the one on the ammonia-wafers, and this becomes more pronounced in the thicker oxide region. This result is similar to the work of [1][2]. Also, as plotted in *fig* 2 the refractive indices (n_f) of thermally grown oxides on HF-wafers (dashed lines) are always smaller than those on ammonia-wafers (solid lines), but the difference in n_f is more pronounced in the thin oxide region.

t (min)	30	180	330
X(HF-wafers)(Å)	198	636	989.7
X(ammonia-wafers)(Å)	197	590	889
ΔX (Å)	1.	46	100.
ΔX/X (%)	0.5	7.5	10.6

Table 1: The oxidation data of the HF-wafers and the ammonia-wafers in dry oxygen

Growth in a chlorine ambient. The oxide thickness versus oxidation time curves of these samples are plotted in *fig* 1 (marked as triangles) and the measured data are listed in *table* 2. It is observed that, in the thin oxide region, the thermally grown oxides of the HF-wafers are thinner than those of the ammonia-wafers. Conversely, for oxides thicker than 500Å, the thermally grown oxides of the HF-wafers are thicker by about 10 to 40 Å compared to those of the ammonia-wafers. The refractive indices of these two groups of samples are almost the same. It seems that the preoxidation cleaning procedure still affects the oxide growth rate in a chlorine ambient, but this effect is less important than in the dry oxidation case.

t (min)	15.	60.	120.	180	240	330
X(HF)(Å)	253.	493.	728.	899.	1078.	1349.
X(ammonia-wafer) (Å)	258.	494.	697.	886.	1057.	1301.
ΔX (Å)	-5.	-1.	31.	13.	23.	48.
ΔX/X (%)	2.	1.3	4.2	1.4	2.	2.3

Table 2: The oxidation data of the HF-wafers and the ammonia-wafers in a chlorine ambient

Growth in a wet oxygen ambient. As plotted in *fig* 1 (marked as stars), the thermally grown oxides of HF-wafers are always about 10Å thinner than those of ammonia-wafers. The experimental data set is listed in *table* 3. The difference of refractive indices between these two groups of samples are negligible. It seems that the oxide growth rate in this oxide thickness range is almost independent of the preoxidation cleaning procedure.

t (min)	5	15	25	45	90
X(HF-wafers)(Å)	382.	792.	1125.	1683.	2747.
X(Ammonia-wafers) (Å)	391	803	1136	1687	2756
ΔX (Å)	-9.	-11	-10.7	-4.0	-9.0
ΔX/X (%)	2.3	1.3	0.9	0.2	0.3

Table 3: The oxidation data of the HF-wafers and ammonia-wafers in wet oxygen

3 The Characteristics of Suboxide States as Measured by ESCA.

As a second part of this work, ESCA measurement of Si $2p$ peaks as a function of the preoxidation cleaning procedure are performed.

Contamination on the Preoxidation Cleaned Silicon Wafer. After wafer cleaning and before the oxidation, both HF- and ammonia-wafers are measured by ESCA to examine the possible contamination of the wafer surface. In the spectrum carbon $1s$ and oxygen $1s$ peaks are observed in addition to silicon $2s$ and $2p$ peaks. However, no chemical species such as fluorine and chlorine, nor metal species such as aluminium are observed in these two kinds of cleaned wafers. This means that the atomic percentage of these species could be under the resolution limit ($\sim$1%) of ESCA. In ammonia-wafers, a shifting of the Si $2p$ peak from Si to SiO_2 is clearly observed. Whereas, in HF-wafers, this Si $2p$ shifting is much smaller, and can only be observed when the take-off angle of photoelectron flux is set at 10°.

Estimation of Ultra Thin Oxide Thickness by Means of ESCA. After wafer cleaning, 'HF-wafers' H1, H2 and H3, and 'ammonia-wafers' A1, A2, A3 are oxidised together at T=900°C in a dry oxygen ambient for 2 min (H1 and A1), 4 min (H2 and A2) and 9 min (H3 and A3), respectively. The oxide thickness of these samples are calculated [3] by the ratio of ESCA spectral intensity of Si $2p$ from elemental silicon I_{si} and oxidised silicon I_{ox}, and listed in *table* 4.

	H1	H2	H3	A1	A2	A3
I_{ox}/I_{si}	3.578	4.70	7.55	4.2	4.81	7.19
X(Å)	31.4	34.9	41.3	33.5	35.3	40.6

Table 4: The oxide thickness estimated by the ESCA spectral intensity of Si $2p$ peaks.

Angular Dependence of the Suboxide States. These samples are studied further in detail by ESCA using different take-off angles θ of the photoelectron flux, namely, 15°, 35°, 55° and 90°. As examples, the high resolution plots of Si $2p$ spectra of sample H1 at θ=15° and θ=90° are shown in *fig* 3a to 3d. It is observed in this angular study of ESCA measurements that, in the thermally grown oxide of HF-wafers, the atomic percentage of suboxide states, especially for Si^{+3} state is higher than those of ammonia-wafer. In the thermal oxide of the HF-wafer, only the Si^{+3} state shows a significant angular dependence, whereas the suboxide $Si^{+1,+2}$ state shows a weak angular dependence. In the thermal oxide of the ammonia-wafer, both Si^{+3} and $Si^{+1,2}$ states show a weak angular dependence.

It is supposed that the SiO_2/Si system consists of an oxide layer on the top, a suboxide layer near the interface and the silicon substrate on the bottom. Si^{+3} has a wide profile towards the surface and $Si^{+1,+2}$ is located almost near the SiO_2/Si interface. It is derived that the ESCA Si $2p$ peak intensity I_{si12} for $Si^{+1,2}$ state and I_{si3} for the Si^{+3} state normalised by the silicon substrate intensity I_{si} can be written as below.

$$\frac{I_{si12}}{I_{si}} \approx \frac{N_{si12}}{\rho_{si}\lambda_{si}} \frac{exp(P_{si12}/sin\theta) - 1}{P_{si12}} \quad (1)$$

$$\frac{I_{si3}}{I_{si}} \approx \frac{N_{si3}}{\rho_{si}\lambda_{si}} [exp(P_{si12}/sin\theta)] \frac{exp(P_{si3}/sin\theta) - 1}{P_{si3}} \quad (2)$$

where, ρ_{si} is the atomic density of Si atoms in the silicon substrate, N_{si12} and N_{si3} are the mean surface densities of the $Si^{+1,2}$ and Si^{+3} states. $P_{si12} = d_{si12}/\lambda_{si12}$ and $P_{si12} = d_{si12}/\lambda_{si12}$, where λ_{si}, λ_{si12} and λ_{si3} is the Si $2p$ electron mean free path in silicon substrate, $Si^{+1,2}$ and Si^{+3} suboxide state profile layer, d_{si12} and d_{si3} is the profile length of $Si^{si+1,2}$ and Si^{+3} state, θ is the incident angle of photoelectron flux to the sample surface. The characteristic values of suboxide states are extracted by the above equations from the

	H1	H2	H3	A1	A2	A3
$N_{si12} \times 10^{14}$	4.17	3.67	4.18	2.89	2.79	0.50
P_{si12}	0.20	0.20	0.20	0.01	0.01	0.05
$N_{si+3} \times 10^{14}$	8.65	1.00	1.03	0.97	1.23	1.18
P_{si3}	0.40	0.60	0.70	0.59	0.10	0.11

Table 5: The characteristic value of suboxide states.

experimental data of angular dependence of Si $2p$ peaks intensity and listed in *table* 5. Curve fitting results are plotted in *fig* 4a and 4b, as well.

It is concluded from this ESCA angular study that in the thermally grown oxide of the HF-wafers, the total amount of suboxide states, especially for Si^{+3} state, is higher than those of ammonia-wafer. In the thermally grown oxides of HF-wafers, the suboxide Si^{+3} state profile is likely to extend wider towards the oxide surface, whereas, the suboxide $Si^{+1,+2}$ states are located near the SiO_2/Si interface. In the thermally grown oxide of ammonia-wafers, the suboxide states, especially the $Si^{+1,2}$ states are likely to be located in a narrow region close to the SiO_2/Si interface.

4 The Correlation of the Suboxide States and the Oxide Growth Rate.

As a third part of this work, the characteristics of suboxide states are correlated to the influence of the preoxidation cleaning procedure on the oxide growth rate, though on this subject already several different mechanisms have been proposed (e.g. [4]). Since the suboxide states are the intermediate states of elemental silicon and oxidised silicon, the suboxide states are related to the available oxidation reaction sites. Therefore, the oxidation reaction process takes place not only at a 'sharp' SiO_2/Si interface, but also within a certain suboxide states profile region. Thus the oxidation reaction constant should be modified as $k = k_i + K(\int_{X_0}^{X_0-d} N_{si12,si3}(y)dy)$, where k_i is the reaction constant of Deal-Grove model, X_0 is the oxide thickness with the original point at the SiO_2/Si interface, K is a constant. The values of mean surface density N times d/λ for each samples is plotted in *fig* 5. Obviously, in dry oxidation, the oxide growth rate of HF-wafer is higher due to the higher density and larger profile length of suboxide states.

In wet oxidation and oxidation in a chlorine ambient, OH and Cl present in the gas phase are the main active species. They diffuse into the oxide layer towards the SiO_2/Si interface, react with silicon and/or oxide network to form a lot of intermediate states such as Si-Cl and Si-OH [5]. Since the total amount of intermediate states is mainly contributed by OH and Cl species in the ambient, the significance of intermediate (suboxide) states due to the difference in the preoxidation cleaning procedure is decreased. Therefore, the influence of precleaning procedures on the oxide growth rate is decreased or even eliminated.

5 Conclusions

It is observed in this work that the preoxidation cleaning procedure significantly influences the oxide growth rate and refractive indices of the thermal dry oxide. However, a reduced influence on the growth rate and refractive indices of the oxide grown in wet oxygen and in a chlorine ambient has been observed. The dependence of the characteristics of suboxide states of thermally dry grown oxide on the preoxidation cleaning procedure has been investigated. However, it is necessary to carry out more extensive studies of the various suboxide states and refractive indices for the thin oxide region grown in different ambients and cleaned in different preoxidation cleaning procedure by means of ESCA and SE.

Acknowledgements

The authors wish to thank J.Vanhellemont for his assistance in the spectroscopic ellipsometry measurements. J. Portillo appreciates the financial support of the Spanish Ministry of Science and Education.

References

1. G.Gould and E.A.Irene, J.Electrochem.Soc., **134**, 1031(1987).
2. J.M.deLarios, D.B.Kao, C.R.Helms and B.E.Deal, Appl. Phys. Lett. **54**, 715(1989).
3. G.J.Grunthaner and P.J.Grunthaner, Material Science Reports 1, 65-160 (1986), North-Holland, Amsterdam.
4. Z.M.Ling, L.H.Dupas and K.M.DeMeyer, Electrochem.Soc., Spring meeting, Atlanta, Ext.Abstr. No.146 (1988).

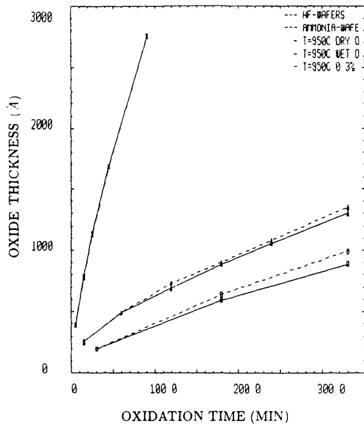

fig.1 The oxide thickness versus oxidation time. The HF-wafer (dashed lines) and ammonia-wafer (solid lines) were oxidised together at T=950° in dry oxygen (square marks), wet oxygen (star marks) and chlorine ambient (triangle marks).

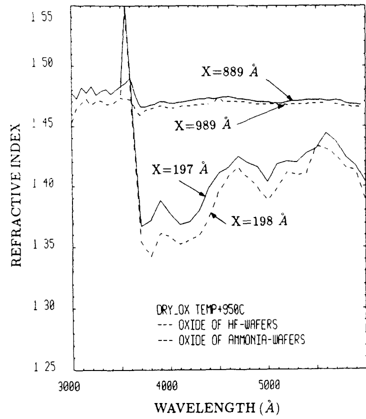

fig.2 The refractive indices of thermally grown oxides at T=950°C of HF-wafers (dashed lines) and ammonia-wafers (solid lines).

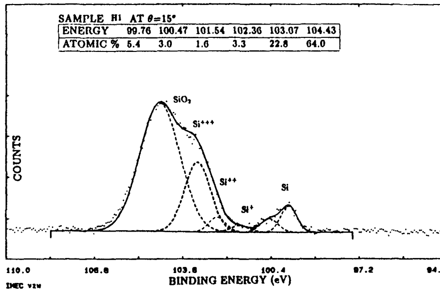

SAMPLE H1 AT θ=15°

ENERGY	99.76	100.47	101.54	102.36	103.07	104.43
ATOMIC %	5.4	3.0	1.6	3.3	22.8	64.0

fig.3a High resolution Si $2p$ spectrum of sample H1. The take-off angle of the photoelectrons is θ=15°.

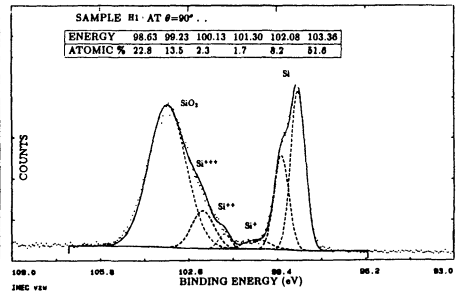

SAMPLE H1 · AT θ=90° . .

ENERGY	98.63	99.23	100.13	101.30	102.08	103.36
ATOMIC %	22.8	13.5	2.3	1.7	8.2	51.6

fig.3b High resolution Si $2p$ spectrum of sample H1. The take-off angle of the photoelectrons is θ=90°.

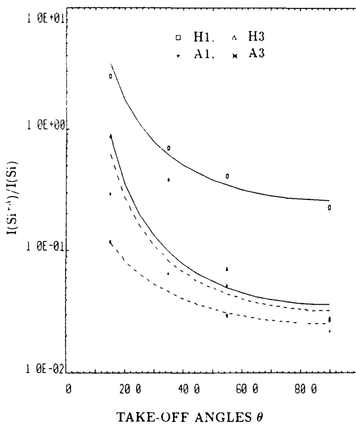

fig.4a **The atomic ratio of Si^{+3} states and substrate silicon versus different take-off angles. The solid and dashed lines are the curve fitting of equation (1) and (2) with the parameters listed in *table* 5.**

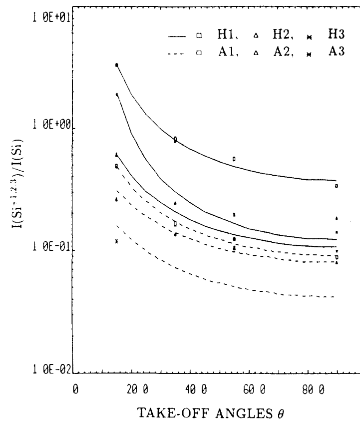

fig.4b The atomic ratio of $Si^{+1,2,3}$ states and substrate silicon versus different take-off angles. The solid and dashed lines are the curve fitting of equation (1) and (2) with the parameters listed in *table* 5.

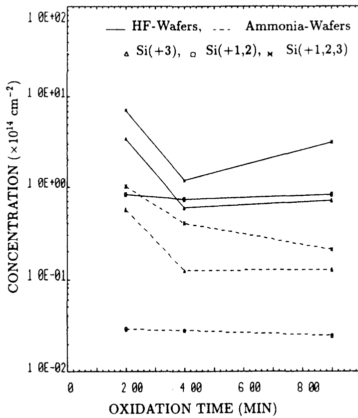

fig.5 **The concentration levels of suboxide states for each sample.**

OXIDATION OF SILICON IN AIR AND NITROGEN AFTER VARIOUS HF ETCHES.

P.A.M. van der Heide, H.W.L. Lindelauf and H.J. Ronde

Philips Research Laboratories,
P.O.Box 80.000,
5600 JA Eindhoven,
The Netherlands

Abstract.

The oxidation of Si(100) as a function of the time (6 minutes-100 hours) in air or nitrogen after various HF-etches was measured using X-ray photoelectron spectroscopy. It is shown that in air after etching in liquid HF in water solutions or after wet HF gas etching about the same oxidation rate and final thickness (0.6 nm) are obtained. After a liquid HF etch followed by a water rinse initially more oxygen is present on the surface and finally a larger thickness (1.1 nm) is obtained.
After wet HF gas etching , storage in dry nitrogen results in very little oxidation (0.2 nm).

1. Introduction.

The etching of SiO_2 layers on silicon using a diluted HF in water solution to remove e.g. native oxide layers is a widely applied step in silicon processing technology. The quality of the resulting surface influences device properties e.g. the breakdown voltages of thin gate oxides. Also for silicon molecular beam epitaxy there is a demand for cleaning methods which can be used at low temperatures (e.g. room temperature).

The HF etch results in a surface with a very low surface recombination velocity, even better than the SiO_2/Si interface (1). In a recent paper (2) we have made a comparison of the liquid HF-etching process and the wet HF-gas etching process (3). The gas etch has the advantages that it introduces less impurities than liquid immersion and also can be used in those applications e.g. 1-2 um contact holes where reproducible etching using liquids is very difficult. It was shown , using X-ray Photoelectron Spectroscopy (XPS) that wet HF gas etching produces clean surfaces with about 0.5 monolayer (ML) of oxygen coverage. The etch did not influence the amount of carbon on the surface. Also the results were more reproducible than the results obtained using e.g. 1% HF in H_2O solutions. The liquid HF etching has also been studied recently by several authors. Grundner and Schulz (4) analysed the etching of p-type silicon in aqueous HF using XPS and high resolution electron energy loss spectroscopy (HREELS). They concluded that the Si(100) surface after etching consists mostly of Si-dihydrides and some hydrocarbons, fluorine and oxygen. The fluorine on the surface increased from 3.10^{13} cm^{-2} to 1.10^{14} cm^{-2}

on going from 0.1% aqueous HF to 40% aqueous HF. Upon rinsing in water the fluorine was replaced by OH-groups.
Graf et al (5) investigated the oxidation of silicon in water after a 40% aqueous HF etch using XPS and HREELS. They conclude that during the water immersion first the fluorine is exchanged by H_2O to form Si-OH, followed by a slower reaction of OH- on Si-H to form Si-OH. The growth is logarithmic up to 3-5 hours of water exposure. Grunthaner et al (6) and Fenner et al. (7) studied the etching of a spinning wafer using a HF-alcohol reagent in a flowing nitrogen atmosphere. In their experiment they conclude that after etching, the amount of oxygen and carbon can be attributed to organic contaminants, which can be removed by heating to 150°C in UHV. This results in contamination levels for all contaminants below 0.1 ML.

After etching usually handling in air is necessary, which results in oxidation. The present paper describes the dependence of the oxidation rate on variations in the HF-etch and the storage atmosphere.
First some experimental details and analysis methods are discussed. Then the results for oxidation after etching in liquid or gaseous HF conditions with or without rinsing are discussed.

Experimental.

The experiments were performed on slices of 2x2 mm^2 n-type silicon with thin oxide layers (1.5-3.0 nm) grown in HNO_3. After being etched they were introduced into the loadlock of a Vacuum Generators Escalab Mk II equipped with facilities for small area XPS (300 um resolution) and Auger. The XPS spectra were obtained using unmonochromatized Mg $K\alpha$ radiation. Electrons emitted perpendicular to the sample surface were analysed (acceptance angle 12°). The resolution was determined by the line width of the $MgK\alpha$ radiation (0.8 eV). As a measure of cleanliness the O1s, F1s, C1s and the Si-SiO_2 2p peaks in the XPS spectra were used.

In the case of (sub) monolayer coverage, 1 ML equals $6.8.10^{14}$ atoms/cm^2 for Si(100), the O1s peak was used for oxide quantification. For thicker oxide layers the SiO_2 2p and the Si2p peaks can be used for quantification using the methods discussed in (2). The sensitivity factors for the materials involved were taken from the Wagner library (8). The value of λ was determined using the Seah and Dench approach (9). No dependence of the width or shape of the O1s peak on layer thickness (10) was observed in our experiments. Therefore the value of (Peakheight/Background), (P/B), can be used for quantification of the O1s peak (λ=1.3 nm) .This leads to the conclusion that an oxygen coverage ((Peakheight)/Background) of 2.0 corresponds with 1-1.2 ML of oxygen. For the determination of the carbon (fluorine) amount on the surface the C1s (F1s) peak was used. The quantitative analysis was based on the formulas for thin overlayers e.g. Briggs (11). In practice no variation of carbon or fluorine peak shapes were observed, indicating that similar to the O1s peak the quantity (P/B) can be used for quantification.

In the case of HF liquid etching the samples were immersed for 2 minutes

in e.g. a 1% HF in demiwater solution held at a fixed temperature of 21.5°C. If the samples were rinsed this was done in a flow of demiwater to remove ionic impurities. This was stopped when a water resistivity of 10 MΩcm was attained.

Subsequently, experiments were performed using wet HF gas etching in the set up described in (2). A flow of nitrogen as a carrier gas was led over a bath with a 10% HF in water solution and directed through a nozzle towards the sample to be etched. This is shown schematically in figure 1. In both type of experiments water was sometimes replaced by methanol. The etching times were the optimum times deduced from the experiments described elsewhere (2). After the etching the samples were left to air, in a glass container (humidity 45%, temperature 23°C) or exposed to a flow of dry N_2 (0-0.1 l/min) from a bottle with nitrogen with 3 ppm H_2O and 3 ppm O_2. The effective water contamination was not measured, but probably above 10 ppm.

Results and discussion.

The experimental results of three different HF etches will be discussed:
-etching in 1% HF (in water) solutions
-etching in 1% HF (in water) solutions followed by a water rinse
-etching using wet HF gas etching (2).
For these three cases the oxidation in air after etching was studied, in the case of HF gas etching also the oxidation in nitrogen was studied.

First experiments were performed using a 1% HF (in water) solution. After the etching the samples were left to air (humidity 45%, temperature 23°C).
The results for the O1s signal (P/B) for samples with and without water rinse are shown in figure 2, curve a and b. Without rinsing an oxide thickness of 0.6 nm is formed after 100 hours , but after a water rinse a thicker oxide (1.1 nm) is formed. At the same time the water rinse removes the fluorine that is present on the sample surface after the HF-etch. After rinsing, the fluorine signal is reduced to about 20% of the original signal (0.1-0.2 ML). As has been shown by Grundner and Schulz (3) using HREELS the Si-F bonds are replaced by Si-OH bonds. The carbon amount slightly increased during the etching (0.3-0.6 ML) but remained stable during the oxidation in air.

Some experiments were performed with etching in HF/methanol mixtures or rinsing in methanol after the HF/H_2O etch, including a water rinse. This did not give much difference in comparison to the results mentioned for etching in HF in water solutions.

Subsequently experiments were performed using wet HF gas etching in the set up described in (2). The results for the oxidation in air are also given in figure 3, curve c. The carbon amount was not changed upon etching (2), and increased only slightly during the first hour in air to a stable value.

The gas etch experiment was also repeated using a 10% HF in methanol solution with some water. This resulted in a surface with less oxygen (0.2 ML), however the oxidation rate was not changed. The methanol pushes water away

of the silicon surface. Immersion in liquid methanol after a gas etch resulted in stronger oxidation , even stronger than curve a in figure 2.

Storage of the silicon in a glass box in a flow of dry nitrogen (0-0.1 l/min) after the gas etch resulted in a much slower oxidation, curve d in figure 3. Variation of the gas flow did not affect the oxide growth.

The oxidation data in figure 2 and 3 could be fitted by:

(1) $d(nm)= A(nm).\log t(hr) + B(nm)$,

where d is the layer thickness, t the time in air, A the regrowth rate and B a constant indicative for the original amount of oxygen present.
A quantitative analysis of the curves in figure 1 results in oxidation constants A and B: table 1.

Table 1.

curve:	a	b	c	d
A(nm/decade)	0.16	0.11	0.16	0.05
B(nm)	0.41	0.21	0.18	0.11

Thus it can be concluded that for storage for about 100 hours three different results can be obtained. For storage in air an oxide thickness of 1.1 nm is obtained after liquid HF etching with rinsing and of 0.65 nm after liquid HF etching without rinsing or HF gas etching. The differences are due to the different starting situations, the oxidation rate constants A are almost equal.
For storage in nitrogen after the gas etch a decrease in oxidation rate of a factor 3 is obtained, resulting in about 1 ML of oxygen on the surface.

The results for liquid HF etching in air can be compared with the results by other authors, they are similar to the results of Mende (12). The oxidation rate was slower than the regrowth rate observed by Lukes (13) and Archer (14). This can probably be attributed to the limited accuracy of ellipsometry ,as used by these authors. Our data are in good agreement with the work by Raider (15) using XPS.

The fact that the oxidation rates for curves a, b and c are almost equal, despite differences in F concentration, indicates that the limiting reaction is the interaction with Si-H. In all cases upon storage in air the fluorine concentration decreased slowly, but the amount of oxide increased faster, indicating also interaction with Si-hydrides. The carbon concentration increased slightly upon exposure but, in our environment did not increase after 1 hour exposure. The much slower oxidation rate in nitrogen is attributed to the absence of water, which is necessary to start oxidation.

Conclusions.

It is shown that upon storage in air oxidation of silicon occurs with about the same oxidation rates after liquid HF etching with and without rinsing and

after HF gas etching . The initial oxide amount after etching is the highest after the liquid HF etch with rinsing. For storage in nitrogen after the gas etch a decrease in oxidation rate of a factor 3 is obtained, resulting in about 1 ML of oxygen on the surface after 100 hours of storage. This is attributed mainly to the removal of H_2O.
Thus handling in nitrogen glove boxes is recommended in those cases where long waiting times after etching are necessary.

References.

(1) E. Yablonovitch, D.L. Allara, C.C. Chang, T. Gmitter and T.B. Bright, Phys.Rev.Lett. 57,249,1986.

(2) P.A.M. van der Heide, M.J. Baan Hofman and H.J. Ronde, J. Vac.Sci. Techn. A 7,1719, 1989.

(3) P.J. Holmes and J.E. Snell, Microelectron. Reliab. 5,337,1966.

(4) M. Grundner and R. Schulz, AIP conf. proc. 167,329,1988.

(5) D. Graf, M. Grundner and R. Schulz, J. Vac.Sci. Techn. A 7,808, 1989.

(6) P.J. Grunthaner, F.J. Grunthaner, R.W. Fathauer, T.F. Lin, F.D. Schowengerdt, B. Pate and J.H. Mazur, in J.C. Beann and L.J. Schowalter(Eds.) Silicon Molecular Beam epitaxy, vol. 88-8, The Electrochem. Soc.Inc. new Yersey, p. 375,1988.

(7) D.B. Fenner, D.K. Biegelsen and R.D. Bringans, J. Appl. Phys. 66, 419, 1989.

(8) C.D. Wagner, L.E. Davis, M.V. Zeller, J.A. Taylor, R.H. Raymond, L.H. Gale, Surface and Interface Analysis 3, 1981,211-225.

(9) M.P. Seah and W.A. Dench, Surface and Interface Analysis, 1,1979,1-11.

(10) F.J. Grunthaner and P.J. Grunthaner, Materials Science Reports 1,65,(1986).

(11) D. Briggs and M.P. Seah, ed.,Practical surface Analysis by Auger and X ray Photoelectron Spectroscopy, Wiley 1985.

(12) G. Mende, J. Finster, D. Flamm and D. Schulze, Surf.Sci. 128,169,1983.

(13) F. Lukes,Surf.Sci. 30,91,1972.

(14) R.J.Archer, J.Electrochem. Soc.104,619,1957.

(15) S.I. Raider, R. Flitsch and M.J. Palmer, J. Electrochem. Soc. 122,413,1975.

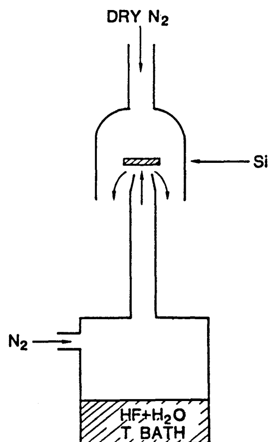

Figure 1: Set up of the HF gas etching system.

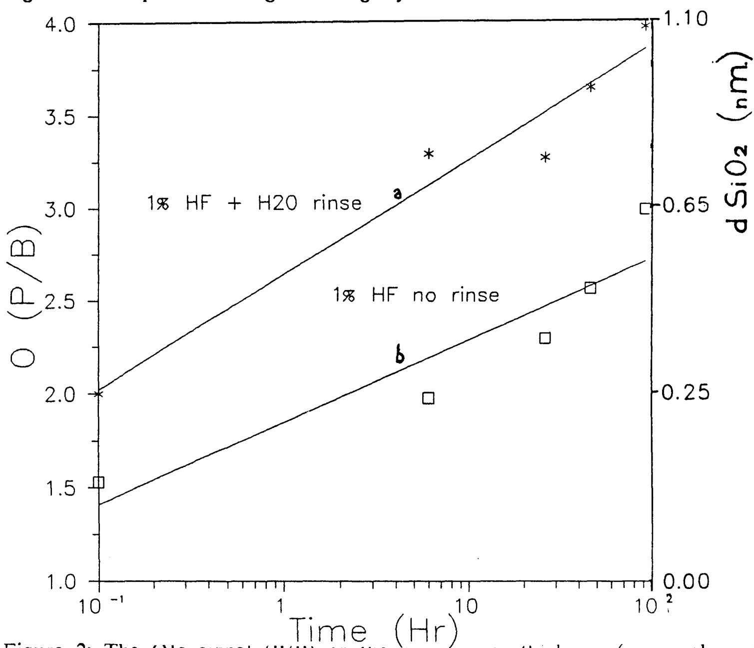

Figure 2: The O1s signal (P/B) or the oxide layer thickness (nm, scale not linear) as a function of exposure time (hours) for storage in air:
curve a: after 1% HF in water etch + water rinse,
curve b: after 1% HF in water etch and no water rinse,

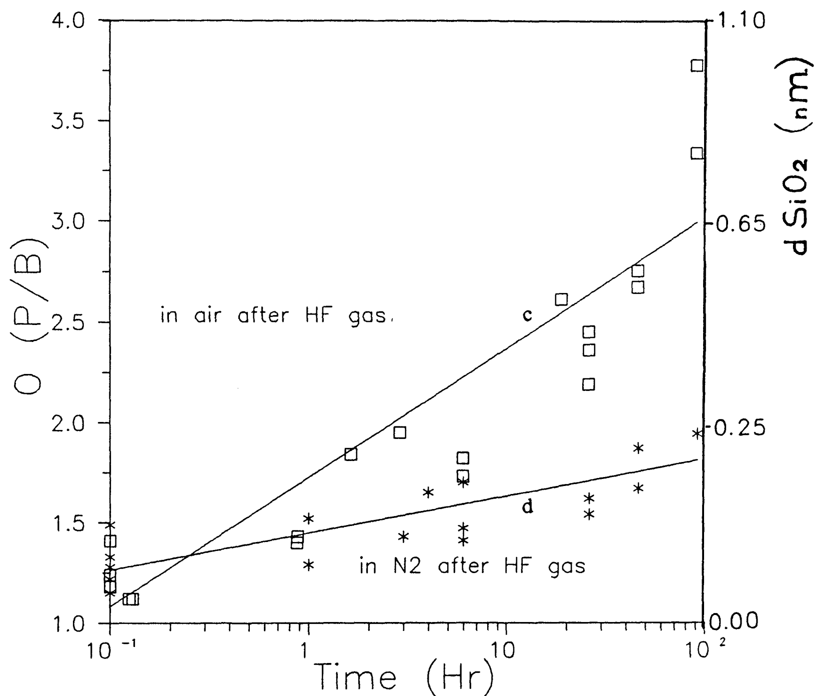

Figure 3 : The O1s signal (P/B) or the oxide layer thickness (nm, scale not linear) as a function of exposure time (hours) for the HF gas etch:
curve c: storage in air
curve d : storage in N_2.

AGING OF HYDROPHILIC SI SURFACES AND ROUGHNESS OF THE SI/SIO_2 INTERFACE AFTER THERMAL OXIDATION.

M. Grundner, P.O. Hahn, I. Lampert
Wacker-Chemitronic GmbH, Research and Development
Postfach 1140, D-8263 Burghausen, Germany

ABSTRACT

Aging of a hydrophilic silicon surface leads to enhanced roughness of the Si/SiO_2 interface after thermal oxidation. Removal of the OH groups before storage by derivatization avoids this effect. Furthermore, a simple H_2O dip before thermal oxidation restores the properties of the as prepared surface. Combined measurements of surface morphology by ARLS (Angle Resolved Lightscattering) and chemical surface composition by HREELS (High Resolution Electron Energy Loss Spectroscopy) lead to the conclusion that inhomogeneous condensation-hydrolization reactions of the hydrophilic surface during storage are responsible for the increase in roughness after thermal oxidation.

I. INTRODUCTION

Effects of pretreatments of the wafer surface on thermal oxidation have been numerously reported in the past. The general observation was a retarded oxide growth rate in the case of the SC1 clean (NH_4OH, H_2O_2, H_2O) (see e.g. 1-3), which has recently been attributed to an Al contamination of the hydrophilic oxide (4). Effects of pretreatments on the interface roughness Si/SiO_2 have been reported, too (5). In this paper it is shown that aging of the hydrophilic oxide influences the roughness of the Si/SiO_2 interface after thermal oxidation. Aging is shown to be correlated with chemical and structural properties of the hydrophilic oxide.

II. EXPERIMENTAL

The roughness of the surface was determined by measurement of the diffuse scattered light of a laser beam (6). Variation of the angle between incident and scattered radiation allows for the detection of different correlation

lengths of the roughness in the range of 0.4 um to 10 um. The chemical state of the surface was investigated by HREELS and additionally by XPS (X-Ray Photoelectron Spectroscopy). The wafers were one side polished, boron doped in the range 1 - 20 Ohmcm with (100) or (111) orientation. The hydrophilic treatment was performed by a modified SC1 clean (NH_4OH, H_2O_2, H_2O) followed by thermal oxidation in dry O_2 at 1000°C to a thickness of about 700 Å. Before the lightscattering measurements the thermal oxide was dissolved in 5% aqueous HF.

III. LIGHTSCATTERING RESULTS

After the hydrophilic treatment wafers were stored for 3, 17 and 27 days, respectively, in conventional wafer boxes in the laboratory. After thermal oxidation and removal of the oxide angle resolved light scattering measurements yielded the results shown in Fig. 1.

The steep increase of the scattered intensity at angles around 160° is due to the proximity of the specular ray. Up to three days of storage no change in lightscattering was observed. After 17 days a pronounced peak had developed with its maximum around a correlation length of 1.5 um. Further storage led to a shift of this peak to longer wavelengths. Storage thus causes roughness increase after thermal oxidation, the distribution of correlation lengths being governed by storage time.

An increase in roughness was not observed for a chemically modified surface. In this case the surface was rendered hydrophobic by a treatment with HMDS (hexamethyldisilazane). Fig. 2 shows the lightscattering at a fixed correlation length of 0.9 um as a function of storage time before oxidation. The additional HMDS treatment obviously protects the surface against changes which lead to increased roughness after oxidation. The scatter of the points in the case of the hydrophilic wafer is presumably due to statistical variations between different wafers.

Dipping an aged hydrophilic wafer in water before oxidation restored the properties of the virgin surface, as is shown by a line scan across a wafer in Fig. 3. One half of the aged wafer received a short (seconds) dip in D.I. water immediately before oxidation. The lightscattering intensity of this part after oxidation was on the level usually observed on freshly prepared wafers. The aged half exhibits a sharp rise in intensity for both light sources, an UV and a He-Ne laser, the UV laser exhibiting more surface sensitivity. The spike in the line scan represents a particle. Obviously the changes on the surface which lead

to roughness increase are reversibel and the active species must be either H_2O molecules or OH^-ions.

The effect of storage on the roughness of the interface after thermal oxidation raises the question whether there is a corresponding effect observable before oxidation. For this purpose an extremely careful prepared wafer was chosen with a small misorientation (0.03°) to yield broad and undisturbed terraces. The width of the latter was 0.6 um, which led to a bragg peak at the correlation length of 0.6 um in the angle resolved measurements and a very low lightscattering level otherwise (Fig. 4). Remeasurement after some days of storage in humid air revealed an increase in diffuse lightscattering. However, after dipping the wafer into D.I. water the original low level was reattained again. This demonstrates that roughness of the Si surface cannot be responsible for the enhanced lightscattering on storage. Rather more some reversible chemical and/or structural inhomogeneity of the oxide has to be responsible for this effect. It should be mentioned that HMDS treated wafers did not show any deterioration on storage, i.e. they retained the state of the as prepared surface.

IV. CHEMICAL AND STRUCTURAL SURFACE COMPOSITION

The hydrophilic surface of a Si wafer is characterized by a thin oxide in the thickness region of 6-10 Å, as described by several authors (e.g. 7, 8). The oxide bears OH groups, which give rise to the peak at 3730 cm^{-1} in the HREELS vibrational spectrum (dashed line) of Fig. 6. Additionally the strong asymmetric Si-O-Si vibration at 1150 cm^{-1} and a weak CH_x (x = 1, 2 or 3) vibration around 2960 cm^{-1}, which corresponds to a coverage of $2x10^{14}/cm^2$ (deduced from XPS measurements) can be detected. In humid air the OH groups are the preferred adsorption sites for water molecules.

Aging of the wafer with respect to OH groups depends on the initial state of the oxide. Fig. 5 shows the relative amount of OH, expressed by the vibrational intensity ratio OH/Si-O-Si, as a function of time. On a freshly prepared wafer the OH intensity diminishes by about 30% during the first hours of storage in air (40% rel. humidity). The further decrease is relatively slow. On the other hand a hydrophilic oxide, which was depleted from OH groups by a rapid thermal anneal under Ar gas and then stored in an atmosphere of 100% rel. humidity, showed an increasing OH coverage corresponding to the dashed curve in Fig. 5. The hydrophilic oxide is therefore no stable system. Besides a slight thickness increase changes in the average OH concentration occur with time.

As for the influence of a short (seconds) water contact we investigated an aged hydrophilic surface before and after a H_2O dip with XPS and HREELS. There was no increase in oxide thickness and the relative concentration of OH groups (OH/Si-O-Si) rose from 0.1 to 0.12. A comparison with Fig. 5 reveals that this value is still characteristic for an aged wafer. We therefore assume that a water dip prevalently homogenizes surface conditions and only to a lesser extent changes the average composition.

The effect of a HMDS (hexamethyldisilazane) treatment on a hydrophilic surface can be seen in Fig. 6. The number of OH groups is reduced by 70% - 80% as gets evident from the OH vibration at 3730 cm^{-1}. At 2960 cm^{-1} a strong CH_3 stretching vibration develops together with a $Si-(CH_3)_3$ rocking mode at 860 cm^{-1}. HMDS reacts with surface OH groups according to (9)

$$(CH_3)_3SiNHSi(CH_3)_3 + 2\ Si\text{-}OH \longrightarrow 2\ Si\text{-}O\text{-}Si\text{-}(CH_3)_3 + NH_3$$

XPS measurements indicate a coverage with CH_3 of $6x10^{14}/cm^2$, hence $2x10^{14}/cm^2$ trimethylsilyl groups are present after the reaction. This corresponds closely to the maximum coverage expected on account of the size of these groups of 0.4 nm^2. The surface is densely covered with $Si-(CH_3)_3$ groups which protect the oxide from reactions with water vapour during storage.

V. DISCUSSION

The surface oxide of a hydrophilic wafer consists of tetrahedral units $Si-[O_x(OH)_y]$ with $x + y = 4$ (7). Oxygen is either bonded in Si-O-Si bridges which connect the tetrahedras or in OH groups which terminate the network. The ratio bridging oxygen to OH groups (x/y) is governed by the condensation-hydrolization equation

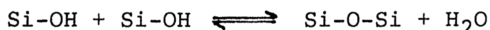

$$Si\text{-}OH + Si\text{-}OH \rightleftharpoons Si\text{-}O\text{-}Si + H_2O$$

which is a function of the water vapour pressure in air or of the pH value in liquids. As long as the surface is not in equilibrium Si-OH will either condense or H_2O will hydrolize Si-O-Si bridges prevailingly, as was observed in Fig. 3. According to light scattering measurements the aged hydrophilic oxide must consist of regions of slightly different optical density. On the other hand the OH depleted $Si-(CH_3)_3$ covered surface, which largely excludes reactions with water vapour, showed no deterioration. The scattered light intensity increased on storage neither before nor after thermal oxidation.

From this observations we conclude that condensation/hydrolization reactions play the major role in generating inhomogeneity on the surface. As the oxide volume shrinks with loss of OH groups or swells with increasing hydrolization, regions with different density (and hence optical density, too) will exist on the surface. They give rise to diffuse lightscattering and their size is of the order of the measured correlation lengths of some microns (see Fig. 1).

The reason for the development of such microregions might be a slight incipient nonuniformity of OH group distribution which is amplified by the fact that adsorption (and hence reaction) with H_2O occurs preferably near already existing Si-OH sites. A nonuniform distribution of hydrocarbons (or other adsorbed species) may result in the same effect. The picture of a surface with microregions of slightly different chemistry and structure is also in line with the dipping experiment in water. In aqueous solutions it is known that OH^- ions or water catalyze the fast rearrangement of silicate networks (10) and the surface will be quickly homogenized.

VI. CONCLUSIONS

Vibrational spectroscopy and lightscattering measurements yield the following model for aging of the hydrophilic surface:

a) The oxide shows condensation - hydrolyzation reactions during storage.
b) The reactions create microregions with different OH/Si-O-Si ratios.
c) The microregions exhibit different optical density, which leads to diffuse lightscattering.
d) The microregions are responsible for enhanced roughness of the interface Si/SiO_2 after thermal oxidation.

The problem why inhomogeneity of the hydrophilic oxide leads to roughness after thermal oxidation is however not yet solved. This requires a detailed knowledge of the reactions at the interface during thermal oxidation, which is at present in an early stage.

REFERENCES

1. F.J. Grunthaner and J. Maserjian, IEEE Trans. Nucl. Sci., NS-24, 2108 (1977)
2. F.N. Schwettmann, K.L. Chiang, and W.A. Brown, Electrochem. Soc. Extended Abstr. 78-1, 688 (1978,
3. G. Gold and E.A. Irene, J. Electrochem Soc. 134, 1031

(1987)
4. J.M. deLarios, D.B Kao, C.R. Helms, and B.E. Deal, Appl. Phys. Lett 54 (8), 715 (1989),
5. P.O. Hahn, M. Grundner, A. Schnegg, and H. Jacob in: The Physics and Chemistry of SiO_2 and the $Si-SiO_2$ Interface (Edited by C.R. Helms and B.E. Deal, Plenum Publishing Corporation), 401 (1988)
6. P.O. Hahn, and M. Kerstan, Proc. SPIE, Vol. 1009, 172 (1988)
7. M. Grundner and H. Jacob, Appl. Phys. A 39, 73 (1986)
8. T. Hattori, K. Takase, H. Yamagishi, R. Sugino, Y. Nara, and T. Ito, Jap. J. Appl. Phys. 28 No. 2, 296 (1989)
9. W. Hertl and M.L. Hair, J. Phys. Chem., 75 (14), 2181 (1971)
10. H. Scholze, J. Non Crystall. Solids 102, 1 (1988)

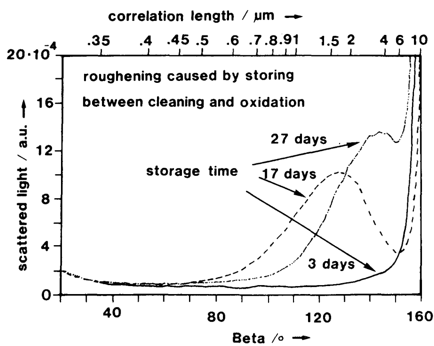

Fig. 1: Scattered light intensity of thermally oxidized wafers after dissolution of the oxide. The oxidation was performed after 3, 17, 27 days of storage of the hydrophilic wafer in air

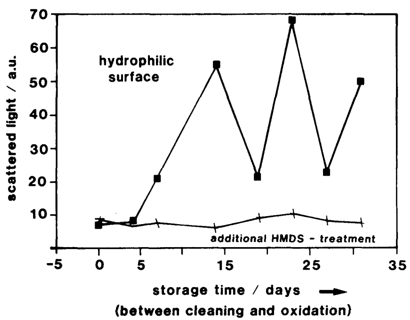

Fig. 2:
Roughness after thermal oxidation at a fixed correlation length of 0.9 µm as a function of storage time in air for a hydrophilic wafer and a HMDS (hexamethyldisilazane) treated wafer.

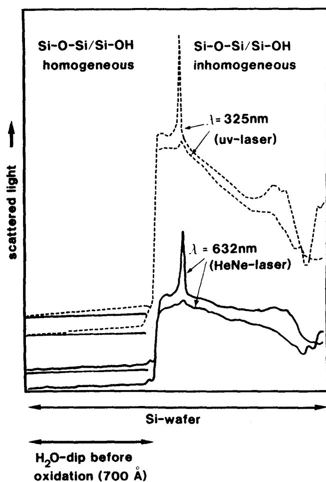

Fig. 3:
Dipping an aged wafer halfway in D.I. water before oxidation results in different roughness on both halves after thermal oxidation.

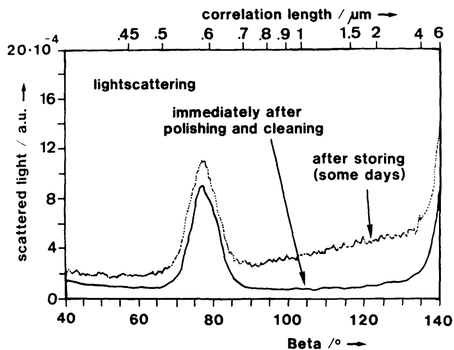

Fig. 4
Change in scattered light intensity due to storage in air. The initial low value is reattained by dipping in water.

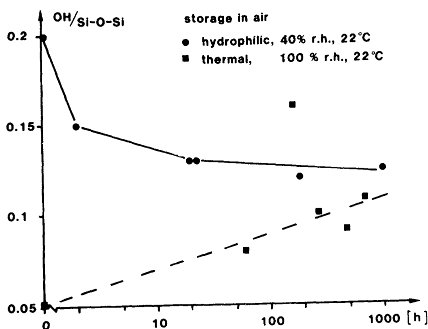

Fig. 5:
Change in OH concentration with storage time of an OH rich and an OH depleted oxide

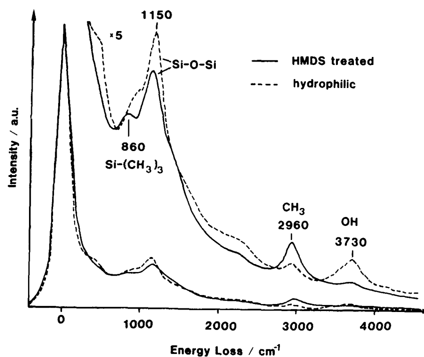

Fig. 6:
Comparison of the spectra of a hydrophilic wafer before and after treatment with HMDS. Si-OH groups are transformed into $Si\text{-}O\text{-}Si(CH_3)_3$ groups by HMDS.

EFFECT OF SILICON WAFER CLEANING ON PRE AND POST THERMAL OXIDATION CHARGES

Allan Resnick and Emil Kamieniecki
SemiTest Incorporated, Billerica, MA 01821

Ara Philipossian and Daniel Jackson
Digital Equipment Corporation, Hudson, MA 01749

ABSTRACT

A controlled study is reported in which a correlation between pre and post oxidation charge is established. This study utilizes a Surface Charge Analyzer (SCA) to measure electrically active contamination on the surface of silicon wafers. The SCA is a new surface photovoltage technique using low intensity light chopped at high frequencies to characterize the electrical properties of a silicon wafer surface. The method does not require any additional processing. By measuring charge values after pre oxidation cleaning, gate oxidation, and anneal it is shown that the contamination left on bare wafers is highly dependent on the last steps of the cleaning process. It is also shown that this contamination has a significant impact on the quality of a subsequent gate oxidation. A higher temperature nitrogen anneal reduces the oxide charge variation observed, but is not sufficient to compensate for charge induced at cleaning.

OBJECTIVE

Wet chemical wafer cleaning processes are highly utilized in the semiconductor industry. It is critical that contamination is periodically removed and that cleaning operations do not add to this contamination, so that yields and reliability are not negatively impacted.

With the advent of surface charge analysis, a new technology to measure the electrically active contamination left on a wafer surface, it becomes feasible to explore effects which have been very difficult to evaluate in the past.

This study applies the use of a Surface Charge Analyzer to the evaluation of a few different cleaning process sequences and examines how they affect the charge residue left on the silicon surface. This cleaning residue is then compared to the oxide charge measured after a gate oxidation process. Variations are explored where the cleaning cycle ends in an oxide removal step, or one in which a native oxide is grown due to exposure in an oxidizing solution.

Correlations are then established between residual contamination from cleaning and oxide charge after a gate oxidation.

EXPERIMENTAL PROCEDURE

Material utilized was 125mm, p-type, <100>, silicon substrates with a resistivity range of 1-25 ohm-cm.

Samples were pulled from the material as received and after each subsequent process step. The total oxide charge (Q_{ox}) was measured using the Surface Charge Analyzer (SCA). This technique is based on photo-electrical measurements (1,2) using low intensity light chopped at high frequencies. The resulting surface photovoltage signal is used to characterize the electrical properties of the silicon, or silicon/oxide, surface region. The oxide charge values presented are determined from the total charge of the semiconductor/oxide system with the silicon surface biased to align the Fermi level with the intrinsic level. Under such conditions, the contribution of interface traps to the charge can be neglected. As no additional processing is required, the measurements directly reflect the variations in the process being evaluated.

Additional wafers were split into six other groups and processed through various wet chemical cleaning cycles ranging from a rinse in deionized (DI) water to a RCA and reverse SC1 cleans. The process sequences for each group are summarized in Table 1. Four of these groups included a dilute Hydrofluoric Acid (HF) dip as the last chemical step. All groups ended with a nine cycle dump rinse in DI water and were then placed into a spin dryer. The Total Organic Carbon readings for the DI water was in the 70 to 80 PPB range.

After the samples were pulled, the remaining wafers (including a non-cleaned sample) were put into a hot wall atmospheric thermal oxidation reactor in which an oxide of 130A was grown. The tube and gas configuration had been previously characterized (3) with the SCA as introducing a minimum amount of charge due to Ambient Air Infiltration.

Oxidized wafers from each cleaning process were then annealed in nitrogen for one hour at 1050C. The same tube configuration was used as above for oxidation.

Evaluation of the bare silicon wafers was made utilizing a voltage sweep direction on the SCA which biased the surface into inversion before data acquisition. The measurements were then taken during a sweep from inversion into accumulation. This was done in order to minimize the effect of tunneling through a thin (2-8Å) oxide. The voltage sweep used on the oxide wafers biases the surface initially into accumulation and the measurements are taken during a sweep from accumulation into inversion. This sweep direction would create a large hysteresis effect on bare wafers and increase the Qox value obtained. This effect is demonstrated in the curve of Figure 2 in which a Qox value of 3.25E10 q/cm^2 was obtained by biasing the surface into inversion initially (Point 1). A value of 7.05E11 q/cm^2 would be obtained with the opposite sweep direction (Point 2).

The reported measurements on bare wafers were taken four days after cleaning. During this time the material was stored in a nitrogen dry box.

Preliminary results indicate that this delay did not influence the results, with the possible exception of the virgin and DI rinse (group 1) wafers.

The data presented represents the average of two to three wafers per process with four readings on each wafer. The error bars on Figure 1 are one standard deviation.

RESULTS AND DISCUSSION

As can be seen from Figure 1, the virgin material exhibited a large negative charge (-6E11 q/cm^2). A DI water rinse had almost no impact on this charge value. Both of these groups had essentially the same charge levels after the gate oxide step (-1E11 q/cm^2).

All cleaning processes which ended in the last acid step of a dilute HF dip displayed very similar SCA plot characteristics. Charge readings were also very similar with values of 6E10 q/cm^2 or less (Figure 2). After thermal oxidation all of these groups again had similar characteristics with oxide charge values in the range of +1E10 to -3E10 q/cm^2 (Figure 3). The HF only process, group 2, had the widest variations of these four recipes.

Group 4, which was processed in a reverse SC1 clean, ending in an oxidizing step of NH_4OH/H_2O_2 had substantially more negative charge, -1E12 q/cm^2 (Figure 4). When these wafers were thermally oxidized they generated the most negatively charged oxide of any process with values of -6E11 q/cm^2 (Figure 5), which is an order of magnitude higher than any other chemically cleaned group.

A one hour nitrogen anneal reduced the variation between groups by decreasing the magnitude of the negative charge on the reverse SC1 group and slightly increasing the negative charge on the processes ending in HF (groups 2,3,5,6).

Typical charge variations of 10% to 30% were found across a wafer, and similar variations existed between wafers of the same process.

CONCLUSIONS

The Surface Charge Analyzer has been demonstrated as an effective technique for the measurement of charge on bare and oxidized silicon wafers. The SCA has been utilized to show the importance of the pre oxidation clean in affecting subsequent charge incorporated into a device oxide.

Various silicon cleaning processes have been characterized for charge before and after an oxidation step. It has been demonstrated that the charge retained after a chemical cleaning step is very highly dependent on the last chemical used in this process.

Cleans which end with an oxidizing agent incorporate much more charge into the native oxide that is grown during this clean.

A correlation has been established which indicates that oxide charge after a specific gate oxidation is substantially affected by the type and quality of the pre oxidation clean.

It was also shown that the charge variation between groups can be reduced with a subsequent nitrogen anneal.

ACKNOWLEDGMENTS

Thanks to Edward Culley for performing the experiments.

REFERENCES

1. E. Kamieniecki, U.S. Patent #4,827,212 "Noninvasive Method and Apparatus for Characterization of Semiconductors," issued May 2, 1989.

2. E. Kamieniecki, "Surface Charge Analysis: A New Method to Characterize Semiconductor/Insulator Structures: Application to Silicon/Oxide System," this symposium.

3. A. Philipossian, D. Jackson, E. Kamieniecki, A. Resnick, "The Effect of Ambient Air Infiltration on Growth Rate and Electrical Characteristics of Ultra-Thin SiO2 Gate Insulators," this symposium.

TABLE 1

PROCESS NUMBER	SEQUENCE
VIR	None
1	DR + Dry
2	HF + DR + Dry
3	SA80/H_2SO_4 + DR + HF + DR + Dry
4	HF + DR + SC1 + DR + Dry
5	SC1 + DR + HF + DR + Dry
6	SC1 + DR + SC2 + DR + HF + DR + Dry

		PROCESS	TEMPERATURE
DR		Dump Rinse	21°C
SC1	7:1:1	$H_2O:NH_4OH:H_2O_2$	85°C
SC2	7:1:1	$H_2O:HCl:H_2O_2$	85°C
HF	10:1	$H_2O:HF$	21°C
SA80/H_2SO_4			85°C

SA80 Ammonium Peroxydisulfate

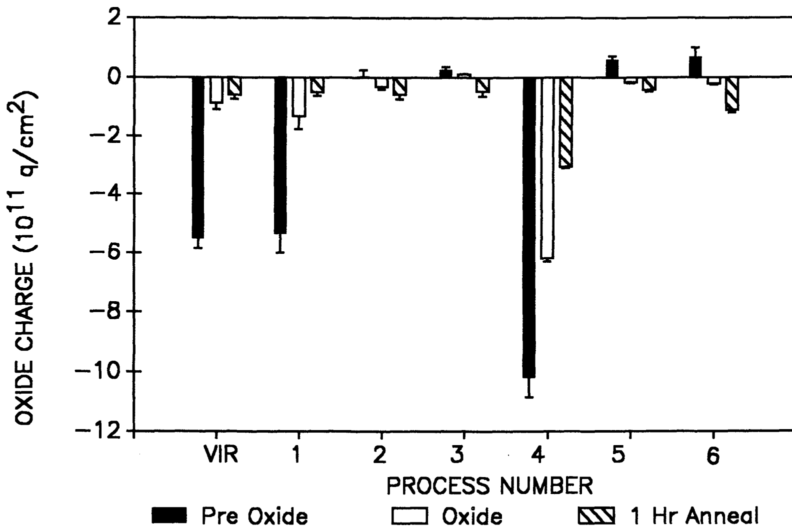

Figure 1 Comparison of charge levels obtained at the various steps for each process.

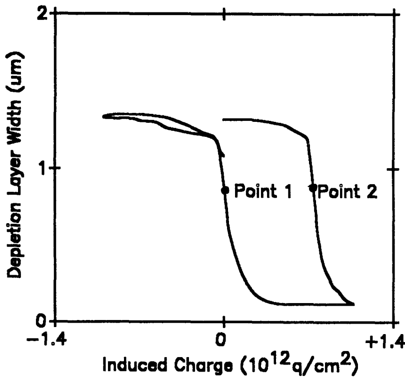

Figure 2 Typical depletion width variation vs. induced charge (SCA plot) for a wafer after a clean ending with an HF dip and rinse. Points 1 and 2 represent the Q_{ox} values that would be obtained with different SCA sweep directions. (Group 3)

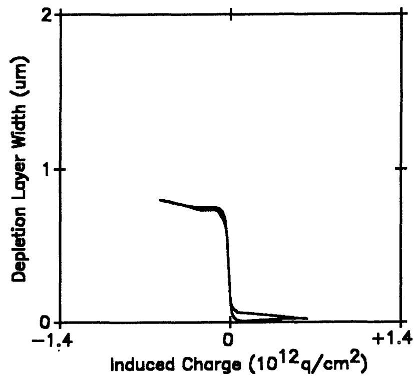

Figure 3 Wafer after thermal oxidation where the pre-oxidation clean ended with an HF dip. (Group 3)

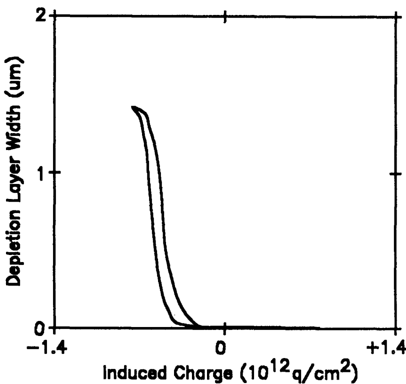

Figure 4 SCA plot of a wafer after cleaning where the last chemical used was ammonium peroxide. (Group 4)

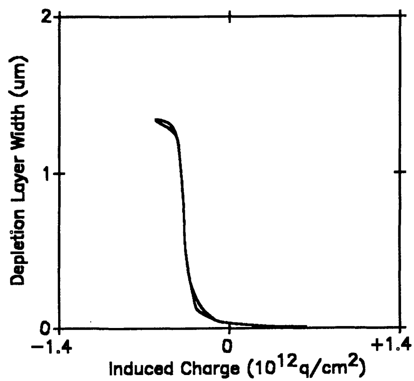

Figure 5 Thermally oxidized wafer where the pre-oxidation clean ended with ammonium peroxide and rinse. (Group 4)

REMOVAL OF SURFACE ORGANIC CONTAMINANTS DURING THERMAL OXIDATION OF SILICON

Sylvia D. Hossain[1] and Carlo G. Pantano[2]
Department of Engineering Science and Mechanics [1]
and Department of Materials Science and Engineering[2]

Jerzy Ruzyllo
Department of Electrical Engineering

Center for Electronic Materials and Processing
The Pennsylvania State University
University Park, PA 16802

The behavior of surface hydrocarbons and carbon during thermal oxidation of silicon is studied. It was established that organic contaminants are readily volatilized and do not affect, in a significant manner, the oxidation kinetics only in the case when the silicon surface during contamination is covered with an oxide at least 5 to 10Å thick. The organic removal process is substantially more effective at the higher temperatures of oxidation (900°C and above) than at the low temperature of 700°C. In the latter case, a noticeable disruption of the oxidation kinetics due to organic contaminants was observed for hydrophobic surfaces, or surfaces subjected to HF step last.

INTRODUCTION

Organic contaminants are very common in the integrated circuits production environment, and as a result, at certain stages of device fabrication, silicon surfaces can be grossly contaminated with hydrocarbons or carbon. In the case of some processes, such as silicon epitaxy or contact metallization, contamination of silicon surfaces with organic materials has a proven adverse impact on the characteristics of the final structures [1,2]. Consequently, cleaning processes applied in silicon device fabrication always include a step aimed specifically at the removal of organic contaminants which is achieved through their oxidation.

A special consideration should be given to the role of organic contaminants in thermal oxidation of silicon.

This is because, first, the exact behavior of surface carbon during thermal oxidation is not yet fully understood, and, second, because thermal oxidation by itself, in contrast to any other processing step, has potential for the removal of organics.

The purpose of this study was to investigate the "cleaning" action that could possibly be taking place during thermal oxidation of silicon, and to evaluate the degree to which surface carbon or hydrocarbons may affect oxide growth rate.

EXPERIMENTAL

The experimental procedure applied in this investigation consisted of the following basic steps: (i) wafer cleaning, (ii) intentional surface contamination with organics, (iii) thermal oxidation, (iv) oxide thickness measurements, and (v) Secondary Ion Mass Spectroscopy (SIMS).

Silicon wafers used were test-grade, p-type, 2-7 ohm-cm, (100) orientation. The samples were cleaned using a standard RCA clean in which step SC-1 consisted of wafer immersion in a solution of $NH_4OH:H_2O_2:H_2O$ for 10 min. at 75°C, and step SC-2 consisted of immersion in a solution of $HCl:H_2O_2:H_2O$ for 10 min. at 75°C. Two different cleaning sequences were applied in this experiment as shown in Table I. In Clean 1, the $HF(1):H_2O(10)$ dip was applied after step SC-1, while in Clean 2, the same was done after step SC-2. The placement of the HF step in the cleaning sequence results in different chemical states of the silicon surface [3,4].

As shown in Table II, clean samples were contaminated with hydrocarbons by immersion in electronic grade isopropyl alcohol (IPA) at various stages of the pre-oxidation process. In Clean 1, the silicon surface after rinsing and before exposure to IPA was expected to be relatively hydrophilic. In Clean 2, due to the HF step performed last, the surfaces were expected to be hydrophobic, and hence, substantially more reactive [5].

Besides dipping in IPA, in this study, silicon wafers were also intentionally contaminated prior to thermal oxidation with about a 150-200Å thick carbon layer, sputtered from a high purity graphite source.

The samples prepared in the manner described above were thermally oxidized at various temperatures in dry oxygen from a pressure tank. A Rudolph Research Auto-El

ellipsometer was used to measure thickness of the resulting films. There is a severe limitation to the ellipsometric measurements performed in this study as the chemical composition of the measured oxide films varies substantially with temperature and time of oxidation. Therefore, we use ellipsometric data as an indication of the compositional changes occurring at the Si surface rather than as an exact measure of the oxide thickness, specially for films thinner than about 100Å. Supporting data concerning chemical composition of the sample surfaces was obtained through SIMS characterization carried out using a O_2^+ or C_s^+ primary beam.

RESULTS AND DISCUSSION

Figure 1 shows results from thermal oxidation following treatments (1-a) and (1-b) outlined in Table II which, in the latter case, involved an IPA treatment of predominantly hydrophilic surfaces, i.e., surfaces covered with an ultrathin chemical oxide. At the oxidation temperature of 1000°C, the two types of processes resulted in virtually identical oxide growth kinetics. Also, the index of refraction for these two sets of samples was identical within experimental error, indicating that the composition and structure of the oxides were similar. This was confirmed by SIMS depth profiles which showed (Fig. 2) that both types of samples had similar carbon and oxygen content in the oxide (difference in oxygen distribution results from a slightly thicker oxide in the sample 1-b). These results indicate, that in the case of hydrophilic surfaces, thickness of chemical oxide prior to IPA immersion was measured at about 15Å, hydrocarbons resulting from the IPA dip have no bearing on the subsequent oxidation of silicon as they are readily oxidized and removed from the surface, in the form of volatile carbon compounds, at a very early stage of oxidation. Worth noting is the fluorine peak at the SiO_2-Si interface in case (1-b) in
Fig. 2. Its possible origin and role will be discussed later.

In the second set of samples, processes (2-a), (2-b), and (2-d) in Table II, the HF step was performed at the end of thecleaning sequence without, except for a D.I. water rinse, any further treatments prior to immersion in IPA. In the case (2-d), the silicon surface is expected to be fully hydrophobic at the time of IPA immersion, while in the process (2-b) somewhat less hydrophobic as, prior to the IPA dip, the surface was rinsed in D.I. water [6]. Final determination with regard to oxide coverage in this last case could not be made as the rinsed wafers were

moved directly into IPA, and the drying process would alter the condition of the surface. Figure 3 shows results obtained after oxidation at 1000°C in dry oxygen for these samples. The differences between reference (no IPA dip) samples and samples immersed in IPA either following a D.I. water rinse or directly after the HF dip, are, in contrast to processes (1-a) and (1-b) in Fig. 1, obvious in this case, stressing the importance of the placement of the HF dip in the cleaning sequence. For samples which were either rinsed and spin dried (2-a), or rinsed and put into IPA (2-b), the oxidation appears to proceed at the same rate with a clear difference in oxide thickness established at a very early stage of oxidation. The reason for this difference is probably related to a combination of factors resulting from the interaction of the wet Si surface with IPA. The expected increase in content of surface hydrogen can be held responsible for the enhanced, as compared to the standard process (2-a), oxide growth rate during the first few minutes of oxidation. It may also result from the catalytic action of fluorine [7] detected in the oxide grown after treatments (2-b) as demonstrated by SIMS profiles in Fig. 4. At a later stage, oxidation appears to be taking place at the same rate: curves (2-a) and (2-b) in Fig. 3 remain parallel throughout the wide range of oxidation times.

The situation is somewhat different in the case of treatment (2-d) where samples after the HF dip were moved directly to IPA. A different slope for curve (2-d) in Fig. 3 for times of oxidation shorter than 30 min. reflects a different oxidation mechanism in this case. We do not have a solid explanation for the probably very complex reactions taking place during oxidation of the silicon surface which was first HF treated and then, without a D.I. water rinse, exposed to IPA. In general however, our results are clear confirmation of the higher vulnerability of the hydrophobic Si surfaces to hydrocarbons which, instead of being readily volatilized in the oxidizing ambient, might be involved in the surface reactions during the oxidation process. The differences in Fig. 3 can not be directly related to the presence of carbon as virtually identical carbon content in the oxide in these three cases was revealed by SIMS profiles (Fig. 4). In addition, as shown later in this paper, carbon would slow down the oxidation rate rather than cause its enhancement as observed in Fig. 3. The differences in oxidation rates are therefore more likely due to the effects of hydrogen during oxidation. After decomposition of IPA molecules and oxidation and volatilization of carbon, the hydrogen may interact with oxygen to form water, or hydroxyl groups, and to enhance oxide growth

rate [8]. This reasoning is supported by the fact that differences in oxide growth rate occur only at the early stage of oxidation (Fig. 3). In other words, factors responsible for the increase of the oxide growth appear to be surface related and do not last throughout the entire oxidation regime. In any case, they come into play only when hydrocarbon molecules are in immediate contact with silicon surfaces, i.e., silicon surface is oxide-free, prior to oxidation. If the silicon surface is passivated with the chemical/native oxide during exposure to hydrocarbons, no disruption of kinetics of subsequent thermal oxidation is observed (Fig. 1).

In this context, an issue which remains to be addressed is a presence of fluorine detected in the oxides grown following some procedures applied in this study. As seen in Fig. 2 and Fig. 4, fluorine shows up in the oxide only after the silicon surface was exposed to IPA prior to oxidation. It is reasonable to assume then, that fluorine either: (i) originates from IPA, or (ii) was present at the surface prior to IPA immersion and subsequent interactions with IPA molecules during oxidation prevented it from leaving the oxide. Addressing the second possibility, we should note that fluorine typically tends to remain in the oxide whenever the silicon surface is fluorinated prior to oxidation [9]. Therefore, in this study, fluorine should also be detected in the oxides grown on the surfaces not exposed to IPA which, as seen in Fig. 2 and Fig. 4, was not thecase. On the other hand, we did not have strong enough evidence to entirely exclude the possibility of IPA molecules aiding in retaining fluorine in the oxide through the complex surface reactions. To resolve this problem, we have tested IPA used in this study for fluorine content using the ion specific electrode method. This test has revealed 0.32 ppm of fluorine in IPA which seems to point to IPA itself as a likely source of fluorine detected in oxides studied.

In the next stage of this experiment, thermal oxidation of silicon wafers covered with a very thin film of sputtered carbon was studied. Figure 5 shows SIMS profiles of the carbon coated Si surface prior to oxidation. The exact thickness of the films resulting from oxidation could not be determined accurately using an ellipsometer because composition of such "oxides" varies continuously with the time of oxidation, and at the early stage of oxidation, consists mainly of carbon. For this reason, we are using ellipsometric data as an indication of the undergoing changes rather than an exact measure of the thickness of the film. In spite of these limitations, for oxidation at 700°C (Fig. 6a) it was possible to

observe somewhat different behavior of the samples covered with carbon, curves (1-c) and (2-c), as compared to the oxidation of the carbon-free surfaces, curve (1-a).

In the former case, both curves (1-c) and (2-c) are essentially flat for up to 100 minutes of oxidation which reflects very little variation in the optical parameters of the film. This may be an indication that the carbon, which gradually undergoes oxidation into the volatile oxides, still remains on the surface. Ellipsometric measurements are expected to yield the same results as long as the coherent, non-transparent film of carbon remains on the silicon surface. In this context, consistently observed for oxidations longer than 120 minutes, somewhat non-aligned ellipsometric reading in the case of process (1-c) in Fig. 6a, may be an indication of the completion of the carbon removal process in this case. In contrast to curves (1-c) and (2-c), a slow increase in the oxide thickness is observed in Fig. 6a in the case of the surface which was not intentionally contaminated with carbon (curve 1-a).

A different situation was observed for the 800°C oxidation (Fig. 6b). Here again, the undisrupted growth of an oxide on thecarbon-free silicon surface was observed (curve 1-a). Also, the same behavior as seen for oxidation at 700°C is observed for the (2-c) process, but not for the process (1-c). In this last case, after the initial retardation, oxide growth seems to follow typical oxidation kinetics exemplified in Fig. 6b by the curve (1-a). This is clearly not the case for process (2-c) where it takes more than 100 minutes of surface exposure to oxygen to see an increase in the oxide growth rate. If the reasoning presented earlier holds, then it can be concluded that the carbon removal during oxidation is more effective in process (1-c) than in process (2-c). As indicated in Table II, the only difference between these two processes is in the placement of the HF dip in the sequence of pre-oxidation surface treatments; in the latter case the HF dip was applied at the end of the sequence. This difference certainly affects the chemical state of the silicon surface prior to carbon deposition. This, in turn, appears to have an impact on the way in which Si-C bonds are formed during the carbon sputtering process. In this context, we should note a fairly well developed oxide phase observed at the carbon coated Si surface which was considered hydrophilic before carbon deposition (Fig. 5). Our SIMS data did not reveal a similarly well defined oxide phase on the surfaces which were HF treated prior to carbon contamination. This difference may be one possible reason for the differences

in curves (1-c) and (2-c) in Fig. 6b. The ultrathin surface oxide in the case (1-c) may prevent direct bonding between carbon and silicon, and hence, allow easier volatilization of carbon during thermal oxidation of silicon.

In the case of oxidation at 900°C (Fig. 6c), curves (1-a) and (1-c) are almost identical while the growth of the oxide on the Si surface coated with carbon after an HF dip, is still initially delayed. Curve (2-c) in Fig. 6c indicate that the carbon removal process during oxidation at this temperature lasts for about 25 minutes. This observation is consistent with earlier discussion as, in the case of oxidation at 800°C, the removal process lasted for over 120 minutes (curve 2-c in Fig. 6b), while at 700°C, even after 150 minutes of oxidation, no indication of the completion of the carbon removal process was obtained (curve 2-c in Fig. 6a).

On the basis of the above considerations, it was reasonable to expect that at the oxidation temperature of 1000°C the impact of surface carbon on the oxide growth rate would be negligible regardless of the sequence in which pre-oxidation treatments were applied. Experimental results confirmed this notion as shown in Fig. 6d where all three processes considered yielded the same oxide growth rate over the wide range of oxidation times. This means that at 1000°C surface carbon is readily removed within a few minutes after exposure to oxygen.

SIMS characterization of the samples subjected to processes referred to in Fig. 6 was carried out to get some additional information regarding the effects observed. These measurements however, did not add much to our interpretation as SIMS could detect elemental carbon, but could not provide direct information on carbon bonded in different configurations. Also, due to the very high rate of sputtering through the very thin surface carbon layer during depth profiling, the detection of differences in carbon coverage at various stages of oxidation process was difficult. Still, in terms of the oxide growth process, SIMS data consistently supported results shown in Fig. 6. An example is shown in Fig. 7 in which distribution of oxygen and carbon in the oxides grown for 50 min. at 800°C following treatments (1-c) and (2-c) is presented. Under these conditions, a difference observed in the oxide thickness, curves (1-c) and (2-c) in Fig. 6b, is reflected in the oxygen profiles shown in Fig. 7.

SUMMARY

The results obtained in this study show that thermal oxidation is effective in removing hydrocarbons and carbon from the silicon surface, but only under certain conditions. The rate of removal depends strongly on the condition of the silicon surface during contamination. In the case of surfaces covered with anultrathin oxide at the time of contamination, the impact of organic contaminants is negligible, particularly at the higher temperatures of oxidation. In contrast, oxide growth on hydrophobic surfaces, or surfaces subjected to the HF step last, can be very clearly disrupted by the presence of hydrocarbons or carbon. Therefore, in the case of cleaning processes with HF step last, including anhydrous HF treatments, it is advisable to consider a process which will lead to a controlled re-growth of an ultrathin, pure, protective oxide immediately following the HF step. The UV/ozone oxidation has been proven to be very useful in this particular application [10]. This oxidation step will convert the silicon surface, in a controlled and reproducible manner, into a hydrophilic state. Also, caution should be exercised in using IPA vapor drying of surfaces subjected in the cleaning procedures to the HF step last.

ACKNOWLEDGMENTS

The authors would like to acknowledge the financial support of this study from IBM T.J. Watson Research Center, Yorktown Heights, New York.

REFERENCES

1. M. Tabe, Appl. Phys. Lett., 45, 1073 (1984).
2. H. Norstrom, M. Ostling, R. Buchta, and C.S. Peterson, J. Electrochem. Soc., 132, 2285 (1985).
3. M. Grundner, P.O. Hahn, I. Lampert, A. Schnegg, and H. Jacob, Proc. this Volume, p. 215.
4. G.T. Duranko, D.J. Syverson, L.A. Zazzera, J. Ruzyllo, and D.C. Frystak, Phys. and Chem. SiO_2 and Si-SiO_2 Interface, Ed. C.R. Helms and B.E. Deal, Plenum Publ. Corp., (1988).
5. D.J. Syverson and G.T. Duranko, Proceedings, Institute of Environmental Sciences, 1988.
6. P.O. Hahn, M. Grundner, A. Schnegg, and H. Jacob, Phys. and Chem. SiO_2 and Si-SiO_2 Interface, Ed. C.R. Helms and B.E. Deal, Plenum Publ. Corp., (1988).
7. M. Morita, T. Kubo, T. Ishihara, and M. Hirose, Appl. Phys. Lett., 45, 1312 (1984).

8. J. Ruzyllo, I. Shiota, N. Miyamoto, and J. Nishizawa, J. Electrochem. Soc., 123, 26 (1976).
9. M. Morita, S. Aritome, M. Tsukude, and M. Hirose, IEEE Intern. Electron Dev. Meeting 1984, Tech. Digest, 144 (1984).
10. J. Ruzyllo, G.T. Duranko, and A.M. Hoff, J. Electrochem. Soc., 134, 2052 (1987).

Table I Two different cleans applied in this study

Clean 1	Clean 2
$NH_4OH:H_2O_2:H_2O$	$NH_4OH:H_2O_2:H_2O$
H_2O rinse	H_2O rinse
$HF:H_2O$	$HCl:H_2O_2:H_2O$
H_2O rinse	H_2O rinse
$HCl:H_2O_2:H_2O$	$HF:H_2O$

Table II Surface treatments applied after Cleans 1 and 2 (Table I)

Process (1-a)	Process (1-b)	Process (1-c)
Clean 1 followed by	Clean 1 followed by	Clean 1 followed by
H_2O rinse Spin Dry	H_2O Rinse IPA	H_2O Rinse Spin Dry Sputtered Carbon

Process (2-a)	Process (2-b)	Process (2-c)	Process (2-d)
Clean 2 followed by	Clean 2 followed by	Clean 2 followed by	Clean 2 followed by
H_2O Rinse Spin Dry	H_2O Rinse IPA	H_2O Rinse Spin Dry Sputtered Carbon	IPA

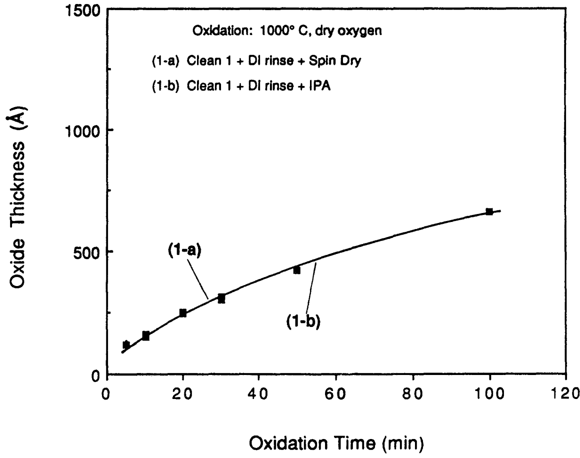

Fig. 1 Oxide thickness vs. oxidation time for Si surfaces subjected to Clean 1 and then exposed to IPA.

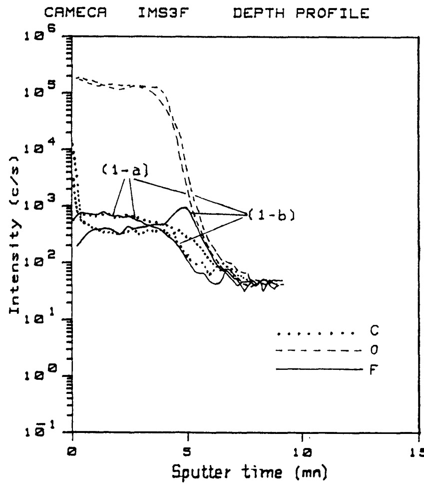

Fig. 2 SIMS profiles of C, O, and F in SiO_2-Si structures formed following processes (1-a) and (1-b).

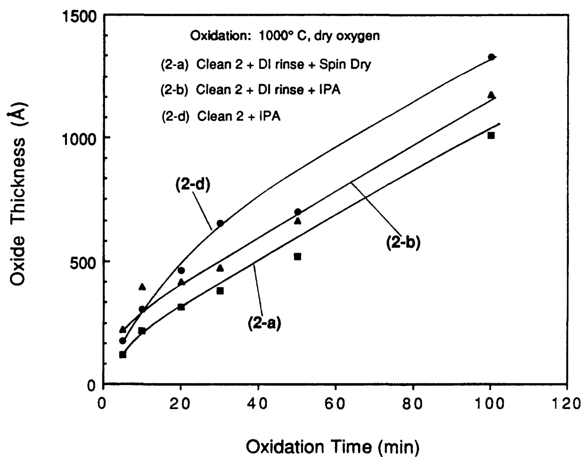

Fig. 3 Oxide thickness vs. oxidation time for Si surfaces subjected to Clean 2 and then exposed to treatments involving an IPA dip.

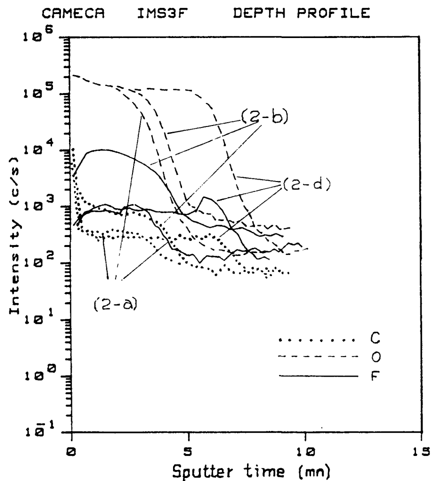

Fig. 4 SIMS profiles of C, O, and F in SiO_2-Si structures formed following processes (2-a), (2-b), and (2-d).

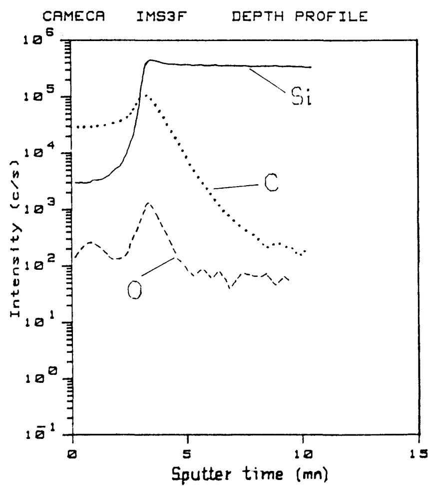

Fig. 5 **SIMS profiles of C, O, and Si of the silicon surface contaminated with sputtered carbon.**

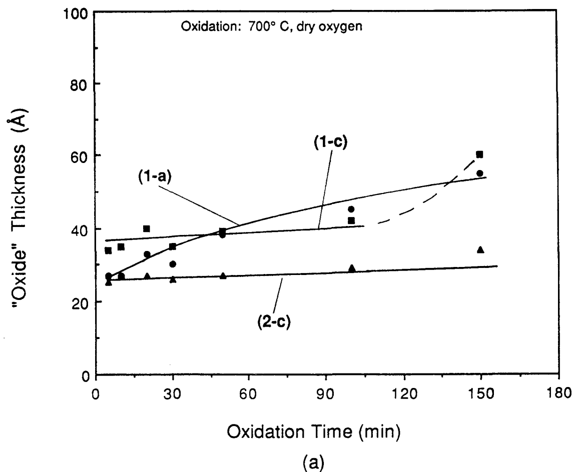

(a)

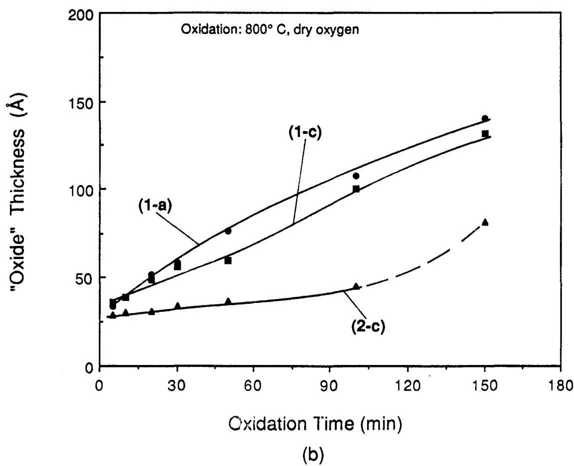

(b)

Fig. 6 **Oxide thickness vs. oxidation time at four different temperatures of oxidation for Si surfaces uncontaminated (1-a), and contaminated with sputtered carbon, (1-c) and (2-c)**

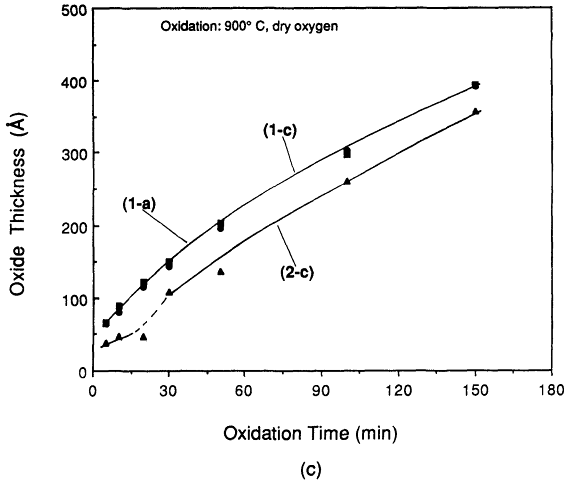

(c)

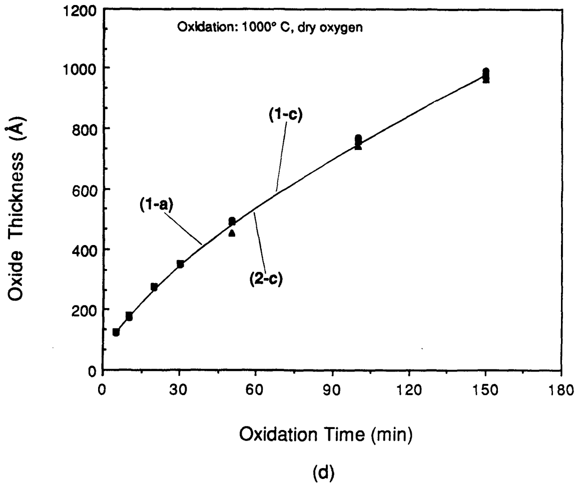

(d)

Fig. 6 (continued).

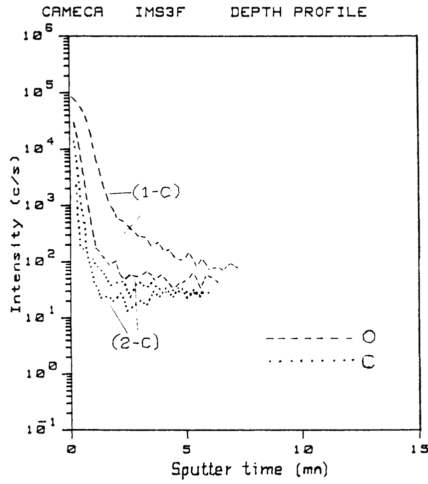

Fig. 7 SIMS depth profiles of O and C in SiO_2-Si structures formed following processes (1-c) and (2-c).

THE EFFECT OF AMBIENT AIR INFILTRATION ON GROWTH RATE AND ELECTRICAL CHARACTERISTICS OF ULTRA-THIN SILICON DIOXIDE GATE INSULATORS

Ara Philipossian and Daniel Jackson
Advanced Semiconductor Development
Digital Equipment Corporation, Hudson, MA 01749

Emil Kamieniecki and Allan Resnick
SemiTest Incorporated, Billerica, MA 01821

Effective chemical cleaning of silicon surfaces prior to gate oxidation is critical in ensuring reliable gate oxide integrity. Of equal importance is the ability to keep the silicon surface free of any contamination during subsequent thermal processing. During the thermal oxidation of silicon, Ambient Air Infiltration (AAI) has been shown to be a significant source of wafer-to-wafer and within wafer thickness variability. AAI has also been shown to be a major factor in affecting the total oxide charge. Increasing reactant gas flow rates, processing the wafers in encapsulated cantilevers, optimum placement of gas baffles, and controlling reactor exhaust rates have helped reduce ambient air infiltration and the detrimental effects of this source of contamination. Over the entire range of operating conditions, this study reports the difference between best and worst results to be up to a factor of 5 improvement in within wafer thickness variation, and a reduction from $3E11/cm^2$ to $-1E10/cm^2$ in total oxide charge.

INTRODUCTION AND OBJECTIVE

Effective chemical cleaning of silicon surfaces prior to gate oxidation is critical in ensuring reliable gate oxide integrity. Of equal importance is the ability to keep the silicon surface free of any contamination during subsequent oxidation intervals. Ambient Air Infiltration (AAI) in the reaction chamber during gate oxidation can cause substantial SiO_2 growth rate uniformity problems. In addition, the introduction of airborne particulates and other contaminants inside the reactor due to AAI can adversely affect the final electrical properties of gate

oxides. This study focuses on the effects of AAI on the growth rate and electrical properties of ultra-thin gate insulators. By offering a quantitative understanding of the possible mechanisms responsible for AAI, the study helps identify the the optimal reactor geometries and process conditions which minimize such external sources of variability.

EXPERIMENTAL APPARATUS AND PROCEDURE

The experiments were performed in a conventional hot-wall atmospheric thermal oxidation reactor with 150, five inch P<100> silicon substrates. The controlled atmosphere tubular quartz cantilever which encapsulates the wafers and the gas baffles, the critical process parameters, and the different baffle configurations adopted in this study are shown in Figs. 1 and 2.

For each run, oxidized P<100> monitor wafers were completely etched to bare silicon in dilute HF, rinsed in DI water and dried. The wafers, having an initial native oxide thickness of about 8 Å, were then distributed throughout the wafer load and processed according to the procedures outlined in Table I and Table II. Ellipsometry and Surface Charge Analysis [1,2] were used to determine the thickness and the total charge of the resulting silicon dioxide films.

Dielectric thicknesses (beyond that of the native oxide) as a function of wafer position in the furnace are reported as the average of 5 measured points per wafer. Within wafer thickness uniformity (WWU) is reported as the range (high minus low) of 5 measurements per wafer. For certain conditions, the average thickness across the entire load was substantially higher than the others. In those cases, the WWU was scaled back by the ratio of the average thicknesses of the wafer load for direct comparison with other process conditions. In all cases the dielectric thicknesses were measured with an ellipsometer at a wavelength of 6328Å, beam angle of 70° and a refractive index of 1.46.

The total oxide charge (Qox) is measured using the Surface Charge Analyzer (SCA). This technique is based on photo-electrical measurements [1,2] using low intensity light chopped at high frequencies. The resulting surface photovoltage signal is used to characterize the electrical properties of the silicon/oxide surface region. The oxide charge values presented are determined from the total charge of the semiconductor/oxide system with the silicon surface biased to align the Fermi level with the intrinsic

level. Under such conditions, the contribution of interface traps to the charge can be neglected. As no additional processing is required, the measurements directly reflect the variations in the particular reactor process sequence being evaluated.

To determine the precision of the experimental techniques adopted in this study, run-to-run oxide thickness and oxide charge uniformity studies were undertaken which involved a five-fold duplication of the experimental results for three different baffle configurations. The runs, which were performed in random order, indicated the precision to be no worse than that of the ellipsometer (±1 Å) and the Surface Charge Analyzer (±5 %).

RESULTS AND DISCUSSION

In a nitrogen environment (Table I, Process Sequence P-1) with a total gas flow rate of 8 liter/min, oxide growth appears to be independent of time. A "Ramp-Up", followed immediately by a "Ramp-Down" results in the same oxide thickness as a 3 hour nitrogen soak (Fig. 3, curve A). This suggests that the oxidizing species deplete rapidly during the initial intervals of the process and are not replenished from sources external to the reactor. The 5 Å difference across the wafer load indicates the direction of oxidant depletion to be from the source end to the load end of the reactor. Such a depletion pattern may be due to the entrance of ambient air during the "Boat In" interval. Once the wafers are loaded and the ambient air is trapped in the reactor, the rate with which the trapped air is purged determines the extent of oxide growth. At nitrogen flow rates of 8 liter/min, the superficial residence time of gases is roughly two minutes and therefore it is quite likely that most of the residual air is purged during the initial stages of "Ramp-Up".

When the nitrogen flow rate is reduced to 4 liter/min, the average oxide growth increases by 5 Å while maintaining the same source to load depletion pattern (Fig. 3, curve B). This is in accordance with the trapped ambient air mechanism, since reducing the flow rate to 4 liter/min, increases the superficial residence time to approximately 4 minutes thus allowing the trapped ambient air longer time to react inside the reactor and yield thicker oxide films.

While the tube to cantilever opening (X) is not a critical parameter at 8 liter/min, the combination of low flows and a 1 inch opening can allow ambient air to enter

the reactor (Fig. 3, curves D and E). Increasing X increases the outer annulus cross sectional area and significantly reduces the nitrogen flow rate through the inner annulus thus letting ambient air in through the inner annulus exhaust port. The fact that oxide growth is a function of time suggests that air is supplied continuously from the ambient. The reversal in the direction of air depletion (load to source) also supports the above mentioned mechanism. Moreover, reducing the number of baffles appears to be creating less of a barrier against AAI since it results in thicker oxides (Fig. 3, curve F). On the other hand, increasing the number of baffles (Fig. 3, curve C), acts to reduce the oxide growth by reducing the extent of ambient air infiltration into the reaction chamber.

Fig. 4a shows the effect of different gas flow rates and reactor geometries on within wafer growth rate uniformities (WWU) following a typical gate oxidation process (Process Sequence P-2). In all cases, a 1 inch tube to cantilever opening (X) has been used. Due to reduced AAI, which occurs with the combination of high flow rates and near optimal baffle configurations, the equipment is capable of delivering WWU of <%_2 Å (Fig. 4a, curves A and B). Despite high flow rates, the 1 baffle configuration does not create a strong barrier to AAI and as a result, WWU starts to show a slight degradation towards the load end of the reactor (Fig. 4a, curve C). At low flow rates (4 liter/min), the severe infiltration of ambient air results in considerable WWU problems at the load end. As expected, worst uniformities occur when minimal number of baffles are used (Fig. 4a, curves D and E).

In addition to being a major source of growth rate variability, AAI can significantly impact the electrical characteristics of ultra-thin gate oxides. The total oxide charge (Qox), plotted as a function of wafer position (Fig. 4b) exhibits trends similar to the WWU curves shown in Fig. 4a. The similarity between Figs. 4a and 4b is quite apparent when the different scales are taken into account (semi-log for Fig. 4b and linear for Fig. 4a).

At the load end of the reactor, high flow rates of 8 liter/min suppress AAI and result in lower total oxide charge in that region (Fig.4b, curves B and C). The same two curves indicate that there is a slight improvement in Qox at the load end of the reactor when the number of baffles is increased from 1 to 4.

For fixed low flow rates (4 liter/min), increasing the number of baffles reduces the amount of ambient air

reaching the wafers, thus resulting in reduced oxide charge at the load end (Fig.4b, curves D and E).

Throughout the course of this study, the process conditions which describe curve A of Figs. 4a and 4b, have consistently yielded negative values of total oxide charge. These conditions, which seem to have minimized ambient air infiltration, further emphasize the strong correlation of Qox to AAI by indicating that drastic reductions in Qox can be expected in the near absence of AAI. For purposes of presentation, curve A has been plotted as the absolute value of total oxide charge.

The conditions which describe curve A in Figs. 4a and 4b, correspond to a 5-baffle configuration with an 8 liter/min total gas flow rate. These conditions yield the best results for both Qox and WWU. The magnitude of the total oxide charge is consistently below $3E10/cm^2$ (below $1E10/cm^2$ for 75% of the load) and WWU is 2 Å or better. Previous studies [3] report that similar process conditions, also result in excellent uniformities both in terms of growth rate and chemical composition across the length of the reactor.

The most significant difference in WWU and Qox profiles is the increase in Qox near the source end. This may be due to exposure of source end wafers (which are substantially hotter) to ambient air as the wafers are removed from the furnace.

CONCLUSIONS

Ambient air infiltration has been shown to be a significant source of wafer-to-wafer and within wafer thickness variability. Ambient air infiltration has also been shown to be a major factor in affecting the total oxide charge. Increasing reactant gas flow rates, processing the wafers in encapsulated cantilevers, optimum placement of gas baffles, and controlling reactor exhaust rates have helped reduce ambient air infiltration and the detrimental effects of this source of contamination. Over the entire range of operating conditions, this study reports the difference between best and worst results to be up to a factor of 5 improvement in within wafer thickness variation, and a reduction from $3E11/cm^2$ to $-1E10/cm^2$ in total oxide charge.

ACKNOWLEDGMENTS

Many thanks to Edward Culley for performing the experiments, and to Kenneth Van Wormer for helpful insights.

REFERENCES

[1] Kamieniecki, E., U.S. Patent No. 4,827,212 "Noninvasive Method and Apparatus for Characterization of Semiconductors", issued May 2, 1989.

[2] Kamieniecki, E., "Surface Charge Analysis: A New Method to Characterize Semiconductor/Insulator Structures: Application to Silicon/Oxide System", this symposium.

[3] Philipossian, A., and K. Van Wormer, "Re-Circulating Gas Cells and their Effect on the Large-Scale Production of Uniform, Ultra-Thin SiO2 Gate Insulators", Extended Abstract No. 161, Proceedings of the 175th Meeting of the Electrochemical Society, Los Angeles, CA 1989.

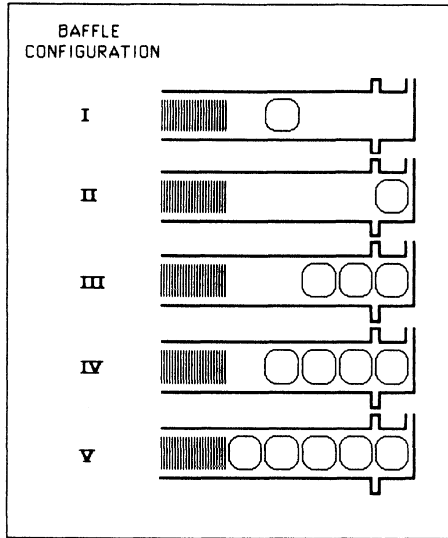

Figure 1 : The different baffle configurations adopted in this study

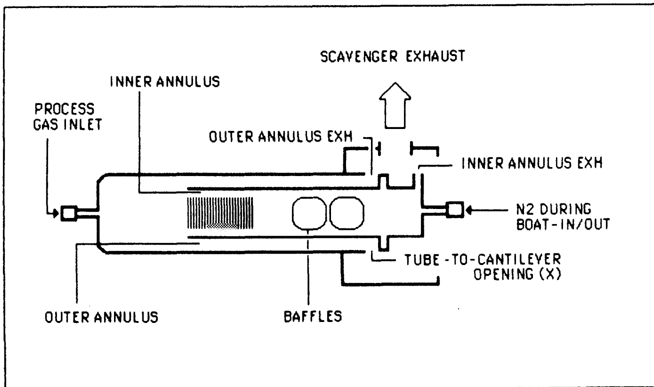

Figure 2 : Experimental apparatus

Curve	Baffle Configuration	Flow Rate (liter/min)	Soak Time (min)	Opening, X (inch)
F	I	4	52	1.0
E	III	4	52	1.0
D	III	4	0	1.0
C	IV	4	52	1.0
B	III	4	0 to 52	0.1
A	III	8	0 to 185	0.1 and 1.0

PROCESS SEQUENCE P-1 :

INTERVAL	TEMP (°C)	TIME (min)	GAS	REMARKS
1	800	10	N2	Boat In
2	800+	20	N2	Ramp-Up
3	950	t	N2	Soak
4	950-	40	N2	Ramp-Down
5	800	10	N2	Boat Out

Table I :

Curve descriptions and thermal processing sequence for Figure 3.

Curve	Baffle Configuration	Flow Rate (liter/min)
E	I	4
D	IV	4
C	II	8
B	IV	8
A	V	8

PROCESS SEQUENCE P-2 :

INTERVAL	TEMP (°C)	TIME (min)	GAS	REMARKS
1	800	10	N2, Dil O2	Boat In
2	800+	20	N2, Dil O2	Ramp-Up
3	950	15	N2, Dil O2	Stabilization
4	950	7	O2, TCA	Oxidation
5	950	30	N2	Anneal
6	950-	40	N2	Ramp-Down
7	800	10	N2	Boat Out

Table II :

Curve descriptions and thermal processing sequence for Figures 4a and 4b.

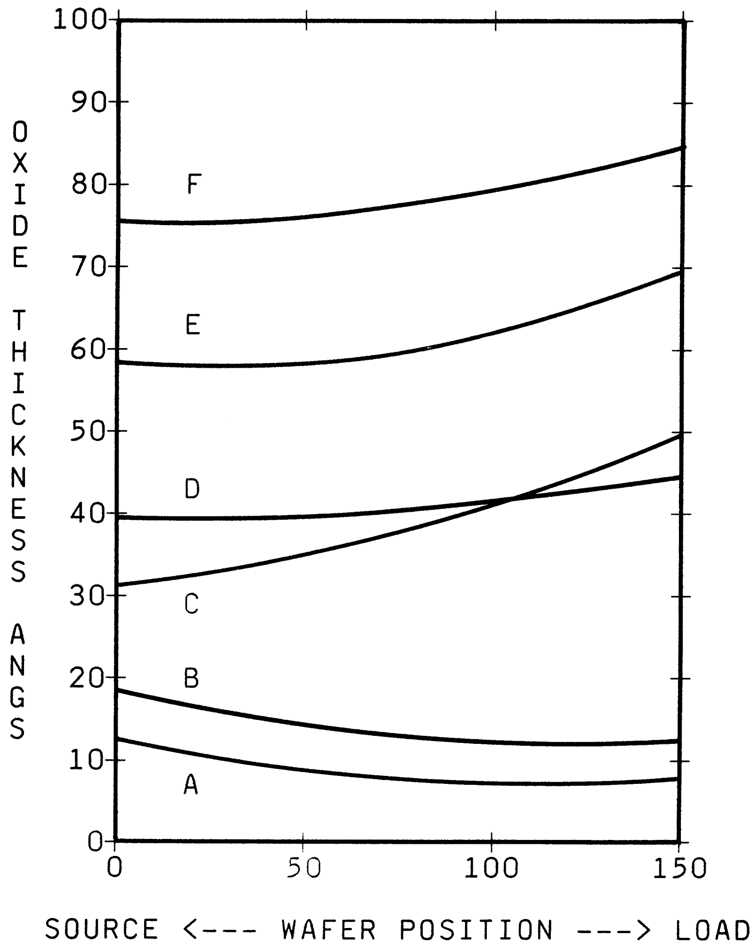

Figure 3 :

Oxide wafer-to-wafer uniformity thickness profiles. Run conditions for each curve are summarized in Table I

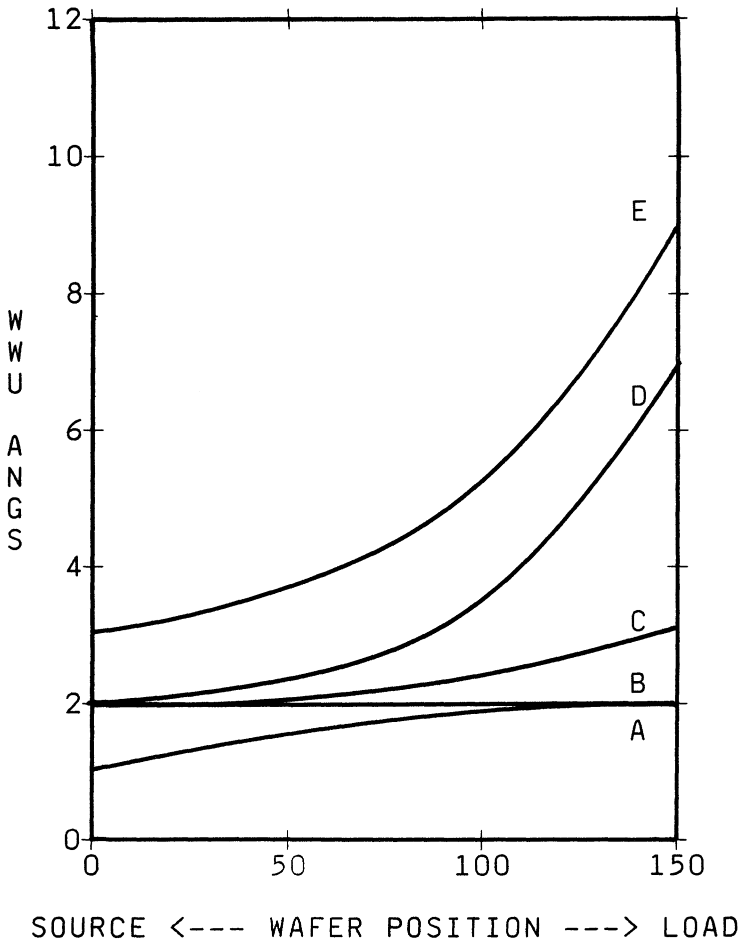

Figure 4a :

Gate oxide within-wafer uniformity thickness profiles. Run conditions for each curve are summarized in Table II (X = 1.0 inch)

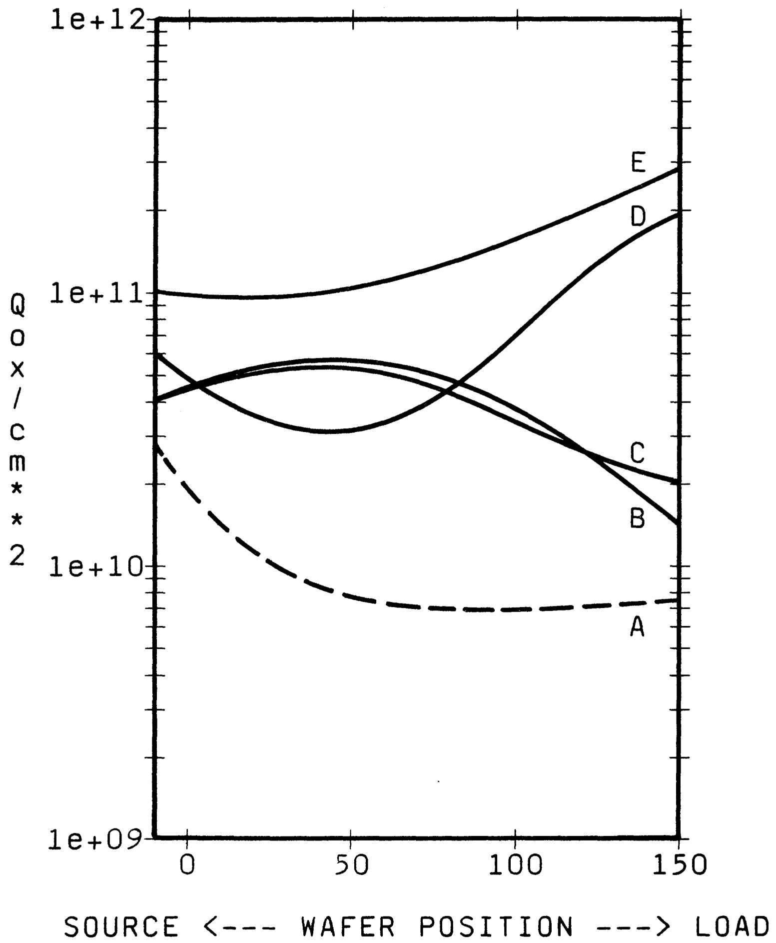

Figure 4b :

Gate oxide total charge uniformity profiles. Run conditions for each curve are summarized in Table II (X = 1.0 inch)

CLEANING OF III - V SEMICONDUCTORS

Epi-GaAs Surface Treatment - Impact of Mixed Phases on Device Performance

A. C. Warren and J. M. Woodall
IBM Thomas J. Watson Research Center, Yorktown Heights, New York 10598

Abstract

Compound semiconductor cleaning and handling procedures are becoming increasingly critical, both before and after epitaxial growth. This is a direct result of both shrinking device dimensions and the advent of novel re-growth techniques. This paper focuses on the connection between various common processing techniques and GaAs surface chemistry, whith emphasis on control of mixed phases. Examples from both electronic properties and recent thermal etch/regrowth results will be used to illustrate problems and solutions in this area.

Introduction

Conventional wafer handling practices with compound semiconductors are largely the result of an accumulation of lore and individual experience - researchers use whatever works for them. This approach has been generally sufficient where a) the pre-epitaxy surface can be etched clean and then buried beneath a thick buffer, and b) where the top surface does not critically impact device performance parameters. With the constant trend toward reduced device dimensions and with the advent of novel etch and re-growth techniques, however, processing and final device performance are becoming increasingly sensitive to the state of the semiconductor surface.

The Si system, for which the greatest body of processing expertise has been collected, is a relatively simple chemical system - upon exposure to air a native oxide is formed which is uniform and easily removed. Compound semiconductors such as GaAs, however, do not have this good fortune. Upon exposure to air (or water), the GaAs surface reacts with O_2 to form a mixed-phase system of Ga and As oxides including Ga_2O, Ga_2O_3(α and β phases), As_2O_3 and As_2O_5. The stoichiometry of this system is dependent upon a number of variables (as will be discussed), and the various constituents affect processing and electronic properties in a variety of ways. It is variations in this stoichiometry resulting from seemingly innocuous processing differences that have produced such controversy as variations in observed Schottky barrier heights to GaAs and probably epitaxial defect density.

Schottky Barriers and Fermi Level Pinning

The problem of high semiconductor interface state densities and resulting "pinning" of the Fermi level has been acknowledged since the advent of microe-

lectronics. In the Si system the problem was mainly one of contamination, and modern processing techniques have essentially eliminated its consideration in most cases. In the GaAs system, however, the pinning is much stronger and appears to be independent of the level of contamination - that is, it is intrinsic to the system itself. For a number of years, it was believed that this was due to the difficulty in terminating a compound semiconductor cleanly, and to the lack of a high quality native oxide for passivation.

In 1985, however, Offsey, et al.[1] demonstrated that a "photowash" technique could be used to prepare the surface of {100} GaAs so that band-bending and Fermi level pinning of air-exposed wafers were greatly reduced. This was attributed to the selective removal of As-containing constituents in the mixed-phase oxide and the formation of a protective passivation that yielded a re-oxidation time constant of minutes to hours (in air). Although the resulting dielectric was unsuitable for MIS (metal-insulator-dielectric) use, this result demonstrated that pinning was not only not an intrinsic property of {100} GaAs, but that processing steps such as rinsing in flowing vs. stagnant deionized water could produce strong variations in the electronic properties of the semiconductor surface. More recently, related treatments using Na_2S have been employed which produce a more stable passivation[2] and which have yielded both low band-bending and low surface recombination velocities.

The specific mechanisms responsible for these results were further clarified by Kirchner, et al.[3] in 1988, when they used Auger and X-Ray Photoemission Spectroscopy (XPS) to clarify the composition of the resulting films. They found that the strong photo-oxidation in the presence of flowing deionized water were almost immediately Ga-rich (Ga:As = 9:1) and were almost As free upon formation of thicker films (Ga:As $\simeq$ 50:1). This As level corresponds directly with the degree of Fermi level pinning and points to As as the contributing species. The processing sensitivity is therefore due to the fact that the As-containg species have a much greater solubility in water than do the Ga-containing ones,[4] indicating that even variations in flow rate (over some range) can affect the resulting dielectric stoichiometry.

GaAs Patterning and Re-growth

A processing step that is extremely sensitive to the state of a semiconductor's surface is that of epitaxial growth. Because of this fact, and the difficulty in obtaining pristine surfaces after air exposure, the accepted practice has been to etch away the top layer to remove contamination, and then grow a buffer layer to isolate devices from the resulting buried interface. With the constant push toward smaller dimensions, and the desire to build high-quality 3D structures, these practices are becoming un-acceptable. One possibile workaround is the use of in-situ processing to avoid contamination and air exposure between critical UHV (ultra-high-vacuum) steps.

One device structure which illustrates this problem is the lateral FET (field-effect-transistor) shown in Fig. 1. In this embodiment, the fabrication consists of an initial heterostructure epitaxial growth and mask patterning (Fig. 1a),

anisotropic etching of the semiconductor (Fig. 1b), and epitaxial re-growth yielding the structure in Fig. 1c. The critical aspect of fabricating advanced devices such as this is the quality of the interface between the original, etched substrate, and the epitaxially re-grown material. This quality depends upon the degree of contamination, damage in the underlying material from the etch process, and crystalline perfection of the re-growth, all of which place severe constraints on the possible alternatives. Chemical etching, for example, can yield anisotropic, damage-free patterning but has problems with contamination and O_2 exposure. A variety of beam and plasma-enhanced techniques are more compatible with UHV processing, but produce damage in the vicinity of the resulting interface that cannot be healed sufficiently for many applications.

Yet another alternative is that of thermally etching the semiconductor substrate in UHV before re-growth. It has been known for a number of years that GaAs could be removed from a substrate surface in a controlled manner at elevated temperatures[5] - the primary difficulty in simple sublimation is that the Ga and As are removed at different rates. If simply heated in UHV to above 650°C., the As comes off easily, while the slower Ga tends to agglomerate on the surface as shown in Fig. 2. The simple inclusion of an As flux, however, is sufficient to suppress the agglomeration and allow uniform etching as has been reported for un-patterned, non-air-exposed substrates.[5]

The difficulty with patterned, thermal etching arises from the condition of the semiconductor top surface after patterning a suitable etch mask. Early results in thermal etching were performed by growing epitaxial GaAs, raising the temperature under an As beam, and evaporation without ever exposing the surface to be etched to ambient. Clearly, with present technology the formation of a patterned mask must entail a) exposure to ambient, and b) exposure to the mask-patterning process which may include reactive ion etching or plasma treatment to remove organic contamination. If, for example, the substrate has SiO_2 deposited, resist patterned, oxide etched, and an oxygen plasma etch to remove resist residue, one obtains thermal etch results such as those shown in Fig. 3. The non-uniformity is a result of exposure of the GaAs substrate surface to the oxygen plasma, producing an oxide stoichiometry that is highly resistant to chemical removal, and which completely precludes uniform thermal etching.

If, however, one protects the GaAs surface properly before the plasma treatment, this difficulty can be avoided. In early studies of GaAs oxide stoichiometries, Massies, et al.[4] showed that a hot plate bake in air of clean GaAs (native oxide removed with HCl) resulted in a uniform oxide that could be removed by heating to around 500°C. in UHV. This results in a clean, oxygen-free surface that exhibits a streaked, 4x2 reconstruction when examined by RHEED. If this hot plate treatment is used before exposure of the GaAs surface to the oxygen plasma, the above thermal patterning process yields results such as those shown in Fig. 4. Here, the GaAs is etched cleanly to expose pristine {110} facets, and upon which high-quality epitaxial re-growth can occur. In this case, the GaAs was etched at 740°C. under and As_2 flux (beam-equivalent-pressure of 8E-6 torr) for one hour, resulting in an etch depth of about one micron, as described in detail by Warren, et al.[6]

Conclusions

When examined closely, exposure of the GaAs surface to air and to a number of processing steps produces a mixed-phase system that is both complex and highly variable. Because of this, such processing steps must be viewed not as passive cleaning or contamination removal, but as active chemical surface preparation. Even the exposure of the semiconductor surface to water at differing flow rates can produce important stoichiometric changes. It has been shown, however, that despite this complexity, proper attention to the formation of this mixed-phase film can produce highly desirable results. Already, the resultant un-pinning of the GaAs surface is leading to advances in GaAs MIS technology. It also suggests the possibility of improved GaAs laser passivation, and the advent of a new class of re-grown, 3D device structures.

References

1. S.D. Offsey, J.M. Woodall, A.C. Warren, P.D. Kirchner, T.I. Chappel and G.D. Pettit, Appl. Phys. Lett., **48**, 475, 1986.
2. E. Yablonovich, C.J. Sandroff, R. Bhat and T. Gmitter, Appl. Phys. Lett., **51**(6) 439, 1987; C.J. Sandroff, R.N. Nottenburg, J.-C. Bischoff and R. Bhat, ibid., **51**, 256, 1987.
3. P.D. Kirchner, A.C. Warren, J.M. Woodall, C.W. Wilmsen, S.L. Wright and J.M. Baker, J. Electrochem. Soc.: Sol. State Sci, and Tech., **135**(7), 1822, 1988.
4. J.Massies and J.P. contour, Appl. Phys. Lett., **46**, 1150, 1985.
5. J.M vanHove and P.I. Cohen, ibid., **47**, 726, 1985.
6. A.C. Warren, J.M. Woodall, E.R. Fossum, G.D. Pettit, P.D. Kirchner and D.T. McInturff, ibid., **51**(22), 1818, 1987.

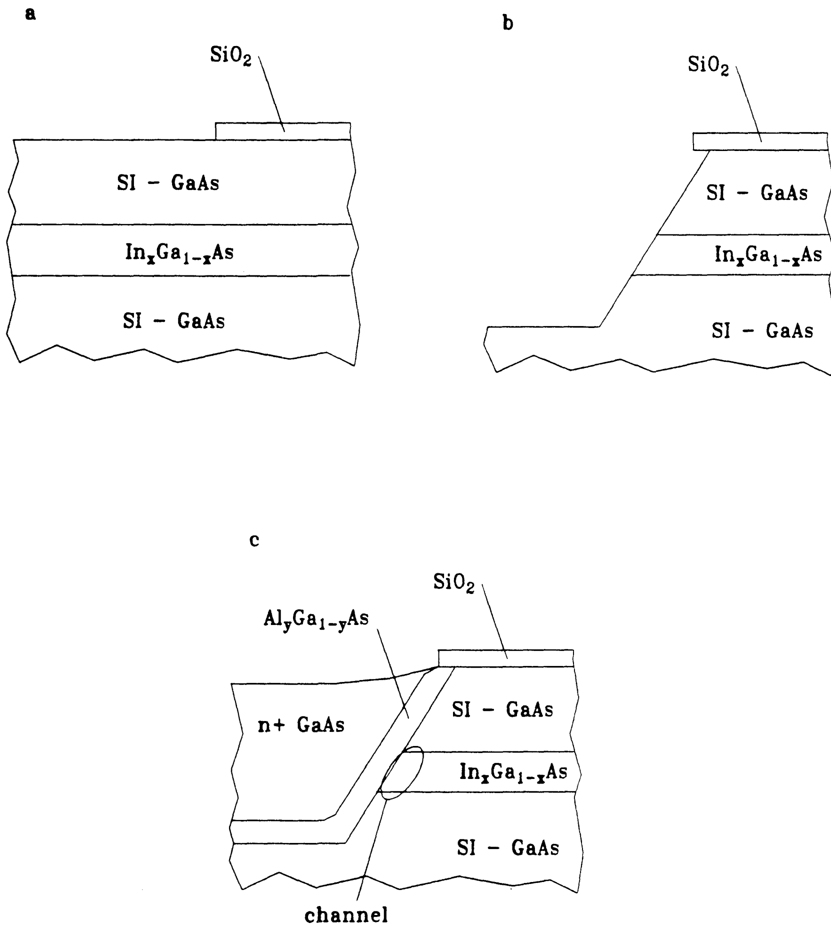

Figure 1. Process for formation of re-grown, lateral FET. A) initial heterostructure with patterned etch mask, b) heterostructure after anisotropic etch, and c) final structure after epitaxial re-growth of barrier and gate layers.

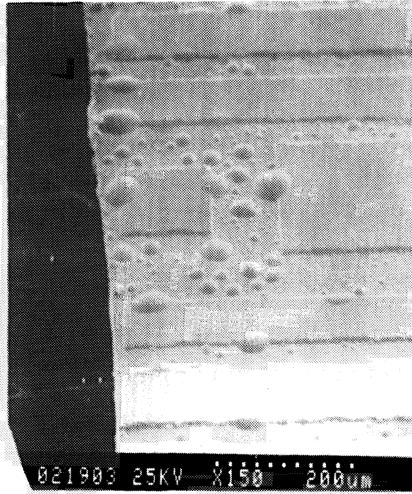

Figure 2. Ga agglomeration after high-temperature exposure of GaAs in UHV.

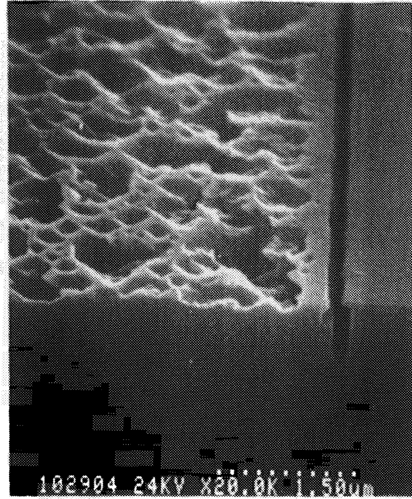

Figure 3. Non-uniform GaAs etch, resulting from plasma exposure of wafer surface.

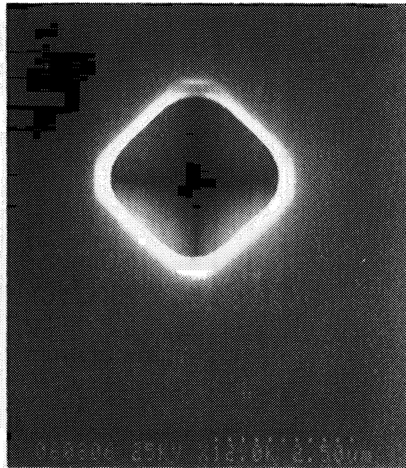

Figure 4. High-quality thermal etch after proper surface treatment. Mask material is SiO_2 and the primary exposed facets are {110} surfaces of GaAs.

PROCESS DAMAGE AND CONTAMINATION EFFECTS FOR SHALLOW Si IMPLANTED GaAs

H.Baratte G.J.Scilla T.N.Jackson A.J.Fleischman H.J.Hovel F.Cardone

IBM Research Division, T.J. Watson Research Center
P.O. Box 218, Yorktown Heights, NY 10598, USA.

During the fabrication of refractory gate MESFET's, the sputter deposition of a WSi_x gate and Reactive Ion Etching (RIE) of the gate pattern can lead to surface damage and contamination. To study these effects, GaAs with a shallow silicon implant was subjected to RIE alone or to both a WSi_x sputter deposition and RIE then annealed. The GaAs surface damage due to the WSi_x sputter deposition and RIE at self-biases under 200V was healed out by 800°C SiN_x capped furnace annealing. Sheet resistance and Hall mobility measurements correlated with the diffusion of compensating impurities into the bulk of the GaAs. The SIMS profiles indicated that the major contaminants (Fe, Cr, Ni, Cu,V, ...) were initially present in the W targets and were thus present in the WSi_x layers. These contaminants were left on the surface of the GaAs after the gate RIE and were driven into the bulk on capped annealing. An HCl etch was found to remove the contaminants, resulting in lower sheet resistances for implanted and processed GaAs. Refractory gate submicron MESFET's with reduced access resistances were fabricated.

Sputtered refractory gate materials are commonly used in the fabrication of submicron self-aligned MESFET's [1-3]. However, the sputter deposition and the subsequent Reactive Ion Etching (RIE) of the gate can result in both damage and contamination of the GaAs surface [4]. Although RIE induced surface damage can be healed out with proper annealing [5], contamination is difficult to avoid, and undesirable impurities may diffuse into the GaAs during high temperatures steps [4]. The impurities that were present in the WSi_x films and at the surface of the GaAs after the gate RIE have been measured by Auger Electron Spectrometry (AES) and Secondary Ion Mass Spectroscopy (SIMS). The redistribution of these impurities in the GaAs during silicon nitride (SiN_x) capped annealing was measured by SIMS and compared to the profiles of shallow silicon implants into GaAs. Sheet resistance and Hall mobility measurements correlated well with the redistribution of these impurities. Cleaning techniques to remove the contamination were developed and tested. Using these techniques, refractory gate MESFET's with reduced source and drain resistances were fabricated.

GaAs samples were initially implanted with ^{29}Si at 30keV $1x10^{13}cm^{-2}$, capped with PECVD silicon nitride (SiN_x) and annealed at 850°C for 20min. The electrical activation and Hall mobility were measured at this first stage after buffered HF decapping of the SiN_x for comparison to values obtained after processing (RIE, WSi_x + RIE, and SiN_x capped re-annealing). The WSi_x deposition process consisted of a gentle oxygen then argon sputter

cleaning of the GaAs surface, followed by DC magnetron sputter deposition of alternating layers from W and Si targets in argon atmosphere at 10mT [3]. The RIE was performed in a parallel plate reactor using a CF_4 (184sccm) / O_2 (16sccm) chemistry at a pressure of 25mT with plasma-induced self-biases ranging from 50V to 250V. The electrical results are summarized in figure 1. A 10% loss in electrical activation was measured after WSi_x sputter deposition and RIE at 100V self-bias (Fig.1-d). The electrical activation dropped to 50% of its initial value and the Hall mobility was 2000 $cm^2V^{-1}s^{-1}$ instead of 3000 $cm^2V^{-1}s^{-1}$ after this sample was further capped with SiN_x and re-annealed at 700°C for 10 minutes. Gradual electrical recovery occured for increased temperatures, with 75% electrical activation and a Hall mobility of $2800cm^2V^{-1}s^{-1}$ for a 850°C- 20min anneal. Surprisingly, the samples that were flash annealed at 800°C for 5s showed 95% activation and a Hall mobility of $2900cm^2V^{-1}s^{-1}$. The blanket exposure of the GaAs surface to RIE only, with no gate sputter deposition, lead to a 5% loss in electrical activation (Fig.1-b). After anneal at 700°C-10min, a 30% degradation in electrical activation and mobility reduction from $3000cm^2V^{-1}s^{-1}$ to $2800cm^2V^{-1}s^{-1}$ were measured. Complete electrical recovery was measured with increasing the annealing temperature to 850°C- 20min. The fact that the sheet resistance and Hall mobility did not improve, but were degraded after a 700°C- 800° 10min annealing, suggested the existence of impurities which would accumulate at the surface and diffuse into the GaAs, thus compensating the ^{29}Si 30keV $1x10^{13}cm^{-2}$ implants. If the GaAs surface had been only damaged by the WSi_x sputter deposition and RIE, the electrical activation and Hall mobility should gradually improve with increasing the annealing temperature above 600°C [5]. This was not the case.

To assess surface damage effects separately from contamination effects, we measured the Shottky I-V and C-V characteristics of GaAs surfaces after processing and capped re-annealing. Ti/Pt/Au dots were evaporated on bulk-doped GaAs surfaces after they had been subjected to RIE or to WSi_x deposition and RIE. Some samples were also capped with silicon nitride (SiN_x) and furnace annealed at 700-850°C prior to TiPtAu deposition to simulate the GaAs surface damage recovery. The surface damage due to the RIE process only (without gate deposition) was significant for RIE plasma self-biases above 200V. The diode ideality factor n and the I-V and C-V barrier heights Φ^{I-V} , Φ^{C-V} were 1.05, 0.7V, and 0.78V respectively after a RIE at 100V self-bias, the same as for an unprocessed GaAs surface (Table I). The diode ideality factor was 2.0 after a RIE at 200V self-bias, the barrier height Φ^{I-V} was reduced from 0.7V down to 0.55V, and Φ^{C-V} increased from 0.78V to 0.95V (Table I). The sputter deposition of WSi_x followed by RIE at 100V self-bias left more damage at the GaAs surface than the RIE process alone with an ideality factor of $n = 1.2$ and barrier heights $\Phi^{I-V} = 0.6V$ and $\Phi^{I-V} = 0.95V$ (Table I). However, the surface damage introduced by the gate sputter deposition and a RIE at less than 200V self-bias could be healed out with a 800°C SiN_x capped furnace anneal, recovering a Schottky barrier height of $\Phi^{I-V} = 0.7V$ and $\Phi^{C-V} = 0.76V$, and an ideality factor of 1.05. This shows that the degradation of electrical activation and Hall mobility measured after a 800°C- 10min capped furnace annealing could not be explained by surface damage only, but was due to contamination of the GaAs by compensating impurities.

A direct correlation was made between the electrical measurements and SIMS analysis of the impurity redistribution into the GaAs during the annealing. Initially, Auger Electron Spectroscopy (AES) of GaAs surfaces showed that extensive RIE at high self-bias (200V self-bias and 60min. etch in a RIE system with Al electrodes) led to a surface accumulation of up to ~15at.% aluminium. For a WSi_x sputter deposition followed by a RIE with a 100V self-bias, SIMS detected Fe, Cr, Ni, Cu, V,... at the surface of the GaAs. A smaller quantity of these impurities accumulated at the surface of GaAs subjected to the RIE only (Fig.2). SIMS analysis of the WSi_x metallurgies showed that the above contaminants were initially

present in the sputtered gate metal (Fig.3). The level of Fe, for instance, was $\sim 1x10^{18}cm^{-3}$ in the WSi_x , which was in agreement with the 8-9wppm Fe measured in the W target. This indicated that the sputter deposition process did not introduce additionnal contaminants into the WSi_x. The Fe, Ni, Cr, Cu, V,... impurities were not seen to move significantly from the WSi_x gate into the GaAs on annealing, but reactive ion etching of the WSi_x left a thin layer of these impurities at the surface of the GaAs, which were driven into the bulk on annealing (Fig.4). The redistribution of ^{56}Fe on annealing was specifically analysed, as ^{56}Fe was present with the highest concentration at the surface of the GaAs. At 800°C- 10min SiN_x capped furnace annealing, the ^{56}Fe was as high as $\sim 5x10^{17}cm^{-3}$ next to the peak of the ^{29}Si implant. After a 850°C- 20min. anneal, the ^{56}Fe had diffused in and the concentration was $\sim 1x10^{17}cm^{-3}$. For a flash anneal at 800°C 5s, the ^{56}Fe was present at $\sim 2x10^{16}cm^{-3}$ into the GaAs. This data was consistent with the electrical sheet resistance and Hall mobility measurements. Little degradation was measured after the gate sputter deposition and RIE. Significant electrical compensation was measured for intermediate furnace anneal temperatures of 700°-800°C (Figure 4 ahows how ^{56}Fe, among other impurities, compensates the ^{29}Si profile), Gradual electrical recovery was measured with a higher anneal temperature of 850°C, for which the contaminants moved deep into the GaAs substrate and met the background level (Fig.4). The flash annealed samples showed good activation, also consistent with SIMS.

An effective method of cleaning the GaAs surface after the gate RIE was found to be a $HCl:H_2O$ (1:1), 1 minute etch. Hall effect measurements indicated that complete electrical activation and maximum Hall mobility were recovered with such HCl clean after the RIE and capped re-annealing at 700°C to 850°C (Fig.1). The $HCl:H_2O$ etch also removed the contamination left after the WSi_x sputter deposition and subsequent RIE. Electrical activation of 90-100% and a maximum Hall mobility were preserved after capped re-annealing at 700°C to 850°C (Fig.1-e). SIMS showed a direct correlation to the removal of contaminants in the GaAs. No accumulation of Fe was detected after the HCl etch for samples subjected to RIE or WSi_x and RIE (Fig.5). The level of Fe in the crystal after SiN_x capped furnace annealing at 850°C-20 minutes dropped from $\sim 1x10^{17}cm^{-3}$ to $\sim 2x10^{16}cm^{-3}$ with the HCl step (Fig.6).

Submicron Lightly Doped Drain (LDD) refractory gate shallow implanted MESFET's were fabricated with theses improved processing techniques by Hovel et al [6]. The introduction of the $HCl:H_2O$ (1:1) 1min. etch after the gate RIE, and prior to the conformal deposition of SiNx, led to a reduction of the source resistances from 1.0Ω-mm to 0.6Ω-mm for devices with source-drain implants of 30keV $1.3x10^{14}cm^{-2}$ ^{29}Si through a 500Å SiN_x dielectric. The edge capacitance increased from 0.4fF/μm to 0.5fF/μm. Assuming some lateral diffusion of the ^{29}Si dopants towards the gate edge, this higher capacitance result implies that there was more active charge under the edge of the gate, consistent with a model of having fewer compensating species available for lateral diffusion under the WSi_x . K-factors were improved at gate lengths greater than 0.7μm, but the advantage was not as pronounced as expected for the shorter gate lengths (0.7μm & 0.5μm), due to the onset of short channel effects, and due to the higher doping concentration achieved at the edges of the WSi_x gate.

These results indicate that contaminants such as Fe, Cr, Ni, Cu, V are responsible for the degradation seen in device characteristics after sputter depositions and dry etching. These contaminants were initially present in the W targets and WSi_x metallurgies and not removed by the RIE gate patterning. Enhanced cleaning procedures, such as the HCl etch of the GaAs surface, reduced the device access resistance. K-factors at submicron gate lengths increased accordingly. Further improved methods to avoid the contamination should lead to the fabrication of better devices.

Acknowledgments:

We wish to thank J.P.DeSouza, A.C.Callegari, and M.Goorsky for their comments. We thank J.F.Degelormo for offering to do comparative tests between his and our sputtering equipments, T.E.McKoy for the ion implantations, D.L.LaTulipe for help with the RIE and D.R.Lombardi for the furnace annealing. We acknowledge the encouragment of J.H.Magerlein and J.H.Greiner during this work.

References

[1] N.Yokoyama, T.Onishi, K.Odani, H.Onodera, M.Abe IEEE Trans. Electron. Devices ED-29, 1541 (1982)

[2] T.N.Jackson, G.Pepper, J.F.Degelormo, "High Performance refractory gate self-aligned GaAs MESFETs fabricated by arsine rapid thermal annealing" - Proc. IEDM, p.600, Washington DC (1987)

[3] J.H.Magerlein, D.J.Webb, A.Callegari, J.D.Feder, T.Fryxell, H.C.Guthrie, P.D.Hoh, J.W.Mitchell, A.T.S.Pomerene, S.Scontras, G.D.Spiers, J.H.Greiner, "Characterization of GaAs self-aligned refractory-gate metal-semiconductor field-effect transistor (MESFET) integrated circuits" J.Appl. Phys., 8(61): 3080-3092, 1987
also : C.J.Anderson, J.H.Magerlein, G.J.Scott, S.Bermon, A.Callegari, J.D.Feder, J.H.Greiner, P.D.Hoh, H.J.Hovel, A.T.S.Pomerene, P.Roche, M.Thomas, "A GaAs MESFET 16x16 crosspoint switch at 1700MBits/sec" GaAs IC symposium, Nashville, Tenessee, (1988).

[4] A.G.Lahav, C.S.Wu, F.Baiocchi "WSix refractory metallization for GaAs metal-semiconductor field effect transistors" J.Vac. Sc. Technol. B6 (6) Nov./Dec. 1988

[5] S.W.Pang, G.A.Lincoln, R.W.McClelland, P.D.DeGraff, M.W.Geis, W.J.Piancnetini, "Effect of dry etching on GaAs" J.Vac.Sc.Tech., pp. 1334-1337, Oct.1983

[6] H.J.Hovel, J.H.Magerlein, S.Bermon, H.Baratte, A.C.Callegari, R.P.Dunne Jr, J.D.Feder, A.J.Fleischman, N.C.LaBianca, D.L.Lacey, D.C.LaTulipe, D.R.Lombardi, T.E.McKoy, D.D.Piazza, A.T.S.Pomerene, D.K.Sadana, J.P.Simons, C.J.Anderson, J.H.Greiner "Enhanced GaAs FET Design for High Speed E/D Circuits" To be published.

Process	Anneal C	n	(IV)	(CV)
Reference	none	1.05	0.71	0.78
RIE 100V	none	1.05	0.69	0.79
RIE 200V	none	2.00	0.65	0.85
RIE 250V	none			
WSix / RIE 100V	none	1.20	0.60	0.95
RIE 100V	700	1.05	0.70	0.78
RIE 200V	800	1.22	0.65	0.82
RIE 200V	850	1.23	0.68	0.85
RIE 250v	850			
WSix RIE 100V	800	1.05	0.69	0.80

Table 1 - Ideality factors, I-V and C-V barrier heights obtained after RIE alone at 100V and 200V self-bias, WSi_x sputter deposition and RIE st 100V.

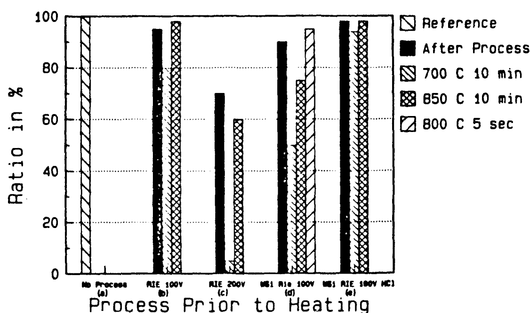

Fig. 1 - Electrical activation degradation after RIE, or WSi_x sputter deposition and RIE at 100V, followed by capped furnace annealing at 700°C and 850°C, implying the diffusion of compensating impurities into the GaAs.
(a) no process, (b) RIE at 100V (c) RIE at 200V (d) WSi_x + RIE 100V (e) WSi_x + RIE, HCl clean

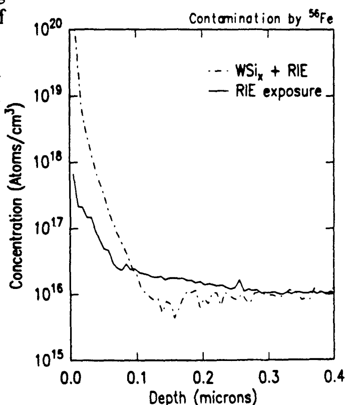

Fig.2 - Accumulation of ^{56}Fe (not shown : Ni, Cr, Cu, V,...) at the surface of the GaAs after RIE at 100V self-bias, and after a WSi_x sputter deposition and RIE.

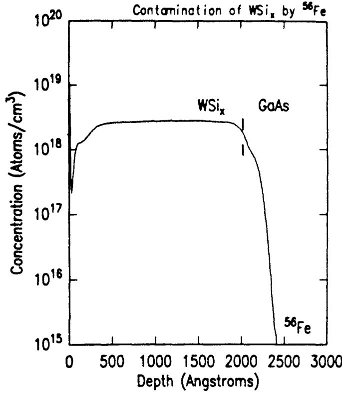

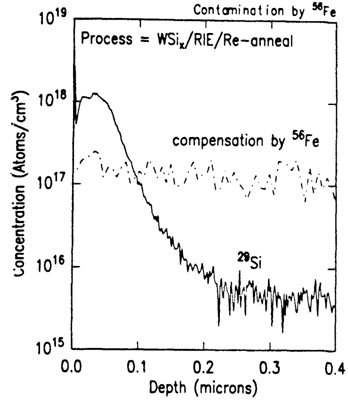

Fig.3 - SIMS analysis of ^{56}Fe in the WSi_x gate metal, showing a level of $1x10^{18}cm^{-3}$ Fe, consistent with the 8-9ppm Fe measured in the W target.

Fig.4 - The contaminants (Fe, Ni, Cu, V,..) were driven into the GaAs during capped annealing and acted as compensating impurities.

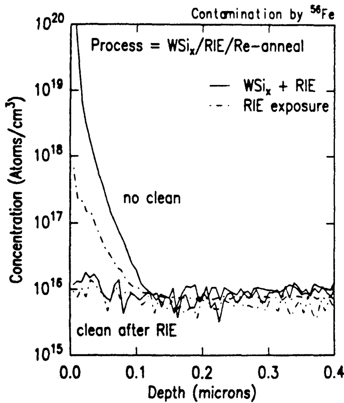

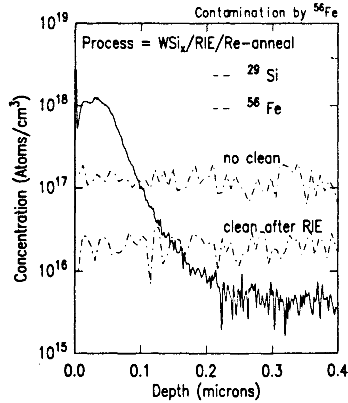

Fig.5 - The contaminants that accumulated at the GaAs surface after RIE or WSi_x sputter deposition and RIE were efficiently removed by a $HCl:H_2O$ 1minute etch.

Fig.6 - The level of ^{56}Fe in the GaAs after SiN_x capped furnace annealing at 850°C for 20 minutes dropped from $\sim5x10^{17}cm^{-3}$ to $\sim5x10^{16}cm^{-3}$ with the $HCl:H_2O$ 1minute etch.

A MEASUREMENT OF OPTICAL PROPERTIES FOR INP SURFACES

X. Liu and E. A. Irene
Department of Chemistry,
University of North Carolina,
Chapel Hill, NC 27599-3290

S. Hattangady and G. Fountain
P.O.Box 12194, Research Triangle Institute,
Research Triangle Park, NC 27709

Abstract

Several chemical cleaning procedures for InP surfaces have been studied using ellipsometry. The strong influence of cleaning on the optical properties of InP surfaces suggests that the measurements involve the formation of surface films. In order to determine the complex index of refraction for InP, a novel method which employs ellipsometry measurements of a thin non-absorbing film on a substrate rather than measurements of a bare surface has been explored. From the knowledge of the refractive index for a series of thicknesses of films on a substrate, the complex refractive index value for the substrate can be determined. Plasma Enhanced Chemical Vapor Deposition(PECVD) SiO_2 and Si_3N_4 films on InP have been used for this experiment, and the complex refractive index for InP has been determined to be 3.521+i0.300 at the wavelength of 632.8 nm.

Introduction

Surface preparation has been shown to have a significant influence on the optical properties of a semiconductor surface(1,2). Chemically reactive, Si, Ge, and III-V semiconductors form a native oxide layer upon exposure to air(3,4). Therefore, an abrupt ambient-substrate boundary is practically unachievable with these surfaces except for a short time with the surfaces in an ultra high vacuum. Recently, it has been shown by in-situ ellipsometry and in-situ contact angle measurements(5) that chemical cleaning left some residue film on Si surfaces. Detailed ex-situ ir spectroscopy studies indicate that the film may be H terminated Si(6,7). All these facts imply that the literature discrepancy of the reported optical properties of Si, Ge, and the compound semiconductors could be interpreted

in terms of different surfaces being measured, i.e. a different surface film on a substrate despite cleaning.

The widely cited values of the complex refractive index of InP in the uv-visible spectral region were obtained from Kramers- Kronig analysis of reflectance measurements by Cardona(8,9). These values are lower than those determined ellipsometrically by Aspnes and Studna(10). Recently, we have examined the InP optical constants at the wavelength 632.8 nm. A discrepancy as large as three percent has been found in the real and ten percent in the imaginary part of the complex index which results in about one degree difference in the ellipsometric variables Ψ and Δ, where Ψ is the change in the amplitude ratio, and Δ is the change in phase difference of polarized light upon reflection from a sample surface.

Due to the high accuracy and the versatile ambient compatibility, ellipsometry has been used to measure the optical properties of semiconductor surfaces(11,12). However, the reported measurements on InP substrates involve, more or less, the dielectric properties of a surface film, which inevitably exists if the sample is not cleaned and kept in a high vacuum system(13-15). Unlike the previous studies, we did not try to eliminate the InP surface layer, instead we measured the surface coated with a thin PECVD film. Taking advantage of the weak dependence of the Ψ and Δ on the film refractive index when the film thickness is less then 20 nm, and even without knowing an accurate value for the film index, the complex refractive index for InP at 632.8 nm was determined with high accuracy by fitting the ellipsometrically measured Ψ-Δ pairs of a series of thicknesses of thin films on the substrate.

It is intended, in this paper, to report the observations of the influence of different chemical treatments on the optical properties of InP, to describe the idea and the experimental results from the novel method for determining the complex index for InP, and to compare our results with literature values.

Experimental Procedures

Commercially available, polished, N-type Sn-doped, (100) oriented InP wafers($n=2x10^{18}cm^{-3}$) were used in the surface cleaning experiments. The wafers were cut into 1 cm^2 pieces. The pretreatments of the InP samples are summarized in Table 1. Group 1 samples were exposed to a 5 minute boiling degrease in tetrachloroethylene, then rinsed in the mixture

of acetone and methanol for about 10 minutes, followed by another 10 minute rinsing in acetone, and blown dry by compressed N_2 gas(16). For convenience, the Group 1 cleaning procedure is called "degreasing". Group 2 samples first received the degreasing, then a 10 second concentrated HF dip, deionized water rinse, and N_2 blow dry. Group 3 samples were cleaned in the way similar to that of the Group 2 samples. However, instead of HF dip and d.i. water rinse, a chemi-mechanical polishing in a 1% Br_2/methanol solution and methanol rinse were employed. Group 4 samples were cleaned in the sequence of degreasing, HF dip, d.i. water rinse, 1% Br_2/methanol polish, methanol rinse, and N_2 dry. Immediately after a chemical cleaning, two ellipsometry measurements were made on different surface spots for each sample.

A manual high precision ellipsometer was used for the measurements. A He-Ne laser was used to provide a stable, highly collimated, monochromatic light beam. A modified McCrackin procedure was applied for the ellipsometer alignment(17). In the alignment procedure, first the optical bench of the ellipsometer was autocollimated, and then the laser and the optical components, i.e., polarizer, compensator, and analyzer, were positioned on the optical axis defined in the autocollimation step. Finally the optical components were calibrated. The full procedure enabled the azimuth angles of the components as well as the incident angle to be known to 0.01^0. A 70.00^0 incident angle was used, and two-zone measurements were employed through out our work, in order to obtain high accuracy(18).

N-type undoped (100) oriented InP wafers($n<10^{16}cm^{-3}$), and P-type B-doped (100) Si wafers were used for the remote PECVD of SiO_2 and Si_3N_4 films. Before the samples were loaded into the deposition chamber, the InP samples were cleaned as Group 2 samples described above, and Si samples were given a modified RCA cleaning(19). For each run, one InP and three Si samples were loaded on the sample stage, which was heated to 250^0C during the deposition. The pressure of the PECVD chamber was 80 mtorr, and the power was 30 watts. For the SiO_2 deposition, a 300/100 sccm Ar/O_2 gas flow was used to generate the plasma, and 5 sccm SiH_4 was supplied as the Si source. For silicon nitride deposition, a 400/10 sccm Ar/N_2 gas flow was used for plasma generation, and 5/100 sccm SiH_4/N_2 was supplied in the deposition chamber. Two spots on each of these PECVD samples were ellipsometrically measured, and the average value for each sample was used in the data analysis.

Results and Discussion

An ideal optically isotropic ambient-film-substrate, three phase, optical model is adequate for our ellipsometry data analysis(20). In the model, the measured Ψ and Δ are related to the optical properties of the system investigated by the relation

$$\tan \Psi \exp(j\Delta) = \rho(N_0, N_1, N_2, L, \phi, \lambda)$$

where N_0, N_1, and N_2 are the complex indices of the ambient, the surface film, and the substrate, respectively. L is the film thickness, ϕ is the angle of the incident beam, and λ is the incident radiation wavelength. With the N_0, ϕ and λ as experimentally controlled variables, and with N_2 fixed, any change in the measured Ψ and Δ reflects a change in the film index N_1 and the film thickness L.

The measured Ψ and Δ values for InP are strongly dependent on the surface chemical treatments, as shown in Table 2. The degreasing of InP in hot tetrachloroethylene, Group 1 samples, altered surface properties, with both Ψ and Δ slightly lower than the values of the as-received InP surface, as listed in the first row under no clean category. The measured Ψ, Δ values were analyzed using a non-absorbing film on an absorbing substrate model to yield a film thickness and refractive index, and these values are in the last two columns of Table 2. The small change due to degreasing could be accounted for by the index change of the surface film due to the exposure to the solvents. The HF dip of the Group 2 samples resulted in a further decrease in Ψ but an increase in Δ. This indicated that the thickness of the surface layer was reduced along with, perhaps, a slight change in film index. The 10 second HF dip removed approximately 1.0 nm of the film. The Group 3 samples, which received the Br_2 methanol polishing, showed a large change in Ψ and Δ. The surface yielded the highest Δ value, thus the lowest film thickness. The cleaning sequence of degreasing, HF dipping, and Br_2 methanol polishing, Group 4 samples, gave the lowest Ψ value.

In order to circumvent the above described difficulty of the influence of the cleaning procedure with the measurement of N_1, we used non-adventitious PECVD films with known properties and with an adjusted film thickness to maximize the sensitivity to the InP substrate. The measured Ψ and Δ of the PECVD SiO_2 films on Si substrates are shown in Figure 1. The solid line was calculated by assuming a particular film index while varying the film thickness, while the value of 3.865+i0.018 was used for the complex index of Si substrate(21,22), and the two dashed lines were derived from two other film index values. From the Figure, the index of the SiO_2 films on Si was determined as 1.39+i0.00, with an

uncertainty of about ±0.05. The deposition temperature of 250^0C and a remote plasma source were used, in order to minimize the substrate damage during the deposition process. Therefore, it was assumed that the SiO_2 films deposited on Si and InP, which were side-by-side in the plasma chamber, have the same optical properties. The assumption enabled the index value, 1.39+i0.00, obtained from the PECVD SiO_2 films on Si to be used for the analysis of the same films on InP. Figure 2 shows the measured Ψ-Δ pairs for SiO_2 films on InP, and the simulated curves using different complex indices for InP while varying the SiO_2 film thickness. The top dashed curve was calculated by using Aspnes' index value 3.536+i0.307 for the InP substrate(10), while the bottom dashed curve came from the Cardona's value of 3.420+i0.278(8). The solid curve with a substrate index value 3.521+i0.300 gave the best fit to all the measured Ψ-Δ data points. The accuracy of this procedure can be simply estimated. The total experimental error was less than 0.02^0 in the measured Ψ and less than 0.05^0 in Δ. A deviation of 0.003 from the real part of the complex index or 0.004 from the imaginary part could independently cause more than 0.02^0 difference in the calculated Ψ, and 0.10^0 in the calculated Δ. To be conservative, the complex index could be represented as (3.521±0.003)+i(0.300±0.004). As mentioned above, there was about ±0.05 uncertainty in the index value for the SiO_2 films, however, this uncertainty did not affect the accuracy of our final result. As seen in Figure 3, the three curves correspond to surface films on InP with indices of 1.34+i.00, 1.39+i0.00, and 1.44+i0.00. As the film thickness goes below 10 nm, all the curves converge into a single one, with a deviation smaller than the measurement uncertainty of our ellipsometry hardware. The convergence ensures that the index value of InP could be determined accurately, even the film index near the origin could be determined reasonably accurately.

Similarly, the index of the PECVD Si_3N_4 films on Si was determined as 1.70+i0.00. Again this value was adopted for the nitride films on InP. Using the procedure described above, the complex index of InP was determined as 3.521+i0.300, which is the same as that determined by using SiO_2 films. The experimental Ψ and Δ data and the simulated curves for the nitride films on InP are shown in Fig.4.

Figure 5 shows the calculated Ψ and Δ curves for SiO_2 and Si_3N_4 on InP using 3.521+i0.300 for the InP while varying film thicknesses. The measured data for both SiO_2 and Si_3N_4 on InP almost perfectly fit the calculated curves. This provides a consistency check on this value for InP. Our complex index value is in good agreement with the Aspnes value(10),

3.536+i0.307, as was determined by the spectroscopic ellipsometry. Our index value is higher, both in the real and the imaginary part, than those determined by reflectance measurements(8). We, therefore, agree with the comment(10) that the Kramers-Kronig analysis of reflectance data could cause notable errors because the extrapolated reflectance data in the experimental unobtainable wavelength ranges were used in the integration.

Conclusions

We have demonstrated that the surface preparation of InP influences the measured optical properties of InP. The influence may be derived from the alteration of either the refractive index or the thickness of a surface layer by the chemical treatments. An in-situ solution ellipsometry study, which could eliminate the ambient effect caused by the interaction of the surface with the ambient air, is needed for further studies of this phenomena and is underway. Among the InP cleaning procedures investigated, the 1% Br_2 in methanol chemi-mechanical polishing produces the thinnest surface layer.

The complex refractive index for InP has been determined to be 3.521+i0.300 by the novel procedure. The new method has two distinguishable advantages over the techniques applying direct measurements of a bare surface. The measurements of a surface covered with a thin film eliminate the influence of the surface preparation, thus a reliable and reproducible result could be expected. The second advantage is that the weak dependence of Ψ and Δ on the film index relieves the requirement for having an accurate index value for the film. Therefore, the uncertainty of the final result is greatly reduced. The ellipsometric method described herein is generally applicable for other solid state materials.

Acknowledgement

This research was supported in part by the Office of Naval Research, ONR, and the Semiconductor Research Corporation, SRC.

REFERENCES

(1). H.R. Philipp, J. Appl. Phys., 43(6), 2835 (1972).
(2). H.J. Mattausch, and D.E. Aspnes, Phys. Rev., B23(4), 1896 (1981).

(3). E. Kuphal and H.W. Dinges, J. Appl. Phys., 50, 4196 (1979).
(4). D.E. Aspnes and A.A. Studna, Appl. Phys. Lett., 39(4), 316 (1981).
(5). G. Gould and E.A. Irene, J. Electrochem. Soc. 135(6), 1535 (1988).
(6). E. Yablonovitch, D.L. Allara, C.C. Chang, T. Gmitter, and T.B. Bright, Phys. Rev. Lett., 57, 249 (1986).
(7). V.A. Burrows, Y.J. Chabal, G.S. Higashi, K.Raghavachari, and S.B. Christman, Appl. Phys. Lett., 53, 988 (1988).
(8). M. Cardona, J. Appl. Phys. 36, 2181 (1965).
(9). B.O. Seraphin and H.E. Bennett, Optical Properties of III-V Compounds, edited by R.K. Willardson and A.C. Beer (Academic,
New York, 1967), P.499.
(10). D.E. Aspnes and A.A. Studna, Phys. Rev., B27(2), 985 (1983). 11. D.E. Aspnes, J.B. Theeten, and F. Hottier, Phys. Rev., B20(8), 3292 (1979).
(12). W.-K. Paik, Marvin A. Genshaw, and J.O'M. Bockris, J. Phys.
Chem., 74(24), 4266 (1970).
(13). G.D. Pettit and W.J. Turner, J. Appl. Phys., 36, 2081 (1965).
(14). H. Burkhard, H.W. Dinges, and E. Kuphal, J. Appl. Phys., 53, 655 (1982).
(15). J.-P. Moy, Appl. Opt., 20(22), 3821 (1981).
(16). J.F. Wager, M.D. Clark, and R.A. Jullens, J. Vac. Sci. Technol. B2(3), 584 (1984).
(17). F.L. McCrackin, E. Passaglia, R.R. Stromberg, H.L. Steinberg, J. Res. of N.B.S.A., 67A(4), 363 (1963).
(18). R.M.A. Azzam and N.M. Bashara, Ellipsometry and Polarized Light(North-Holland), 1977, P.208.
(19). W. Kern and D.A. Puotinen, RCA Rev., 31, 187 (1970).
(20). R.M.A. Azzam and N.M. Bashara, Ellipsometry and Polarized Light(North-Holland), 1977, P.288.
(21). H.R. Philipp, J. Appl. Phys., 43(6), 2835 (1972).
(22). D.E. Aspnes and J. Theeten, J. Electrochem. Soc., 127(6), 1359 (1980).

Table 1: The summary of the cleaning procedures for InP surfaces. The cleaning of the Group 1 samples is called "degreasing" for convenience.

Group	Cleaning Procedure
1	"degreasing"--- 5 min in hot tetrachloroethylene, 10 min in 1:1 acetone:methanol, 10 min in acetone N_2 dry.
2	degreasing, 10 second concentrated HF dip, d.i. water rinse, N_2 dry.
3	degreasing, 1% Br_2 in methanol chemi-mechanical polish, methanol rinse, N_2 dry.
4	degreasing, 10 second HF dip, d.i. water rinse, 1% Br_2 in methanol polish, methanol rinse, N_2 dry.

Table 2: The ellipsometry measured Ψ and Δ values, and the corresponding standard deviations for InP surfaces after receiving wet chemical cleaning. The thicknesses and refractive indices of the surface films are listed in the last two columns.

Sample Prep.	Ψ (^{0})	Std.Dev. (±)	Δ (^{0})	Std.Dev. (±)	Thickness (nm)	Refractive Index
No Clean	8.553	0.003	155.808	0.11	2.5	1.30
Group 1	8.495	0.09	155.254	0.80	1.8	1.75
Group 2	8.343	0.03	157.511	0.22	1.1	2.30
Group 3	8.314	0.14	158.938	0.56	0.7	2.40
Group 4	8.308	0.05	157.695	0.50	1.0	2.40

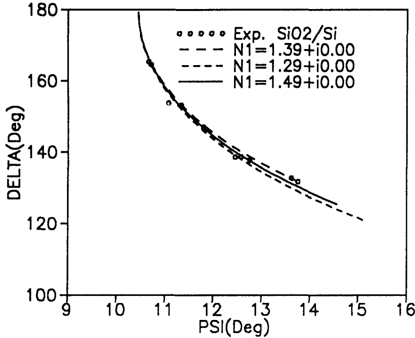

Figure 1: The experimental and simulated Ψ and Δ data for PECVD SiO_2 films on Si. The complex refractive index for Si is 3.865+i0.018, and N_1 is the film index.

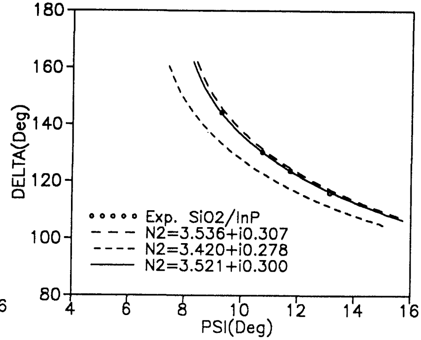

Figure 2: The simulated and experimental Ψ and Δ for silicon dioxide on InP. N_2 is the index for InP, where N1=1.39+i0.00.

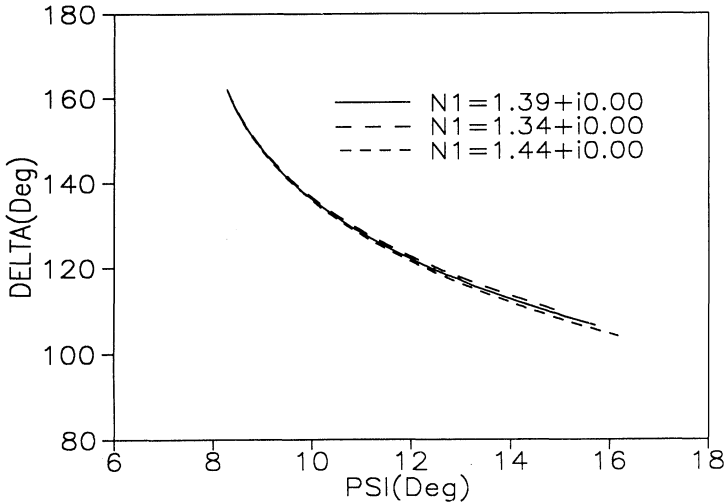

Figure 3 : The calculated Ψ and Δ curves for films on InP, where N2=3.521+i0.300. For each curve, the top most point corresponds to a bare InP surface, and the other end represents a 30 nm film on it.

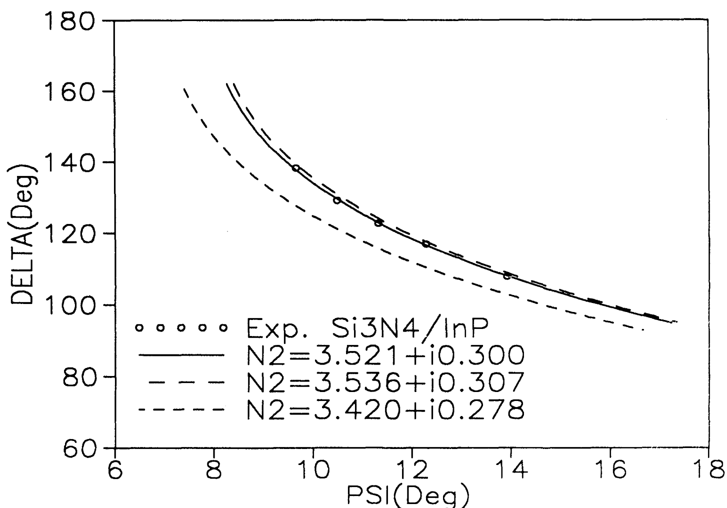

Figure 4: The simulated Ψ and Δ and experimental Ψ-Δ pairs for silicon nitride film on InP, where N1=1.70+i0.00.

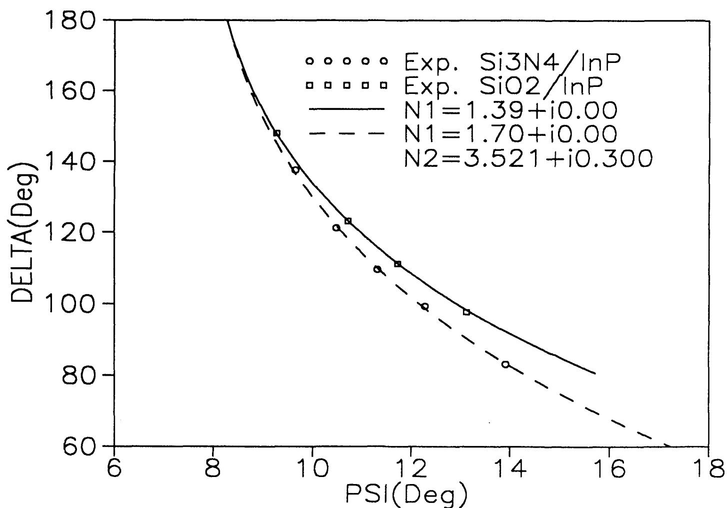

Figure 5: The measured Ψ-Δ for PECVD silicon dioxide and silicon nitride films on InP and the simulated curves.

Author Index

Atsumi, J.	59
Baratte, H.	377
Becker, L. S.	43
Bowling, R. A.	33
Cardone, F.	377
Davison, J.	83
de Larios, J. M.	121,283
Deal, B. E.	121,283
DeKeersmaecker, R.	293
DeMeyer, K. M.	313
Donovan, R. P.	167
Dupas, L. H.	313
Eberle, W. J.	43
Falster, R.	293
Fleischman, A.	377
Frystak, D. G.	129
Fukumoto, T.	182
Golland, D. I.	23
Grundner, M.	215,328
Hahn, P. O.	215,328
Hasenack, C.	293
Helms, C. R.	283
Heyns, M.	293
Hockett, R. S.	227
Hossain, S. D.	341
Hovel, H.	377
Hsu, C.	83
Irene, E. A.	251,383
Ito, T.	114
Jackson, D.	335,357
Jackson, T.	377
Jacob, H.	215
Kajiyama, K.	59
Kamieniecki,E.	273,335,357
Kao, D. B.	121,283
Kato, T.	182
Katz, W.	43
Kawabata, A.	243
Kawaguchi, T.	182
Kawanabe, I.	95
Kern, W.	3
Kikuyama, H.	95
Kren, G.	192
Krusell, W. C.	23
Kunii, Y.	156
Lampert, I.	215,328
Lee, H.	83
Lindelauf, H. W. L.	321
Ling, Z. M.	313
Liu, X.	383
Lowenstein, L. M.	148
Matsuda, K.	141
McNeilly, M. A.	121
Menon, V. B.	167
Miki, N.	95
Minegishi, K.	265
Miyashita, M.	95
Morita, M.	265
Morrison, P. W.	204
Muller, A. J.	204
Munehira, S.	59
Nara, Y	114
Neukermans, A.	192
Nishihagi, K.	243
Ohmi, T.	95,265
Ohmori, T.	182
Ohsawa, A.	75
Ohtsuka, S.	59
Onishi, S.	141
Pahk, U. S.	251
Pantano, C. G.	341
Parimi, P. M.	260
Pecen, J.	192
Philipossian, A.	335,357
Portillo, J.	313
Psota-Kelty, L. A.	204

Resnick, A.	335,357
Ronde, H. J.	321
Ross, D.	67
Ruzyllo, J.	129,341
Saadat, S.'	192
Saito, K.	265
Sakiyama	141
Sato, Y.	114
Schnegg, A.	215
Scilla, G.	377
Sinclair, J. D.	204
Snee, P. M.	306
Sobol, P. E.	43
Sugino, R.	114
Sundarsingh, V. P.	260
Tada, M.	182
Takizawa, R.	75
Tanaka, K.	141
Tipton, C. M.	33,148
Trautmann, E.	83
van der Heide, P.A.M.	321
van Oekel, J. J.	306
Vandervorst, W.	313
Vig, J. R.	105
Warren, A. D.	371
Watanabe, S.	114
Woodall, J. M.	371
Yabumoto, N.	265
Zazzera, L. A.	43

SUBJECT INDEX

accumulation 275
AES 46
adhesion force 171
adsorbed molecules 265
adsorption 144
air 324
airborne concentration 207
aluminum contamination 60, 308
arrival rates 207
arsenic flux 373
atomic absorption spectorphotometry 62, 76
atomic absorption spectroscopy 116, 243
Auger effect 262
automatic analysis 246

backscattered electron imaging 35
bacteria 26
bare wafers 337
bias-temperature test 142

capillary drying 14
capillary forces 33
carbon, removal 341
carbon, sputtered 342
carrier lifetime 60, 116
centrifugal spraying 6
charcoal 206
chemical inhomogeneity 330
chemical oxide 133
chemisorb 268
chlorine gas 115, 132
choline 12, 23, 34, 228
cleaning, efficiency 296
cleaning, fluid jet 12
cleaning, mechanical 11
cleaning, RCA 7, 23, 59, 75
complexing 5
condensation 332
contact angle 47
contact angle measurements 34
copper contamination 59, 130
cumulative histograms 193

damage 131
depth profile 246
detection limit 245
dielectric layer 277
differential reflectance 251
dopant activation 378
dry ice 13
drying 13, 172
dual thresholding 194

electrochemical field 283
ellipsometry 149, 345, 384
epitaxial silicon film 117
ESCA 315
ESCA, angular dependence 316
ESCA/HREELS 216
etch mechanism 123
etching 132
etching, downstream 149
etching, dry 149
etching, H_2 gas 158
etching, isotropic 149
etching, Si 75, 129
etching, SiO_2 252
etching, wet 152

Fermi level pinning 371
filtration 168
fluorine 345
fluorine removal 98
Freundlich's adsorption formula 76

GaAs, native oxide 373
GaAs, regrowth 372
GaAs, thermal etch 373
gas chromatography 205
glancing angle 244
grease removal 186

Halogen radical 114
HCl plasma 130
heavy metals 59, 114, 129
hexamethyldisilazane 331
HF dip 216, 296
HF etch 321
HF gas 266, 323
HF solution 266

HF/H_2O attack 219
HMDS treatment 221
hydride coverage 217
hydrocarbons 267, 342
hydrogen 267
hydrogen peroxide mixtures 5
hydrolization 332
hydrophilic 49
hydrophilic surface 25, 220, 328, 343
hydrophobic 49
hydrophobic surface 217, 343
hydroxides 4

ice particle 182
Indium phosphide 383
initial oxide 286
InP, ambient effect 388
InP, refractive index 386
interface change 279
interface state density 117
inversion 275
ion exchange 85
ion exchange film 51
iron adsorption 75
iron contamination 60
isopropyl alcohol 14, 173, 342

laser defect scanner 45
light scattering 192
lightly doped drain devices 379
liquid surface tension 33
local oxidation 148

mass spectrometry 205
mass transfer 208
megasonics 7, 171
metallic contaminants 25, 59, 116, 130, 232
metallics analysis 46
microwave plasma 130
Mirau optical profilometer 76
monochromator 244
MOS structures yield 293

native oxide 71, 115, 124, 156, 268
non-destructive characterization 276

optical model 253
optical properties 383
organic contaminants 204, 341
organic film 182
organic vapors 204
oxidation kinetics 283
oxidation mechanism 306
oxidation mode 284
oxide breakdown 87, 131, 303
oxide etch back 123
oxide removal 48
oxygen afterglow 133
oxygen concentration 151, 159
oxygen plasma ashing 141
ozone 29
ozone ashing 141

particles 4, 25, 167, 182, 192, 204, 297
particles, characterization 45
particles, control 26
particles, density 70
particles, measurement 27
particles, sizing 192
photosensitized-oxidation 107
photovoltage 273, 336
plasma HCl 130

quartz cleaning 83
quartz tube 130

radioactive tracer measurements 5
reflection electron microscopy 76
remote plasma 129
reprocessed HF 89
RIE 377
rinsing 13, 172
rotating anode 244
Rutherford backscattering 151, 233

sacrificial oxidation 298
scan averaging 194
scattering cross-section 195
Schottky barrier 371
scrubbing 11
SEM 35
Si-hydride coverage 217

Si-OH coverage 221
silica 51
SIMS 60, 116, 143,157, 227, 347, 379
SIMS, polyencapsulation 229
single acetic solution 43
single bit failures 89
sodium 50
solid phase epitaxy 156
spectrochemical analysis 261
spectroscopic ellipsometry 314
spray etching 67
sputter deposition 377
statistical effects 193
STM 304
structural inhomogeneity 330
suboxide states 313
substrate effects 297
sulfuric acid 4
surface charge 273, 335
surface characterization 43
surface film 256
surface recombination velocity 117
surface roughness 76, 129, 298
surfactants 170

TEM 157
tensiometer 34
TEOS CVD 68
thermal desorption 206
thermal desorption spectroscopy 265
thermal oxidation 68, 341
trace contaminants 271
trench etching 33
TRXRF 48, 227, 243, 302
tungsten silicide 380

ultrapure HF 86
UV irradiation 105, 115
UV/ozone 13, 105, 348

wafer fingerprint 299
water concentration 158
wetability 45

XPS 47, 322

yield 89
yield, MOS structures 293